Mass Transport In Oxides

Proceedings of a Symposium

October 22–25, 1967

United States Department of Commerce

National Bureau of Standards

Special Publication 296

UNITED STATES DEPARTMENT OF COMMERCE
C. R. SMITH, *Secretary*
NATIONAL BUREAU OF STANDARDS · A. V. Astin, *Director*

Mass Transport In Oxides

Proceedings of a Symposium
Held at Gaithersburg, Maryland
October 22 - 25, 1967

Edited by

J. B. Wachtman, Jr. and A. D. Franklin
Institute for Materials Research
National Bureau of Standards
Washington, D.C. 20234

Sponsored by
Advanced Research Projects Agency
and
National Bureau of Standards

National Bureau of Standards Special Publication 296
Issued August 1968

For sale by the Superintendent of Documents, U.S. Government Printing Office, Washington, D.C. 20402
Price $3

Abstract

This Monograph presents the Proceedings of the Conference on Mass Transport in Oxides, held at the National Bureau of Standards in Gaithersburg, Md., from October 22 to October 25, under the joint sponsorship of the Bureau and the Advanced Research Projects Agency. Invited papers reviewed mass transport in alkali and silver halides as background, and topics relating to oxides including point defects, (both experiment and theory), lattice dynamics and ionic interactions, atomistic mechanisms of diffusion and ionic conduction, chemical diffusion, defect complexes, assessments of the experimental situation for diffusion and ionic conduction, and the availability of good research materials. In contributed papers, attention was focused on color centers in alkaline earth oxides, cation diffusion in MgO, transport of both cations and anions in transition metal oxides, and coulometric and emf techniques for obtaining transport data. A panel discussion summarized the work of the conference.

Key Words: Crystal defects, diffusion, ionic conductivity, mass transport, oxides, stoichiometry.

Library of Congress Catalog Card Number: 68-60030

Foreword

The National Bureau of Standards has as a major responsibility the task of ensuring that basic, urgently needed data on the properties of materials are available to meet the requirements of the Nation's scientists and engineers. In this context, data is a rather broad term, implying experimentally measured numbers, experimental procedures, theory, and the specification of the dependence of important properties upon controlling variables.

In an immediate sense, this responsibility is met in part through measurements and calculations done in NBS laboratories, in part through compilation and publication of critically evaluated data gathered from the literature, and in part through survey articles including compiled data. To respond to the long-range needs, emphasis is placed on stimulating the development of fields where data will be increasingly needed in the future.

Mass transport in oxides is an important factor controlling the properties and use of ceramic materials at high temperatures and in controlling the processing of ceramics to achieve the properties needed for use at any temperature. Reliable data on diffusion coefficients and the factors controlling them are needed; however, this requires the development of reliable measurement techniques, understanding of the relationship of structural defects to diffusion coefficients, and high-quality, well-characterized research materials. In recognition of this need, the National Bureau of Standards, through its Institute for Materials Research, and the Advanced Research Projects Agency of the Department of Defense organized this Symposium on Mass Transport in Oxides, bringing scientists interested in diffusion together with those interested in such underlying fields as point defect studies and crystal growth. The intent was to provide a forum where the problems currently limiting progress in obtaining reliable diffusion data might be more clearly understood.

The National Bureau of Standards presents these Proceedings of the Conference in order to assist those attending the Conference in further research and to make the results available to a wider audience. On behalf of the recipient of these Proceedings, the National Bureau of Standards would like to express appreciation to the participants, whose time, energy, and thought are embodied in these Proceedings, and to the Advanced Research Projects Agency, whose sponsorship made the Conference possible.

A. V. Astin, Director
National Bureau of Standards.

Introduction

The Symposium on Mass Transport in Oxides was held at the National Bureau of Standards laboratories at Gaithersburg, Maryland, on October 22–25, 1967. It brought together approximately 100 scientists and engineers from the United States, Great Britain, the Netherlands, Canada, Australia, and France.

Mass transport in solid, crystalline oxides is an important factor controlling the properties and use of ceramic materials, directly when ceramics are used at high temperatures and indirectly at any temperature, through influence on the processing and, therefore, the final properties of the ceramic.

Mass transport processes are directly important in high temperature applications involving creep, ionic conductivity, or protection from corrosion including oxidization. They are also directly involved in fuel cell operation.

The indirect influence of mass transport processes arises through the dependence of such structure-sensitive properties as strength, electrical and magnetic parameters, thermal conductivity, and optical properties upon the microstructure produced by processing. Most polycrystalline ceramics are produced either by solid state sintering or by a process involving partial or complete melting followed by controlled crystallization. Domination of the resulting microstructure is effected through careful control of the heat treatment (which may be rather complex) and through the use of chemical additives to affect the rates of mass transport. An empirical approach has generally been followed, sometimes quite successfully, but much effort is being devoted to improving ceramic processing, including the development of better quantitative descriptions in terms of the basic processes at work. An extensive survey of ceramic processing is given in the report of the National Academy of Science-National Research Council Materials Advisory Board ad hoc committee on Ceramic Processing, publication 1576 of the National Academy of Sciences. Knowledge of mass transport rates and the factors controlling them is an area where improvement is badly needed. Lack of reproducibility of diffusion data for oxides is a problem extensively discussed in the present conference report and illustrated in a recent compilation of diffusion data [A. L. Dragoo, Diffusion Rates in Inorganic Nuclear Materials, J. Res. NBS (Phys. and Chem.) **72A,** 157 (1968)].

The field of mass transport in oxides at the present time contains much of importance and opportunity to the basic science of materials, in addition to its technological significance. Detailed mechanisms for similar processes in the "model" alkali halides have been rather well-worked out. While these models provide some guidance to understanding the behavior of oxides, they are basically ideal-solution models and cannot be applied without perhaps very extensive modification to the oxides, where defect concentrations are often much larger and where higher ionic charges imply larger interactions among the defects themselves. It can be expected that considerable progress in understanding the basic properties of solids would result from more intensive study of mass transport in oxides. The time appears ripe for expanding effort in this field, particularly since recent advances in crystal growth techniques (particularly in the use of chemical vapor transport) should now make it possible to prepare adequate research specimens.

There are a number of detailed problems concerning mass transport in oxides that should be considered. First, there is the question of the validity for oxides of the basic model developed for alkali halides, in which diffusion is described in terms of the concentration and jump frequencies of isolated point defects. Evidently, means of identifying and measuring the concentration of different species of point defects are important, as are means of calculating their properties. The status of such calculations, especially for alkali halides, was recently surveyed in "Calculation of the Properties of Vacancies and Interstitials," National Bureau of Standards Miscellaneous Publication 287, issued November 17, 1966. It is of interest to inquire how successfully the theories described there apply to oxides. In particular, can the powerful new tools of lattice dynamics be used to obtain the basic materials parameters needed for calculation of the properties of the defects themselves? Theory taking into account details of the defect motion is then needed to express the rate of mass transport in terms of point defect properties. Oxide structures are in many cases

more complex than the simple alkali halide structures; applications to these structures are essentially extensions of the traditional model within its conceptual framework. There is some doubt about the adequacy of this framework, however. The effect of the partially-covalent bonding in oxides upon defect properties is an open question and the existence of microdomains in many oxides, which may be regarded as resulting from an ordering of defects, is a warning that the traditional model may be too simple.

Second, how well do the phenomenological descriptions of chemical diffusion, developed largely for alloys, describe behavior in oxides where in addition to the chemical composition gradients directly associated with diffusing species there are effects associated with nonstoichiometry and with gradients of electrical potential?

Third, to what extent can ionic conductivity be separated from electronic conductivity and used as a tool in the study of oxides in the same way that ionic conductivity has been so extensively used in alkali halides? Conversely, can studies of electronic conductivity as a function of composition, environment, and temperature be used to infer the type and property of point defects and to throw light on the mechanisms of mass transport?

This conference was intended to provide a review of current understanding of mass transport in oxides, and an opportunity to see where new research efforts might be fruitful. It consisted of a framework of invited papers chosen to cover most of the questions mentioned above, around which were grouped contributed papers representing current work. The entire conference was summarized by a panel discussion, the report of which is included in these Proceedings.

The program began with a review of mass transport in alkali and silver halides and then turned to the theoretical and experimental study of point defects in oxides, including the use of lattice dynamics in the investigation of interionic interactions. The atomistic mechanisms underlying the phenomenological diffusion equations were then discussed, as well as the treatment of chemical diffusion. The occurrence of defect complexes in oxides was treated and a general assessment was given of the state of existing data and the conditions needed to obtain reliable data. The remaining invited papers dealt with ionic conductivity, coulometric studies, and the current availability and the perfection of oxide single crystals.

No simple answers to the questions and problems previously mentioned were expected, but suggested directions for work aimed at solving these problems were sought. The report of the panel discussion summarizes the results. A few general points are mentioned here for emphasis:

1. The impurity level in the best currently available research specimens of oxides is high enough that intrinsic behavior should not be expected in nearly stoichiometric oxides much below the melting point. Better oxide single crystals are badly needed.

2. Departures from stoichiometry frequently occur in oxides. The most likely possibility for intrinsic and reproducible behavior is in systems where the nonstoichiometry is large enough to dominate impurity effects. Very careful control of thermodynamic variables and allowance of time to equilibrate are necessary to fix the state of the specimen. This requirement holds for transport work in oxides in general.

3. A difference of opinion exists concerning the emphasis which should be placed on detailed study of atomic mechanisms of mass transport in simple and generally pure systems on the one hand and on phenomenological study of transport in engineering materials on the other hand. It appears essential to continue both, and probable that creative tension between proponents of the two types of study will benefit both.

J. B. Wachtman, Jr.
A. D. Franklin

Acknowledgment

The editors would like to thank the following for their help in organizing and conducting the Symposium:

C. E. Birchenall	University of Delaware
R. E. Carter	General Electric Company
J. H. Crawford, Jr.	University of North Carolina
R. E. Howard	National Bureau of Standards
J. R. Manning	National Bureau of Standards
A. S. Nowick	Columbia University
D. H. Whitmore	Northwestern University

Contents

*Invited Paper.

Mass Transport in the Face-Centered Cubic Alkali and Silver Halides*

Lawrence Slifkin

Department of Physics, University of North Carolina, Chapel Hill, N.C. 27515

Some current concepts and problems relating to mass transport in alkali and silver halide crystals are discussed: (1) There are contributions from several types of defects to ionic conductivity and tracer diffusion; thus, the analysis of such data to yield energies and entropies of formation and migration is not a trivial matter. (2) In a few cases, the energy and entropy of formation of the defect pair have been resolved into the components associated with each member of the pair. (3) Bound Schottky pairs have been identified, and in a few materials their characteristics have been measured. (4) The diffusion of impurity ions in ionic crystals still presents some unanswered questions. (5) Several other problem areas are listed, the study of which thus far is in a relatively early stage.

Key Words: Alkali halides, diffusion, ionic conductivity, silver halides, tracer diffusion.

1. Why Halide Crystals?

Our present understanding of mass transport in oxide crystals is very limited indeed. Not only are pure crystals difficult to prepare, but the melting points of many of these materials are much higher than the range of the usual high-temperature furnaces. As a result, although there have been a number of experiments on diffusion in the extrinsic, impurity-sensitive range, one can only speculate as to the nature of intrinsic defect phenomena.

In contrast, the alkali halides have readily accessible melting points and may be prepared as crystals of very high purity; studies of the intrinsic mass transport properties are thus quite feasible. During the past 20 years there has been an intensive investigation of these materials [2, 67].[1] mainly by means of measurements of ionic conductivity and tracer diffusion, but also employing dielectric loss and magnetic resonance techniques. The materials which have been examined in most detail are NaCl, KCl, and KBr, all exhibiting Schottky defects; and AgCl and AgBr, in which Frenkel defects predominate. Our understanding of these materials, while certainly not flawless, has reached a level that is not likely to be attained for the oxides for some time to come. It thus seems reasonable that the concepts, problems, and difficulties that have emerged from the study of these halides may well provide a useful guide in the development of a science of ionic transport phenomena in oxide crystals.

2. Ionic Diffusion and Conductivity

Let us consider, for concreteness, a crystal containing Schottky defects (dissociated cation and anion vacancies), along with a small concentration of divalent metal ion impurity. The diffusion coefficient of either type of vacancy is given by [1, 2]

$$D_v=\frac{1}{6}\lambda^2\nu.$$

Here, λ is the jump distance, presumably the distance to the nearest equivalent site; ν is the number of jumps made per second by the vacancy, and is equal to

$$\nu=12\nu_0\cdot\exp\left[-(H_m-TS_m)/kT\right].$$

The factor 12 enters because there are 12 equivalent neighbors in the face-centered cubic lattice; ν_0 is an attempt frequency, usually taken to be the Debye frequency because of lack of a more exact description; H_m is the enthalpy (or, for most purposes at atmospheric pressure, an energy) of activation for migration; and the entropy of migration, S_m, results from transient changes in lattice mode frequencies during the jump process.

Motion of these vacancies produces self-diffusion of the corresponding ion, with a coefficient given by

$$D=f\cdot D_v\cdot x,$$

where f, the correlation factor, allows for the fact that the tracer does not make successive jumps at random, even though the vacancies do (for f.c.c. lattices, $f=0.78$); x is the fractional concentration of this type of vacancy (i.e., either cation or anion vacancy). The concentrations of anion and cation vacancies satisfy a relation of the mass-action type:

$$x_1x_2=\exp\cdot\left[-(H_f-TS_f)/kT\right],$$

the subscript f referring to the process of formation

*Preparation of this manuscript supported by the U.S. Atomic Energy Commission (Contract No. AT(40-1)-2036), the Office of Aerospace Research (Grant No. AF-AFOSR-450-66) and the Advanced Research Projects Agency (Contract No. SD-100).

[1] Figures in brackets indicate the literature references at the end of this paper.

of the dissociated Schottky pair of vacancies. Thus, if the crystal is sufficiently pure and the temperature sufficiently great that the concentrations of impurities are negligible compared to x_1 and x_2, so that the two types of vacancy are present in equal concentrations, then either concentration increases with increasing temperature as exp $(-H_f/2kT)$. On the other hand, if the concentration of, say, divalent cation impurity is not negligible, then the cation vacancy concentration is increased and the anion vacancy concentration is suppressed. Although each such impurity ion must, because of charge neutrality, introduce a cation vacancy, not all of these extra vacancies will be free. There will be at least a coulombic attraction between impurity and vacancy, and in the simplest model we may consider the two to form a new species, a "complex," when they are nearest neighbors, and to be free otherwise. This equilibrium is similarly described by a mass-action equation.

$$\frac{x_k}{x_1(c-x_k)} = 12 \cdot \exp\left[(H_a - TS_a)/kT\right],$$

where x_k is the fractional concentration of complexes, c is the total fractional concentration of divalent cation impurity, and H_a and S_a are the enthalpy and entropy given up in the association process. In addition, electrical neutrality of the crystal requires that

$$x_1 = x_2 + (c - x_k).$$

Ionic mobility is more frequently studied by means of the resulting electrical conductivity than by self-diffusion experiments. If charge and the tracer are both transported by the same mechanism, then the Nernst-Einstein equation leads to the following relation between D and conductivity, σ:

$$\sigma = \frac{Nq^2}{fkT} D,$$

where N is the number of molecules per unit volume and q is the magnitude of the charge transported by each carrier.

From these relations, and on the simple association model which we have considered, it is thus possible to calculate as a function of c and T, the contribution from each defect to the ionic conductivity and self-diffusion—provided one knows the values of the three sets of enthalpies and entropies introduced above. In practice, of course, we wish to invert the calculation; we know the total conductivity and/or various diffusion coefficients, and from this it is necessary to extract the various enthalpies (essentially energies) and entropies for each defect.

3. Defect Formation and Migration Energies

If the concentration of impurities is small and if only one type of defect, say the cation vacancy, contributes to the conductivity, then the Arrhenius plot of log (σT) versus $1/T$ would be a straight line at high temperatures, with a slope equal to $-(\frac{1}{2} H_f + H_m)/k$. At lower temperatures, where the concentration of intrinsic, thermally induced defects falls well below that of divalent cation impurity, then if one could neglect the impurity-vacancy association the slope should be equal to $-H_m/k$. At still lower temperatures, the formation of complexes becomes significant, and the slope would increase again, reaching the value $-(H_m + \frac{1}{2} H_a)/k$. It should therefore be possible to determine the values of these three energies from such an Arrhenius plot of the conductivity, and this has indeed been done for many of the halides [3, 4]. Typical values for the common alkali halides are: 2 to 2½ eV for the formation of a Schottky defect, 0.6 to 0.8 eV for the activation energy for migration of the cation vacancy, and 0.3 to 0.5 eV for the impurity-vacancy association energy. Unfortunately, however, the expected linear region below the intrinsic range and above the association region is often so short that there may be considerable ambiguity in determining the slope. Various studies of the same material have thus occasionally resulted in values of H_m differing by about 0.1 eV, with comparable uncertainties produced in the other energies. Moreover, it is difficult to be certain that only one type of defect is moving in the high temperature region.

An alternative approach has been to examine the variation of ionic conductivity with increasing impurity concentration. The analysis of such conductivity isotherms is based on manipulation of the several equations given above, and has been lucidly formulated by Lidiard [2]. Generally, certain approximations must be made, such as the assumption that single cation vacancies are solely responsible for the conductivity—at least in the lower temperature region of the intrinsic range—or that the entropy of the impurity-vacancy association can be taken as zero. Moreover, the simple model which we have considered does not adequately account for extended, or "excited," configurations of the complexes nor for long-range electrostatic screening effects of the Debye-Hückel type, which Lidiard [2] has shown to be important at high concentrations of point defects.

For the silver halides, self-diffusion experiments [5, 6] have conclusively demonstrated that anion transport is negligible in comparison with cation mobility, but the situation is complicated by a marked upward curvature in the Arrhenius plots

at high temperatures, a curvature that has been interpreted in terms of Debye-Hückel interactions [7] and also partially as an effect of an excess lattice expansion [8]. There are two recent extensive studies of silver chloride, Abbink and Martin's analysis of conductivity isotherms [7] and Müller's [9] analysis of the temperature-dependence of the conductivity in the region of the "knee" between intrinsic and extrinsic ranges; the results from the two differ considerably. Abbink and Martin performed a careful experiment, but the results of their analysis are sensitive to the accuracy of the Debye-Hückel treatment. The resolution of this conflict is certainly not obvious.

Additional information on silver ion transport in AgCl and AgBr has been gleaned from detailed and precise comparisons of ionic conductivity with the silver tracer diffusion coefficient, looking at apparent deviations from the Nernst-Einstein equation [6, 10, 11, 12]. The main point of interest here is that in an "interstitialcy" jump, where the interstitial ion replaces an ion in an adjacent normal site, the jump distance for the electrical charge is greater than that for the radioactivity. Recent work of Friauf and co-workers [11, 12] has actually been able to specify the contributions from collinear and from noncollinear interstitialcy jumps. Studies of halide self-diffusion in these materials, however, have not yet given such a complete picture. In both the chloride [13] and the bromide [14], the Arrhenius plots are quite curved at low temperatures, suggestive of several alternative diffusion mechanisms.

The alkali halides present somewhat different problems. Since the concentrations of thermal defects here are appreciably smaller than in the silver halides, Debye-Hüchel screening effects are not expected to be as important (although Kanzaki [15] has interpreted deviations from predictions of the simple theory of the conductivity isotherms for calcium-doped NaCl as due to long-range electrostatic interactions). On the other hand, a contribution to the ionic conductivity from anion vacancies poses a worrisome problem. This sometimes appears as a curvature in the intrinsic region of the Arrhenius plot [16, 17], but a straight line is no guarantee of a single process. Thus, in KBr [18], although both types of vacancy make comparable contributions, and the activation energy for the anion vacancy is 0.2 eV larger than that for the cation vacancy, nevertheless, the intrinsic region of the Arrhenius plot appears to be quite linear. Another difficulty that plagues the analysis of conductivity isotherms is accurate knowledge of the effective impurity concentration. This is not only a problem of measuring the magnitudes of deliberate additions, but also of determining the presence of background impurities which can react with a portion of the added dopant; e.g., small quantities of OH^-, which may react with added Sr^{++} [17].

How, then, must one deal with the alkali halides? One approach applied by Rolfe [18] to KBr, is to determine conductivity isotherms of crystals doped with divalent anions as well as with divalent cations. This procedure, however, has not been generally extended because no other f.c.c. alkali halide has been found to offer an appreciable solubility for a divalent anion. A second recent approach is to instruct a computer to obtain those values of the various energies and entropies which will provide the best fit to carefully measured Arrhenius plots for various concentrations of impurity [19, 20, 21]. There are two energies and entropies of migration (one set for each type of vacancy), along with corresponding parameters involving Schottky defect formation and impurity-vacancy binding (the binding entropy is sometimes hopefully set equal to zero). With so many adjustable parameters to be employed in fitting a rather unspectacular, monotonic Arrhenius plot, it is not at all obvious that the procedure should work. Nonetheless, unique values do emerge, values which are consistent among Arrhenius plots involving different impurity concentrations. The method is not without its hazards, however, as Dawson and Barr [21] have shown that the best set of values may be rather sensitive to the extent of the temperature range used in fitting theoretical to experimental conductivities.

By far the most reliable and convincing procedure would seem to be a combination of ionic conductivity measurements with tracer studies of anion and cation self-diffusion, as has been done recently by Fuller and Reilly [20] and by Dawson and Barr [21]. Diffusion experiments have the advantage that they are not influenced by mobility of vacancies of the opposite type. On the other hand, mobile neutral species, such as impurity-vacancy complexes and bound vacancy pairs, which would be invisible in a conductivity measurement, may make an appreciable contribution to tracer diffusion. The importance of the impurity-vacancy complex may be minimized by working at high temperatures; the contribution from bound vacancy pairs must be separately evaluated. This is accomplished by observing the effect of additions of divalent cation on the diffusion coefficient of the anion. The cation impurity adds cation vacancies, thereby suppressing the anion vacancies, but leaves unchanged the concentration of bound pairs [20, 21, 22, 23]. In particular, Dawson and Barr [21] have recently obtained excellent agreement between results of tracer diffusion studies in KBr and computer fits of Arrhenius plots.

The end products of such experiments are values

of H_f, H_m for both anion and cation vacancy, H_a for complexes involving various impurities, and all of the corresponding entropies. Perhaps one of the most valuable uses of the enthalpies is to provide a guide for the theoretician: the interionic potentials and polarization corrections in these materials are somewhat uncertain, and trial functions can be tested by comparing the predicted energies with the experimental ones. The entropies, however, presently are by-products for which little use has been found. One can qualitatively understand that these entropies are so much larger than in metals because of the large relaxations which occur when an ion is removed from an electrostatically bound structure; a quantitative theory, unfortunately, is still lacking. It is also becoming apparent from recent work that anion vacancies and bound pairs often make a significantly larger contribution to transport phenomena than had previously been appreciated. Lidiard [24] has further pointed out that the defect formed by addition of a vacancy to a bound pair should have some stability and mobility, and may make a nontrivial contribution.

4. Resolution of H_f and S_f into Their Components

The separate components of a Schottky or Frenkel pair can be individually created or annihilated at certain jogs on dislocations and surfaces. The dislocation, for example, must therefore be in equilibrium separately with both component point defects, and this will usually leave it with a net charge [25]. If there is an excess of cation vacancies in the crystal, because of the presence of divalent cation impurities, some of these will condense onto the dislocation, giving it a negative charge. At high temperatures, on the other hand, one can neglect the effects of impurities and if the free energy of formation of the cation vacancy is less than that for the anion vacancy, the dislocation will produce an excess of cation vacancies and will acquire a positive charge. At some intermediate temperature, the isoelectric point, the dislocation is electrically neutral; from the dependence of this temperature upon impurity concentration it is possible to deduce the energy and entropy of formation of the cation vacancy. These quantities may then be subtracted from those for the complete Schottky or Frenkel pair to give the parameters characterizing the other component of the pair.

Kanzaki, Kido, and Ninomiya [26] studied the effects of dislocation density on the ionic conductivity of very pure and doped KCl. They interpreted the results in terms of the effect of the compensating space charge surrounding the charged dislocations, and were able thereby to deduce the vacancy formation free energy at one particular temperature. Davidge [27], Strumane and DeBatist [28], and Kliewer and Koehler [29] determined the concentration dependence of the isoelectric point in NaCl by observation of potential differences produced by dislocation displacement and by studies of the effect of dislocations on the elastic modulus. Their results are essentially in agreement with one another and indicate that the formation energy of the cation vacancy is only slightly less than that for the anion vacancy, but that the formation entropy for the cation vacancy is considerably larger than that for the anion vacancy. Plint and Breig [30] have deduced vacancy formation free energies from light scattering, but for NaCl the result does not agree with Kliewer, etc.

Charged dislocation effects in silver chloride have been calculated by Kliewer [31]. He shows how the vacancy formation entropy can be obtained from Wakabayasi's data [32] on the temperature dependence of contact potential and he gives an estimate for the energy of formation. This energy has recently been measured [33], and the probable effects of the surface charge on the mechanism of the photographic process are cited. As in sodium chloride, the cation vacancy has a smaller formation energy and a larger formation entropy than does its complementary defect (the interstitial silver ion, in this case). Saunders, Tyler, and West [34] have been able to probe the potential near the surface of AgBr crystals by an ingenious experiment in which photographic development techniques are exploited to follow the drift of photoelectrons in thin specimens. They find that at room temperature the surface is negatively charged, as in AgCl [33], but their results are interpreted by Trautweiler [35] in terms of intrinsic, rather than impurity effects. This seems somewhat questionable, since it would then be necessary that a purity of 0.1 ppm be preserved in AgBr slabs only a few tens of microns thick, formed by melting between glass plates.

5. Bound Schottky Pairs

Effects of bound Schottky pairs in ionic crystals were perhaps first seen by Tannhauser [5] in 1958, who was puzzled by curvature extending over the entire temperature range of the Arrhenius plot for diffusion of bromide in silver bromide. In various alkali halides, bound pair contributions to anion diffusion were found by Morrison and coworkers [36], Laurance [22], and Fuller [20]. The vacancy pair diffusion contribution in KBr has recently been measured by Barr and Dawson [14]. Downing and Friauf [37] compared the ionic conductivity in NaCl with the diffusion of sodium tracer

and have found an "anomalous" contribution to diffusion which is attributed to bound pairs.

Dielectric loss experiments in several of the alkali halides by Sastry, Srinivasan, and Economou [38] have shown peaks which have many of the characteristics of vacancy pair relaxation processes. The pair formation energies, rotation activation energies, and rotation preexponential factors are all consistent with what would be expected for pairs. Doping with divalent cation impurity, which would perturb the monovacancy concentrations and the conductivity but not the concentration of pairs, was found not to affect the results. Also, measurements on crystals of different thicknesses seem to show that the effect is a bulk one and not a surface phenomenon of the type studied by Wimmer and Tallan [39]. The one disturbing fact, and it is quite disturbing indeed, is that the intensities of the losses are larger than expected, by a factor of about 50 to 100. Boswarva and Franklin [40] have concluded that extending the simple Debye theory to include long range interactions cannot patch up the discrepancy. Recently, Chandra and Agrawal [41] have calculated the entropies of formation of bound pairs in alkali halides, have found them to be quite large, and have concluded that the very large concentrations of pairs implied by the experiment are really correct. This leads to predictions, however, of startlingly large density anomalies, specific heat anomalies, discrepancies between diffusion and conductivity, etc., in conflict with the lack of experimental observation of such anomalies. Sack and Smith [41a] have observed, in several halides, an extra dielectric loss at high temperatures and at microwave frequencies which is attributed to relaxation by vacancy pairs and which does not show an anomalously large intensity. It thus seems rather likely that the large concentrations of vacancy pairs deduced by Sastry et al. and by Chandra and Agrawal are erroneous.

If the rotational activation energy for vacancy pairs could indeed be convincingly determined from a relaxation experiment of this sort, a comparison could be made with the pair migration energy obtained from diffusion studies. The two energies are not the same. Of the two types of jump which a bound vacancy pair can make, the relaxation experiment would measure the faster, while the diffusion experiment is limited by the slower. If both activation energies could thus be obtained, a comparison with the predictions of Tharmalingam and Lidiard [23] would be of interest.

Vacancy pairs were studied in AgCl by Layer [42], by quenching very pure material from temperatures near to the melting point. Correction of the original data for more recent values of the vacancy migration energy, etc., yields a binding energy of the pair of 0.5 eV, a migration activation energy of 1.0 eV, and a quenched in concentration of approximately 10^{-4}. This concentration presumably refers to dissociated Schottky pairs at the original quench temperatures. It is sufficiently small not to contradict the nonobservance of Schottky defects in AgCl by mass-transport studies [12] or combined measurements of lattice parameter and density [43]. The results are consistent with self-diffusion experiments [6, 13] and with the observation of very large dislocation loops in nearly perfect regions of AgCl crystals which appear to have been produced by condensation of Schottky defects [44].

6. Impurity Ion Diffusion

The diffusion of impurity ions is considerably more complicated than is self-diffusion. Except for a measurement by Batra [45] of the diffusion of bromide and iodide tracers in silver chloride (in which it was—surprisingly—found that they both have the same activation energy as does the chloride ion), there has been virtually no recent work on the diffusion of anionic impurities. The remainder of this discussion is thus concerned only with cation diffusion.

It is generally assumed that metallic ions in alkali halide crystals simply substitute for the alkali ions. That this may not always be true is indicated by the optical absorption spectrum of Co^{++} which in several halides is that characteristic of the symmetry of an interstitial, not substitional, site [46, 47]. There is also some evidence from electrolysis experiments [48] that Pb^{++} forms a negatively charged complex in KCl, or at least in KCl with certain impurities present. In the silver halides, in view of the well-known ease with which the silver ion enters interstitial sites, one is not surprised that Cu^{+} [49] and Au^{+} [50] also diffuse interstitially. It is, however, somewhat unexpected that Fe^{+++} resides interstitially in AgCl in a complex involving, at least at low temperatures, a tetrahedron of silver vacancies [51, 52].

It has been emphasized by Lidiard [2] that for the usual, substitutional case, the impurity ion can only migrate when it is part of an impurity-vacancy complex. Also since a polyvalent ion affects the local concentration of vacancies, the diffusion behavior depends very much on whether the concentration of the diffusing ion is large or small as compared to the "background" concentration of vacancies. This discussion has been extended recently by Howard and Lidiard [53].

The treatment of divalent cation impurity diffusion centers about the properties of the impurity-

vacancy complexes. These have been studied by a variety of techniques: ionic conductivity, dielectric loss, depolarization effects, anelasticity, electron paramagnetic resonance, and tracer diffusion. Reported binding energies are generally in the range 0.3 to 0.5 eV in the alkali halides and somewhat less in the silver halides, but there is little agreement within this range among the various experiments on a given system. Watkins [54] has shown, by means of magnetic resonance and dielectric loss experiments, that in Mn-doped NaCl the binding energy at the next-nearest-neighbor site is almost as large as at the nearest-neighbor site. It is also known that larger complexes may be formed by aggregation of simple impurity-vacancy pairs, the initial step being production of a trimer [55].

The cation vacancy in the neighborhood of a metallic impurity ion has a number of different jump probablilites: it may exchange with the impurity, rotate about the impurity, dissociate from the impurity, and jump from a more distant site to a site adjacent to the impurity. The ratio of these last two, of course, is determined by the binding free energy. The frequencies of all four types of jump, however, must be known if a complete understanding of impurity diffusion is to be attained. It is expected that the extra charge on the divalent impurity ion would increase the activation energy for its exchange with an adjacent vacancy, and experiments by Dreyfus and Laibowitz [56] on anelasticity and dielectric loss as a function of crystal orientation do show that the vacancy-impurity exchange frequency is less than that for the jumping of the vacancy around the impurity. The complex is thus able to rotate about the impurity much faster than it can actually diffuse. Further details about these jump frequencies are lacking.

With the analysis of impurity diffusion in terms of the various jump frequencies presently impossible, recent work on impurity diffusion in halide crystals has been concerned with the dependence of the diffusion coefficient on impurity concentration, as in the experiments of Keneshea and Fredericks [57] and of Rothman, Barr, Rowe, and Selwood [58] on diffusion in KCl and NaCl. In general, most of these results can be described by the simple association theory of Lidiard. There are available three studies of divalent cation diffusion in silver halides. Hanlon [59] measured the diffusion of cadmium in pure and in cadmium-doped AgBr, and found that the data required the assumption that the vacancy mobility increased by a factor of two for each 1 atomic percent cadmium present. Reade and Martin [60] diffused cadmium tracer into pure AgCl; Laskar [61] diffused manganese tracer into pure AgCl. In all three cases of tracer diffusion in pure silver halide, the Arrhenius plots appear to consist of two segments, with a break at approximately 325 °C. It is possible that the tracer may be diffusing by both vacancy and interstitial mechanisms, but at present this is at best only speculation.

7. Several Other Problem Areas

In addition to those problems which have been discussed in the preceding sections, there are several others which are of considerable interest. Most of these are in rather early stages of development.

(a) Electrode polarization effects [62] have been studied both experimentally and theoretically, but there are still wide gaps between the two.

(b) Effects of high pressure, described by activation volumes, have been measured in only a few cases [4, 63].

(c) Thermoelectric effects have been discussed by Howard and Lidiard [53]. Most of the data that are available are for the silver halides; Christy's results [64] on AgCl indicate that the heats of transport are quite large and are temperature dependent.

(d) Little is known of the diffusion along dislocations in ionic crystals; how wide are the "pipes"? what are the activation energies? what are the effects of the charge on the dislocations? what effects arise from impurity segregation? [66].

(3) Lüty [65] has measured the migration energy for the anion vacancy in KCl by means of color center reactions at low temperatures. The experiments quite conclusively give 0.6 eV, or only approximately 2/3 the value obtained at high temperatures from tracer diffusion and ionic conductivity experiments. If the ionic configuration around the vacancy does indeed change at some intermediate temperature, so that the two experiments are observing different kinds of anion vacancy, then a new dimension will have been introduced into the study of mass transport in ionic crystals.

8. Concluding Remark

The alkali and silver halides thus still pose a few mysteries and many unanswered questions, but these are, after all, quite detailed and intimate questions. It would appear that we now have both a sound conceptual base and also the techniques necessary for obtaining the answers. This is a position which justifies cautious optimism; it has been reached, however, only as a result of interpretation of measurements extending over large ranges of temperature and purity, penetrating well into both the intrinsic and extrinsic regions. Had one

been limited to temperatures below half of the melting point and to purities poorer than a hundred parts per million, as has so far been the case in research on oxides, then it is doubtful whether many of the present concepts could have been developed, or whether we would even know what questions to ask. The road ahead for the oxides thus appears to be long and difficult indeed.

9. References

[1] See, for example, P. Shewmon, Diffusion in Solids (McGraw-Hill Book Co., New York, N.Y., 1963).

[2] A particularly useful discussion of mass transport in ionic crystals is: A. Lidiard in Handbuch der Physik, **XX**, p. 246, ed. by S. Flügge (Springer-Verlag, Berlin, 1957).

[3] See, for example, R. Dreyfus and A. Nowick, J. Appl. Phys. **33**, 473 (1966); S. Jain and S. Dahake, Phys. Letters **3**, 308 (1963); Indian J. Pure & Appl. Phys. **2**, 71 (1964).

[4] A. Abey and C. T. Tomizuka, J. Phys. Chem. Solids **27**, 1149 (1966).

[5] D. Tannhauser, J. Phys. Chem. Solids **5**, 224 (1958).

[6] W. D. Compton and R. Maurer, J. Phys. Chem. Solids **1**, 191 (1956).

[7] H. Abbink and D. Martin, Jr., J. Phys. Chem. Solids **27**, 205 (1966).

[8] P. Müller, Phys. Stat. Sol. **21**, 693 (1967).

[9] P. Müller, Phys. Stat. Sol. **12**, 775 (1965).

[10] A. Miller and R. Maurer, J. Phys. Chem. Solids **4**, 196 (1958).

[11] R. Friauf, J. Phys. Chem. Solids **18**, 203 (1961); J. Appl. Phys. **33**, 494 (1962).

[12] M. Weber and R. Friauf, to be published.

[13] E. Lakatos and K. Lieser, Z. Physik. Chem. **48**, 213 (1966).

[14] L. Barr and D. K. Dawson, private communication.

[15] H. Kanzaki, K. Kido, S. Tamura, and S. Oki, J. Phys. Soc. Japan **20**, 2305 (1965).

[16] A. Allnatt and P. Jacobs, Trans. Faraday Soc. **58**, 116 (1958).

[17] P. Jacobs and J. Maycock, Jr., J. Phys. Chem. Solids **24**, 1693 (1963).

[18] J. Rolfe, Can. J. Phys. **42**, 2195 (1964).

[19] J. Beaumont and P. Jacobs, J. Chem. Phys. **45**, 1496 (1966).

[20] R. Fuller, Phys. Rev. **142**, 524 (1966); R. Fuller and M. Reilly, Phys. Rev. Letters **19**, 113 (1967).

[21] D. K. Dawson and L. Barr, Phys. Rev. Letters **19**, 844 (1967).

[22] N. Laurance, Phys. Rev. **120**, 57 (1960).

[23] K. Tharmalingam and A. Lidiard, Phil. Mag. **6**, 1159 (1961).

[24] A. Lidiard, oral comments, this conference.

[25] J. Frenkel, Kinetic Theory of Liquids (Oxford University Press, 1946); K. Lehovec, J. Chem. Phys. **21**, 1123 (1953).

[26] H. Kanzaki, K. Kido, and T. Ninomiya, J. Appl. Phys. **33**, 482 (1962).

[27] R. Davidge, Phys. Stat. Solidi **3**, 1851 (1963).

[28] R. Strumane and R. DeBatist, Phys. Stat. Solidi **6**, 817 (1964).

[29] K. Kliewer and J. Koehler, Phys. Rev. **157**, 685 (1967).

[30] C. Plint and M. Breig, J. Appl. Phys. **35**, 2745 (1964).

[31] K. Kliewer, J. Phys. Chem. Solids **27**, 705, 719 (1966).

[32] H. Wakabayasi, J. Phys. Soc. Japan **15**, 2000 (1960).

[33] L. Slifkin, W. McGowan, A. Fukai, and J. Kim, Phot. Sci. & Eng. **11**, 79 (1967); J. Kim, Ph.D. Thesis, University of N.C., 1967; W. McGowan, Ph.D. Thesis, University of N.C., 1965.

[34] V. Saunders, R. Tyler, and W. West, to be published.

[35] F. Trautweiler, to be published.

[36] J. Morrison and R. Rudham, J. Phys. Chem. Solids **6**, 402 (1958); L. Barr, J. Morrison, and P. Schroeder, J. Appl. Phys. **36**, 624 (1965).

[37] H. Downing and R. Friauf, private communication.

[38] P. Sastry and T. Srinivasan, Phys. Rev. **132**, 2445 (1963); N. Economou, Phys. Rev. **135**, A1020 (1964); N. Economou and P. Sastry, Phys. Stat. Solidi **6**, 135 (1964).

[39] J. Wimmer and N. Tallan, J. Appl. Phys. **37**, 3728 (1966).

[40] I. Boswarva and A. Franklin, Phil. Mag. **11**, 335 (1965).

[41] S. Chandra and V. Agrawal, J. Phys. Chem. Solids **28**, 1055 (1967).

[41a] H. Sack and G. Smith, J. Phys. Soc. Japan **18**, Suppl. 3, 124 (1963).

[42] H. Layer, M. Miller, and L. Slifkin, J. Appl. Phys. **33**, 478 (1962).

[43] R. Fouchaux and R. Simmons, Phys. Rev. **136A**, 1664 (1964).

[44] C. Childs, A. Fukai, W. McGowan, and L. Slifkin, to be published.

[45] A. Batra and L. Slifkin, to be published; see also J. Laurent and J. Bénard, J. Phys. Chem. Solids **3**, 7 (1957).

[46] M. Hills, J. Phys. Soc. Japan **19**, 760 (1964); K. Lal, Phys. Stat. Solidi **22**, 141 (1967).

[47] M. Musa, Phys. Stat. Solidi **16**, 771 (1966).

[48] W. Fredericks and A. Scott, J. Chem. Phys. **28**, 249 (1958).

[49] P. Süptitiz, Phys. Stat. Solidi **7**, 653, 667 (1964).

[50] A. Batra, A. Laskar, and L. Slifkin, to be published.

[51] W. Hayes, J. Pilbrow, and L. Slifkin, J. Phys. Chem. Solids **25**, 1417 (1964).

[52] M. Satoh and C. Slichter, Phys. Rev. **144**, 259 (1966).

[53] R. Howard and A. Lidiard, Rept. Prog. Phys. **XXVII**, 161 (1964).

[54] G. Watkins, Phys. Rev. **113**, 79, 91 (1959).

[55] J. Cook and J. Dryden, Proc. Phys. Soc. **80**, 479 (1962); Y. Chiba, K. Veki, and M. Sakamoto, J. Phys. Soc. Japan **18**, 1092 (1963); H. Symmons and R. Kemp, Brit. J. Appl. Phys. **17**, 607 (1966); K. Shrivastava, Nuovo Cimento **47B**, 251 (1967).

[56] R. Dreyfus and R. Laibowitz, Phys. Rev. **135**, A1413 (1964).

[57] F. Keneshea and W. Fredericks, J. Chem. Phys. **38**, 1952 (1963); **41**, 3271 (1964); **43**, 2925 (1965); **46**, 2000 (1967); J. Phys. Chem. Solids **26**, 501, 1787 (1965).

[58] S. Rothman, L. Barr, A. Rowe, and P. Selwood, Phil. Mag. **14**, 501 (1966).

[59] J. Hanlon, J. Chem. Phys. **32**, 1492 (1960).

[60] R. Reade and D. Martin, Jr., J. Appl. Phys. **31**, 1965 (1960).

[61] A. Laskar and L. Slifkin, Bull. Am. Phys. Soc. **11**, 838 (1966).

[62] For recent work, see A. Allnatt, P. Jacobs, and J. Maycock, J. Chem. Phys. **43**, 2526 (1965); **44**, 3644 (1966); J. Beaumont and P. Jacobs, J. Phys. Chem. Solids **28**, 657 (1967); H. Wintle and J. Rolfe, Can. J. Phys. **44**, 965 (1966); **45**, 2253 (1967); D. Kahn and J. Maycock, J. Chem. Phys. **46**, 4434 (1967).

[63] S. Kurnick, J. Chem. Phys. **20**, 218 (1952); W. Taylor, W. Daniels, B. Royce, and R. Smoluchowski, J. Phys Chem. Solids **27**, 39, 1196 (1966); C. B. Pierce, Phys Rev. **123**, 744 (1961).

[64] R. Christy, J. Chem. Phys. **34**, 1148 (1961); R. Christy, Y. Hsueh, and R. Mueller, J. Chem. Phys. **38**, 1647 (1963); see also P. Jacobs and J. Maycock, Trans. AIME **236**, 165 (1966); and M. Shimoji and H. Hashino, J. Phys. Chem. Solids **28**, 1155, 1169 (1967).

[65] F. Lüty, in The Physics of Color Centers, ed. W. D. Compton. to be published.

[66] R. Tucker, A. Laskar, and R. Thomson, J. Appl. Phys. **34**, 445 (1963); see also various recent papers of Ya. Geguzin and co-workers, such as Sov. Phys.—Dok. **11**, 626 (1967). Sov. Phys.—Solid State **8**, 2599 (1967); ibid. **7**, 2826 (1966).

[67] P. Süptitiz and J. Teltow, Phys. Stat. Solidi **23**, 9 (1967)

Diffusion of Sodium in Sodium Chloride in an Applied Electric Field [1]

Robert J. Friauf and Vaughn C. Nelson [2]

University of Kansas 66045

1. Statement of the Problem

Ionic conductivity and diffusion in NaCl are both due to the movement of vacancies. Conductivity and diffusion can be compared by the Einstein relation, corrected for correlation, but there are differences which can be attributed to diffusion by vacancy pairs. Vacancy pairs are electrically neutral and would not contribute to the conductivity. If the drift mobility of the cation could be measured by diffusing Na in an electric field, the amount of vacancy pair diffusion could be obtained from this measurement and checked against the measured conductivity and the Na and Cl diffusion without an electric field.

2. Procedure

(*a*) The ionic conductivity was measured in the extrinsic and intrinsic ranges (275 to 797 °C) with an ac bridge at 1000 Hz. (*b*) The diffusion of Na was measured (640 to 790 °C) with radioactive tracers and the sectioning method. (*c*) The mobility of radioactive tracers was measured (600 to 772 °C) by diffusing Na in an applied electric field. The amount of charge passed through the sample was measured with a silver coulometer. Considerable difficulties were encountered because of the poor contact at the interface between the two crystals.

[1] Work supported by the U.S. Atomic Energy Commission.

[2] Present address: Universidad de Oriente, Cumana, Venezuela.

3. Results

(a) The Na diffusion (no electric field) is given by $D = 1300\ e^{-2.27/kT}$ (cm²/sec). (b) The diffusion of Na in an applied field gives a drift mobility of Na ions $M_p = (1 \times 10^6/T)\ e^{-2.06/kT}$ (cm²/volt sec). (c) The best two exponential fit of the conductivity is

$$\sigma T = 3.6 \times 10^9\ e^{-2.06/kT} + 2.5 \times 10^9\ e^{-2.08/kT}$$

($^\circ K$ ohm^{-1} cm^{-1})

where the cation parameters in the first term have been calculated from the measured drift mobility of Na tracers. (d) The activation energy for diffusion of Na by vacancy pairs is 2.6 eV, and approximately 50 percent of the Na diffusion near the melting point is due to vacancy pairs.

4. Conclusions

Measuring mobility in alkali halides by diffusion in an electric field is promising as a tool in actually delineating the contributions of single vacancies. The importance of anion vacancy conductivity in NaCl is confirmed by these results. The overall picture for NaCl shows an appreciable contribution of vacancy pairs to the diffusion of both anion and cation.

290-621 O-68—2

Characterization of Point Defects in Oxides [1]

John E. Wertz

Department of Chemistry, University of Minnesota, Minneapolis 55455

This review describes the geometry of numerous point defects which have been observed in oxides. Experimental evidence for their existence and for their configuration is briefly cited. Attention is concentrated primarily upon the alkaline earth oxides, for which most defect structural information is available. Some defects in ZnO and in Al_2O_3 are also mentioned. Defects may be categorized as involving impurities, vacancies, or interstitial atoms. These may exist in isolation or in association with other defects. Numerous examples are given of cation vacancies associated with one or with two other defects; the latter are neutral in each case. One may further categorize defects as to whether they require radiation of the solid for their production. Valuable information about some stable defects has been obtained by correlating them with closely related unstable defects. Some defects may be studied by optical or electron spin resonance techniques if they are caused to trap electrons or holes. An example is the determination of the site geometry of OH^- ions which in MgO show an infrared band at 3296 cm^{-1}. Measurement of the concentration of trapped-electron-or trapped-hole centers after appropriate sample treatments may give minimum estimates of the numbers of cation or anion vacancies present. For some defects, electron spin resonance studies have permitted correlation with optical absorption, luminescence or uniaxial stress measurements. Known trapped-hole and trapped-electron defects in oxides are enumerated.

Key Words: Electron spin resonance, impurities, interstitials, optical spectra, point defects, vacancies.

1. Introduction

The perceptive experimentalist or theorist who concerns himself with mass transport in oxides recognizes the significance both of line- and of point-defects. Notwithstanding his recognition of the latter, he may disdain confrontation with defects resulting from various kinds of irradiation. If nature had provided us with observation capabilities of atomic resolution for direct detection of such defects as vacancies, one might not have to resort to irradiation and other procedures for their characterization. It is a simple fact that the geometry of a number of stable defects in oxides is known because they were converted by irradiation to unstable defects amenable to study by optical or electron spin resonance methods. In the process, it has been possible in some cases to provide unambiguous analytical procedures for measuring the numbers of the stable defect. Alternatively, for some oxides these studies make it clear that it is naive to refer to Schottky pairs, for anion vacancies have been shown to be far outnumbered by cation vacancies at temperatures below 1200 °C. To demonstrate this, it was necessary to create anion vacancies by neutron irradiation, populate them singly with electrons, and identify them with one or more measurable properties. Thus it was established that not even ionizing radiation could generate such vacancies at room temperatures (at least in the alkaline earth oxides). In the conviction that many students of mass transport will wish to know which defects may be detected in oxides as well as the nature of the evidence for their existence, this review is presented without apology for inclusion of unstable point defects.

Outside of the group of alkaline earth oxides, there are relatively few oxides in which the geometry of point defects (except perhaps impurity ions) is known with reasonable certainty. The simple rock-salt structure and the ready availability of single crystals of MgO, CaO, and SrO makes these—especially the stable MgO—ideally suited for characterization of defects. In a number of instances, the characterization of a particular defect in MgO led to reports of observation of the analogous defect for another type of oxide. Hence much of this review is devoted to defects in MgO.

2. Substitutional and Interstitial Defects

2.1. Substitutional Impurities

The nature of the impurities present in a sample, their distribution and their interaction with other

[1] Some previously unpublished results cited herein were obtained with the support of the Solid State Sciences Division of the Air Force Office of Scientific Research under grant 200–66.

defects are vital to one who seeks to make meaningful measurements of mass transport in oxides. In ionic crystals, the impurities are predominantly found in substitutional sites. Even if the charge on an impurity ion differs from that in the host lattice, one may still find a significant fraction of ions without a compensating impurity or vacancy nearby. Such statements may be made with considerable confidence if the ion belongs to transition metal or rare earth groups, in a paramagnetic state readily studied by electron spin resonance. For such ions the number and anisotropy of the lines in the electron spin resonance (ESR) spectrum reflect the electric field symmetry about the ion. If the angular dependence of the spectrum is precisely that which is expected from the symmetry of the host, the ion is likely to have no nearby compensating defects.

The existence of ions without an associated compensating vacancy is especially common in the oxides of formula MO. Here one cation vacancy compensates for two trivalent ions, and at least one of these may be remote from the vacancy. Monovalent cations may serve to compensate impurity cation charge in some oxides. Even if one detects no departure from the octahedral or tetrahedral symmetry of the host ions, there may be a symmetrical distortion of the lattice about an impurity ion because of a different fractional covalency of an impurity-oxygen bond.

The ESR behavior of ions with an associated compensating defect is considered in section 3. It is important to recognize that a number of the transition metal ions may exist in two or more valence states. An outstanding example is iron, which in the alkaline earth oxides may exist stably in the divalent or trivalent forms; irradiation leads to a significant concentration of monovalent iron.

No attempt will be made here to enumerate the substitutional transition-metal or rare-earth impurity ions which have been identified in various oxides by ESR techniques. A compilation has recently been made of ESR parameters for ions in MgO, CaO, SrO, Al_2O_3, TiO_2, and ZnO, as well as some compounds having perovskite, spinel, or garnet structures [1].[2] However, section 3 is devoted to those impurity ions for which there is evidence of association with vacancies or with other defects, both stable and unstable.

Very little is known about the sites occupied by a number of impurities detected by standard analytical techniques. Many of these are diamagnetic and further have not modified the ESR spectrum of a paramagnetic defect in so obvious a way as to announce their presence. They are especially likely to remain undetected by optical methods as well as by ESR techniques if there is no abundant nuclide of nonzero spin. One long-known defect shows the presence of aluminum in association with a vacancy at which a hole is trapped by its hyperfine splitting pattern [2]. More recently, the effects of an aluminum ion associated with a vacancy were detected by its reduction of the zero-field splitting of a Cr^{3+} ion also associated with the vacancy [3, 4, 5]. This defect is considered in section 3. The association of a lithium ion with a cation vacancy in ZnO is obvious from a hyperfine quartet from ^7Li ($I=3/2$) which becomes a triplet from ^6Li when the sample is doped with the latter [6, 7].

2.2. Interstitial Defects

Relatively few interstitial defects have been established with reasonable certainty in the oxides. The presence of interstitial zinc in ZnO heated at elevated temperatures has long been accepted. In the alkaline earth oxides one infers the presence of interstitial alkaline earth metal atoms and of oxygen atoms only after neutron- or ion-irradiation. However, there seems to be little direct or detailed evidence of such atoms. For one impurity, the OH^- ion, remote from a cation vacancy, it seems reasonable to infer an interstitial position for the hydrogen atom of the OH^- ion [8]. This location is consistent with the relatively great width of the infrared band (~ 100 cm^{-1}) presumed to be correlated with it; the widths of OH stretching bands for an $O\cdots H\cdots O$ system increases with reduced separation of the oxygen atoms [9]; for hydrogen between two oxgyen atoms at approximately the normal lattice spacing of 4.20 Å, the width of the infrared band is roughly one-tenth as great. These defects are described in section 4.

3. Association of Vacancies With Impurities

The defects of greatest interest for mass transport studies in most oxides are the anion and cation vacancies. As pointed out earlier, it is erroneous to assume that these are present in equal concentrations in oxides except perhaps at very high temperatures. One presently has no technique for direct observations on isolated vacancies in oxides. However, an estimate of their number may be made if the cation vacancy is caused to trap a positive hole or an anion vacancy an electron. These types of defects will be described in sections 4 and 5 respectively. Evidence from trapped electron

[2] Figures in brackets indicate the literature references at the end of this paper.

defects will also be adduced for the presence of a divacancy and of a trivacancy (section 5).

Vacancies which are associated with other point defects may be illustrated for the alkaline earth oxides as follows:

a. Cation vacancy-trivalent cation, impurity as next-nearest neighbor (nnn).

b. Cation vacancy-trivalent cation, impurity as nearest neighbor (nn).

c. Cation vacancy-monovalent anion impurity.

d. Cation vacancy plus two trivalent cations, each as next-nearest neighbor.

e. Cation vacancy plus two trivalent cations, each as nearest neighbor.

f. Cation vacancy plus trivalent cation plus monovalent anion.

g. Cation vacancy plus trivalent cation plus trapped hole.

h. Cation vacancy plus monovalent anion plus trapped hole.

These various defects are illustrated in figure 1 for an alkaline earth oxide. For simplicity, only deviations from the normal site charge of the rocksalt-type lattice are shown. Thus, M^+ represents a trivalent impurity cation, A^+ a monovalent anion and OH^+ and O^+ represent the ions OH^- and O^- respectively. The symbols [=] and [++] refer respectively to unoccupied cation and anion vacancies. Since each of the associated defects considered here is a linear array of simple defects, only the minimum number of atoms will henceforth be used to represent them in the text.

The relative proportions of isolated, singly-associated and of doubly-associated vacancies observed at room temperature depends upon the temperature at which equilibrium is attained if quenching occurs at a sufficiently rapid rate. In MgO, there is an appreciable mobility of cation vacancies at 400 °C, and hence if isolated defects are to predominate, one should rapidly quench crystals from some temperature of the order of 1000 °C. In the temperature region near 400 °C, a considerable association of vacancies with one or more impurity ions will occur [4]. One may obtain binding energies of associated defects by studying their concentrations at room temperature, following a quench from successively higher temperatures [10]. Anion vacancies are normally present at very low concentrations in the alkaline earth oxides. However, if they are produced by neutron irradiation in a reactor, one may follow the disappearance of isolated vacancies and detect the presence of increasing numbers of vacancy pairs as the temperature is increased up to 900 °C. This association is detected from the disappearance of F-centers and the formation of F_2 centers (sec. 5).

3.1. Structural Data from Electron Spin Resonance

The centers

Cr^+ O [=] [001] or equivalent

and Cr^+ [=] [011] or equivalent

in MgO were among the early point defects in oxides for which there was evidence of association of a vacancy with another defect [11, 12]. As in figure 1, only deviations from normal site charge are shown. The first defect, with a vacancy in the nnn position has a principal axis of the crystal as an axis of tetragonal symmetry. For brevity, this will be referred to as a Cr_T defect. The second defect, with a nn vacancy, shows an ESR spectrum interpretable in terms of rhombic symmetry; it will be called a Cr_R defect. Additional there are Cr^{3+} ions which show an isotropic ESR spectrum, and are therefore

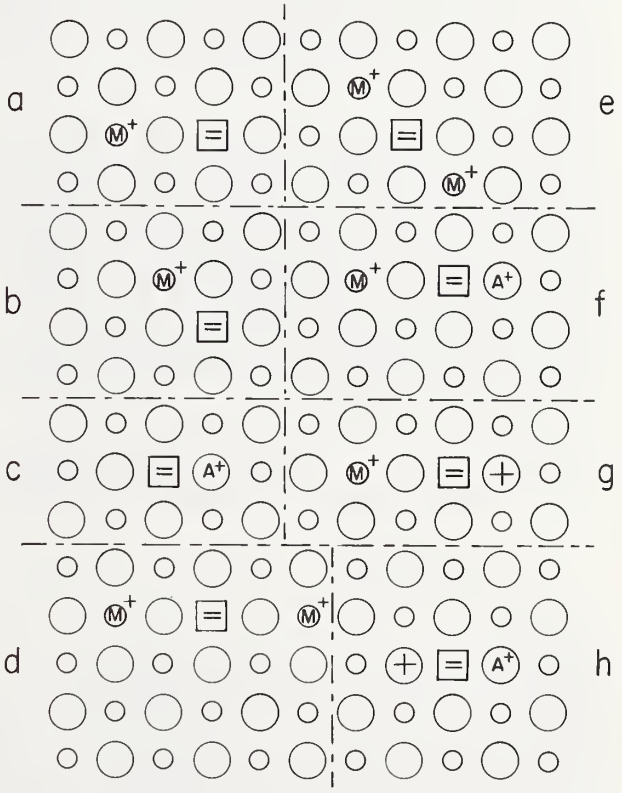

FIGURE 1. *Geometries of known associated-cation-vacancy point defects in alkaline earth oxides.*

One cation vacancy is associated respectively with:

a. One nnn trivalent cation, ⟨001⟩ or equivalent axis.
b. One nn trivalent cation, [011]-type direction.
c. One nn monovalent anion.
d. Two trivalent nnn cations.
e. Two trivalent nn cations.
f. One nnn trivalent cation and one nn monovalent anion.
g. One nnn cation and one nn positive hole.
h. One nn anion and one nn positive hole.

regarded as unassociated ions in octahedral symmetry. These will be represented by Cr_O.

The ESR spectrum of the Cr_O ion consists of a single line with $g=1.980$ for the even isotopes of Cr. A hyperfine quartet from the ^{53}Cr in its natural abundance of 10.53 percent shows a characteristic splitting constant of about 17.9 G [11].

Upon association with a nnn cation vacancy in MgO, the $M_S=\pm 1/2$ states of Cr^{3+} are split from the $M_S=\pm 3/2$ states by about 0.16 cm^{-1} in zero magnetic field, due to the lowering of the symmetry from octahedral to tetragonal. This splitting is given by $2D$ in the spin Hamiltonian for Cr^{3+} (S=3/2):

$$\mathcal{H}=\beta[g_xH_xS_x+g_yH_yS_y+g_zH_zS_z]$$
$$+D[S_z^2-S(S+1)/3]+E(S_x^2-S_y^2). \qquad (1)$$

Here $g_x=g_y=g_\perp$, $g_z=g_{||}$, and $E=0$ because of the tetragonal axis of symmetry. The g components for the several ions associated with vacancies are given in table 1, together with zero-field splitting parameters D. The ESR spectrum is shown in figure 2 with the lines belonging to the Cr_T center labeled with a T.

For Cr^{3+} with a nn cation vacancy, the site symmetry is rhombic. Hence the g-components will not be identical, and the asymmetry parameter E will be different from zero. The zero-field splitting resulting from the close proximity of the vacancy to the Cr^{3+} ion in MgO is about 0.8 cm^{-1}. Since the microwave photon energy for the spectrum shown in figure 2 is only about 0.3 cm^{-1}, one observes only a few of the allowed transitions occurring where energy levels come sufficiently close together. These are marked with an R in figure 2.

If the Cr^{3+} concentration is small, i.e., <0.01 percent, one expects that most of these ions will be widely separated in samples quenched from perhaps 1000 °C. Because of the double charge of the vacancy, one must serve for two Cr^{3+} ions. Hence for low concentrations, only half of the Cr^{3+} ions may be associated with a vacancy. The normal relative populations are:

$$[Cr_O]>[Cr_T]>[Cr_R],$$

where the square brackets imply concentration of the enclosed species. Only recently has the ESR spectrum of the nnn Cr_T center been observed in CaO [13]. The rhombic Cr_R defect has not been reported in any crystal other than MgO.

Analogous associated vacancy centers have been observed for Fe^{3+} in MgO, although ordinarily the concentrations of nnn or nn centers is at least an order of magnitude smaller than that of Fe^{3+} in octahedral symmetry [14]. It is not clear why the relative fraction of Fe^{3+} associated with vacancies is less than that for Cr^{3+}. The ESR parameters are given in table 1.

Association of vacancies with Ti^{3+} represents an interesting case [15]. Unlike iron, which may be incorporated in either the +2 or +3 states, both of which are detectable by ESR spectra, Ti appears to be incorporated in the tetravalent form in MgO. One therefore requires x-irradiation to create Ti^{3+} ($3d^1$) ions. If any of the latter were simply substitutional ions in octahedral symmetry, they would not be detected in the ESR spectrum because

TABLE 1. *ESR parameters for associated vacancy centers in* MgO

Geometry	$g_{||}$	$g_\perp$	|D| ($\times 10^4$ cm^{-1})	|E|	Ref.
Cr^+ O [=]....[001]...	1.9782		819.2		[11]
Cr^+ [=]....[011]...			338.5	2511	[12]
Fe^+ O [=]....[001]...	2.0037		5000		[14]
Ti^+O [=]....[001]...	1.9533	1.8993			[15]
Mn^{++} O Li^-?....[001]...	1.995		280		[5]
Mn^{++} O [=]....[001]...	1.9926		528.3		[13]
Cr^+ O [=] O M^+....[001]...	1.9782		798.3		[4, 5]
Cr^+ [=] M^+....[011]...			331.1	2207	[5]
Cr^+ [=] H^+O....[001]...	1.9786	1.9815	746.5		[13]
For CaO:					
Cr^+ O [=]....[001]...	1.9697	1.9751	1360.6		[13]

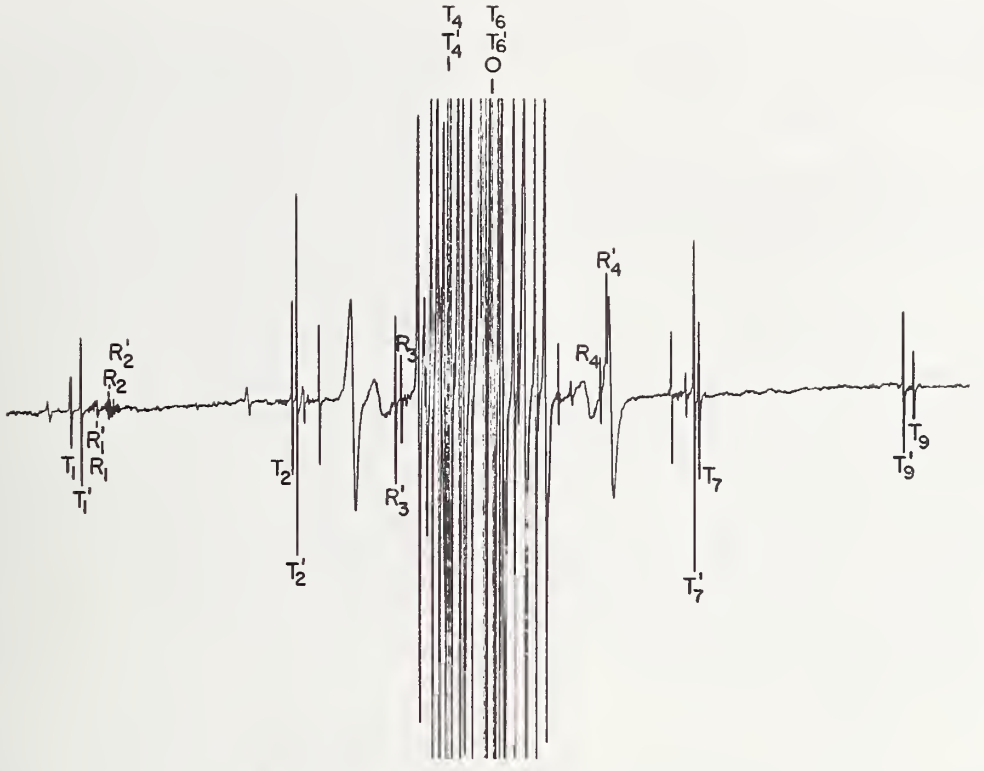

FIGURE 2. *ESR spectrum of* Cr^{3+} *in* MgO.

Lines marked with symbols O, T, R, T′ and R′ refer respectively to Cr^{3+} in octahedral symmetry, to defects a, b, d and e of figure 1. The unusual aspect of this spectrum is the inversion of relative intensity of primed and unprimed defects. This results from heating at 400 °C to enhance vacancy association.

of the orbital degeneracy of the ground state. However, the tetragonal crystal field distortion from the nnn vacancy lifts the degeneracy. It seems reasonable to expect that unless samples were quenched from a high temperature (perhaps > 1200 °C) that most Ti^{4+} ions should have an associated vacancy.

The ESR spectrum of Mn^{4+} in a site of tetragonal symmetry has been observed for Li-doped MgO powder; the parameters are given in table 1 [5]. However, the zero-field splitting parameter D is very much lower than that of any of the other ions. It is suggested that perhaps in this case Li^+ is the associate of Mn^{4+} [5]. Perhaps one may write

$$Mn^{2+}\ O\ Li^-$$

as the configuration. Another Mn^{4+} spectrum of tetragonal symmetry has been observed in a single crystal [13]. The magnitude of the parameter D (table 1) makes it appear that this is likely corresponds to the defect

$$Mn^{2+}\ O\ [=].$$

In addition to the Cr_T or Cr_R centers which have a net negative charge because of overcompensation by the associated cation vacancy, there are the neutral, doubly-associated centers shown in figure 1d and 1e. Evidence for these in the ESR spectrum is found in the form of satellites to the Cr_T or Cr_R spectra of figure 2. These satellite spectra contain precisely the same number of lines as the Cr_T or Cr_R spectra respectively, but with the slightly smaller zero-field-splitting constants given in table 1 [3, 4, 5]. These are interpreted as indicating a reduced crystal field at the Cr^{3+} ion because of another trivalent ion symmetrically located on the opposite side of the vacancy. The linear arrays for these centers are thus:

$Cr_{T'}$:	$Cr^+\ O\ [=]\ O\ M^+$	⟨ 001 ⟩ axis
$Cr_{R'}$:	$Cr^+\ [=]\ M^+$	[011]-type direction.

In an aluminum-doped MgO crystal the ion M^+ is very likely to be Al^{3+}. By extended heating of this crystal at 400 °C, it was possible to obtain a $Cr_{T'}$ spectrum 90-fold as intense as the Cr_T spectrum. This temperature of 400 °C has previously been mentioned as lying within the range in which there is a significant mobility of positive ion vacancies. Subsequent heating at 700 °C reduces the $Cr_{T'}$ intensity many-fold. The $Cr_{R'}$ concentration changes qualitatively in the same way as that of $Cr_{T'}$. In undoped crystals it was possible to get a ratio of $Cr_{T'}/Cr_T$ concentrations of about 2.2.

In MgO crystals which are known to have a significant concentration of the defect

$$O[=]H^+O$$

which shows an OH-stretching line at 3296 cm^{-1} [16, 17], one sees still a third Cr^{3+} spectrum of tetragonal symmetry. It appears to be the neutral defect

$$Cr^+O[=]H^+O.$$

Here the compensating charge is still closer to the vacancy than in the $Cr_{T'}$ center and the zero-field splitting constant (table 1) is the smallest of the three doubly-associated centers involving Cr^{3+} [13].

In the infrared spectrum of MgO, the OH line at 3296 cm^{-1} is always accompanied by another at 3310 cm^{-1} [16, 17]. The latter line appears to increase with the concentration of trivalent ions in the crystal. If any such trivalent ion is associated to form the center

$$M^+O[=]HO^+,$$

then one may understand the lack of a change in intensity of the 3310 cm^{-1} line on x-irradiation of the sample, since the center is neutral [8]. This behavior is unlike that of the defect

$$O[=]HO^+$$

which may trap a positive hole on the oxygen atom opposite to the HO^+, and thus shift the OH stretching frequency from 3296 cm^{-1} to 3323 cm^{-1}. It remains to be established that there is a correspondence between the $Cr^+O[=]H^+O$ center, for which the ESR spectral parameters are given in table 1, and the one responsible for the 3310 cm^{-1} line. Presumably Al^{3+} might be the trivalent ion in some of these defects.

It is known that there may be an appreciable concentration of F^- (fluoride) ions in some crystals. Presumably they may also associate themselves with a cation vacancy, for one may detect a defect with the structure $O^+[=]F^+$ (sec. 4).

3.2. Associated Vacancy Data From Luminescence

Some valuable structural data on point defects of Cr^{3+} may be obtained from sharp-line luminescence studies on oxides. A pair of very narrow lines ("R lines") observed in ruby (Cr^{3+}-doped Al_2O_3) corresponds to $^2E_g \rightarrow {}^4A_{2g}$ transitions. In the alkaline earth oxides, a single line at 6981 Å is observed for octahedral symmetry [18–21]. (Phonon sidebands are also present, but they will be ignored in this discussion.) It has been established that in MgO the line from Cr^{3+} ions in octahedral symmetry may be split by the action of a uniaxial stress [22]. If the symmetry about the Cr^{3+} ion is lowered to tetragonal, both the ^2E_g and $^4A_{2g}$ states are split. The magnitude of the ground state splittings is given from ESR data (in the previous section) by $2D \approx 0.16$ cm^{-1} [11]. This splitting is so small as to be unresolved even at 4 °K; it serves to broaden lines relative to the R line. At low concentrations of chromium ($\sim 10^{-4}$) in MgO there is a weaker pair of lines at 6992 Å and at 7038 Å; their intensity increases with Cr^{3+} concentration. These are attributed to Cr^{3+} ions associated with a *nnn* cation vacancy, i.e., the Cr_T center [20]. Uniaxial stress experiments verify the tetragonal symmetry [21]. External stress along the axis of the defect causes additional splitting of the two lines, and hence the internal stress is compressive. That is, the vacancy-Cr^{3+} distance is less than the normal lattice constant of 4.20 Å. No splitting occurs for a stress applied along a [111]-direction. The ratio of the intensities of the lines at 6992 Å and 7038 Å varies with temperature according to the Boltzmann factor. This is strong evidence that the 6992 and 7038 Å lines arise from a 94 cm^{-1} splitting of the ^2E_g state [21].

A pair of emission lines occurring at 6989 and 7034 Å are very weak at low Cr^{3+} concentrations but their intensity increases rapidly with concentration. Uniaxial stress experiments show that the symmetry axis is a principal axis of the crystal [21]. Likewise, no splitting is observed for stresses applied along a [111]-direction; relative intensities of 6989 and 7034 Å lines again vary with temperature approximately as the Boltzmann factor. These lines have been attributed to a doubly associated center involving two Cr^{3+} ions, i.e., $Cr^+O[=]OCr^+$. A small exchange interaction would be expected for two Cr^{3+} ions thus disposed, and structure about both the 6989 and 7034 Å lines has been interpreted as evidence for such interaction. Comparison at 18 °K and at 4 °K of the intensities of the satellites about the 7034 Å line suggests a 2.0 cm^{-1} exchange splitting of the ^2E_g level and a 2.6 cm^{-1} splitting of the $^4A_{2g}$ ground state [21].

An additional Cr^{3+} luminescence line has been reported at 7088 Å in MgO [10]. Its relative luminescence intensity is reported to be correlated with that of the ESR spectrum of the Cr_R center. The large shift in position from the 6981 Å line for Cr^{3+} in octahedral symmetry is qualitatively to be expected from the large distortion of the crystal field by the *nn* vacancy. Hence one appears to have luminescence data which are in accord with expectation for defects 1a, 1b, 1d, and 1e of figure 1.

Ions which are isoelectronic with Cr^{3+} might be expected to show characteristic $^2E_g \rightarrow {}^4A_{2g}$ lines appropriate to the octahedral symmetry of an isolated substitutional ion or a distortion to lower symmetry by vacancy association. The emission line of V^{2+} in octahedral symmetry in MgO at 8696 Å at 77 °K is accompanied by a group of phonon sidebands; it corresponds to the Cr^{3+} line system originating at 6981 Å [23]. No emission lines corresponding to a V^{2+} ion associated with a cation vacancy has yet been established. x-irradiation does result in electron trapping by numerous V^{3+} ions in octahedral symmetry. It appears likely that V^{2+} luminescence lines reflecting vacancy association resulting from the parent V^{3+} ion will yet be established.

The Mn^{4+} ion fluorescence or cathodoluminescence spectrum in MgO shows numerous lines [5, 8, 17]. Of these, the line at 6545 Å is attributed to ions in octahedral symmetry [5]; another at 6593 Å is attributed [8] to the center

$$Mn^{2+}\,O[=].$$

It remains to be established by correlation with the ESR spectrum of Mn^{4+} in tetragonal symmetry that the latter assignment is correct.

4. Trapped-Hole Defects

The term "color center" applied to the alkali halides is linked with defects having an electron in an anion vacancy, i.e., "F-centers." Such defects may readily be generated by irradiation or by heating in metal vapors. Though complicated by the relatively more pronounced effects of impurities, the alkaline earth oxides do show a characteristic color center on irradiation. This center is the hole trapped on an oxygen atom adjacent to a cation vacancy (fig. 3) [24]; it is here referred to as the V_1 center. Though the model was proposed for the alkali halides [25], it has not been observed in them.

At 77 °K, MgO crystals which have been subjected to 2537 Å or x-irradiation show an ESR spectrum of three lines at random orientation of the magnetic field [24]. The angular dependence of these lines is that for a system of tetragonal symmetry. The positions of the lines at several field orientations is given in figure 4. The ESR parameters for this defect and for others akin to it are given in table 2. The positive deviation of the g-components from the free-electron value and the tolerance of high levels of microwave power are consistent with the assumption of a positive hole located on an oxygen atom adjacent to a cation vacancy, i.e., an O^- ion. From the width of the

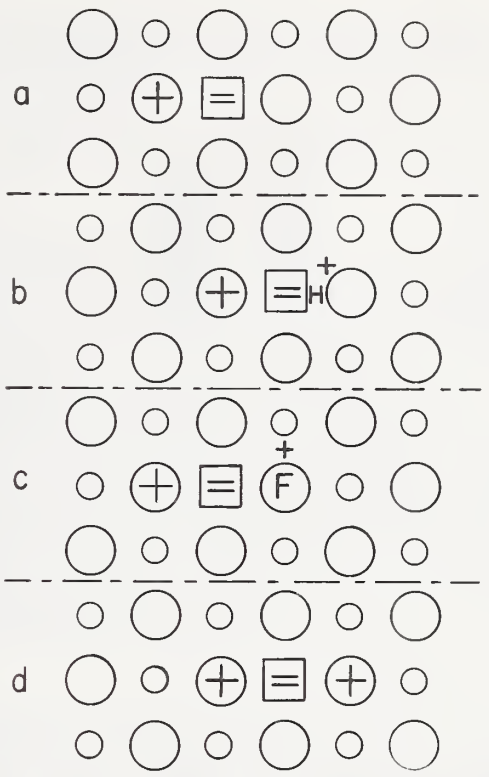

FIGURE 3. *Models of trapped holes in alkaline earth oxides.*
a. V_1 center.
b. V_{OH} center.
c. V_F center.
d. W center.

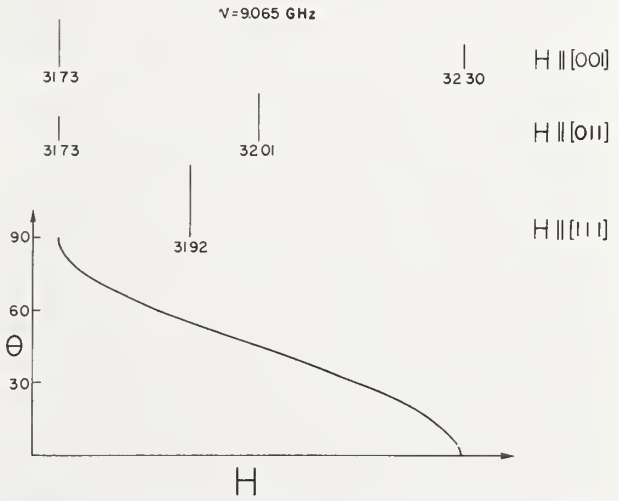

FIGURE 4. *Line positions in the ESR spectrum of the* V_1 *center in* MgO *for* H∥[001], H∥[011] *and* H∥[111].
The variation of line position as a function of angle between the magnetic field and a principal axis is shown at the bottom of the figure.

lines, which may be as little as 0.4 G, one may infer that the lifetime of a positive hole along a particular axis is long compared with 10^{-7} sec. This relatively long lifetime is presumably the result of

TABLE 2. *ESR parameters of* V-*centers*

	$g_{\|\|}$	$g_{\perp}$	D (cm^{-1})	Ref.
V_1, MgO	2.0032	2.0385		[24]
V_1, CaO	2.0011	2.0710		[27]
V_{OH}, MgO	2.0033	2.0396		[16, 13]
V_F, MgO	2.0031	2.0388		[28]
W, MgO	2.0032	2.0408	0.02125	[24, 13]
ZnO (Li-doped)	2.0026	2.0254		[7]
Al_2O_3	2.02	2.006		[36]
$Al_2O_3(O^+?)$	2.018	2.011		[29]

an extensive relaxation along the hole-vacancy axis. At room temperature the lines are roughly thirty-fold broader, suggesting a much more rapid hole migration among the three principal axes. While this representation of the V_1 center geometry in MgO gives the impression of localization of the hole upon one oxygen atom, the V_1-ESR data require only that the fractional localization of the hole on the two axial atoms differ from that on the four equatorial atoms.

If the lifetime of a hole upon a particular oxygen atom were at least of the order of seconds, one might hope selectively to populate or bleach V_1 centers along a particular axis. Failure of such experiments even at 4 °K suggests that there is considerable hopping of a hole about a particular cation vacancy [13, 26].

That MgO becomes violet colored upon irradiation was reported in 1937 [30]. The color corresponds to a broad absorption band at 5320 Å. Since the coloration of several specimens varies widely for a given irradiation, it was concluded understandably that the coloration is due to an impurity. However, parallel optical absorption and ESR experiments have shown that the 18000 cm^{-1} band is that of the V_1 center [31]. In some samples the crystals appear brown in varying degrees after x-irradiation. Such behavior is attributable to an additional absorption band appearing at 3940 Å. This band may be induced in any MgO crystal by heating in air at 1200 °C. Its origin is unknown.

While the negative ion vacancy of the F-center may be produced in the alkali halides by ionizing radiation, neither a cation nor an anion vacancy is generated by such irradiation of the alkaline earth oxides. However, positive ion vacancies occur in significant numbers in all magnesium oxide crystals which have been available to this time; these are the inevitable counterparts of trivalent impurity ions which are always present. The aluminum ion is an important contributor of cation vacancies, though it does not make its presence as obvious as the paramagnetic ions Cr^{3+} and Fe^{3+}. The two latter ions (and others derived from them on irradiation) affect a considerable number of the physical properties of MgO. Other impurities in MgO which may help to incorporate positive ion vacancies are Ti^{4+}, V^{3+} and Mn^{4+}. Iron is doubtless the most important impurity controlling the number of positive ion vacancies. In MgO crystals grown from the melt, the predominant fraction of iron is in the Fe^{2+} form, as judged both by the ESR- and the optical absorption spectra. Extended heating in oxygen at 1200 °C converts a significant fraction to Fe^{3+} [32], presumably accompanied by the inward diffusion of cation vacancies [33]. We have noted that the cation vacancy may be associated with defects such as Ti^{3+}, Cr^{3+}, Fe^{3+}, OH^-, or F^-. Heating to 700 °C or above and quenching may serve to dissociate such centers and increase the number of isolated positive ion vacancies. Hence such heating and quenching before irradiation with x rays or with ultraviolet light of energy 5 eV or more gives an enhanced concentration of V_1 centers. It has tacitly been assumed that there exists also a number of defects adequate to accept the electrons removed by UV or x-irradiation [26]. Probably most of the holes are generated at normal oxygen sites. These would move rapidly through the crystal until trapped by a transition metal impurity ion or by a cation vacancy.

Before proceeding to a description of the ESR spectra of other hole centers for which the spectral parameters are given in table 2 and the models are given in figure 3, it is profitable to consider data concerned with the distribution of hydrogen as an impurity in MgO.

A narrow O–H stretching band appears at 3296 cm^{-1} in many MgO crystals before these have undergone any treatment. It is accompanied by a band at 3310 cm^{-1} only partially resolved from it and appearing as a shoulder [16]. Other crystals merely give a very broad band in this region upon heating at 400 °C. These show an apparent transformation of the broad band into the 3296–3310 cm^{-1} pair, in addition to weaker lines. In some cases one sees a strong line at 3700 cm^{-1}. The close correspondence of this line with that in $Ca(OH)_2$ suggests that one may have local regions of $Mg(OH)_2$ in an MgO crystal. This has been confirmed from the diffraction pattern in MgO of a small region observed to diminish in size under the electron beam of an electron microscope [34]. The broad band in the OH-stretching region presumably arises from OH^- in isolated sites. For these the hydrogen atom would probably be interstitially oriented [8]. These infrared bands are especially strong in crystals which have been made from MgO powders prepared from $Mg(OH)_2$. Crystals showing strong 3296 cm^{-1} bands are also found to produce lentic-

ular cavities when heated at 1000 °C in a reducing gas such as H_2, D_2, or CO. The source of the hydrogen appears to be primarily derived from OH centers having the 3296 cm^{-1} line [34].

Upon x-irradiation of such samples at 77 °K one observes a reduction of intensity of the 3296 cm^{-1} line by a factor of two or more, while a new line appears at 3323 cm^{-1}. The latter has an intensity approximately equal to that lost by the 3296 cm^{-1} line. At room temperature the 3323 cm^{-1} line bleaches with a time constant of 80 min at 32 °C, with a corresponding regrowth of the 3296 cm^{-1} line. The interpretation of the infrared line behavior is based upon a correlation with ESR behavior.

In all crystals showing a strong 3296 cm^{-1} line, one sees doublet satellites on one side of each of the V_1 center ESR lines. These doublets decay with the same time constant as that of the 3323 cm^{-1} infrared line. Their angular dependence likewise indicates a center of tetragonal electric field symmetry. The suggestion is strong that the defect is a hole trapped at a positive ion vacancy, but with a perturbing nucleus of spin one-half. This nucleus is required by the axial dependence of the hyperfine splitting to lie along the axis defined by the positive hole and the cation vacancy. Electron-nuclear double resonance experiments unambiguously demonstrate the nucleus to be hydrogen. The magnitude of the anisotropic component of the hyperfine splitting is a measure of the dipole-dipole interaction of the positive hole and the nucleus. From this interaction one may calculate $r = 3.2$ Å, confirming the proton position indicated for the V_{OH}-defect in figure 3, i.e., adjacent to the cation vacancy. This distance is fortuitously close to that obtained by assuming that the oxygen atoms are undisplaced from their normal distance of 4.20 Å and that the OH distance is 0.94 Å as in $Ca(OH)_2$. The intensity of the ESR lines of this V_{OH} center correlates well with that of the 3323 cm^{-1} line. Decay of the V_{OH} center is undoubtedly due to the loss of the hole from the oxygen adjacent to the cation vacancy. Hence the transfer of line intensity from the 3323 cm^{-1} to the 3296 cm^{-1} line of decay of the V_{OH} center implies that the 3296 cm^{-1} line is appropriate to the geometry O[=]H^+O. Here, although the V_{OH} center produced by irradiation was the primary defect of ESR study, the by-product—more important perhaps than the V_{OH} center—was the unambiguous identification of a stable defect present in significant concentrations in crystals subjected to a wide variety of studies by many investigators.

Even in some MgO crystals which have not been x-irradiated there may exist weak 3323 cm^{-1} lines which suggest the presence of V_{OH} centers [8, 13]. Their presence in Li-doped MgO was interpreted as due to raising of the Fermi level by lithium [8].

It has been surmised that the 3310 cm^{-1} infrared line arises from OH^- adjacent to a cation vacancy and associated with a trivalent impurity cation, corresponding to the model of figure 1f [8], i.e.,

$$M^+O[=]H^+O.$$

The ESR data for a center in which the trivalent cation is Cr^{3+} were given in section 4, and Al^{3+} was mentioned as another possible cation. Such an assignment is consistent with the observation that the intensity of the 3310 cm^{-1} line is unaltered upon x-irradiation [16].

Another defect which may be present in non-irradiated MgO has an analogous structure and could be described in detail because a trapped hole could be associated with it. This trapped hole defect is labeled V_F in figure 3, and has the configuration [28]

$$O^+[=]F^+$$

Again, a doublet, V_{OH}-like ESR spectrum is observed. The identification was made when the g-components of HF-treated MgO powder samples were found to coincide with those of the spectrum in a single crystal. Fluoride ion is a common impurity in MgO, and within the range in which the temperature is high enough to permit cation vacancy migration but low enough to permit stable association, one may expect considerable association of the two defects.

Following establishment of the V_1 center in MgO, it is obvious to ask about the possible occurrence of a center formed by trapping two holes at a single cation vacancy. This W center (i.e., double-V) shown in figure 3 has indeed been observed in MgO x-irradiated and observed at 77 °K [24]. The ESR spectrum of this system with $S = 1$ may roughly be described by the statement that each line of the V_1 center is replaced by a pair of widely separated lines. Having a spin of 1, the energy levels of the system are split in zero magnetic field, with $D = -0.02125$ cm^{-1}. From the magnitude of the dipolar interaction one calculates a separation of 4.9 Å for the two holes. The axis is again along a [001] or equivalent direction. It is apparent that on a localized model the two holes tend to be as far apart as possible. This center is far less stable than the V_1 center, probably due to a reduced binding energy for the second hole. It is the least stable of the various neutral centers which contain a cation vacancy.

There appears to be one other example of a pair of holes trapped on two oxygen atoms adjacent to

a cation vacancy. This is observed in a reactor-irradiated Al_2O_3 crystal in which at 77 °K for $H \perp \langle c \rangle$, one observes a pair of lines for each of six inequivalent orientations of a line joining two oxygen sites [35]. For $H \| \langle c \rangle$, only two lines are observed either at 77 °K or at 300 °K. However, for $H_\perp \langle c \rangle$, as one raises the temperature above 230 °K, the twelve lines are observed to broaden at an increasing rate. This is attributed to jumping of the holes among the equivalent positions. For this center with $S=1$, $D \approx 0.13$ cm^{-1}. From this D value, an internuclear distance of about 3.0 Å has been computed for the two interacting holes, in satisfying accord with expectation. The same spectrum had previously been given a more doubtful interpretation [36].

It is reported that when lithium is substituted for zinc in ZnO that a positive hole may be trapped on an oxygen atom adjacent to the lithium [6, 7]. The hyperfine splitting pattern is appropriate to the overlap of the hole wave function on the lithium. Doping with ^{6}Li gives rise to the expected triplet splitting for ^{6}Li with I=1 [7].

5. Electrons Trapped at Anion Vacancies

5.1. Electron Spin Resonance Evidence for *F*-Centers

The first documented example of an electron trapped in an anion vacancy in an oxide appears to be that in MgO [37]. Subsequently, ESR absorption of similar centers was detected in CaO, SrO and BaO [38, 39], ZnO [7], Al_2O_3 [36] and in some complex oxides [35, 40]. ESR data for electron centers in some of these oxides is given in table 3. The ESR spectrum in MgO has an isotropic g-factor of 2.0023. Since most of the Mg^{2+} neighbors of an anion vacancy are ^{24}Mg or ^{26}Mg with I=0, there is an intense central line. However, for a natural abundance of ^{25}Mg of 10.11 percent, the probability is about 0.36 that one of six Mg neighbors is ^{25}Mg with I=5/2. Hence one would expect a hyperfine sextet, but with marked anisotropy. Since the axis of hyperfine interaction may be parallel or perpendicular to the applied field if $H \| [001]$, the spectrum is not immediately obvious. However, for $H \| [111]$, all hyperfine interactions are equivalent and one sees a nicely resolved sextet as in figure 5. The probability of having two ^{25}Mg ions as neighbors to an anion vacancy is about 0.10, and for $H \| [111]$ one expects a spectrum of eleven lines. Some of these are seen in figure 5, and the remainder (except for the central line) can be seen at higher gain. The intensities of the hyperfine lines are in accord with expectation. Hence, the identification of the defect as an electron in an anion vacancy would seem to be established. The small hyperfine splittings that are observed indicate that the electron is far more localized in the MgO F-center than in those of the alkali halides.

Electron-nuclear double resonance (ENDOR) experiments on F-centers in MgO agree in detail with the expectations for interaction of a nn ^{25}Mg nucleus with an electron in an anion vacancy. The additional information which only ENDOR provides is evidence for outward motion of nn Mg nuclei by 0.04 to 0.08 of the normal Mg-O distance [11]. This conclusion results from an interpretation of the magnitude of the quadrupole coupling constant; ENDOR measurements of the F-center in SrO give similar conclusions [42].

In the alkali halides one observes an optical band for a defect (F'-center) in which two electrons are trapped at an anion vacancy. The existence of a stable F' center in additively colored CaO is suggested by an optical band at 3.1 eV and by bleaching experiments [43, 44]. Irradiation with light of energy > 2.8 eV causes bleaching of the 3.1 eV band and an enhancement of the F

TABLE 3. *ESR parameters of trapped-electron centers* [a]

F	F_2		F' excited state	F_t	
g	$g_\|\|$	$g_\perp$	g	g	D (cm^{-1})
MgO 2.0023	2.0004	2.0012	2.000	2.0033	0.0287 [47]
CaO 2.0001	1.995	1.9980 [35]	1.995 [35]	2.00	[46]
SrO 1.9846	1.9816 (g_{av})				
BaO 1.936					

[a] Values for which no other references are cited are taken from reference [39].

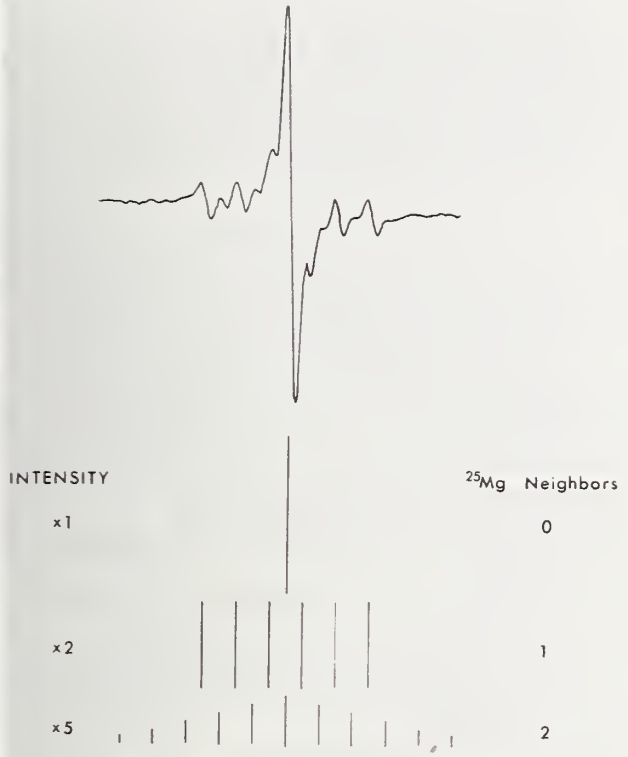

FIGURE 5. *ESR spectrum of the* F*-center in* MgO.

H∥[111]. The central line arises from centers with no ^{25}Mg neighbors. The uniformly spaced sextet arises from centers having one nn ^{25}Mg nucleus. The remaining lines belong to a set of eleven lines from centers having two nn ^{25}Mg nuclei.

band at 3.6 eV. There is simultaneously an enhancement of the number of F-centers seen by electron spin resonance. Irradiation of such samples with light of energy < 2.5 eV reduces the intensity of the 3.6 eV F band and enhances that of the 3.1 eV F' band. It is presumed that the low-energy light causes release of electrons from shallow traps and that these are then captured by F-centers to form F'-centers.

The F'-centers do not show ESR absorption in their singlet ground states. However, upon illumination with light of energy > 3.5 eV, a doublet ESR signal is observed both for MgO and for CaO, corresponding to an excitation of the triplet state [35].

An F-like center which apparently has no counterpart in the alkali halides is an electron trapped at a cation-anion vacancy pair (F_2-center) [38]. At ~ 9 GHz, its ESR spectrum in MgO, CaO, SrO and BaO consists of a narrow, but asymmetric, line underlying the central component of the F-center line. The F_2 line is enhanced at the expense of the F-line by heating at temperatures up to 900 °C, followed by x-irradiation at room temperature to populate the anion vacancy of the vacancy pairs. After such treatment, no F-centers are detected. Resolution of parallel and perpendicular ESR line components is achieved at 35 GHz, both for MgO and for CaO; the g-components are given in table 3 [35]. Unlike the simple F-center, the F_2 center may be depopulated by optical irradiation over a broad range of energies peaking at 3.5 eV in MgO [45].

A remarkable three-vacancy, two-electron F-center has been called the F_t center, the subscript t suggesting that ESR observations are made on the triplet (excited) state. It appears to be a linear array of a cation vacancy between two anion vacancies, each having one electron. The axis lies along [001] or equivalent directions [46]. Exchange coupling of the electrons leads to a singlet ground state. However, the energy separation J/k of the triplet level is reported to be only 80 °K for MgO [47] and 50 °K for CaO [46]. Hence at 300 °K the triplet levels are thermally populated. For CaO at 1.6 or 4.2 °K, light in the F-band (3.6 eV) was found effective in producing polarization of excited spin levels [46]. The anisotropy of the spectrum unambiguously identifies the axes. The separation of electrons is calculated from the zero-field splitting parameter D to be 4.47 Å in MgO and 5.5 Å in CaO, assuming D arises wholly from dipole-dipole interaction. A central cation vacancy is interposed to attain stability for the aggregated vacancies. For MgO, it was found necessary to use doses of $> 2\times 10^{19}$ nvt at 150 °C in order to see the F_t spectrum.

5.2. Optical Absorption of Trapped-Electron Defects

After a moderate dose of fast-neutron radiation, MgO exhibits a blue color quite distinct from the violet appearance after x-irradiation. It was soon established that this blue color is unrelated to the simple F-center. The absorption spectrum of neutron-irradiated MgO shows an intense peak at 2500 Å as well as a large number of bands extending to 1.2 μ. Unlike the alkali halides for which the electron trapped at an anion vacancy (F-center) gives rise to absorption in the visible region of the spectrum, the F-center in MgO absorbs at 2500 Å. This has been established by correlated ESR and optical absorption studies [15, 48]. This shift to a much higher binding energy for an electron in an oxygen vacancy was predicted remarkably well [49]. For MgO crystals which have been heated in magnesium vapor or electron irradiated, there appears to be a second band very nearly superimposed upon the F band [50]. Tentatively, this may be interpreted as the F′ band (two electrons in one anion vacancy).

Doubtless the most impressive evidence of correlation of the 4.9 eV optical band in MgO with the ESR spectrum comes from the combination of

Faraday rotation measurement with ESR observation. There is a marked change in the Faraday rotation amplitude under conditions of microwave saturation of the F-center resonance [51, 52].

The optical absorption band of the F-center in CaO is centered at 3350 Å [35, 44, 51, 52]. Though it was not detected at first, a sharp zero-phonon line at 3555 Å appears to be associated with this band [53, 35]. Very recently it has been shown that the Faraday rotation in the zero-phonon line also is affected by microwave saturation of the electron spin resonance of the F-center. This appears to be the first example of a zero-phonon line associated with a center of simple symmetry. Its sharpness and its associated phonon bands should permit many incisive inquiries of the details of geometry, of the absorption process and of vibrational modes.

The optical absorption band for SrO is found to peak at 3 eV [35]. It has as yet received little attention.

MgO samples which have been neutron-irradiated at elevated temperatures or which are heated to 300 °C or more after irradiation show a remarkable number of bands with sharp zero-phonon transitions. It was predicted that these arise from F-aggregate centers [15]. A number of uniaxial stress investigations have been carried out to establish the symmetry properties of the centers responsible [54, 55, 56, 45, 35]. A number of these bands are found to be oriented along a [110] direction, as is the two-electron M center in the alkali halides. Others have symmetry characteristics resembling those of the three-electron R center [45, 35]. Detection and identification of an ESR signal for those defects in which either the ground state or an attainable excited state is predicted to be paramagnetic would be most desirable for identification of the defects.

Interaction of an oxide surface with oxygen may lead to modification of existence defects or generation of new ones upon adsorption. The former case is typified by MgO, in which the concentration of F-centers in the bulk crystal may be diminished by neutron irradiation in oxygen. This effect is pronounced if the MgO is in powder form [57, 58]. Destruction of a surface defect (S-center) by O_2 is apparently total. Neutron irradiation of alkaline earth powders in vacuo leads to the S-center described as an electron trapped at a negative ion vacancy with five Mg^{2+} neighbors. An intense color and the associated ESR spectrum both disappear rapidly on admission of oxygen. A surface center labeled S′ and having rather different g-components is generated by UV irradiation of MgO in vacuum [59]. Admission of oxygen leads to a new defect showing rhombic symmetry. Its g-components are $g_{xx}=2.077$, $g_{yy}=2.0011$ and $g_{zz}=2.0073$ [60]. These are similar to the values for O_2^- observed in KO_2 and in alkali halides having the O_2^- defect. The same O_2^- center is observed on a ZnO surface to which oxygen has been admitted without UV irradiation.

6. References

[1] W. Low and E. L. Offenbacher in Solid State Physics, F. Seitz and D. Turnbull, eds., **17,** 135 (1965).
[2] J. H. E. Griffiths, J. Owen and I. M. Ward, Repts. Conf. on Crystalline Solids, Bristol 1954, p. 81.
[3] P. Auzins and J. E. Wertz, Bull. Am. Phys. Soc. **9,** 707 (1964).
[4] J. E. Wertz and P. V. Auzins, J. Phys. Chem. Solids **28,** 1557 (1967).
[5] B. Henderson and T. P. P. Hall, Proc. Phys. Soc. **90,** 511 (1967).
[6] J. Schneider and O. Schirmer, Z. Naturf. **18A,** 20 (1963).
[7] P. H. Kasai, Phys. Rev. **130,** 989 (1963).
[8] A. M. Glass and T. M. Searle, J. Chem. Phys. **46,** 2092 (1967).
[9] E. R. Lippincott and R. Schroeder, J. Chem. Phys. **23,** 1099 (1955).
[10] A. M. Glass, J. Chem. Phys. **46,** 2080 (1967).
[11] J. E. Wertz and P. Auzins, Phys. Rev. **106,** 484 (1957).
[12] J. H. E. Griffiths and J. W. Orton, Proc. Phys. Soc. (London) **73,** 948 (1959).
[13] J. E. Wertz, unpublished data.
[14] J. W. Orton, P. Auzins and J. E. Wertz, Bull. Am. Phys. Soc. **9,** 739 (1964).
[15] J. E. Wertz, G. S. Saville, L. Hall and P. Auzins, Proc. Brit. Ceram. Soc. **1,** 59 (1964).
[16] P. W. Kirklin, P. Auzins and J. E. Wertz, J. Phys. Chem. Solids, **26,** 1067 (1965).
[17] J. E. Ralph, unpublished reports, AERE, Harwell.
[18] O. Deutschbein, Ann. Phys. **14,** 712 (1932).
[19] A. L. Schawlow, D. L. Wood and A. M. Clogston, Phys. Rev. Lett. **3,** 544 (1959).
[20] A. L. Schawlow, J. Appl. Phys., Suppl. **33,** 395 (1962).
[21] G. F. Imbusch, A. L. Schawlow, A. D. May and S. Sugano, Phys. Rev. **140** A 830 (1965).
[22] A. L. Schawlow, A. Piksis and S. Sugano, Phys. Rev. **122,** 1469 (1961).
[23] M. D. Sturge, Phys. Rev. **130,** 639 (1963).
[24] J. E. Wertz, P. Auzins, J. H. E. Griffiths and J. W. Orton, Disc. Faraday Soc. **28,** 136 (1959).
[25] F. Seitz, Rev. Mod. Phys. **26,** 7 (1954).
[26] Y. Chen and W. A. Sibley, Phys. Rev. **154,** 842 (1967).
[27] A. J. Shuskus, J. Chem. Phys. **39,** 849 (1963).
[28] J. E. Wertz and P. V. Auzins, Phys. Rev. **139** A 1645 (1965).
[29] F. T. Gamble, R. H. Bartram, C. G. Young, O. R. Gilliam and P. W. Levy, Phys. Rev. **138** A 577 (1965).
[30] J. H. Hibben, Phys. Rev. **51,** 530 (1957).
[31] J. E. Wertz, G. Saville, P. Auzins and J. W. Orton, J. Phys. Soc. Japan **18,** Supp. II, 305 (1963).
[32] R. W. Soshea, A. J. Dekker and J. P. Sturtz, J. Phys. Chem. Solids, **5,** 23 (1958).
[33] J. E. Wertz, J. W. Orton and P. Auzins, J. Appl. Phys. Suppl. **33,** 322 (1962).
[34] D. H. Bowen, Symposium on Mass Transport in Oxides, Washington, D.C. 1967, p.
[35] B. Henderson, Proceedings of the Symposium on Mass Transport in Oxides, Washington, D.C. (1967).
[36] F. I. Gamble, C. G. Bartram, C. G. Young, O. R. Gilliam and P. W. Levy, Phys. Rev. **134** A 577 (1964).
[37] J. E. Wertz, P. Auzins, R. A. Weeks and R. H. Silsbee, Phys. Rev. **107,** 1535 (1957).

[38] J. E. Wertz, J. W. Orton and P. Auzins, Disc. Faraday Soc. **30**, 40 (1961).
[39] P. Auzins, J. W. Orton and J. E. Wertz, Symposium on Paramagnetic Resonance, **I**, p. 90, W. Low, ed. (Academic Press, N.Y. 1963).
[40] T. Takeda and A. Watanabe, J. Phys. Soc. Japan **21**, 267 (1966).
[41] W. P. Unruh and J. W. Culvahouse, Phys. Rev. **154**, 861 (1967).
[42] J. W. Culvahouse, L. V. Holroyd and J. L. Kolopus, Phys. Rev. **140** A 1181 (1965).
[43] J. C. Kemp, W. M. Ziniker and E. B. Hensley, to be published.
[44] W. C. Ward and E. B. Hensley, Bull. Am. Phys. Soc. **10**, 307 (1965).
[45] R. D. King and B. Henderson, Proc. Brit. Ceram. Soc. **9**, to be published.
[46] D. H. Tanimoto, W. M. Ziniker and J. C. Kemp. Phys. Rev. Letters, **14**, 645 (1965).
[47] B. Henderson, Brit. J. Appl. Phys. **17**, 851 (1966).
[48] B. Henderson and R. D. King, Phil. Mag. **13**, 1149 (1966).
[49] J. C. Kemp and V. I. Neeley, Phys. Rev. **132**, 215 (1963).
[50] W. Sibley, to be published.
[51] J. C. Kemp, W. M. Ziniker and J. A. Glaze, Phys. Letters, **22**, 37 (1966).
[52] J. C. Kemp, W. M. Ziniker and J. A. Glaze, Proc. Brit. Ceram. Soc. **9**, 109 (1967).
[53] J. C. Kemp and W. M. Ziniker, These proceedings.
[54] R. D. King and B. Henderson, Proc. Phys. Soc. **89**, 153 (1966).
[55] I. K. Ludlow and W. A. Runciman, Proc. Phys. Soc. **86**, 1081 (1965).
[56] I. K. Ludlow, Proc. Phys. Soc. **88**, 763 (1966).
[57] R. L. Nelson and A. J. Tench, J. Chem. Phys. **40**, 2736 (1964).
[58] R. L. Nelson, A. J. Tench and B. J. Harmsworth, Trans. Faraday Soc. **63**, 1427 (1967).
[59] J. H. Lunsford, J. Phys. Chem. **68**, 2312 (1964).
[60] J. H. Lunsford and J. P. Jayne, J. Chem. Phys. **44**, 1487 (1966).

Theory of the Energetics of Simple Defects in Oxides

I. M. Boswarva

Queens College, Flushing, New York 11367

and

A. D. Franklin

National Bureau of Standards, Washington, D.C. 20234

Currently, defect formation energy calculations for ionic crystals rest upon the applicability of (1) two-body short-range interactions, (2) additivity rules that allow assignment of ionic parameters, such as radius, charge, polarizability, etc., independent of ionic displacement, and (3) a simple functional form to express the dependence of the short-range interaction potentials on the distance between the two ions. An examination of the properties of the alkaline-earth chalcogenides shows that additivity rules for ionic radii and polarizabilities apply as well to them as to the alkali halides. Further, shell-model fits to both the static and dynamic properties of MgO, UO_2, and ThO_2 indicate that a model based upon two-body potentials can be used to describe these simple oxides. However, attempts to calculate formation energies of vacancies in MgO have been unsuccessful. The problem may lie with the functional dependence for the oxygen-oxygen interactions, which are attractive in the shell model fits and are therefore not likely to be well described by the exponential dependence upon ion separation used in the defect calculations.

Key Words: Oxide crystals, point defects, formation energy, theory, Born model, additivity rules.

1. Introduction

The Born model of an ionic solid has been used rather successfully for the calculation of formation and motional energies of simple defects in alkali halides and the alkaline earth halides. Recently, models such as the shell model have been able to provide a reasonable fit to the lattice dynamic properties of simple oxides such as MgO [1],[1] UO_2 [2], and ThO_2 [2]. It therefore seems appropriate to examine the nature of the Born model calculation of defect energies with respect to its possible application to oxides.

In this model, the lattice energy is expressed as a sum over two-body interaction energies between all pairs of ions in the crystal. The pair energies are assumed to depend on the distance between the ions, the charges of the ions, and their electronic dipole moments. Parameters describing the properties of the ions, including ionic charge, polarizability, van der Waals coefficients, and overlap energy parameters are needed for the calculation, and are obtained by fitting the elastic and dielectric properties of the same crystal with the model.

In this paper, we shall first describe briefly the mechanics of the defect calculations in order to focus on the basic assumptions involved, then examine the applicability of the concepts of ionic polarizability and radii to a family of compounds that includes simple oxides (the alkaline earth chalcogenides), and finally discuss some attempts at calculating defect formation energies in MgO and VO_2.

2. Defect Formation Energy Calculations

In the Born model, the crystal is considered to be static, with separate charged ions situated at positions of equilibrium with respect to the (ionic) potential energy of the crystal. The electrons are considered to be localized upon particular ions and to move with the ions. Changes in electron states are included via induced dipole moments, deformation dipoles, etc. In what follows we will describe the special case of a vacancy, but the argument applies, with trivial modification, to other point defects.

A vacancy is formed by removing an ion from an otherwise perfect crystal. The zero of energy is thus the energy of the perfect crystal. When the vacancy is formed, the surrounding ions are displaced from their lattice sites and become polarized. The defect formation energy then contains three

[1] Figures in brackets indicate the literature references at the end of this paper.

290-621 O-68—3

types of terms: Coulombic, polarization and short-range closed-shell interactions.

Expressions for the first two groups of terms can readily be written down:

$$E_c=-\frac{1}{2}\sum_{\substack{i\neq j\\ i,j}}^{\text{Defect Crystal}}\frac{e_ie_j}{|\mathbf{R}_i-\mathbf{R}_j|}+\frac{1}{2}\sum_{\substack{i\neq j\\ i,j}}^{\text{Perfect Crystal}}\frac{e_ie_j}{|\mathbf{r}_i-\mathbf{r}_j|},$$

where $\mathbf{R}_i$, $\mathbf{R}_j$ indicate relaxed positions of the ions, $\mathbf{r}_i$, $\mathbf{r}_j$ perfect lattice positions and the summations are over all ions of the crystals, including defects in the first term;

$$E_p=-\frac{1}{2}\sum_i \mathbf{m}_i\cdot\mathbf{F}_i^{(1)},$$

where $\mathbf{m}_i$ is the electronic dipole induced on ion i and $\mathbf{F}_i$ [1] is that part of the total field $\mathbf{F}_i$ at the ion i due to monopole sources in the crystal, and is given by

$$\mathbf{F}_i^{(1)}=\sum_{j\neq i}\frac{e_j(\mathbf{R}_j-\mathbf{R}_i)}{|\mathbf{R}_j-\mathbf{R}_i|^3}.$$

Further, $\mathbf{m}_i=\alpha_i\mathbf{F}_i$, where α_i is the polarizability of the ion i, and

$$\mathbf{F}_i=\mathbf{F}_i^{(1)}-\sum_{j\neq i}\left\{\frac{\mathbf{m}_j}{|\mathbf{R}_j-\mathbf{R}_i|^3}-\frac{3[(\mathbf{R}_j-\mathbf{R}_i)\cdot\mathbf{m}_j](\mathbf{R}_j-\mathbf{R}_i)}{|\mathbf{R}_j-\mathbf{R}_i|^5}\right\}.$$

The third group present the major problem, insofar as their form must be obtained from detailed consideration of perfect crystal properties. However, this difficulty may be separated from the mechanics of the defect calculation and will be discussed later. For the present, we will assume that the short range interactions are of the central, two body type and can be represented by an analytic form, $\phi_{ij}(R)$. Then

$$E_{SR}=\sum_{\substack{i,j\\ i\neq j}}\{\phi_{ij}(|\mathbf{R}_i-\mathbf{R}_j|)-\phi_{ij}(|\mathbf{r}_i-\mathbf{r}_j|)\}.$$

Because of the short-range nature of these interactions only those between close ions, normally nearest neighbors and next nearest neighbors, are included.

Now the total formation energy

$$E=E_c+E_p+E_{SR}$$

must be minimized with respect to the ionic relaxations $\mathbf{R}_i-\mathbf{r}_i$ to solve the problem. Apart from the short-range interactions mentioned above and the problem of obtaining values of polarizabilities α_i from perfect lattice data, the only difficulties remaining are computational ones.

The most satisfying way of doing the problem would be to construct a model crystal containing the defect plus such a large collection of ions that all of the important displacements and moments are explicitly included in the expression for the total energy. Unfortunately, for ionic crystals this has been possible only for neutral defects. For a charged defect E_c and E_p contain long-range terms, making the computational problem in such an entirely explicit calculation prohibitively complex. Instead, the model used consists of an inner region (I), in which the displacements and moments are treated explicitly, embedded in an outer region (II), treated in a quasi-continuum manner, with the properties of the crystal. The latter is treated in the harmonic approximation, the total energy of the crystal depending only quadratically on the ionic displacements and moments.

Until very recently only calculations in which region I was just the nearest neighbors of the defect had been carried out. However, these have been fairly successful for a number of simple defects, as shown by table 1.

TABLE 1. *Recent defect energy calculations*

Formation	Schottky pair.	NaCl-type alkali halide.	Boswarva and Lidiard [3]. Tosi and Doyama [4].
Formation	Schottky pair.	CsCl-type alkali halide.	Boswarva [5].
Formation	Frenkel pairs and Schottky trios.	CaF_2-type alkaline earth halides.	Franklin* [6].
Motion	Vacancy pairs.	NaCl-type alkali halide.	Tharmalingam and Lidiard [7].
Formation	Interstitials.	NaCl-type alkali halide.	Tharmalingam [8].
Formation	Substitutional impurity.	NaCl-type alkali halide.	Tosi and Doyama [4].
Motion	Vacancy.	NaCl-type alkali halide.	Tosi and Doyama [4].
Formation	Vacancies.	NaCl-type alkali halide.	Scholz [9].

*Region I contains nearest and next-nearest neighbors.

In general the results are slightly less than the experimental energies where these are known. But in this age of large, high-speed computers these small region I's are unduly restrictive. One of the authors has just completed a calculation of the Schottky pair in NaCl extending region I to include next-neighbors and finds this movement of the I-II boundary typically increases W_s by about 0.3 eV, from 1.8 eV for a region I containing only nearest neighbors to 2.1 eV for the more extended region I. This large change clearly indicates an unsatisfactory situation. In a detailed examination of the internal consistency of the model as applied to CaF_2, we have found that the electric fields calculated on the basis of the final configuration deviate significantly from those assumed in the quasi-continuum treatment of region II as far out as the sixth shell of neighbors to the defect. Calculations using a more extended region I, such as those now being done by Scholz at Harwell and Hatcher et al., at Brookhaven, are clearly needed.

The major issues to be resolved in carrying over this model to the oxides, then, involve the application of two-body short-range interaction potentials and ionic polarizabilities, and the determination of suitable parameters describing these from experimental data. It should be noted that once these issues have been resolved, computer programs developed for the alkali halides can be applied directly to the alkaline earth oxides, and those for CaF_2 to the oxides of the transuranic elements U and Th, of some of the rare earths such as Ce, and of the alkali metals.

3. Evaluation of Short-Range Interionic Potentials

3.1. Semiempirical Approach [2]

It can readily be shown that if the energy E of a pair of hydrogen atoms with parallel spins is calculated quantum mechanically as a function of their internuclear distance, r, using first-order perturbation theory and the antisymmetrized product of a pair of ls wave functions, the interaction is repulsive and the E dependence on r is almost exponential. A similar dependence has also been found for the interaction of a pair of He or Ne atoms. As a result it is often assumed that the short-range interaction between any pair of closed shell ions has the form

$$\phi = B \exp(-r/\rho)$$

where B, ρ are constants. Then, if only nearest neighbors are included, the lattice energy/ion pair is

$$W_L(r) = \frac{-\alpha_M e^2}{r} + MB \exp(-r/\rho)$$

where α_m is the Madelung constant and M is the number of nearest neighbors that each ion possesses. The parameters B and ρ can be simply evaluated, neglecting temperature effects, by the relations

$$\left(\frac{dW_L}{dV}\right)_{r=r_0} = 0 \text{ and } \left(V\frac{d^2W_L}{dV^2}\right)_{r=r_0} = \beta^{-1}$$

where V is the volume/ion pair, r_0 the equilibrium interionic distance and β the compressibility.

To include next-nearest neighbor short-range interactions one needs either: (a) to assume some relations among the six parameters B_{+-}, B_{++}, B_{--}, ρ_{+-}, ρ_{++}, ρ_{--}; (b) to employ more experimental information; or (c) to find a reasonable combination of both. The traditional Born-Mayer approach, so successful in alkali halides, is of the first kind. It is assumed that B_{ij} is given by $b\beta_{ij} \exp[(r_i + r_j)/\rho]$, where the ionic radii r_i and r_j are chosen to give as close a fit as possible between $(r_+ + r_-)$ and the interionic separations throughout the family. The Pauling coefficients β_{ij} are given by

$$\beta_{ij} = 1 + Z_i/n_i + Z_j/n_j$$

where Z_i, Z_j are the valences, and n_i, n_j the number of electrons in the outer shell, of the two ions. Under these assumptions, the short-range part of the perfect-lattice energy can be written as

$$W_{SR} = M\beta_{+-}b \exp[(r_+ + r_-)/\rho] + \tfrac{1}{2} M'b[\beta_{++} \exp(2r_+/\rho) + \beta_{--} \exp(2r_-/\rho)] \exp(-r'/\rho)$$

where M' and r' are the number of and distance to the next-nearest neighbors to a given ion, so that it is still only necessary to evaluate the two parameters, b and ρ. It can be appreciated that, while this approach has been fruitful for the alkali halides, the assumptions involved may not carry over to other substances.

In particular, even though the basic framework may be applicable to other classes of substances, there is no guarantee that the same parameters, including ionic radii and polarizability, need describe one ion in two different families of substances with different structures. Thus when moving to a new substance, for which the same de-

[2] See M. P. Tosi in Solid State Physics, 16, p. 1, Ed., F. P. Seitz and D. Turnbull (Academic Press, N.Y., 1964).

tailed family relationships either don't exist or have not been worked out, one has little alternative to increasing the amount of experimental data and decreasing the number of assumptions. This is the approach taken by one of us in work on CaF_2. Still assuming constant hardness parameter ρ, the four parameters ρ, $A+-$, $A++$, $A--$ were fitted using the quantities

$$r_o,\ \tfrac{1}{2}(C_{12}+C_{44}),\ C_{11},\ \bar{M}\omega_o^2\left(\frac{\epsilon_o+2}{\epsilon_\infty+2}\right)$$

where C_{12}, C_{44}, C_{11} are the elastic constants, $\bar{M}$ the reduced mass of an ion pair, ϵ_o and ϵ_∞ the static and high frequency dielectric constants, and ω_0 the circular frequency of the transverse optic mode. This dispenses with the use of the additivity rule for ionic radii and the Pauling relations.

Apart from this CaF_2 work all the workers quoted in the table above have used the Born-Mayer derivation with next nearest neighbors or some elaboration of it. Frequently, however, the simple exponential dependence has given too weak an interaction dependence with respect to the change in interionic distance and it has been necessary to include other terms such as ones to represent the Van der Waals interaction. In this case

$$W_{SR}^{ij}=B_{ij}\exp(-r_{ij}/\rho)-c_{ij}r_{ij}^{-6}-d_{ij}r_{ij}^{-8}$$

where the Van der Waals coefficients c_{ij}, d_{ij} are derived from refractive index data.

3.2. Quantum-Mechanical Approach

In 1948 Lowdin [11] published the results of a quantum mechanical treatment of the cohesive energy, interionic distance and elastic constants of a number of alkali halides. He considered a system of closed shell ions containing the total number of electrons N, for which the Hamiltonian operator, omitting relativistic effects, is

$$H_{op}=\frac{e^2}{2}\sum_{g,g'}\frac{Z_gZ_{g'}}{r_{gg'}}+\sum_{i=1}^{N}\left(\frac{p_i^2}{2m}-e^2\sum_g\frac{Z_g}{r_{ig}}\right)+\frac{e^2}{2}\sum_{i,k=1}^{N}\frac{1}{r_{ik}}$$

where Z_g is the atomic number of nucleus g, $r_{gg'}$ the distance between the nuclei g and g', r_{ig} the distance between electron i and nucleus g, r_{ik} the distance between electrons i and k, and p_i the momentum of electron i. Neglecting the mutual deformation of the ions, he used Hartree-Fock free-ion wave functions. Only short-range interactions between nearest-neighbors ions were included. Even within this framework his task presented sizable numerical problems which necessitated several mathematical approximations. However he found good agreement with experimental values of cohesive energy and lattice parameters for salts with cations and anions of about the same size. He also found that the three-body interaction arising from part of the last term of H_{op} qualitatively accounted for the observed difference in elastic constants C_{12} and C_{44}, which for a model with only two-body effects should be equal. Even more encouraging to workers using the Born-Mayer model, he found that the short-range interaction varied exponentially with interionic distance.

Unfortunately, current work by a group of Lowdin's colleagues at Uppsala (about to be published in Arkiv Fysik **34**, 199 (1967)), in which the required two and three electron overlap integrals are found exactly and next-nearest neighbor interactions included, no longer supports the purely exponential dependence of the short-range interactions. Such results strongly reopen the question of how much the success of the Born-Mayer model has been fortuitous and certainly indicate that the first step in the study of a new material such as an oxide should be at least a limited exploration of the quantum mechanical aspects.

4. Applicability of the Born Model to Oxides

The use of any ionic model in defect calculations rests on the assumption that ionic properties such as polarizability or short range interaction parameters, which in part are expressible as ionic radii, can be assigned to individual ions and remain unchanged as the ion is displaced from its lattice site. Very similar to this criterion is the "additivity" rule, in which unvarying ionic properties are assigned to ions within a family of substances. It is traditional to use the additivity rule to derive the properties of alkali and halogen ions from alkali halide data, and then on the assumption that these ions retain these values, to use the rule to derive properties of other ions from data on their compounds with the alkali or halogen ions.

When this is done to produce parameters for the oxygen ion, it is found that they are not constant but vary markedly from compound to compound. This lack of constancy is usually interpreted to mean failure of the oxygen ion generally to follow "additivity" rules. It seems worthwhile, however, to explore an alternative possibility. The alkali and halogen ions, while retaining essentially constant ionic properties within the single family of the rock salt-type alkali halides, may have different prop-

erties from one family of compounds to another. A fairer test of the applicability of the additivity rules to oxides would be to do what was done with the alkali halides—to test them while remaining within a given family of compounds, all with the same structure. Fortunately, enough of the basic data now is available for the alkaline earth chalcogenides to perform such a test.

4.1. Ionic Polarizabilities

Two semi-empirical approaches to the evaluation of electronic polarizabilities in ionic crystals are well established. The first, pioneered by Tessman, Kahn, and Shockley (TKS) [12], assumes (i) that within a family of salts the electronic polarizabilities of each substance is the sum of the electronic polarizabilities of the individual ions and that each ion polarizability is constant within the family. Under the further assumption (ii) that the electrostatic interactions between ions are purely of the dipole-dipole type, the effective field acting on an ion is $E_{\text{eff}}=E+LP$ where E is the externally applied field, P the electronic polarization and the Lorentz factor L is given a value of $4\pi/3$ for cubic crystals with at least tetrahedral site symmetry.

The polarizability per ion pair α_m is then related to the refractive index, n, of the salt through the Clausius-Mossotti relation

$$\alpha_m=\frac{3V_m}{4\pi}\frac{n^2-1}{n^2+2}=\alpha_i+\alpha_j$$

where V_m is the volume occupied by an ion pair. The polarizabilities α_i, are chosen to attain a best fit to α_m values throughout the family and the achievement of such a fit is taken as a measure of the validity of the assumptions. This fit is found by minimizing the standard relative deviation

$$F=\left\{\frac{1}{N}\sum_{m=1}^{N}\left(\frac{\alpha_m-\alpha_i-\alpha_j}{\alpha_m}\right)^2\right\}^{1/2}$$

with respect to the variables α_i, α_j when applied to the family of alkaline earth chalcogenides (13 members included). This analysis produces the results in table 2.

TABLE 2. *Electronic polarizabilities in (angstroms)* [a]

Mg^{2+}	0.094 (Fixed)	O^{2-}	1.657
Ca^{2+}	1.157	S^{2-}	4.497
Sr^{2+}	1.795	Se^{2-}	5.686
Ba^{2+}	3.188	Te^{2-}	7.317

[a] Standard relative deviation, $F=2.53$ percent.

It should be noted that the minimum value of F defines the ionic polarizabilities only to within an additive constant. Therefore one polarizability must be fixed by other considerations. In this work the Mg^{2+} polarizability is taken as 0.094 Å^3, the value found for the gaseous ion by Pauling [13]. However, this particular ion has a value so much smaller than the other seven ions in the family that even a 100 percent error in its value would have little effect on the other ions. The minimum value of F is lower than that obtained with the alkali halide polarizabilities, indicating excellent adherence to the additivity rule by the alkaline earth chalcogenides.

These figures have been obtained using the normal Lorentz factor of $L=4\pi/3$, which is found by considering the ions as independent dipoles. If, on the other hand, the charge clouds of neighboring ions overlapped substantially a smaller value of L would be appropriate. A plot of different L values against the minimum of F for each L itself shows a sharp minimum at $4\pi/3$ thus giving further evidence for the appropriateness of the point ion model.

The second approach to finding ionic polarizabilities starts from the relation between the ion polarizability and the optical absorption due to that ion

$$\alpha=\frac{C}{N}\int_0^\infty\frac{\mu(\Delta E)}{(\Delta E)^2}\,d(\Delta E)$$

where $\mu(\Delta E)$ is the absorption coefficient per unit energy increment ΔE; $\Delta E=E_{n'}-E_n$, the energy difference between the two states involved in the absorption process; N is the number of ions per unit volume; and C is a material-independent constant. As the absorption due to the cation and the anion in an ionic solid are in widely separated regions of the spectrum this approach should give polarizabilities directly without the assumptions needed in the first approach. Unfortunately, the absorption spectra required lie in the far ultraviolet and are not available for most materials (including the oxides), although Hajj [14] has successfully used the data of Eby, Teegarden and Dutton [15] to find halide polarizabilities in the alkali halides.

4.2. Van der Waals Coefficients

The equation above for α can be used to obtain van der Waals coefficients. It is assumed that the bulk of the absorption due to a particular ion occurs near some characteristic energy $\bar{E}$ so that the equation reduces to

$$\alpha_i=\frac{e^2h^2n}{4\pi^2m\bar{E}}$$

where n is the number of electrons in the ion, e the electronic change, m the electron mass, and h is Planck's constants. With characteristic energies gotten from the polarizabilities previously determined the following relations (Mayer [16]) can be employed to find the dipole-dipole and dipole-quadrapole coefficients of the van der Waals interaction between ions i and j

$$c_{ij}=\frac{3E_iE_j\alpha_i\alpha_j}{2(\bar{E}_i+\bar{E}_j)}$$

$$d_{ij}=\frac{27\alpha_i\alpha_j\bar{E}_i\bar{E}_j}{8e^2(\bar{E}_i+\bar{E}_j)}\left[\frac{\alpha_i\bar{E}_i}{n_i}+\frac{\alpha_i\bar{E}_j}{n_j}\right].$$

Table 3 shows the results obtained.

The only other published values for these oxides, which are about a factor of 4 smaller, are those published by Huggins and Sakamoto [17] who used a method of extrapolating from the constants for isoelectronic ions in alkali halides.

TABLE 3. *Van der Waals coefficients*

	$C_{+-}(A^6)$	$C_{--}(A^6)$	$C_{++}(A^6)$	$d_{+-}(A^8)$	$d_{--}(A^8)$	$d_{++}(A^8)$
MgO	4.86	53.0	0.72	4.01	70.6	0.23
CaO	45.6		41.5	49.3		34.4
SrO	74.2		113	76.5		82.9
BaO	136		329	136		261

4.3. Ionic Radii

Fumi and Tosi [10] (FT) (1964) have shown that within the framework of the Born model of ionic solids it is possible to determine completely the radii of ions within a family of salts using only solid state experimental data. This is in contrast to all earlier evaluations of ionic radii (e.g., Goldschmidt [1]) which, although similarly using the concept of approximate additivity of interionic distances, fixed one ion radius either arbitrarily or by appeal to free ion properties. Further, for the alkali halides FT found radii for the cations of about 0.2 Å larger than the traditional values with their anion values correspondingly about 0.2 Å smaller. Work already cited by Boswarva and Lidiard [3], and Tosi and Doyama [4] found that satisfactory values of characteristic energies of simple point defects in the alkali halides could only be obtained using FT radii. Therefore it is probably essential to derive ionic radii in the alkaline earth chalcogenides using the FT approach for the study of the applicability of the Born model to defect calculations in this family.

The table 4 gives the results obtained along with Goldschmidt's values for these ions. The relative standard deviation for the ionic separation calculated from these radii compared to observed values in this family is 6.5 percent compared with 4.4 percent for FT's results for the alkali halides. Bearing in mind (i) the greater uncertainty in experimental data used, especially the compressibilities, and (ii) the greater reliance placed on the evaluation of βij through the Pauling relation for doubly charged ions, it appears that the "additivity" rule in the interionic distance is well obeyed for this family, another indication of distinct ions in the substances. The good agreement with Goldschmidt values should be noted so that FT's conclusion for the alkali halides that the older values of the cations are too small by about 0.2 Å and the anion values similarly too large is not mirrored in the alkaline earth chalcogenides.

TABLE 4. *Ionic radii in the alkaline earth chalcogenides, angstroms*

	Ours	Goldschmidt
Mg^{2+}	0.73	0.78
Ca^{2+}	1.08	1.06
Sr^{2+}	1.21	1.27
Ba^{2+}	1.43	1.43
O^{2-}	1.40	1.32
S^{2-}	1.75	1.74
Se^{2-}	1.87	1.91
Te^{2-}	2.02	2.11

5. Defect Formation Energy Calculations

5.1. Alkaline Earth Oxides

Yamashita and Kurosawa [19] performed an early calculation of vacancy formation energies in MgO, CaO, and SrO. They used the *TKS* values for the ionic polarizabilities, and evaluated the short-range interaction potentials by fitting to cohesive energy, interionic separation, compressibility, and dielectric data. It is interesting to note that they found the oxygen-oxygen short range interactions to be attractive, rather than repulsive, thus ruling out any use of the traditional Born-Mayer treatment involving ionic radii. Furthermore, they found it necessary to assume that the polarizability of the oxygen ions immediately surrounding the cation vacancy was a half or less the normal value in order to give Schottky pair formation energies of reasonable magnitude.

We have attempted to use the computer programs, with region I containing the nearest neighbors to the defect, worked out for the alkali halides to calculate vacancy formation energies in the alkaline earth oxides. The purpose of these very preliminary calculations is to explore the effect of various ways of evaluating the short-range interactions. Four methods of obtaining these interactions were studied, all assuming exponential dependence upon the interionic distances. The resulting Schottky pair formation energies are shown in the table 5, along with results for NaCl using the same techniques.

TABLE 5. *Schottky pair formation energies, eV*

	Only 1st n.n.	With 2d n.n. via ionic radii	C_{11}, C_{12} and r_0	C_{11}, C_{12}, r_0 and $\bar{M}\omega_0^2 \frac{\epsilon_0+2}{\epsilon+2}$
NaCl	1.81	1.79	1.84	1.84
MgO	2.1–2.9	Fails	3.97	Fails
CaO	2.5	0.99	.....	.....
SrO	4.5	3.58	.....	.....
BaO	0.97	Fails	.....	.....

Column 2 contains the results when only nearest neighbor short-range interactions are included, the only experimental data needed for evaluating the parameters being the compressibility β and the interionic distance r_0. The value for BaO appears to be wholly unrealistic and that SrO unreasonably high compared to the values for MgO and CaO.

For the results in column 3, short-range oxygen-oxygen interactions were included by using the ionic radii and the Pauling coefficients in the Born-Mayer formulation. Again only β and r_0 were needed to evaluate the short-range interactions. Failure implies a negative formation energy for the Schottky pair, the same anamolous result that led Yamashita and Kurosawa to propose a reduced polarizability for the oxygen ions immediately neighboring the cation vacancy.

In column 4 are the results obtained when the ionic radii were abandoned and the short-range interaction parameters were determined by fitting the two elastic constants C_{11} and C_{12}, and r_0. An exponential form was assumed for the short-range potentials for the cation-anion and anion-anion interactions, with the same hardness parameter ρ for each, but different values of the intensity factor B_{ij}. The cation-cation interactions were neglected. Only for MgO are the necessary elastic constant data available. Here the oxygen-oxygen short-range interaction was found to be attractive.

Under these circumstances, there is no justification for assigning the same values of ρ to the anion-anion as to the cation-anion interaction. To remove this condition, a fourth experimental equation, that first deduced by Szigeti [20] involving the dielectric constants and the frequency ω_0 of the transverse optic mode, was invoked. $\bar{M}$ is the reduced mass of the ions and ϵ_0 and ϵ are the static and high frequency dielectric constants. The result for MgO was again failure of the model to give a positive Schottky formation energy, again in agreement with the results of Yamashita and Kurosawa.

It is interesting to note that while the results for MgO are fluctuating wildly with the method of evaluating the short-range interactions, the results for NaCl are very little influenced. This may be related to the apparent attractive nature found for the oxygen-oxygen interaction. Peckham [1] has also found an attractive interaction in his shell model fit to both the static and dynamic properties of MgO. Certainly the assumption of an exponential functional form for these oxygen interactions must be highly suspect if they are attractive.

5.2. Uranium Dioxide

Dolling, Cowley, and Woods [2] have obtained neutron scattering data for UO_2 and have derived therefrom the phonon spectra. They have fitted these data with several sets of shell model parameters (see the preceding paper by J. Slater for a discussion of the shell model). J. D. Axe [21] has pointed out that some confusion exists as to the units in which these parameters are presented in the paper of Dolling et al., but that if the shell-shell force constants as given in their table II be divided by 2 and their ionic charges by $\sqrt{2}$, then the agreement with experiment noted in their paper can be reproduced. With these corrections, it is found that their model IV appears to fit the cohesive energy as well, and to provide a reasonable basis from which to attempt some defect energy calculations.

Here again, the oxygen-oxygen parameters indicate an attractive interionic short-range potential. In the case of UO_2 an important defect is the oxygen interstitial. There is no hope of calculating the formation energy of the oxygen interstitial with this attractive oxygen-oxygen potential because in the interstitial the oxygen ion is enclosed in a cubic cage of lattice oxygen ions, and nothing in the model would prevent the interstitial oxygen ion from collapsing into one of the lattice ions. Even for an oxygen vacancy, preliminary attempts to calculate formation energies using a program developed for CaF_2 have failed because of inward collapse of next-nearest neighbor oxygen ions.

6. Summary

Defect formation energy calculations for ionic crystals, as currently being done, rest upon the applicability of (1) two-body short-range interionic potentials, (2) additivity rules that allow assignment (independent of displacement) of parameters, such as ionic charge, polarizability, and those determining the short-range interactions, to the individual ions, and (3) a simple functional form, such as exponential, to express the dependence of the short-range interionic potential on the distance between two ions. An examination of the properties of the alkaline earth chalcogenides as a family shows that additivity rules for ionic radii and polarizabilities apply as well to them as to the alkali halides. Furthermore, shell-model fits to both the static and dynamic properties of MgO, UO_2, and ThO_2 indicate that a model based upon two-body potentials can be used to describe these simple oxides.

Attempts to calculate vacancy formation energies in the alkaline earth oxides have, however, been notably unsuccessful. Since the shell-model parameters indicate attractive oxygen-oxygen short-range interactions, it appears likely that the problem lies with the choice of the functional dependence of these interactions upon the interionic separation. While the exponential form has theoretical backing for closed-shell ions and appears to be valid for the alkali and alkaline-earth halides, it probably is not valid for the oxygen-oxygen interactions in the oxides. Thus the key problem in the oxides is to obtain and evaluate expressions for these interactions.

7. References

[1] G. Peckham, Proc. Phys. Soc. **90,** 657 (1967).
[2] G. Dolling, R. A. Cowley and A. D. B. Woods, Can. J. Phys. **43,** 1397 (1965) J. D. Axe, Bull. Am. Phys. Soc. **11,** 244 (1966).
[3] I. M. Boswarva and A. B. Lidiard, Phil. Mag. **16,** 805 (1967).
[4] M. P. Tosi and M. Doyama, Phys. Rev. **151,** 642 (1966).
[5] I. M. Boswarva, Phil. Mag. **16,** 827 (1967).
[6] A. D. Franklin, Submitted to J. Phys. Chem. Sol.
[7] K. Tharmalingam and A. B. Lidiard, Phil. Mag. **6,** 1157 (1961).
[8] K. Tharmalingam, J. Phys. Chem. Sol. **24,** 1380 (1963); Ibid, **25,** 255 (1964).
[9] A. Scholz, Phys. Stat. Sol. **7,** 973 (1964).
[10] F. G. Fumi and M. P. Tosi, J. Phys. Chem. Sol. **25,** 31 (1964); M. P. Tosi and F. G. Fumi, Ibid **25,** 45 (1964).
[11] P. Lowdin, A Theoretical Investigation into Some Properties of Ionic Crystals (Uppsala, 1948).
[12] J. R. Tessman, A. H. Kahn and W. Shockley, Phys. Rev. **92,** 890 (1953).
[13] L. Pauling, Proc. Roy. Soc. **A114,** 181 (1927).
[14] F. Hajj, J. Chem. Phys. **44,** 4618 (1966).
[15] J. E. Eby, K. J. Teegarden and D. B. Dutton, Phys. Rev. **116,** 1099 (1959).
[16] J. E. Mayer, J. Chem. Phys. **1,** 270 (1933).
[17] M. L. Huggins and Y. Sakamoto, J. Phys. Soc. Jap. **12,** 241 (1957).
[18] V. M. Goldschmidt, Skrifter det Norske Videnskaps Akademie No. 2 (1926), No. 8 (1927).
[19] J. Yamashita and T. Kurosawa, J. Phys. Soc. Jap. **9,** 944 (1954).
[20] B. Szigeti, Proc. Roy. Soc. **A, 204,** 52 (1950).

Lattice Dynamics and Ionic Interactions

John Slater, J. J. Thomson Physical Laboratory,

Whiteknights Park, Reading, England

A very brief review is made of topics relating to the use of models of forces between atoms in insulating crystals. The topics include elastic constants, lattice dynamics, lattice energy, pair potentials and ionic radii.

Key Words: Elastic constants, ionic radii, lattice dynamics, lattice energy, pair potentials.

1. Introduction

The title of this review allows a great deal of scope, and no single topic will be dealt with in much detail. The question to be answered is roughly, "What sorts of models can be used for the forces between atoms in insulators?" The point of view will be that of a physicist who knows little about mass transport: the aim will be to reiterate things that are "well-known" to provide a background for subsequent papers. Work on this subject has progressed along a few rather distinct lines, some offering more detail than others. The headings will be—lattice vibrations and force constants; anharmonicity; elastic constants; defect applications; lattice energy; ionic radii, and miscellaneous topics.

2. Lattice Vibrations and Force Constants

The dynamics of crystal lattices is usually discussed [1] [1] in terms of the crystal potential energy expanded about the equilibrium positions of the ions in the ionic displacements $u_\alpha \begin{pmatrix} l \\ k \end{pmatrix}$. Small vibrations of the lattice are then controlled by the second derivatives

$$\left\{ \frac{\partial^2 v}{\partial u_\alpha \begin{pmatrix} l \\ k \end{pmatrix} \partial u_\beta \begin{pmatrix} l' \\ k' \end{pmatrix}} \right\}_0 .$$

If we ignore the higher terms we have the "harmonic" approximation—the forces are linear in the displacements—the "springs" are Hookean. The above derivative is the force on the ion $\begin{pmatrix} l \\ k \end{pmatrix}$ when the ion $\begin{pmatrix} l' \\ k' \end{pmatrix}$ is displaced a unit amount, all other ions being fixed. It is usually called an interatomic force constant and work in lattice dynamics aims to determine these from experimental observations on lattice waves.

The experimental data which have to be explained are several: thermal effects, for example conductivity, infrared absorption, Raman effect and especially x-ray diffuse scattering and neutron inelastic scattering. The last is the most important. It is convenient to deal with plane waves of propagation vector **k**. If there are n atoms per unit cell in the crystal there will be $3n$ kinds of wave with a given **k** and we want to know the frequencies ω associated with each of these. It is clear that figure 1, which shows the experimental dispersion curves for UO_2 determined by neutron diffraction [2], contains a great deal of implicit information about the crystal forces. The procedure used is to assume some model for the forces with suitable parameters and then either fit these by least squares to the experimental dispersion curves (as in fig. 1) or determine the parameters from macroscopic constants, and then see how the agreement with the neutron results looks.

The simplest model used is the "rigid-ion" model [3], with point-ion long-range Coulomb forces and arbitrary short-range forces, usually restricted to first or second neighbours. The comparison with experiment of a nearest neighbour rigid-ion treatment [4] of NaI is shown in figure 2. For a crystal like germanium, this would imply short-range forces only, and this approach was found to be incorrect: it emerged that the polarisation of the ions had to be introduced. This gave rise to the "deformation-dipole" and "shell" models, which are essentially equivalent [5]. In the

[1] Figures in brackets indicate the literature references at the end of this paper.

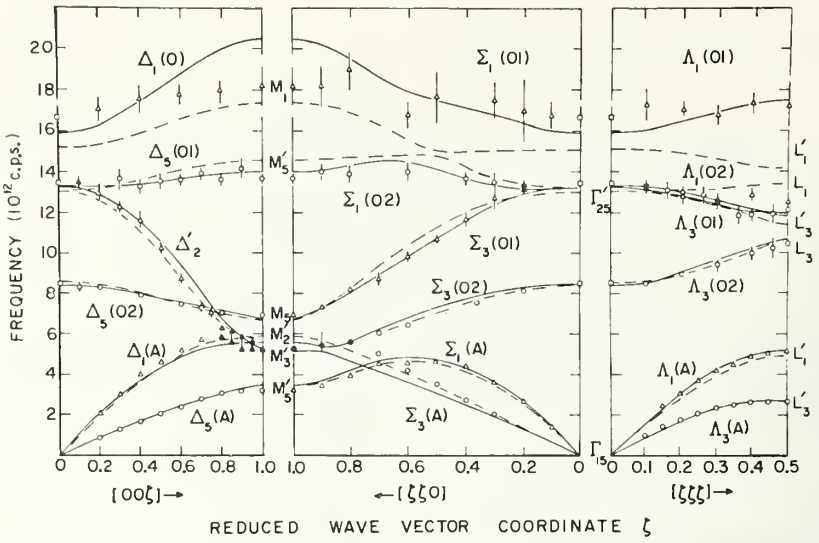

FIGURE 1. *Phonon dispersion in uranium dioxide measured by Dolling, Cowley and Woods* [2].
Reproduced from Can. J. Phys. **43**, 1402 (1965).

shell model one supposes that the outer electrons of an ion can be represented as a rigid shell attached to the nucleus and core by an isotrópic spring. The polarisation of an ion is then represented by the relative displacement of shell and core. Figure 2 shows the improvement this gives for NaI.

Both models, however, give a bad fit for the longitudinal optic branch (highest branch) at the (111) zone boundary. This point corresponds to a wave in which the anions are essentially stationary and alternate planes of cations move in opposite directions [6]. The rigidity of the anion shell seems to be raising the frequency. The so-called "breathing-shell" model introduced by Schröder and coworkers [7, 8] allows a compressible shell and appears to give significant improvement over the simple shell model for some substances (for example, NaI) without introducing more parameters. All of these models are classical, although they can be given a quantum-mechanical basis.

For MgO, Peckham [9] used a shell model fitted to the elastic and dielectric constants: the agreement is shown in figure 3. The fit here was not improved significantly by the introduction of a breathing shell model. The number of oxides which have been investigated is small: MgO, UO_2, ThO_2, a few branches in quartz [10] and some work on crystals like MnO and NiO, where the main interest is in magnetic properties. It is expected that CaO will be treated in the near future. There are three reasons for this lack of information: the experiments are slow and expensive, it is difficult to obtain good crystals of sufficient size, and difficult to observe high-frequency optic branches where phonon populations are low at room temperature.

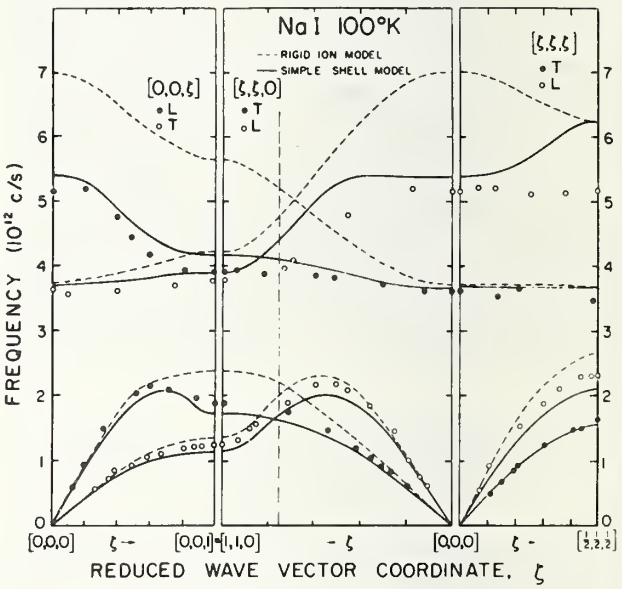

FIGURE 2. *Phonon dispersion in sodium iodide* [4].
Reproduced from Phonons p. 66 Ed. R. W. H. Stevenson, Oliver and Boyd, Edinburgh (1966).

3. Anharmonic Contributions to the Crystal Forces

In the perfect crystal lattice, anharmonic terms like the third derivatives

$$\left\{\frac{\partial^3 v}{\partial u_\alpha\begin{pmatrix}l\\k\end{pmatrix}\partial u_\beta\begin{pmatrix}l'\\k'\end{pmatrix}\partial u_\gamma\begin{pmatrix}l''\\k''\end{pmatrix}}\right\}_0$$

give rise to macroscopic effects such as thermal expansion and the temperature dependence of elastic and dielectric constants, while on the quasi-particle model, anharmonicity accounts for the short life times of phonons, observed in thermal conductivity and neutron scattering. The number of short range anharmonic constants allowed by symmetry is large and, in planning calculations, simplifications have to be made, usually an assumption of axially symmetric nearest neighbour interactions or a Born-Mayer potential. The Coulomb part of the anharmonicity is ignored. Nevertheless these fairly crude models have been quite successful in explaining, for example, thermal expansion [11] and the behaviour of neutron groups with change in temperature [12, 13]. The number of calculations which have been carried out is relatively small.

4. Elastic Constants

The extent of the deviation of a crystal from the radial potential type of behaviour is traditionally estimated from the agreement of the elastic constants with the Cauchy relations. For crystals with complex structures, like SiO_2, one can hardly expect these to be satisfied, and indeed they are not. For an inert gas configuration like MgO, one might hope for better, but the values given in table 1 are not encouraging. On the other hand it is not clear that the deviation from the Cauchy relations implies any form of covalent bonding: for example, it appears that Schröder's "breathing-shell" model, mentioned in section 2, gives a deviation even if only central forces are allowed.

TABLE 1. *Elastic constants (dyn. cm$^{-2}\times 10^{11}$) of some crystals in the sodium chloride structure*
Showing the deviation from the Cauchy relations.

	C_{12}	C_{44}	C_{44}/C_{12}
NaCl	1.23	1.26	1.03
LiF	4.04	5.54	1.37
MgO	8.7	14.8	1.70

5. Defect Applications

It is clear from figure 3 and others that the agreement between theory and experiment for lattice vibrations can be very close. It would be a pity then, even in the absence of a complete physical justification for the forces involved, not to use this information for something, and a very convenient by-product for some defect applications is Green's-function information. Figure 4 shows what is essentially the mechanical impedance of a magnesium ion in an MgO crystal. What is convenient is that one can convert this in a trivial manner to the case where an atom of different mass is substituted, or the force constants around the defect changed. This sort of function is particularly convenient for comparison with impurity infrared absorption and the vibrational side-band structure on optical absorption lines of impurity ions. The rich detail of these together with the reliability of the lattice dynamical calculations permits information to be obtained about the defect environment. For example, it can be established from the sideband structure that V^{2+} and Ni^{2+} substituted in the MgO

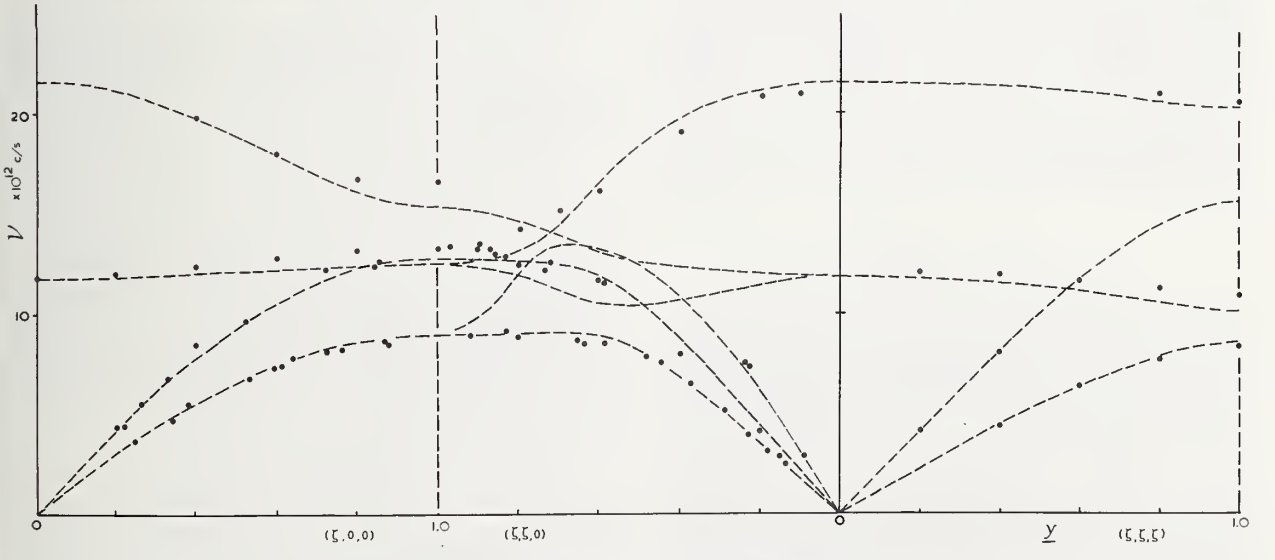

FIGURE 3. *Phonon dispersion in magnesia.*
A composite of points measured by Peckham [9] and Buckland and Saunderson [29]. The curve is the theoretical shell-model prediction of Peckham.

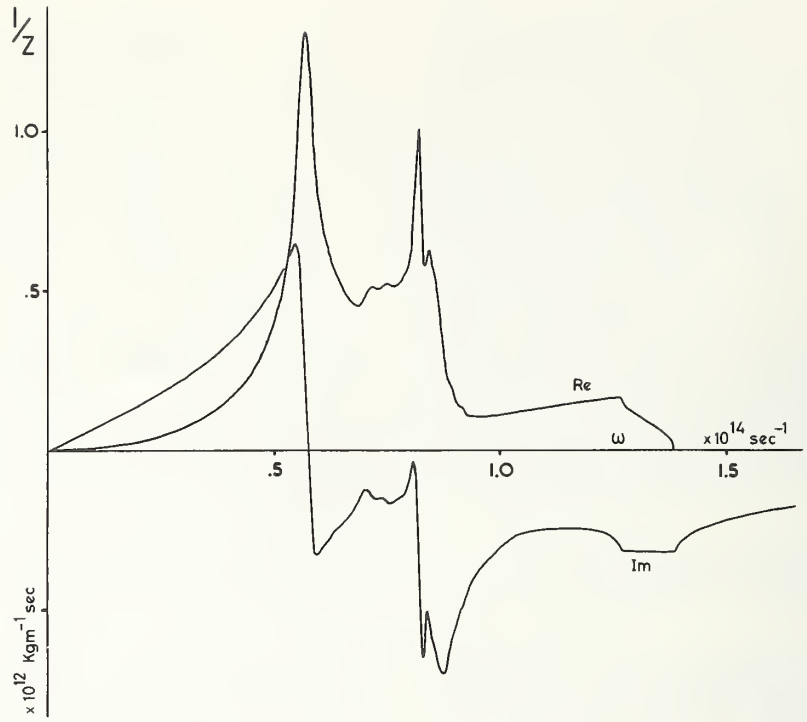

FIGURE 4. *The mechanical admittance for radial* (A_{1g}) *motion of the anions surrounding a magnesium ion in a magnesium oxide crystal.*

lattice have greater force constants to neighbours than the Mg^{2+} ion itself [14].

6. Interatomic Potentials and Lattice Energy

Various potential functions have been used to describe the repulsive forces which balance the Coulombic attraction of the ions in an ionic crystal. These repulsive forces arise essentially from the Pauli principle—from the increase in electron kinetic energy as the electron density in the crystal increases.

a. For rare gas solids the Lennard-Jones potential is usually used.

$$V(r) = -\frac{c}{r^6} + \frac{b}{r^n} \qquad (1)$$

the first term being the van der Waals attractive potential; n is usually about 12. Exponential and polynomial two-part potentials have also been used, and it is hard to find solid arguments for preferring one to another [15].

One reason for mentioning work on the inert gases is that it is probably here that the great progress made recently in formal quantum mechanical theory of atoms will first show results for solids. Several calculations have been made using variational methods of the interaction of inert gas atoms; for example D. Y. Kim [16] has calculated the potential for two interacting He ions, obtaining the following analytic form (r in Å, V in eV):

$$V(r) = 387e^{-4.42r} + 366e^{-7.15r} - 0.58/r^{5.9}. \qquad (2)$$

The second exponential term, which becomes important for $r \leqslant 3$ Å, is worthy of note, even if helium is a rather special case.

b. For ionic crystals in the sodium chloride structure the time-honoured form is the Born-Mayer potential [1]

$$V(r) = -\frac{A}{r} + \mathrm{Be}^{-r/\rho}. \qquad (3)$$

The exponential dependence can be justified by consideration of the falling off with distance of the electronic charge density.

c. The most generalised potential in common use is obtained by adding van der Waals terms to the Born-Mayer potential

$$V(r) = \frac{A}{r} + \mathrm{Be}^{-r/\rho} - C/r^6 - D/r^8. \qquad (4)$$

This potential has been used recently by Ladd and Lee [17] for the discussion of lattice energies in a wide range of ionic crystals, including oxides.

d. There are miscellaneous other potentials used of logarithmic and polynomial form in $1/r$ for which it is hard to find physical justification. One can also regard the Born-Mayer-Verwey [30] potential as rather unphysical: it is essentially a Born-Mayer potential in which the forces are strengthened inside the equilibrium distance. Perhaps another exponential term as in eq (2) would be preferable.

It is worth emphasising that these potentials apply to simple structures in the electrostatic model. In more complex structures direct polarisation can play a very important part. For example in the spinel structure oxygen ion polarisation is estimated to give 25 percent of the cohesive energy [18]. Also the use of the electrostatic model implies that one can associate a particular electron with a particular atom and treat the forces then as arising from the interaction of charge distributions on these distinct ions. If one is dealing with a crystal like MgO which may approximate a closed-shell configuration then one can perhaps hope that this will work, and the success of the shell model for the lattice dynamics of MgO offers some evidence that it does.

When one considers oxides which are more interesting in practice, the oxides of transition metals, for example, the electrostatic model can tell only part of the story. Molecular orbital theory has had considerably more success in explaining the spectra of transition metal ions in crystals than the older, essentially electrostatic crystal field theory, and one must expect that work on ion motion will have to rely upon this sort of theory, at least in a qualitative way, if it is to give results. Quite extensive work of this kind has been done on the wide range of materials of the spinel structure [18, 19].

7. Ionic Radii

So far the impression has perhaps been given that the situation in interionic forces is unchanged since thirty years ago, and to redress the balance, something should be said about recent moves away from the older forms. A. R. Ruffa [20] has worked on the polarisabilities and susceptibilities of ions in crystals. On the basis of quantum mechanical arguments of an approximative kind, he has shown that the additivity rule for the polarisabilities of the ions in the alkali halides is something of an accident, and suggests that the cation polarisability may be considerably larger than the free ion value. He has used related arguments for rutile polarisability and in explaining the magnetic susceptibilities of the alkali halides.

It is now some time since Tosi and Fumi [21] published their ionic radii, but it is perhaps worth reiterating their conclusions, because they seem very important. The use of ionic radii for alkali halides is justified because of the success of the additivity in prediction of interatomic spacings in the crystals. However the additivity cannot alone provide a unique set of ionic radii. One more condition is necessary. For the Pauling and Goldschmidt radii this is obtained in effect from the polarisability of the ions in solution. It can be argued that this gives a free ion radius rather than a crystal ion radius, and Tosi and Fumi have calculated ionic radii from crystal data alone using the assumption of an interatomic potential of the Born-Mayer type. They have obtained in this manner radii which differ by amounts between 0.15 and 0.3 Å from the traditional values, the cations being larger and the anions smaller than in the traditional case. Table 2 shows an example. The radii agree well with those obtained from x-ray measurements of electron density. The radius of a given ion varies somewhat from one crystal to another.

TABLE 2. *Comparison of ionic radii*

Ion	Traditional radius	Radius of Fumi and Tosi
Na^+	0.95–0.98 Å	1.21 Å
Cl^-	1.81 Å	1.65 Å

It has always been the philosophy, of course, to use ionic radii with some caution. Wyckoff writes in the introduction to his tables of crystal structures: "We nowadays talk about ionic, covalent and other bond 'sizes' with an assurance that may exceed our knowledge of the physical realities of the situation." One supposes that the radii traditionally used are to be questioned also for less simple ions. J. C. Slater has recently reviewed the subject of radii obtained by these older methods [25].

8. Miscellaneous Topics

A great deal of work of a quantum mechanical kind has been done falling roughly within the scope of this talk, which the writer has neither the space nor the authority to deal with. Four of these are mentioned here.

a. Quantum mechanical calculations have been carried out by several Scandinavian workers on non-stoichiometric oxides like zirconia and praseodymia [22, 23].

b. A large amount of detailed work has been done by physical chemists on molecules like MgO, SrO etc. Recently Tosi and Doyama [24] have applied a model borrowed from lattice dynamics to treat the alkali halide molecules and obtain good results. One supposes that some flow of information is possible in the other direction.

c. The fact that the free O^{--} ion does not exist has inspired calculations of form factors and electronic states of oxygen ions and the associated cations in crystals like MnO and MgO [27, 28].

d. The work of Benneman, Kleinman and Phillips should also be mentioned as offering the promise of a better understanding of binding in insulating crystals [26].

In summary, it seems that for a crystal of MgO (inert gas) type the Tosi and Fumi radii and Born-Mayer potential, with Van der Waals terms if these can be estimated, offer as reliable a model as is available, though this simple model may well turn out to be mistaken (see remarks by Boswarva and Franklin). For more complex structures, the situation is more uncertain, although all is not yet lost; polarisation energies and bonding energies can be estimated; Madelung energies can be computed trivially. Great progress is being made in the detailed relation of theory and experiment in the field of lattice dynamics and thermal properties for simple crystals. With regard to other perfect lattice properties that have been mentioned, work is being done on many fronts, and it is encouraging to note that much of the progress is comparatively recent. With the great strides that have been made recently both in computing techniques and in formal quantum mechanics there is reason to look forward to detailed fundamental treatments of the nature of forces in crystals.

9. References

[1] M. Born and K. Huang, Dynamical Theory of Crystal Lattices (Oxford University Press, 1954).
[2] G. Dolling, R. A. Cowley and A. D. B. Woods, Can. J. Phys. **42**, 1397 (1965).
[3] E. W. Kellerman, Phil. Trans. Roy. Soc. A **238**, 513 (1940).
[4] W. Cochran, Phonons Ed. R. W. H. Stevenson, Oliver and Boyd, Edinburgh (1966).
[5] R. A. Cowley, Proc. Roy. Soc. A **268**, 109 (1962).
[6] A. D. B. Woods, B. N. Brockhouse, R. A. Cowley and W. Cochran, Phys. Rev. **131**, 1038 (1963).
[7] U. Schröder, Solid State Commun. **4**, 347 (1966).
[8] V. Nüsslein and U. Schröder, Phys. Stat. Sol. **21**, 309 (1967).
[9] G. Peckham, Proc. Phys. Soc. **90**, 657 (1967).
[10] M. M. Elcombe, Proc. Phys. Soc. **91**, 947 (1967).
[11] R. A. Cowley, Proc. Phys. Soc. **88**, 473 (1966).
[12] R. A. Cowley, Phonons Ed. R. W. H. Stevenson, Oliver and Boyd, Edinburgh (1966).
[13] B. Dawson, A. C. Hurley and V. W. Maslen, Proc. Roy. Soc. A. **298**, 289 (1967).
[14] M. J. L. Sangster, Reading University (unpublished).
[15] G. L. Pollack, Revs. Mod. Phys. **36**, 765 (1964).
[16] D. Y. Kim, Revs. Mod. Phys. **35**, 443 (1963).
[17] M. F. C. Ladd and W. H. Lee, Progress in Solid State Chemistry, Ed. Reiss. **1** (1964) and **2** (Pergamon Press, Inc., New York, N.Y., 1965).
[18] G. Blasse, Phil. Res. Repts. Suppl. (1963–4).
[19] S. Iida and H. Miwa, J. Phys. Soc. Japan **21**, 2505 (1966).
[20] A. R. Ruffa, Phys. Rev. **159**, 742 (1967).
[21] F. G. Fumi and M. P. Tosi, J. Phys. Chem. Solids **25**, 31 (1964).
[22] B. Roos, Ark. Fys. **25**, 363 (1963).
[23] B. G. Hyde, D. J. M. Bevan and L. Eyring, Phil. Trans. Roy. Soc. **259**, 583 (1966).
[24] M. P. Tosi and M. Doyama, Phys. Rev. **160**, 716 (1967).
[25] J. C. Slater, J. Chem. Phys. **41**, 3199 (1964).
[26] J. C. Phillips, Phys. Rev. Letters **19**, 415 (1967).
[27] S. Nagai, J. Phys. Soc. Japan **22**, 457 (1967).
[28] P. M. Raccah and R. J. Arnott, Phys. Rev. **153**, 1028 (1967).
[29] R. J. Buckland and D. H. Saunderson, Harwell Research Report A.E.R.E.–R5467 (1967).
[30] R. Guccione, M. P. Tosi and M. Asdente, J. Phys. Chem. Solids **10**, 162 (1959).

On Electron-Lattice Interaction in the CaO *F* Center [1]

James C. Kemp and William M. Ziniker [2]

Department of Physics, University of Oregon, Eugene, Oregon 97403

The sharp vibronic structure in several absorption bands of point defects in alkaline earth oxides has gotten considerable study, because of the relationship to the phonon spectrum. Unhappily, none of the vibronic structure analyzed to date has been identified with any very simple point defect, such as the *F* center, nor with any center of established structure. Thus electron-phonon coupling coefficients to specific lattice modes could not be seriously estimated; nor could local modes be discussed.

Recently we identified the zero-phonon peak [3] (3555 Å) and associated band [4] (center 3350 Å) of the CaO *F* center, by the method of microwave-sensitive Faraday rotation. One has an opportunity with the simple electronic structure involved here to understand the optical, vibronic, and magneto-optic properties in detail. The spectral Faraday rotation, $\theta(E)$, for example, seems to have an obvious interpretation. The observed overall band rotation pattern is quite analogous to that in alkali halide *F* centers. On the other hand the $\theta(E)$ structure accompanying the zero-phonon peak is absorption derivative-like, i.e., dispersion-like, with (in particular) a positive lower-energy peak. The zero-phonon transition is evidently to an orbital singlet, indicating a large Jahn-Teller splitting of the excited *p* state, so that orbital magnetism is quenched. We invoke non-cubic modes, such as a local Γ_{3g} mode of the first cation shell. The associated $\theta(E)$ should then be simply $-\lambda/2\epsilon$ times the spectral dispersion angle of the zero-phonon peak, where λ is the spin-orbit constant and ϵ is a (mean) Jahn-Teller splitting. (This pertains to the paramagnetic θ seen at helium temperatures.) From moments of the overall *F*-band magneto-optic pattern we know $\lambda = -(8 \pm 1) \times 10^{-3}$ eV. The observed zero-phonon $\theta(E)$ curve is correctly fitted, where we use $\epsilon \cong 0.15$ eV—a reasonable value if strong noncubic relaxation is assumed. A picture using a noncubic configuration coordinate (added to interaction with other modes such as the familiar breathing mode) is thus consistent with the rotation patterns of both the broad band and the zero-phonon line. The negative λ needed incidentally strongly supports our identification of the *F*-center optical spectrum in CaO: Another species which we have suspected might have many properties similar to those of the *F* center is interstitial Ca^{1+}; but this would doubtless have positive λ in the *p* state.

Other structure on the CaO F band consists of peaks at 3531 Å and 3518 Å and some weaker peaks, including some possible barely resolved weak structure just to the high energy side of the zero phonon line. The interval 3555 to 3531 Å is about four times the CaO reststrahl energy of 0.045 eV. Actual comparison with the lattice spectrum cannot yet be reported.

We wish to speculate that a model in terms of bulk lattice modes may not be appropriate in alkaline earth oxide *F* centers. The degree of local distortion would seem to favor strong local modes, electron lattice coupling being then indirect, via a broadening of the local modes. The latter can be treated theoretically in this structure using point ion-lattice techniques and simple *F*-electron wave functions, and the frequencies and couplings predicted for at least two or three of the simplest modes. (The Γ_{1g} mode has already been dealt with in MgO, etc., in different contexts.)

[1] Research supported by the U.S. Air Force Office of Scientific Research.

[2] Present address: Ceramic Engineering Department, University of Washington, Seattle, Washington.

[3] W. M. Ziniker, Bull. Am. Phys. Soc., Ser. II, **12**, 896 (1967).

[4] J. C. Kemp, W. M. Ziniker, and J. A. Glaze, Proc. Brit. Cer. Soc. **9**, 109 (1967).

Electronic States of Defects in Irradiated Oxides

B. Henderson

Physics Dept., Keele University, Keele, England

This paper reviews some of the progress made during the last few years in understanding the electronic states of defects in irradiated oxides. The discussion refers particularly to the alkaline earth oxides. A short introduction indicating the scope of the work on oxide materials, is followed by a description of the main types of experiment proving useful in the simple cubic oxides. In particular the following topics are discussed: (i) the electron-phonon interaction in the MgO F-centre, (ii) the evidence for the F'-centres in the oxides, (iii) the annealing of radiation damage and the production of aggregate centres, (iv) the investigation of the structure of defects in oxides using uniaxial stress splitting of optical zero-phonon lines.

Some novel results of the e.p.r. spectrum of a triplet ($S=1$) state defect in neutron irradiated Al_2O_3 are also discussed: a new model is proposed for this defect.

Key Words: Annealing, defects, electron-phonon, electronic states, interaction, radiation damage.

1. Introduction

Irradiation of insulating solids may produce varied changes in their physical properties consequent upon the introduction of defects of atomic dimensions into the lattices. These defects, which trap electrons or holes, may be investigated by the techniques of optical absorption and/or electron spin resonance. Such techniques have been especially fruitful in the alkali halides, and in these compounds the electronic properties of many defects (F-centres, F-aggregate centres and V-centres) are well understood. Similar studies on oxide systems form a natural extension of this work. However, the additional trapping potential of the oxygen ion vacancy as well as the variety of crystal structures in which it might be found provide complexities which are not normally met with in the alkali halides. In addition, most oxides are relatively resistant to radiation damage by ionising radiation so that reactor irradiation is frequently necessary, with the result that defect sites are produced on both the anion and cation sublattices. Unfortunately, most commercially available oxides are relatively impure compared with the alkali halides, and consequently great care has to be taken to recognise effects due to impurity ions.

Unlike the alkali halides, oxide systems have been the object of few serious optical studies and the absorption spectrum of many defects is completely unknown. Thus for many defects the only source of identification is their paramagnetic resonance spectrum. Many such spectra in oxides have been attributed to electrons trapped at oxygen ion vacancies. The paramagnetic states of these defects will have their orbital momentum quenched and thus their g-values are close to the free electron value. In the alkaline earth oxides there is a small negative shift from the free electron g-value [1];[1] a somewhat larger shift is observed in barium titanate [2]. In alumina [3], calcium tungstate and lithium niobate [4], and in numerous vitrous oxides [5], significant positive g-shifts are observed. This subject will not be discussed further except to note that no satisfactory theory exists for the g-value of electrons trapped at oxygen ion vacancies. Instead the discussion will be centred on the recognition of oxygen ion vacancies, and vacancy aggregates in the alkaline earth oxides, and of a trapped hole centre in Al_2O_3.

2. Single Vacancies in the Alkaline Earth Oxides

2.1. The F-Band in MgO and CaO

The spectral position of the F-band in MgO (4.9 eV), CaO (3.65 eV) and SrO (3.0 eV) has now been determined with some certainty. The electron bound to the anion vacancy is in many ways analogous to a hydrogen atom, and the localised electronic states of the F-centre are conveniently described by a Is (A_1) ground state and a $2p$ (T_1) excited state. An electric dipole transition between these levels gives rise to a broad bell-shaped

[1] Figures in brackets indicate the literature references at the end of this paper.

absorption band, whose width and shape reflects the strength of the coupling between the electronic states of the centre and vibrational modes of the lattice. In the configurational coordinate model, which we use here, it is assumed that the coupling is to only one normal mode of the lattice. The model predicts that the half-width (H_o) at 0 °K is related to the vibrational frequency ν_g by

$$S=\left\{\frac{H_o}{2.36\ h\nu_g}\right\}^2 \tag{1}$$

where S is a vibrationless quantity representing the effective number of phonons excited in the transition. The breadth of the band $H(T)$ is then related to the absolute temperature (T) by

$$H(T)^2=H(O)^2\ \coth\frac{h\nu_g}{2kT}. \tag{2}$$

The peak position of the band also shifts with temperature. This shift is produced by the combined effects of the change in lattice constant with temperature and the change in force constants of the oscillators in the ground and excited states. The shift consequent upon the variation in lattice parameter may be estimated from the thermal expansion data and by assuming an Ivey-Mollwo Law to apply to the oxide F-bands as in the alkali halides. The change produced by the difference in force constants may be estimated by applying the method of moments to the band shape. Applying this to the first moment we see that the shift of the band centroid to lower frequencies as a function of temperature is

$$\Delta E=\tfrac{1}{2}fh\nu_g\ \coth\frac{h\nu_g}{2kT} \tag{3}$$

where f is the fractional change in force constants [6]. In terms of the ν_g and ν_e, which refer to the vibrational frequencies interacting with the lattice in the ground and excited states, respectively,

$$f=\frac{\nu_e^2-\nu_g^2}{\nu_g^2}. \tag{4}$$

If we have sufficient experimental data to determine S, ν_g and f, we can construct the configurational coordinate diagram for the ground and excited states of the F-centre by methods of Klick et al. [7].

The experimental data, $H(T)$ and $E(T)$ for the F-centre in MgO are shown in figure 1. The half-width can be fitted accurately to a curve of the form (2) with $\nu_g=7.8\times10^{12}S^{-1}$. Thus the Huang-Rhys factor determined by substitution for ν_g in (1) is $S=39$. Consideration of the peak position

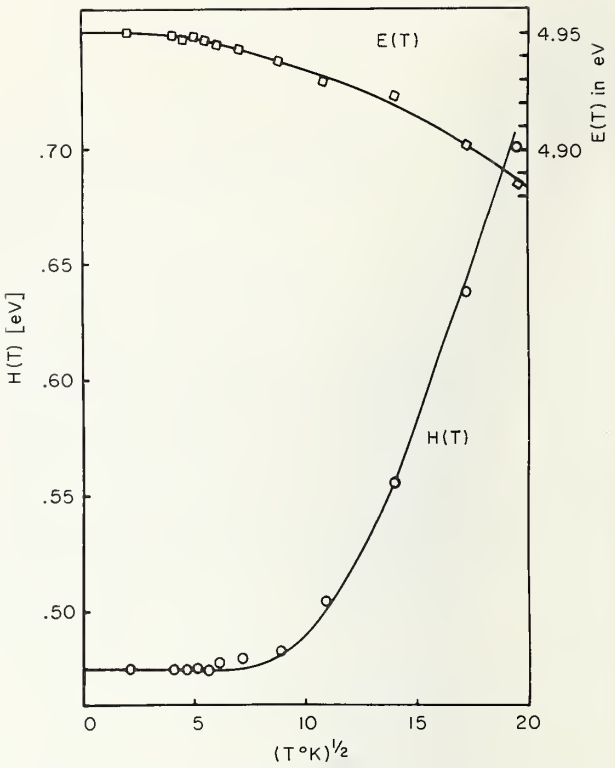

FIGURE 1. *The experimentally determined* F-*band peak* E(T) *and half-width* H(T) *plotted as a function of* $T^{1/2}$.

The solid line through the half-width data is the curve $H(T)^2=(H(0)^2\ \coth\frac{h\nu_g}{2kT}$ where $\nu_g=7.8\times10^{12}$ sec^{-1}. This frequency occurs just below a peak in the experimental phonon density of states curve.

temperature dependence leads to $\nu_e=7.4\times10^{12}S^{-1}$. The most important predictions based upon the configurational coordinate curves which may be constructed from this data relate to the probability of observing luminescent emission from the F-centre excited state. Consideration of the criterion for luminescence discussed by Dexter et al. [8], suggests that in the present case, the return of the F-centre electron to the ground state should be via a luminescent transition of high probability at a photon energy of about 3.0 eV. Such a transition has not so far been observed in MgO F-centres.

It is of some interest to note the relatively large value of the Huang-Rhys factor for the F-centre in MgO ($S=39$). In CaO, Bennett has calculated that $S=3.6$ which agrees well with the value predicted from the zero-temperature half-width assuming that the vibrational frequencies coupled to the F-centre in the ground state are the fundamental longitudinal optic modes. Now at $T=0$ °K the probability of observing a transition involving n-vibrational quanta is then given by [9]

$$P_n=\frac{e^{-S}S^n}{n!}. \tag{5}$$

Thus when P_n is normalized to unity, the transition probability of the zero-phonon line relative to the whole band is e^{-S}. Thus, for the F-centre in MgO, the zero-phonon line transition probability is very small (since $S=39$). However, for CaO the zero-phonon line has a quite reasonable probability since S is of order only $\simeq 6$. These ideas *seem* to be in agreement with experimental results since no structure is associated with the F-band in MgO whereas in CaO zero-phonon lines have been observed in the appropriate position with respect to the F-band in both absorption and emission. The recent measurements of the zero-phonon line under uniaxial stress applied along [100], [110] and [111] axes show that the transition is $A \rightarrow T$ within a centre with cubic symmetry [10]. The stress splitting pattern for such a centre is simple and unmistakable [8, 9]. Thus this assignment is contrary to the report by Kemp and Ziniker (this conference) that this zero-phonon transition, in the presence of strong Jahn-Teller interaction is to an orbital singlet. Further experimental evidence is required to reconcile these data and to confirm (or otherwise) that the zero-phonon line at 3557.3 Å is indeed due to the F-centre.

2.2. F'-centres in MgO and CaO

In the alkaline earth oxides, the F'-centre is an oxygen ion vacancy containing two trapped electrons. Unlike the F-centre it is, therefore, electrically neutral and would be the stable anion defect in an otherwise perfect crystal. Studies of these centres are few. Ward and Hensley [11] have identified an optical band at 3.1 eV with the F'-centre in CaO and Kemp et al. [12] have observed interconversion between the F and F'-centres in CaO using photo-excitation techniques. We have recently observed spin resonance spectra under ultra-violet illumination which we believe to be due to excited spin triplet states ($S=1$) within the helium-like F'-centres in MgO and CaO. The MgO specimens used in the experiments had been annealed in hydrogen at 1600 °C prior to irradiation to doses in the range $2-20\times10^{18}$ nvt. The CaO single crystals used were taken from the region of the molten pool closest to the graphite electrodes; the reducing effect of the graphite produced excess Ca in the samples as evidenced by the copious numbers of F and F'-centres apparent from the optical absorption spectrum.

The bound electronic states of the F'-centre are expected to be similar to the states of the two electrons bound to the radial potential of a helium like atom. The ground state is a spin singlet ^{1}S state in which both electrons are in the lowest energy

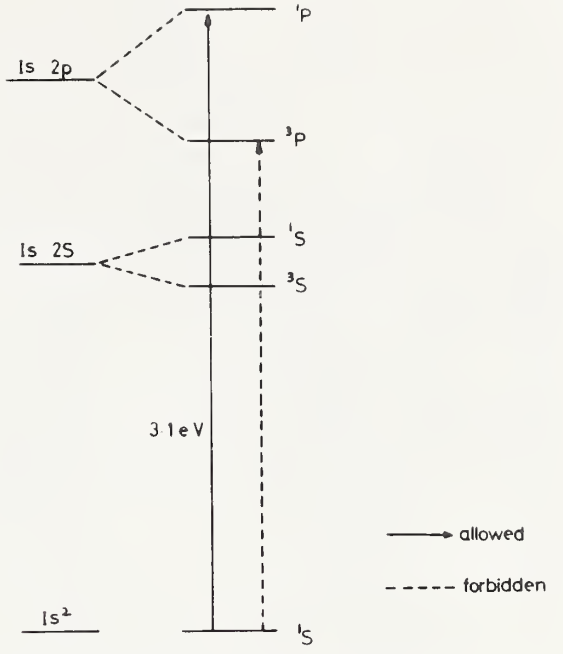

FIGURE 2. *Possible energy of levels of the helium-like* F′*-centres: in absorption only* $^1S \rightarrow {}^1P$ *is allowed.*

spatial state (1s). The excited states correspond to one of the electrons having spatial symmetry appropriate to 2s or 2p states. Figure 2 shows that the next states in order of increasing energy will be ^{3}S, ^{1}S, ^{3}P, and ^{1}P. The only allowed optical transition is then from the ground state ^{1}S to the ^{1}P state. This transition occurs at 3.1 eV in CaO [11] although the process by which the triplet state becomes occupied in both CaO and MgO is not yet understood. In figure 3 the photo-excited resonance observed in CaO is shown. A similar resonance is observed in MgO with a clearly defined hyperfine structure associated with Mg^{25} attending the central single line. The g-values are respectively 1.9866 for CaO and 2.000 for MgO. It should be noted that in the case of MgO all light below 3.5 eV was filtered out thus giving a lower bound for the $^1S \rightarrow {}^1P$ transition energy. The CaO photo-excitation was accompanied by a strong, long-lived red luminescence at room temperature. The evidence, although not conclusive, strongly supports the interpretation that these photo-excited resonances are due to excited ^{3}S-states of the F'-centre. Further studies of these resonances are in progress.

3. Annealing Studies

3.1. F_2-Centres

When neutron irradiated MgO is annealed at temperatures above 300 °C, changes in the e.p.r.

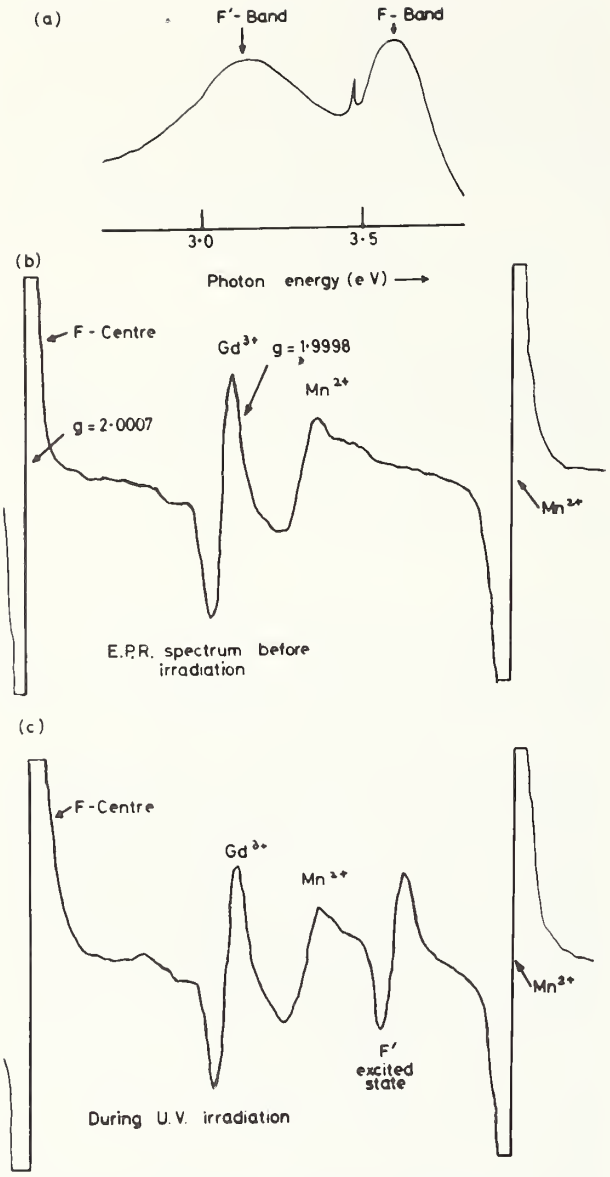

FIGURE 3. *The resonance absorption at 300 °K due to photo-excited triplet state of the* F'*-centre in CaO.*

Only a single line spectrum is observed since the $M_s = 1$ levels are not split in cubic field. The line occurs at $g = 1.995$ and its presence is accompanied by a strong long-lived fluorescence. The exciting light was obtained from a high-pressure mercury lamp suitably filtered to cut out all energy below 2.5 eV.

and optical absorption spectrum are readily observable. Although there is a general decrease in the concentration of point defects due to recombination processes, other defects are also produced as a result of thermally induced defect migration. Wertz et al. [1], have reported the magnetic resonance spectra of F_2-centres in MgO, CaO, SrO, and BaO. According to the model proposed by Professor Wertz and his associates [1], the defect consists of a single electron trapped at a positive-negative ion vacancy pair. Thus the g-tensor is expected to be axially symmetric. At X-band the $g_\perp$ and $g_{||}$-components cannot be resolved with any great precision: we have, however, resolved them at Q-band. For MgO our measurements give $g_\perp > g_{||}$, the respective values being $g_\perp = 2.0012$ and $g_{||} = 2.0004$. For CaO we obtain $g_{||} = 1.995$ and $g_\perp = 1.9980$. The axially symmetric g-tensors substantially support the proposed model. The hyperfine constant for the F_2-centre in MgO is somewhat larger than for the simple F-centre. Surface centres similarly observed in MgO and CaO powders also have axial symmetry [13]. A comparison of the g-values of the surface centres (see ref. 13) with those recorded here indicates that the closeness of these centres to the surface merely enhances the crystal field effects, resulting in larger g-shifts.

The approximate eigenstates of the F_2-center have been calculated by Stoneham [14] using a dielectric continuum model in which the electron is bound to an electric dipole field. This is essentially the approach used in earlier computations by Herman, Wallis and Milnes [14]. As is common in F-centre calculations, Stoneham uses the high frequency dielectric constant ϵ since use of the static constant ϵ_0 yields no bound states for the F_2-centre. The principal conclusions are that the binding energies are 2.42 eV in MgO, 1.92 eV in CaO, 1.70 eV in SrO and 1.24 eV in BaO, and that no other bound states exists within ~ .01 eV of the conduction bands. The reduced binding energy in the case of CaO and SrO is presumably reflected in the decreasing importance of surface F-centres in the overall oxygen absorption processes on surfaces of these oxides [13]. These calculations, although only approximate, do give important information about the optical absorption properties of F_2-centres since it is expected that optical absorption by the defect results in electron excitation into the conduction band. Consequently, it seems probable that the F_2-centres may be optically bleached using photons of the appropriate energy. King and Henderson [15] have observed such bleaching in the MgO F_2-centre by monitoring the changes in intensity of the F_2-centre spin resonance signal during irradiation from a high pressure mercury lamp. A peak in bleaching efficiency is observed at photon energies of about 3.5 eV as shown in figure 4. Dichvoic effects in bleaching with polarized light were not observed in accord with expectations for an excitation from a bound state to the conduction band.

3.2. Studies of Zero-Phonon Lines in Annealed Crystals

The change in optical absorption spectrum which follows annealing at temperatures above 300 °C

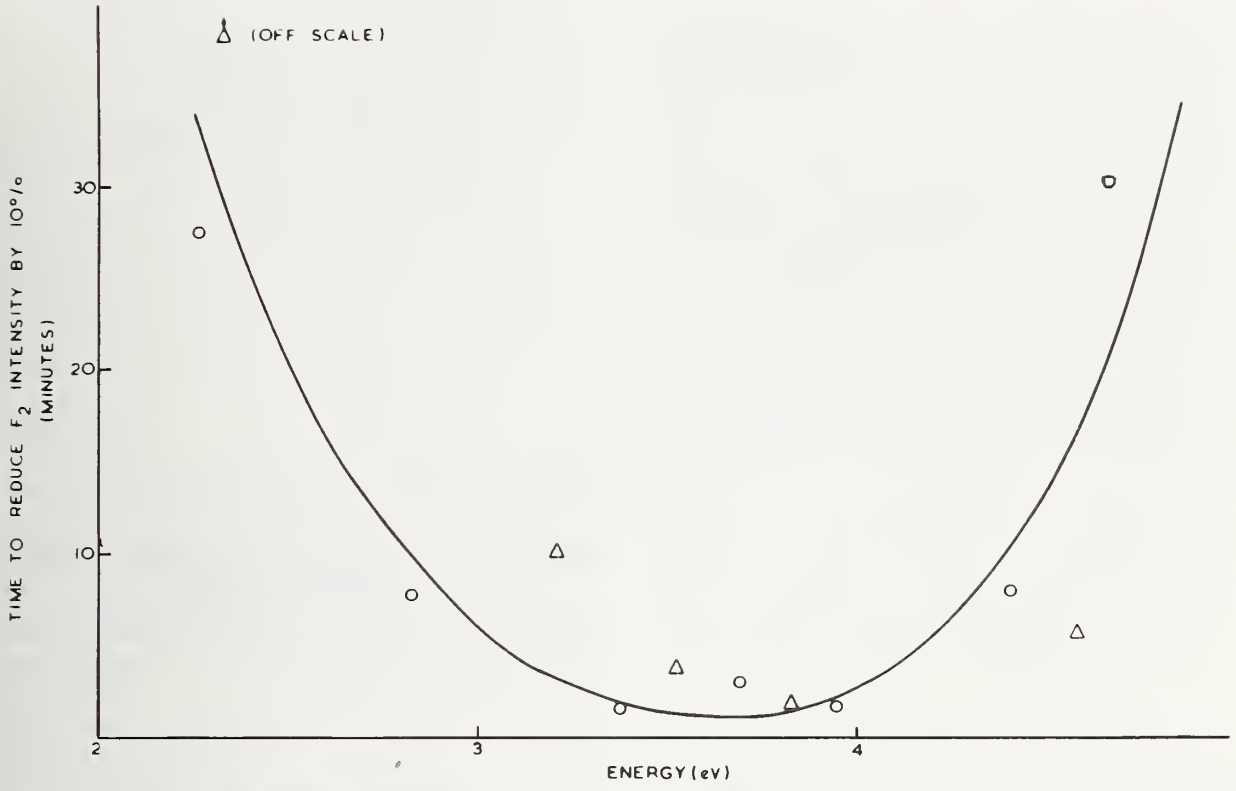

FIGURE 4. *The bleaching of the* F_2*-centre in MgO.*

Monochromatic radiation was obtained by filtering the radiation from a high pressure mercury lamp. Allowance was made for the strong emission lines in the radiation and for the self absorbance of the specimen. The peak efficiency of bleaching occurs at about 3.7 eV, which corresponds to the separation between the ground state of the F_2-centre and the conduction band. The symbols are: ○ close to strong emission line in the radiation; Δ not close to strong emission line.

was first discussed by Wertz et al. [16]. At low temperatures the complex absorption spectrum showing many overlapping bands is highlighted by a large number of zero-phonon lines (fig. 5). The technique of uniaxial stress splitting, discussed independently by Kaplianskii [19] and by Runciman [18] has been used to investigate the symmetry properties of defects giving rise to these lines. Using such techniques it has been shown that zero-phonon lines at 4684 and 4700 Å are due to defects having identical symmetry properties [15]. The analysis of the experimentally determined splitting pattern for these lines, shown in figure 6, confirms that the defects have [110] orientation, orthorhombic symmetry and a linear electric dipole oscillator along a [110] direction. Such symmetry properties are identical with those expected for *M*-centres.

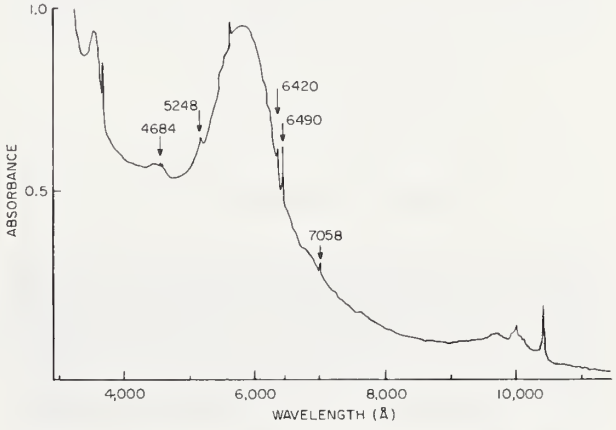

FIGURE 5. *The optical absorption spectrum of magnesium oxide neutron irradiated to a dose of* 2×10^{20} *nvt at 600 °C.*

This spectrum has many identical features of samples irradiated at 150 °C and annealed at 300 to 600 °C.

The stress splitting patterns of the lines at 5248, 6419, and 6490 Å show that they are due to $A \leftrightarrow E$ transitions within defects having trigonal symmetry and [111] symmetry axes. Thus the defects have properties analogous to the *R*-centres in the alkali halides [8], and models for these centres are correspondingly similar [19]. Figure 7 shows that the defects consist of three anion vacancies forming an equilateral triangle on the [111] plane and containing different populations of trapped electrons. It seems that from electrostatic consideration the

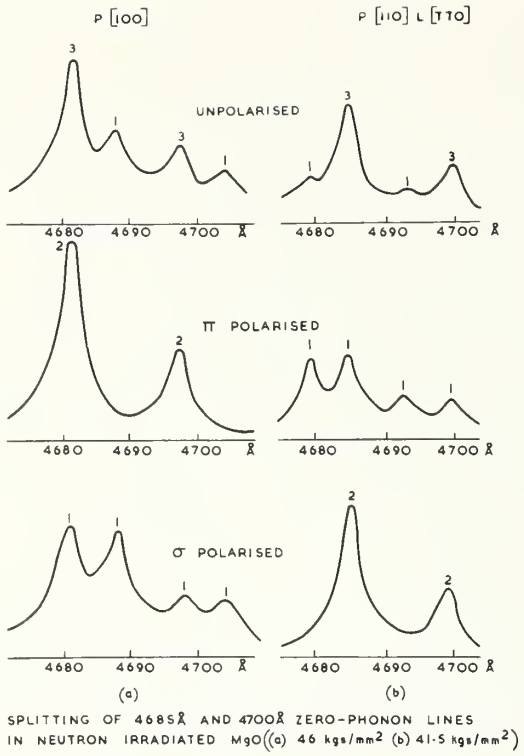

SPLITTING OF 4685Å AND 4700Å ZERO-PHONON LINES IN NEUTRON IRRADIATED MgO((a) 46 kgs/mm² (b) 41·5 kgs/mm²)

FIGURE 6. *The experimental splitting patterns for the 4684 and 4700 Å lines for two directions of applied stress at 77 °K.*

(π refers to E parallel to stress, σ to E perpendicular to stress.)

centre will trap more than 3 or 4 electrons; more likely is the recent suggestions [19] that such a vacancy aggregate will trap 5, 6, or 7 electrons. Using a molecular orbital approach to construct the most likely one-electron ground states we obtain:

R^+ 5 electrons—$^2E\ (1a)^2(1e)^3$

R 6 electrons—$^1A_1\ (1a_1)^2(1e)^4$

R^- 7 electrons—$^2A_1\ (1a_1)^2(1e)^4(2a_1)$.

The line at 5248 Å is apparently due to the 5 electron centre since at low temperatures it is strongly dichroic under uniaxial stress [19]. This behavior is associated with the stress induced removal of the ground state orbital degeneracy, and the intensity ratios between the two optical transitions

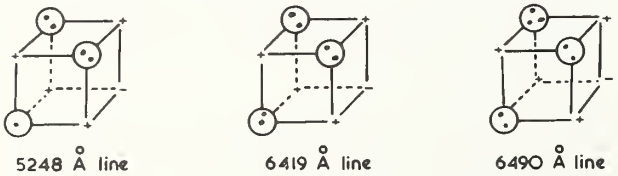

FIGURE 7. *This shows the proposed models for the three defects whose optical absorption is due to* A ↔ E *transitions within defects trigonal symmetry.*

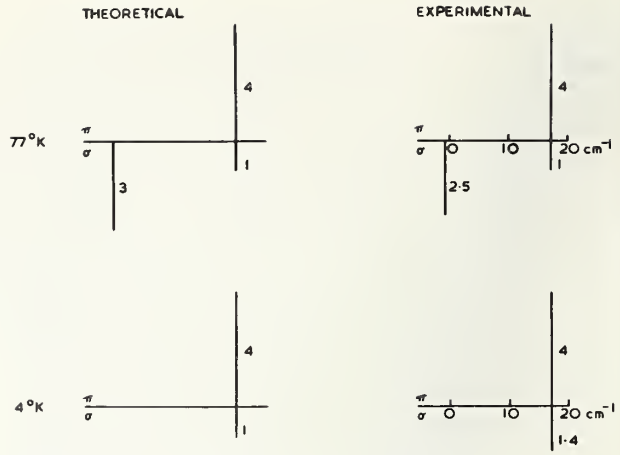

STRESS INDUCED DICHROISM OF 5248 Å ZERO-PHONON LINE IN NEUTRON IRRADIATED MgO ([100] STRAIN 50 hgs/mm²)

FIGURE 8. *The stress induced dichroism in the 5248 Å line under [100] strain (50 kg/mm).*

(a) Dichroism expected for an $E \rightarrow A$ transition of a trigonal centre with ⟨110⟩ and ⟨112⟩ dipoles under [100] stress (b) Experimentally observed behaviour of the 5248 Å line.

will then be proportional to $\exp -\left(\frac{\Delta E}{kT}\right)$, where ΔE is the stress induced splitting in the ground state. The comparative intensities under stress at 77 and 4 °K are shown in figure 8 and are consistent with those expected for a trigonal defect with optical dipole moments along [110] and [112] directions in the plane perpendicular to the trigonal axis. No such dichroism is observed for the 6419 and 6490 Å lines, and these have been assigned to the 6 electron centre and 7 electron centre, respectively [19, 20].

The description of the electronic ground states discussed above suggests that both the R^+ and R^- centres are paramagnetic. Kemp et al. [21], have shown that such is the case for the R^+ centre using Faraday rotation techniques. The magnetic properties of this centre are expected to be similar to the R-centre in KCl discussed recently by Krupka and Silsbee [22]. In fact, strong coupling of the ^{2}E ground state to the vibrations of the lattice lead to an unusually short relaxation time in KCl which explains the absence of the resonance signal even at low temperatures. The paramagnetic resonance spectrum of the R-centre in KCl is observed only under strong uniaxial pressure and at 2 °K. Thus the previous suggestion [19] by the author that a spectrum in MgO with trigonally symmetric g-tensor was due to the R^+ centre is likely to be incorrect. However, the 7 electron centre R' which has a $^2A_1$ ground state is not expected to present such problems and therefore it would seem appropriate to assign this spectrum to the R^--centre. The spectrum shown in figure 9 is recorded in the [110] and [100] orientations and consists of four equally intense lines.

The presence of hyperfine interactions with Mg^{25} is shown clearly, although it has not yet been fully investigated. The g-tensor has axial symmetry, the axes of symmetry being [111]. We obtain $g_{||}=2.0026$ and $g_{\perp}=2.0039$. It is difficult to prove that this spectrum is due to the R-like centre containing 7 trapped electrons although the circumstantial evidence is quite strong. It is evident from figure 5 which shows the optical absorption spectrum from the same sample, that the 6419 Å line is much more intense than the other trigonal centres. Further studies of this centre are currently in progress.

4. A Trapped Hole Centre in Al_2O_3

Although optical absorption and spin resonance studies of irradiation induced defects in alumina have been reported by numerous authors [3, 23, 24], no correlation has been made of the various optical bands to the paramagnetic resonance spectra. In reactor irradiated Al_2O_3, a twelve line spectrum from a triplet state in six inequivalent sites was attributed by Gamble et al. [3], to the molecule ion AlO^{3-} situated in a pair of oxygen ion sites. The present results, and those of Cox [25], suggest that a more probable model, involves a pair of holes trapped on adjacent oxygen ion sites: the line joining the two O^- ions defines the paramagnetic z-axis, while the x-axis points towards a cation vacancy. It is apparent in figure 10, that the hole pair may be trapped on any two of three equivalent anions. Thus there are three equivalent magnetic z-axes for the defect which are rotated through $+3°$ with respect to the a-directions of the crystal. In other Al_2O_3 molecular units in the lattice these axes are rotated through $-3°$ so that in all there are six inequivalent sites for this defect giving a twelve line spectrum for a spin triplet state. Clearly this model has the same symmetry as the AlO^{3-} molecule ion discussed by Gamble et al. [3] and the evidence against the molecule ion model is obtained from temperature dependent properties of the spectrum.

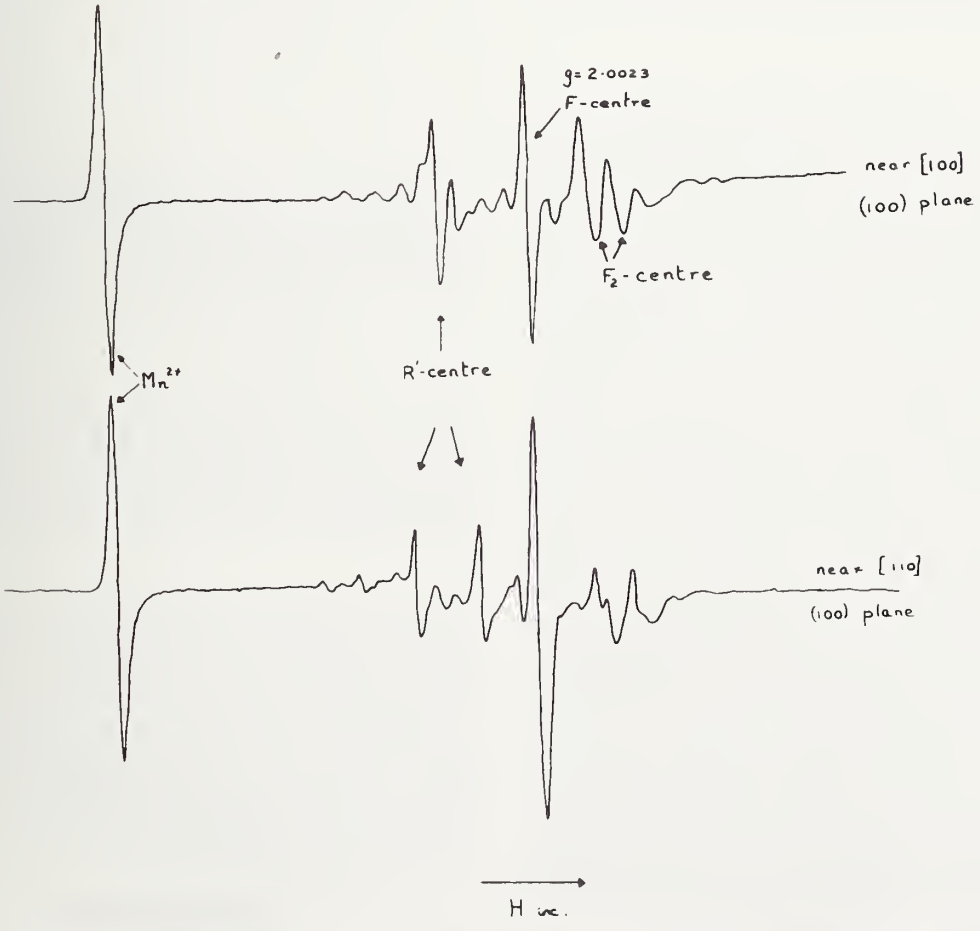

FIGURE 9. *Derivative of the resonance absorption at 35* Gcs *of the magnesium oxide crystal used to obtain the optical absorption spectrum shown in figure 8.*

The spectrum was measured at 77 °K with H_o parallel to (*a*) a [100] crystal axis and (*b*) a [110] crystal axis.

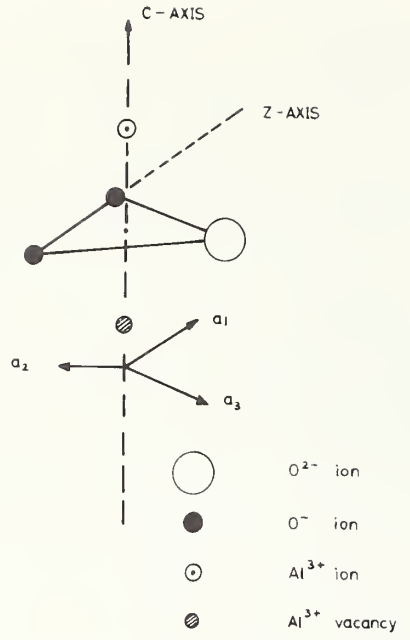

FIGURE 10. *Symmetry properties of the hole-pair trapped on neighbouring oxygen ions in Al_2O_3.*

Figure 11 shows the spectrum measured at 77 and at 300 °K. At 77 °K it is identical with that reported earlier [3]. When the Zeeman field is perpendicular to the crystal c-axis the spectrum consists of 12 equally intense resonance lines whose widths were of order 30 to 35 G depending on the irradiation dose. The spectrum corresponding to one orientation with the field H parallel to the c-axis consists of only two lines: this spectrum remains unaffected when measurements are recorded at 300 °K. However, the 12 lines of the c-axis spectrum are absent at this temperature. This effect is concerned with the thermally activated jumping between the three equivalent hole sites at the higher temperature. The jump rate increases with temperature and thus the lines in the c-axis spectrum will broaden with temperature since the magnetic energy changes when the defect z-axis changes. Clearly this does not affect the $H||$ c-axis spectrum since in this orientation all possible sites for the defect are degenerate. Cox [25] has noted that the broadening becomes detectable at 230 °K and estimates that at this temperature the jump frequency is of order 10^7 sec^{-1}. If we assume weak dipolar coupling between the hole pair then the magnetic dipole strength should be approximately equal to the magnitude of D, the crystal field splitting. Thus it can be shown that

$$D \simeq 11.1 \frac{g^2\beta^2}{\langle r^3 \rangle} \qquad (7)$$

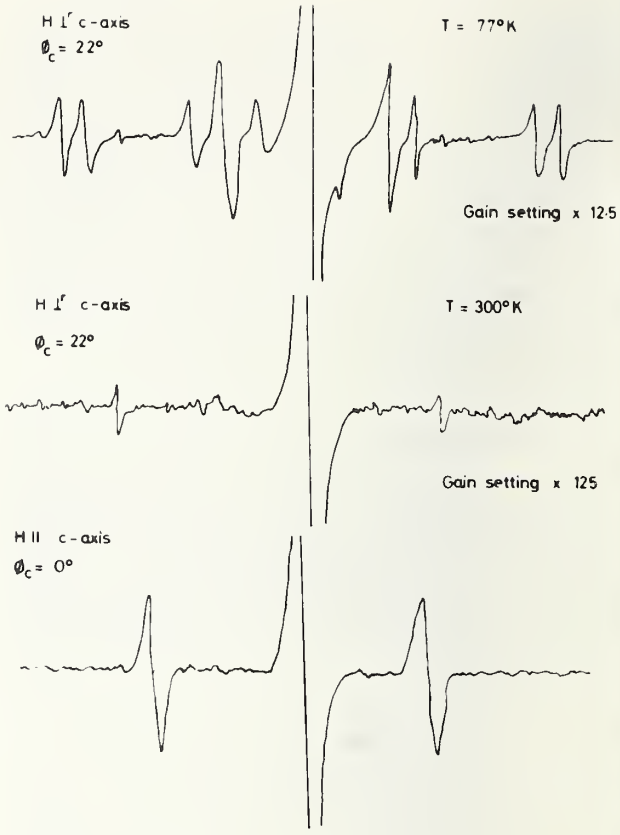

FIGURE 11. *The derivative absorption spectrum of a reactor irradiated Al_2O_3 crystal at 77 and 300 °K in two orientations.*

Here θ_c refers to the angle between H_o and the crystal c-axis, and ϕ_c is the azimuthal angle measured in the basal plane where $\phi_c = \theta_c = 90°$ corresponds to the [100] hexagonal crystal axis. The energy level for the system may be described by a spin-Hamiltonian

$$\mathcal{H} = \beta H \cdot g \cdot S + D(S_z^2 - \tfrac{1}{3}S(S+1)) + E(S_x^2 - S_y^2),$$

in which $S = 1$, $g_\perp = 2.019$, $g_{||} = 2.010$, $D = 710 \times 10^{-4}$ cm^{-1} and $E = 25 \times 10^{-4}$ cm^{-1}.

where r is the separation between the holes. We find since $D \sim 1400g$ that $r = 3.00$ Å. This is very close to the 0–0 separation in the corundum lattice, strongly supporting the proposed model for the defect.

It is a pleasure to record my indebtedness to R. D. King of the Ceramic Division, U.K.A.E.A., Harwell with whom I collaborated on some of the work discussed here. I would also thank A. M. Stoneham, A. E. Hughes, and D. Pooley of U.K.-A.E.A., Harwell, for many stimulating discussions, and R. Cox of Centre d'Etudes Nucleaires de Grenoble for communicating his results on Al_2O_3 to me prior to publication.

5. References

[1] Wertz, J. E., Orton, J. W. and Auzins, P., Disc. Farad. Soc. **30**, 40 (1961).

[2] Takeda, T., and Watanabe, A., J. Phys. Soc. Jap. **21**, 267 (1966).
[3] Gamble, F. I., Bartram, C. G., Young, C. G., Gilliam, O. R., and Levy, P. W., Phys. Rev. **134**, A577 (1964).
[4] Henderson, B., unpublished data.
[5] Weeks, R. A., Interaction of Radiation With Matter, Ed. A. Bishay, Plenum Press, New York (1967).
[6] Pryce, M. H. L, Phonons (Scottish Universities Summer School, 1965), Oliver and Boyd (1966).
[7] Klick, C. C., Paterson, D. A., and Knox, R. S., Phys. Rev. **133**, A1717 (1964).
[8] Dexter, D. L., Klick, C. C., Russell, G. A., Phys. Rev. **100**, 603 (1955).
[9] Hughes, A. E., J. de Phys. **28** (supp), 55 (1967).
[10] Hughes, A. E., private communication.
[11] Ward, W. C. and Hensley, E. B., Bull. Amer. Phys. Soc. **10**, 307 (1965).
[12] Kemp, J. C., Ziniker, W. M. and Hensley, E. B., Phys. Lett. **25A**, 43 (1967).
[13] Nelson, R. L., Tench, A. J., and Harmsworth, B. J., Trans. Far. Soc. **63**, 1427 (1966).
[14] Stoneham, A. M., private communication.
[15] King, R. D. and Henderson, B., Proc. Brit. Ceram. Soc. **9**, 63 (1967).
[16] Wertz, J. E., Saville, G., Auzins, P., and Orton, J. W., J. Phys. Soc. Jap. Supp. z. **18**, 305 (1963).
[17] Kaplianskii, A. A., Optics Spectrosc. **16**, 329 and 557 (1964).
[18] Runciman, W. A., Proc. Phys. Soc. **86**, 629 (1965).
[19] Henderson, B., and King, R. D., J. de Phys. **28** (supp), 75 (1967).
[20] Ludlow, I. K., unpublished.
[21] Kemp, J. C., Ziniker, W. M. and Glaze, J. A., Proc. Brit. Ceram. Soc. **9**, 109 (1967).
[22] Krupka, D. C. and Silsbee, R. H., Phys. Rev. **152**, 816 (1966).
[23] Levy, P. W., Phys. Rev. **123**, 1226 (1961).
[24] Mitchell, E. W. J., Rigden, J. D. and Townsend, P. W., Phil. Mag. **5**, 1013 (1960).
[25] Cox, R., private communication (1967).

Covalency in Metal Oxides

B. E. F. Fender and B. C. Tofield

Inorganic Chemistry Laboratory, Oxford University

Recent developments in our understanding of neutron diffraction by antiferromagnetic solids have made it possible to obtain in a relatively direct way a quantitative measure of covalency—including the determination of electron delocalization in some simple transition metal oxides. Theory predicts [1] [1] that in an octahedral "complex," and for a molecular orbital model involving only d electrons of the metal and s and p electrons of the ligand,

$$S/S_o = 1 - a(bA_\sigma^2 + cA_\pi^2 + dA_s^2)$$

where S is the effective spin quantum number of the metal ion in an antiferromagnetic solid; S_o is the expected value of the spin quantum number in a fully ionic lattice; A_σ, A_π, and A_s are covalency or admixture parameters describing σ overlap of d and p atomic orbitals, π overlap of d and p orbitals and σ overlap of d and s orbitals, respectively; and a, b, c, d, are constants which depend on the number of outer d electrons in the cation.

The intensities of neutron Bragg peaks have been measured to evaluate S and thus the covalency parameters in MnO [2, 3] and NiO [1, 3, 4] (see table).

TABLE. *Covalency parameters*

NiO $(A_\sigma^2 + A_s^2)$	*6.0% [4]	3.8 ± 0.2% [3]
MnO $(A_\sigma^2 + 2A_\pi^2 + A_s^2)$	*3.3% [2]	3.5 ± 0.6% [3]
CoO $\left(A_\sigma^2 + \frac{2}{3}A_\pi^2 + A_s^2\right)$		2.8%

*Not corrected for zero point spin deviation.

In a similar way the two independent determinations of the effective spin of Co^{2+} in CoO [5, 6] can be used to calculate covalency parameters. Using the average value of $S = 1.915$ together with an appropriate value of the spectroscopic splitting factor ($g = 4.278$ from Co^{2+} in MgO) [7] and allowing for magnetic disorder at 0 °K [8], the sum of the covalency parameters is calculated to be 2.8 percent. The similarity of the sum of the covalency parameters for all three oxides suggests that the type of bonding is not important and the dominant factor is merely a reduction of charge at the cation. The magnitude of the covalency parameters indicates that the charge in the region of the cation is reduced by about $0.2e$ in each oxide, even though the π bonding contribution varies from zero in NiO to > 50 percent in MnO.

If the total covalency in metal oxides is governed mainly by the electron affinities of the metal ions, one would expect the covalency parameter sum for trivalent ions of the first transition series to be larger, but similar to each other. The present evidence does not appear to support this view. The results of Nathans [2] when corrected for zero point spin deviation [3, 8] give $A_\pi^2 = 3.5$ percent for Cr^{3+} in $LaCrO_3$ and $A_\sigma^2 + 2A_\pi^2 + A_s^2 = 7.8$ percent for Fe^{3+} in $LaFeO_3$. (The transition metal ions are in a near octahedral arrangement of oxygen ions [13]). A similar single set of measurements on the same systems [9] appear to confirm the results for Cr^{3+} ($A_\pi^2 \approx 2$ percent) but indicate that covalency may be higher for Fe^{3+} (≈ 18 percent).

It is important to note, however, that both $LaFeO_3$ and $LaCrO_3$ has distorted perovskite structures, though neither have been subjected to a full structural analysis. The present covalency parameters, and presumably those of Nathans, have been calculated assuming the atom positions in both $LaFeO_3$ and $LaCrO_3$ to be the same as in $La(Mn_{0.8}Co_{0.2})O_3$ [10]. The unit cell parameters [10, 11, 12] indicate that this may be a better approximation for $LaFeO_3$ than for $LaCrO_3$. As the determination of covalency parameters by neutron diffraction depends on an accurate knowledge of the nuclear structure factors, if these are not well known, the covalency parameters obtained may be in error. In addition, deviation of the compounds from stoichiometry can introduce a further source of uncertainty. Further progress towards the determination of covalency in trivalent oxides must therefore be linked with improved characterisation of the compounds investigated.

[1] Figures in brackets indicate the literature references at the end of this paper.

References

[1] J. Hubbard and W. Marshall, Proc. Phys. Soc. **86**, 561, (1965).

[2] R. Nathans, G. Will and D. E. Cox, Proc. Int. Conf. Magnetism, Nottingham (1964).

[3] B. E. F. Fender, A. J. Jacobson and F. A. Wedgwood, J. Chem. Phys. (to be published).

[4] H. A. Alperin, J. Phys. Soc. Japan, Suppl. B III, **17**, 12, (1962).

[5] W. L. Roth, Phys. Rev. **110**, 1333 (1958).

[6] D. C. Khan, Ph.D. Thesis, Ohio State University (1965).

[7] A. D. Liehr and C. J. Ballhausen, Ann. Phys. (N.Y.) **6**, 134 (1959).

[8] T. Ogushi, Phys. Rev. **111**, 1063 (1958).

[9] B. E. F. Fender and B. C. Tofield (unpublished results).

[10] M. A. Gilleo, Acta Cryst. **10**, 161 (1957).

[11] S. Geller and E. A. Wood, Acta Cryst. **9**, 563 (1956).

[12] S. Geller, Acta Cryst. **10**, 243 (1957).

[13] P. Coppens and M. Eibschutz, Acta. Cryst. **19**, 524 (1965).

Diffusion and Ionic Conductivity: Kinetic Theory

John R. Manning

Institute for Materials Research, National Bureau of Standards, Washington, D.C. 20234

Kinetic expressions for the tracer diffusion coefficient D_i^* of species i and the ionic conductivity σ_i from species i are derived in terms of atom jump frequencies by making suitable modifications in the random walk diffusion equations. Also, D_i^* and σ_i are related to each other. The tracer diffusion coefficient is found from the Fick's Law term in the kinetic equation for the flux J_i, whereas σ_i is derived from the drift velocity term in this equation. Nonrandom effects which must be included are those from kinetic driving forces, correlation effects, and the vacancy wind effect. The correlation factor f is derived from an equation for the effective frequency of independent displacements. It is shown that isotope effect measurements, which measure a quantity $f\Delta K$, and/or measurements of σ_i/D_i^* can help to distinguish experimentally between different diffusion mechanisms. In the case of impurity diffusion, measurements of f and σ_i/D_i^* yield information about the vacancy jump frequencies for exchange with solvent atoms in the vicinity of the impurity. A brief description is given of Lidiard's pair association treatment for vacancy-impurity complexes.

Key Words: Atom transport, diffusion in crystals, diffusion coefficient, diffusion mechanisms, ionic conductivity, jump frequencies, kinetic theory.

1. Introduction

1.1. Kinetic Equations for Diffusion Coefficient and Ionic Conductivity

In the present paper, kinetic expressions in terms of the atom jump frequencies will be derived for the tracer diffusion coefficient D_i^* of species i and the ionic conductivity σ_i from this species. By use of these kinetic expressions, the experimental D_i^* and σ_i can be related to each other. In addition, information about diffusion mechanisms and about jump frequencies near an impurity can be obtained.

Diffusion and ionic conductivity both arise from atom transport. From a kinetic viewpoint, both of these effects are proportional to the atom (or ion) jump frequencies. For planar diffusion in the x direction, the jump frequencies for diffusing atoms of species i can be defined to be Γ_R in the $+x$ direction and Γ_L in the $-x$ direction. Then, D_i^* is proportional to the sum $\Gamma_R+\Gamma_L$, whereas σ_i is proportional to the difference $\Gamma_R-\Gamma_L$. The kinetic equation for the flux J_i of species i contains two terms, one proportional to $\Gamma_R+\Gamma_L$ and hence to D_i^*, the second proportional to $\Gamma_R-\Gamma_L$ and hence to σ_i. Thus, D_i^* and σ_i are closely related and can be obtained from the two terms in the kinetic diffusion equation for J_i.

1.2. Tracer Profiles

D_i^* and σ_i also can be related to the moments of the concentration profile $c_i(x, t)$ for diffusion of a layer of tracer atoms. Here, D_i^* is proportional to $\langle x^2\rangle$, the mean square displacement of the diffusing i atoms, whereas σ_i is proportional to the mean displacement $\langle x\rangle$.

If a layer of radioactive tracer atoms originally at plane 0 is allowed to diffuse by means of a random walk, the atom concentration $c_i(x, t)$ after time t is given by

$$c_i(x, t) = S_o(\pi D_i^* t)^{-1/2} \exp(-x^2/4D_i^* t), \qquad (1)$$

where x is the displacement from plane 0, S_o is the original concentration per unit area on plane 0, and D_i^* is the tracer diffusion coefficient. It is assumed here that jumps in the $+x$ and $-x$ directions are equally probable so that the mean atom displacement $\langle x\rangle$ equals zero. The concentration profile for eq (1) is shown in figure 1a. It is a symmetric profile centered on plane 0. The mean square displacement $\langle x^2\rangle$ of the atoms provides a measure of the width of the tracer profile. It is related to the tracer diffusion coefficient by

$$\langle x^2\rangle = 2D_i^* t. \qquad (2)$$

Whenever the probability of jump in the $+x$ direction is larger than that in the $-x$ direction, $\langle x\rangle$ is no longer zero. If each jump is still independent of previous jumps,

$$c_i(x, t) = S_o(\pi D_i^* t)^{-1/2} \exp[-(x-\langle x\rangle)^2/4D_i^* t]. \qquad (3)$$

Here D_i^* is the same quantity as that in eq (1).

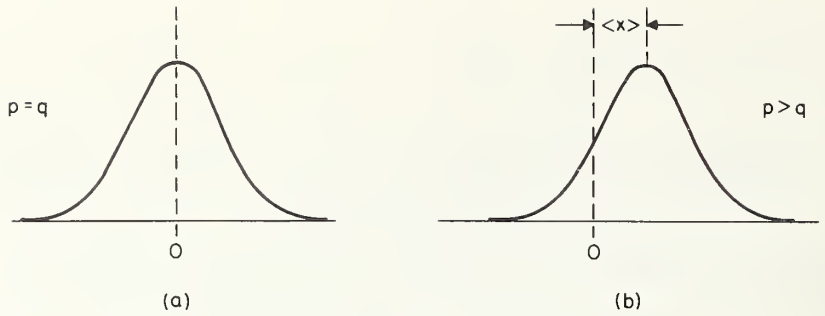

FIGURE 1. *Concentration profiles for a layer of radioactive tracer atoms originally at plane* 0 *with* p *being the probability of jump to the right and* q *being the probability of jump to the left.*

(a) Random walk, no kinetic driving force.
(b) With kinetic driving force.

The concentration profile for eq (3) is shown in figure 1b. This profile has the same shape and width as that for the truly random walk of figure 1a, but the whole profile is shifted a distance $\langle x \rangle$. Instead of there being only one parameter D_i^* to be measured, there now are two parameters D_i^* and $\langle x \rangle$.

An electric field acting on charged ions provides a driving force which makes $+x$ and $-x$ jumps unequal in number. The resulting $\langle x \rangle$ is directly proportional to the field and to σ_i. When a constant electric field is the only driving force, the ionic conductivity σ_i for species i can be calculated directly from $\langle x \rangle$.

1.3. Nonrandom Effects

The basic equations which will be used in the following discussion are the random walk diffusion equations. The introduction of a driving force by itself introduces a nonrandom effect into the kinetic equations. This is easily included in random walk equations by allowing Γ_R to be unequal to Γ_L, as in eq (3) and section 2.1. Even in the absence of driving forces, however, atoms often do not follow random walks. Instead, if diffusion occurs by a vacancy or interstitialcy mechanism, they follow correlated walks, where the direction of one atom jump depends to a certain extent on the directions of previous jumps by that atom. This introduces a correlation factor f into the diffusion equations and influences both D_i^* and $\langle x \rangle$. In addition, if there is a net flux of vacancies or interstitialcies, the influence of the flux will change the atom jump frequencies. This can greatly affect $\langle x \rangle$ but does not influence D_i^*.

The modifications of the random walk equations introduced by correlation effects and a vacancy flux are considered in separate sections on the correlation factor and the "vacancy wind". These nonrandom effects make the relations between the experimental quantities (D_i^* and σ_i) and the atom jump frequencies somewhat more complex. Nevertheless, they also can help one to distinguish experimentally between different diffusion mechanisms and to calculate jump frequency ratios for jumps in the vicinity of an impurity.

2. Kinetic Diffusion Equations Assuming Independent Displacements

2.1. Random Walk Diffusion Equations Modified by a Driving Force

Although atoms do not necessarily follow random walks in actual crystals, many of the random walk ideas can be applied to correlated walks. As a first step, the random walk diffusion equations will be discussed.

The random walk diffusion equations modified by a driving force can be derived by considering two neighboring atom planes which are normal to the diffusion direction. The number of atoms of the diffusing species i per unit area on plane 1 can be called n_1 and that on plane 2, which is the neighboring plane in the $+x$ direction, can be called n_2. Then, if Γ_{12} is the jump frequency for a jump of a given i atom from plane 1 to plane 2 and Γ_{21} is the jump frequency in the opposite direction from plane 2 to plane 1, the net flux J_i of species i in the $+x$ direction is

$$J_i = n_1\Gamma_{12} - n_2\Gamma_{21}. \tag{4}$$

Here $n_1\Gamma_{12}$ is the number of atoms jumping in the $+x$ direction per unit area per unit time and $n_2\Gamma_{21}$ is the number jumping in the $-x$ direction.

Equation (4) can be written in terms of two differences: (1) the difference between the concentrations n_1 and n_2 and (2) the difference between the jump frequencies Γ_{12} and Γ_{21}. If planes 1 and 2

(and all such neighboring planes) are separated by a distance d

$$n = cd, \tag{5}$$

where c is the number of atoms per unit volume. Also the difference $n_2 - n_1$ equals d times the gradient $\partial n_i/\partial x$. Thus,

$$n_2 - n_1 = d^2(\partial c_i/\partial x). \tag{6}$$

Equation (4) then reduces to

$$J_i = -\Gamma d^2(\partial c_i/\partial x) + c_i d(\Gamma_{12} - \Gamma_{21}), \tag{7}$$

where Γ is the average of Γ_{12} and Γ_{21}, equal to $\frac{1}{2}(\Gamma_{12} + \Gamma_{21})$, and c_i is the average concentration $\frac{1}{2}d(n_1 + n_2)$, equal to the concentration associated with the region midway between planes 1 and 2.

A more familiar form of the diffusion equation can be obtained by writing

$$D_i^* = \Gamma d^2, \tag{8}$$

and

$$\langle v_F \rangle_i = d(\Gamma_{12} - \Gamma_{21}). \tag{9}$$

Here, D_i^* is the tracer diffusion coefficient for species i measured in a homogeneous system, and $\langle v_F \rangle_i$ is the average drift velocity of species i as a result of kinetic driving forces acting on the atoms. (By definition, a kinetic driving force is any influence which makes the jump frequency Γ_{12} in one direction between two planes differ from the frequency Γ_{21} for a jump in the opposite direction between these same two planes.) This yields

$$J_i = -D_i^*(\partial c_i/\partial x) + c_i \langle v_F \rangle_i. \tag{10}$$

The first term on the right in eq (10) is the normal Fick's Law diffusion term with D_i^* being related to the width of the tracer profiles shown in figures 1a and 1b. The second term is the drift term with $\langle v_F \rangle_i$ being related to the displacement $\langle x \rangle$ of the tracer profile shown in figure 1b and also related to the ionic conductivity σ_i for this species.

2.2. Effect of Diffusion Coefficient Gradient

In the derivation of eq (10), it was assumed that each atom jump was independent of previous jumps; but no assumption was made about the relation between Γ_{23} and Γ_{12}, where Γ_{23} is the jump frequency in the $+x$ direction from plane 2 and Γ_{12} the similar frequency from plane 1. If the jump frequency depends on the starting position as well as the direction of the jump, Γ_{23} and Γ_{12} may differ. This circumstance can arise, for example, when the energy of motion (and/or formation) depends on the composition of the crystal and the composition is a function of position. This would make the diffusion coefficient depend on position, and conceivably could strongly affect the diffusion process. Nevertheless, it can be shown that such a dependence of diffusion coefficient on position does not affect eq (10). Thus, this equation is valid in general, even when there is a non-constant diffusion coefficient.

One quantity which is affected by a diffusion coefficient gradient is the total drift velocity $\langle v \rangle_i$ of the i atoms. This velocity depends on differences, such as $\Gamma_{23} - \Gamma_{21}$, between the frequencies for jumps in the $+x$ and $-x$ directions from a given plane (in this case, plane 2). If $\Gamma_{12} \neq \Gamma_{23}$, the expression for $\langle v \rangle_i$ differs from the expression for $\langle v_F \rangle_i$. In general, [1, 2][1]

$$\langle v \rangle_i = \langle v_F \rangle_i + (\partial D_i^*/\partial x), \tag{11}$$

where $\partial D_i^*/\partial x$ is the diffusion coefficient gradient. The measured drift velocity $\langle v \rangle_i$ equals the drift velocity $\langle v_F \rangle_i$ arising from the driving forces only if $\partial D_i^*/\partial x$ equals zero.

D_i^* is defined by eq (8), which is valid whenever individual displacements are independent of one another. In general, Γ and hence D_i^* can depend on local conditions in the crystal. Nevertheless, Γ and D_i^* often do not depend on position, making $\partial D_i^*/\partial x$ equal zero. For simplicity, it is assumed in the following two sections (3 and 4) that Γ is independent of position.

3. Correlation Effects

For diffusion by a vacancy or interstitialcy mechanism, neither eq (8) for D_i^* nor eq (9) for $\langle v_F \rangle_i$ is accurate if Γ is assumed to equal the actual jump frequency. The correlation factor influences D_i^*, and both the correlation factor and vacancy wind effects influence $\langle v_F \rangle_i$. In the present section correlation factor effects are considered.

3.1. Correlation Factor

After an atom has exchanged places with a given vacancy, the vacancy is in the proper position to allow the atom to make a reverse jump back to its original site. Thus, the second exchange of an atom with a given vacancy is not random in direction. Instead, the atom has a greater-than-random probability of making a reverse jump. This situation, which arises whenever diffusion proceeds by

[1] Figures in brackets indicate the literature references at the end of this paper.

a vacancy mechanism, creates a correlation between the directions of successive atom jumps and introduces a correlation factor into the diffusion equations.

A similar correlation arises for diffusion by an interstitialcy mechanism. After an atom has jumped from an interstitial to a lattice site, the atom which was just displaced from the lattice site is still on a neighboring site and is in the proper position to cause a reverse jump. By contrast, no such correlation arises for self-diffusion by an exchange mechanism or by a direct interstitial mechanism.

Mathematically, the correlation factor can be calculated as follows: In general, regardless of whether there is a random walk, eq (2) is valid in the limit where t goes to zero [3]. The total displacement x of an atom is the sum of the displacements x_j from the individual jumps made by the atom,

$$x = x_1 + x_2 + x_3 + \ldots + x_n. \tag{12}$$

Thus,

$$x^2 = \sum_{j=1}^{n} x_j^2 + 2 \sum_{j=1}^{n-1} \sum_{k=j+1}^{n} x_j x_k. \tag{13}$$

If each jump is independent of previous jumps, the summations of $x_j x_k$ on the average equal zero. For this case,

$$D_i^{\text{random}} = (2t)^{-1} \sum_{j=1}^{n} x_j^2. \tag{14}$$

In cubic crystals, eq (14) reduces to

$$D_i^{\text{random}} = \frac{1}{6} \lambda^2 \nu, \tag{15}$$

where λ is the jump distance and ν is the atom jump frequency (including jumps in all possible directions).

For a correlated walk, one obtains instead

$$D_i^* = f D_i^{\text{random}}. \tag{16}$$

Here the correlation factor f is defined as equalling the ratio $D_i^*/D_i^{\text{random}}$; and, from eq (13),

$$f = 1 + \frac{2 \sum_{j=1}^{n-1} \sum_{k=j+1}^{n} \langle x_j x_k \rangle}{\sum_{j=1}^{n} x_j^2}. \tag{17}$$

In cubic crystals, it follows that the tracer diffusion coefficient can be expressed simply as

$$D_i^* = \frac{1}{6} \lambda^2 \nu f. \tag{18}$$

Equation (17) is the equation which is usually used to calculate the correlation factor. A number of investigators have calculated values of f for various circumstances from this equation [4]. In particular, very general matrix equations have been developed by Howard [5].

3.2. Correlation Effects in Terms of Effective Jump Frequencies

The calculation of f from eq (17) is directly applicable only to the D_i^* or $\langle x^2 \rangle$ terms in the diffusion equations [i.e., the width of the tracer profile in figure 1 and first term on the right in eq (10)]. By itself, eq (17) does not provide information about the effect of a correlated walk on $\langle v_F \rangle_i$ or $\langle x \rangle$ [i.e., the shift of the tracer profile in figure 1b and the second term on the right in eq (10)]. In addition, the mathematical equations leading to eq (17) do not provide a convenient physical model for discussion of correlation effects. For these reasons, an alternate but still rigorous approach for calculation of correlation effects will be presented here. The majority of the discussion will be in terms of diffusion by a vacancy mechanism, but the same reasoning can be applied to diffusion by an interstitialcy mechanism.

If diffusion normal to a set of sufficiently close-packed planes is considered, the correlated walk equations can be expressed in terms of an equivalent random walk with the actual jump frequencies, Γ_{12} and Γ_{21}, in eqs (8) and (9) being replaced by effective frequencies of independent displacement, Γ_{12}^e and Γ_{21}^e. Each close-packed plane must be such that a vacancy on one side of the plane cannot pass to the other side of the plane without at some time stopping at a lattice site on this plane. In cubic crystals, the (100) planes are suitable planes. Any vacancy which arrives on the same plane as a particular tracer atom can be said to have randomized its position with respect to the tracer, since in the absence of driving forces the vacancy is just as likely to cause future jumps of the tracer in the $-x$ direction as the $+x$ direction. Even with a driving force, the distortions of the vacancy flux introduced by the tracer will not change the vacancy concentration on this plane. Thus, vacancy paths which start from this plane can be treated as being uncorrelated to previous jumps of the vacancy and the tracer.

With this background, let us consider a series of exchanges of a tracer with a given vacancy V. After an initial exchange which moves the atom a distance d in the $+x$ direction, the vacancy V is

in the proper position to allow a reverse jump taking the atom back to its original plane. There is probability P that such a jump will be caused by vacancy V (this may occur either immediately or after the vacancy has wandered through the lattice for some time) and probability $1-P$ that the vacancy instead moves to a vacancy sink or to a site on the plane containing the tracer. In these latter cases, the correlated series of atom-vacancy exchanges is terminated and the next tracer jump starts a new jump series which is uncorrelated to previous jumps. Unless at some time the correlated jump series is terminated in this way, the atom and vacancy will continue to jump back and forth between the two neighboring planes, contributing many atom jumps but resulting in almost no net x displacement of the atom.

If a series of correlated jumps contains an odd number of jumps, there is net displacement d, and if the series contains an even number of jumps there is zero net x displacement. The probability U that a correlated series results in a net x displacement of magnitude d is given by

$$U = 1-P+P^2-P^3+\ldots=(1+P)^{-1}. \quad (19)$$

Here the nth term in the series equals the probability that the correlated series contains at least n jumps.

Only a fraction of the jumps will be the first jump in a series. This fraction equals $1-P$, the probability that another series terminated on the previous jump. Therefore, the probability that a given jump starts a series which results in net displacement d equals $U(1-P)$. Displacements resulting from separate series are independent of one another. As a result, when there are no kinetic driving forces, an effective frequency Γ^e of independent displacements (all of magnitude d) can be defined in terms of the actual jump frequency Γ^a as

$$\Gamma^e=\Gamma^a[U(1-P)]=\Gamma^a\frac{1-P}{1+P}. \quad (20)$$

or

$$\Gamma^e=\Gamma^a f, \quad (21)$$

where the correlation factor f is given by

$$f=\frac{1-P}{1+P}. \quad (22)$$

For crystals to which the present treatment applies, eq (22) for the correlation factor is the same as that obtained from eq (17). It can be seen that the correlation factor equals the fraction of jumps which result in independent displacements, with the displacement neither canceling previous jumps nor being cancelled by succeeding, correlated jumps.

Substituting the value of Γ^e from eq (21) in place of Γ in eq (8) yields

$$D_i^*=\Gamma^a f d^2. \quad (23)$$

For cubic crystals, this is equivalent to eq (18).

3.3. Values of the Correlation Factor

The probability P can be calculated from the crystal geometry in terms of the vacancy jump frequencies in the crystal. For self-diffusion, P and hence the correlation factor f are numerical constants depending on the crystal structure. To first order, P for self-diffusion equals z^{-1}, where z is the number of nearest neighbors to which a vacancy can jump. More careful calculations show that P for self-diffusion is somewhat larger than z^{-1} since even those vacancy paths which do not cause an immediate vacancy-tracer exchange can eventually allow such an exchange to occur. To two significant figures, f is 0.78 for self-diffusion in face-centered cubic crystals (or NaCl sub-lattices), 0.73 in body-centered cubic crystals, 0.65 in simple cubic crystals (or CsCl sublattices), and 0.50 in diamond [6].

Values of f when diffusion is by an interstitialcy mechanism differ from those for a vacancy mechanism. For example, in the face-centered-cubic case, f equals $\frac{2}{3}$ when diffusion is by a collinear interstitialcy mechanism. For self-diffusion by exchange or direct interstitial mechanisms, f equals unity. This dependence of f on the diffusion mechanism can help in experimental determination of the diffusion mechanism.

For anisotropic diffusion, the correlation factor usually will be different for diffusion along each principal axis. Values for the aluminum sublattice in corundum are given in table 1. Here the correlation factors f_x and f_z depend strongly on the jump frequency ratio ν_z/ν_x. If f_x or f_z were measured, the corresponding value of ν_z/ν_x could be found.

For diffusion of impurities, the correlation factor depends on the vacancy jump frequencies near the impurity. For example, in a face-centered cubic crystal (or NaCl sublattice), the vacancy jump frequencies can be defined in a 5-frequency model as w_1 for a jump which moves the vacancy from one site neighboring on the impurity to another such site, w_2 for exchange with the impurity, w_3 for dissociation from the impurity by a jump from a nearest neighbor site to a nonnearest neighbor site, w_4 for

290-621 O-68—5

Table 1. *Correlation factors for diffusion via vacancies in the aluminum sublattice of corundum* [a]

ν_z/ν_x [b]	$f_x=f_y$ [c]	f_z [d]
0	0.33	1.00
10	0.50	0.65
∞	0.66	0.36

[a] After Compaan and Haven. These and additional values are given in reference [6].
[b] ν_z = jump frequency along z-direction.
ν_x = jump frequency in xy plane.
[c] $f_x=f_y$ = correlation factor for jumps in xy plane.
[d] f_z = correlation factor for jumps along the z-direction.

the reverse of a w_3 jump, and w_0 for all other jumps. Then

$$P=\frac{w_2}{w_2+2w_1+7Fw_3}, \tag{24}$$

where F depends on the ratio w_4/w_0 and ranges from 2/7 to unity [7], and

$$f=\frac{2w_1+7Fw_3}{2w_2+2w_1+7Fw_3}. \tag{25}$$

For a fast-diffusing impurity, where w_2 is much larger than w_1 or w_3, f can become nearly equal to zero, yielding a large correlation effect. Then the tracer diffusion coefficient D_i^* in eq (18) is proportional to $w_1+3.5Fw_3$ rather than to w_2 (ν itself is proportional to w_2, but νf in this case is proportional to $w_1+3.5Fw_3$). On the other hand, if w_2 is much smaller than w_1 or w_3, f can become almost unity, and there is only a small correlation effect.

The introduction of the additional jump frequencies w_1, w_3, etc., into the relation between D_i^* and ν prevents a direct determination of ν from measurements of D_i^*. If the factor f can be measured, however, not only are calculations of ν again possible but also eq (25) provides a relation between the three ratios w_1/w_2, w_1/w_3, and w_4/w_0 (for jumps of solvent atoms near the impurity). Other relations between these ratios can be found by measuring μ_i/D_i^*, as described later in this paper; by measuring D_i^*/D_s^*, where D_s^* is the solvent diffusion coefficient; or by measuring the coefficient b which describes the change in solvent diffusion coefficient upon the addition of impurities [8]. Where vacancy-impurity complexes are formed, dielectric and mechanical relaxation experiments also can yield relations between these jump frequency ratios.

3.4. Isotope Effect

One means of measuring the correlation factor experimentally is by isotope effect experiments. Two isotopes of the same diffusing element will have different masses and hence can be expected to have different jump frequencies. In crystals where each jump vector lies along an axis of at least two-fold or three-fold rotational symmetry [9],

$$\frac{\Delta D^*}{D_\alpha^*}=f_\beta\frac{\Delta w_2}{w_{2\alpha}}. \tag{26}$$

Here $\Delta D^*=D_\beta^*-D_\alpha^*$ and $\Delta w_2=w_{2\beta}-w_{2\alpha}$, where subscripts α and β refer to the two isotopes and w_2 is the isotope jump frequency.

According to classical rate theory, w_2 is proportional to the inverse of the square root of the isotope mass, making

$$\frac{\Delta w_2}{w_{2\alpha}}=\left(\frac{m_\alpha}{m_\beta}\right)^{1/2}-1. \tag{27}$$

In applying eq (27) to real cyrstals, however, the masses m_α and m_β should be reduced masses which take into account the masses of the other atoms in the crystal which must move to allow the diffusing isotopes to jump [10]. The usual procedure is to treat m_α and m_β as being the actual masses of the isotopes but then to multiply the right-hand side of eq (27) by a factor ΔK to correct for the reduced masses [11, 12]. Thus,

$$\frac{\Delta D^*}{D_\alpha}=f_\beta\Delta K\left[\left(\frac{m_\alpha}{m_\beta}\right)^{1/2}-1\right]. \tag{28}$$

It is predicted [11, 12] that ΔK will equal approximately 0.5 for diffusion by an interstitialcy mechanism, since approximately half the kinetic energy for the interstitialcy jump is carried by each of the two atoms cooperating in the jump. Also, in general, if n atoms participate equally in a jump, such as by a ring mechanism, ΔK would equal n^{-1}. For direct interstitial and vacancy mechanisms, value of ΔK near unity might be expected since only one atom really makes a jump.

The product $f_\beta\Delta K$ can be determined by measuring $\Delta D^*/D_\alpha$ with the true isotope masses m_α and m_β in eq (28) being known. For diffusion of small interstitial atoms, which certainly diffuse by a direct interstitial mechanism, it is usually found that $f_\beta\Delta K$ equals unity within experimental error. Since f_β for the direct interstitial mechanism is unity, it follows that ΔK also is near unity, as expected. For a vacancy mechanism in a face-centered cubic crystal or NaCl sub-lattice, f_β equals 0.78. Values somewhat smaller than this

have been measured for $f_\beta \Delta K$ ($\simeq 0.7$) in NaCl [13], indicating that $\Delta K \simeq 0.9$ in this case if it is assumed that diffusion occurs entirely by means of free vacancies.

Experimentally determined values of the product $f_\beta \Delta K$ can be used to distinguish between different possible diffusion mechanism, since predicted values of this product for self-diffusion depend strongly on the diffusion mechanism [14]. Here the factor ΔK, although it makes the relation between $\Delta D^*/D^*_\alpha$ and m_β/m_α more complex, greatly aids in distinguishing between the possible mechanism. For example, the correlation factors for self-diffusion by direct interstitial and ring mechanisms are both unity but the values of ΔK differ greatly.

For self-diffusion in an isotropic crystal, the correlation factors are known numerical constants. Thus, if the diffusion mechanism is known, ΔK can be calculated from measured values of $f_\beta \Delta K$. For impurity diffusion, however, values of f_β are normally not known. Since only the product of $f_\beta \Delta K$ can be measured, an estimate must be made of ΔK, perhaps by assuming that it is the same as for self-diffusion, if one wishes to determine f_β from isotope effect measurements.

4. The Drift Term and Ionic Conductivity

To this point, the discussion of non-random effects has been concerned mainly with the effect of correlation on the tracer diffusion coefficient D_i^*, which appears in the first term on the right in eq (10). Equally important are effects on $\langle v_F \rangle_i$, the quantity which appears in the *second* term on the right in eq (10).

4.1. Correlation Effects on $\langle v_F \rangle_i$

In the discussion of correlation factor effects in terms of the probability P, it was shown that in the absence of driving forces the actual jump frequency Γ^a for a given type of jump is related to an effective frequency Γ^e of independent displacements. It can be shown [2] that this type of discussion is valid even when there is a driving force. Thus, one can write

$$\Gamma^e_{12} = f \Gamma^b_{12} \tag{29}$$

$$\Gamma^e_{21} = f \Gamma^b_{21} \tag{30}$$

where f is given by eq (22) with P evaluated in the absence of driving forces. The frequencies Γ^e of independent displacement can be substituted into eq (9) to yield $\langle v_F \rangle_i$. The basic jump frequencies Γ^b equal the actual jump frequencies Γ^a in the absence of kinetic driving forces multiplied by $[1 + (F_i x_i / 2kT)]$, where F_i is the net kinetic driving force, x_i is the x displacement resulting from the jump, k is Boltzmann's constant, and T is the absolute temperature. These relations can be substituted into eq (9) with Γ^e taking the place of Γ to yield,

$$\langle v_F \rangle_i = \Gamma^a f d^2 (F_i / kT), \tag{31}$$

where d is the interplanar spacing.

It may be noted that the same correlation factor appears in eq (31) as in eq (23). Thus, eq (31) can be rewritten as

$$\langle v_F \rangle_i = \frac{D_i^* F_i}{kT}, \tag{32}$$

where D_i^* is the tracer diffusion coefficient measured in a homogeneous system in the absence of kinetic driving forces.

4.2. Vacancy Wind Effect in an Electric Field

By definition, the kinetic driving forces are any influences which make a jump by an atom in one direction between two neighboring sites more likely than a jump in the opposite direction between these same two sites. An electric field E acting on the charged ions in a crystal can provide such a driving force F_i^E with

$$F_i^E = q_i E, \tag{33}$$

where q_i is the charge of the diffusing ion. In kinetic terms, such a field changes the effective energy of motion for jumps with and opposed to the field.

In addition to the direct force exerted on the ions, there also can be an indirect force. This indirect force arises if the field also acts on the other ions in the sublattice in which a given ion is diffusing. If diffusion is by a vacancy mechanism and the field drives these other ions in the $+x$ direction, there will be an equal flow of vacancies in the $-x$ direction. As a result, vacancies will approach any given ion more frequently from the $+x$ direction than the $-x$ direction. This causes the given ion to begin a series of vacancy-ion interchanges more frequently with a $+x$ jump than with a $-x$ jump.

In the discussion of correlation effects, it was found that a correlated series can be treated as giving either zero net x displacement (if there are an even number of jumps in the series) or a displacement equal to that from the first jump (if there are an odd number of jumps in the series). Detailed analysis [2] shows that if the first exchange is more likely to be in the $+x$ direction an additional kinetic

driving force F_i^β in effect is exerted on the ion, with the force for an isolated impurity being given by

$$F_i^\beta = 2q_s E\langle n_{jp}\rangle, \tag{34}$$

where q_s is the charge of the other (solvent) ions in the sublattice and $\langle n_{jp}\rangle$ is a complex kinetic quantity, expressions for which are given in reference [15]. In kinetic terms, $\langle n_{jp}\rangle d$ equals the average net x displacement a vacancy which starts its path on a site on the $+x$ side of the impurity would undergo upon traveling to a vacancy sink if exchanges with the impurity were not allowed and there were no kinetic driving forces. This same equation applies for diffusion by an interstitialcy mechanism if "interstitialcy" is substituted for "vacancy" in the definition of $\langle n_{jp}\rangle$.

If the only driving forces are those arising from the electric field, eqs (32) to (34) yield for a vacancy mechanism

$$\langle v_F\rangle_i = \frac{ED_i^*}{kT}\left(q_i + 2q_s\langle n_{jp}\rangle\right). \tag{35}$$

Here the first term inside the parenthesis arises from the direct force on the charged ions, and the second term from the influence of the vacancy flow. This latter effect can also be called a "vacancy wind" effect.

Vacancy wind effects arise whenever there is a flow of vacancies. The relation of vacancy wind effects to correlation effects is discussed in reference [16]. For self-diffusion, q_i equals q_s and $1+2\langle n_{jp}\rangle = f^{-1}$, where f is the correlation factor. In eq (35) correlation effects introduce a factor f into the expression for D_i^*, whereas the vacancy wind effect makes the factor in parentheses equal f^{-1}. Thus, in the expression for $\langle v_F\rangle_i$, the factor arising from vacancy wind effects exactly balances f in D_i^* arising from correlation effects. In other words, the vacancy wind and correlation factor effects on $\langle v_F\rangle_i$ exactly cancel one another for self-diffusion, being equal and opposite effects in this case. For impurity diffusion, however, these effects usually do not cancel each other. For impurity diffusion, the vacancy wind term $2q_s\langle n_{jp}\rangle$ makes the factor in parentheses in eq (35) differ from q_i but usually does not make this factor equal exactly $q_i f^{-1}$. Explicit equations for impurity diffusion are given in section 4.4.

4.3. Drift Mobility and Ionic Conductivity

The ionic drift mobility μ_i of species i in an electric field is defined as the average drift velocity $\langle v_F\rangle_i$ per unit field. Thus,

$$\mu_i E = \langle v_F\rangle_i. \tag{36}$$

When there is a constant electric field and no driving forces except those from the electric field, the shift $\langle x\rangle$ in the tracer profile shown in figure 1b is given by

$$\langle x\rangle = \mu_i E t. \tag{37}$$

Also, the ionic conductivity σ_i contributed by species i is

$$\sigma_i = c_i\mu_i q_i, \tag{38}$$

where c_i is the number of i atoms per unit volume and q_i is their charge.

Experimentally, μ_i could be determined from either eq (37) or eq (38). The total conductivity σ is given by

$$\sigma = \Sigma_i\sigma_i, \tag{39}$$

where the summation is over all charge carriers in the crystal, including electrons. Thus, the fraction of the conductivity contributed by species i must be known before measurements of σ can be used to determine μ_i.

For diffusion by a vacancy mechanism, eqs (35) and (36) yield

$$\frac{\mu_i}{D_i^*} = \frac{q_i}{kT}\left[1 + 2\langle n_{jp}\rangle\frac{q_s}{q_i}\right]. \tag{40}$$

The similar equation for diffusion by a collinear interstitialcy mechanism (where both cooperating atoms move along the same line) is

$$\frac{\mu_i}{D_i^*} = \frac{q_i + q_s}{kT}\left[1 + 2\langle n_{jp}\rangle\frac{q_s}{q_i + q_s}\right]. \tag{41}$$

Here the direct force affecting a jump of the impurity is $E(q_i + q_s)$, since a solvent ion must also move during the interstitialcy jump.

In the special case of self-diffusion, the quantities inside the square brackets in eqs (40) and (41) equal f^{-1}, where f is the correlation factor [15]. Then, for a vacancy mechanism,

$$\frac{\mu_i}{D_i^*} = \frac{q_i}{kTf}. \tag{42}$$

For self-diffusion (where $q_i = q_s$) by a collinear interstitialcy mechanism,

$$\frac{\mu_i}{D_i^*} = \frac{2q_i}{kTf}. \tag{43}$$

Equation (43) for the collinear interstitialcy mechanism differs by a factor 2 from eq (42) for the vacancy mechanism. In addition, the numerical values of the correlation factor depend on the diffusion mechanism, being 0.78 for a vacancy mechanism in a face-centered cubic structure and $\frac{2}{3} \simeq 0.67$ for a collinear interstitialcy mechanism in this structure. Thus, measurements of μ_i/D_i^* provide information about the diffusion mechanism.

For self-diffusion, the ratio μ_i/D_i^* can be derived by noting that the net flux of ionic charge in a given sublattice is proportional to the vacancy or interstitialcy flux. When there are no impurities, motion of these defects is not correlated; whereas motion of the ions, which contributes to D_i^*, is correlated. Thus, the ratio of μ_i/D_i^* contains the factor f^{-1}. In addition, the jump vector of the interstitialcy imperfection differs from that of either ion cooperating in the jump. Thus, the ratio μ_i/D_i^* also contains a displacement factor S, where

$$S = \frac{\lambda_{\text{defect}}^2 \nu_{\text{defect}} c_{\text{defect}}}{\lambda_{\text{atom}}^2 \nu_{\text{atom}} c_{\text{atom}}}. \tag{44}$$

Here λ is the jump distance of the atom or the defect during an elementary jump, ν the jump frequency per atom or defect, and c the number of atoms or defects per unit volume. For interstitialcies, there are two atom jumps for each interstitialcy jump, making $\nu_{\text{atom}} c_{\text{atom}} = 2\nu_{\text{defect}} c_{\text{defect}}$. Also, for a collinear interstitialcy mechanism, $\lambda_{\text{defect}} = 2\lambda_{\text{atom}}$, making $S = 2$. On the other hand, for a vacancy mechanism, $S = 1$.

In general, equations such as (42) and (43) relating μ_i to D_i^* for self-diffusion by means of isolated defects can be written as

$$\frac{\mu_i}{D_i^*} = \frac{q_i S}{kTf}. \tag{45}$$

Also, one can define a quantity D_σ in terms of the measured conductivity σ,

$$D_\sigma = \frac{\sigma kT}{c_i q_i^2}. \tag{46}$$

If only one species contributes to the ionic conductivity and eq (45) is valid for this species,

$$\frac{D_\sigma}{D_i^*} = Sf^{-1}. \tag{47}$$

Values of S, f^{-1} and Sf^{-1} for various mechanisms are listed in table 2. Because of the difference in these values for the different mechanisms, a measurement of Sf^{-1} can help to establish the diffusion mechanism.

As in the case of the isotope effect, it is not just the correlation factors which enter here. Instead there is an additional factor, S in this case and ΔK in the isotope effect case, which has an important influence on the results.

TABLE 2. *Correlation and displacement factors for self-diffusion in silver chloride*

Diffusion mechanism	f^{-1}	S	$D_{\sigma i}/D_i^* = Sf^{-1}$
Direct interstitial	1.00	1.00	1.00
Vacancy	1.28	1.00	1.28
Noncollinear interstitialcy ($\theta \cong 70.5°$) [a]	1.03	1.33	1.37
Collinear interstitialcy ($\theta = 0$) [a]	1.50	2.00	3.00

[a] θ = angle between the jump vectors of the two atoms cooperating in the interstitialcy jump.

Measurements on silver diffusion in AgCl and AgBr indicate that Sf^{-1} is less than 3.00 but larger than 1.37. It is thought that a combination of collinear and noncollinear interstitialcy jumps is present in these cases [17].

If diffusion proceeds in part by means of bound anion vacancy–cation vacancy pairs, the motion of these pairs will contribute to D_i^* but not to μ_i or D_σ. This situation would make μ_i/D_i^* and D_σ/D_i^* smaller than the values predicted in eqs (45) and (47). Thus, if vacancies are known to be the dominant defect, values of D_σ/D_i^* (or $\mu_i kT/D_i^* q_i$) smaller than the f^{-1} value for a vacancy mechanism may suggest the presence of vacancy pairs, as for example in TlCl [17].

On the other hand, larger values of D_σ/D_i^* may be obtained if the total conductivity σ is larger than σ_i, as will occur when electrons or ions on the other sublattice carry appreciable current. In such a case, it is necessary to know the transport number of species i and substitute σ_i in place of σ in eq (46) if one wishes to measure Sf^{-1}. The ratio μ_i/D_i^* may provide a more definite measurement of Sf^{-1} in this case, since it is not affected by these other contributes to σ.

4.4. Drift Mobility for Impurity Diffusion

For diffusion of impurities, the quantities in square brackets in eqs (40) and (41) in general do not equal f^{-1} and can differ greatly from this value. For example, in a NaCl sublattice, the vacancy jump frequencies near an impurity are defined above eq (24). For these frequencies [15],

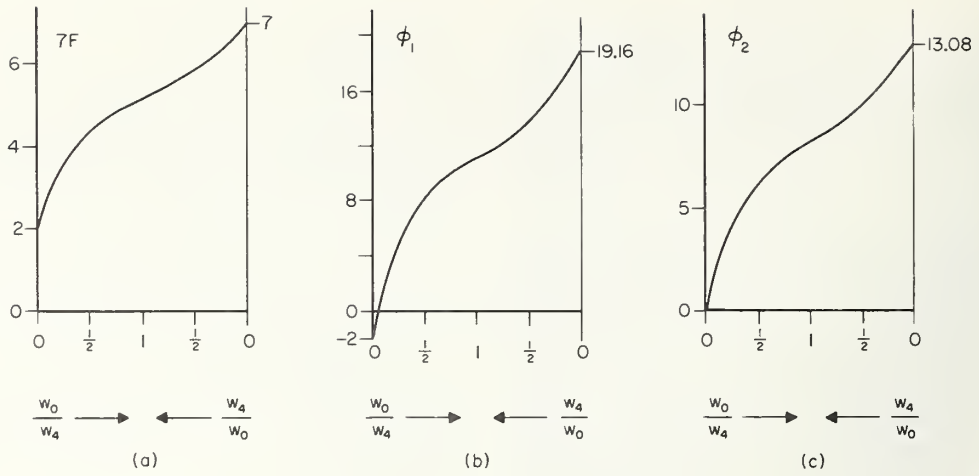

FIGURE 2.
(a) Value of $7F$, which appears in eqs (24) and (48) to (52), as a function of w_4/w_0 and w_0/w_4.
(b) Value of ϕ_1, which appears in eq (49), as a function of w_4/w_0 and w_0/w_4.
(c) Value of ϕ_2, which appears in eq (51), as a function of w_4/w_0 and w_0/w_4.

$$\langle n_{jp}\rangle = \frac{-2w_1 + w_3[3 - 7(1-F)(w_4 - w_0)w_4^{-1}]}{2w_1 + 7Fw_3}. \tag{48}$$

For a divalent impurity diffusing in a divalent cation sublattice, $q_i = q_s = 2e$. With diffusion by a vacancy mechanism on a sublattice of a crystal with the NaCl structure, eqs (40) and (48) then yield

$$\frac{\mu_i}{D_1^*} = \frac{2e}{kT}\left[\frac{-2w_1 + \phi_1 w_3}{2w_1 + 7Fw_3}\right], \tag{49}$$

where

$$\phi_1 = 6 + 7F - 14(1-F)(w_4 - w_0)w_4^{-1}. \tag{50}$$

Values of $7F$ and ϕ_1, which depend only on the ratio w_4/w_0, are presented in figures 2a and 2b.

For a tetravalent impurity diffusing in a divalent cation sublattice, $q_i = 4e$ and $q_s = 2e$. With diffusion by a vacancy mechanism on a sublattice of a crystal with the NaCl structure, it follows in this case from eqs (40) and (48) that

$$\frac{\mu_i}{D_i^*} = \frac{4e}{kT}\left[\frac{\phi_2 w_3}{2w_1 + 7Fw_3}\right], \tag{51}$$

where

$$\phi_2 = 3 + 7F - 7(1-F)(w_4 - w_0)w_4^{-1}. \tag{52}$$

Values of $7F$ and ϕ_2, which depend only on the ratio w_4/w_0, are plotted in figures 2a and 2c. Here it is assumed that there is a uniform vacancy concentration much larger than the concentration of tetravalent impurities i.

4.5. Cross Terms in the Thermodynamic Diffusion Equations

It can be seen from eqs (48) to (52) and figure 2 that the vacancy wind contribution to μ_i/D_i^* [the term containing $\langle n_{jp}\rangle$ in eq (40)] can be large and in fact can even be larger than the contribution from the direct force exerted by the electric field on the charged ions. As a result, the deviation from the Nernst-Einstein relation ($\mu_i/D_i^* = q_i/kT$) can be large.

For a system with two atom species (A and B) and with vacancies in equilibrium, the general thermodynamic diffusion equations can be written as

$$J_A = L_{AA}X_A + L_{AB}X_B,$$

$$J_B = L_{BA}X_A + L_{BB}X_B. \tag{53}$$

Where X_A and X_B are the thermodynamic driving forces for species A and B. Howard and Lidiard [18] have shown that, if the cross-coefficient L_{BA} is non-zero, deviations from the Nernst-Einstein relation can be expected. In the present equations, the quantity $2\langle n_{jp}\rangle$ in eqs (40) and (41) equals L_{BA}/L_{BB}, and L_{BB} for diffusion of the dilute impurity B equals $D_B^* c_B/kT$. Thus, explicit values of L_{BA} can be determined.

The vacancy wind contribution to $\langle v_F\rangle_i$ appears here entirely as a contribution to L_{BA}. As expected, this term causes deviations from the Nernst-Einstein relation. Even for self-diffusion, this cross term is not negligible, since then $2\langle n_{jp}\rangle$ equals $(1-f)/f$.

5. Vacancy-Impurity Complexes

When an aliovalent impurity is introduced into an ionic crystal, vacancies may also be introduced in order to maintain charge neutrality, making the concentration of vacancies depend on the concentration of impurities. In this case, it is convenient to consider the vacancy-impurity complexes as the diffusing units, with the probability that an impurity is part of a complex being a function of impurity concentration. Lidiard [19] has treated in detail the diffusion of divalent impurities in monovalent sub-lattices (which is similar to tetravalent impurities in divalent sub-lattices). Two effects which enter these calculations are the diffusion potential and the variation with impurity concentration of the probability p that an impurity is associated with a vacancy in a complex.

The diffusion potential arises because vacancies tend to diffuse down their gradient faster than do the impurities, causing a separation of charge and hence a local electric field. The resulting diffusion potential prevents a further separation of charge. This keeps the vacancies in the vicinity of the impurities and thus allows the diffusion problem to be treated entirely in terms of the vacancy-impurity complexes. The homogeneous thermoelectric power arises from the same type of internal electric field as does the diffusion potential. In the case of the homogeneous thermoelectric power, there is a separation of charge by diffusion of two kinds of defects, cation and anion vacancies if there is Schottky disorder or vacancies and interstitials if there is Frenkel disorder.

The variation of p with concentration can have a strong effect on the diffusion coefficient. One can distinguish two types of experiments: (1) Tracer experiments can be performed where the number of aliovalent ions and accompanying vacancies introduced with the tracer is small compared to the vacancy concentration already present in the crystal. This already-present vacancy concentration may be the intrinsic concentration for a given temperature; or, in doped crystals, it can arise from vacancies introduced by other aliovalent ions present in uniform concentration throughout the crystal. In the latter case, p depends on the uniform concentration of aliovalent ions and not on the tracer concentration. Since the jump frequency ν equals $w_2 p$, where w_2 is the vacancy-impurity exchange frequency in the complex, eq (18) becomes

$$D_i^* = \frac{1}{6} \lambda^2 w_2 p f. \tag{55}$$

(2) In the other limit, experiments can be performed in which a large number of aliovalent ions are introduced along with the radioactive tracer ions as carrier (being nonradioactive ions of the same chemical element as the tracer ions), making the additional vacancy concentration much larger than that normally present. In this limit, Lidiard [19] has shown for a divalent impurity diffusing in a monovalent sublattice that

$$J_i = -D_i^* \frac{2}{1+p} \frac{\partial c_i}{\partial x}. \tag{56}$$

The factor $2/(1+p)$ arises because the concentration gradient of complexes is not directly proportional to the concentration gradient of tracer. Also, p is determined by the total concentration of aliovalent ions, i.e., tracer plus carrier, in the particular part of the crystal.

Lidiard's pair-association model [19] is especially useful in treating vacancy-impurity complexes and in deriving equations such as eq (56) above. Also, this model can be applied in general to dilute alloys if dissociation of vacancy-impurity complexes is taken into account. When this is done, the pair association model and the correlated walk model presented earlier in this paper give identical results.

6. References

[1] A. D. LeClaire, Phil. Mag. **3**, 921 (1958).
[2] J. R. Manning, Phys. Rev. **139**, A126 (1965).
[3] A. Einstein, Ann. Physik **17**, 549 (1905).
[4] See for example discussions in Y. Adda and J. Philibert, La Diffusion dans les Solides. (Presses Universitaires de France, Paris, 1966) Chapter 7; or in J. R. Manning, Diffusion Kinetics for Atoms in Crystals, Ch. 3 (D. Van Nostrand Co., Inc., Princeton, 1968).
[5] R. E. Howard, Phys. Rev. **144**, 650 (1966).
[6] K. Compaan and Y. Haven, Trans. Faraday Soc. **52**, 786 (1956); **54**, 1498 (1958).
[7] J. R. Manning, Phys. Rev. **136**, A1758 (1964).
[8] R. E. Howard and J. R. Manning, Phys. Rev. **154**, 561 (1967).
[9] A. H. Schoen, Phys. Rev. Letters **1**, 138 (1958); K. Tharmalingam and A. B. Lidiard, Phil. Mag. **4**, 899 (1959).
[10] G. H. Vineyard, J. Phys. Chem. Solids **3**, 121 (1957).
[11] J. G. Mullen, Phys. Rev. **121**, 1649 (1961).
[12] A. D. LeClaire, Phil. Mag. **14**, 1271 (1966).
[13] L. W. Barr and A. D. LeClaire, Proc. Brit. Ceram. Soc. **1**, 109 (1964).
[14] L. W. Barr and J. N. Mundy, Diffusion in Body-Centered Cubic Metals, p. 171 (American Society for Metals, Metals Park, Ohio, 1965).
[15] J. R. Manning, Phys. Rev. **139**, A2027 (1965).
[16] J. R. Manning, Can. J. Phys. (to be published).
[17] See for example the review article, R. J. Friauf, J. Appl. Phys. **33** (Suppl. 1), 494 (1962).
[18] R. E. Howard and A. B. Lidiard, J. Phys. Soc. Japan **18** (Suppl II), 197 (1963); Reports on Progress in Physics **27**, 161 (1964).
[19] A. B. Lidiard, Phil. Mag. **46**, 815 (1955); **46**, 1218 (1955).

Chemical Diffusion Coefficients for Some Nonstoichiometric Metal Oxides

J. Bruce Wagner, Jr.

Department of Materials Science, Northwestern University, Evanston, Illinois 60201

The chemical diffusion coefficient, $\tilde{D}$, is the proportionality constant in Fick's law when the diffusion process occurs under a concentration (activity) gradient.

The chemical diffusion coefficients may be obtained from: (1) data of parabolic oxidation of a metal when certain stringent boundary conditions are met, (2) measurement of the change in weight as a function of time for an initially homogeneous oxide crystal which is exposed isothermally to an oxidizing or reducing atmosphere, (3) measurement of the electronic conductivity as a function of time under the same conditions as in (2), and (4) measurement of a color change as a function of time under the same conditions as in (2).

Available values of $\tilde{D}$ in cm^2/sec using methods (2) and (3) are:

$\tilde{D}_{MnO} \approx 10^{-6}$	(1150 °C)
$\tilde{D}_{FeO} = 74.1 \exp[-15.36\ (O/Fe)]$	(1100 °C)
$\tilde{D}_{CoO} = 4.33 \times 10^{-3} \exp(-24{,}000)/RT$	(800–1100 °C)
$\tilde{D}_{NiO} = 7.52 \times 10^{-4} \exp(-21{,}900)/RT$	(800–1100 °C)

Under the assumption that the self diffusion coefficient of the anion is much less than that of the cation, values of the cation tracer diffusion coefficient have been calculated from the chemical diffusion coefficient using the analyses of C. Wagner [Z. physik Chem. **B32,** 447 (1936)] and of Darken [Trans. AIME **175,** 184 (1948)]. These calculated values of tracer diffusion coefficients are in good agreement with experimental values reported in the literature.

Key Words: Chemical diffusion, electronic conductivity, self diffusion, tracer diffusion.

1. Introduction

Diffusion processes occurring under a chemical potential gradient are important in the preparation of semiconductors, oxidation of metals, reduction of ores, reactions in the solid-state, and sintering of oxides.

In the present context, the chemical diffusion coefficient is important in (1) materials characterization, i.e., it allows a calculation of the time necessary to equilibrate an oxide crystal with a given partial pressure of oxygen and (2) in certain cases the data can be used to help verify a particular lattice defect model in the crystal.

Examples are presented in which a nonstoichiometric oxide crystal is heated in a given oxygen partial pressure. The oxygen gas is removed from the experimental apparatus containing the crystal, and oxygen gas of a different partial pressure is admitted. So long as the crystal is stable in both these atmospheres, oxygen will be removed or added to the crystal as the case may be and for sufficiently thick samples, the addition or removal of oxygen will be controlled by diffusion. The proportionality constant in Fick's law for such processes will be termed the chemical diffusion coefficient and denoted by the symbol, $\tilde{D}$. It is sometimes termed an effective or interdiffusion coefficient.

2. Definition of Terms

We begin by defining some terms used in the present paper. The term, self diffusion coefficient, D_i^S, means here the coefficient in Fick's law when diffusion of the ith species in a crystal of which i is a component takes place in a crystal of constant composition and no chemical potential gradient of any of the components. Thus,

$$D_i^S = \lim_{(\partial c_i/\partial x)\to 0} \left[\frac{J_i}{(\partial c_i/\partial x)}\right]_{c_i} \tag{1}$$

where concentration, c, is used in place of activity, J_i denotes the flux and x is the distance into the crystal in the case of one-dimensional diffusion. The particles are assumed to move independently, i.e., cross terms in the flux equation are neglected. The self diffusion coefficient is in turn related to

the tracer diffusion coefficient, D_i^T, through a correlation factor, f, by

$$D_i^T = fD_i^S \tag{2}$$

where $f \leq 1$. Thus, tracer diffusion refers to diffusion of a tracer in a crystal of constant composition under no chemical potential gradient. Of course tracer diffusion can be and has been measured in crystals having a chemical potential gradient. However, the above terminology [eqs. (1) and (2)] seems generally accepted. The self diffusion coefficient of the ith species, D_i^S, is proportional to the diffusion coefficient for the defect responsible for the migration of the ith species. In the present paper only oxides with majority lattice defects as cation vacancies will be considered. Hence

$$D_i^S = X_{V_i} D_{V_i} \tag{3}$$

where X_{V_i} denotes the mole fraction of vacancies and D_{V_i} denotes the diffusion coefficient of vacancies.

In the present context, the process of chemical diffusion refers to diffusion which occurs in a concentration gradient or to the flow of a "deviation from stoichiometry" [1][1] through a crystal. The total flux $\tilde{J}$, is given by the algebraic sum of the two fluxes in a binary compound as

$$\tilde{J} = J_1 + J_2 \tag{4}$$

where the subscripts 1 and 2 denote the cation and anion, respectively. The chemical diffusion coefficient, $\tilde{D}$, is the proportionality constant in Fick's law,

$$\tilde{J} = \tilde{D}(\partial \tilde{c}/\partial x) \tag{5}$$

where $\tilde{c}$ is the absolute value of the concentration of the excess of one of the two components expressed in appropriate units. For example, for a metal deficit compound such as CoO, $\tilde{c}$ represents the excess of oxygen above that of the stoichiometric compound expressed in equivalents per cubic centimeter.

3. Methods of Determining the Chemical Diffusion Coefficient

The chemical diffusion coefficient can be determined by (1) the isothermal parabolic oxidation of a metal when stringent boundary conditions are met; (2) the change in weight of a crystal as a function of time when a crystal is initially equilibrated in a given atmosphere of oxygen and then the partial pressure of oxygen changed to a new value; (3) the change in electrical conductivity as a function of time for conditions as in (2); and (4) the movement of a color front in a crystal as a function of time for conditions as in (2).

Data obtained from the parabolic oxidation kinetics can be used to determine the self-diffusion coefficients as well as chemical diffusion coefficients. This method requires that the oxide growing on a metal be compact, exhibit no porosity, and maintain good contact with the metal, Moore [2, 3] has used this method to obtain the chemical diffusion coefficient in cuprous oxide and recently Pettit [4] has summarized the relation between activities and diffusion coefficients in a p-type oxide growing on a metal.

The thermogravimetric [5] and electronic conductivity [6, 7] methods of measuring the chemical diffusion coefficient are based upon the measurement of a property of the oxide crystal as the gradient in composition or the gradient in the deviation from stoichiometry is changed. The crystal is initially brought into equilibrium with a given partial pressure of oxygen. A different partial pressure of oxygen is introduced to the crystal at time zero. The surface of the crystal is assumed to come immediately into equilibrium with the gas phase, i.e., the chemical potential of oxygen at the oxide surface and gas phase are equal. A physical parameter is measured as a function of time as the crystal attains its new equilibrium state. In the case of a weight change, the solution to Fick's second law for a thin plate is

$$\log(1 - \Delta m/\Delta w) = \log\left(\frac{8}{\pi^2}\right) - \frac{\pi^2 \tilde{D} t}{9.2 a^2} \tag{6}$$

where Δm denotes the weight change of the crystal at any time, t; Δw denotes the weight change at the new equilibrium state (i.e., the total change in weight at the end of the experiment); and a is the half thickness of the slab. The equation for a brick-shaped sample of dimensions $2a$, $2b$, $2c$ is,

$$\log(1 - \Delta m/\Delta w) = \log\left(\frac{512}{\pi^6}\right) - \frac{\pi^2 \tilde{D} t}{9.2}\left(\frac{1}{a^2} + \frac{1}{b^2} + \frac{1}{c^2}\right). \tag{7}$$

In eqs (6) and (7) $\tilde{D}$ is assumed to be independent of composition. The applicability of this assumption will be discussed below.

[1] Figures in brackets indicate the literature references at the end of this paper.

When certain boundary conditions are fulfilled, the measurement of the weight change yields an unambiguous result for the chemical diffusion coefficient. For oxides where the change in weight is small, i.e., where there are small deviations from stoichiometry as is the case for NiO, CoO and MnO, it is more convenient to measure the electronic conductivity. This method is suitable when there is predominantly only one type of carrier, electrons or holes, and neither the mobility of the carrier nor the degree of ionization of lattice defects changes over the composition range of interest. In such cases, the ratio, $\Delta m/\Delta w$ in eqs (6) and (7) may be replaced by the ratio of the corresponding electronic conductivities $\Delta\sigma/\Delta\sigma_\infty$, as will be shown below.

Equations (6) and (7) are the solutions for diffusion into or out of a finite crystal. A useful cross check is to treat the initial kinetic data, Δm or $\Delta\sigma$ versus time for the beginning of the reequilibration, as diffusion into a semi-infinite crystal. Consider the solution for a slab. The initial kinetics before the center of the crystal changes composition, can be represented (5) by,

$$\left(\frac{\Delta m}{A}\right)^2 = k_p t \tag{8}$$

where k_p is a parabolic rate constant and

$$k_p = \frac{4\tilde{D}}{\pi}(\Delta c)^2. \tag{9}$$

In eq (9), Δc is the total change in cation concentration for a given experiment.

For the thermogravimetric method, an automatic recording balance is employed. For the electronic conductivity method, the crystal is wrapped with four platinum wires, two for current leads and two for the IR drop. A conventional d-c measuring circuit is used. The gases may be mixtures of CO and CO_2 or argon and oxygen metered in known amounts by means of capillary flow meters. In order to minimize thermal segregation, a minimum linear flow velocity of 0.9 cm/sec is recommended [8]. Initially the crystal is equilibrated at a given temperature and oxygen partial pressure. The gas flow is terminated and a new gas mixture of a different oxygen partial pressure is admitted. The time when the new gas front reaches the crystal is taken as time zero for the experiment, i.e., when the sample just begins to change weight or conductivity. Weight changes or conductivity changes are taken as a function of time until the new equilibrium state is attained.

The movement of a color front as a function of time in single crystals of nickelous oxide has been used by Slack [9] to obtain the diffusion coefficient of cation vacancies. A detailed description of this experiment is not available.

It is the purpose of the present paper to discuss available data for a series of nonstoichiometric oxides, MnO, FeO, CoO, and NiO. Emphasis will be placed on methods (2) and (3) listed above.

4. Relation Between the Chemical Diffusion Coefficient, Self-Diffusion Coefficient and Tracer Diffusion Coefficient

The relation between the chemical diffusion coefficient and the self-diffusion coefficients was first formulated by C. Wagner [10], especially for the understanding of oxidation of metals. However, his theoretical analysis was not restricted to the oxidation of metals. His equation for a binary compound semiconductor that is predominantly an electronic conductor and that exhibits only small deviations from stoichiometry is,

$$\tilde{D} = \{|z_1|D_1^s + |z_2|D_2^s\} \cdot \frac{c_{eq}}{\tilde{c}} \cdot \left[\frac{1}{RT}\frac{\partial \mu_{Me}}{\partial \ln \tilde{c}}\right] \tag{10}$$

where the subscripts 1 and 2 denote respectively the cation and anion, z denotes the valence of the indicated species, c_{eq} denotes the total concentration of cations or anions in equivalents per cubic centimeter (the molar volume times the number of equivalents per mole), $\tilde{c}$ denotes the absolute value of the excess concentration of the metal or metalloid in the same units, μ_{Me} denotes the chemical potential of the metal in ergs per gram atom and the other terms have their usual significance.

Darken [11] derived a similar expression particularly for binary metallic alloys. It is,

$$\tilde{D} = [X_2 D_1^s + X_1 D_2^s] \cdot \left[1 + \frac{\partial \ln \gamma_1}{\partial \ln X_1}\right] \tag{11}$$

where the symbols 1 and 2 denote the respective components of the binary metallic alloy, γ denotes an activity coefficient and X denotes the concentration of the indicated species in terms of mole fraction.

More recently, Brebrick [1] has derived a more detailed equation applicable to a binary compound semiconductor that exhibits Schottky disorder and is in the "exhaustion region." His equation is,

$$\tilde{D} = \Gamma_2 \lambda^2 \{1 + (\Gamma_1/\Gamma_2 - 1)\delta\} \left[1 + \left(\frac{\Delta^2 + 4K_s}{\Delta^2 + 4n_i^2}\right)^{1/2}\right] \tag{12}$$

where the subscripts 1 and 2 denote the cation and anion, respectively, Γ denotes a jump frequency, λ denotes a jump distance, δ is the fraction of vacancies that are cation vacancies, Δ denotes a deviation from stoichiometry and is equal to the difference between the cation and anion concentrations, K_s denotes the Schottky constant and n_i the intrinsic carrier concentration. Brebrick's equation has been successfully applied to lead sulfide. Unfortunately, this equation has not been tested for oxides presumably due to the lack of necessary parameters such as the value of the lattice disorder constant or the intrinsic carrier concentration. Moore [2] has discussed this equation with application to cuprous oxide but the lack of the previously mentioned parameters allowed only an order of magnitude calculation.

4.1. Limiting Case for a Predominantly Electronic Conductor Which Has Cation Vacancies as Majority Lattice Defects and $D_0^S \ll D_{Me}^S$

When $D_0^S \ll D_{Me}^S$, one term in eq (10) or (11) may be neglected. This approximation appears to be valid for the oxides considered here. The equation of Darken becomes,

$$\tilde{D} = [X_2 D_1^S] \cdot [1 + \partial ln\gamma_1 / \partial ln X_1]. \tag{13}$$

It should be emphasized that this equation was derived for metallic alloys and not for ionic or partially polar semiconductors. The equation due to C. Wagner which was derived for semiconductors becomes,

$$\tilde{D} = [|z_1| D_1^S] \cdot \frac{c_{eq}}{\tilde{c}} \cdot \left[\frac{1}{RT} \frac{\partial \mu_{me}}{\partial ln \tilde{c}}\right]. \tag{14}$$

Equation (10) and therefore eq (14) were derived on the basis of the tarnish layer theory for the rate of parabolic oxidation of metals. In this case the amount of oxide in equivalents, $\tilde{n}$, formed per unit time, t, per unit area, A, was

$$\frac{d\tilde{n}}{dt} \frac{1}{A} = \tilde{J} = \frac{k_r}{\Delta x} \tag{15}$$

where $\tilde{J}$ is the flux, Δx is the oxide layer thickness and k_r is the rational rate constant in equivalents per second for a layer one centimeter thick. C. Wagner showed that:

$$k_r = \frac{300}{96{,}500} \cdot \frac{1}{Ne} \int_{\mu_{Me}^a}^{\mu_{Me}^i} (t_1 + t_2) t_3 \cdot \sigma \frac{d\mu_{Me}}{|z_1|} \tag{16}$$

[2] The Kroger-Vink notation is used. The subscripts refer to the indicated lattice site, super primes denote the effective negative charges, super dots denote effective positive charges relative to the normally occupied lattice site and $\oplus$ and $\ominus$ denote electron holes and electrons, respectively.

where

N = Avogadro's number,
e = elementary electronic charge in esu,
μ_{Me} = chemical potential of the metal at the inner (superscript i) and outer (superscript a) surfaces of the oxide, respectively,
t = transference number,
σ = total electrical conductivity,
z = valence,

and the subscripts 1, 2, or 3 denote the cation, anion or electron, respectively.

According to C. Wagner [10], eq (15) may be written in differential form as,

$$\tilde{J} = \left\{\frac{300}{96{,}500} \frac{(t_1 + t_2) t_3 \sigma}{Ne} \frac{1}{|z_1|} \left[\frac{\partial \mu_{Me}}{\partial \tilde{c}}\right]\right\} \left[\frac{\partial \tilde{c}}{\partial x}\right] \tag{17}$$

where $\tilde{c}$ is the absolute value of the excess concentration of metal or metalloid expressed in equivalents per cm^3. Thus the expression in the curly brackets in eq (17) is the phenomenological chemical diffusion coefficient, $\tilde{D}$, in Fick's first law.

In the case of the oxides considered in this paper, $t_3 \approx 1$. Furthermore the chemical potential of the metal is related to the chemical potentials of the cations and electrons by,

$$d\mu_{Me} = d\mu_1 + |z_1| d\mu_3. \tag{18}$$

Under the assumption that the particles migrate independently, the partial conductivity for each species, $t_i \sigma = \sigma_i$, can be related to the self-diffusion coefficient by the Nernst-Einstein equation,

$$D_i^S = B_i RT/N \tag{19}$$

where B_i is the mobility and given by C. Wagner [10] as,

$$B_i = \frac{300}{96{,}500} \frac{\sigma_i}{|z_i| e c_i} \tag{20}$$

In this way the expression in curly brackets, $\tilde{D}$, of eq (17) can be related to self-diffusion coefficient.

To a first approximation, the majority lattice defects in the oxides considered here are cation vacancies. The equation [2] is,

$$\tfrac{1}{2}\, O_{2(g)} = O_O + V''_k + k\oplus. \tag{21}$$

Hence eq (3) becomes,

$$D_{Me}^S = X_{V_{Me}} D_{V_{Me}} \tag{22}$$

with the state of ionization not denoted. The diffusion coefficient of the vacancies is,

$$D_{V_{Me}} = B_{V_{Me}} RT/N \tag{23}$$

and the mobility of the cation vacancies, $B_{V_{Me}}$, is given [10] by eq (20). For this limiting case where in addition to the assumption that $D_O^S \ll D_{Me}^S$, the activity of the vacancies can be set equal to their concentration (dilute solution), eq (10) becomes

$$\tilde{D} = (1+z_1)\frac{1}{f} D_{Me}^T \frac{1}{X_{V_{Me}}} \tag{24}$$

where the concentration is now expressed in terms of mole fraction $X_{V_{Me}}$. The term $(1+z_1)$ is due to the diffusion potential, i.e., the ions are accelerated by the more rapidly moving electrons (as electron holes) and conversely, the electrons are decelerated.

5. Experimental Results and Discussion

5.1. Wustite, Fe_xO

Wustite is particularly well suited for the determination of the chemical diffusion coefficient because the phase field is wide, and the thermodynamics of the system are well known [8]. See figure 1. The thermogravimetric technique was used by Levin and J. B. Wagner [5]. Single crystals were not available. Rectangular sheets of iron, about 0.3 by 0.5 by 0.02 to 0.05 in where oxidized completely to wustite. The resulting grains were columnar and the lateral grain size diameter was about 0.3 cm. The wustite was oxidized or reduced within the limits of the phase field. Typical plots of raw data for reduction of undoped wustite from an oxygen to iron atomic ratio (O/Fe) of 1.125 to 1.050 at several temperatures are shown in figure 2. These data are replotted in accord with eq (8) in figure 3. From the initial slopes a value of $\tilde{D}$ was obtained. These same data are replotted in accord with eq (6) in figure 4. Again $\tilde{D}$ was evaluated. The values of the chemical diffusion coefficients obtained from eq (8) were labeled $\tilde{D}_i$ and those from eq (6) labeled $\tilde{D}_l$. Values for several different reduction increments are shown in table 1. The agreement between the two sets of values, $\tilde{D}_i$ and $\tilde{D}_l$, is good. In this series of experiments, the initial composition of the wustite was always O/Fe = 1.125. The final composition was O/Fe = 1.100, or 1.075 or 1.050. For a given temperature the values of $\tilde{D}$ decrease as the O/Fe ratio increases, i.e. $\tilde{D}$ is a function of composition. In order to establish this compositional dependency Hembree [12] carried out a series of experiments at

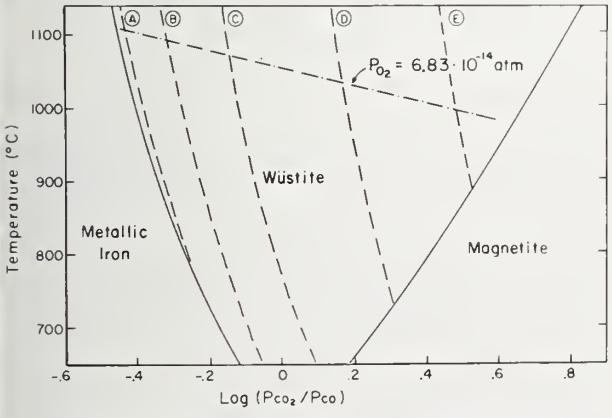

FIGURE 1. *Phase diagram for the wustite phase field.*

The dashed lines are lines of constant composition. In terms of the atomic ratio of oxygen to iron, O/Fe, these are:

A. O/Fe = 1.050
B. O/Fe = 1.060
C. O/Fe = 1.075
D. O/Fe = 1.100
E. O/Fe = 1.125

The dashed-dot line represents the composition of wustite when heated at equilibrium with a constant oxygen pressure (6.83×10^{-14} atm).

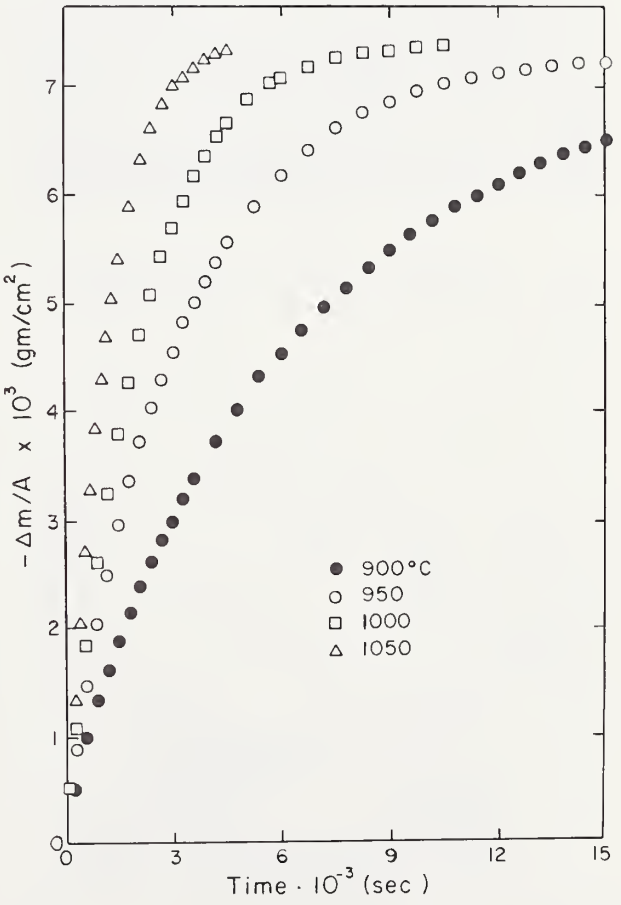

FIGURE 2. *Typical plot of data for the reduction of wustite from an initial O/Fe ratio of 1.125 to a final ratio of 1.050. After Levin and J. B. Wagner* [5].

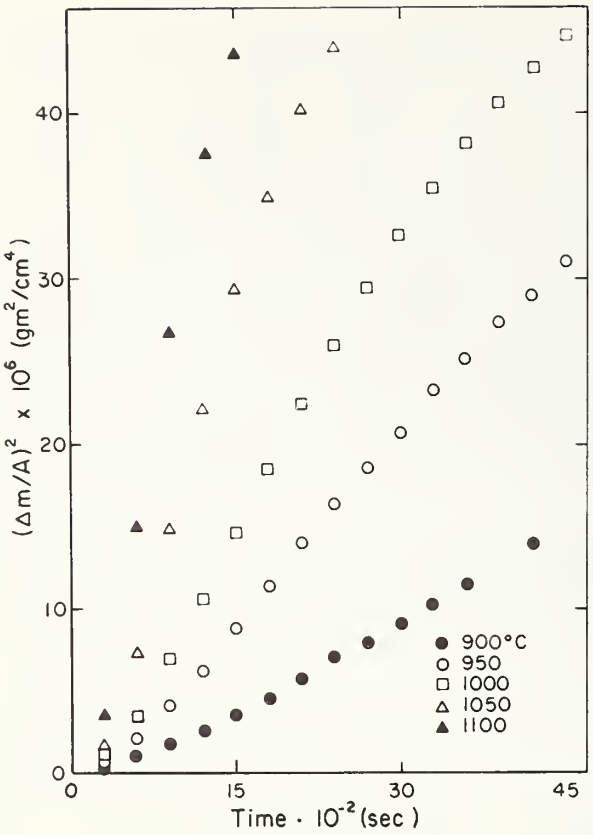

FIGURE 3. *Parabolic rate curves for reduction of wustite from O/Fe = 1.125 to 1.050. After Levin and J. B. Wagner* [5].

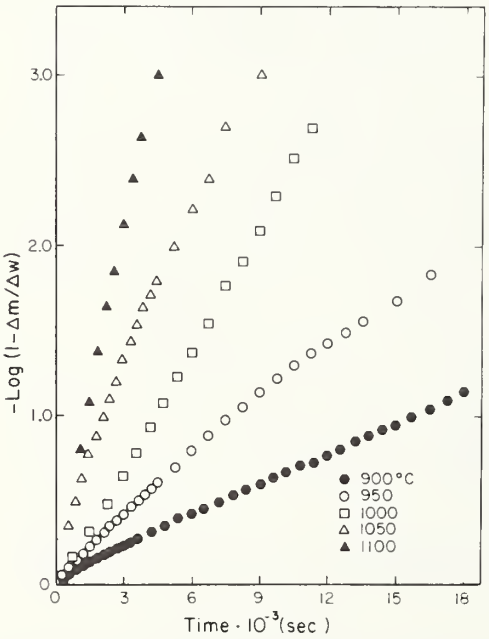

FIGURE 4. *Plot of data for reduction of wustite from O/Fe = 1.125 to 1.050 according to eq (6). After Levin and J. B. Wagner* [5].

TABLE 1. *Values of the "Parabolic Rate Constant," K_p, and the chemical diffusion coefficients from the initial, $\tilde{D}_i$, and later $\tilde{D}_l$ stages of the reduction of undoped wustite for various experimental conditions* [5]

Temperature, °C	K_p g^2 per cm^4/sec	$\tilde{D}_i$ cm^2 per sec	$\tilde{D}_l$ cm^2 per sec
(A) Reduction of undoped wustite, O/Fe = 1.125 to 1.050 $\Delta c = 0.0885$ g per cm^3			
1100	3.11×10^{-8}	3.1×10^{-6}	3.3×10^{-6}
1050	2.43×10^{-8}	2.4×10^{-6}	2.6×10^{-6}
1000	1.27×10^{-8}	1.3×10^{-6}	1.4×10^{-6}
950	8.21×10^{-9}	8.2×10^{-7}	7.0×10^{-7}
900	3.85×10^{-9}	3.8×10^{-7}	3.5×10^{-7}
(B) Reduction of undoped wustite, O/Fe = 1.125 to 1.075 $\Delta c = 0.0624$ g per cm^3			
1100	9.22×10^{-9}	1.9×10^{-6}	2.5×10^{-6}
1050	6.97×10^{-9}	1.4×10^{-6}	1.3×10^{-6}
1000	4.19×10^{-9}	8.4×10^{-7}	8.0×10^{-7}
950	2.77×10^{-9}	5.6×10^{-7}	5.6×10^{-7}
900	1.55×10^{-9}	3.1×10^{-7}	3.1×10^{-7}
(C) Reduction of undoped wustite, O/Fe = 1.125 to 1.100 $\Delta c = 0.0296$ g per cm^3			
1100	9.81×10^{-10}	8.8×10^{-7}	8.6×10^{-7}
1050	6.13×10^{-10}	5.5×10^{-7}	5.7×10^{-7}
1000	3.85×10^{-10}	3.5×10^{-7}	3.8×10^{-7}
950	2.50×10^{-10}	2.2×10^{-7}	2.7×10^{-7}
900	1.37×10^{-10}	1.2×10^{-7}	1.8×10^{-7}

1100 °C whereby the reduction increments were 0.01 in terms of the O/Fe ratio. The phase field of wustite was divided into ten increments from O/Fe = 1.150 to O/Fe = 1.050. See figure 5. Between a composition change of 0.01 in O/Fe ratio, the chemical diffusion coefficient was assumed to be constant. Figure 6 shows a plot of log $\tilde{D}$ versus the O/Fe ratio obtained by P. Hembree [12]. The values of $\tilde{D}$ at 1100 °C obey an equation,

$$\tilde{D} = 74.1 \times 10^{-6.67(O/Fe)} = 74.1 e^{-15.36(O/Fe)}. \quad (25)$$

Over the entire phase field, the value of $\tilde{D}$ varies by a factor of four. Thus an oxidation experiment and a reduction experiment, both within the phase field from the same initial composition but to different final compositions, yield different results. Most of the previous work involved composition ranges which spanned one-third to two-thirds of the entire phase field, a difference in O/Fe ratio of 0.03 to 0.06. During the process of equilibrating a sample, the crystal spends about two-thirds of the time of the experiment at a composition near the final composition [12]. Thus, two experiments on two crystals having identical initial compositions in the center of the phase field, one being oxidized to a higher O/Fe ratio and the other being reduced to a lower O/Fe ratio will give different values of $\tilde{D}$. The reverse situation whereby the same two

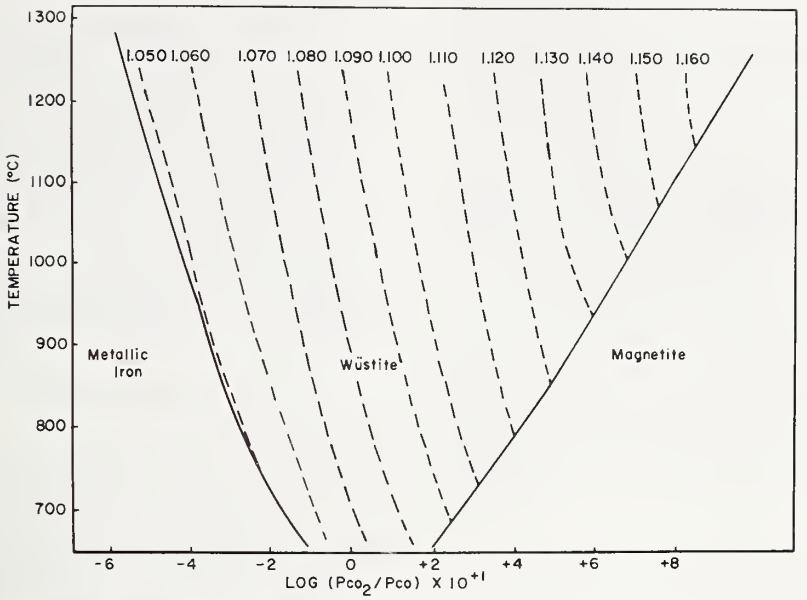

FIGURE 5. *Wustite phase field with lines of constant composition (dashed lines).*
The numbers at the top of the dashed lines are the atomic ratios of oxygen to iron. After Hembree [12].

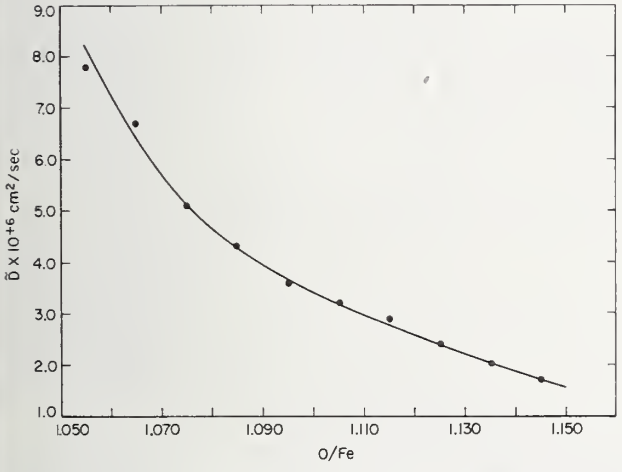

FIGURE 6. *Compositional dependence of* $\tilde{D}$ *for undoped wustite as a function O/Fe ratio at 1100 °C according to Hembree [12].*

crystals now are brought back to the same initial composition will yield approximately the same value of $\tilde{D}$.

In a dilute solution of cation vacancies in a lattice, the cation vacancy can jump to any filled cation lattice site. When the concentration of cation vacancies is four to eleven percent of the total cation sites, then each vacancy has some neighbors as vacancies. The vacancies have a charge relative to the lattice and are repelled from one another.

For such high concentrations of vacancies, the migration of vacancies is impeded by one another. Thus it is understandable that the chemical diffusion coefficient which is proportional to the vacancy diffusion coefficient should decrease with increasing vacancy concentration. P. Hembree [12] has constructed a "hard sphere" model for cation vacancies in wustite which explains qualitatively the decreasing $\tilde{D}$ with increasing vacancy concentration at high vacancy concentrations.

Landler and Komarek [14] explain a similar observation for the reduction of wustite in H_2-H_2O mixtures by a change in the mobility of the vacancies as a function of composition.

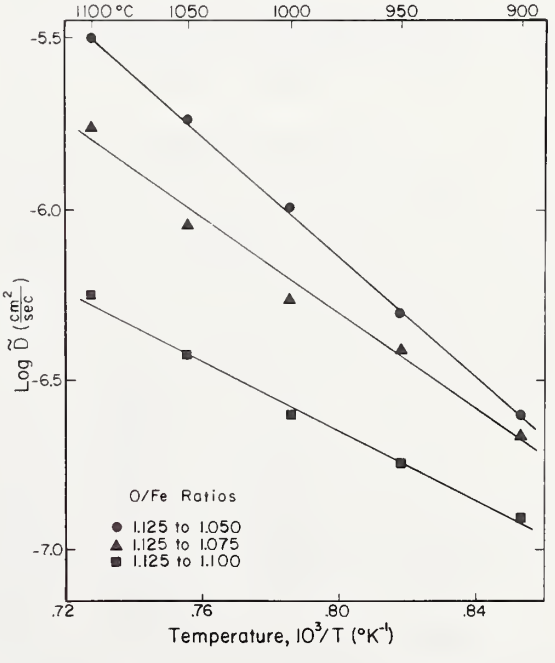

FIGURE 7. *Temperature dependence of the chemical diffusion coefficient of wustite for several composition increments according to Levin and J. B. Wagner [5].*

The temperature dependence of $\tilde{D}$ for Fe_xO has thus far only been evaluated for large reduction increments in CO-CO_2, viz. O/Fe from 1.125 to 1.050, 1.075 or 1.100 as the case may be. An Arrhenius plot for $\tilde{D}_l$ is shown in figure 7 and values of the corresponding "activation energies" are composite quantities containing both the energy for motion of the cation vacancies and the partial molar enthalpy of dissolution of oxygen from CO_2.

Landler and Komarek [14] report a value of 38 kcal for the activation energy for reduction of undoped wustite in H_2-H_2O mixtures. Their value was not a function of the wustite composition. They considered the rate controlling steps to involve the combined processes of solid state diffusion and a phase boundary reaction at the gas-oxide surface.

5.2. Relation Between $\tilde{D}$ and D^T_{Fe}.

The value of $\tilde{D}$ for Fe_xO is easily obtained and relatively unambiguous. The equation (24) of C. Wagner relating $\tilde{D}$ and D_i^T was made expressly for compounds exhibiting small deviations from stoichiometry and Darken's equation (13) was not derived for partially polar compounds. Nevertheless, both equations provide an order of magnitude agreement in relating the experimentally determined values of $\tilde{D}$ with experimentally determined values of D^T_{Fe}. In table 2 are values of $\tilde{D}$ for wustite calculated using the tracer diffusion data of Himmel, Mehl and Birchenall [13] and the thermodynamic data of Darken [8]. The metal-metal oxide boundary was taken as a standard state for the oxygen activity. Both the limiting equation of Wagner [eq (24)] and the equation of Darken [eq (13)] were tested. These values are to be compared with experimental values obtained by Levin and J. B. Wagner shown in table 3. The agreement is good, expecially so when one realizes that wustite exhibits super-lattice lines by x-ray studies which suggests that the vacancies are ordered into "clusters" [15], and a p to n transition is found in the center of the phase field [16, 17].

Using the more recent data of Hembree [12] for $\tilde{D}$ at 1100 °C, and taking O/Fe = 1.07 as an average value,

$$\tilde{D}(\text{expt'l}) = 74.1 \times 10^{-6.67(\text{O/Fe})}$$

$$= 5.3 \times 10^{-6}\ \text{cm}^2/\text{sec}. \qquad (26)$$

As a comparison one may use equation (24) of C. Wagner and the tracer diffusion data of Hembree [18] and calculate the chemical diffusion coefficient using eq (25). According to Hembree,

$$D^T_{Fe} = 1.1 \times 10^{-7}\ \text{cm}^2/\text{sec} \qquad (27)$$

at O/Fe = 1.07 and 1100 °C. Because the iron sublattice is f.c.c., as a first approximation $f = 0.78$, and $z_1 = 2$. Thus,

$$\tilde{D}(\text{calc'd}) = 3\frac{D^T_{Fe}}{f}\frac{1}{X_{V''_{Fe}}} = \frac{3ND^T_{Fe}}{fv_m[V''_{Fe}]}$$

$$= 5.5 \times 10^{-6}\ \text{cm}^2/\text{sec} \qquad (28)$$

where N is Avogadro's number, f is the correlation factor = 0.78, v_m is the molar volume = 11.84

TABLE 2. *Calculated values of the chemical diffusion coefficient for wustite* [5]

O/Fe	N_o	Temp. °C	Himmel et al. [13]	From Wagner, eq (24)	From Darken, eq (13)	
			D^T_{Fe}, cm² per sec [b]	$\tilde{D}$, cm² per sec	$\left[1+\frac{\partial ln\gamma_{Fe}}{\partial ln N_{Fe}}\right]$	$\tilde{D}$, cm² per sec
1.050	0.512	1100	[c] 9.1×10^{-8}	7.2×10^{-6}	58.2	3.5×10^{-6}
		1000	3.6×10^{-8}	2.8×10^{-6}	57.9	1.4×10^{-6}
		900	2.0×10^{-8}	1.5×10^{-6}	51.0	6.7×10^{-6}
1.075	0.518	1100	[c] 2.0×10^{-7}	10.3×10^{-6}	58.2	7.7×10^{-6}
		1000	4.9×10^{-8}	2.6×10^{-6}	57.9	1.9×10^{-6}
		900	2.6×10^{-8}	1.3×10^{-6}	51.0	0.9×10^{-6}
1.100	0.524	1100	[c] 2.2×10^{-7}	8.6×10^{-6}	58.2	8.6×10^{-6}
		1000	7.4×10^{-8}	2.8×10^{-6}	57.9	3.0×10^{-6}
		900	3.6×10^{-8}	1.4×10^{-6}	51.0	1.2×10^{-6}

[b] These values are to be divided by 0.78 to yield the self-diffusion coefficient.
[c] By extrapolation.

TABLE 3. *Experimental results obtained from the Arrhenius curves for the reduction of undoped wustite* [5]

Experiment	Activation energy from $\log \tilde{D}_i$ vs. $1/T$, kcal per mole	Activation energy from $\log \tilde{D}_t$ vs. $1/T$, kcal per mole
Reduction of undoped FeO:		
O/Fe = 1.125 to 1.050	[a] 34.0 ± 2.4	37.4 ± 3.1
O/Fe = 1.125 to 1.075	29.2 ± 2.9	32.1 ± 1.4
O/Fe = 1.125 to 1.100	31.5 ± 0.4	24.8 ± 0.7

[a] The errors represent 80 percent confidence limits.

cm^3/mole, and $[V''_{Fe}]$ is the vacancy concentration per $cm^3 \approx 4 \times 10^{21}$. The agreement is remarkable in view of the assumption of an ideal solution and the assumption that $f = 0.78$.

In the studies by Levin and J. B. Wagner [5], by Landler and Komarek [14] and by Hembree [12], $\tilde{D}$ *decreases* as the O/Fe ratio (which is proportional to the cation vacancy concentration) *increases*. Although a calculation such as that presented by eq (28) yields the correct order of magnitude, if values of the tracer diffusion coefficient are calculated using eq (13) from the experimental values of $\tilde{D}$, the calculated values of D^T_{Fe} also *decrease* with *increasing* O/Fe ratio [14]. This is not in accord with radiotracer experiments which show that values of D^T_{Fe} increase with increasing O/Fe ratio [13, 18, 31]. Landler and Komarek [14] have discussed this problem in terms of the mobility of cation vacancies which is not a constant but a function of the composition.

5.3. Cobaltous Oxide, CoO

Cobaltous oxide has a narrower range of homogeneity than does wustite. The maximum vacancy concentration is about 1 percent at 1000 °C [19]. The chemical diffusion coefficient could be obtained from a thermogravimetric technique, but the d-c electronic conductivity was more convenient. In order to use this technique, the ratio of the conductivity change at any time t to that at infinite time, $\Delta\sigma/\Delta\sigma_\infty$, must be substituted for the ratio $\Delta m/\Delta w$ as was discussed previously. In this case the evaluation of $\tilde{D}$ requires that the mobility of the carrier remains constant and the particular model for the point defects in the crystal must be known. In the case of CoO, the model has been shown to be [19, 20],

$$\tfrac{1}{2}\, O_2(g) = O_O + V'_{Co} + \oplus. \tag{29}$$

Consequently, a weight change per unit volume is equal to the oxygen pickup (or evolved) per unit volume and this in turn is related to the change in the electronic conductivity, $\Delta\sigma$, by

$$\frac{\Delta w}{\text{Unit volume}} = \Delta[O_O] = \Delta[\oplus] = \frac{1}{e}\frac{\Delta\sigma}{u} \tag{30}$$

where e denotes the electronic change and u, the mobility of the electron holes. Then using the subscripts a and b for an initial and final states,

$$\frac{\Delta w_a}{\Delta w_b} = \frac{\Delta\sigma_a}{\Delta\sigma_b}\cdot\frac{u_b}{u_a}. \tag{31}$$

If the electron hole mobility is independent of oxygen pressure over the pressure range in question, then the ratio u_b/u_a will be unity. The conductivity is written as

$$\sigma = [\oplus]\, eu = K' p_{O_2}^{1/4} \exp\left[\frac{-\Delta G_f^\circ/2 - \Delta G^*_\oplus}{RT}\right] \tag{32}$$

and the concentration of electron holes is

$$[\oplus] = K'' p_{O_2}^{1/4} \exp\left(-\Delta G_f^\circ/2RT\right). \tag{33}$$

The terms, ΔG_f° and $\Delta G^*_\oplus$ are the free energies of dissolution of oxygen in the crystal and that for motion of the electron holes respectively and K' and K'' are two constants dependent only on temperature. The electron hole mobility may be expressed by

$$u = \text{constant} \cdot \exp\left[-\frac{\Delta H^*_\oplus}{RT} - \frac{\Delta S^*_\oplus}{R}\right] \tag{34}$$

where $\Delta G^*_\oplus = \Delta H^*_\oplus - T\Delta S^*_\oplus$. Tannhauser and Fisher [20] report that both u and $\Delta H^*_\oplus$ are independent of oxygen pressure for the experimental conditions reported here. Furthermore, Eror [19], found that $\Delta S^*_\oplus$ also was independent of oxygen pressure. These data suggest that u is independent of the oxygen partial pressure and therefore $\Delta\sigma/\Delta\sigma_\infty$ may be substituted for $\Delta m/\Delta w$ in eqs (6) or (7). The foregoing model depends on the hopping process for the movement of the electron holes. If this model is not valid, the substitution may still be used provided that the mobility ratio is unity.

Equation (7) as modified was used by Price and J. B. Wagner [7] to determine $\tilde{D}$ for CoO at 800, 900, 1000 and 1100 °C. The data may be expressed by

$$\tilde{D} = 4.33 \times 10^{-3} \exp\left(-24{,}000/RT\right)\ cm^2/sec. \tag{35}$$

The relation between $\tilde{D}$ and D^T_{Co} was obtained using the thermodynamic data of Eror [19] and the equa-

290-621 O-68—6

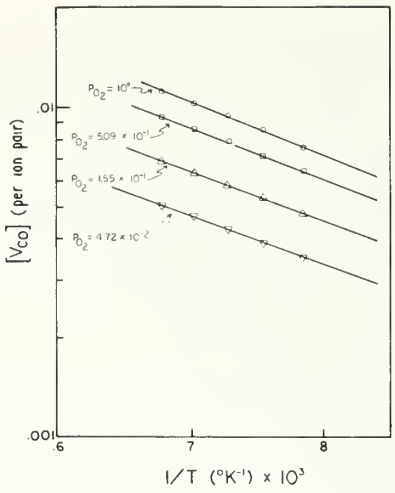

FIGURE 8. *Cation vacancy concentration in cobaltous oxide as a function of oxygen pressure and temperature according to Eror [19].*

tions of Darken or C. Wagner. The thermodynamic data of Eror are shown in figure 8. The metal, metal-oxide phase boundary [21] was used as the reference state for the oxygen activity. A comparison of the calculated values of D^T_{Co} and the experimental data are shown in table 4. Again the agreement is satisfactory.

5.4. Nickelous Oxide, NiO

Of the series of oxides under consideration, nickel oxide exhibits the smallest deviation from stoichiometry, about 0.1 percent at 1000 °C. It was assumed that because NiO has the same structure as CoO that the conductivity method could be applied. Price and J. B. Wagner [7] determined $\tilde{D}$ for NiO between 800 and 1100 °C to be

$$\tilde{D} = 7.52 \times 10^{-4} \exp(-21{,}900/RT) \text{ cm}^2/\text{sec}. \quad (36)$$

For the calculation of the tracer diffusion coefficient, the data of Mitoff for the concentration of cation vacancies in NiO was used. These data were extrapolated to the lower temperatures of interest in the present work. At 1300 °C Mitoff [30] obtained

$$[V''_{Ni}] = \left[\frac{1 \text{ atm}}{0.2 \text{ atm}} P_{O_2}\right]^{1/6} 6 \times 10^{-3} \exp(-11{,}400)/RT \text{ vac/ion pair}. \quad (37)$$

The data of Eror [19] suggested that singly ionized vacancies may be the majority defects in NiO between 800 to 1100 °C. Therefore the equation of Mitoff may be modified to yield

$$[V'_{Ni}] = \left[\frac{1 \text{ atm}}{0.2 \text{ atm}} P_{O_2}\right]^{1/4} 6 \cdot 10^{-3} \exp(-11{,}400/RT) \text{ vac/ion pair}. \quad (38)$$

The mole fractions of oxygen and nickel were calculated from this equation. The standard state for the activity of oxygen was the metal oxide phase boundary as determined by Kiukkola and C. Wagner [21]. Values of D^T_{Ni} were computed using the Darken equation. The use of the limiting equation (24) of C. Wagner, gave lower values of D^T_{Ni}. On using the more general equation (14) of C. Wagner with no assumption of ideality, the values of D^T_{Ni} were very nearly the experimental values of tracer diffusion. See table 5.

TABLE 4. *Comparison of calculated and experimental values of* D^T_{Co} *(cm²/sec) at one atmosphere of oxygen* [7]

Temperature °C	Price [7] eq (13)	Calculated eq (24)	Experimental Carter and Richardson [24]
1100	13.9×10^{-9}	1.54×10^{-9}	6.50×10^{-9}
1000	4.07×10^{-9}	0.62×10^{-9}	6.50×10^{-9}
900	0.906×10^{-9}	0.22×10^{-9}	0.742×10^{-9}
800	0.391×10^{-9}	0.06×10^{-9}	0.180×10^{-9}

TABLE 5. *Comparison of calculated and experimental values of* D^T_{Ni} *(cm²/sec) at 0.209 atmospheres of oxygen* [7]

Temperature °C	1100	1000	900	800
Price and Wagner [7] eq (13)	3.59×10^{-11}	1.12×10^{-11}	0.429×10^{-11}	0.077×10^{-11}
Price and Wagner [7] eq (25)	0.80×10^{-11}	0.22×10^{-11}	0.08×10^{-11}	0.02×10^{-11}
Linder and Åkerstrom [25]	3.31×10^{-11}	0.55×10^{-11}	0.036×10^{-11}	0.005×10^{-11}
Fueki and Wagner [26]	0.842×10^{-11}	0.198×10^{-11}	0.036×10^{-11}	0.005×10^{-11}
Shim and Moore [27]	3.60×10^{-11}	0.999×10^{-11}	[d] 0.227×10^{-11}	[d] 0.039×10^{-11}
Choi and Moore [28]	9.55×10^{-11}	2.49×10^{-11}	[d] 0.534×10^{-11}	[d] 0.085×10^{-11}

[d] By extrapolation.

5.5. Manganous Oxide, MnO

Manganous oxide exhibits an apparent p to n transition in its phase field [19]. See figure 9. Therefore conductivity measurements can only be used for an evaluation of $\tilde{D}$ over those composition ranges where the mobilities of the predominant carriers are independent of oxygen pressure and only one type of carrier is responsible for the majority of the electronic conductivity. It has been assumed that the mobilities of the electrons or of the holes are constant at oxygen partial pressures near either extreme of the composition range, e.g., at 1150 °C for p-type, $10^{-11} \leq P_{O_2}$ (atm) $\leq 10^{-8}$, and

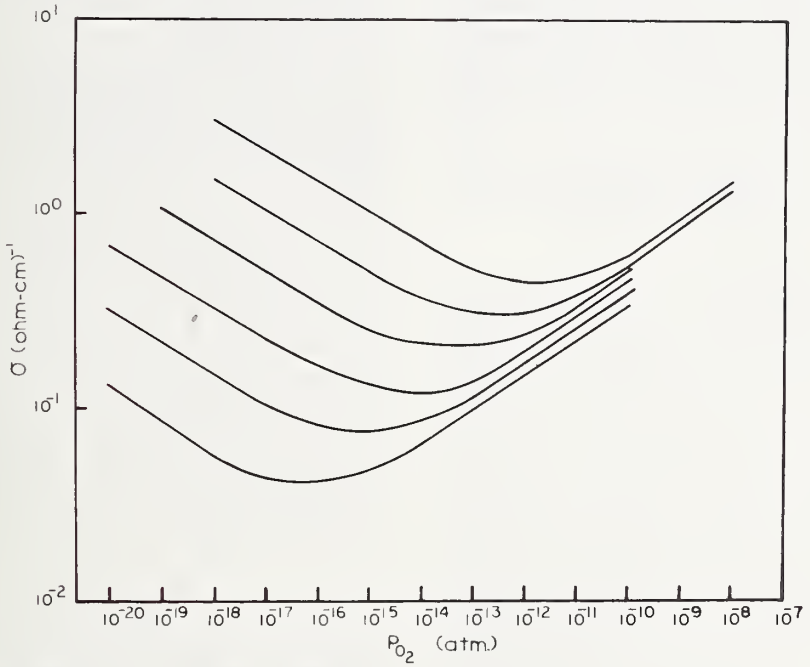

FIGURE 9. *Electronic conductivity of manganous oxide as a function of oxygen pressure at temperature increments of 50 °C.* The lowest curve corresponds to 900 °C. After Eror [19].

for n-type, $10^{-18} \leq P_{O_2}$ (atm) $\leq 10^{-15}$. Thus far tentative values for p-type MnO yield $\tilde{D} \approx 10^{-6}$ cm²/sec at 1150 °C [22]. The temperature dependence of this value over the temperature interval of 850 to 1150 °C is very small. The reason for this is not known, but these values are preliminary and must be regarded as such. As a comparison, the value of D^{T}_{Mn} has been calculated by Fueki and J. B. Wagner [23] to be about 10^{-9} cm²/sec for p-type MnO for 1150 °C.

6. Effect of Impurities, Intentionally Added or Not

Wustite is the only oxide in which a systematic study of the effects of trace impurities on $\tilde{D}$ has been made. Wustite doped with titanium, with chromium, or with lithium has been studied. As a first approximation it is assumed that the majority lattice defects in wustite are doubly ionized cation vacancies. Accordingly the following models hold

$$TiO_2 = Ti^{\cdot\cdot}_{Fe} + 2O_0 + V''_{Fe} \tag{39}$$

$$Cr_2O_3 = 2\ Cr^{\cdot}_{Fe} + 3O_0 + V''_{Fe} \tag{40}$$

$$Li_2O = 2\ Li'_{Fe} + O_0 + 2\oplus. \tag{41}$$

On an atom for atom basis, titanium should create twice as many vacancies as chromium, each for a given oxygen pressure and temperature. Conversely, lithium should destroy vacancies. Because $\tilde{D}$ is inversely dependent upon the vacancy concentration, the addition of higher valence solutes is expected to lower the value of $\tilde{D}$ and conversely for lower valence solutes. Levin [5] and Hembree [12] have shown that the addition of chromium decreased the value of $\tilde{D}$ relative to undoped wustite. Likewise titanium decreases and lithium increases $\tilde{D}$ relative to undoped wustite [12]. The results are in agreement with the simple lattice models given by (39), (40) and (41). The samples doped with lithium were prepared by evaporation of metallic lithium onto a wustite slab and subsequently annealing in a CO-CO_2 gas mixture. The samples containing titanium or chromium were made by oxidizing an alloy to a given oxygen to

metal ratio. This procedure is subject to experimental problems due to the phenomenon of internal oxidation during the preparation of the doped wustite. Even if there was a precipitate of another oxide formed initially, the samples were annealed for periods of weeks and the results were clearly in accord with theory.

The nickel oxide crystals were impure. Samples were sent to different companies for spectrographic analyses and to one company for neutron activation analysis. The results were not consistent. Accurate and consistent values of analyses are needed to test the role of trace impurities. It must be emphasized that trace impurities could act as traps for electron holes and in so doing change the oxygen pressure dependence of conductivity. Experiments are needed to test the dependence of $\tilde{D}$, D_i^T and σ on added impurities in CoO and MnO as well as NiO.

7. Remarks on Other Experimental Errors and Precautions

The obvious precautions for measurement of weight, of sample geometry or of probe spacing are relatively easily made. Other precautions, in addition to an awareness of the crystal purity cited previously, include a test of the assumption that the oxide surface comes into equilibrium with the gas phase virtually instantaneously when a new gas mixture is admitted to the surface. Especially for the case of wustite in CO-CO_2 mixtures, there have been suggestions [14] that a surface reaction is rate-controlling even though the data can be fitted to diffusion controlled kinetics. The data for wustite are self-consistent and the doping experiments should be carried out whereby the chemical potential of oxygen in the gas phase is maintained constant but the CO-CO_2 mixture is diluted with an inert gas. In such a case, the kinetics should remain unchanged if the reaction is diffusion controlled because the rate depends only on the gradient of chemical potential in the oxide. Such studies are underway for the case of wustite.

In the case of using the electronic conductivity method at low oxygen pressures provided by oxygen-argon mixtures, e.g., NiO at $p_{O_2} \leq 10^{-6}$ atm, and 1100 °C, the voltage drop across the probes occasionally did not stabilize over a long time period but fluctuated, e.g. by a factor of two and one half. In these cases, it is suspected that the surface is not completely equilibrated with the oxygen pressure. This phenomenon cannot be avoided so long as this method is used. A check on the precision and accuracy of the data can be made by comparing the final (equilibrium) value of the conductivity to equilibrium values on plot of log σ versus p_{O_2} where the data have been extended to higher pressures where this fluctuation phenomenon is not observed. Likewise gas mixtures, e.g., CO/CO_2, where the ratio of one gas to the other is less than about one to one hundred will have a very small "buffer capacity" against small fluctuations in composition [4].

In the solution of Fick's second law, $\tilde{D}$ was assumed to be constant. This assumption is better the smaller the composition ranges over which the data are computed as was determined for wustite. Thus the composition dependence of $\tilde{D}$ can be determined by the evaluation of $\tilde{D}$ for composition increment which are sufficiently small so that the error in assuming $\tilde{D}$ a constant is less than the experimental error.

The relations between $\tilde{D}$ and D_i^T were derived by C. Wagner for compounds exhibiting small deviations from stoichiometry. In such cases the values of the valence of the cation is relatively well-defined. In case of large deviations from stoichiometry, the assumption of integer values may not be correct. Meussner and Birchenall [29] and Carter and Richardson [24] considered this problem for iron sulfide, and for cobaltous oxide, respectively. For the most part other investigators have neglected this consideration. On the other hand, the thermodynamics are best known for oxides exhibiting large deviations from stoichiometry owing to the relative ease of the experimental procedure. These competing factors must be weighed when the equations relating $\tilde{D}$ and D_i^T are used.

8. Summary

It has been shown that the chemical or interdiffusion coefficient for oxygen in crystals of manganous oxide, ferrous oxide, cobaltous oxide and nickelous oxide can be determined by a thermogravimetric or electronic conductivity technique. Values so obtained can be used to calculate tracer diffusion coefficients in these oxides. The calculated values are in good agreement with experimental values reported in the literature.

These studies have been supported by the Advanced Research Projects Agency through a grant from the Materials Research Center of Northwestern University. The author expresses his sincere thanks to helpful discussions with P. Hembree, F. S. Pettit, and J B Price.

10. References

[1] R. F. Brebrick, J. Appl. Phys. **30**, 811 (1959).
[2] W. J. Moore, J. Chem. Educ. **38**, 232 (1961).

[3] W. J. Moore, J. Electrochem. Soc. **100,** 302 (1953).
[4] F. S. Pettit, J. Electrochem. Soc. **113,** 1249 (1966).
[5] R. L. Levin and J. B. Wagner, Jr., Trans. Am. Inst. Min. Met. Engrs. **233,** 159 (1965).
[6] H. Dunwald and C. Wagner, Z. physik Chem. **B24,** 53 (1934).
[7] J B Price and J. B. Wagner, Jr., Z. physik Chem. (N.F.) **49,** 257 (1966).
[8] L. S. Darken and R. W. Gurry, J. Am. Chem. Soc. **67,** 1398 (1945).
[9] G. Slack, private communication to S. P. Mitoff, J. Chem. Phys. **35,** 882 (1961).
[10] C. Wagner, Z. physik Chem. **B11,** 139 (1930); Z. physik. Chem. **B32,** 447 (1936).
[11] L. S. Darken, Trans. Am. Inst. Min. Met. Engrs. **175,** 184 (1948).
[12] P. L. Hembree, Masters Thesis, Northwestern University. Paper submitted to Trans. Am. Inst. Min. Met. Engrs. May 1967.
[13] L. Himmel, R. F. Mehl and C. E. Birchenall, Trans. Am. Inst. Min. Met. Engrs. **197,** 827 (1953).
[14] P. F. J. Landler and K. L. K. Komarek, Trans. Am. Inst. Min. Met. Engrs. **236,** 138 (1966).
[15] F. Koch, Ph. D. Thesis, Northwestern University (1967).
[16] I. Bransky and D. S. Tannhauser, Trans. Am. Inst. Min. Met. Engrs. **239,** 75 (1967).
[17] W. J. Hiflegas and J. B. Wagner, Jr., Phys. Ltrs. **25A,** 742 (1967).
[18] P. L. Hembree, Ph. D. Thesis, Northwestern University (1967).
[19] N. Eror, Ph. D. Thesis, Northwestern University (1965).
[20] D. S. Tannhauser and B. Fisher, J. Chem. Phys. **44,** 1663 (1966).
[21] K. Kiukkola and C. Wagner, J. Electrochem. Soc. **104,** 379 (1957).
[22] J B Price, Ph. D. Thesis Research in Progress, Northwestern University.
[23] K. Fueki and J. B. Wagner, Jr., J. Electrochem. Soc. **112,** 970 (1965).
[24] R. E. Carter and F. D. Richardson, J. Metals **200,** 1244 (1954).
[25] R. Lindner and Å. Åkerstrom, Disc. Faraday Soc. **23,** 133 (1957).
[26] K. Fueki and J. B. Wagner, Jr., J. Electrochem. Soc. **112,** 384 (1965).
[27] M. T. Shim and W. J. Moore, J. Phys. Chem. **26,** 802 (1957).
[28] J. S. Choi and W. J. Moore, J. Phys. Chem. **66,** 1308 (1962).
[29] R. Muessner and C. E. Birchenall, Corrosion **13,** 677 (1957).
[30] S. P. Mitoff, J. Chem. Phys. **35,** 882 (1961).
[31] P. Desmarescaux and P. Lacombe, Mem. Sci. Rev. Metallurg. **LX,** No. 12, 899 (1963).

The Use and Limitations of the Concept of an Effective Binary Diffusion Coefficient for Multi-Component Diffusion

Alfred R. Cooper

Case Western Reserve University Cleveland, Ohio 44106

An "effective binary diffusion coefficient" is frequently used for treating kinetics of mass transport controlled reactions in multicomponent systems. The concept is examined and the relation of an EBCD to the matrix of phenomological coefficients is determined. It is shown that the EBCD are useful parameters in that Fick's laws are meaningful if:

(i) the concentration gradients of all species are in the same direction.

(ii) either a steady state exists or there is no characteristic distance involved in the problem (i.e., infinite or semi-infinite diffusion).

When these conditions are obeyed, use of the EBCD gives considerable convenience dealing with mass transport in particular cases. This convenience is gained at the expense of a loss in generality, because the EBCD depend on direction (in composition space) as well as composition.

Key Words: Composition dependence of diffusion, diffusion, effective binary diffusion coefficient.

Introduction

The kinetics of many important processes, e.g., dissolution, precipitation, solid-solid reaction, and homogenization depend on interdiffusion, and frequently technically important systems are multi-component. Fortunately, the phenomenology of multi-component diffusion seems reasonably well understood [1].[1] However, there have been relatively few examples [2] of unambiguous determination of the matrix of coefficients necessary to describe the diffusion process in multi-component systems (possibly none in oxide systems) and few [3] efforts to predict, by solution of the simultaneous differential equations of multi-component diffusion, the behavior of a non-uniform multi-component system that is tending toward uniformity. Typically, the determinations and predictions have involved the often questionable assumption of composition independent coefficients.

Because of the complexity of the usual approach, we deem it advisable to critically examine a somewhat simpler approach to multi-component diffusion, involving the concept (perhaps first considered by Hougen and Watson) [4] of an effective binary diffusion coefficient for multi-component diffusion (henceforth EBDC). Since the EBDC are often used without concern as to their validity, our goal will be to determine the relationship of an EBDC to the matrix of phenomenological coefficients and the appropriateness of an EBDC when used in Fick's equations. It is hoped that this will permit a better understanding of limitations of the EBDC's and lead to increased utility of the EBDC in appropriate circumstances.

[1] Figures in brackets indicate the literature references at the end of this paper.

Multi-Component Systems

To be consistent with common usage, a system is termed "*multi-component*" *if it has two or more components that may vary independently*, and "*binary*" *if only one component can vary independently*. Thus, for example, a silver-gold alloy would be considered a binary unless the defect concentration can vary from its equilibrium value. Then and only then can it be considered multi-component (ternary if there is only one species of non-equilibrium defect). Likewise, an oxide is a binary if it is stoichiometric and contains two cations (although there are three species, two cations and oxygen, electrical neutrality and the fact that the sum of cation fractions is unity reduce the number of species that are independently variable). On the other hand, because it is not stoichiometric, iron oxide, $Fe_{(1-\delta)}0$, which has received so much attention at this conference [5] is also a binary oxide system even though it has a single cation species. A different viewpoint of $Fe_{(1-\delta)}0$, leading to the same conclusion, would be to consider Fe^{++} and Fe^{+++} as different species.

With these definitions, a binary system is one which has "composition space" that is unidimensional, i.e., a single number will describe the com-

position, X. In general, in a system of r components, compositional space has $(r-1)$ dimensions as the composition, $X=(x_1, x_2 \ldots x_{r-1})$, is given by a set of $(r-1)$ values of the fraction x_i of the individual components. In what follows, the rth species has always been chosen to be the dependent. Where necessary the dependent species is specified in the notation used in this paper by a presuffix, i.e.,

$$_rD_{ij} \text{ or } _rF_i.$$

A continuous "path" in composition space is given by a one-dimensional set of connected compositions. This is illustrated schematically for a ternary system by figure 1a. At a particular composition, the "direction", $_rf_i$ of a continuous path in this space is defined by a set of $(r-2)$ derivatives with respect to x_i, i.e.,

$$_rF_i = (f_{1i}, f_{2i}, \cdots f_{(i-1)i}, f_{(i+1)i}, \cdots f_{(r-1)i})$$

where

$$f_{ki} = \frac{dx_k}{dx_i}.$$

(We are not concerned with $f_{ki} \to \infty$ because this has explicit meaning in terms of direction.) Various directions, $_cF_B = f_{AB}$, in composition space in a ternary system are shown in figure 1b.

Since it will be necessary to refer to positions, paths, and directions in both real space and composition space in the following, an effort has been made, even at the expense of awkward language, to make clear whether composition space or real space is involved.

Multi-Component Diffusion

In 1945 Onsager [6] suggested extending Fick's law to multi-component systems by allowing the flux density,[2] j_i, of species i to be a linear combination of the concentration [2] gradients, $\nabla\rho_k$ $(k=1 \to r)$ of all species. Reducing this idea to a set of equations relating independent flux densities [2] (by establishing a reference frame) and independent fraction [2] gradients ∇x_j (by noting that $\sum_{j=1}^{r} \nabla x_j = 0$) gives what has come to be known as the phenomenological equations for multi-component diffusion. For an r component system the following $(r-1)$ equations are obtained:

$$j_i = -\sum_{j=1}^{r-1} {}_rD_{ij}\rho\nabla x_j \qquad (1)^3$$

$$\text{for } i \text{ from 1 to } r-1.$$

The validity of this linear combination is confirmed by the experimental demonstration that at a given composition the coefficients $_rD_{ij}$ appear to be independent of time [7] and direction [2d].

Another approach to multi-component diffusion is to use the concept of an EBDC. For species i the EBDC, D_{im}^*, defined as follows:

$$j_i \equiv -D_{im}^* \rho\nabla x_i \qquad (2)^3$$

is the proportionality constant between the flux density of species i and the product of density, ρ, and the gradient, ∇x_i, of fraction of i.

It is clear that the EBDC, D_{im}^*, for species i, treats the system as if all of the other constituents can be combined together as a single species, m, standing for mixture. Thus it is like a binary diffusion coefficient between i and the remainder of the constituents. While the notion of an EBDC arose in multi-component gas systems, it has been used explicitly in condensed systems [8].

Conservation of species i and assumption of constant density, ρ, allows us to write the $(r-1)$ transient diffusion equations from eq 1 as follows

$$\frac{\partial x_i}{\partial t} = \nabla \sum_{j=1}^{r-1} {}_rD_{ij}\nabla x_j \qquad (3)$$

$$i = 1 \to (r-1).$$

Similar treatment yields the following equations:

$$\frac{\partial x_i}{\partial t} = \nabla D_{im}^* \nabla x_i \qquad (4)$$

$$i = 1 \to (r-1)$$

from equation 2.

We turn to the relation between the matrix of phenomenological coefficients, $_rD_{ij}$, and the EBDC, D_{im}^*. This is readily determined because combination of eqs 1 and 2, with the assumption that the gradient of all species is in the same direction in real space, yields

$$D_{im}^* = \sum_{j=1}^{r-1} {}_rD_{ij}(dx_j/dx_i). \qquad (5)$$

[2] Concentration, density, fraction and flux density can be defined so as to use any quantity; mols, number, mass, or volume to describe the amount of the species, but consistency is essential.

[3] The reference frame for the flux densities, j_i, must be well-defined and in what follows it is assumed that the reference frame is identical for equations 1 and 2.

(The assumption is obviously fulfilled if we are concerned only with diffusion that is confined to a single direction in real space. Henceforth, we confine ourselves to this situation and allow y to represent distance in this direction in real space.)

Thus, in principle, the EBDC for species, i, D^*_{im}, is calculable from $(r-1)$ values of ${}_rD_{ij}$ and the set of $(r-2)$ independent components of the direction vector ${}_rF_i$ on composition space.

In addition to being functions of composition X, the EBDC are also functions of direction ${}_rF_i$ in composition space. This is not surprising because in an r component system there are $(r/2)(r-1)$ irreducible independent phenomenological coefficients and only $(r-1)$ independent EBDC.[4] Thus the phenomenological coefficients must be more general.

A linear (Fickean) treatment of diffusion implies that the coefficient, D^*_{im}, is independent of the gradient, ∇x_i. Thus for the EBDC to be useful coefficients, in the sense that equations 2 and 4 have their usual meaning, the EBDC must be independent of the gradient, i.e., they must be functions[5] of composition. Since, by definition, the phenomenological coefficients, ${}_rD_{ij}$, are functions of composition, according to equation 5 the EBDC, D^*_{im}, will be functions of composition if the direction, ${}_rF_i$, is a function of composition.

We know that in general the direction, ${}_rF_i$, cannot be a function of composition X because typically there are an infinity of possible directions (see fig. 1b) at a particular composition. However, for a specific experiment described by its initial and boundary conditions, the direction may be a function of composition. If it is and if the end point compositions are constant, there is one and only one diffusion path for each pair of end point compositions, $X_o^{(-)}$ and $X_o^{(+)}$.

We will now consider the use of the EBDC in three different classes of experiments: (i) steady state, (ii) transient without a characteristic length, and (iii) transient with a finite characteristic length.

Steady State

In one sense this can be a somewhat trivial consideration, because, by definition, at steady state the diffusion path is a function only of the pair of end point compositions $X_o^{(-)}$ and $X_o^{(+)}$. Thus, when these are fixed, the directions are a function of composition, i.e., $F=F(X)$ and the concept of an EBDC is valid for steady state diffusion.

[4] Actually, although the Onsager Reciprocal Relations [1] do not apply directly to the phenomenological coefficients, along with the thermodynamics they reduce the number of independent coefficients from $(r-1)^2$ to $\frac{1}{2}r(r-1)$.

[5] We use function of composition in the sense that for a given value of the composition there is one and only one value of the function.

It only remains to inquire whether steady state is ever attained in multi-component diffusion. This is a question which needs an experimental answer. Although an unequivocal experiment (one in which it is shown that the diffusion path remains constant) has perhaps not been conducted, indications are that a steady state is attained in multi-component diffusion.

Steady state in liquid systems can occur from a balance between the diffusive and convective flux densities. For a multi-component system with a velocity, V_y, in the diffusion direction, the assumption of a steady state along with the use of eqs 3 and 4 gives:

$$V_y\left(\frac{dx_i}{dy}\right)=\frac{d}{dy}\sum_{j=1}^{r-1}{}_rD_{ij}\left(\frac{dx_j}{dy}\right) \tag{6}$$

and

$$V_y\left(\frac{dx_i}{dy}\right)=\frac{d}{dy}D^*_{im}\frac{dx_i}{dy}. \tag{7}$$

Solution of these equations is important in analyzing the kinetics of dissolution or precipitation with free or forced convection.

To obtain the flux density of species i from eq 1 requires the solution of $(r-1)$ simultaneous equations like eq 6. It is clear that this would be a difficult task and it is not known if there are cases for which this has been achieved.

On the other hand, use of the EBDC requires only a single equation 7 to be solved. In the fortuitous case where the EBDC varies only slightly with composition, analytical solutions [9] of equation 7 are available for conditions appropriate to several important processes. Some support for the existence of a steady state in multi-component diffusion is obtained from the fact that for given end member compositions, the D^*_{im} has been found to be independent of V_y [8a].

Transient Without a Characteristic Length

So-called infinite and semi-infinite diffusion couples permit the use of the "Boltzmann transformation," $y^*=y/t^{1/2}$, where y is distance in the diffusion direction, because none of the "boundaries" are at some characteristic finite length, L. Substituting this into eq 3 yields

$$\sum_{j=1}^{r-1}\frac{d}{dy^*}{}_rD_{ij}\frac{dx_j}{dy^*}+\frac{1}{2}y^*\frac{dx_i}{dy^*}=0 \tag{8}$$

$$i=1\rightarrow(r-1).$$

Solution of $(r-1)$ simultaneous total differential equations of equation 8 has been achieved in ternary systems ($r=3$) for cases where the ${}_rD_{ij}$'s are constant [3] and suggestions as to how to proceed when the coefficients depend on composition have recently been advanced [3d].

The existence of a solution (determined or not) to equation 8 implies that for given boundary conditions, the composition, X, is a function of y^*, i.e., $X=X(y^*)$. Thus, the diffusion path is a function of the Boltzmann variable, y^*.

If we restrict attention to a single phase region (thermodynamically speaking), then there is a one-to-one relationship between y^* and X as every value of composition, X, corresponds to one and only one value of y^*. This permits the conclusion that the diffusion path is a function of the pair of boundary conditions to equation 8[6] (i.e., the end member compositions). With this established, it follows that the direction is a function of composition, i.e., $F=F(X)$, and therefore that the EBDC are valid Fickean diffusion coefficients for transient unidirectional diffusion when there is no characteristic length. Thus, rewriting equation 3 as follows

$$\frac{d}{dy^*}D^*_{im}\ \frac{dx_i}{dy^*}+\frac{1}{2}y^*\frac{dx_i}{dy^*}=0 \qquad (9)$$

is permissible and solutions from heat transfer and binary diffusion are appropriate. Because of the simplicity of equation 9 relative to equation 8, it is convenient to use equation 9 along with equation 2 when it is necessary to calculate the flux density of a particular species in unidirectional multi-component diffusion in the absence of a characteristic distance, L.

Transient With a Characteristic Length

In so-called finite diffusion experiments where a characteristic length, L, prevents all the boundary conditions and initial conditions being expressed in terms of y^*, eqs 8 and 9 cannot be used. The existence of a characteristic length, L, also permits the end member compositions $X_o^{(+)}$, $X_o^{(-)}$ to vary and thus the diffusion path will not be constant. Therefore, we cannot be certain that the directions, ${}_rF_i$, will remain functions of composition during the experiment and, in general, caution need be exercised to assure that a change in end member composition will not markedly influence the EBDC. To consider this point, we rewrite eq 5

$$D^*_{im}={}_rD_{ii}+{}_rf_{1i}\,{}_rD_{i1}+{}_rf_{2i}\,{}_rD_{i2}+\cdots$$

and notice that if either the changes of direction ${}_rF_i$ are only very slight or if the cross terms, ${}_rD_{ij}$, $i\neq j$ are very much less than the diagonal term ${}_rD_{ii}$, then we still may have D^*_{im} sufficiently insensitive to factors other than composition so as to be useful. Particular care has to be exercised in cases such as illustrated in figure 1b where a component of the direction can reach infinity.

Guy, Leroy and Lindemer [3d], in considering ternary alloys with the usual phenomenological equations 1 and 3, have shown how, when the ratio of the magnitude of the diagonal term to the cross terms is great, homogenization of lamina of discreet thickness, L, proceeds almost identically to that predicted using a single EBDC.

Uphill Diffusion of One Species

The EBDC for a particular pair of end member compositions can be obtained by making an infinite diffusion experiment and using eq 9 to interpret the results, as in terms of $D_{im}(X)$.

At times,[7] a species in a multi-component system in a stable single phase region will behave as if its EBDC is $<O$. This is sometimes termed "uphill diffusion" [3c]. It may occur, for example, when the flux of a species is caused primarily by the random "hopping" of other species. It results in a diffusion path in composition space which is S-shaped, as shown schematically in figure 1a, and has regions where some of the components of the direction, f_{iB}, (see fig. 1a) go to infinity.

For an infinite diffusion experiment we have shown that composition is a function of y^*. To be consistent with figure 1, a graph of one component, x_B, of the composition would appear as is shown schematically in figure 2. This profile of the x_B component versus composition requires drastic behavior of the EBDC for species B as can be determined by expanding eq 9 to obtain

$$D^*_{Bm}\frac{d^2x_B}{dy^{*2}}+\frac{dD^*_{Bm}}{dy^*}\ \frac{dx_B}{dy^*}+\frac{1}{2}\frac{y^*dx_B}{dy^*}=0. \qquad (10)$$

Since $x_B(y^*)$ is known, it is convenient to write equation 6 as a linear first order differential equation in D^*_{Bm}

$$\frac{dD^*_{Bm}}{dy^*}+p(y^*)D^*_{Bm}=q(y^*) \qquad (11)$$

[6] This conclusion has been verified because it has been found both in multi-component metal [7] and oxide glass systems [10] that the diffusion path in "infinite" diffusion couples does not vary with time.

[7] A particularly clear example is found in Path 5 of figure 8 and figure 9 of reference [2d].

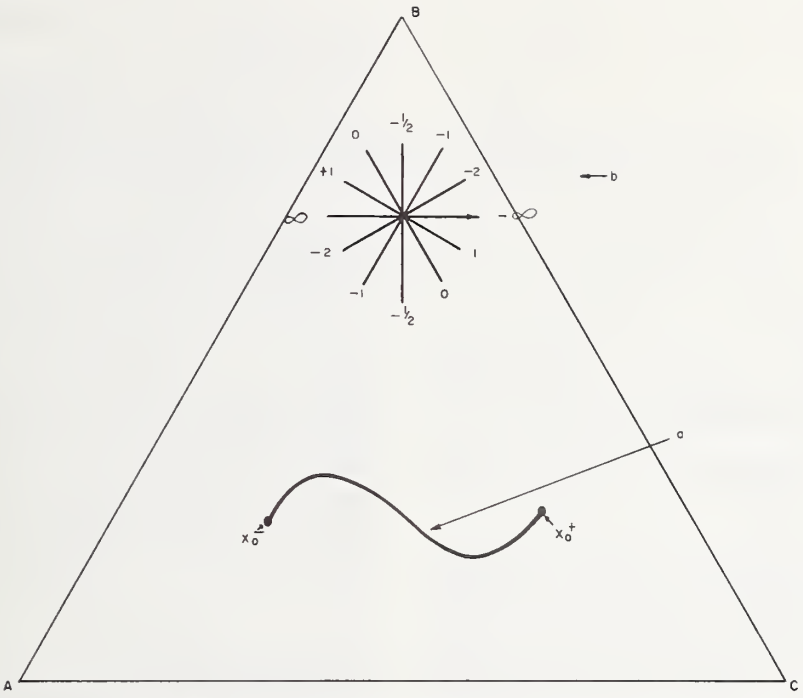

FIGURE 1. *Ternary composition space (a) A curved diffusion path. (b) Various directions,* f_{AB}, *on composition space.*

where

$$p(y^*) = \left(\frac{d^2x_B}{dy^{*2}} \Big/ \frac{dx_B}{dy^*}\right) \text{ and } q(y^*) = -\frac{1}{2}y^*$$

While eq 11 is, in principle, solvable by use of an integrating factor, it is difficult for cases where the concentration profile is similar to that shown in figure 2, because as indicated by figure 3, p (obtained from the concentration profile of figure 2) has discontinuities. An estimate [10] of D^*_{Bm} as a function of y^* can be obtained which is qualitatively consistent with figure 3, with eq 7, and also with eq 3. This is shown as figure 4 and the "bad" behavior (discontinuities, infinite values and negative values) is obvious.

The erratic behavior of the EBDC, D^*_{BM}, in special cases, limits its usefulness, i.e., for the diffusion path in figure 1a it would be difficult to characterize the functional dependence of D^*_{Bm} on composition. However, two factors moderate this limitation. (1) In a ternary system there is usually

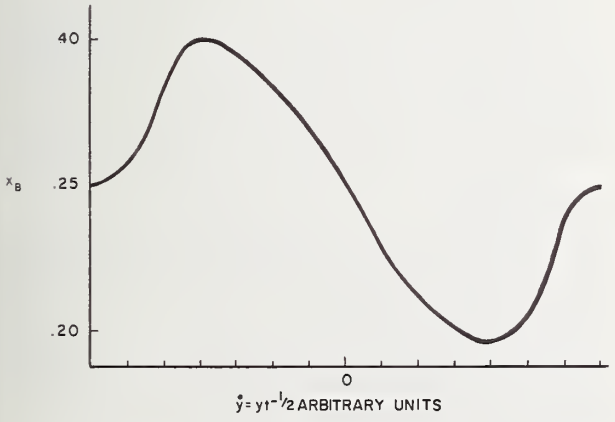

FIGURE 2. *A schematic diffusion profile of fraction of component* B, x_B, *versus Boltzmann variable,* $y^* = yt^{-1/2}$.

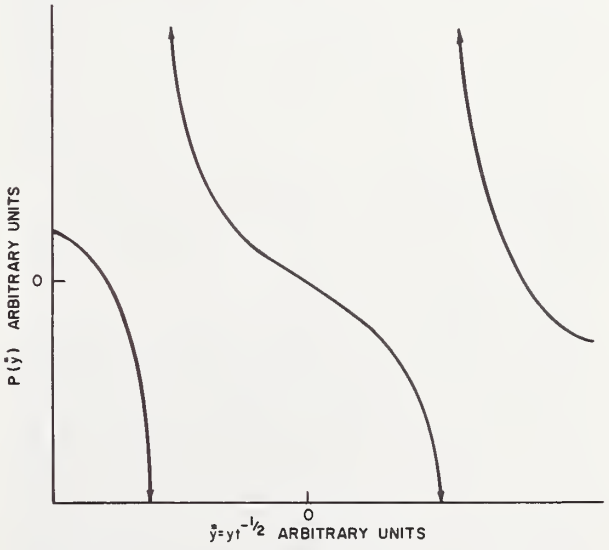

FIGURE 3. *Schematic of the function* p(y*) *versus* y*.

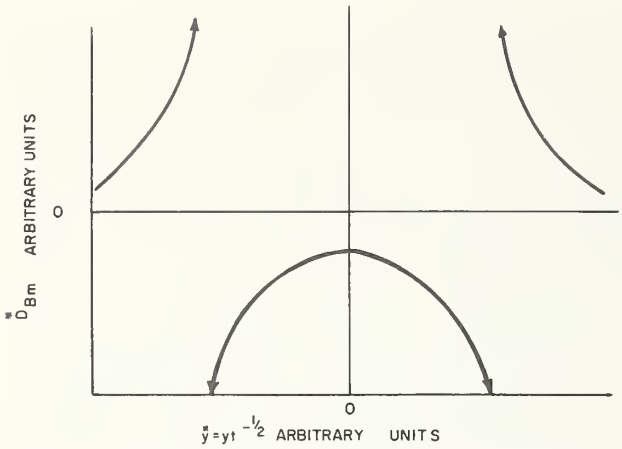

FIGURE 4. *Schematic of* D^*_{BM} *versus* y*. (*Note* y* *scale identical on figures 2, 3, 4).*

only at most a single species in a given experiment that has an EBDC that is erratic. The diffusion behavior of the system can be described by choosing the EBDC of the other two species. (2) Even when the EBDC behaves erratically, it still follows eq 10, and such important values as flux densities integrated across a given plane can be calculated.

Summary and Conclusions

The EBDC approach to multi-component diffusion (eqs 2 and 4), is in no way contradictory to the usual phenomenological approach (eqs 1 and 3). In fact, when the gradient vector in real space of all species is in the same direction, the EBDC can be derived from the phenomenological coefficients and the direction F in composition space. Conversely, the $(r-1)^2$ phenomenological coefficients can be determined from the directions and the EBDC of $(r-1)$ experiments. The EBDC are useful for describing mass transport in steady state and transient behavior when the boundary and initial conditions can be described in terms of a variable, $y^* \equiv yt^{-1/2}$, that combines distance and time. They may be useful in other cases as a close approximation of reality, but care has to be taken to be sure that the EBDC are insensitive to factors other than composition before using them in Fick's diffusion (equations 2 and 4).

Using the EBDC we obtain the convenience of having to deal with a single coefficient (the EBDC) to relate the flux density of a species to its gradient (eq 1) or to predict the transient behavior in a particular infinite or semi-infinite diffusion couple experiment (eq 10). It is much easier (1 experiment) to determine the concentration dependence of an EBDC along the diffusion path in composition space than it is to determine ($r-1$ experiments at each composition) the concentration dependence of the matrix of phenomenological coefficients along this path.

We do not obtain something for nothing. We have gained convenience of the EBDC at the expense of generality. Thus, while the EBDC may be very useful for characterizing the kinetics of a process in a multi-component system where mass transport is rate controlling, on the other hand it would be impractical to characterize the diffusion behavior at a particular composition by the EBDC, because of their direction dependence. In a ternary, for example, at a specific composition, it requires a matrix of four coefficients [8] to characterize the diffusion behavior using the usual phenomenological approach. Two EBDC's are required for the same purpose. These, however, are not simple coefficients, but functions of direction in composition space, and hence they are much less efficient in characterizing the general behavior.

The help of Milton Lees, Arun K. Varshneya and the support of NASA, Research Grant No. NGR 36–003–100, are gratefully acknowledged. Critical comments by A. Lidiard provoked important improvements in the paper and editorial suggestions by A. Franklin increased its readability.

References

[1] D. Fitts, Non-Equilibrium Thermodynamics, McGraw-Hill Book Company, New York, 1962.
[2] (a) J. S. Kirkaldy, G. R. Mason, and W. J. Slater, Canadian Mining & Metallurgical Bulletin, **64**, 53 (1961).
(b) A. G. Guy and J. Philibert, Z. Metallkunde, **56**, 841 (1965).
(c) T. O. Ziebold and R. E. Ogilvie, Trans. AIME, **239**, 942 (1967).
(d) J. P. Sabatier, A. Vignes, Memoires Scientifigues Rev. Metallurg., **64**, 225 (1967).
[3] (a) L. J. Fujita and H. Gosting, J. Amer. Chem. Soc. **79**, 1099 (1956).
(b) J. S. Kirkaldy, Can. J. Phys. **37**, 30 (1959).
(c) Y. Oishi, J. Chem. Phys. **43**, 1611 (1965).
(d) A. G. Guy, V. Leroy and T. B. Lindemer, A.S.M. Transactions Quarterly, **59**, 517 (1966).
[4] O. Hougen & K. Watson, Chemical Process Principles, Vol. III, Wiley, New York, 1947, pp. 97–99.
[5] FeO Papers at this Conference: J. B. Wagner, Jr.; H. F. Rizzo, et al.; L. Himmel and J. B. Holt; R. H. Campbell M. O'Keefe.
[6] L. Onsager, Ann. N. Y. Acad. Sci., **46**, 241 (1945).
[7] T. O. Ziebold, Ternary Diffusion in Copper-Silver-Gold Alloys, Doctoral Thesis, M.I.T., Cambridge, Mass., 1965.
[8] (a) A. R. Cooper, Jr. and W. D. Kingery. J. Amer. Ceram. Soc. **47**, 37 (1964).
(b) A. R. Cooper, Jr., J. Chem. Eng. Sci., **21**, 1095 (1966).
[9] V. G. Levich, Physicochemical Hydrodynamics, Prentice Hall, 1962, chapter 2.
[10] A. R. Cooper, Jr. and A. K. Varshneya, to be published in J. Amer. Ceram. Soc. **51**, 103 (1968).

[8] Only three of these are truly independent.

Divalent Cation Impurity Diffusion in MgO

A. J. Mortlock

Australian National University, Canberra.

1. Introduction

Direct measurements are now available of the diffusion in MgO of Mg^{2+}, Ni^{2+}, Co^{2+}, Fe^{2+}, Zn^{2+}, Ca^{2+}, Be^{2+} and Ba^{2+} [1 to 6].[1] In the single case of Ba^{2+} the penetration profiles could be analysed into two components yielding different activation energies (Q) and pre-exponential factors (D_o). With the exception of Mg^{2+}, and Ba^{2+} at small penetrations ($\lesssim 20\,\mu$), all the observed Q's lie in the range 1.6 to 2.1 eV and the D_o's are roughly of the order of 10^{-5} cm^2/sec. The data for Mg^{2+}, and Ba^{2+} at small penetrations, yield Q's of approximately 3.4 eV and D_o's of the order of 10^{-1} cm^2/sec.

Harding [6] considers that the lower Q's and D_o's are strongly influenced by dislocations. Furthermore, in the case of Ba^{2+} the higher Q and D_o measured at small penetrations are associated with lattice diffusion in this region and are only observed because of the relatively high resolution ($\sim 1\,\mu$) of the grinding technique used to analyse the penetration profiles. Lidiard [7] on the other hand has interpreted the Ni^{2+}, Co^{2+}, Fe^{2+}, Ca^{2+} and Be^{2+} results as being characteristic of extrinsic diffusion and, therefore, the observed Q's as energies of motion, H_m. This conclusion was reached on the basis of the maximum annealing temperatures used, 1700 to 1800 °C, and the purity of the MgO crystals, nominally 99.99 percent for the Ca^{2+}, Be^{2+} and Ba^{2+} investigations. Thus, for crystals with a concentration of aliovalent impurities of 10^{-4} the extrinsic-intrinsic transition is at approximately 1700 °C. The relatively high Q for Mg^{2+} was explained as intrinsic diffusion due to the unusually high purity of the crystals used in these particular experiments.

The incompatibility of these two interpretations of the experimental data requires closer examination. This is particularly so as the problem cannot be easily resolved at the present time by using higher purity MgO crystals because these are unavailable or, because of vaporization losses, annealing at much higher temperatures. It is also of interest to consider the reason for the unusual two-component nature of the Ba^{2+} penetration profiles.

[1] Figures in brackets indicate the literature references at the end of this paper.

2. Evidence for Extrinsic Diffusion

The following points throw light on the first of these problems:

(i) The MgO crystals used for the Ca^{2+}, Be^{2+} and Ba^{2+} diffusion experiments came from the same source and were of the same nominal purity. Therefore, as Lidiard's calculations indicate that the measured diffusion of Ca^{2+} and Be^{2+} is in the extrinsic region, this should also apply to the Ba^{2+} data, the temperature range being approximately the same in all three cases.

(ii) With the single exception of the large penetration Ba^{2+} results, all the available Q measurements can be fitted by the equation

$$Q = H_m = 1.34 + (1.05 \times 10^{16})r^2 \text{ eV} \qquad (1)$$

where r is the cation radius in Å; see figure 1. For this fitting Lidiard's [7] value of 1.5 eV for H_m for Mg^{2+} was used and the upward-pointing arrow attached to the plotted point indicates, following Lidiard, that this could possibly be a few tenths of an eV higher. The operation of this equation demonstrates a simple variation of H_m with cross-sectional area of the diffusing cation. This in turn indicates a consistent dependence of H_m on elastic strain energy at the saddle point.

(iii) The relatively large D_o factor for the small penetration Ba^{2+} measurements does not appear to be entirely inconsistent with the much smaller D_o's for the other impurities when due account is taken of the relatively large size of this cation: $r = 1.35$ Å. This is more clearly seen if it is supposed following Lawson [8] that S_m, the entropy of motion, is proportional to the activation volume of motion and then, as a very rough approximation, that this is a linear function of r^3. Under these circumstances $\log D_o$ should increase linearly with r^3, particularly for the larger values of r: the experimental data scatter badly but are not inconsistent as a whole with the predicted tendency.

The combined evidence represented by (i) to (iii) points very strongly to the conclusion that all the impurity cation diffusion measurements so

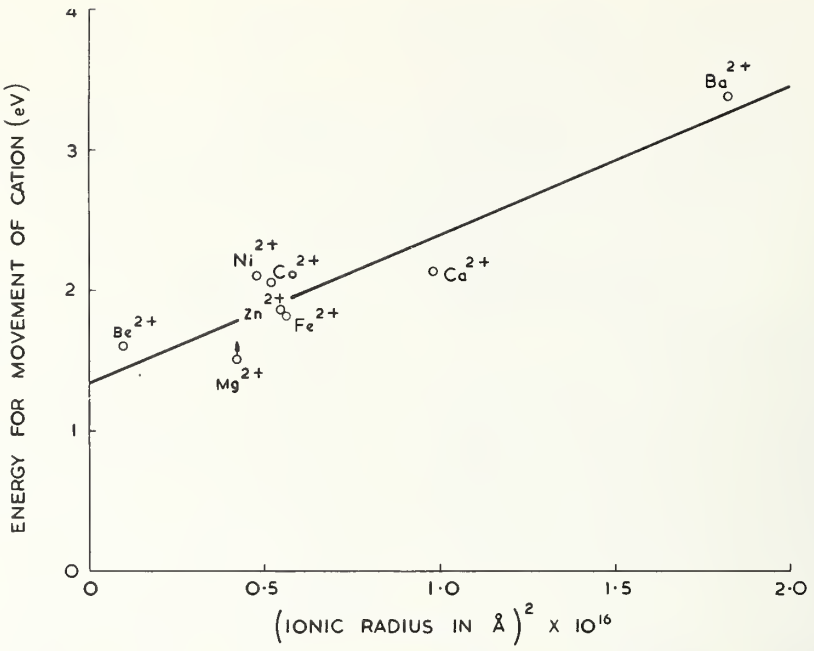

FIGURE 1. *Correlation between movement energies for cation diffusion in MgO and cation radius.*

far reported in MgO have been made in the extrinsic region. This extends and further supports the similar conclusion reached earlier by Lidiard [7] on the basis of a smaller amount of experimental data.

The problem of the two component nature of the Ba^{2+} penetration profiles can be explained by noting that a similar behaviour has been observed by Gupta and Weirick [10] for the self-diffusion of Ca in CaO. The near-surface diffusion region (0–20 μ) is attributed in this case to extrinsic diffusion and the deeper diffusion region to the super position of extrinsic and dislocation diffusion. The reason why Ba^{2+} alone shows this effect in MgO could be due to the enhanced effect of a smaller density of dislocations, in this case, caused by the unusually large segregation to them by the large Ba^{2+} ions, Mortlock [11]. The observed very small solubility of BaO in MgO, Harding [12], is consistent with this.

3. Mullen's Equation

In view of the success of eq (1) in fitting the experimental data, it is of interest to examine the performance in this connection of more complex equations which have been derived from strain energy considerations. Mullen [13] has shown that the energy of motion for cation self-diffusion in an ionic solid, H_{mo}, is given by

$$H_{mo} = K\,(1-1/\sqrt{2})^2\, r_o^2 \qquad (2)$$

where K is an empirical constant and r_o is the nearest-neighbour distance. It is also shown that the energy of motion for an impurity cation which is larger than the host ion it replaces is given by

$$H_m = K\,\{[(r_i - r_+) + (1-1/\sqrt{2})\, r_o]^2 - 3(r_i - r_+)^2\} \qquad (3)$$

where we now distinguish between the radius of the impurity cation r_i and that of the host cation, r_+. The second term in this equation arises out of the gain in strain energy resulting from the relaxation of the anion sublattice which takes place when the cation moves away from its equilibrium position.

If we put

$$\Delta r = r_i - r_+$$

$$\Delta H_m = H_m - H_{mo}$$

then we can eliminate the constant K to write

$$\Delta H_m = H_{mo}\left\{6.83\left(\frac{\Delta r}{r_o}\right) - 23.3\left(\frac{\Delta r}{r_o}\right)^2\right\} \qquad (4)$$

In figure 2 the experimental data for cation diffusion in MgO are plotted. The dashed line in this figure corresponds to the first term only in eq (4) while the full line represents both terms.

This equation shows some agreement with experiment up to and including ions as large as Ca^{2+} for which $(\Delta r/r_o)$ is 0.16. For larger ions, however, the only data available (Ba^{2+}) suggests that the reduction

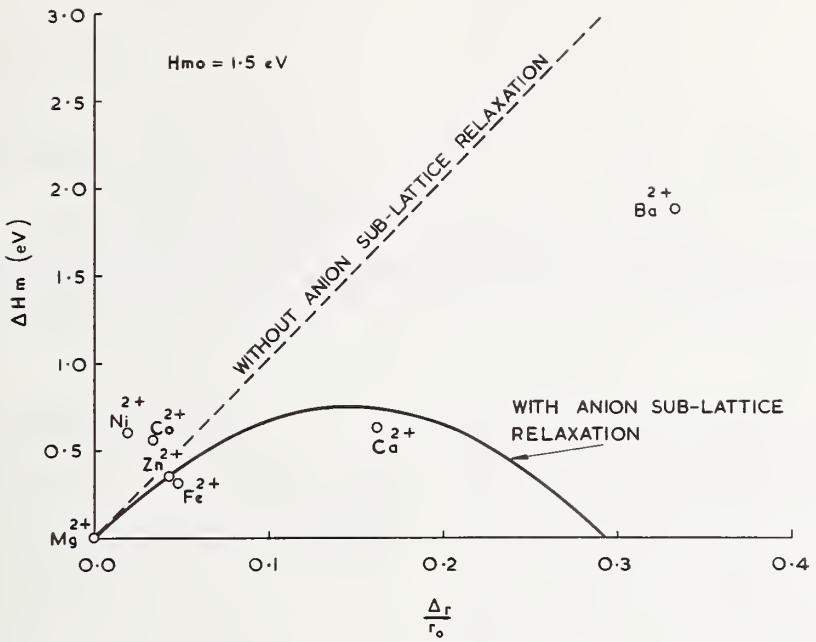

FIGURE 2. *Comparison between the observed and predicted increase in energy for the movement of divalent cation impurities in MgO relative to that for self-diffusion.*

in the energy of motion due to relaxation of the anion sub-lattice is over estimated. Overall, the semi-empirical equation (1) seems to describe the effect of ionic size variations on the motion energy better than eq (4).

4. References

[1] R. Lindner and G. D. Parfitt, J. Chem. Phys. **26,** 182 (1957).
[2] B. J. Wuensch and T. Vasilos, J. Chem. Phys. **36,** 2917 (1962).
[3] B. J. Wuensch and T. Vasilos, J. Chem. Phys. **42,** 4113 (1965).
[4] J. Rungis and A. J. Mortlock, Phil. Mag. **14,** 821 (1966).
[5] B. C. Harding and A. J. Mortlock, J. Chem. Phys. **45,** 2699 (1966).
[6] B. C. Harding, Phil. Mag. **16,** 1039 (1967).
[7] A. B. Lidiard, Proc. British Ceramic Soc. No. 9, July, 1967, p. 9.
[8] A. W. Lawson, J. Phys. Chem. Solids **3,** 250 (1957).
[9] R. W. Keyes, J. Chem. Phys. **29,** 467 (1958).
[10] Y. P. Gupta and L. J. Weirick, J. Phys. Chem. Solids **28,** 811 (1967).
[11] A. J. Morlock, Acta Met. **8,** 132 (1960).
[12] B. C. Harding, M. Sc., Thesis Australian National University, Canberra (1967), p. 27.
[13] J. G. Mullen, Phys. Rev. **143,** 658 (1966).

Diffusion of Iron and Nickel in Magnesium Oxide Single Crystals [1]

Stuart L. Blank and Joseph A. Pask

Inorganic Materials Research Division, Lawrence Radiation Laboratory, and Department of Mineral Technology, College of Engineering, University of California, Berkeley, California 94720

1. Literature Data

The vacancy mechanism is the most widely accepted mechanism for diffusion among oxides. The self-diffusion coefficient of Mg^{+2} in MgO was reported by Lindner and Parfitt [1] [2] as

$$D = 0.249 \exp(-79.0 \text{ kcal}/RT)$$

in the temperature range of 1400 to 1600 °C. If the MgO was "sufficiently pure," the value for the activation energy represents that for the intrinsic diffusivity region. Self-diffusion measurements of Ni^{+2} in NiO by Choi and Moore [2] in the temperature range of 1000 to 1470 °C showed

$$D = 1.82 \times 10^{-3} \exp(-45.6 \text{ kcal}/RT)$$

Self-diffusion measurements of Fe^{+2} in $Fe_{0.907}O$ by Himmel et al. [3] in the temperature range of 700 to 1000 °C showed

$$D = 0.118 \exp(-29.7 \text{ kcal}/RT)$$

Diffusion measurements of iron in α-Fe_2O_3 in air by Izvekov et al. [4] in the temperature range 950 to 1050 °C showed

$$D = 1.3 \times 10^{6} \exp(-100.2 \text{ kcal}/RT)$$

It has been found by several investigators that addition of Mg^{+2} ions to Fe_xO results in a decrease of the Fe^{+3}/Fe^{+2} ratio indicating that magnesium ions do not act purely as a diluent. Diffusion studies on the Fe_xO-MgO system, which forms a complete solid solution, are contradictory. Wuensch and Vasilos [5] have shown that

$$D = 8.83 \times 10^{-5} \exp(-41.6 \text{ kcal}/RT)$$

indicating no compositional dependency. Rigby and Cutler [6] found that the diffusivity but not the activation energy is concentration dependent.

In reaction studies between Fe_2O_3 and MgO Carter [7] concluded that the solid-state reaction forming $MgFe_2O_4$ occurred by counterdiffusion of the Mg^{+2} and Fe^{+3} ions through a relatively rigid oxygen lattice. He found the ratio of $MgFe_2O_4$ formed on the MgO side of the initial interface to that formed on the Fe_2O_3 side to be 1:2.7. Fresh and Dooling [8] indicated that the rate controlling step in this reaction is the diffusion of the oxide components through the ferrite product layer. Schaefer and Brindley [9] found that "isolated islands" of $MgFe_2O_4$ developed inside crystals of (Fe, Mg)O upon oxidation.

2. Experimental Procedure

2.1. NiO-MgO Diffusion Couples

Reagent grade NiO powder was used for all of the polycrystalline NiO-single crystal MgO diffusion runs. Single crystal NiO vs. single crystal MgO runs were also made. Diffusion anneals were made in the temperature range 1200 to 1400 °C both at atmospheric pressure and at 10^{-6} torr.

2.2. Fe-MgO Diffusion Couples

Single crystals of MgO were packed in reagent grade iron powder and annealed at temperatures from 1100 to 1350 °C at a pressure of 10^{-6} torr.

2.3. Fe_2O_3-MgO Diffusion Couples

Reagent grade ferric oxide was used for all polycrystalline Fe_2O_3 diffusion runs. Single crystals of MgO packed in Fe_2O_3 powder were annealed in air in the temperature range 1020 to 1500 °C. A run of single crystal Fe_2O_3 versus single crystal MgO was also made at 1330 °C. Diffusion runs were either air-cooled or cooled with the furnace rather

[1] Extended abstract; complete paper has been submitted for publication in the Journal of the American Ceramic Society.
[2] Figures in brackets indicate the literature references at the end of this paper.

290-621 O-68—7

than quenched into water in order to prevent shattering of the MgO single cyrstals. Several samples, however, were quenched into cold water from 1350 °C and 1500 °C for the purpose of obtaining EPR and optical absorption specimens.

2.4. Analytical Studies

An Applied Research Laboratories electron microprobe was used to determine diffusion profiles. The K_α x-ray emission line was monitored for all the cations present. Specimen currents were set at 0.03 μa. The data output from the microprobe was fed to a CDC 6600 computer where the various correction factors necessary to quantitatively convert counts to concentrations were applied.

Specimens of the Fe-MgO and Fe_2O_3-MgO systems were prepared for the electron paramagnetic resonance studies in the same manner as for the diffusion studies. Crystals of MgO containing gradients of iron were either cleaved or ground to obtain varying concentrations of iron ions in the crystals. EPR spectra were also obtained for the MgO crystals as received and after various treatments. The EPR spectrometer was calibrated by using two standards: Diphenyl-picryl hydrazyl (D.P.P.H.) with a g value of 2.0037 and 5×10^{14} spins of Cr^{+3} in MgO ($g=1.987$).

Optical absorption spectra were taken on specimens obtained from the diffusion zone of several Fe_2O_3-MgO and Fe-MgO couples. A Beckman IR–4 was used for the 1–10 μ region and a Cary 14 for the 250 $m\mu$-1μ region. Patterns were taken using the double beam.

A Fe_2O_3 single crystal versus MgO single crystal diffusion couple was examined using the Laue back reflection technique in order to determine whether the resulting $MgFe_2O_4$ zone formed by reaction was a single crystal. Its relative orientation was also determined.

3. Diffusion Mathematics

The Boltzmann-Matano approach was applied for solution of the diffusion equations in the Fe-MgO and NiO-MgO systems. A computer was used to reduce error to a mimimum in solving the equation:

$$D_{c=c_1}=-\frac{1}{2t}\cdot\left(\frac{dx}{dc}\right)_{c=c_1}\int_o^{c_1}x\,dc$$

The mathematics needed in order to calculate the diffusivities in the Fe_2O_3-MgO system involve a 3-phase 2-moving boundary solution. Figure 1 shows the phase diagram and diffusion profile for this system. The theoretical solution to this problem was determined by Dorn and Blank [10].

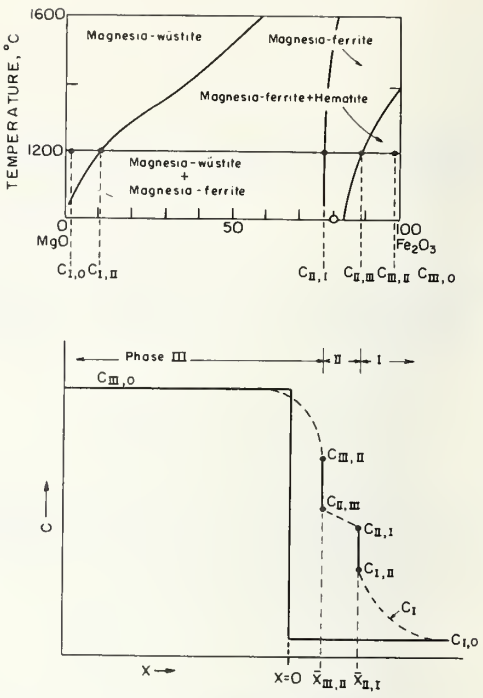

FIGURE 1. *Phase diagram and diffusion profile for three phase diffusion problem.*

The data needed for the analytical solution is not known either from this study or from the literature. An approximation thus had to be made to calculate the D values for the interdiffusivity of Fe^{+3} and Mg^{+2}. If we assume that the original interface between the Fe_2O_3 and the MgO is located at the boundary $\bar{X}_{II,I}$ we can calculate D_I (D of Fe^{+3} in MgO).

$$C_I=C_{I,o}+\left[\frac{C_{I,II}-C_{I,o}}{1-\text{erf}\,(\gamma_I)}\right]\left[1-\text{erf}\left(\frac{x}{\sqrt{4D_It}}\right)\right]$$

where γ_I is defined by the relation

$$\bar{X}_{II,I}=\gamma_I\sqrt{4D_It}$$

and all other quantities are defined on the diffusion profile shown in figure 1. Since for all practical purposes $C_{I,o}=0$, then

$$\frac{C_I}{C_{I,II}}\left[1-\text{erf}\,(\gamma_I)\right]=\left[1-\text{erf}\left(\frac{x}{\sqrt{4D_It}}\right)\right].$$

Knowing $C_{I,II}$, x, t, C_I and using the approximation stated above that $\bar{X}_{II,I}$ is the initial interface, we can calculate D_I from

$$\frac{C_I}{C_{I,II}}=\left[1-\text{erf}\left(\frac{x}{\sqrt{4D_It}}\right)\right].$$

The resulting diffusivities are therefore indicative of some average composition within the diffusion zone in MgO. This approximation prevents the determination of concentration dependence if it exists, but it is thought that it is more applicable in this case than the Boltzmann-Matano solution would be to a 3-phase problem.

4. Results

4.1. Fe-MgO System

In a vacuum from 1100 to 1350 °C iron enters MgO by the redox reaction

$$x\mathrm{Fe} + \mathrm{MgO} = \mathrm{Fe}_x\mathrm{O} + \mathrm{Mg}\uparrow .$$

The relationship between ln D and the concentration of Fe, in terms of the atomic percent (a/o) of Fe, at a given temperature was found to be linear from 2 a/o Fe to the iron concentration in MgO at the interface which was constant for all times at a given temperature. In this system, thus, there is no moving boundary on diffusion, and the actual and Matano interfaces are identical. Table 1 lists the diffusivity results.

The above results show a trend in activation energies which is opposite to that expected on the basis of the energies found for the end components, 79 kcal for MgO and 30 kcal for Fe_xO. The observed trend in activation energy values prompted investigations of the NiO-MgO and Fe_2O_3-MgO systems.

4.2. NiO-MgO Systems

Figure 2 shows a typical diffusion profile obtained in the NiO-MgO system using single crystals in an air atmosphere. The Boltzmann-Matano interface at approximately 290μ which corresponds to the initial interface lies on the higher nickel side of the 25 a/o concentration (the actual interface) indicating that a flow of excess Mg^{+2}, and an equivalent amount of $O^{=}$ ions in order to maintain electroneutrality, occurred across the actual moving NiO-MgO interface. The results of the diffusion study in an air atmosphere are listed in table 2.

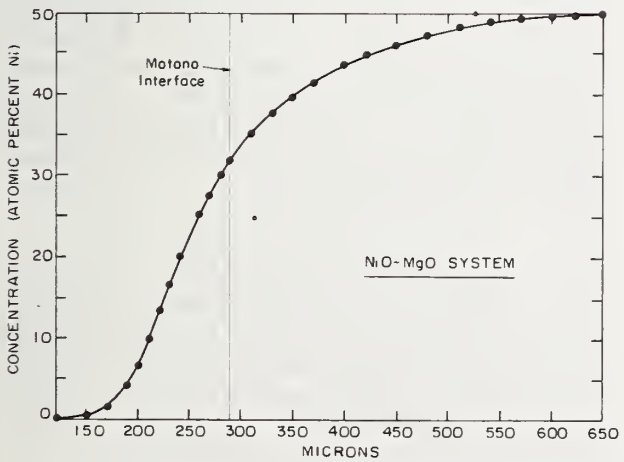

FIGURE 2. *Typical diffusion profile in the NiO-MgO system annealed in air at 1370 °C.*

TABLE 1.

C (a/o Fe)	D_o (cm²/sec)	ΔH (kcal/mole)
5	6.34×10^{-7}	29.6
10	4.49×10^{-6}	32.9
15	5.04×10^{-5}	37.7
20	8.40×10^{-4}	43.5

TABLE 2.

C (Ni a/o)	D_o (cm²/sec)	$\Delta H^{\ddagger}$ (kcal/mole)
10	6.31×10^{-6}	42.8
20	1.05×10^{-5}	42.8
30	1.96×10^{-5}	42.8
40	3.16×10^{-5}	42.8

In vacuum the relation $D = 9.82\times10^{-6}$ exp (-45.5 kcal/RT) was found to hold with the activation energy and diffusivities concentration independent. The activation energy values for diffusion in vacuum and in air are not significantly different to warrant postulation of any mechanism change.

These results suggest that the concentration of vacancies in the air experiments increases with an increase of nickel concentration due to the formation of Ni^{+3}. Since the activation energy was found to be independent of composition and atmosphere, it is postulated that no structural changes occur in this system and that diffusion proceeds by counter-diffusion of Ni^{+2}, Ni^{+3} and Mg^{+2} ions on octahedral sites. Substitutional solid solutions are therefore to be expected.

4.3. Fe_2O_3-MgO System

Figure 3 shows a computer-drawn typical diffusion profile in the Fe_2O_3-MgO system obtained in air. The irregularities in the profile starting at a concentration of approximately 1 a/o Fe represent precipitates in the crystal which probably formed on cooling. The discontinuous increase in iron concentration seen at 900μ is due to the presence of the $MgFe_2O_4$ phase, and the increase near the 1000μ region is due to the transition to the Fe_2O_3 phase. Optical examination of the

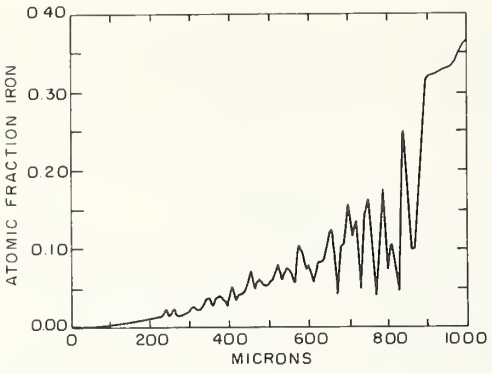

FIGURE 3. *Diffusion profile in the Fe_2O_3-MgO (air) system annealed at 1460 °C for 42 hours (computer drawn).*

diffusion specimens at room temperature indicated that the precipitates in the MgO single crystal region were coherent since they were not visible but that the precipitates of α-Fe_2O_3 in the $MgFe_2O_4$ phase were incoherent.

The x-ray analysis of a single crystal versus single crystal couple showed that the $MgFe_2O_4$ phase formed by reaction was a single crystal oriented with the (100) face of the $MgFe_2O_4$ coincident with the (100) face of the MgO. The observation with the electron microprobe that several Fe_2O_3 precipitates were in contact with the MgO region without reaction substantiated the conclusion that the precipitates in the $MgFe_2O_4$ region were formed on cooling. A large solubility of Fe_2O_3, probably as Fe_3O_4, in the $MgFe_2O_4$ at high temperatures is therefore indicated. The data also showed that the solubility of MgO or $MgFe_2O_4$ in α–Fe_2O_3 is very small. Because the limit of detection of precipitates by the electron probe was on the order of 1μ, the precipitates were of that order of size in the 1 *a/o* Fe concentration region. The results of the diffusion analysis showed the relationship

$$D = 8.83 \exp(-74.6 \text{ kcal}/RT)$$

to hold over the temperature range 1000 to 1460 °C. This expression is the mathematical approximation for some average composition within the diffusion zone in MgO. The analysis did not allow a determination of any concentration dependence of either the D_o or the activation energy terms if it existed.

4.4. Electron Paramagnetic Resonance Studies

Examination of the MgO starting crystals by EPR showed that octahedrally coordinated Fe^{+3} ions were present. These could be reduced to Fe^{+2} by heating in vacuum (10^{-6} torr) for 48 hours at 1200 °C. The spectroscopic analysis showed a total iron concentration of 0.01 percent. The *g*-value for Fe^{+3} at the 0.01 percent total iron concentration was found to be 1.993. Further studies by EPR on crystals to which small amounts of iron were added by diffusion showed that the *g* value for the Fe^{+3} ions moves from 1.993 ($1/2 \rightarrow -1/2$ transition) to higher *g* values as the trivalent iron concentration increases. These studies also showed that at 0.2 *a/o* Fe^{+3} and below it is relatively easy to reduce all the Fe^{+3} ions to Fe^{+2} by heating in a vacuum.

Specimens were also investigated from the diffusion zone in MgO of the Fe_2O_3-MgO couples. The EPR spectra of a sample from a couple run in air and containing a high iron concentration shows two important features: a sharp transition occurring at $g=2.56$ and a broad absorption starting at approximately 1000 gauss. The spectra of the same specimen after reduction at 1300 °C for 10 hours in vacuum (10^{-6} torr) shows that the sharp transition at $g=2.56$ disappears, and that the broad absorption remains but is shifted to the $g=2.44$ region. In both cases the specimen was ferrimagnetic, indicating that some Fe^{+3} ions were in tetrahedral sites. From the spectra discussed and other EPR experiments the following assignments were made for the important features observed in the patterns. The peak at $g=1.993$ which broadens and shifts to $g=2.56$ is the $1/2 \rightarrow -1/2$ transition of Fe^{+3} coordinated in a distorted octahedral site. The *g*-value shift is due to the ferrimagnetic $MgFe_2O_3$ elements which form at the higher iron concentrations. The field as seen by an Fe^{+3} ion in such an environment will be considerably different from the field seen by an Fe^{+3} ion in a paramagnetic environment. The ferrimagnetic centers tend to concentrate the field and therefore cause the $1/2 \rightarrow -1/2$ transition to occur at a lower externally applied field. The broad absorption starting about 1000 G is related to the ferrimagnetic material in the crystals.

EPR spectra in the Fe-MgO system showed similar features. Both octahedral Fe^{+3} and ferrimagnetic material were present.

4.5. Optical Studies

The optical investigation showed that Fe^{+2} (octahedrally coordinated) has a broad absorption band centered at 1μ. Trivalent iron shows a band in the region of 0.5μ. Specimens from an Fe_2O_3-MgO couple quenched from 1350 °C in air showed a different composition when compared with similar specimens that were slow-cooled indicating that compositions at the annealing temperatures are

not necessarily the same as those measured at room temperature. The quenched samples were higher in Fe^{+2} content than those that were slow-cooled.

5. Discussion

The results of the Fe-MgO diffusion experiments under vacuum conditions indicated that both D_o and the activation energy vary with iron concentration. Of particular interest are the values for the activation energy which increase from 29 kcal at 5 *a/o* to 43 kcal at 20 *a/o* Fe. The EPR and optical studies on specimens cooled in vacuum have shown that the introduction of Fe^{+2} ions into MgO is associated with the appearance of Fe^{+3} ions by reaction, with some unknown amount in tetrahedral sites.

The concentration of thermally created vacancies in the MgO was compared with that chemically created due to the presence of original trivalent impurities. Assuming that the heat of formation of a Shottky defect in MgO is 5 eV, the equilibrium concentration of vacancies in theoretically pure MgO at 1200 °C would be about $10^{14}/cm^3$. If the only trivalent impurities in our crystals were the 0.005 wt percent Al_2O_3 indicated by spectroscopic analysis, then the calculated concentration of chemically created vacancies is a minimum of $10^{18}/cm^3$, or 4 orders of magnitude greater than the equilibrium concentration of the thermally created vacancies. The existing impurities therefore place all diffusion experiments into the extrinsic rather than intrinsic region. This result then provides an explanation for the ΔH value of 29.6 kcal/mole at the low iron concentrations rather than the expected 79 kcal for the intrinsic region.

Examination of the MgO structure indicates that the four octahedral sites adjoining a tetrahedral site filled with an Fe^{+3} ion must be vacant in order to avoid extremely high cation-cation repulsive forces. The resulting defect in the MgO matrix is now an embryonic element of the inverse spinel structure whose size initially would be less than one unit cell of the $MgFe_2O_4$ structure. These embryonic units, however, could act as nucleation sites for subsequent precipitation in the system on cooling. It would be expected that the bond strength of the Mg^{+2} ions coordinated with oxygens associated with such filled tetrahedral sites would be significantly increased. This would result in an increased heat of motion term when these Mg^{+2} ions move since counterdiffusion must occur to maintain electroneutrality. This structural change occurring inside the crystal could then provide an explanation for the increasing activation energy with increase of iron seen in this system.

The results obtained in the NiO-MgO system, however, suggest a different mechanism. In this case the diffusivity but not the activation energy is a function of the nickel concentration in air; in vacuum there is no concentration dependence. These results and the absence of precipitates in the system suggest that no structural changes occur and that most, if not all, of the cations remain on octahedral sites. In this case a true substitutional solid-solution exists.

The optical studies have shown the existence of Fe^{+2} in the Fe_2O_3-MgO system. The mechanism for formation of Fe^{+2} from the Fe^{+3} ions is believed to be related to the formation of $MgFe_2O_4$ in the system. In this process a driving force is established for the reduction of some Fe^{+3} to Fe^{+2} with the release of oxygen at the surface. The oxidation-reduction process should be relatively easy due to the small energy necessary to transfer an electron between neighboring octahedrally coordinated Fe^{+3} and Fe^{+2} ions. This mechanism could also be used to explain the effect observed with addition of Mg^{+2} ions on the Fe^{+3}/Fe^{+2} ratio in magnesio-wüstite crystals.

6. References

[1] K. Lindner and G. D. Parfitt, Diffusion of Radioactive Magnesium in Magnesium Oxide Crystals, J. Chem. Phys. **26,** 182 (1957).

[2] J. S. Choi and W. J. Moore, Diffusion of Nickel in Single Crystals of NiO, J. Phys. Chem. **66,** 1308 (1962).

[3] L. Himmel, R. F. Mehl and C. E. Birchenall, Self-Diffusion of Iron in Iron Oxides and the Wagner Theory of Oxidation, Trans. Am. Inst. Min. Met. Eng. **197,** 827 (1953).

[4] V. I. Izvekov, N. S. Gorbunov and A. A. Babed Zakhryapin, Diffusion of Iron in Hematite, Fiz. Metal. i Metalloved **14,** 195 (1962).

[5] B. J. Wuensch and T. Vasilos, Diffusion of Transition Metal Ions in Single-Crystal MgO, J. Chem. Phys. **36,** 2907 (1962).

[6] E. B. Rigby and I. B. Cutler, Interdiffusion Studies of Fe_xO-MgO, J. Am. Ceram. Soc. **48,** 95 (1965).

[7] R. E. Carter, Mechanism of Solid-State Reaction Between Magnesium Oxide and Aluminum Oxide and Between Magnesium-Oxide and Ferric Oxide, J. Am. Ceram. Soc. **44,** 116 (1961).

[8] D. L. Fresh and J. S. Dooling, Kinetics of the Solid-State Reaction Between Magnesium Oxide and Ferric Oxide, J. Phys. Chem. **70,** 3198 (1966).

[9] W. L. Schaefer and G. W. Brindley, Oxidation of Magnesio-wüstite Single Crystals, J. Phys. Chem. Solids **24,** 919 (1963).

[10] J. Dorn and S. L. Blank (to be published).

Impurity Cation Diffusion in Magnesium Oxide

B. J. Wuensch

Ceramics Division, Department of Metallurgy and Materials Science
Massachusetts Institute of Technology, Cambridge, Massachusetts 02139

and

T. Vasilos

Avco Corporation, Space Systems Division
Lowell, Massachusetts 01887

Diffusion coefficients for Ca^{2+} in single-crystal MgO have been determined in the range 790 to 1850 °C from concentration gradients obtained with the aid of electron microprobe spectroscopy. Step-function distributions of solute provided artificial Gaussian gradients with an apparent Dt product of 1.7 10^{-8} cm^2, and demonstrated that the microprobe technique could not be reliably used for the analysis of gradients less than 10μ in extent. A procedure for correction of the gradients for this effect was developed, and will be applied to the data. The diffusion coefficients obtained are tentatively represented by an activation energy of 2.76 eV, and a pre-exponential term D_o of 8.9 10^{-4} cm^2/sec. Diffusion coefficients obtained above 1200 °C are in good agreement with recent results of Rungis and Mortlock.

Data are available for both anion and cation self-diffusion in MgO, and for the diffusion of 9 different impurity cations. None of these results have revealed a change of slope in the temperature variation of the diffusion coefficient. Unequivocal identification of the diffusion processes as extrinsic or intrinsic is difficult. Available estimates of the energy required for Schottky pair formation in MgO indicate the purity of the crystals employed in most studies should result in extrinsic behavior at all temperatures up to the melting point of the material. This view is supported by activation energies for impurity ion diffusion which are less than half the energy required for defect formation, and small D_o values characteristic of extrinsic diffusion. The Mg^{2+} self-diffusion data appears to represent intrinsic transport. The energy for Mg^{2+} self-diffusion should therefore display no correlation with energies for impurity ion diffusion or for cation self-diffusion in transition metal oxides. Recent cation diffusion data do not display a regular variation with the ratio of ionic radius to polarizability, as previously proposed by the writers. It is concluded that the early agreement with this relationship was fortuitous. Interpretation of the variation of impurity cation activation energy in terms of a size effect explains the difference in values observed for ions of greatly different size, but cannot explain smaller differences between ions of similar radius. It is proposed that different correlations may apply to spherical-shell ions and to ions, such as the transition metals, with highly polarizable d electrons.

Wuensch & Vasilos:

Key Words: Cation diffusion, electron microprobe, magnesium oxide, Schottky pair.

1. Introduction

Many properties of ceramic oxides are controlled by the rates of diffusion of one of the constituent ions. Both anion and cation self-diffusion rates have therefore been determined for a number of materials in order to gain insight into the kinetics of such processes. Study of impurity ion diffusion, on the other hand, affords the possibility of determining the influence of the nature of the diffusing atom on diffusion in a given oxide when such measurements are made for a series of different ions. Correlations between diffusion rates and properties of the migrating species have been observed for metals. No completely satisfactory relationship has been established for ionic crystals.

Diffusion rates have now been determined for a number of impurity cations in single-crystal MgO. This oxide has been studied for a number of reasons. Magnesium oxide has the NaCl-type structure common to many of the alkali halides. Transport has been extensively studied in these materials and is relatively well understood. Single crystals of MgO, although of questionable character, are readily available. Oxides of a number of divalent cations display complete or appreciable solid solu-

bility in MgO, and thus are amenable to study. The present paper describes preliminary results of a study of diffusion of Ca^{2+} in single-crystal MgO, and summarizes the data presently available for the diffusion of other impurity ions in this material.

2. Experimental

2.1. Sample Preparation

Diffusion couples in the system CaO-MgO were prepared with single crystals obtained from the Norton Company, Worcester, Mass. Specimens of two varieties were employed. In a first type, a 1μ layer of 50 wt percent CaO-MgO solid solution was placed between two polished (100) surfaces of MgO single crystals. The vapor pressure of CaO was appreciable at the higher temperatures investigated, and it was necessary to encapsulate the entire specimen in a cylinder of pressed MgO powder. This compact sintered to high density during the early portion of the diffusion annealing and prevented loss of solute through vaporization. Annealing of the thin-film type of diffusion couple produces a Gaussian distribution of solute. If the diffusion coefficient, D, is independent of concentration, a plot of the logarithm of solute concentration as a function of the square of penetration is linear, and has slope given by $(4Dt)^{-1}$, where t is the time of the diffusion annealing.

In a second type of specimen a polished (100) surface of a MgO crystal was placed over a small well of sintered MgO in which a pellet of 50 wt percent CaO-MgO solid solution had been placed. The surface of the crystal was thus in equilibrium with a vapor of the solute and was maintained at constant concentration throughout the course of the annealing. If the diffusion coefficient is independent of concentration, these boundary conditions produce a solute distribution given by C_o erfc $x(4Dt)^{-1/2}$, where C_o is the surface concentration and erfc is the complementary Gaussian error function. The inverse complementary error function of C/C_o is a linear function of penetration into the sample, and has a slope given by $(4Dt)^{-1/2}$.

All diffusion annealings were conducted in air. Samples were prepared in the temperature range 790 to 1850 °C. The duration of the annealings ranged from 24 hr, at the higher temperatures investigated, to as long as 1.2 yr.

2.2. Diffusion Couple Analysis

After completion of the diffusion annealing, the MgO crystals were cleaved along a (100) plane parallel to the diffusion direction. The cleaved surface was then polished. The distribution of CaO solute was determined with the aid of electron microbeam probe spectroscopy. The samples were analyzed with a 30 kV electron beam having a diameter of approximately 1μ. Intensities of CaK_α radiation were recorded relative to the intensity obtained from a $CaCO_3$ standard to eliminate possible variations in beam characteristics. The intensity ratios were converted to concentrations of CaO through comparison with intensities obtained from a set of fine-grained sintered CaO-MgO standards.

Diffusion rates at the lower temperatures which were investigated were extremely small. Diffusion annealings in excess of a year in duration produced measurable concentration gradients of only 10 to 15μ in extent. Since the diffusion coefficients obtained from the initial samples prepared at these temperatures were believed to be less accurate than those obtained at the higher temperatures, additional samples were prepared which employed diffusion annealings of longer duration. The latter samples usually provided diffusion coefficients which were smaller than those obtained from comparable specimens annealed for shorter times.

It was therefore suspected that the short gradients which had been measured had been influenced by lack of resolution of the microprobe. This was experimentally confirmed by coating MgO crystals with a thin layer of solute in the manner used to prepare diffusion couples. These specimens were not subjected to a diffusion annealing. Normal microprobe analysis of crystals with such a step-function distribution of solute provided an apparent concentration gradient approximately 8μ in extent. The apparent solute distribution was Gaussian in nature, and thus was difficult to distinguish from actual solute penetration into the material. The form of the apparent distribution was independent of the concentration of CaO in the step function, and corresponded to an apparent product Dt of $1.7\ 10^{-8}$ cm^2.

This effect provides an example of the caution which must be exercised in examining small-scale features through microprobe spectroscopy. In matrices of low atomic number, such as MgO, penetration of the electron beam into the specimen and secondary fluorescence may decrease the effective resolution of the electron beam to several times the nominal diameter of the electron beam.

2.3. Correction of the Data

The concentration gradients measured with the microprobe correspond to the convolution of the true concentration gradient with an instrumental

broadening function which was approximately Gaussian in nature. The form of the apparent concentration gradient obtained upon analysis of step-function distributions of solute was reproducible and independent of concentration in the step. It was therefore assumed to represent a reliable measure of the instrumental broadening.

Correction for the effect is simple for thin film diffusion couples in which all solute concentrations fall within the permissible range of solid solution of CaO in MgO. The convolution of two Gaussian functions is a Gaussian function with an exponential parameter equal to the sum of the exponential parameters of the two original functions. A true value of the product Dt may therefore be obtained by subtracting from the apparent value the product $1.7\ 10^{-8}$ cm^2 obtained from the step functions. This procedure unfortunately is not valid for the complementary error function distributions, or for several of the thin-film specimens which displayed a surface layer of CaO which had not been completely dissolved in the MgO crystal.

For these specimens it was assumed that each apparent concentration, C^a, experimentally determined at a discrete penetration x_i, was given by the sum of the true concentration, C^o, plus a linear combination of the true concentrations at neighboring penetrations. This relation may be expressed

$$C^a(x_i) = C^o(x_i) + \sum k_j C^o(x_{i+j})$$

where the proportionality constants, k, are determined from the apparent concentration distribution obtained from the step function. This provides a set of simultaneous equations which may be solved for the unknown concentrations C^o. Details of this procedure, and comparison of the corrected and apparent concentration gradients will be described elsewhere [1].[1]

3. Results

Figure 1 presents a concentration distribution typical of those obtained from analysis of the vapor-deposition specimens prepared at higher temperatures. Surface concentrations ranged between 0.1 and 0.9 atomic percent CaO. The inverse complementary error function of C/C_o varies linearly with penetration into the specimen indicating that, within experimental error, D is not a function of concentration. A representative concentration distribution for the thin-film type of specimen is given in figure 2. The corrections for instrumental broadening of the distributions were negligible for the more extensive penetrations obtained at high temperatures. The diffusion coefficients obtained are plotted as a function of reciprocal temperature in figure 3.

Rungis and Mortlock [2] recently performed a similar set of measurements using MgO crystals obtained from a different source. The techniques employed in their study were quite different than those of the present work. Diffusion of the radioactive tracer Ca^{45} was studied, and concentration distributions were measured through autoradiography. Despite these differences in approach, the results of the two studies are in reasonable agreement in the temperature range 1200 to 1850 °C. For lower temperatures, however, the present work provides diffusion coefficients which are considerably smaller. The results of the present study are therefore described by

$$D = 8.9\ 10^{-4} \exp(-2.76\ \text{eV}/kT)$$

while Rungis and Mortlock's data are represented by

$$D = 2.95\ 10^{-5} \exp(-2.13\ \text{eV}/kT).$$

Our low temperature data, however, are based on concentration gradients not yet corrected for instrumental broadening. The correction will increase these diffusion coefficients and bring the results of the two studies into closer accord.[2]

4. Discussion

4.1. Comparison of Diffusion Parameters

Both cation [3] and anion [4] self-diffusion rates have been determined for single-crystal MgO. Data are also available for the diffusion of a number of impurity ions. These include Ni^{2+} [5], Co^{2+} [5], Fe^{2+} [5, 6], Mn^{2+} [6], Zn^{2+} [7], Be^{2+} [8], and Cr^{3+} [6]. The properties of these ions, and the parameters describing their diffusion in MgO are summarized in table 1. Not included in this compilation are the results of several additional studies which have employed diffusion couples of different geometry. In these experiments a single crystal of MgO was placed in contact with an extended source of polycrystalline solute oxide. These samples provide coefficients for interdiffusion *between* MgO and a pure solute oxide which, being polycrystalline, is more difficult to characterize. Measurements of

[1] Figures in brackets indicate the literature references at the end of this paper.

[2] It might be expected that the correction procedure would provide diffusion coefficients which would be still smaller, since the apparent gradient is larger in extent than the true distribution of solute. Most of the low-temperature specimens, however, retained a layer of undissolved CaO at the surface of the crystal because of the reduced range of solid solubility at these temperatures. The true concentration gradient is therefore masked by a steep apparent gradient contributed by this layer. The corrected gradient, while smaller in extent, has a much smaller slope. The corrected diffusion coefficient is therefore larger.

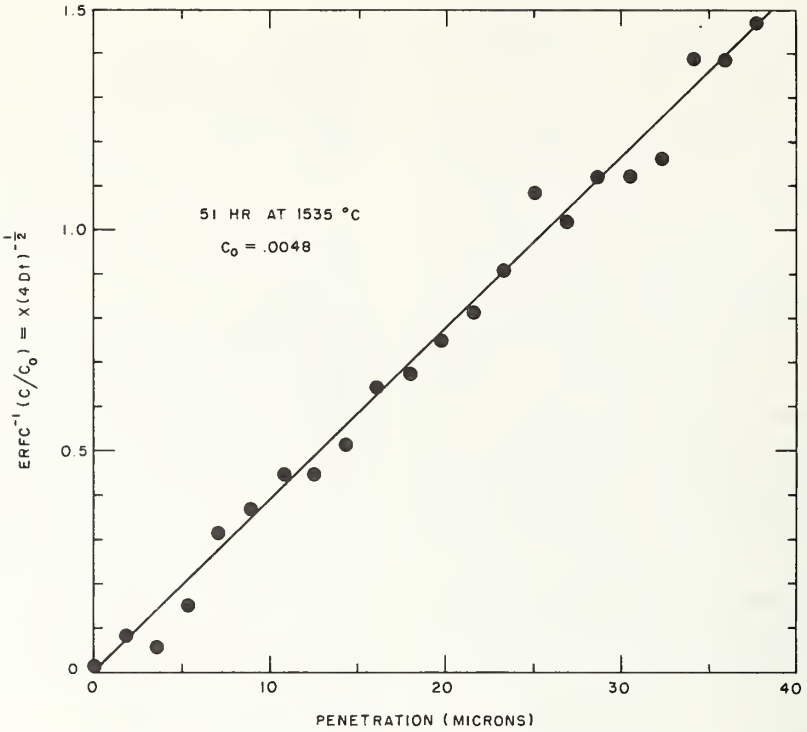

FIGURE 1. *Plot of the inverse complementary error function of CaO concentration divided by concentration at the sample surface as a function of penetration into single crystal MgO for a specimen with constant surface-concentration boundary conditions* (C_0 *expressed as atomic fraction CaO*).

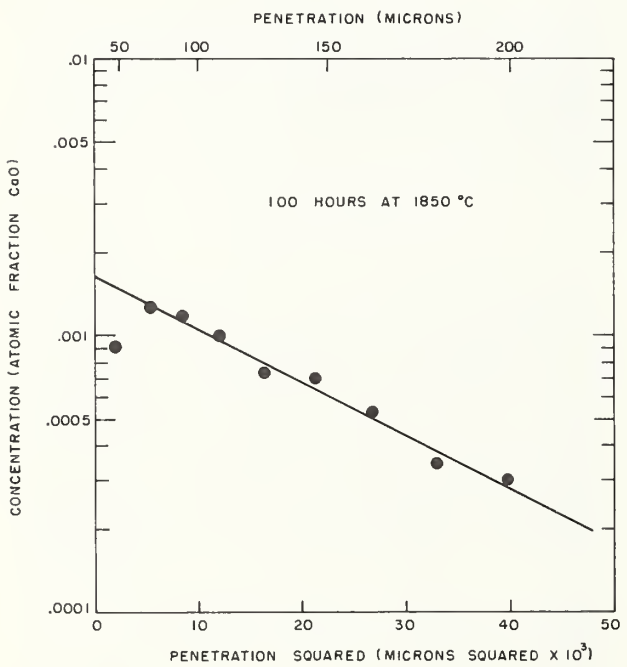

FIGURE 2. *Plot of the logarithm of concentration of CaO as a function of the square of penetration into single-crystal MgO for a specimen with thin-film boundary conditions.*

this type have been conducted for Ni^{2+} [9–11], Co^{2+} [9], Fe^{2+} [11, 12], and Mn^{2+} [13]. The principal difference between the results obtained from this type of specimen and those obtained from the thin-film or vapor-deposition type is that the diffusion coefficients obtained from the former have been found to be a marked function of concentration. None of the experiments with vapor-deposition or thin-film diffusion couples [2, 5–8], have provided evidence for a concentration-dependent diffusion coefficient. The explanation for this apparent discrepancy may be in the range of concentrations explored with the differing types of specimens. The work summarized in table 1 has been concerned with low solute concentrations. In previous work by the writers, for example, *surface* concentrations of solute oxide rarely exceeded 10 atomic percent. The principal portion of the concentration profiles consisted of concentrations of the order of fractions of an atomic percent.

In early work [5] the writers noted that the activation energies for diffusion of transition metal ions in single-crystal MgO decreased as the radius of the migrating ion increased. To explain this behavior, it was assumed that the contributions to the barrier to diffusion which differed most for

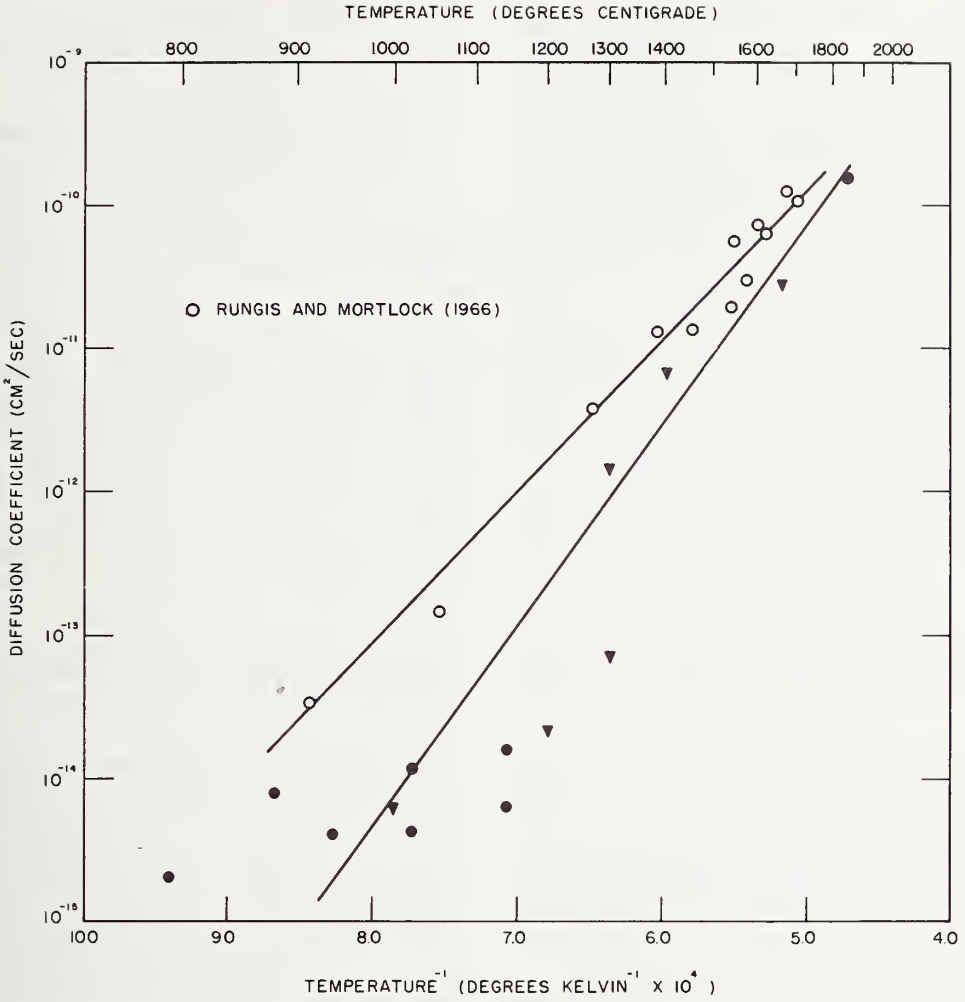

FIGURE 3. *Plot of diffusion coefficients for Ca^{2+} in single-crystal MgO as a function of reciprocal temperature.*
Triangles represent diffusion coefficients obtained from constant surface-concentration specimens, circles values obtained from thin-film samples.

TABLE 1. *Data for diffusion in single crystal MgO*

Ion	Ionic radius, r (10^{-8} cm)	Polarizability, α (10^{-24} cm^3)	r/α (10^{16} cm^{-2})	E (eV)	D_o (cm^2/sec)	Material	Reference
Be^{2+}	.31	.012	25.83	1.60	$1.41\ 10^{-5}$	M	Harding & Mortlock [8]
Cr^{3+}	.63	.852	.74	2.95	$9.8\ 10^{-4}$	N	Tagai, et al. [6]
Mg^{2+}	.65	.111	5.86	3.43	$2.49\ 10^{-1}$	N, I	Linder & Parfitt [3]
Ni^{2+}	.69	.246	2.80	2.10	$1.80\ 10^{-5}$	N	Wuensch & Vasilos [5]
Co^{2+}	.72	.289	2.49	2.06	$5.78\ 10^{-5}$	N	Wuensch & Vasilos [5]
Zn^{2+}	.74	.250	2.96	1.85	$1.48\ 10^{-5}$	N	Wuensch & Vasilos [7]
Fe^{2+}	.75	.456	1.64	1.81	$8.83\ 10^{-5}$	N	Wuensch & Vasilos [5]
				1.82	$3.2\ 10^{-4}$	N	Tagai, et al. [6]
Mn^{2+}	.80	.543	1.47	1.21	$4.1\ 10^{-7}$	N	Tagai, et al. [6]
Ca^{2+}	.99	.551	1.80	2.13	$2.95\ 10^{-5}$	M	Rungis & Mortlock [2]
				2.76	$8.9\ 10^{-4}$	N	Present work
O^{2-}	1.40	2.63	.53	2.71	$2.5\ 10^{-6}$		Oishi & Kingery [4]

I = Infra Red Development Co., Welwyn Garden City, England
M = Monocrystals Co., Cleveland, Ohio
N = Norton Co., Worcester, Massachusetts

the series of ions were the repulsive overlap energy between the jumping ion and its neighbors, and the polarization of the migrating ion. Increased radius of the diffusing ion should increase the contribution of the first term and increase the barrier to diffusion, while increased polarizability should decrease the barrier. When the logarithm of the activation energy for diffusion was plotted as a function of the ratio of ionic radius, r, to polarizability, α, for the diffusing ion, a linear relation was found for Ni^{2+}, Co^{2+}, Fe^{2+}, and Mg^{2+}. A similar relation [17] figure 4, exists between r/α and the activation energies for cation self-diffusion in the oxides MgO [3], NiO [14, 15], CoO [16], CaO [17], and FeO [16, 18]. Later data [2, 7] obtained for diffusion of the impurity ions Zn^{2+} and Ca^{2+} provided less convincing correlation. As shown in figure 4, the data for Mn^{2+} diffusion [6], Be^{2+} diffusion [8], and Ba^{2+} diffusion [19] in MgO fail completely to fit into this scheme. It must be concluded that the correlation observed between activation energy and r/α for the limited amount of early data was fortuitous, and this parameter is of questionable value in establishing relations between activation energies.

Assumption that the activation for diffusion should increase as a function of ionic radius alone satisfactorily explains the large difference in activation energies for ions of greatly dissimilar radius (e.g., Be^{2+} and Ba^{2+}). This cannot account, however, for the smaller (but apparently significant) uniform decrease of activation with increasing radius in a series of ions of similar radius (e.g., Ni^{2+}, Co^{2+}, Zn^{2+}, and Fe^{2+}). It will probably be necessary to consider additional contributions to the activation energy for diffusion in order to satisfactorily explain these variations. Changes in activation energy for spherical-shell ions (e.g., Be^{2+}, Zn^{2+}, Ca^{2+}, and Ba^{2+}) might be explained solely in terms of a size effect. Polarization of the d electrons of the transition metal ions, however, will provide an additional contribution to the activation energy for diffusion which could easily be of the order of a few tenths of an electron volt. Such ions might therefore depart significantly from correlations among data for spherical-shell ions.

4.2. Nature of the Diffusion Process

Interpretation of the mechanism of diffusion is complicated by the fact that none of the studies performed to date have revealed ranges of temperature within which diffusion could be described by different activation energies. This has prevented unambiguous identification of the activation energy in any one diffusion study as representing intrinsic or extrinsic behavior.

A theoretical estimate of the energy required for the formation of Schottky defects in MgO [20] has provided a value of 5 ± 1 eV. On the basis of this value one would predict that a concentration of aliovalent impurity of the order of 200 ppm would be sufficient to cause transport in MgO to be extrinsic for all temperatures up to the melting point of the material. Most of the diffusion studies performed with MgO, table 1, have employed crystals obtained from the Norton Company. Several independent analyses of this material have shown that these crystals may contain from 0.06 to 0.3 percent impurity oxides [6, 21]. There would be little possibility of observing intrinsic diffusion in such crystals. The low values (ca. 10^{-5} cm^2/sec) obtained for D_o for the diffusion of all impurity ions and for O^{2-} is also indicative of extrinsic diffusion. All activation energies are of the order of, or less than half the energy for Schottky pair formation. This would preclude possibility of intrinsic diffusion via a Schottky defect mechanism.

In contrast, the data for Mg^{2+} self-diffusion are represented by a D_o characteristic of intrinsic diffusion. Furthermore, the activation energy for diffusion may be satisfactorily interpreted as the sum of half the estimated energy for Schottky defect formation (2 to 2.5 eV) plus a reasonable energy (1.4 to 0.9 eV) energy for ion migration. The data for Mg^{2+} self-diffusion, unlike all other studies of diffusion in MgO, therefore appear to represent intrinsic diffusion. The Mg^{2+} self-diffusion data should therefore display no correlation with either the extrinsic data obtained for impurity ion diffusion or that obtained for cation self-diffusion in transition metal oxides. (In the latter oxides it is known that stoichiometry controls the defect concentration, and the activation energy for diffusion represents the energy for ion migration.) This provides further evidence that the r/α correlation must be fortuitous. If the bulk of the available data indeed represent extrinsic diffusion, there is no basis for comparison of D_o values. Such results will primarily reflect the impurity content of the particular crystals employed.

Problems still remain in relating the Mg^{2+} self-diffusion data with the results for impurity ion diffusion. The activation energies for impurity ion diffusion, if assumed to represent the energy for migration of the ion, are rather high compared to that estimated for Mg^{2+}. The available Mg^{2+} self-diffusion data were measured with crystals obtained from two different sources [3]. The manufacturer of one set of crystals stated purity of a level for which intrinsic behavior could be expected. The other crystals which were employed were obtained from the Norton Company. No difference between diffusion rates in the two materials was

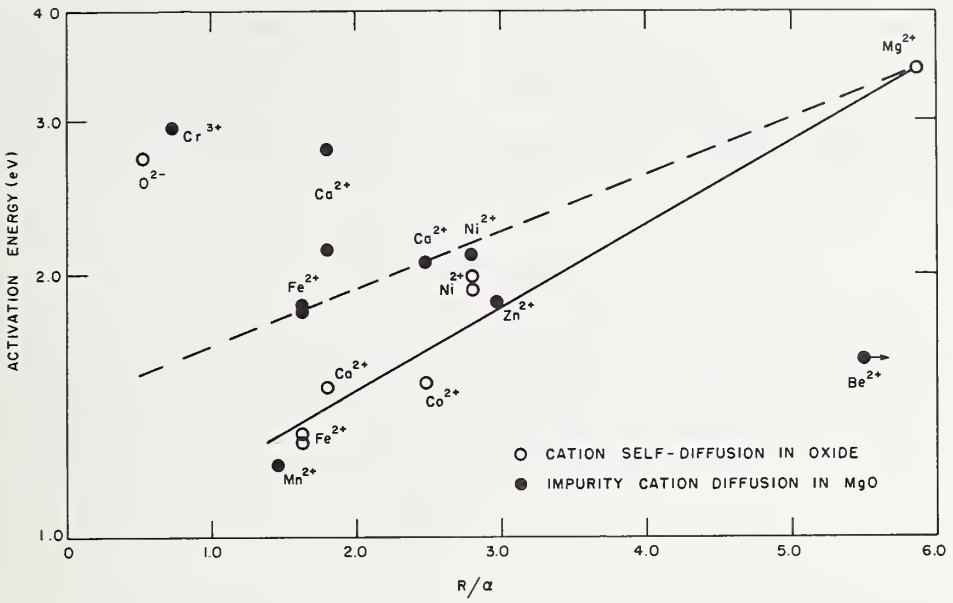

FIGURE 4. *Plot of the activation energy for impurity ion diffusion in MgO and for self-diffusion in oxides with the rock-salt structure as a function of the ratio of ionic radius to ionic polarizability for the migrating ion.*
More recent data for impurity ions do not agree with the correlation previously observed for the transition metal ions.

noted, as should be expected for intrinsic behavior. Curiously, however, all other investigations conducted with the Norton crystals appear to have produced extrinsic behavior.

Cation self-diffusion measurements are extremely difficult to perform with MgO because the longest-lived radioisotope of Mg has a half-life of only 21.3 hr. This has restricted measurement of diffusion coefficients to a narrow range of temperatures (1400 to 1600 °C) for which appreciable tracer penetrations could be obtained within a short period of time. The relation between the Mg^{2+} self-diffusion data and the data now available for impurity ion diffusion would be considerably clarified if the self-diffusion measurements could be extended to lower temperatures to reveal extrinsic behavior or, alternatively, impurity ion diffusion measurements with crystals of higher quality could be extended to high temperatures to reveal an intrinsic region of behavior.

The writers are pleased to acknowledge the assistance of W. R. Mitchell in the preparation of samples. This work was supported, in part, by contract Nonr–4267(00) with the Office of Naval Research.

5. References

[1] B. J. Wuensch and T. Vasilos, Diffusion of Ca^{2+} in Single Crystal MgO (to be published).

[2] J. Rungis and A. J. Mortlock, The Diffusion of Calcium in Magnesium Oxide, Phil. Mag. **14,** 821–827 (1966).

[3] Roland Lindner and Geoffrey D. Parfitt, Diffusion of Radioactive Magnesium in Magnesium Oxide Crystals, J. Chem. Phys. **26,** 182–185 (1957).

[4] Y. Oishi and W. D. Kingery, Oxygen Diffusion in Periclase Crystals, J. Chem. Phys. **33,** 905–906 (1960).

[5] B. J. Wuensch and T. Vasilos, Diffusion of Transition Metal Ions in Single-Crystal MgO, J. Chem. Phys. **36,** 2917–2922 (1962).

[6] H. Tagai, S. Iwai, T. Iseki and M. Saho, Diffusion of Iron, Manganese and Chromium Oxides into Single Crystal Magnesia, Radex Rundschau **4,** 577–583 (1965).

[7] B. J. Wuensch and T. Vasilos, Diffusion of Zn^{2+} in Single-crystal MgO, J. Chem. Phys. **42,** 4113–4115 (1965).

[8] B. C. Harding and A. J. Mortlock, Diffusion of Be in MgO, J. Chem. Phys. **45,** 2699–2700 (1966).

[9] I. Zaplatynsky, Diffusion of Co^{2+} and Ni^{2+} in Magnesium Oxide, J. Am. Ceram. Soc. **45,** 28–31 (1962).

[10] J. S. Choi, Diffusion of Nickel in Nickel Oxide and Magnesium Oxide, Ph. D. thesis, Indiana University (1963).

[11] Stuart L. Blank and Joseph A. Pask, Diffusion of Iron and Nickel in Magnesium Oxide Single Crystals, These Proceedings.

[12] E. Bertrand Rigby and Ivan B. Cutler, Interdiffusion Studies of the System Fe_xO-MgO, J. Am. Ceram. Soc. **48,** 95–99 (1965).

[13] John T. Jones and Ivan B. Cutler, Interdiffusion Studies in the System Mn_xO-MgO, Bull. Am. Ceram. Soc. **45,** 363 (1966).

[14] Moon Taik Shim and Walter J. Moore, Diffusion of Nickel in Nickel Oxide, J. Chem. Phys. **26,** 802–804 (1957).

[15] Jae Shi Choi and Walter J. Moore, Diffusion of Nickel in Single-crystals of Nickel Oxide, J. Phys. Chem. **66,** 1308–1311 (1962).

[16] R. E. Carter and F. D. Richardson, An Examination of the Decrease of Surface-activity Method of Measuring Self-diffusion Coefficients in Wustite and Cobaltous Oxide, J. Metals **6,** 1244–1257 (1954).

[17] Y. P. Gupta and L. J. Weirick, Self-diffusion of Calcium in Single Crystal Calcium Oxide, J. Phys. Chem. Solids **28**, 811–821 (1967).

[18] L. Himmel, R. F. Mehl, and C. E. Birchenall, Self-diffusion of Iron in Iron Oxides and the Wagner Theory of Oxidation, J. Metals **5**, 827–843 (1953).

[19] A. J. Mortlock, Divalent Cation Impurity Diffusion in MgO, These proceedings.

[20] Jiro Yamashita and Tatumi Kurosawa, Formation Energy of Lattice Defect in Simple Oxide Crystals, J. Phys. Soc. Japan **9**, 944–953 (1954).

[21] R. J. Stokes, Thermal-mechanical History and the Strength of Magnesium Oxide Single Crystals: I, Mechanical Tests, J. Am. Ceram. Soc., **48**, 60–67 (1965).

Cavity Formation in Magnesium Oxide

A. Briggs and D. H. Bowen

Ceramics Division, Harwell, Didcot, Berks.

Cavities have been produced in single crystals of MgO by two different processes; by annealing certain crystals in a reducing atmosphere and by annealing crystals irradiated with fast neutrons to doses in excess of 10^{20} nvt. Cavities produced by the first process are lenticular in shape with diameters up to $\sim 100\mu$m, and contain hydrogen at pressures up to 250 atm, even when annealing is conducted in a hydrogen-free reducing atmosphere. Those produced by the second process are cuboidal, with sides ~ 200 Å long, and contain helium and neon produced by transmutation.

Preliminary studies of the cavities by a number of techniques are described and their modes of formation and the behaviour of the associated gases are discussed.

Key Words: Annealing, cavities, diffusion, magnesium oxide.

1. Introduction

The formation of a cavity in a crystalline solid requires an adequate supply of vacancies. The vacancies may result either from lattice displacements produced by ionising or heavy particle radiation or from departures from stoichiometry, as for example, in crystals containing impurity ions of different valence from those of the host lattice. These processes may be accompanied by the formation of a gaseous phase by conversion of the anion constituent to free gas, decomposition of impurities or by transmutation. Studies of the mechanisms of cavity formation and the behaviour of the associated gases may prove valuable as a means of gaining information on transport processes in solids.

Cavities are known to form in alkali halides under a variety of treatments such as X and electron irradiation, (Hibi et al. [1],[1] Tanaka et al. [2]), neutron irradiation, (Gilman and Johnston [3]) and annealing in hydrogen, (Amelinckx et al. [4]) but apart from studies of gas bubble formation, (Whapham [5]), (Woollaston and Wilks [6]), comparable phenomena do not appear to have been reported hitherto in oxides. This paper described the formation of cavities in single crystals of magnesium oxide by two methods; by annealing in a reducing atmosphere and by annealing after irradiation with fast neutrons to doses in excess of 10^{20} nvt ($\geq$1 MeV). In both cases the resulting cavities contain gases.

2. Cavities Produced by Annealing in a Reducing Atmosphere

Certain MgO crystals, after annealing for periods of several hours in a reducing atmosphere at temperatures above 1000 °C have been found to contain cavities $\sim 100\mu$m in diameter. These lie parallel to {100} planes, are lenticular in cross-section and, in the plane of the cavity, are bounded by ⟨110⟩ directions. (Figs. 1 and 2.) The figures also show that the crystal surrounding a cavity is heavily dislocated and contains a high concentration of impurities, (Bowen [7]). Smaller cavities, ~ 1000 Å in size, are also observed that initially are octahedral with {111} facets. (Fig. 3.) At a slightly later stage in growth, these cavities may also develop {100} facets.

Figure 4, showing different cavities in various stages of formation observed by ultramicroscopy, indicates a possible sequence for growth of the lenticular cavities. Figure 4 (1) is a region of crystal having roughly the shape and dimensions of the final cavity but consisting of a large number of small cavities that act as scattering centres and hence show as bright spots. Formation of the final cavity then appears to take place by amalgamation of the small cavities. The amalgamation (dark area) occurs preferentially at the centre of the region (fig. 4(3)) or sometimes in lobes directed along either ⟨110⟩ or ⟨100⟩. Figure 5 is a scanning electron micrograph of an embryonic lenticular cavity cleaved through its mid-plane. In this case, amalgamation has occurred in lobes along ⟨100⟩ and stereo photographs confirm that the dark areas a, b, c, d, are depressions while the bright areas are prominences, i.e., the cruciform structure consists of small cavities separated by walls of crystal.

Bubbles of gas are liberated from cavities in both slowly and rapidly cooled crystals when dissolved in acid and comparison of the sizes of cavities in the solid and corresponding bubbles in

[1] Figures in brackets indicate the literature references at the end of this paper.

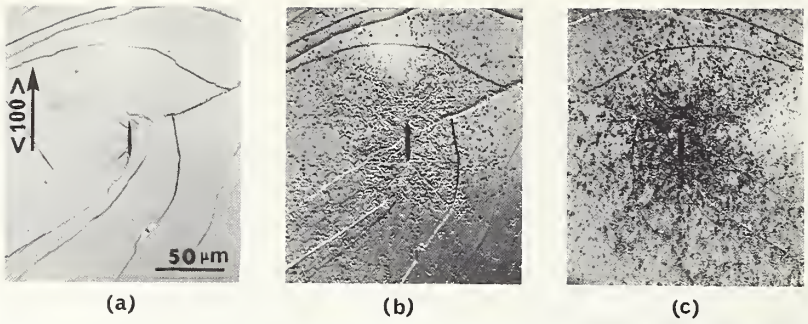

FIGURE 1. *a. Crystal cleaved on {100} plane to reveal cross-section of a lenticular cavity.*
b. As (a) after etching to reveal dislocations.
c. Matched cleavage face after etching to reveal impurities.

the acid shows that the gas pressure in a cavity at room temperature is ~ 250 atm. Analysis, by mass spectrometer, of the gas released when the crystals are crushed shows that it is invariably hydrogen even when the annealing atmosphere is hydrogen-free deuterium or carbon monoxide. Not all MgO crystals yield cavities when annealed, but those that do exhibit a relatively large OH^- absorption in the infrared which decreases considerably on formation of the cavities (fig. 6). In crystals showing the most intense absorption (produced by W. & C. Spicer Ltd., Winchcombe, Gloucestershire from MgO supplied by Kanto Chemical Co.) the estimated concentration of OH^- centres (see below) is $\sim 10^{18}cm^{-3}$.

The cavities are not distributed uniformly throughout the crystal. They appear in a band whose thickness increases with time but whose outer edges are at a constant depth below the surface, irrespective of the annealing time. The number of lenticular cavities (average diameter 20μm) within the band in crystals having a high OH^- centre concentration is typically $\sim 2.5 \times 10^5 cm^{-3}$.

The fact that hydrogen-filled cavities result from annealing in deuterium, carbon monoxide or hydrogen indicates that the gas in the cavities stems from an internal source. The presence of OH^- as an impurity in MgO single crystals has previously been reported by Wertz et al. [8], Kirklin et al. [9] and by Glass and Searle [10]. These observations, together with the correlation between the incidence of cavities and the intensity of the OH^- absorption obtained in the present work suggest that the effect of the reducing atmosphere is to create vacancies for cavity growth and to liberate hydrogen from the hydroxyl ion impurity of the crystals. Since the presence of hydrogen in the cavities in both slowly and rapidly cooled crystals indicates that the gas does not precipitate during cooling, any mechanism for cavity formation must explain the accumulation of hydrogen during growth of the cavity. A tentative explanation, based on the OH^--type centres described by

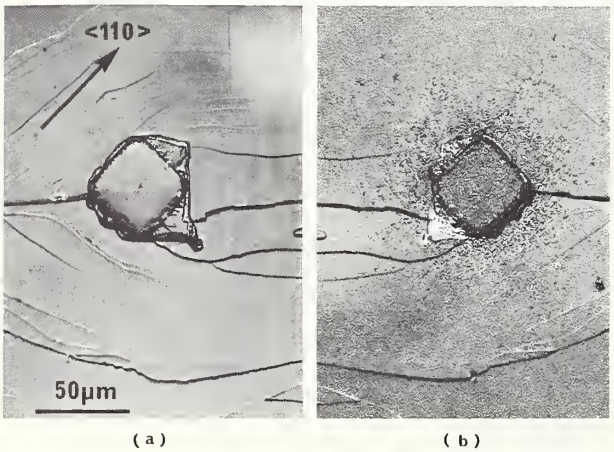

FIGURE 2. *a. Cavity cleaved through its mid-plane.*
b. Matched cleavage face after etching to reveal impurities.

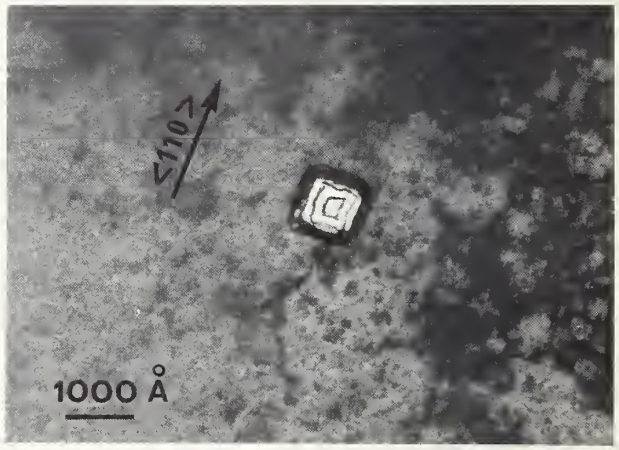

FIGURE 3. *Bright field transmission electron micrograph of an octahedral cavity with {111} facets. Operating reflection (200).*

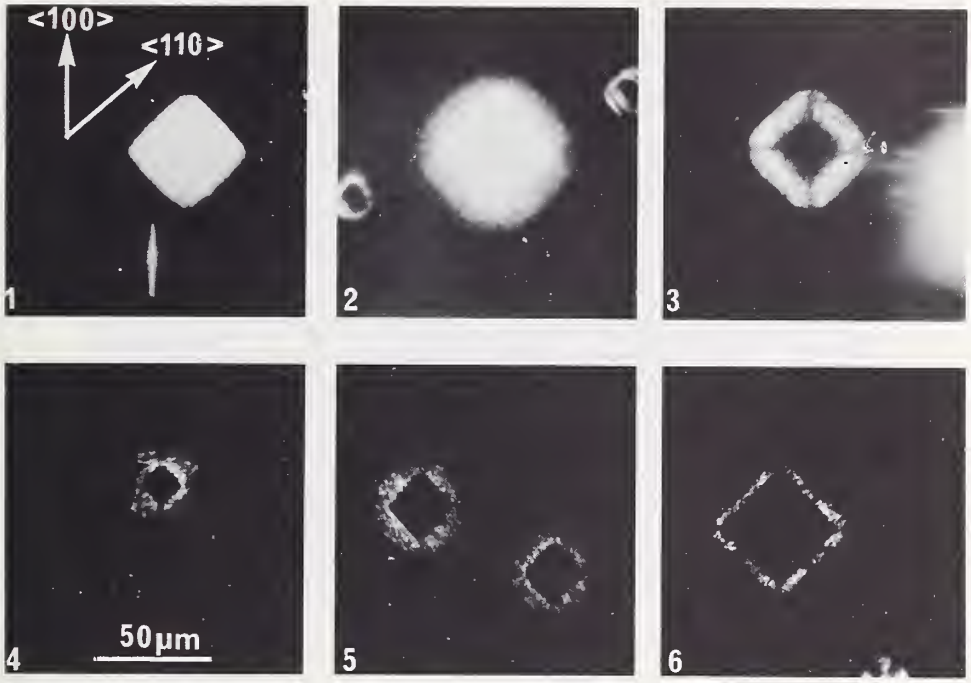

FIGURE 4. *Ultramicroscope photographs showing a possible growth sequence of a lenticular cavity.*

Kirklin et al. [9] and by Glass and Searle [10] is as follows.

The function of the reducing atmosphere is to remove oxygen atoms from the surface of the MgO, thereby creating anion vacancies and liberating electrons in the crystal. Wertz et al. [8] showed that this could occur at 1200 °C even *in vacuo* (in that work trapping of the electrons by trivalent impurities was considered). The anion vacancies and electrons then diffuse into the crystal, possibly in association, until they meet an OH^- centre where the following reaction occurs.

$$\boxed{Mg}\text{---}HO^- + \boxed{O} + e \rightarrow \boxed{Mg}\boxed{O} + O^{2-} + H.$$

A divacancy containing a hydrogen atom results which may become the nucleus for condensation of other vacancies to form a cavity. On this basis, the number of cavities that could be formed would be related to the concentration of OH^- ions within the crystal. The OH^- centre concentration determined in the present work would provide sufficient vacancies for approximately 10^5 cavities per cm^3 of average diameter 20μm. Furthermore, the calculated pressure in a cavity assuming that each OH^- ion released a hydrogen atom is ~ 500 atm. These figures are in reasonably good agreement with the experimental results.

The possibility of precipitates of $Mg(OH)_2$ in the crystals cannot be discounted. Glass and Searle have associated the absorption band at 3700 cm^{-1} with the presence of precipitates since this frequency is the stretching frequency for OH^- in $Mg(OH)_2$. (C. Cabannes-Ott. [11].) It may be noted that the band at 3700 cm^{-1} is prominent in crystals in which cavities are formed (fig. 6). In the present

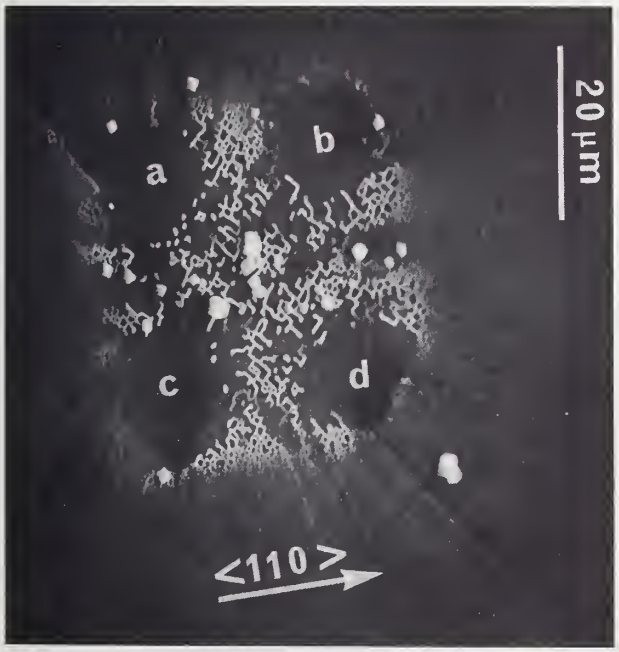

FIGURE 5. *Scanning electron micrograph of a lenticular cavity showing development of lobes. (a, b, c, d).*
Normal to the plane of the specimen inclined at 35° to the electron beam.

290-621 O-68—8

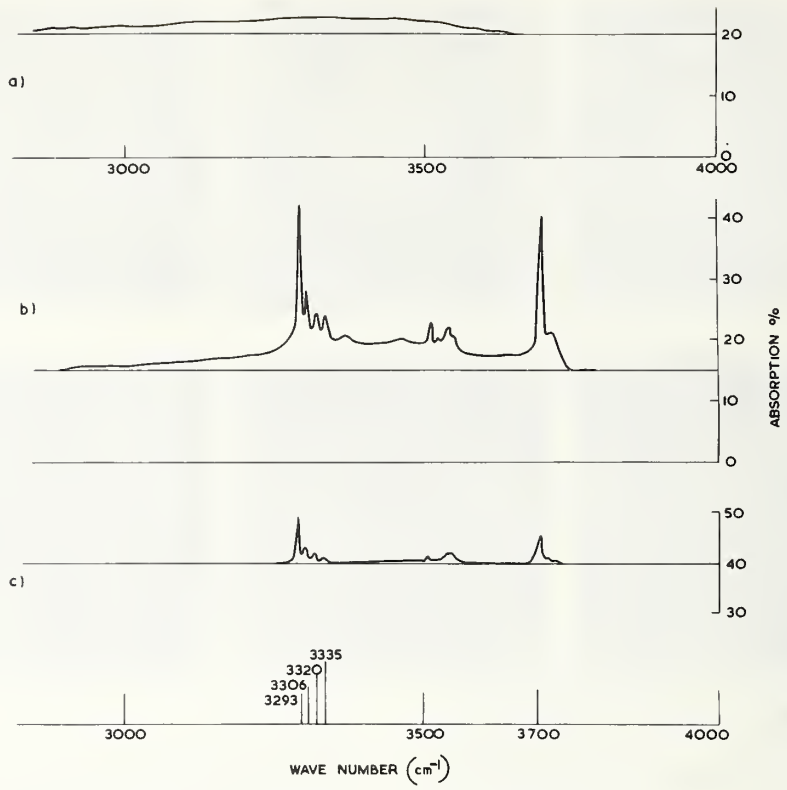

FIGURE 6. *Infrared absorption spectra of MgO crystals.*
a. For a crystal that does not produce cavities.
b. For a crystal that does produce cavities; prior to annealing in hydrogen.
c. For the same crystal as *b*: after annealing in hydrogen.

work one precipitate that gave a selected area diffraction pattern consistent with crystalline $Mg(OH)_2$ has so far been found in a thin foil of MgO. The precipitate was oriented with the *c* axis parallel to [111] and the *a* direction parallel to $[1\bar{1}0]$. This orientation is identical with that deduced by Garrido [12], Brindley [13] and Ball and Taylor [14] for the topotactic transformation of $Mg(OH)_2$ to MgO.

3. Cavities Produced by Post-Irradiation Annealing

These have been observed by transmission electron microscopy (Morgan and Bowen [15]) in the form of cuboids bounded by {100} planes with a mean length of side of ~ 200 Å (fig. 7). They are formed in samples irradiated to doses in excess of 10^{20} nvt (≥ 1 MeV) by annealing in argon at temperatures above 1500 °C. Cavities are not observed in similarly annealed samples irradiated to lower doses or in high-dose samples annealed below 1500 °C. From observations of the size distribution of the cavities and the fact that, in pulse anneals at 1800 °C, the cavities formed in periods as short as 30 seconds, Morgan and Bowen concluded that the cavities formed by a vacancy condensation process but that a certain critical vacancy concentration and mobility were required before condensation could begin.

In the present work, high precision lattice parameter measurements have been used to gain information about the temperature range over which this condensation occurs and the distribution of the vacancies prior to the formation of cavities. Measurements were made on a crystal (irradiated to a dose of 8.8×10^{20} nvt) to a precision of ± 2 parts in 10^6 using the Harwell Automatic Precision X-ray Goniometer (Baker et al. [16]). The results are shown in figure 8. The initial steep fall in lattice parameter on annealing between 200 and ~ 1000 °C is due primarily to the annealing of interstitials, partly by recombination with vacancies and partly by clustering to form interstitial dislocation loops on {110} planes (Bowen and Clarke [17]). Approximately equal numbers of anion and cation displacements are to be expected since the fast neutron cross-sections for Mg^{2+} and O^{2-} are nearly equal. Above ~ 1100 °C, the lattice parameter falls below the value for unirradiated MgO. In this temperature region, electron microscopy shows that very few fresh interstitial loops are being nucleated and

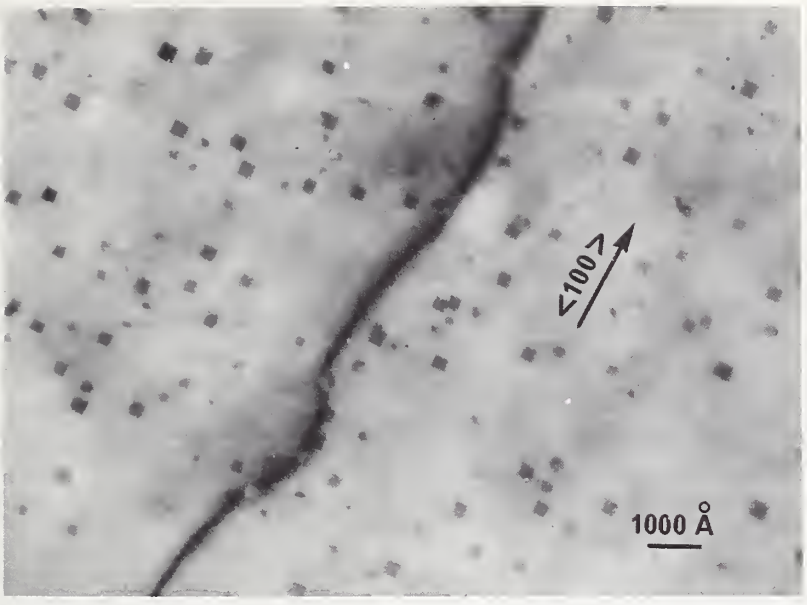

FIGURE 7. *Transmission electron micrograph of cavities in irradiated MgO after annealing for 1 hour at 1800 °C.*

it is assumed that the majority of interstitials have already migrated to existing loops. It is then reasonable to associate the negative change in lattice parameter with lattice dilatations resulting from the presence of vacancies or vacancy clusters. Condensation of these clusters into relatively large cavities would result in removal of their dilatations with a consequent increase in parameter. The temperature at which recovery begins of the negative change in parameter correlates well with the electron microscope observation that cavity formation occurs after annealing at temperatures above 1500 °C but it is evident that the process is not complete until the annealing temperature reaches ~ 1750 °C.

The negative change in parameter implies that the dilatations associated with the defects are such as to produce a net contraction of the lattice. Theoretical (Kemp and Neeley [18]) and experimental (Unruh and Culvahouse [19]) evidence for the *F* centre in MgO indicates that the nearest neighbour relaxations are outwards and it is possible that the x-ray measurements in this region reflect the presence of vacancy clusters with a net inward relaxation rather than single vacancies. Martin [20] has deduced, from cold neutron scattering measurements, the presence of clusters containing up to ~ 100 vacancies for similar dose samples annealed in the same temperature region.

Helium and neon are produced during neutron irradiation by transmutation of magnesium and oxygen ions (Wilks 1966). The total number of gas atoms generated by a dose of 8.8×10^{20} nvt, calculated from cross-section data, is $\sim 3 \times 10^{17}$ cm^{-3}. In contrast to the production of cavities by OH^- ions where the number of hydrogen atoms is comparable to the number of vacancies produced, the number of rare gas atoms produced by transmutation is considerably less than the number of irradiation-induced vacancies contributing to cavity formation ($\sim 3 \times 10^{21}$ cm^{-3}). Furthermore, gas atoms are not necessarily produced at the nucleation sites of cavities. Consequently, the accumulation of gas in the cavities is expected to continue after the cavities have been formed rather than as an intrinsic part of the cavity formation process. Morgan and Bowen concluded, from studies of the gas released by crushing crystals following various periods of anneal at 1800 °C, that despite the presence of cavities, the majority of gas atoms were initially trapped at dislocations and that diffusion of appreciable amounts of gas into the cavities occurred only after the annealing period was sufficiently long to remove the majority of dislocations.

We are grateful to Dr. P. J. Anderson and Mr. R. D. King for discussions and assistance with the infrared and mass-spectrometer work and to Mr. T. W. Baker for the lattice parameter measurements. We wish to thank Dr. J. Williams for his support and interest in this work.

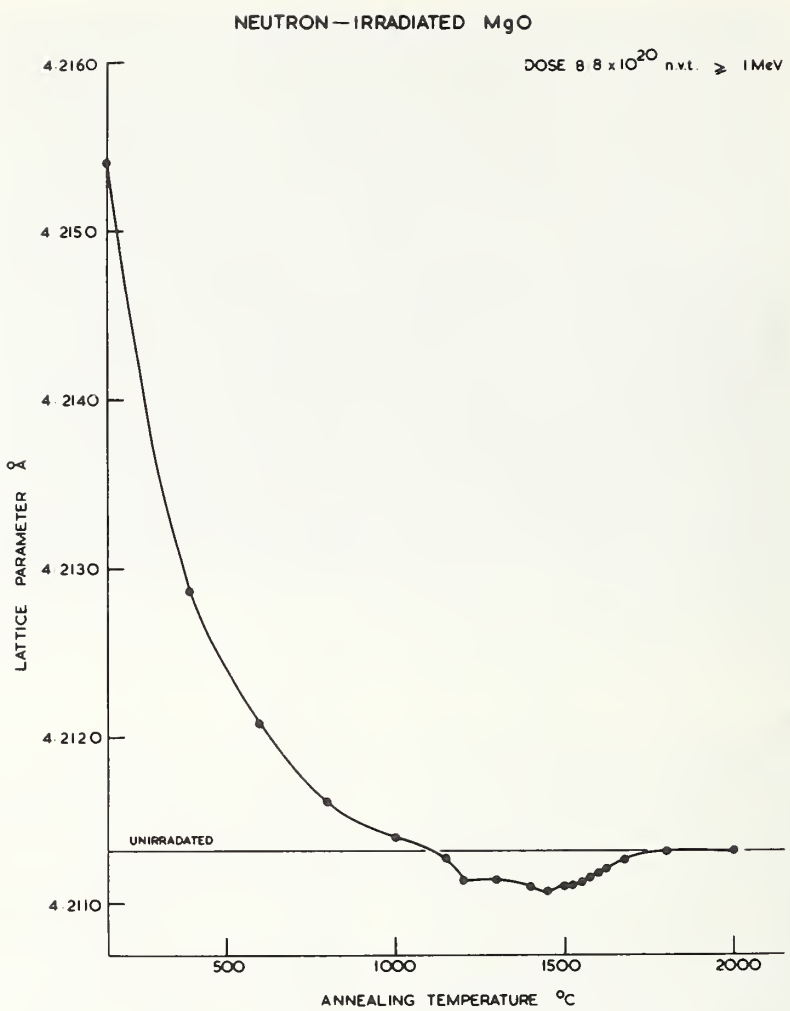

FIGURE 8. *Annealing of lattice parameter changes in irradiated MgO.*

4. References

[1] T. Hibi, K. Yada, and Y. Kawamata, J. Phys. Soc. Japan, **18,** Suppl. III, 345 (1963).

[2] K. Tanaka, M. Mannami, K. Izumi, and O. Akisue, Japan J. Appl. Phys. **3,** 164 (1964).

[3] J. J. Gilman and W. G. Johnston, J. Appl. Phys. **29,** 877 (1958).

[4] S. Amelinckx, W. Maenhout-van der Varst and W. Dekeyser, Acta Met. **7,** 8 (1959).

[5] A. D. Whapham, Trans. Am. Nucl. Soc. **8,** 21 (1965).

[6] H. J. Woollaston and R. S. Wilks, J. Nuclear Materials, **12,** 305 (1964).

[7] D. H. Bowen, Trans. Brit. Ceram. Soc. **62,** 771 (1963).

[8] J. E. Wertz, P. Auzins, J. H. E. Griffiths, and J. W. Orton, Discussion Faraday Soc. **26,** 66 (1958).

[9] P. W. Kirklin, P. Auzins and J. E. Wertz, J. Phys. Chem. Solids. **26,** 1067 (1965).

[10] A. M. Glass, and T. M. Searle, J. Chem. Phys. **46,** 2092 (1967).

[11] C. Cabannes-Ott, Compt. Rend. **242,** 355 (1956).

[12] M. J. Garrido, Compt. Rend. Acad. Sci. **203,** 94 (1936).

[13] G. W. Brindley, Progress in Ceramic Science. (ed. Burke, J. E., Pergamon Press) **3,** 7 (1963).

[14] M. C. Ball, and H. F. W. Taylor, Min. Mag. **32,** 754 (1961).

[15] C. S. Morgan, and D. H. Bowen, Phil. Mag. **16,** 165 (1967).

[16] T. W. Baker, J. D. George, B. A. Bellamy, and R. Causer, Nature, **210,** 720 (1966).

[17] D. H. Bowen, F. J. P. Clarke, Phil. Mag. **9,** 413 (1964).

[18] J. C. Kemp, and V. D. Neeley, Phys. Rev. **132,** 215 (1963).

[19] W. P. Unruh, and J. W. Calvahouse, Phys. Rev. **154,** 861 (1967).

[20] D. G. Martin, U.K.A.E.A. Res. Rept. AERE R5521 (1967).

Defect Complexes and Microdomains in Nonstoichiometric Oxides. An Analysis of Wüstite, $Fe_{1-\delta}O$

G. G. Libowitz

Ledgemont Laboratory, Kennecott Copper Corporation
Lexington, Massachusetts 02173

The deviation from stoichiometry in oxides of the transition elements generally are attributed to an excess of one type of point defect. Consequently, mass transport in nonstoichiometric oxides is usually discussed in terms of mechanisms involving the movement of simple point defects. However, there is evidence that, at least in some cases, the nonstoichiometry is due to defect complexes and to clusters of defects (microdomains) randomly distributed in the lattice, rather than to simple point defects. The evidence for defect complexes or microdomains in nonstoichiometric FeO, UO_2, TiO, and rare earth oxides is reviewed.

A statistical thermodynamic analysis of defects in wüstite has been carried out and the resulting expressions relating thermodynamic activity to deviation from stoichiometry were compared with available oxygen activity data. The results indicate that above 1000 °C the predominant defects are complexes consisting of two Fe vacancies and one Fe^{+3} interstitial, rather than simple Fe vacancies. Recent electrical conductivity data are also in better agreement with the defect complex model.

Key Words: Defect complexes, microdomains, nonstoichiometry, point defects, statistical thermodynamics, wüstite.

1. Introduction

Nonstoichiometry in oxides usually is attributed to an excess of one type of point defect. An apparent excess in oxygen may be due to interstitial oxygen or metal vacancies; and conversely, an apparent deficiency in oxygen may be attributed to oxygen vacancies or metal interstitials. Consequently, mass transport in nonstoichiometric oxides generally is interpreted in terms of mechanisms involving the movement of the particular type of simple point defect which is responsible for the deviation from stoichiometry. There is evidence, however, that at least in some cases, the nonstoichiometry is due to defect complexes and to large clusters of point defects, rather than to simple point defects. These should not be confused with the so-called Magneli compounds [1][1] which are separate compounds, closely spaced in composition, whose related crystal structures may be viewed as made up of different arrangements of ordered defects. The oxides which we will be concerned with in this paper vary in composition over a measurable single phase existence range, and the defect complexes or clusters present are, to a large extent, randomly distributed in the crystal lattice.

Thus, in order to properly understand mass transport phenomena in such oxides, the possibility of the presence of complexes or clusters should be taken into consideration and the conditions under which they exist should be evaluated. In this paper, the evidence for defect complexes and clusters will be reviewed and the case of wüstite, FeO, will be discussed in detail.

[1] Figures in brackets indicate the literature references at the end of this paper.

2. Defect Complexes

2.1. Wüstite

It has been shown [2] that wüstite always contains an apparent excess of oxygen; i.e., the stoichiometric composition, FeO, does not exist. The composition of closest approach to stoichiometry is $FeO_{1.05}$, and the deviation from stoichiometry may be as high as $FeO_{1.19}$ at 1400 °C. x-ray and density studies [3] have established that there is an excess of Fe vacancies in the lattice so that the apparent excess in oxygen is actually a deficiency in iron.

A more recent neutron diffraction study of wüstite by Roth [4] revealed that the apparent concentration of vacancies in $Fe_{1-\delta}O$ exceeds the value of δ as determined by chemical analysis. Also, the observed diffraction intensity data did not agree with values calculated on the basis of a model containing simple iron vacancies. However, the intensity data were consistent with a model in which defect complexes consisting of two vacancies and an interstitial Fe ion are present as shown in

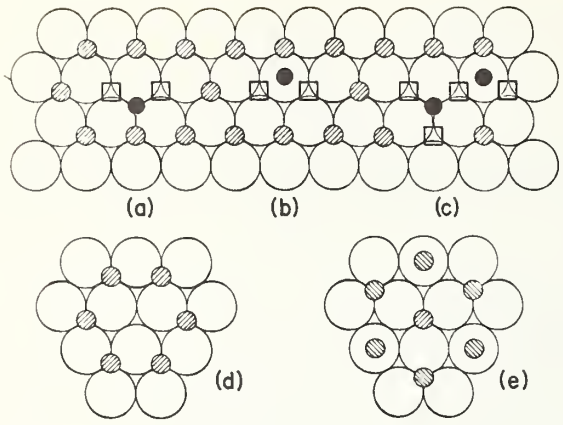

FIGURE 1. (a, b *and* c)—*(111) planes of wustite.* (d *and* e)—*(111) planes of magnetite,* Fe_3O_4. ⊘ *Fe ions on normal sites,* ● *interstitial Fe ions,* □ *vacancies,* ○ *oxygen anions.*

figure 1 (a and b). The defect complexes can cluster [as shown in (c)] in such a manner as to form regions which resemble the Fe_3O_4 spinel structure (d and e). Since Fe_3O_4 is the oxide which coexists with wustite at the oxygen-rich side of the phase diagram, the clusters may act as nuclei for the precipitation of magnetite when the overall oxygen content exceeds the saturation limit of oxygen in wüstite.

Because Roth's studies were on quenched samples of wüstite, there is some question as to whether these defect complexes actually exist at high temperatures. Recent x-ray studies at elevated temperatures by Koch, reported by Swaroop and Wagner [5], indicate some sort of clustering does occur. Further evidence for these defect complexes will be given later.

2.2. Uranium Dioxide

UO_2 exhibits both positive and negative deviations from stoichiometry. From density and x-ray measurements [6], diffusion studies [7] and magnetic investigations [8], it was concluded that the positive deviations from stoichiometry (which may extend up to the composition $UO_{2.25}$ at 1300 °C [9]) were due to additional oxygen atoms (or ions) situated in the octahedral interstices of the fluorite structure. However, neutron diffraction studies [10] which permit determination of the positions of the oxygen atoms showed that, as in the case of wüstite, the situation in nonstoichiometric uranium dioxide was not that simple. The extra interstitial oxygen atoms do not occupy the octahedral interstices (e.g., 1/2, 1/2, 1/2 positions) but rather are displaced in the (110) direction to the 1/2, 0.4, 0.4 positions. The two nearest oxygen atoms are shifted along the (111) direction from their normal positions about 1 Å towards adjacent interstices. The entire configuration may be considered to be a defect complex consisting of three interstitial oxygen atoms and two oxygen vacancies. Here again, the structure of the next higher oxide phase [11], U_4O_9, is apparently an ordered arrangement of these complexes, since the oxygen atoms in U_4O_9 occur in positions similar to the ones occupied in the nonstoichiometric dioxide.

3. Microdomain Theory

Anderson [12] has suggested that defect complexes or clusters such as those described above may be considered microdomains whose structures are similar to the next adjacent phase of the compound under consideration, and it is the ordering or aggregation of these randomly distributed microdomains as the composition of the compound changes which leads to the formation of the new phase. These microdomains may even exist at the stoichiometric compositions, such that the lattice of a stoichiometric oxide may contain microdomains of both the next higher oxide and the next lower oxide (or metal phase).

On the basis of thermodynamic considerations, Ariya and Morozova [13] proposed a similar concept of nonstoichiometric compounds which they referred to as submicroheterogeneity. Ariya and Popov [14] later suggested a modification of this concept whereby a nonstoichiometric oxide would consist solely of microdomains resembling the next higher and lower oxides. For example, in TiO, which has an existence range of $TiO_{0.86}$ to $TiO_{1.20}$, the nonstoichiometry has been attributed [15] to oxygen vacancies for oxygen deficient compositions and titanium vacancies for oxygen excess compositions. Ariya and Popov proposed that the vacancies cluster into microdomains in the NaCl-type TiO lattice as shown in figure 2. In one type of microdomain, half of the oxygen sites are vacant and the vacancies arrange themselves to resemble the Ti_2O structure (hexagonal) although the structure remains cubic. Conversely, the other type of microdomain has one-third of the Ti sites vacant arranged such that the structure resembles the orthorhombic Ti_2O_3 structure, although here again the actual structure remains cubic. At the stoichiometric composition, the size of the average Ti_2O_3-type microdomain is about one and one-half times that of the Ti_2O-type microdomain. As the overall oxygen content of the sample increases towards positive deviations from stoichiometry, $TiO_{1+\delta}$, the average size of the Ti_2O_3-type microdomains increases at the expense of the Ti_2O-type microdomains. The converse is true as the overall oxygen content decreases to $TiO_{1-\delta}$ compositions. The

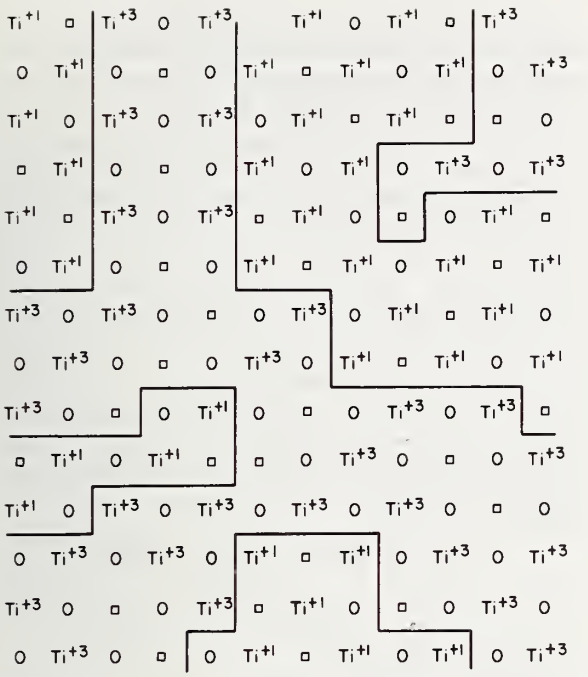

FIGURE 2. *Microdomains in TiO according to Ariya and Popov [14].*

boundaries between the two types of microdomains are continually shifting such that a dynamic situation exists between microdomains. From the overall concentration of vacancies [15], Ariya and Popov have estimated that the average size of a microdomain in TiO ranges from three to nine unit cells on edge, depending upon the stoichiometry. Therefore, the microdomains are too small to be seen by normal x-ray techniques which just show the NaCl-type structure. It may be of interest that some preliminary electron diffraction studies [16] of nonstoichiometric TiO (> 900 °C) revealed diffuse lines indicative of a disordered complex superlattice structure, in addition to lines of the normal NaCl-type structure. Similar type microdomains were also proposed by Ariya for vanadium monoxide.

The concept of microdomains has been invoked to explain hysteresis in phase transformation of the rare earth oxides [17]. This may be illustrated by referring to figure 3 which shows the partial phase diagram of the praseodymium-oxygen system and the results of an isobaric measurement of temperature as a function of oxygen content. The horizontal portions of the isobar represent two-phase regions, and the sloping sections represent single-phase regions. It is seen that the experimental isobar exhibits a hysteresis effect across the 2-phase ($\sigma+\iota$) region. The heating cycle accurately reflects the phase diagram, but on cooling, the segment representing the two-phase

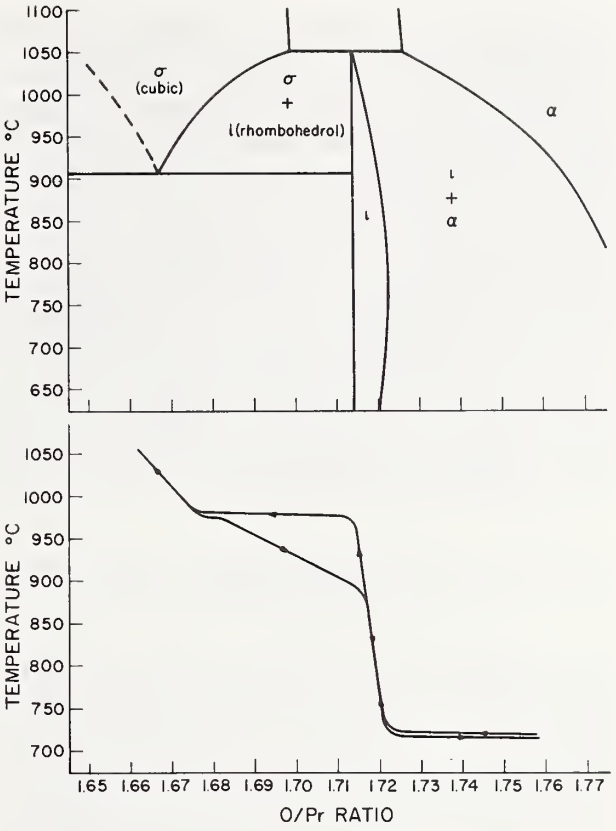

FIGURE 3. *Partial phase diagram and representative isobar in the praseodymium-oxygen system (from Hyde, Bevan and Eyring [17]).*

region is no longer horizontal. The σ-phase of praseodymium oxide is cubic and may be viewed as a derivative of the fluorite-type structure with oxygen vacancies ordered such that there are strings of oxygen octahedrally coordinated Pr^{3+} ions symmetrically arranged in all four (111) directions of the fluorite lattice (the four 3-fold axes). The ι-phase has a similar structure except that it is slightly distorted to a rhombohedral structure where the strings of regular oxygen octahedra are now all parallel to only one of the (111) directions of the pseudo-cube (one 3-fold axes). In passing from the ι-phase to the σ-phase (heating cycle), these "strings" which are ordered along one (111) direction become randomly oriented along all four (111) directions and the transformation is relatively sharp as shown. However, in passing from the disordered σ-phase to the more ordered ι-phase (cooling cycle), there is a chance selection of the one rhombohedral 3-fold axis from the four 3-fold axes of the σ-phase so that different regions of the crystal have different orientations of the 3-fold axis. Thus, instead of a sharp formation of the ι-phase, at 975 °C microdomains of the ι-phase are formed adjacent with microdomains of the residual

σ-phase. As the temperature continues to decrease, the ι-phase microdomains grow at the expense of σ-phase microdomains and finally at 875 °C, the transformation to ι-phase is complete. A similar hysteresis effect is observed at higher oxygen contents in the transformation from the rhombohedral ι-phase to a triclinic phase.

Finally it should be emphasized that the microdomain concept is only a hypothesis since the existence of microdomains has only been deduced from indirect evidence. However, the concept does provide an appealing explanation of phase transformations in nonstoichiometric oxides and is worthy of further investigation. The nature of the microdomains may be similar to that of the antiphase structures observed in some intermetallic compounds such as CuAu [18].

4. Statistical Thermodynamic Analysis of Wüstite

The remainder of this paper will be concerned with the defect structure of wüstite. As mentioned earlier, there is some uncertainty as to whether simple Fe vacancies or the defect complexes proposed by Roth (or even some other types of defects) are responsible for the nonstoichiometry in wüstite. As a further complication, Vallet and Raccah [19] have proposed, as a result of thermodynamic activity measurements, that there are three forms of wüstite within the single phase field as shown in figure 4. Despite the phase boundaries shown, the authors have pointed out that there is a good possibility that some of the phases may exist in a metastable state within the phase field of others. Additional evidence for the existence of these phases has been obtained from x-ray [20] and dilatometric [21] studies, but they have not been observed in subsequent activity measurements [22, 23]. No structures have been reported, but it has been suggested [24] that the different forms of wüstite are due to various modes of ordering of the defects.

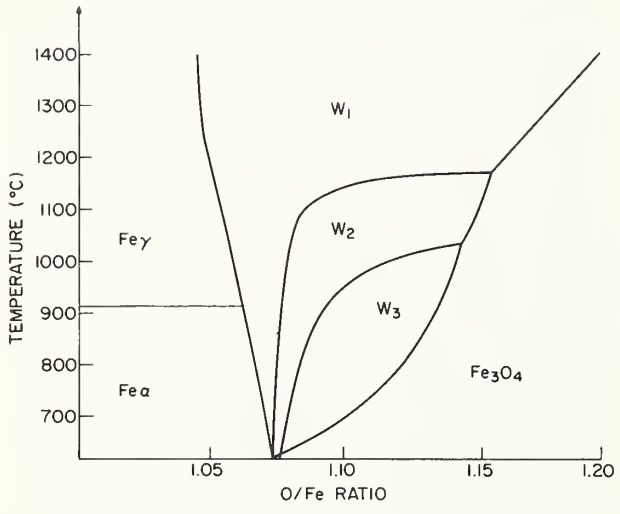

FIGURE 4. *Partial phase diagram of the Fe-O system according to Vallet and Raccah [19].*

Recent interpretations [25, 26] of electrical conductivity data at elevated temperatures ($\geq$ 1000 °C) indicate, on the basis of a mass action law treatment, that the defect in wüstite is a doubly ionized Fe vacancy. However, at the large concentrations of defects present in wüstite, a simple mass action law analysis is not valid. More accurate relationships for the dependence of electrical conductivity and thermodynamic activity on oxygen pressure may be obtained from a statistical thermodynamic treatment of defects in wüstite.

4.1. Derivation of Equations

The free energy of a wüstite crystal containing an excess of Fe vacancies may be written:

$$G = N\mu_{FeO} + N_{\square Fe} g_{\square Fe} + zN_{\square Fe} I_h - kT \ln \left[\frac{N!}{N_{\square Fe}!(N - N_{\square Fe})!} \cdot \frac{(N - N_{\square Fe})!}{(zN_{\square Fe})!(N - zN_{\square Fe} - N_{\square Fe})!} \right] \quad (1)$$

where N is the total number of Fe sites in the lattice and $N_{\square Fe}$ the number of Fe vacancies. μ_{FeO} is the free energy of a formula unit of FeO in an ideal defect-free crystal; $g_{\square Fe}$ is the free energy of formation of an Fe vacancy (exclusive of the contribution from configurational entropy) by the addition of an oxygen atom to the crystal from some standard state (e.g., O_2 gas at one atm.); I_h is the average energy necessary to ionize a positive hole from an Fe vacancy, and z is the degree of ionization. If the vacancies are assumed to be doubly ionized, z becomes equal to two. Since electrical conductivity in FeO occurs by a hopping mechanism [27], the holes manifest themselves as Fe^{+3} ions distributed among the Fe^{+2} sites in the lattice. The first ln term in eq (1) represents the number of ways of distributing vacancies over Fe sites in the lattice, and the second ln term is the number of ways of distributing positive holes over the remaining Fe atoms.

At large positive (excess oxygen) deviations from stoichiometry, it can be assumed that the concentrations of defects other than Fe vacancies are negligible. Then, we may write:

$$N = N_O = N_{Fe} + N_{\square Fe} \quad (2)$$

where N_O and N_{Fe} are the number of oxygen atoms and iron atoms in the crystal, respectively. If we consider vacancies to be formed by the addition of oxygen atoms to the lattice, N_{Fe} remains constant. However, the other quantities in eq (2) change on vacancy formation.

The chemical potential of oxygen in the FeO crystal, μ_O, is:

$$\mu_O = \frac{\partial G}{\partial N_O} = \frac{\partial G}{\partial N_{\square Fe}} \cdot \frac{\partial N_{\square Fe}}{\partial N_O} = \frac{\partial G}{\partial N_{\square Fe}} \tag{3}$$

since $\frac{\partial N_{\square Fe}}{\partial N_O} = 1$ from eq (2).

Bearing in mind that the total number of sites does not remain constant on vacancy formation (i.e., $\partial N/\partial N_{\square Fe} = 1$), we may apply eq (3) to eq (1) using Stirlings approximation to obtain:

$$\mu_O = \mu_{FeO} + g_{\square Fe} + I_h + kT \ln \frac{4N^3_{\square Fe}}{N(N-3N_{\square Fe})^2}. \tag{4}$$

Since $\mu_O = kT \ln a_O$, we may write:

$$a_O = C_{\square Fe} \left[\frac{N^3_{\square Fe}}{N(N-3N_{\square Fe})^2}\right] \tag{5}$$

where a_O is the activity of oxygen relative to the same standard state of oxygen as was used in the definition of $g_{\square Fe}$, and where

$$C_{\square Fe} = 4 \exp\left[(\mu_{FeO} + g_{\square Fe} + I_h)/kT\right]. \tag{6}$$

Since the concentration of Fe vacancies is usually measured in terms of the amount of excess oxygen in $FeO_{1+\delta}$, we may express eq (5) in terms of δ utilizing the definition:

$$\delta = N_{\square Fe}/(N - N_{\square Fe}) \tag{7}$$

$$a_O = C_{\square Fe} \frac{\delta^3}{(1-2\delta)^2(1+\delta)} \tag{8}$$

We now will consider the possibility that the nonstoichiometry in FeO is due to the defect complexes proposed by Roth [4]. In the NaCl-type structure, the coordination number of Fe sites around an Fe site is 12. Therefore, for each Fe site, there are 12/2 ways of forming a vacancy pair. For each vacancy pair, there are two ways of placing an Fe ion into an adjoining tetrahedral interstice. Therefore, there are $12N$ possible ways in which a defect complex may be incorporated into the FeO lattice. However, every defect complex in the lattice will block an additional number of sites or configurations for occupancy by another defect complex. Each vacancy of the complex restricts twelve possible vacancy pairs. However, the vacancy pair of the complex is counted twice so that there are $2(12) - 1 = 23$ restricted vacancy pairs. Since each vacancy pair may be associated with an interstitial Fe ion in two ways, there are 46 restricted or blocked configurations. Also, the interstitial Fe ion of the original complex blocks one additional vacancy pair to give a total of 47 blocked configurations. It can be shown [28] that the number of ways of distributing N_c complexes over $12N$ configurations with each complex blocking 47 configurations is:

$$w_c = \left[47^{N_c}\left(\frac{12N}{47}\right)!\right] \Big/ \left[N_c!\left(\frac{12N}{47} - N_c\right)!\right]. \tag{9}$$

This expression does not take into account the fact that two or more complexes may exclude the same site (or configuration). However, this overlapping effect should only be important at very high defect concentrations. The free energy of a wüstite crystal containing the defect complexes may then be written:

$$G = N\mu_{FeO} + N_c g_c + N_c I'_h - kT \ln\left[w_c \frac{(N-2N_c)!}{(N_c)!(N-3N_c)!}\right] \tag{10}$$

g_c is the term corresponding to $g_{\square Fe}$ in eq (1) for the formation of a defect complex. I'_h is the ionization energy of a positive hole from the defect complex. It is assumed that the interstitial Fe ion is trivalent (i.e., Fe^{+3}), in which case there is only one hole per complex available for ionization. In addition to w_c, the configurational entropy term includes the term for the number of ways of distributing positive holes over Fe ions on normal lattice sites.

For the case of only defect complexes in the lattice, eq (2) can be rewritten as:

$$N = N_O = N_{Fe} + N_c$$

where N_{Fe} represents Fe ions, both on normal sites and in interstices, and eq (3) may be rewritten as:

$$\mu_O = \frac{\partial G}{\partial N_c} \tag{11}$$

Application of eqs (11) and (4) to eqs (10) and (9) yields:

$$a_O = C_c \left[\frac{N_c^2 (N - 2N_c)}{(N - 3N_c)^2 (12N - 47N_c)^{0.745} (12N)^{0.255}} \right] \tag{12}$$

where

$$C_c = \exp\left[(\mu_{FeO} + g_c + I_h')/kT \right] \tag{13}$$

In terms of deviation from stoichiometry, δ, eq (12) becomes:

$$a_O = C_c \left[\frac{\delta^2 (1 - \delta)}{(1 - 2\delta)^2 (12 - 35\delta)^{0.745}} \right] \tag{14}$$

4.2. Comparison With Data

In order to determine which defect is in better agreement with experimental data, eqs (8) and (14) were compared with the recent measurements of Rizzo, Gordon, and Cutler [22] on oxygen activity in wüstite as a function of oxygen content. If the standard state of oxygen is taken as oxygen gas at one atm pressure, the oxygen activity, a_O, may be expressed as the square root of the oxygen pressure in atm, $P_{O_2}^{1/2}$. The results for several isotherms above 1000 °C are shown in figures 5 through 9. The dashed curves were obtained from eq (8) and the solid curves from eq (14) by computing the values

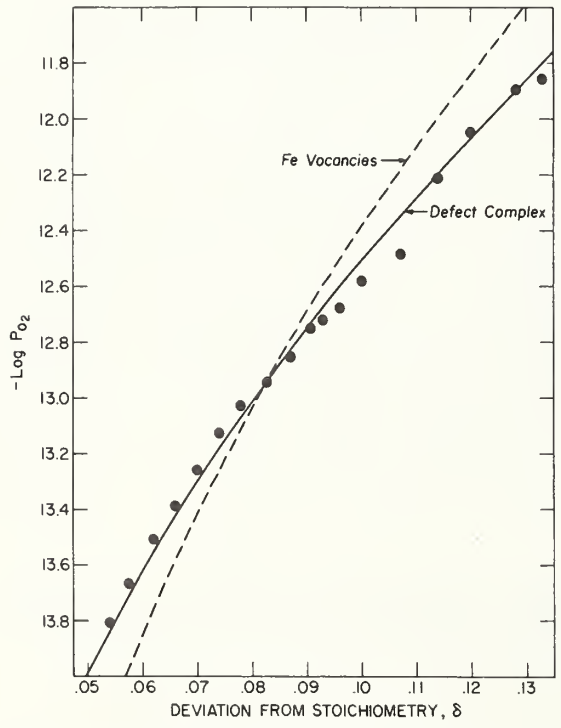

FIGURE 5. *Comparison of computed activities from eqs. 8 and 14 with oxygen activity data of Rizzo et al. [22] at 1057 °C.*

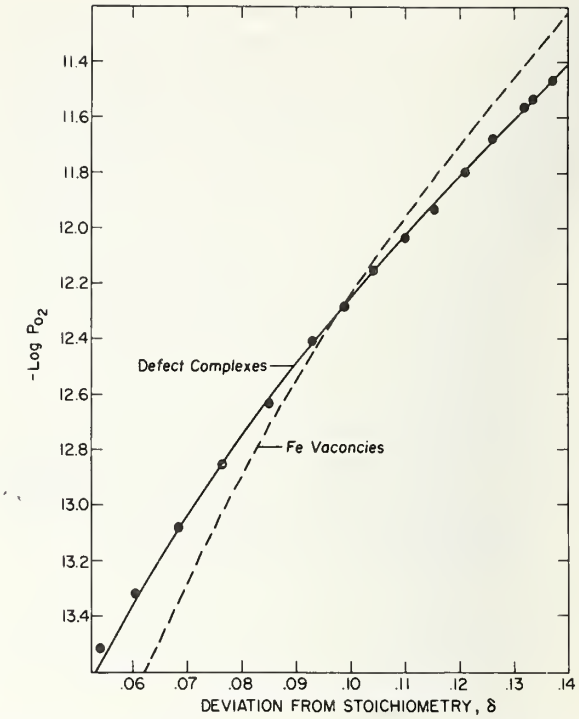

FIGURE 6. *Comparison of computed activities from eqs. 8 and 14 with oxygen. activity data of Rizzo et al. [22] at 1075 °C.*

of the constants $C_{\square Fe}$ and C_c which give the best fit with the experimental data. These constants merely determine the relative heights of the curves. The shapes or slopes are determined by the particular function of δ in each case. It is seen that the data are in better agreement with the defect complex model than with the doubly ionized vacancy model at each temperature. The agreement at 1075 °C (fig. 6) and for Run #7 at 1150 °C (fig. 8) is particularly striking. The data shown in figure 7 are the result of four separate runs, thus accounting for the large amount of scatter. However, the experimental points are in consistently better agreement with the curve for defect complexes.

The data at 1139 °C (not shown) and 1200 °C (fig. 9) do not show a clear-cut preference for either model. In the case of 1200 °C, the highest temperature studied by Rizzo et al., it may be that the complexes begin to dissociate into single vacancies. However, recent data of Swaroop and Wagner [5] show good agreement with the defect complex model at 1200 and 1250 °C, as shown in figures 10 and 11.

In the derivation of eqs (8) and (14), it was implicitly assumed that there was no interaction between defects. If, however, one assumes a pair-wise Bragg-Williams type of interaction between metal vacancies (i.e., the number of vacancy pairs is independent of the interaction energy), it can be

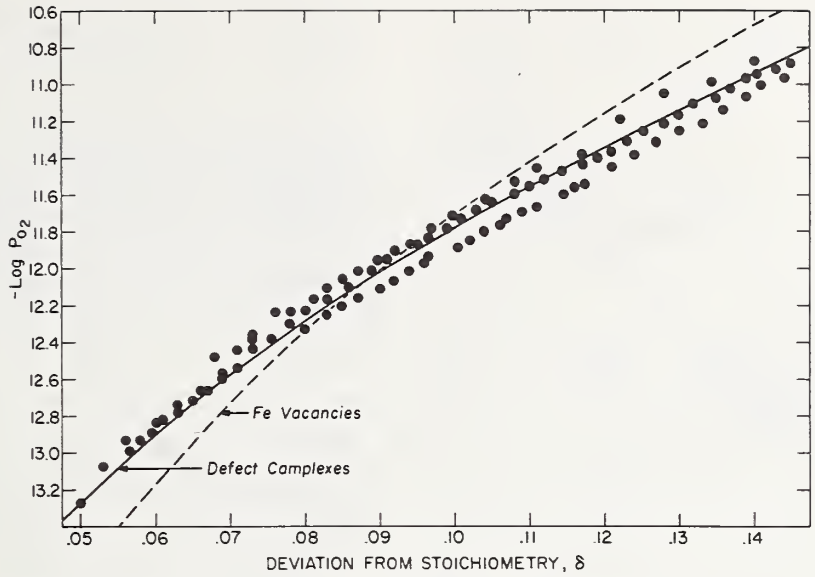

FIGURE 7. *Comparison of computed activities from eqs. 8 and 14 with oxygen activity data of Rizzo et al. [22] at 1100 °C.*

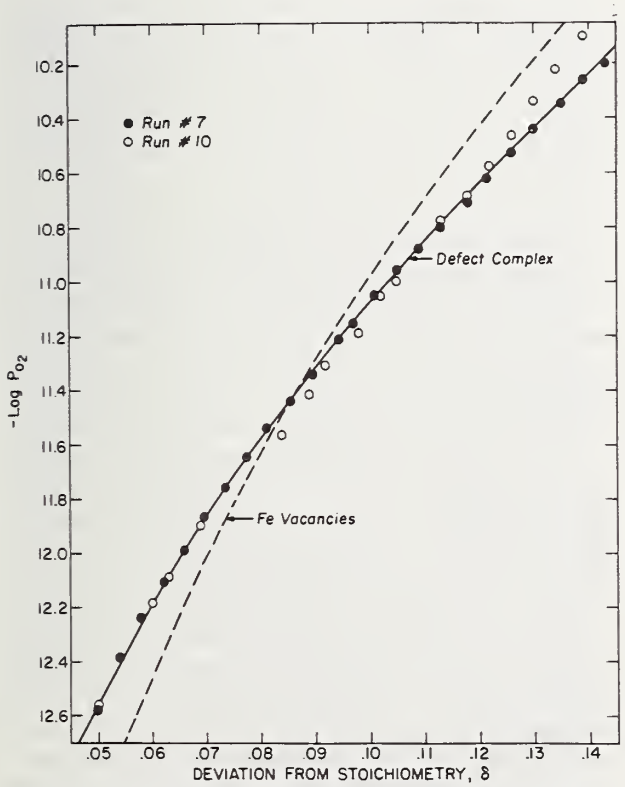

FIGURE 8. *Comparison of computed activities from eqs. 8 and 14 with oxygen activity data of Rizzo et al. [22] at 1150 °C.*

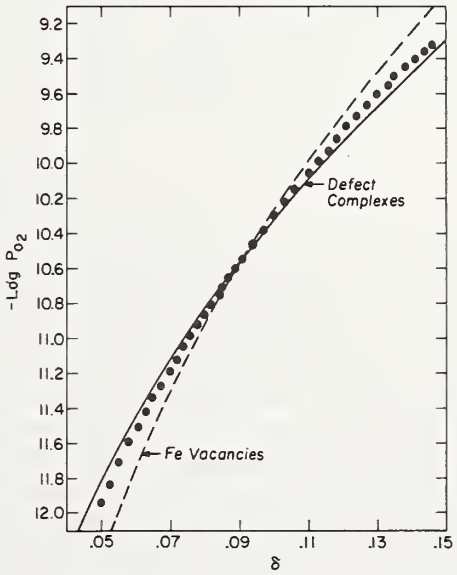

FIGURE 9. *Comparison of computed activities from eqs. 8 and 14 with oxygen activity data of Rizzo et al. [22] at 1200 °C.*

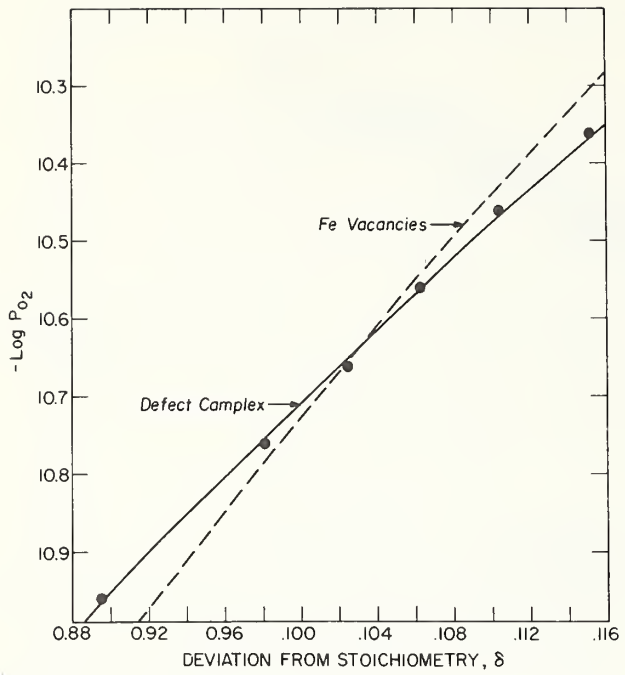

FIGURE 10. *Comparison of computed activities from eqs. 8 and 14 with oxygen activity data of Swaroop and Wagner [5] at 1200 °C.*

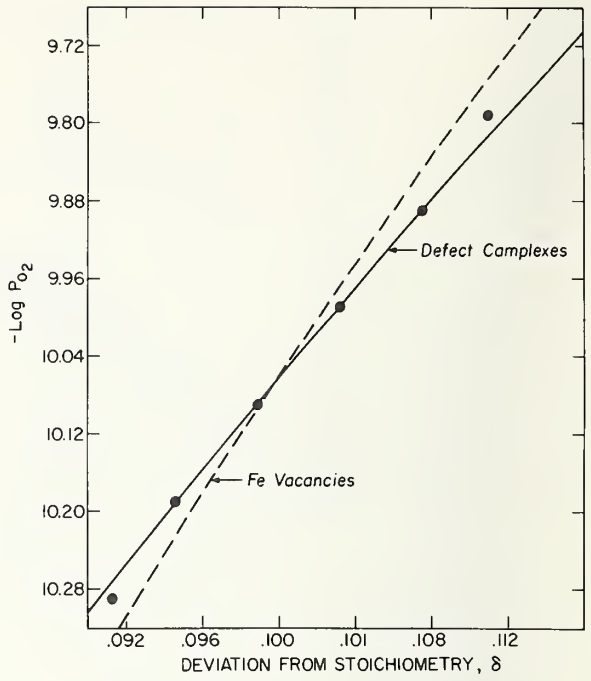

FIGURE 11. *Comparison of computed activities from eqs. 8 and 14 with oxygen activity data of Swaroop and Wagner [5] at 1250 °C.*

shown [29] that eq (8) will have an additional interaction term as follows:

$$\ln a_O = \ln C_{\square Fe} + \ln \left[\frac{\delta^3}{(1-2\delta)^2(1+\delta)} \right] + \frac{zE_\square}{2kT} \frac{\delta(2+\delta)}{(1+\delta)^2}$$

where $E_\square$ is the free energy of interaction between a pair of Fe vacancies and z is the coordination number of Fe sites. Thus, the effect, on eq (8), of neglecting interactions would be an apparent variation of $C_{\square Fe}$ with δ. Rizzo et al. [22] calculated the partial molal enthalpies of oxygen, $\Delta\bar{H}_O$, in wüstite across the homogeneity range of the compound. Although there is a great deal of scatter in their data, there appears to be a slight variation in $\Delta\bar{H}_O$ across the existence range. This means that $g_{\square Fe}$ in eq (6), and consequently $C_{\square Fe}$, do indeed vary to some extent with δ. From the above relation, we see that the overall effect of interaction will be larger at higher values of δ, and will depend upon the magnitude of $E_\square$. From activity measurements at the phase boundaries of wüstite and a simplified Bragg-Williams treatment, Hoch et al. [30] have obtained a value of 2.7 kcal/mole for $zE_\square/2$. Because of the assumptions made by Hoch, this is only an approximate value, but it can be used to estimate the effect of defect interaction on the curves in figures 5 through 11. For the temperatures considered here, log P_{O_2} would change by only 0.1 from $\delta = 0.05$ to $\delta = 0.14$. It can be seen that this would not lead to a significant difference in the shapes of the Fe vacancy curves in figures 5 through 11.

For the case of defect complexes, estimation of the effect of interaction between complexes is somewhat more difficult since there will be several types of defect pairs, each type representing a different relative orientation of the two complexes with respect to one another. Consequently, there will be a different interaction energy for each type of defect pair. However, in view of the excellent agreement of the experimental data with the theoretical curves shown in eqs 5 through 11, it appears that for defect complexes, the overall effect of defect interactions is no greater than for the vacancy case.

Equations (8) and (14) did not give satisfactory agreement with experimental data at 1000 °C and below. This was true for the oxygen activity data of Ackerman and Sandford [23] and Vallet and Raccah [31] as well as those of Rizzo et al. Therefore, it appears that the phase diagram proposed by Vallet and Raccah (fig. 4) is applicable below 1000 °C, and some other type of defect ordering occurs [24] at lower temperatures.

4.3. Conductivity Dependence on Oxygen Pressures

Recent measurements of the electrical conductivity of wüstite as a function of oxygen pressure by Geiger et al. [25] and Bransky and Tannhauser [26] show an approximate pressure dependence of $P_{O_2}^{1/6}$ over a limited composition range at temperatures of 1000 °C and above, as illustrated in figure 12. The reaction for the formation of a doubly ionized Fe vacancy may be written:

$$\tfrac{1}{2}O_2 \rightarrow O_O^{=} + \square_{Fe} + 2h^{+} \text{ (or } 2\ Fe^{+3}) \qquad (15)$$

where $\square_{Fe}$ represents an Fe vacancy and h^{+} represents a hole or an Fe^{+3} ion. The equilibrium constant for this reaction is:

$$K = \frac{[\square_{Fe}][h^{+}]^2}{P_{O_2}^{1/2}} = \frac{\tfrac{1}{2}[h^{+}]^3}{P_{O_2}^{1/2}}. \qquad (16)$$

If the mobility of carriers is constant with composition, the conductivity is proportional to the hole concentration:

$$\sigma \propto [h^{+}] \propto P_{O_2}^{1/6}. \qquad (17)$$

For the formation of defect complexes, we may write:

$$\tfrac{1}{2}O_2 + Fe_{Fe}^{+2} \rightarrow O_O^{=} + (\square_{Fe} - Fe_I^{+3} - \square_{Fe}) + h^{+}. \qquad (18)$$

A similar treatment of eq (18) yields a pressure dependence of $P_{O_2}^{1/4}$ for the conductivity. Since the data in figure 12 indicated a pressure dependence of $P_{O_2}^{1/6}$ rather than $P_{O_2}^{1/4}$ over most of the composition range studied, the authors concluded, on the basis of this simple mass action law treatment, that the predominant defects were doubly ionized Fe vacancies rather than defect complexes.

However, at the high concentrations of defects present in this system, a simple mass action law treatment is not valid. In order to form Fe^{+3} ions (or positive holes) on the right hand side of eq (15), Fe^{+2} ions must appear on the left hand side. It is implicitly assumed that the concentration of Fe^{+2} ions remains constant and that the activity or mole fraction of Fe^{+2} is approximately unity in eq (16). However, at the high defect concentrations in this system (5 to 15 percent defects), 10 to 30 percent Fe^{+3} ions are formed and consequently the mole fraction of Fe^{+2} ions must vary from 0.9 to 0.7. A similar objection applies to eq (18). In addition, the

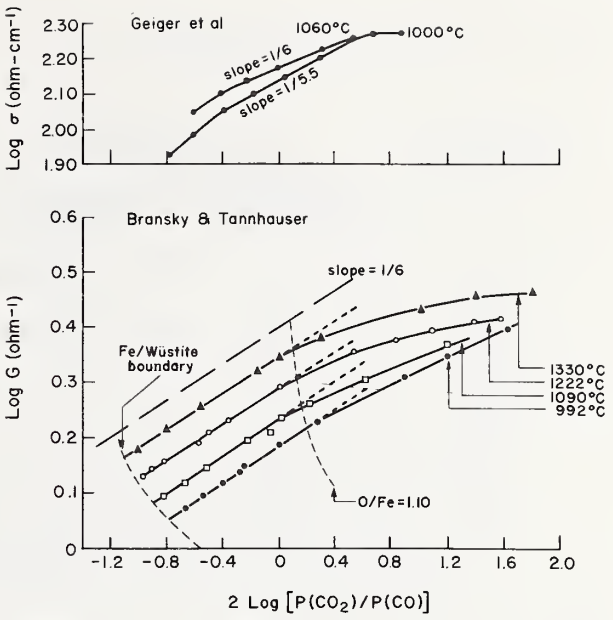

FIGURE 12. *Log conductivity, σ, and conductance, G, in wüstite as a function of log oxygen partial pressure.*
The dashed portions of the curves have slopes of 1/6. From Geiger et al. [25] and Bransky and Tannhauser [26].

mass action law treatment does not take into account the possible orientations of the defect complex in the lattice as discussed in section 4.1.

A more correct pressure dependence of conductivity may be obtained as follows. Let us assume that the conductivity is proportional to the $1/n$th the power of oxygen pressure, and we wish to determine n. We may write:

$$P_{O_2}^{1/n} \propto \sigma \propto [h^{+}] \propto N_D/N.$$

Therefore: $\ln P_{O_2} = n \ln (N_D/N) + \text{constant}$ where N_D/N represents the defect concentrations $N_{\square Fe}/N$ or N_c/N. Hence:

$$n = \frac{N_D}{N} \frac{\partial \ln P_{O_2}}{\partial (N_D/N)}. \qquad (19)$$

Application of eq (19) to eqs (5) and (12) using the relation $a_O = P_{O_2}^{1/2}$, reveals that n does not remain constant at 6 or 4 as implied by the mass action law treatment, but varies across the existence range of wüstite as shown by the calculated values given in table 1. For the case of doubly ionized vacancies, the pressure dependence of conductivity varies from approximately the 1/7th to 1/9th power. One-sixth power dependence would never be observed if simple vacancies were present. On the other hand, the defect complex model leads to 1/5th to 1/7th power dependence of conductivity on oxygen pressure. Thus, if defect complexes were present in wüstite, ln σ versus ln P_{O_2} curves should show a

TABLE 1. *Variation of oxygen pressure dependence of conductivity of wüstite;* $\sigma \propto P_{O_2}^{1/n}$

Deviation from stoichiometry δ	n	
	For doubly ionized vacancies	For defect complexes
0.05	6.7	4.8
0.06	6.8	5.0
0.07	7.0	5.2
0.08	7.1	5.4
0.09	7.3	5.6
0.10	7.5	5.9
0.11	7.7	6.2
0.12	7.9	6.4
0.13	8.1	6.7
0.14	8.3	7.1
0.15	8.6	7.4

sharp slope at low oxygen contents, an approximate 1/6 power dependence of conductivity on oxygen pressure in the midrange, and a leveling off of the curve at high oxygen contents. This is in accord with the curves shown in figure 12. Recently, Wagner [32] has obtained some additional conductivity data and found that there is indeed a continuous variation in slope for the data in the upper half of figure 12 rather than a straight line portion as shown. Thus, it appears that conductivity data are also in much better agreement with the defect complex model than with the model of doubly ionized simple vacancies.

5. Conclusion

Thermodynamic oxygen activity data and electrical conductivity measurements strongly indicate that the predominant defects in wüstite above 1000 °C are the defect complexes proposed by Roth [4], rather than the simple Fe vacancies previously supposed. Below 1000 °C there appears to be some other type of ordering in wüstite. Evidence has also been presented that defect complexing and microdomain formation may be quite prevalent in nonstoichiometric oxides. These effects should be considered in the interpretation of mass transport measurments on nonstoichiometric oxides.

6. References

[1] A. Magneli, Proc. Buhl. Intl. Conf. on Materials, E. Schazt, ed., Gordon and Breach, New York, 1964, p. 109; A. D. Wadsley, Chap 3, Nonstoichiometric Compounds, L. Mandelcorn, ed., Academic Press, New York, 1964, pp. 98–209.

[2] L. S. Darken and R. W. Gurry, J. Am. Chem. Soc. **67,** 1398 (1945).

[3] E. R. Jette and F. Foote, J. Chem. Phys. **1,** 29 (1933).

[4] W. L. Roth, Acta Cryst. **13,** 140 (1960).

[5] B. Swaroop and J. B. Wagner, Jr., Trans. AIME **239,** 1215 (1967).

[6] L. Lynds, W. A. Young, J. S. Mohl, and G. G. Libowitz, Advances in Chem. Series No. 39, 58 (1963).

[7] A. B. Auskern and J. Belle, J. Nucl. Matls. **3,** 267 (1961).

[8] A. Arrott and J. E. Goldman, Phys. Rev. **108,** 948 (1957).

[9] L. E. J. Roberts and A. J. Walter, J. Inorg. Chem. **22,** 213 (1961).

[10] B. T. M. Willis, Nature **197,** 755 (1963).

[11] B. T. M. Willis, J. Phys. (Paris) **25,** 431 (1964).

[12] J. S. Anderson, Advances in Chem. Series No. 39, pp. 1–22 (1963); Proc. Chem. Soc. 166 (1964).

[13] S. M. Ariya and M. P. Morozova, J. Genl. Chem. **28,** 2647 (1958).

[14] S. M. Ariya and Y. G. Popov, ibid. **32,** 2054 (1962).

[15] M. E. Straumanis and H. W. Li, Z. Anorg. Chem. **305,** 143 (1960).

[16] J. M. Cowley, Paper presented at Intl. Symp. on High Temperature Chemistry, Argonne Natl. Lab., May 1967.

[17] B. G. Hyde and L. Eyring, Rare Earth Research, vol. 3 (L. Eyring, ed.), Gordon and Breach, New York, 1964, pp. 623–64; also B. G. Hyde, D. J. M. Bevan and L. Eyring, Phil. Trans. Roy Soc. (London) **259,** 583 (1966).

[18] D. W. Pashley, Modern Developments in Electron Microscopy, B. M. Siegel, ed., Academic Press, 1964, p. 238.

[19] P. Vallet and P. Raccah, Compt. Rend. **258,** 3679 (1964).

[20] C. Carel, D. Weigel, P. Vallet, ibid. **260,** 4325 (1965).

[21] C. Carel and P. Vallet, ibid. **258,** 3281 (1964).

[22] H. Rizzo, R. S. Gordon and I. B. Cutler, Paper presented at Symposium on Mass Transport in Oxides, N.B.S., Gaithersburg, Md., Oct. 1967.

[23] R. J. Ackermann and R. W. Sandford, Jr., Argonne Natl. Lab. Report ANL–7250, Sept. 1966.

[24] P. Raccah, private communication.

[25] G. H. Geiger, R. L. Levin, J. B. Wagner, Jr., J. Phys. Chem. Solids **27,** 947 (1966).

[26] I. Bransky and D. S. Tannhauser, Trans. AIME **239,** 75 (1967).

[27] D. S. Tannhauser, J. Phys. Chem. Solids **23,** 25 (1962).

[28] R. Speiser and J. W. Spretnak, Trans. Am. Soc. Metals **47,** 493 (1955).

[29] J. B. Lightstone and G. G. Libowitz, Bull. Am. Phys. Soc. **12,** 389 (1967).

[30] M. Hoch, A. S. Iyer and J. Nelkin, J. Phys. Chem. Solids **23,** 1463 (1962).

[31] P. Vallet and P. Raccah, Mém. Sci. Rev. Métallurg. **62,** 1 (1965).

[32] J. B. Wagner, Jr., private communication.

Diffusion in Oxides: Assessment of Existing Data and Experimental Problems [1]

C. E. Birchenall

Professor of Metallurgy, University of Delaware

and

Metallurgist, Lawrence Radiation Laboratory, Livermore, California 94550

Ideal conditions for the direct measurement of diffusion coefficients in oxides are described. The need for careful measurement, whether the object is to measure intrinsic properties of pure oxides or the engineering properties of commercial materials, is emphasized. Oxides are classified as impurity-tolerant, impurity-sensitive or borderline to judge the likelihood that intrinsic properties have been measured. A survey of several oxide structure types is given to illustrate the state of the empirical literature.

Key Words: Diffusion, engineering properties, intrinsic properties, nonstoichiometry, thermodynamics.

1. Introduction

A clear point, mathematically expressed and backed by conclusive and consistent data, can be made quickly. To deal appropriately with the opposite case will take me a little longer. The assigned topic poses several problems: (1) The allocated time could easily be squandered on the measurements on just one oxide, e.g., BeO. (2) Assessment implies value judgements—that is, do the data satisfy my desires, the desires of the investigator, or of his employer? Not all of us have the same concerns. Instead of raising a single, high ideal, I shall try to anticipate a part of the range of these concerns. (3) I could exhaust the time and your patience enumerating and describing experimental methods and the steps that determine the quality of data. I shall make a few such remarks. However, most detail is omitted. (4) Finally, if this review stimulates controversy, hopefully even some thought, I shall fulfill another aspect of my assignment.

The nature of the defects supporting diffusion, the transport equations, and some ideal model crystals have been discussed in preceding papers. Assessment of data requires that we inquire what the actual materials are, intrinsically or extrinsically. Who needs to know their properties and for what purposes? The latter proposition can be dissected into the scientific approach (what are the properties of the absolutely pure compound?) and the engineering approach (what are the properties of the stuff I can buy or make?). Between these legitimate extremes are many tenable intermediate positions. The point is that sloppy measurements serve neither of the ends nor any of the middle adequately.

2. Experimental Methods

2.1. Direct and Indirect Methods

The most direct experiment, that in which only a single process occurs and in its analysis requires the fewest unverified assumptions, must be the standard. For diffusion coefficients, a well-defined simple initial and final geometry and the direct verification of composition as a function of distance and time at temperature are the minimum requirements for a primary standard measurement. The stated conditions are seldom easy or convenient to achieve, but in the long run they save time, controversy and journal pages. Sooner or later someone does it right anyway. In this sense, there is no standard other than the one described.

Some indirect measurements conform to the geometrical conditions, but make assumptions about the spatial distribution of the diffusing

[1] Work performed under the auspices of the U.S. Atomic Energy Commission.

substance. The surface activity method and the gaseous exchange method, often used for oxygen diffusion, are of this type. Both of these techniques are subject to surface transport resistance that may be difficult to verify and correct for. Vaporization losses can affect the surface activity method. Exchange with other parts of the vacuum system, desorption and leakage may affect the exchange method. Naturally, good technique can minimize all of these shortcomings, but in the long run the success of the measurement will be judged by how it agrees with the more direct measurements.

Still less direct measurements result from inferring diffusivities from processes in which several mechanisms may contribute simultaneously to the rate and in which the rate measurement itself is supposed to distinguish the controlling mechanism. Oxide growth rates and sintering rates are the most common measurements in this category. Experience indicates that these methods are only reliable under the most ideal circumstances and careful application.

The invited paper to follow deals with ionic conductivity measurements as a method for studying transport. The difficulties in correlating diffusivities from conductivity measurement with those from direct measurement are almost legendary. However, the combination of these techniques for studying correlation factors contributes powerfully to a deeper insight into the diffusion mechanism.

2.2. Specimen Preparation

Assume that the direct method of measurement has been chosen. It consists of several distinguishable steps, the most significant of which is the preparation of the crystal and its characterization. The presence and distribution of pores, cracks, grain boundaries, and impurities should be determined before and after diffusion, or preferably excluded. For noncubic single crystals, orientation should be determined and appropriate faces prepared with minimum distortion. Somewhere in this sequence the specimen should be equilibrated with a known activity of one of its constituents[2] under conditions comparable with those to be used in the diffusion anneal.

Alternatively, the crystal should be enclosed in such a small inert container during the diffusion anneal that it establishes its own equilibrium atmosphere by dissociation without a significant change in composition of the surface layer. Packing the container with chips of the working substance of identical composition and large specific surface area minimizes superficial changes. The diffusing substance is established either by preparing a second crystal of different composition to be welded to the first or by depositing a thin layer of the diffusing substance on the surface of the specimen. Often the deposited substance is a radioactive tracer to keep the amount small, or to measure self-diffusion of one of the basic constituents. Vapor deposition is perhaps the most common method, but evaporation of a solution containing the tracer in a compound is also done. Occasionally electrodeposition may be possible. In any case a uniform deposit to avoid hold-up in clumps is necessary. The necessity to convert the deposit to the same chemical form as the substrate is not so obvious, but it may be critical for measurements in all but the most variably composed oxides. Some attempts should be made to establish the distribution and form of the initial deposit. Microscopic inspection, autoradiography (for radioactive tracers), microprobe scanning (for chemically different diffusant) are some of the useful methods.

2.3. Diffusion Anneal

The diffusion anneal should be done in a nonreactive system with a uniform and constant hot zone, including good thermal baffling (radiation shielding). The atmosphere or intimate contact with a second condensed phase should fix the thermodynamic activity of the specimen throughout the run. "Vacuum" or "inert flowing gas" are not satisfactory conditions for establishing a fixed activity of oxygen over the oxide. Heating and cooling should not be so slow that composition changes can occur in these steps, nor so fast that mechanical damage results.

2.4. Sectioning and Analysis

Determination of the spatial distribution of the diffusing substance after the anneal may be done in a variety of ways. Slices parallel to the original surface may be taken by cutting or grinding. Such cuts must be uniform in thickness. The material in the slice must be analyzed or the composition of the exposed surface must be determined. The amount of material removed in each slice may be measured or the thickness of the remaining sample determined. The choices should be taken to optimize precision. Instead of parallel sections, a single perpendicular or oblique section may be useful for autoradiographic or microprobe analysis. The oblique angle gives mechanical magnification of the penetration distance which may be very desirable when the total penetration by diffusion is small. In most cases it is now better, quicker and cheaper

[2] Equilibration with one constituent suffices for a binary system. A ternary system requires positive control of two activities. For a discussion of this problem with special application to the spinels, see [1].[3]

[3] Figures in brackets indicate the literature references at the end of this paper.

to use the single sectioning method on nonporous specimens.

Autoradiography and microprobe scanning both reveal whether diffusion has occurred preferentially along cracks or grain boundaries, and to what extent. Autoradiography requires careful calibration of the emulsion if quantitative compositions are to be obtained. Care must be taken also to correct for absorption of radiation in the specimen regardless of the detection method. When the radiation is very weakly absorbed by the specimen over the penetration distance into the sample, the detector records the total activity remaining below it in the sample. When the radiation is very strongly absorbed, that is, the penetration distance by diffusion is much greater than the range of the radiation, the activity measured is nearly proportional to the surface concentration. Intermediate cases require more complicated corrections than these limiting cases. If experimental conditions can be adjusted to take advantage of the limiting cases, enhanced precision usually justifies extra effort. Even when parallel sectioning is used, after the last section is taken in the diffusion zone, it is wise to take an autoradiograph or microprobe scan, whichever is appropriate, in order to look for preferred diffusion paths.

3. Specimen Purity

I have postponed the question of impurities in the specimen because all of the preceding points affect the utility of the data independent of the purity. The effect of impurities, however, depends on the purpose of the study and the substance under study. I shall divide the oxides roughly into two classes—impurity-tolerant and impurity-sensitive. Given a choice, concentrate your research on impurity-tolerant compounds. These are the substances that can or do deviate more from stoichiometry than the usual limit below which the impurity content is readily reduced. A few other oxides or types of oxides may have mechanisms for tucking away some impurities so that they have little effect on the diffusivities of the basic ions. The spinels seem to have this capacity to some extent. It might appear that these impurity-tolerant oxides, because of their variable composition ranges, require more careful atmosphere control than the oxides with more sharply defined composition ranges. Such is not automatically the case. The apparent insensitivity of impurity-sensitive oxides to atmosphere variation (usually oxygen partial pressure) often has its origin in the fact that the impurity concentration exceeds both the intrinsic disorder of the stoichiometric substance and the composition range of the phase field of the perfectly pure oxide. Diffusivities ordinarily vary with oxygen partial pressure to some power $\pm 1/n$, where n generally lies between 2 and 8, frequently between 3 and 6. Thus the sensitivity to P_{O_2} often is not great, and positive control of P_{O_2} is likely to be adequate. Pumping alone or blowing CO_2, H_2O or an inert gas alone, through the system leaves P_{O_2} undetermined by orders of magnitude, which is very undesirable.

For those who must apply impure oxides in a practical device the transport properties in the working substances are the pertinent quantities, not the properties of hypothetical ideal crystals. Sintered oxide parts are examples where diffusivities on real materials should be useful in understanding and controlling processing. For oxide growth on slightly impure metals or on alloys it is important to remember that impurities or alloying elements are fractionated at each interface and that they are not uniformly distributed through the growing oxide phases. Application of diffusion data to such cases requires more than the determination of diffusivity in a single composition, pure or impure. Also oxides for application may have irreducible variabilities owing to the methods by which they are produced and handled. If these factors affect diffusivity the study of the property must have a statistical sampling basis from the outset.

Tentative examples of oxides that illustrate relative tolerance to impurities are:

Impurity-sensitive:	BeO, CaO, MgO, Al_2O_3
Impurity-tolerant:	CoO, FeO, Fe_3O_4, cubic-stabilized zirconia
Borderline:	CdO, ZnO, NiO, αCr_2O_3, αFe_2O_3.

The list includes several oxides that are regarded as model compounds.

Repeating for emphasis that those who need to know how fast ions move in materials of commercial purity must and should study diffusion in those materials just as carefully as they would study the purest materials conceivable, I turn to the attempt to find out what the transport properties of pure oxides are—composition variation within a single field and temperature dependence particularly. It is largely from these two dependencies that mechanisms of diffusion are deduced.

4. Crystal Structure

The first consideration governing intrinsic transport behavior is the crystal structure. I deal mainly with (1) oxides with the sodium chloride structure (oxides of the alkaline earths and the iron group

290-621 O-68—9

transition metals), (2) the spinel oxides, especially the ferrites, chromites and aluminates, (3) the rhombohedral sesquioxides with the α corundum structure, and (4) cubic stabilized zirconia. You will recognize that several of my examples are repeat performances, up-dated and amended.

Recall that the structures of many oxides can be described crudely as nearly close-packed anions with cations arranged in orderly, or occasionally disorderly, fashion in the interstices. The description applies even better to many sulfides.

5. Assessing the Data

It is much easier to write directions for a good diffusion measurement than it is to follow the prescription. I doubt if any set of measurements on oxides meets all of the criteria I laid down. It is even more difficult to judge the value of a single set of measurements. You can ask whether they are internally consistent, if the procedures appear to have been carefully applied, and whether the magnitudes reported are reasonable. But eventually, assessment of data comes down to the simple question, can other people get the same results by similar and by different approaches?

Long ago, when diffusion data on metals were as unreliable as those on oxides are now, I learned that it is more important to compare actual magnitudes of diffusivities than it is to compare activation energies. It is more important at this stage to know that a set of values is approximately right than it is to know that they are internally consistent but might be off an order of magnitude or so. Also, when the published data and Arrhenius-type equation occasionally disagree, the data are usually right and the equation miscalculated.

5.1. Calcium Stabilized Zirconia

To illustrate, consider calcium-stabilized zirconia, a valuable material because it can be almost exclusively an ionic conductor. Figure 1 shows two sets of data and one line. The line is log D vs. $1/T$ resulting from Carter and Roth's [2] conductivity measurements converted through the Nernst-Einstein relation, assuming that the oxide ion transport number is unity and the correlation coefficient for oxide vacancies on the fluorite structure is 0.65, which is appropriate for a simple cubic network [3]. The filled circles are diffusivities determined by mass spectrometric analysis for diffused ^{18}O in sectioned single and polycrystals by Simpson and Carter [4]. The open circles were determined [5] by the time-lag permeability method [6] on sintered tubes of about 95 percent density. The compositions are not precisely the same in

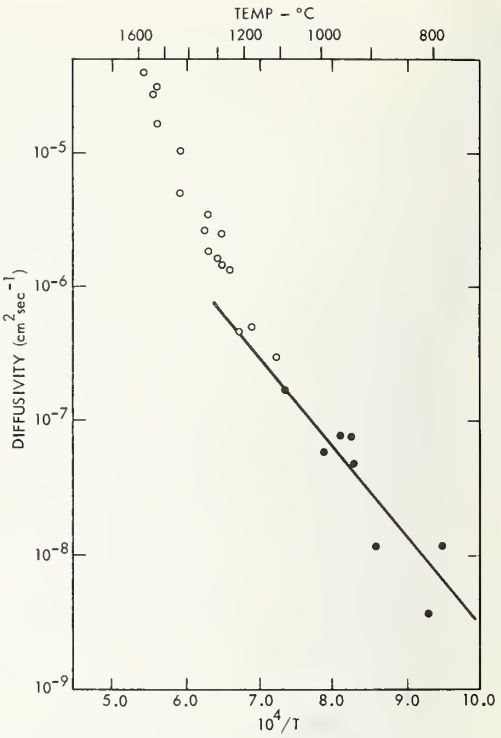

FIGURE 1. *Oxygen diffusivity in calcium-stabilized zirconia.*
— Calculated [2] from electrical conductivity measurements on $Ca_{0.142}Zr_{0.858}O_{1.858}$ assuming only oxide ion conduction and a correlation coefficient for anion vacancies in the fluorite structure of 0.65.
● ^{18}O diffusivities [4] in dense single and polycrystals of $Ca_{0.142}Zr_{0.858}O_{1.858}$ by mass spectrometric analysis of sections.
○ Diffusivities from permeability measurements [5] in 95 percent dense tubes of $Ca_{0.08}Zr_{0.92}O_{1.92}$ by the time-lag procedure [6].

the permeability specimens as in the others. There are big differences in apparent activation energy. (Possibly the dissociative gaseous transport across pores at high temperatures contributes to abnormally high diffusivities.) Nevertheless, the whole picture gives considerable confidence that the magnitudes of the oxide ion diffusivity are about right.

In making this statement, I do not mean to imply that the defect structure, the stabilizing mechanism, or the conditions of stability of calcium-stabilized zirconia are understood. For example, the conductivity in the lime-rich region decreases with increasing CaO concentration [7] in spite of the fact that the vacancy concentration is increasing. The activation energy for conductivity increases substantially over this same compositon range. The conductivity decrease may result from the stability of complexes larger than single vacancies and lower in mobility. The structure appears to be in the early stages of phase separation or ordering under some conditions that have been investigated.

At 1700 °C the calcium and zirconium ion diffusivities are at least six orders of magnitude lower than the oxide ion diffusivities [8]. Although the grain boundary diffusivities are about 10^5 times

greater than the cation bulk diffusivities, the total cation transport should be negligible even in fine-grained material.

5.2. Ion Transport in the Growth of αFe_2O_3

Having mentioned grain boundary diffusion, let me emphasize that while the theory of intrinsic diffusion behavior may be advanced most efficiently by the study of good single crystals, applications may involve grain boundary transport in an important way. Now that ^{18}O marker studies [9] show that αFe_2O_3 grows predominantly by cation diffusion, it appears that growth rates of αFe_2O_3 on Fe_3O_4 calculated [10] by the Wagner equation from self-diffusion of iron values are several orders of magnitude too low to agree with the measured growth rates. Previously this discrepancy did not seem to be significant.

I do not intend to suggest that grain boundary diffusion in αFe_2O_3 has been shown to be the growth mechanism, although that is one possible way to reconcile the discrepancy. However, the αFe_2O_3 case history is revealing concerning the state of knowledge of diffusion in oxides. Lindner [11] first measured iron self-diffusion into a porous, sintered-powder compact in air. As an afterthought to measurements on wüstite (along with a pass at magnetite), Himmel et al. [10] made one actual measurement and one measurement that gave only an upper limit for iron self-diffusion in a natural hematite single crystal in one atmosphere of oxygen, and the results were consistent with those of Lindner. At about the same time, Davies et al. [12] observed the disappearance of ^{110}Ag markers during the growth of hematite on magnetite. They attributed the disappearance of the silver markers to vaporization from the external surface (which was probably correct), and they concluded that hematite grew predominantly by oxide ion diffusion inward (which is probably not correct). Himmel and Holt [9] used the ^{18}O activation method [13] to show that oxygen is practically immobile in αFe_2O_3 during its growth. Hagel [14] measured oxygen self-diffusion by exchange with single-crystal spheres, and reported values comparable with those reported for iron ions in hematite [10, 11]. All of these values are several orders of magnitude too low to explain the hematite growth rates.

Izvekov et al. [15] report iron diffusivities in hematite that are about two orders of magnitude above the earlier results for similar atmospheric conditions (fig. 2). These coefficients are still more than an order of magnitude too low to account for the growth of hematite. Either these results are still too low in spite of direct disagreement with earlier measurements, or the iron diffusivity is much greater in hematite in equilibrium with magnetite, or grain boundary transport is mainly responsible for the transport supporting oxide growth. However, the growth morphology of hematite is not always that characteristic of simple volume diffusion control, suggesting that some step is rate-limiting other than the resistance to diffusion in some circumstances.

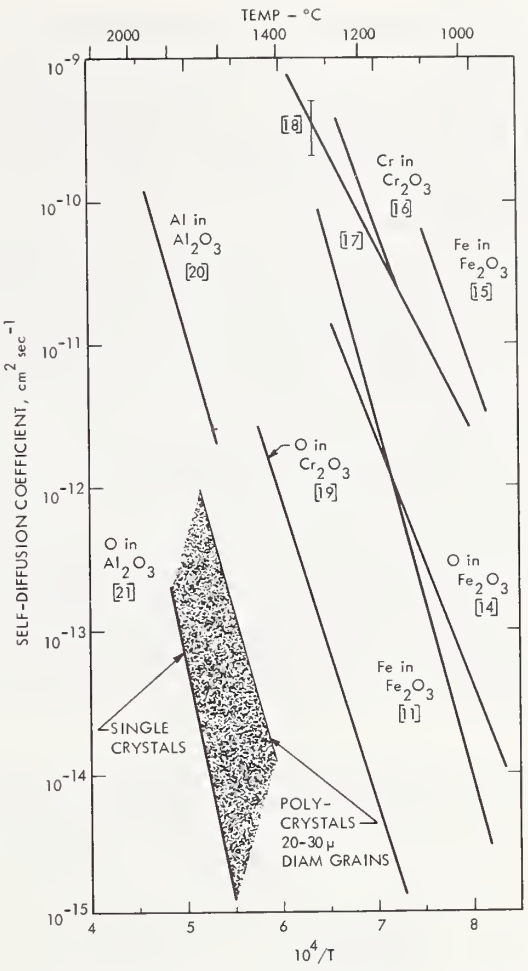

FIGURE 2. *Self-diffusion in sesquioxides with the alpha corundum structure.*

Impurities may have affected strongly the measurements on natural hematite. During oxidation of iron, cationic impurities usually diffuse more slowly through the lower oxides than does the iron ion. Fractionation of impurities at the interfaces also occurs. It appears that Fe_2O_3 is normally the purest of the oxides if the lower oxides intervene between it and the metallic phase. Whether differences in purity between growing hematites and those used for diffusion studies can account for the large discrepancy noted is not known. It is a factor to consider in future work, but it is not yet an explanation for past results.

5.3. Diffusivities in αCr_2O_3 and Al_2O_3

Chromium diffusivities in αCr_2O_3 are in substantial agreement in three measurements [16–18] (fig. 2). They are clearly much greater than oxide ion diffusivities [19] and are in good agreement with the growth rate constants as they are related through Wagner's theory.

In αAl_2O_3 the cation diffusivity [20] is also greater than the anion diffusivity [21]. Anion diffusivity shows a strong preference for grain boundary paths. The growth process of oxide scale on aluminum is so complex that a direct comparison of rates is not appropriate at this time.

5.4. Cation and Anion Self-Diffusion in Oxides With the NaCl Structure

Figure 3 contains results for cation self-diffusion in the oxides FeO [10], CoO [22], NiO [23–25], MgO [26], and CaO [27], each of which crystallizes with the NaCl structure. Oxide ion diffusivities as reported for NiO [28], CoO [29], and MgO [30] are also recorded in the figure. The activation energies Q are obtained by fitting the lines to the Arrhenius equation

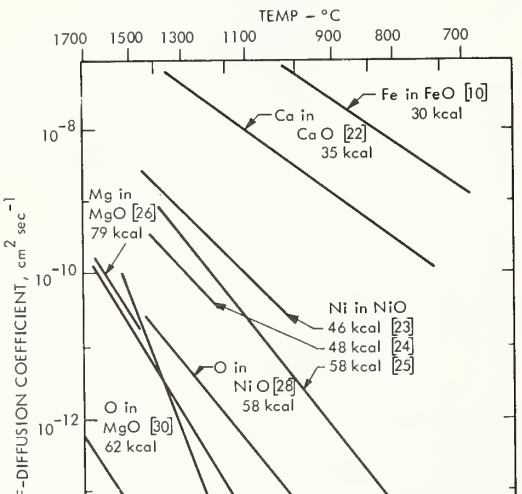

FIGURE 3. *Self-diffusion of cations and anions in some oxides with NaCl structures.*

$$D = D_0 \exp(-Q/RT). \tag{1}$$

Activation energies for the self-diffusion of cations in FeO and CoO are probably reliable to 1 or 2 kcal/gram-ion. For the other measurements, the sensitivities of the point defect concentrations to small concentrations of impurities and the susceptibility of oxygen exchange methods to surface transport control contributions makes the estimation of uncertainty ranges hazardous. Probably the activation energy for the self-diffusion of nickel ions in NiO lies within the range of values given. Intrinsic activation energies for the other cases in the lower left part of the figure may differ from the quoted values by 20 or 30 percent, which could result in large deviations in the diffusion coefficients from the reported values.

When excess oxygen is added to a stoichiometric crystal MgO, one filled anion site O_0 may be added to the crystal and one unfilled cation site V_M is created simultaneously. If the temperature is sufficiently high, the vacancy may have an excess negative charge residing on the surrounding anions, compensated by electron holes that are dissociated to the extent that they can migrate independently as current carriers when an electrostatic field gradient is imposed.

At high temperatures, it seems to be appropriate to assume double ionization of at least FeO [31] and CoO. The other oxides might even follow a different pattern because of the difficulty of forming valence states greater than 2 for Ni, Mg and Ca. Nevertheless, FeO, CoO and NiO are treated here tentatively as if they formed doubly-ionized cation vacancies and electron holes. The appropriate reaction equation is

$$\tfrac{1}{2} O_2(g) \rightleftarrows V_M'' + 2p^+ + O_0^{2-} \tag{2}$$

where $''$ indicates a virtual doubly-negative charge associated with the neighboring ions. The virtual charges are not counted in the charge balance, just as V_M contributes nothing in the mass balance.

The enthalpy change ΔH_f for the formation of one gram ion of cation vacancies also results in the formation of two gram equivalents of electron holes. For reaction 2 the standard free energy change is

$$\Delta G^0 = \Delta H_f - T\Delta S^0,$$

and the mass action constant is given by

$$K = \exp\left(\frac{\Delta S^0}{R}\right) \exp\left(-\frac{\Delta H_f}{RT}\right) \tag{3}$$

When the mass action relation for the reaction is written assuming that the oxide ion concentration remains substantially unchanged, and that the concentrations of vacancies and holes are a satisfactory approximation for their activities, it is found that the vacancy concentration and the hole

concentration are both proportional to the sixth root of the oxygen partial pressure. Also

$$[V''_M] = 4^{-1/3} p_{O_2}^{1/6} \exp\left(\frac{\Delta S^0}{3R}\right) \exp\left(-\frac{\Delta H_f}{3RT}\right)$$
$$[p^+] = 2^{1/3} p_{O_2}^{1/6} \exp\left(\frac{\Delta S^0}{3R}\right) \exp\left(-\frac{\Delta H_f}{3RT}\right) \quad (4)$$

If the cation diffusivity is proportional to $[V''_M]$ and the electronic conductivity is proportional to $[p^+]$, it is to be expected that measurements of these properties made over a range of temperatures at constant composition not too near the stoichiometric composition will depend only on the activation energy for motion of the corresponding carrier, ΔH_M for cation mobility, ΔH_μ for hole mobility [32]. If instead the measurements are done at constant p_{O_2} the activation energy in each case must be augmented by $\Delta H_f/3$, because the composition-controlled concentration of carriers is temperature dependent through eq (4). Measurements that are made at neither constant p_{O_2} nor constant composition depend for their utility mainly on the slow variation implied by $p_{O_2}^{1/6}$. For other mechanisms of defect formation, this dependence may be more or less critical. It is good practice to avoid this question by fixing pressure or composition in addition to temperature.

Table 1 collects the data for diffusivity of cations and conductivity by electron holes for FeO, CoO, and NiO. The data are shown to be consistent by inserting in the boxes for which no measurements are available reasonable numbers in parentheses that are compatible with the measured values. No stronger claim than consistency can be made because comparisons of reported values and uncertainties quoted by the authors suggest that ranges of 25 to 30 percent or plus or minus several kilocalories, whichever is larger, should be associated with some experimental values. CaO and MgO are omitted from this table because their conductivities appear to be mixed electronic-ionic in nature, varying with temperature, and very sensitive to small concentrations of impurities [40]. The increasing difficulty of oxidizing the stoichiometric crystal, the reaction implied by eq (2), is seen in the progression of ΔH_f from FeO, which has a negative value, through a small positive value for CoO, to a larger positive value for NiO. These numbers measure the relative stabilities of divalent and trivalent cations in these crystals.

5.5. Diffusion in Some Spinel Oxides

Figures 4, 5, and 6 collect available diffusion data on ferrites (fig. 4, also includes O in Co_3O_4), chro-

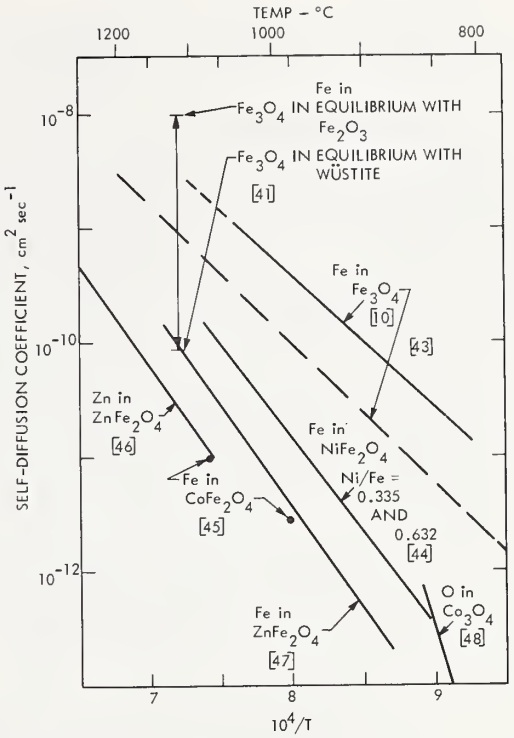

FIGURE 4. *Self-diffusion of cations in ferrites with the spinel structure and of oxygen in Co_3O_4.*

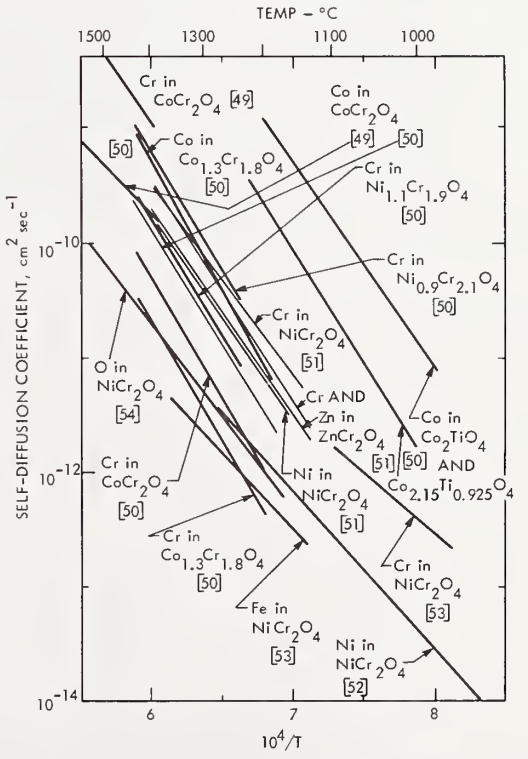

FIGURE 5. *Diffusivities of ions in chromites with the spinel structure and in cobalt titanate.*

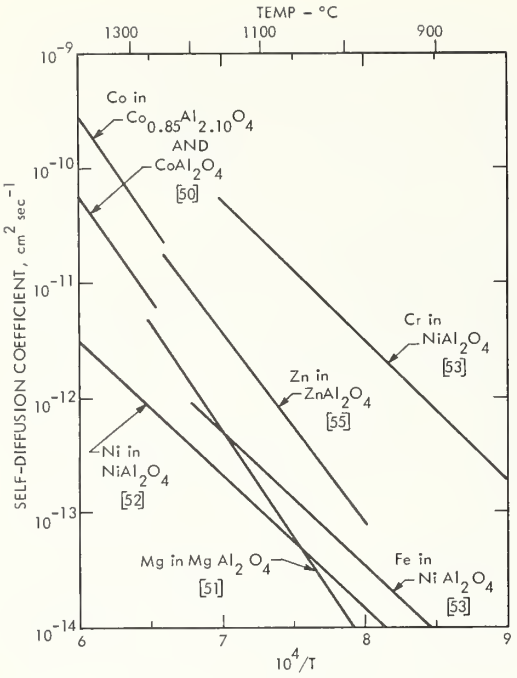

FIGURE 6. *Cation diffusivities in aluminates with the spinel structure.*

mites (fig. 5, also includes Co in two compositions of cobalt titanate) and aluminates (fig. 6). These figures are all on the same scale. They may be compared directly as long as the shift in origin is made properly. A number of tentative conclusions may be drawn from these comparisons, but it is important to note that the experiments are less than ideal in several respects, notably that sintered powder specimens with residual porosity were often employed, grain boundary contributions were not checked, and the thermodynamic activities of the components were usually uncontrolled.

TABLE 1. *Energies associated with cation self-diffusion and p-type conduction in FeO, CoO and NiO. References are in brackets. Estimated values that make the table internally consistent are in parentheses. All values are in kcal/g mole.*

Oxide	ΔH_m	$\Delta H_m + \Delta H_f/3$	ΔH_μ	$\Delta H_\mu + \Delta H_f/3$	$\Delta H_f/3$
FeO	30 [10, 22]	−10 [10]	10 [19]	(−18)	−28 [10]
					−17 [33]
CoO	35 [22]	(40)	(7)	12 [34]	5.1 [22]
		46 [23]	1.6 [35]	23 [37]	
NiO	(38)	48 [24]	2.3 [36]	18 [38]	24 [37]
		58 [25]	5.5 [37]	21 [39]	

In general, diffusion of iron in magnetite is much faster than it is in the heavily alloyed ferrites. The iron ion diffusivity is very sensitive to the oxygen partial pressure [41]. When iron is heavily substituted by ions with less labile valence states, the cation diffusivities fall to or below the lowest part of the magnetite diffusion range (that is, for magnetite in equilibrium with wüstite or a low oxygen partial pressure). The fact that a variety of cations in a variety of ferrites show roughly comparable diffusivities (in air) suggests that once iron becomes predominantly divalent or predominantly trivalent as a result of substituting cations with valence three or greater or cations with valence two or smaller, respectively, further composition change is not large in its effects [42].

Cobalt titanate [50] has cobalt diffusivities comparable to the cation diffusivities in alloyed ferrites. They show a strong dependence on the ratio of cobalt to titanium but very little dependence on the oxygen partial pressure [43]. Perhaps the strong effect of oxygen partial pressure on cation mobility in magnetite is through its effect on the ratio of Fe^{2+} to Fe^{3+} and not directly on the cation to anion ratio.

Clearly the general mobility of cations in ferrites is greater than that in chromites which in turn is slightly greater than that in aluminates. This trend agrees with the relative growth rates of these products on ferrous alloys at high temperatures; that is, alloying with chromium reduces the oxidation rate of iron-base alloys that form predominantly spinels, while alloying with aluminum reduces the rate even more. The activation energies for individual materials are probably not very significant. If a rough average slope is taken through each set of data, a characteristic activation energy is found for ferrites to be about 67 kcal, for chromites to be about 88 kcal, and for aluminates to be about 92 kcal/gram-mole of cations.

Diffusion coefficients of the two cations in the same spinel may be quite different. Although the data are not totally consistent, it appears that D^*_{Co} is greater than D^*_{Cr} in cobalt chromite and that the difference increases with increasing ratio of Co to Cr. D^*_{Ni} appears to be lower than D^*_{Cr} in $NiCr_2O_4$, and D^*_{Cr} appears to decrease as the ratio of Cr to Ni increases. Oxygen diffusivity in $NiCr_2O_4$ is lower than either cation diffusivity, but it may not be as low as the diffusivity of iron in this substance. These wide mobility differences explain in part the nonuniform distribution of the metallic elements in scales on alloys. They also suggest the possibility that scales might exist in which cation dominance of growth gives way to anion dominance within the scale layer because of composition changes. However, I know no real example at this time.

In nickel aluminate, the chromium diffusivity exceeds the iron diffusivity which in turn exceeds the nickel diffusivity.

6. Conclusion

I have not cited at all several oxide systems that illustrate good agreement among investigators, as in Cu_2O, or poorer agreement, as in ZnO. I have overlooked the pseudo-oxides, such as Ag_2S, which have such high intrinsic disorder in the cation sites that cation mobilities have little concentration dependence and very low temperature dependences. Nor have I discussed another pseudo-oxide, FeS, that illustrates the demobilizing effect of a vacancy superlattice in the cation sites at low temperatures at about composition Fe_7S_8.

Nevertheless, I think I have represented fairly the state of this art by the examples chosen. There are some measurements that are reliable because of the care with which they were done or the confirmation they have subsequently received or both. Other measurements must be regarded as tentative until independent confirmation of a direct or correlative sort develops. Correlations of the type I have offered will become increasingly useful and suggestive as the amount and range of the data increase. Some of the values I presented will be omitted from the later compilations because they failed to stand the test of repetition, correlation or consistency with the better theories that we hope will be available in the near future.

7. References

[1] H. Schmalzried and C. Wagner, Z. Physik Chem. N.F. **31**, I98 (I962).

[2] R. E. Carter and W. L. Roth, unpublished research quoted in reference [4].

[3] C. Compaan and Y. Haven, Trans. Faraday Soc. **52**, 786 (1956).

[4] L. A. Simpson and R. E. Carter, J. Am. Ceram. Soc. **49**, 139 (1966).

[5] A. W. Smith, F. W. Mezaros and C. D. Amata, J. Am. Ceram. Soc. **49**, 240 (1966).

[6] R. M. Barrer, Diffusion in and Through Solids, Cambridge University Press, 1941, pp. I8–I9.

[7] J. M. Dixon, L. D. LaGrange, U. Merten, C. F. Miller and J. T. Porter II, J. Electrochem. Soc. **110**, 276 (1963); T. Y. Tien and E. C. Subbarao, J. Chem. Phys. **39**, 1041 (I963).

[8] W. H. Rhodes and R. E. Carter, J. Am. Ceram. Soc. **49**, 244 (1966).

[9] L. E. Himmel and J. B. Holt, Chicago Meeting, AIME, October, I966.

[10] L. E. Himmel, R. F. Mehl and C. E. Birchenall, Trans. Met. Soc. AIME **197**, 827 (1953).

[11] R. Lindner, Arkiv Kemi **4**, 381 (1952).

[12] M. Davies, M. T. Simnad and C. E. Birchenall, Trans. AIME, J. Metals **3**, 889 (1951); **5**, I250 (1953).

[13] R. H. Condit and J. B. Holt, J. Electrochem. Soc. **111**, 1192 (1964).

[I4] W. C. Hagel, Trans. Met. Soc. AIME **236**, 179 (1966).

[15] V. I. Izvekov, N. S. Gobunov and A. A. Babad-Zakhrapin, Fiz. Met. i Metalloved. **14**, I95 (1962).

[I6] I. M. Fedorchenko and Y. B. Ermolovich, Ukrain. Chim. Zhur. **26**, 429 (1960).

[17] W. C. Hagel and A. U. Seybolt, J. Electrochem. Soc. **108**, 1146 (1961).

[18] L. C. Walters and R. E. Grace, J. Appl. Phys. **36**, 2331 (1965).

[19] W. C. Hagel, J. Am. Ceram. Soc. **48**, 70 (1965).

[20] A. E. Paladino and W. D. Kingery, J. Chem. Phys. **37**, 957 (1962).

[21] Y. Oishi and W. D. Kingery, J. Chem. Phys. **33**, 480 (1960).

[22] R. E. Carter and F. D. Richardson, Trans. Met. Soc. AIME **200**, I244 (1954).

[23] J. S. Choi and W. J. Moore, J. Phys. Chem. **66**, 1308 (1962).

[24] M. Klotsman, A. N. Timofeev and I. Sh. Trakhtenberg, Fiz. Met. i Metalloved. **14**, 91 (1962).

[25] R. Lindner and A. Akerstrom, Disc. Faraday Soc. **23**, I33 (1957).

[26] R. Lindner and G. Parfitt, T. Chem. Phys. **26**, I82 (I957).

[27] R. Lindner, St. Astrumdal and A. Akerstrom, Acta Chem. Scand. **6**, 468 (I952).

[28] M. O'Keefe and W. J. Moore, J. Phys. Chem. **65**, I438 (1961). The line is calculated from the corrected equation given on p. 2277.

[29] W. K. Chen and R. A. Jackson, Am. Ceram. Soc. Bull. **46**, 357 (1967).

[30] Y. Oishi and W. D. Kingery, J. Chem. Phys. **33**, 905 (1960) and **34**, 688 (1961).

[31] I. Bransky and D. S. Tannhauser, Trans. Met. Soc. AIME **239**, 75 (1967). The ΔH_μ value in table 1 is calculated from conductivity values for $Fe_{0.95}O$.

[32] C. E. Birchenall, Met. Rev. **3**, 235 (1959).

[33] K. Hauffe and H. Pfeiffer, Z. Elektrochem. **56**, 390 (1952), and Z. Metallkunde **44**, 27 (1953).

[34] C. Wagner and E. Koch, Z. Physik Chem. **32B**, 439 (1936).

[35] R. Uno, J. Phys. Soc. Japan **22**, 1502 (1967). His measurements are consistent with singly ionized vacancies instead of the doubly ionized vacancies assumed. That is, conductivity is proportional to $\rho_{O_2}^{1/3.8}$.

[36] F. J. Morin, Phys. Rev. **93**, 1199 (1954).

[37] S. P. Mitoff, J. Chem. Phys. **35**, 882 (I96I).

[38] H. H. von Baumbach and C. Wagner, Z. Physik Chem. **24B**, 59 (1934).

[39] M. G. Harwood, N. Herzfeld and S. L. Martin, Trans. Faraday Soc. **46**, 650 (1950).

[40] S. P. Mitoff, J. Chem. Phys. **41**, 2561 (1964).

[41] H. Schmalzried, Z. Physik Chem. N. F. **31**, 184 (1962).

[42] In addition to the data given, some unpublished results in my laboratory support this conclusion.

[43] V. I. Izvekov, Inzh. fiz. Zh. Akad. Nauk. Belorus. SSR **1**, No. 11, 64 (1958).

[44] R. H. Condit, M. J. Brabers and C. E. Birchenall, Trans. Met. Soc. AIME **218**, 768 (1960).

[45] R. H. Condit, M. J. Brabers and C. E. Birchenall, unpublished data.

[46] R. Lindner, D. Campbell and A. Akerstrom, Acta. Chem. Scand. **6**, 457 (1952).

[47] R. Lindner, Arkiv Kemi **4**, 381 (1952).

[48] Barbara A. Thompson, Ph. D. Thesis, Renssalaer Polytechnic Institute, 1962.

[49] R. Sun, J. Chem. Phys. **28**, 290 (1958).

[50] A. Morkel and H. Schmalzried, Z. physik Chem. N. F. **32**, 76 (1962).

[51] R. Lindner and A. Akerstrom, Z. physik Chem. N. F. **6**, I62 (I956).

[52] R. Lindner and A. Akerstrom, Z. physik Chem. N. F. **18**, 303 (1958).

[53] I. N. Belokurova and D. V. Ignatov, Soviet J. Atom. Energy **4**, 399, transl. p. 301 (1958).

[54] W. D. Kingery, D. C. Hill and R. P. Nelson, J. Am. Ceram. Soc. **43**, 473 (1960).

[55] N. S. Gorbunov and V. I. Izvekov, Uspekhi. Fiz. Nauk **72**, 273 (1960).

The Determination of Thermodynamic Properties in Single Phase Wüstite by Coulometric Titration in a High Temperature Galvanic Cell

H. F. Rizzo[1], R. S. Gordon, and I. B. Cutler

Department of Ceramic Engineering
University of Utah
Salt Lake City, Utah 84112

The thermodynamic properties of wüstite were determined as a function of composition between 1050 and 1200 °C by coulometric titration in a high temperature galvanic cell using a stabilized zirconia electrolyte. Isothermal plots of the oxygen pressure versus composition (O/Fe) were sigmoidal in shape with a pronounced negative deviation from Raoult's Law below the inflection point ($FeO_{1.10}$-$FeO_{1.12}$) and a positive deviation above. The partial molal enthalpy of oxygen, $\Delta\bar{H}_O$, varied between −64.5 kcal/mole ($FeO_{1.05}$) and −74.5 kcal/mole ($FeO_{1.14}$). A statistical mechanical model, developed by Libowitz and based on Fe^{+3} interstitials, each associated with two Fe vacancies, predicted correctly the P_{O_2} versus O/Fe dependence at temperatures between 1057 to 1200 °C. The usefulness of a solid electrolyte galvanic cell in determining phase boundaries and thermodynamic functions in the iron-oxygen system was demonstrated.

Key Words: Composition-versus-pressure, defect complexes, galvanic cell, wüstite.

Introduction

The high temperature galvanic cell is especially suited for studying the thermodynamic properties of defect oxide phases. By varying the composition electrochemically (i.e., coulometric titration) the activity of oxygen can be obtained as a continuous function of composition over the entire phase field of a nonstoichiometric phase. Coulometric titration provides the experimental flexibility and control necessary to delineate the composition and phase boundaries in a number of oxide systems.

With respect to the study of defect phases, two basic techniques have been employed.

1. Measurements have been conducted on numerous samples of a defect phase, each prepared at a specific composition [1–5].[2]
2. Measurements have been made on a single sample, in which the composition is varied electrochemically by a coulometric titration technique [1, 6–8].

The first technique has been used to study regions of homogeneity in the defect phases Fe_xO [4], WO_{2-x} [5], TiO_{2-x} [3], UO_2-U_3O_8 [1], and Nb_2O_{5-x} [2]. The second technique has been used by Kiukkola and Wagner [7] to determine single and two-phase regions in the Ag-Te system. It has also been used in the UO_{2+x} [6], UO_2-U_3O_8 [1], TiO_{2-x} [8], $NbO_{2\pm x}$ and $Ti_{0.5}Nb_{0.5}O_{2\pm x}$ [8] systems.

The objective of this study was to determine the feasibility of coulometric titration in determining phase boundaries and oxygen activities in oxide systems. The iron-oxygen system was selected since there is considerable information, principally the work of Darken and Gurry [9], on the phase boundaries and thermodynamic properties of the wüstite phase as a function of temperature and composition.

Experimental

Two types of experimental cells were employed in the studies: (1) a closed-end tube cell and (2) a three-electrode cell. The closed-end tube cell consists of a dense stabilized zirconia (.85 ZrO_2 + .15 CaO) tube (~ 1″ OD by ~ 10″ long) closed at one end. (See fig. 1.) The inside of the tube is open to the atmosphere (Salt Lake City, Utah) which is used as the standard reference oxygen potential ($P''_{O_2\,(air)} = 0.18$ atm). The other side is sealed in a chamber in which the atmosphere is purified argon. A detailed description of the closed-end tube cell and the fabrication of the electrolyte can be found elsewhere [10]. With the foregoing type of cell arrangement, three different compositions were studied:

[1] Presently Staff Scientist (Lt. Col., USAF), Air Force Weapons Laboratory, Kirtland Air Force Base, New Mexico 87117.

[2] Figures in brackets indicate the literature references at the end of this paper.

$$\text{Pt, Fe-Fe}_x\text{O} \left| \begin{matrix} 0.85\ \text{ZrO}_2 \\ + \\ 0.15\ \text{CaO} \end{matrix} \right| \text{O}_2\ (\text{air}, P''_{\text{O}_2} = 0.18\ \text{atm}), \text{Pt} \qquad \text{I}$$

$$\text{Pt, Fe}_z\text{O-Fe}_3\text{O}_4 \left| \begin{matrix} 0.85\ \text{ZrO}_2 \\ + \\ 0.15\ \text{CaO} \end{matrix} \right| \text{O}_2\ (\text{air}, P''_{\text{O}_2} = 0.18\ \text{atm}), \text{Pt} \qquad \text{II}$$

$$\text{Pt, FeO}_y{}^{3} \left| \begin{matrix} 0.85\ \text{ZrO}_2 \\ + \\ 0.15\ \text{CaO} \end{matrix} \right| \text{O}_2\ (\text{air}, P''_{\text{O}_2} = 0.18\ \text{atm}), \text{Pt} \qquad \text{III}$$

The anode compositions FeO_y and Fe_zO-Fe_3O_4 were obtained by titration of oxygen into Fe-Fe_xO sample electrodes.

The cell emf (E) for cell I, II, and III is related to the equilibrium partial pressures in atmospheres of diatomic oxygen at the anode (P'_{O_2}) and cathode (P''_{O_2}) by equation (1), in which R is the gas constant, $\mathcal{F}$ is the Faraday constant and

$$E = \frac{RT}{4\mathcal{F}} \ln \frac{P''_{\text{O}_2}}{P'_{\text{O}_2}}. \qquad (1)$$

T is the absolute temperature. Using cells I and II the oxygen activity (P'_{O_2}) was measured for the two phase mixtures, Fe-Fe_xO and Fe_zO-Fe_3O_4 (II). In addition, the oxygen activity was measured (using cell III) for any arbitrary composition (y) in the wüstite phase (FeO_y) by coulometric titration.

The three-electrode cell (fig. 2) consists of three electrodes in a stabilized zirconia cylinder (1 in.-diameter, 3/4 in.-height). In the coulometric titration studies, one of the bottom Fe-Fe_xO electrodes was used to titrate oxygen in or out of the top electrode, while the other bottom electrode was used to record the emf. Two compositions were studied in this cell:

$$\text{Pt, Fe-Fe}_x\text{O} \left| \begin{matrix} 0.85\ \text{ZrO}_2 \\ + \\ 0.15\ \text{CaO} \end{matrix} \right| \text{Fe}_z\text{O-Fe}_3\text{O}_4, \text{Pt}; \qquad \text{IV}$$

$$\text{Pt, Fe-Fe}_x\text{O} \left| \begin{matrix} 0.85\ \text{ZrO}_2 \\ + \\ 0.15\ \text{CaO} \end{matrix} \right| \begin{matrix} \text{FeO}_y \\ \\ z < 1/y < x \end{matrix} \qquad \text{V}$$

Isothermal titration experiments were conducted in both directions with cell V across the entire wüstite phase between 800 and 1200 °C. In order to calculate the activity of oxygen at the cathode (Fe_zO-Fe_3O_4), the activity at the anode must be known. The oxygen potentials for the Fe-Fe_xO equilibrium are reasonably well established [9, 11–15] and were also measured in this study [16] with the closed-end tube (cell I).

In the titration studies the cell voltages and currents were measured on a cyclic basis. Using an electromechanical timer the cell voltage was recorded automatically after each titration period.

The normal procedures in the titration experiments were as follows: (1) Start titration from the iron-rich boundary of wüstite; (2) vary the titration current for a fixed titration time so that the time after titration required for the cell voltage to stabilize at a constant emf (equilibrium) would be within the time allowed; (3) reverse titration direction and compare the ratio of change in emf per

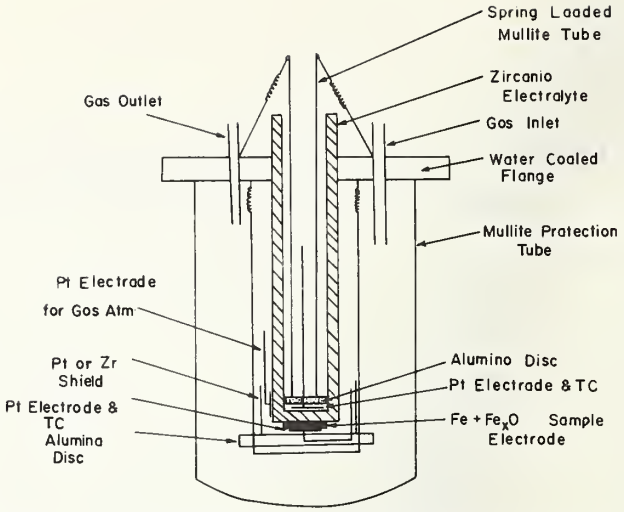

FIGURE 1. *Schematic of galvanic cell with zirconia electrolyte closed-end tube cell.*

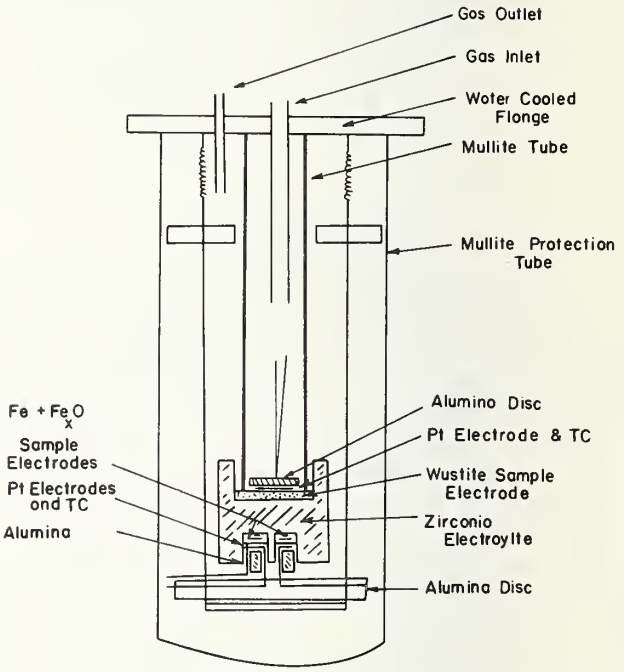

FIGURE 2. *Schematic of galvanic cell with three-sample electrode, cylindrical shaped zirconia electrolyte.*

[3] The compositions in the phase field of wüstite are signified FeO_y where y is the O/Fe ratio.

coulomb titrated in both directions; (4) periodically interrupt titration cycles and measure cell voltage for extended periods (1–24 hours). Analysis of data from items (1) through (4) was the basis for determining if the titration experiment was a reversible process and if equilibrium cell voltages were being measured. Measurement of cell voltages during the titration period provided information on the degree of polarization. Titrations in both directions were performed between the wüstite boundaries. Minimal hystersis and equality of the number of coulombs titrated in both directions were indications of reliable experiments.

One of the principal experimental difficulties was the reduction or oxidation of the single-phase wüstite sample by the cell atmosphere. The apparent rate-controlling mechanism was the transfer of oxygen from the surface of the sample to the gas phase. Reduction and oxidation rates could be changed by varying the gas flow rates and gettering conditions. Verification of the gas atmosphere as a controlling factor was determined by monitoring the cell atmosphere surrounding the wüstite electrode by the use of a platinum electrode on the zirconia tube next to the wüstite electrode. It was noted that during titration of oxygen into wüstite the oxygen pressure increased in the cell atmosphere and decreased during titration of oxygen out of the wüstite electrode. The reduction of the wüstite electrode was also noted in the three-electrode cell and was most probably due to the presence of the two Fe-Fe_xO sample electrodes.

Corrections for reduction or oxidation of the wüstite electrode were made on a cyclic basis. Two methods were used. One was to measure the rate of change of cell voltage for extended times (45 min. to 24 hrs.) for a known change in the number of coulombs (i.e., composition). From this measurement, the change in the number of coulombs per unit time for a given voltage range was calculated and used in each titration cycle to estimate the change in the number of coulombs due to oxidation or reduction taking place during the emf measuring period. The second method was to compare the change in the cell emf during a titration step with the net change in cell emf between adjacent cycles. If these voltages were different, an effective number of coulombs to account for the difference was either added to or subtracted from the number passed in the titration period. The details describing these corrections are found in the thesis of the principal author [10]. The magnitude of these corrections in establishing the oxygen-partial pressure-composition isotherms for the single-phase region varied between three and twenty percent.

The electrode samples used in this study varied from pure Fe (less than 25 ppm) to samples containing 77.0 weight percent Fe. Compositions containing 85 and 82 weight percent iron were prepared by dry mixing and pressing mixtures of reagent grade Fe_2O_3 (99.0 percent minimum) and iron powder (GAF HP carbonyl 99.6 to 99.9 percent) in ½ inch steel dies and then heating in a tungsten vacuum furnace (2×10^{-5} mm Hg) between 950 to 1000 °C for 19 hours. A sample containing 77 wt percent iron was prepared by oxidation of iron (99.96 percent) in a H_2O/H_2 atmosphere at 900 °C. This powdered sample was used in the three-electrode cell for the variable composition wüstite. The weights, dimensions, and total iron determined by chemical analysis for the electrode samples used in the titration experiments are presented in table 1.

Results

A. Fe-Fe_xO, Fe_zO-Fe_3O_4 Phase Boundaries

In the progress of the titration experiments on cells I, II, and IV, the oxygen potentials were determined for both the Fe-Fe_xO and Fe_zO-Fe_3O_4 (i.e.,

TABLE 1. *Summary of electrode samples used in titration experiments*

	A	*B*	*C*	*D*	*E*
Composition of electrode (wt % Fe)	85.5	82.0	100	77.0	85.5
Weight of electrode (g)	0.2222	0.3385	0.0922	0.2336	0.221 0.265
Sample dimensions (cm)	1.5 length 0.26 width 0.10 thick	1.1 diam. 0.070 thick	0.6 length 0.3 width 0.065 thick	powder compact 1.5 diam. 0.023 thick	powder compact 0.6 diam.
Surface area (cm^2)	0.39	0.95	0.18	1.77	0.28

A, B, C Electrode sample—closed-end tube
D Electrode sample—three-electrode cell
E Reference electrode—three-electrode cell

composition O/Fe ~ 1.33)[4] two phase equilibria. The experimental details and results are reported extensively elsewhere [10, 16]. For the purpose of this paper the standard free energy of formation (calories) of Fe_xO and log P_{O_2} for the Fe-Fe_xO equilibrium (x Fe + 1/2 O_2 = Fe_xO) are given by equations (2) and (3) and are valid between 540 and 1200 °C [10, 16]:

$$\Delta F_2 = -62{,}452 \pm 46 + 15.127(\pm 0.05)T(°K); \quad (2)$$

$$\log P_{O_2} = \frac{-27{,}295 \pm 85}{T} + 6.6115 \pm 0.0218. \quad (3)$$

Equation (4) is an expression for log P_{O_2} for the Fe_zO-Fe_3O_4 equilibrium between 900 and 1200 °C [10, 16]:

$$\log P_{O_2} = \frac{-33{,}210 \pm 20}{T} + 13.354 \pm 0.064. \quad (4)$$

B. Titration in Single Phase Wüstite

Two principal techniques were employed: (1) At a constant temperature oxygen was titrated into the wüstite phase for a prescribed time, followed by measurements of the cell emf for a fixed time sufficient for equilibrium to occur. Repeated titration-emf measurement cycles resulted in the establishment of an oxygen pressure-composition isotherm. (2) The same basic procedure was followed, but after each titration period an emf-temperature profile was made for each new composition, giving the oxygen potential as a function of both temperature and composition. The latter method proved more difficult because of the tendency for the single-phase wüstite to become oxidized or reduced by the surrounding cell atmosphere.

The reaction for cell III with the oxygen pressure corrected to one atmosphere is given by equation (5):

$$1/s\ FeO_y + 1/2\ O_2\ (1\ atm) = 1/s\ FeO_{y+s} \quad y >>> s. \quad (5)$$

The equilibrium oxygen pressure for any wüstite phase FeO_y is related to E_{III} by equation (6):

$$\ln P_{O_2} = \frac{-2N\mathcal{F}E_{III}}{RT} + \ln\ (0.18). \quad (6)$$

The cell reaction for the three-electrode zirconia cell (V) is given by equation (7):

$$x\text{Fe} + \frac{y' + u}{u}\ Fe_{y'}O = Fe_xO + \frac{y'}{u}\ Fe_{y'+u}O. \quad (7)$$

By subtracting the reaction (xFe + 1/2 O_2 (1 atm) = Fe_xO) from equation (7) the activity of oxygen in wüstite can be determined, assuming that $y' \gg u$. The equilibrium pressure of oxygen computed from E_V and ΔF_f° of Fe_xO is given by equation (8):

$$-\log P_{O_2} = \frac{1}{2.303\ RT}[-N\mathcal{F}E_V + 62{,}452 - 15.127T]. \quad (8)$$

Oxygen pressure-composition isotherms were determined in coulometric titration experiments at 800, 894, 950, 1000, 1057, 1075, 1100, 1139, 1150, and 1200 °C. Selected isotherms are presented in figures 3–6 for the temperatures 1075, 1100, 1139, and 1200 °C, respectively. One interesting feature of all the P_{O_2} vs. O/Fe plots is their sigmoidal shape. The correlation of the inflection points in the curves with the p–n transition (represented by the arrows on figures 3–6) in wüstite will be dis-

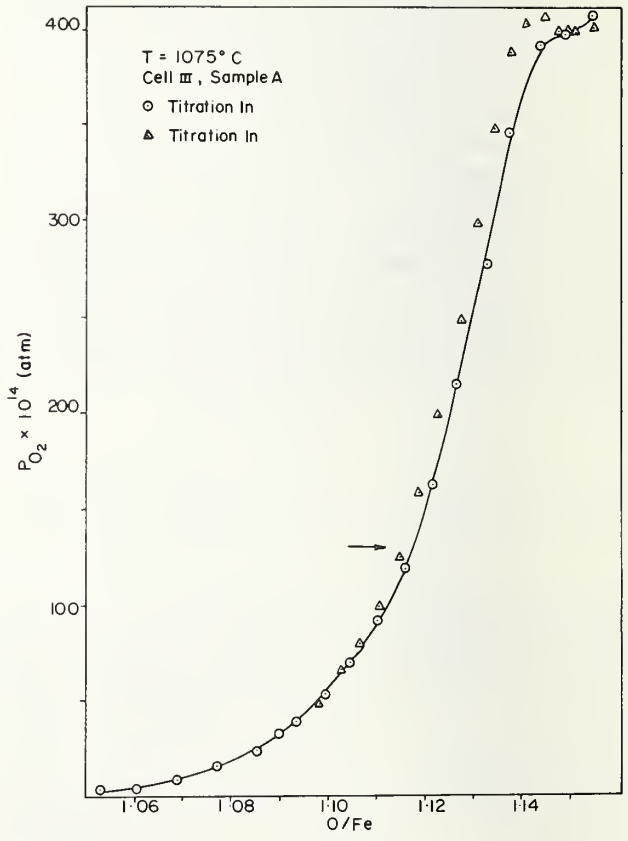

FIGURE 3. *1075 °C isotherms of* P_{O_2} *versus composition, O/Fe.*

[4] Evidence, which is reported elsewhere [17], was found in the titration experiments of this study that several defect phases exist between the presently reported oxygen-rich boundary of wüstite and magnetite [9]. Therefore, reference to the Fe_zO-Fe_3O_4 equilibrium in this paper corresponds to the most oxygen-rich wüstite-type phase in equilibrium with magnetite or a composition slightly less oxygen rich than $FeO_{1.33}$ (i.e., Fe_3O_4).

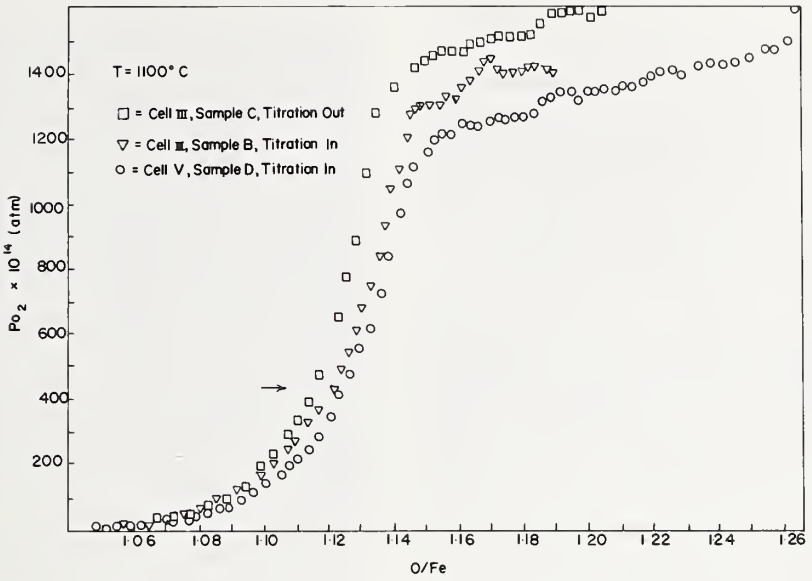

FIGURE 4. *1100 °C isotherms of* P_{O_2} *versus composition, O/Fe.*

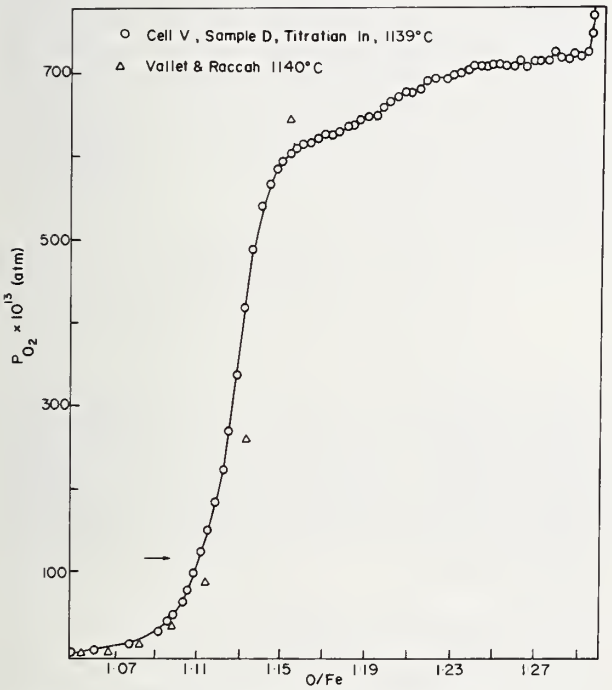

FIGURE 5. *1139 °C isotherms of* P_{O_2} *versus composition, O/Fe.*

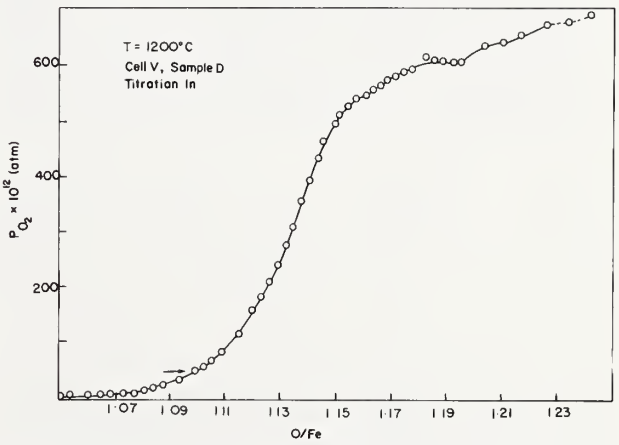

FIGURE 6. *1200 °C isotherms of* P_{O_2} *versus composition, O/Fe.*

cussed later. Plots of log P_{O_2} versus composition were employed in the Gibbs-Duhem graphical integrations. The raw data and the experimental conditions used to construct the isotherms are tabulated in the thesis of the principal author [10]. The compositions were determined from a knowledge of the weight of the iron in a particular sample and the assumptions that the composition of the iron-rich boundary was $FeO_{1.050}$ and was constant in the temperature range of measurements. The validity of these assumptions is discussed elsewhere [10, 16].

In general the oxygen-wüstite composition isotherms presented in figures 3 through 6 indicated higher partial pressures than those previously reported for the single-phase region, except in a few cases. This discrepancy is difficult to explain unless the cell voltage measurements did not correspond to equilibrium conditions. Nonequilibrium voltages could result from (1) side reactions between the electrolyte and the wüstite, (2) a reaction between the platinum electrode and wüstite, (3) insufficient time for diffusion to occur after titration, and (4) polarization of the cell.

The first two can be dismissed when one considers the reproducibility of measurements in the

two-phase regions Fe-Fe_xO and Fe_2O-Fe_3O_4 combined with the excellent agreement of the partial pressures of oxygen with other investigations [10]. Polarization of the cell could occur at low temperatures and high titration currents. For example, in establishing a partial pressure composition isotherm at 800 °C, titration currents greater than 0.4 milliamps required times longer than the allowed 35 minutes for stabilization of the voltage. In the course of a titration experiment the voltage drops across all components of the cell were measured and titration currents were reduced whenever there was an indication of polarization at one of the sample electrodes. The fundamental experimental criterion used to establish that equilibrium measurements were being made was that the cell voltage was time-invariant. Hysteresis effects due to direction of titration were small and the reproducibility of oxygen pressure composition isotherms was good. For example, the 1100 °C isotherms (fig. 4) were obtained from four separate experiments which employed different cells, samples, and titration currents (0.4 to 2.1 milliamps), titrations in both directions, different times to measure cell emf after titration (9–35 min), varying sample thickness and starting compositions. The composition where the first two-phase region occurred (constant oxygen activity) compared to within ± 0.005 O/Fe of the reported oxygen-rich boundary of wüstite ($FeO_{1.154}$). This agreement confirms the validity of determining the actual phase boundary composition by coulometric titration. The series of plateaus for compositions greater than $FeO_{1.154}$ correspond to the multiphase region previously mentioned [17]. The temperature of 1100 °C was certainly high enough to dispel the question of diffusion and, although there was scatter between experiments there is little doubt that the partial pressure of oxygen was higher than reported values. It is noted that all reported data were obtained with CO-CO_2 or H_2O-H_2 atmospheres, so the effect of the presence of carbon or hydrogen on the activity of oxygen in wüstite could perhaps provide the explanation for the lower partial pressures measured by these methods. The data reported by Barbi [4] on wüstite, which were determined by emf measurements, also showed higher oxygen pressures than those reported by others.

The difference in partial pressure of oxygen between this study and other investigations is even more pronounced for isotherms obtained between 800 and 1000 °C. This observation is again difficult to explain since in this temperature range there was very little oxidation or reduction of the sample and thus, if diffusion was not a rate-limiting step in achieving equilibrium, the measurements should be valid. However, it was observed many times throughout this investigation that the emf-temperature coefficient would undergo a change in slope between 800 and 950 °C for all compositions more oxygen-rich than $FeO_{1.06}$. It is also noted that Kleman [12] has proposed the existence of more than one wüstite defect phase in this temperature and composition range. Therefore, to avoid the question of nonequilibrium isotherms and the possibility of other defect phases being present, only the isotherms between 1057 and 1200 °C were employed to calculate the thermodynamic properties of wüstite. The data at the lower temperatures can be found elsewhere [10]. It will also be shown that use of a defect model for wüstite proposed by Libowitz [30] supports the use and validity of the higher temperature isotherms.

C. Thermodynamic Treatment of Wüstite

From the relationship between the pressure of oxygen and the composition of wüstite at various temperatures the partial molal thermodynamic functions can be calculated. The partial molal quantities are particularly useful for describing the variation of thermodynamic quantities with the deviation from stoichiometry. The choice of components is somewhat arbitrary. For example, the following reactions describe the formation of wüstite:

$$Fe + (y/2)O_2 = FeO_y{}^5; \tag{9}$$

$$FeO_{1.05} + \frac{y-1.05}{2} O_2 = FeO_y. \tag{10}$$

The first reaction requires a knowledge of the activity of iron in wüstite which can be obtained by a Gibbs-Duhem integration of the oxygen activity. Darken and Gurry, using Fe and O_2 as components, determined the activity of iron in wüstite from the following relation:

$$\log a_{Fe} = -1/2 \int_{1.05}^{y} [(O/Fe - 1) d(\log P_{O_2})] - 1/2 \log P_{O_2} + 1/2 \log P'_{O_2}. \tag{11}$$

They defined the activity of Fe at the Fe-Fe_xO boundary to be unity, which is actually the standard state for iron because of the low solubility of oxygen in iron (2–3 ppm at 950 °C and 25 ppm at 1350 °C [18]). P'_{O_2} is the partial pressure of oxygen corresponding to the two-phase Fe-Fe_xO equilibrium.

[5] The use of FeO_y rather than Fe_yO is preferred since the O/Fe ratio is used in the Gibbs-Duhem integrations.

The second reaction described by eq (10) was used in this study to determine the partial molal quantities. In this case $FeO_{1.05}$ was selected as one of the components and the formation of wüstite was based on the solution of oxygen in the most oxygen deficient wüstite phase, $FeO_{1.05}$. It should be pointed out that for a definite wüstite composition the solid solution under consideration is that of oxygen in the wüstite phase, not oxygen in iron. Thus, this selection of components appears to have a better physical meaning than Fe and O_2 except perhaps for the use of magnetite and wüstite in describing the binary solution. The composition of oxygen-deficient wüstite does not vary appreciably with temperature and can be considered constant over the temperature range 1050 to 1200 °C [16]. The standard state for oxygen was defined as an ideal gas at one atmosphere, and the activity of $FeO_{1.05}$ at the oxygen-deficient composition was defined to be unity for all temperatures. The standard free energy of formation and other thermodynamic properties of the most oxygen-deficient wüstite ($FeO_{1.05}$) were obtained from data in cell I [16].

The free energy of mixing of one mole of $FeO_{1.05}$ with $\frac{y-1.05}{2}$ moles of O_2 at any particular temperature is given by eq (12):

$$\Delta F_{mix} = RT \ln a_{FeO_{1.05}} + \frac{y-1.05}{2} RT \ln P_{O_2}. \quad (12)$$

From the knowledge of oxygen activity across the variable composition of wüstite, the activity of $FeO_{1.05}$ can be determined by a Gibbs-Duhem integration of the following equation:

$$\ln a_{FeO_{1.05}} = -\int_{1.05}^{y} (y-1.05) d(\ln P_{O_2}). \quad (13)$$

Graphical integrations were performed on the isotherms at 1057, 1075, 1100, 1139, 1150, and 1200 °C.

The partial molal free energies, $\Delta\bar{F}_{FeO_{1.05}}$ and $\Delta\bar{F}_O$, were calculated from the following relations:

$$\Delta\bar{F}_{FeO_{1.05}} = \bar{F}_{FeO_{1.05}} - F^\circ_{FeO_{1.05}} = RT \ln a_{FeO_{1.05}};$$

$$\Delta\bar{F}_O = \bar{F}_O - 1/2F^\circ_{O_2} = \frac{RT}{2} \ln P_{O_2}. \quad (14)$$

The free energies for $\Delta\bar{F}_{FeO_{1.05}}$ are tabulated in table 2, and those for $\Delta\bar{F}_O$ can be calculated from partial pressure of oxygen data contained in table 3. The total free energy of formation of wüstite, $\Delta F_{f(FeO_y)}$, from the elements in their standard states of any composition y greater than 1.05 is given by

TABLE 2. *Partial molal free energy of $FeO_{1.05}$ in Wüstite*

Composition O/Fe	1.06	1.07	1.08	1.09	1.10	1.11	1.12	1.13	1.14	1.15
Isotherm Temp °C	$-(\bar{F}_{FeO_{1.05}} - F^\circ_{FeO_{1.05}})$[a](Cal)									
1057	6.6	21.2	41.8	64.2	91.5	136.5	190.0	227.0	242.0	285.0
1075	4.5	17.9	41.1	69.3	101.0	140.0	180.0	233.0	275.0	284.0
1100 Sample A, B, C	6.1	22.1	44.2	72.8	106.7	148.0	193.0	295.0	288.0	306.0
1139	7.0	21.5	37.7	62.5	103.2	156.4	217.0	273.0	326.0	344.0
1150	7.2	19.9	41.0	69.5	106.0	154.0	211.0	281.0	345.0	351.0
1200	8.2	25.0	51.9	85.0	124.3	172.5	225.0	278.0	333.0	368.0

[a] $\Delta\bar{F}_{FeO_{1.05}} = \bar{F}_{FeO_{1.05}} - F^\circ_{FeO_{1.05}} = 2.303RT \log a_{FeO}$.

TABLE 3. *Partial pressure of oxygen obtained from P_{O_2}–O/Fe isotherms*

Composition O/Fe	1.05	1.06	1.07	1.08	1.09	1.10	1.11	1.12	1.13	1.14	1.15
Isotherm Temp °C	$-\log P_{O_2}$										
1057	13.93	13.58	13.26	12.98	12.78	12.58	12.32	12.01	11.87	11.81	11.79
1075	13.63	13.32	13.04	12.74	12.50	12.25	12.04	11.81	11.59	11.43	11.40
1100 Samples A, B, C	13.25	12.88	12.56	12.26	12.00	11.77	11.56	11.27	11.05	11.02	10.93
1100 Sample D	13.25	12.93	12.66	12.40	12.10	11.89	11.68	11.46	11.25	11.02	10.93
1139	12.73	12.32	12.00	11.80	11.62	11.29	10.98	10.73	10.47	10.28	10.23
1150	12.58	12.18	11.87	[b] 11.61	[b] 11.35	[b] 10.10	10.88	10.64	[b] 10.39	[b] 10.18	10.12
1200	11.99	11.51	11.18	10.85	10.57	10.29	10.04	9.82	9.61	9.42	9.30

[b] Average values between Samples A, D.

eq (15). $\Delta F^{\circ}_{f(FeO1.05)}$ is the standard free energy of formation,

$$\Delta F_{f(FeO_y)} = \Delta F^{\circ}_{f(FeO1.05)} + \Delta F_{mix}, \qquad (15)$$

of one mole of the most oxygen-deficient wüstite phase, $FeO_{1.05}$. It is known very accurately from cell measurements of Fe-Fe_xO equilibrium described previously [16]. The values for free energy of formation of FeO_y are given in table 4.

The partial molal enthalpies ($\Delta\overline{H}_O$ and $\Delta\overline{H}_{FeO_{1.05}}$) were evaluated from a linear least-squares fit of the log a_O and log $a_{FeO_{1.05}}$ data as a function of $1/T$. The values of log P_{O_2}, which were extracted from the log P_{O_2}-O/Fe isotherms and used in all the thermodynamic calculations, are listed in table 3. The use of a linear fit of log P_{O_2} versus $1/T$ to determine the partial molal enthalpy of oxygen was justified on the basis of the linear emf-temperature coefficients obtained for different wüstite compositions. The determination of the partial molal enthalpy of $FeO_{1.05}$ as a function of composition was also made using a linear fit of log $a_{FeO_{1.05}}$ versus $1/T$. Although there was no physical basis for a linear fit, the errors are small because the slopes of log a_{FeO} versus $1/T$ plots are very small.

The partial molal entropies were determined from the temperature derivatives of the partial molal free energies using a least-squares analysis of the data. The partial molal enthalpies and entropies of oxygen at different compositions are given in table 5 along with the least-square analysis of the log P_{O_2} versus $1/T$ data. A similar tabulation for $\Delta\overline{H}_{FeO_{1.05}}$, $\Delta\overline{S}_{FeO_{1.05}}$, and log $a_{FeO_{1.05}}$ versus $1/T$ are found in table 6.

The enthalpies of mixing were calculated from equation (16) and are given in table 7:

$$\Delta H_{mix} = (y - 1.05)\Delta\overline{H}_O + \Delta\overline{H}_{FeO_{1.05}}. \qquad (16)$$

TABLE 4. *Free energy of formation for FeO_y*

Composition O/Fe	1.05	1.06	1.07	1.08	1.09	1.10	1.11	1.12	1.13	1.14	1.15
Isotherm Temp °C	$-(\Delta F_{f(FeO_y)} = \Delta F_{f(FeO_{1.05})} + \Delta F_{mix}$ (cal))										
1057	44,447	44,865	45,275	45,675	46,070	46,455	46,835	47,195	47,565	47,930	48,325
1075	44,161	44,575	44,985	45,380	45,775	46,150	46,530	46,890	47,255	47,615	47,965
1100 Samples A, B, C	43,764	44,175	44,575	44,965	45,345	45,720	46,090	46,435	46,785	47,175	47,505
1139	43,144	43,550	43,940	44,325	44,710	45,070	45,428	45,785	46,125	46,465	46,795
1150	42,970	43,375	43,765	44,145	44,520	44,885	45,250	45,605	45,955	46,305	46,620
1200	42,175	42,470	42,955	43,325	43,685	44,035	44,380	44,715	45,045	45,370	45,680
	$\Delta F_{f(Fe_{y'}O)} = \dfrac{\Delta F_{f(FeO_y)}}{y}$										
1100	41,680	41,675	41,660	41,635	41,600	41,565	41,520	41,460	41,400	41,380	41,310
1200	40,165	40,065	40,145	40,115	40,075	40,030	39,980	39,925	39,865	39,800	39,720

TABLE 5. *Partial molal enthalpy and entropy of oxygen as a function of wüstite composition*

Composition O/Fe	$-\log P_{O_2} = A + B\left(\frac{1}{T}\right) \times 10^4$		$-(\Delta\overline{H}_O)^{d} = -\left(\overline{H}_O - \frac{1}{2}H^{\circ}_{O_2}\right)$	$-(\Delta\overline{S}_O)^{d} = -\left(\overline{S}_O - \frac{1}{2}S^{\circ}_{O_2}\right)$
	A	*B*	*cal*	*cal/mole deg*
1.06	−7.831 ± 0.230	2.846 ± 0.032	65,139 ± 730	17.9
1.07	−8.371 ± .491	2.879 ± .068	65,862 ± 1,550	19.2
1.08	−8.875 ± .713	2.912 ± .091	66,197 ± 2,080	20.3
1.09	−9.566 ± .914	2.975 ± .127	68,068 ± 2,900	21.9
1.10	−10.512 ± .573	3.071 ± .080	70,253 ± 1,830	24.0
1.11	−10.924 ± .596	3.093 ± .083	70,772 ± 1,900	25.0
1.12	−10.680 ± .722	3.024 ± .100	69,200 ± 2,290	24.4
1.13	−11.514 ± .480	3.111 ± .067	71,180 ± 1,530	26.4
1.14	−12.844 ± .583	3.275 ± .081	74,927 ± 1,850	29.4
1.15	−13.690 ± .500	3.384 ± .070	77,426 ± 1,600	31.3

[d] $\Delta\overline{H}_O = \dfrac{-2.303 \times 1.987}{2} B \times 10^4$ and $\Delta\overline{S}_O = \dfrac{2.303 \times 1.987}{2} A$.

TABLE 6. *Partial molal enthalpy and entropy of $FeO_{1.05}$ as a function of composition*

Composition O/Fe	$-\log a_{FeO_{1.05}} = A + B\left(\frac{1}{T}\right)\times 10^4$		$\Delta\bar{H}_{FeO_{1.05}}$ [c]	$\Delta\bar{S}_{FeO_{1.05}}$ [c]
	A	$B\times 10^3$	*cal*	*cal/mole deg*
1.06	0.00397±0.0019	−0.409±0.265	19.0± 12.0	0.0182
1.07	.00594± .0043	−0.363±0.609	17.0± 28.0	.0272
1.08	.01005± .0096	−0.463±1.33	21.0± 61.0	.0460
1.09	.02080± .0142	−1.36 ±1.98	62.0± 90	.0952
1.10	.03919± .0115	−3.16 ±1.61	144.0± 73	.179
1.11	.05250± .00515	−4.01 ±0.72	183.0± 32	.240
1.12	.06775± .0162	−5.00 ±2.26	229.0±103	.311
1.13	.0944 ± .0208	−7.56 ±2.89	346.0±132	.432
1.14	.1505 ± .0403	−14.40 ±5.0	660.0±228	.690
1.15	.1465 ± .0188	−13.35 ±2.6	611.0±120	.670

[c] $\Delta\bar{H}_{FeO_{1.05}} = -2.303\times 1.987\times 10^4 B$ and $\Delta\bar{S}_{FeO_{1.05}} = 2.303\times 1.987 A$.

TABLE 7. *Enthalpy and entropy of mixing $FeO_{1.05}$ and oxygen and enthalpy and entropy of formation of FeO_y*

Composition O/Fe	$-\Delta H_{mix}$	$-\Delta H_{f(FeO_y)}$	$\frac{-\Delta H_{f(FeO_y)}}{1+y}$	$-\Delta S_{mix}$	$-\Delta S_{f(FeO_y)}$
	cal/mole	*cal/mole*	*cal/g atom*	*cal/mole deg*	*cal/mole deg*
1.05	0	65,609± 50	32,005	0	15.13
1.06	636	66,245± 70	32,155	0.163	15.29
1.07	1,309	66,920±110	32,300	0.361	15.39
1.08	1,985	67,595±180	32,495	0.569	15.70
1.09	2,673	68,280±250	32,670	0.785	15.91
1.10	3,386	68,995±220	32,855	1.031	16.16
1.11	4,080	69,690±210	33,030	1.272	16.40
1.12	4,615	70,225±335	33,125	1.425	16.56
1.13	5,350	70,960±330	33,315	1.672	16.80
1.14	6,095	71,705±450	33,505	1.956	17.09
1.15	7.141	72,750±330	33,835	2.460	17.59

The total enthalpies of formation for any particular composition of wüstite were calculated from equation (17) and are given in table 7:

$$\Delta H_{f(FeO_y)} = \Delta H^{\circ}_{f(FeO_{1.05})} + \Delta H_{mix}. \qquad (17)$$

The entropies of mixing and formation as a function of composition were calculated in a similar manner and are tabulated in table 7.

Additional thermodynamic data were obtained by performing emf-temperature profiles for successively titrated compositions. Using cell IV, a number of oxygen-pressure versus temperature profiles were obtained between 700 and 1150 °C at a constant heating or cooling rate which was varied between 0.30 and 1.25 °C/min. Within the wüstite single-phase region it was difficult to retrace the emf profiles upon heating. This problem was probably due to variations in gas atmosphere as a result of outgassing effects upon heating. Thus, for most of the profiles taken, only the cooling curves were used. A typical profile is shown in figure 7. Note that upon heating the increase in voltage indicates that the sample is being oxidized. It was also observed that breaks in the emf-temperature curves occurred between 800 and 1000 °C and did not appear to be a function of the heating or cooling rates. However, there was considerable hysteresis in the temperature break and the slopes in the lower temperature regions. The slopes for the high temperature regions were reproducible. A linear least-square fit of log P_{O_2} versus $1/T$ was made on each profile in selected temperature regions where a break in the curve occurred. The least-square analysis (see table 8) confirmed the existence of more than one slope.

Because of the problem of the oxidizing-reducing cell atmosphere it was difficult to establish the actual composition. An alternate method of determining the composition for a particular emf-temperature profile was to match the partial pressure of oxygen with each of the oxygen pressure-composition isotherms (1057 to 1200 °C). For example, the logarithm of the partial pressure for composition "*C*" at 1057 °C determined from $-\log P_{O_2} = -7.206 + 2.777\ (1/T)\times 10^4$ (table 8) was −13.674. The composition (O/Fe) corresponding to this pressure on the 1057 °C isotherm is $FeO_{1.0575}$. This procedure

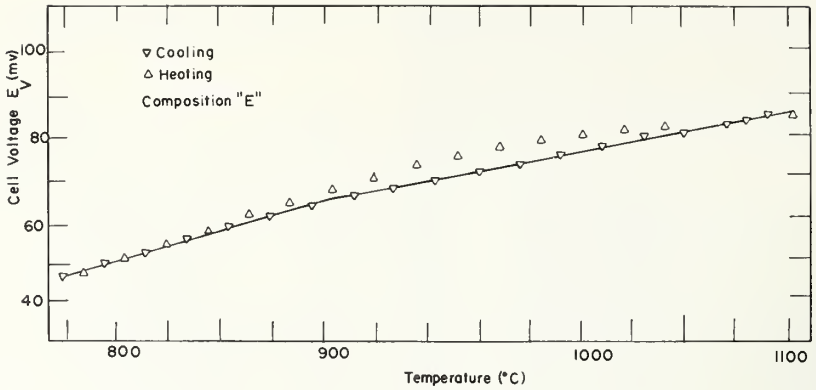

FIGURE 7. *Temperature profile of cell V for composition* "E".

was repeated for each isotherm and the results are recorded in table 9. The high-temperature isotherms were selected in order to eliminate any ambiguity due to changes in slopes or possible nonequilibrium conditions that occurred below 1000 °C. It was noted that the compositions determined from low-temperature isotherms (800 and 894 °C) did not agree with the determined average composition.

The partial molal enthalpies ($\overline{H}_O - 1/2\overline{H}^\circ_{O_2}$) were determined from least-squares analysis of log P_{O_2} versus $1/T$ and are presented in table 8. The partial molal entropies were determined from the intercept of the equation for log P_{O_2}, which agreed well with the values obtained from the emf-temperature coefficients.

The partial molal enthalpies and entropies, $\Delta\overline{H}_O$ and $\Delta\overline{S}_O$, for these compositions are plotted with other data obtained from the isothermal titration experiments in figure 8. Although the error limits plotted with the data from the titration experiments are rather large compared with these data, the two sets of data appear to follow the same trend. That is, the partial molal enthalpy for oxygen levels off at a composition between $FeO_{1.10}$ to $FeO_{1.13}$ before again becoming more negative. This change in slope of $\Delta\overline{H}_O$ could be indicative of a change in the defect structure of wüstite. This change in slope occurs in the composition range in which a positive deviation from Raoult's Law was noted. The inflection point of P_{O_2} versus O/Fe also corresponds to

TABLE 8. *Linear least-squares fit of log* P_{O_2} *in equilibrium with* FeO_y *compositions determined from cell V*

Composition[e]	Temp range	$-\log P_{O_2} = A + B\left(\frac{1}{T}\right)\times 10^4$		$-(\overline{H}_O - 1/2H^\circ_{O_2})$	$\overline{S}_O - 1/2S^\circ_{O_2}$
		A	*B*		
	°C			*cal/mole*	*cal/mole deg*
"B"	850–1040	−7.0725 ± 0.0083	2.7763 ± 0.0010	63,522 ± 25	−16.18
"C"	850–1125	−7.2061 ± .0720	2.7774 ± .0094	63,547 ± 215	−16.49
"D"	825–1150	−7.845 ± .020	2.8224 ± .0025	64,577 ± 58	−17.94
"M"	950–1000	−9.187 ± .10	2.92 ± .02	66,810 ± 460	−21.00
	800–900	−10.966 ± .105	3.1294 ± .0118	71,601 ± 270	
	800–1000	−10.019 ± .180	3.0427 ± .02106	69,617 ± 480	
"E"	875–1100	−8.7394 ± .0110	2.8555 ± .0014	65,334 ± 30	−19.97
	750–875	−9.6092 ± .0360	2.9559 ± .0039	67,631 ± 890	
"K"	750–1100	−9.054 ± .060	2.8956 ± .0071	66,251 ± 160	
"F"	925–1100	−9.8815 ± .0346	2.9623 ± .0044	67,777 ± 100	−22.61
	800–900	−9.7042 ± .0630	2.9403 ± .0071	67,274 ± 160	
	800–1100	−9.7704 ± .0238	2.9479 ± .0029	67,450 ± 65	
"G"	750–1100	−9.840 ± .013	2.9188 ± .0017	66,782 ± 40	−22.45
"H"	1000–1200	−8.997 ± .071	2.7989 ± .0098	64,039 ± 220	−20.40
"I"	950–1050	−12.46 ± .1	3.23 ± .01	73,904 ± 230	−28.51
	800–900	−11.992 ± .059	3.1792 ± .0066	72,740 ± 150	
	800–1050	−12.440 ± .064	3.2294 ± .0076	73,889 ± 175	
"J"	1000–1150	−12.791 ± .106	3.2619 ± .0143	74,632 ± 325	−29.2
"K"	950–1100	−12.826 ± .021	3.2653 ± .0027	74,710 ± 60	−29.3
	775–975	−11.847 ± .047	3.145 ± .0054	71,958 ± 125	
	775–1100	−12.222 ± .079	3.187 ± .0095	72,919 ± 215	

[e] See Table 9 for actual compositions.

TABLE 9. *Composition of wüstite derived from comparison of P_{O_2} with various P_{O_2}-FeO_y isotherms*

Temp. °C of P_{O_2}-O/Fe Isotherm	Composition Designation										
	B	C	D	E	F	G	H	I	J	K	L
	O/Fe Ratio[f]										
1057	1.054	1.0575	1.067	1.091	1.094	1.108	1.118	1.120	1.136	1.163	1.163
1075	1.054	1.058	1.069	1.091	1.093	1.108	1.121	1.124	1.136	1.146	1.143
1100		1.058	1.067	[g]1.089	[g]1.091	[g]1.106	[g]1.119	[g]1.120	[g]1.134	[g]1.138	[g]1.138
1139	1.0528	1.056	1.066							1.138	
1150	1.0535	1.058	1.066							[g]1.152	
1200	1.0535	1.057	1.067							1.145	
Avg O/Fe Ratio	1.0536	1.058	1.067	1.090	1.093	1.107	1.119	1.121	1.135	1.148	1.148

[f] O/Fe ratio determined from matching P_{O_2} of each composition (C, D, etc.) to that of P_{O_2}-O/Fe isotherms.
[g] Average values based on more than one sample.

the composition where wüstite changes from a *p*- to *n*-type semiconductor [19–21].

The results of Darken and Gurry [9] at 1250 °C show that $\Delta\bar{H}_O$ varies from −61.72 kcal/mole ($FeO_{1.055}$) to −63.78 kcal/mole for $FeO_{1.14}$ compared to −64.5 and −74.5 kcal/mole in this study. This comparison may not be valid since the data reported here extend from 1057 to 1200 °C compared with the 1100 to 1400 °C range studied by Darken and Gurry. The thermodynamic properties of wüstite determined by Kleman, Raccah, and Vallet [12, 22] were based on the presence of three wüstite phases, and are described by equation (18):

$$\log P_{O_2} = (a/T + b)(\text{O/Fe}) + c/T + d. \qquad (18)$$

The coefficients (a, b, c, d) were defined for each of the three wüstite phases proposed. Kleman showed how the results of Darken and Gurry for $\Delta\bar{H}_O$ could be duplicated by the average partial molal enthalpy for each of the three phases. The proposed phase diagram and plot of partial molal enthalpies of oxygen for the three phases are shown in figure 9. Note that wüstite III is stable below 1010 °C. The partial molal enthalpies $\Delta\bar{H}_O$ for wüstite II (−65 kcal/mole $FeO_{1.05}$, −67 kcal/mole, $FeO_{1.14}$) are similar in magnitude to those reported in this study. However, for wüstite I, which should correspond to data of Darken and Gurry (1100 to 1400 °C), $\Delta\bar{H}_O$ varies from −68 kcal ($FeO_{1.05}$) to −60 kcal/mole ($FeO_{1.14}$). Other $\Delta\bar{H}_O$ values reported vary between −66.5 to −69.6 kcal [20, 33, 34]. The partial molal enthalpies of oxygen determined by two different methods in this study were consistent in calculating higher values than those reported by Darken and Gurry.

A comparison of the enthalpy of formation as a function of composition with Darken and Gurry's results at 1250 °C indicated agreement within 500 cal. It has been proposed by Ariya and Morozova [33] that nonstoichiometric compounds can be considered to be solid solutions of one stoichiometric

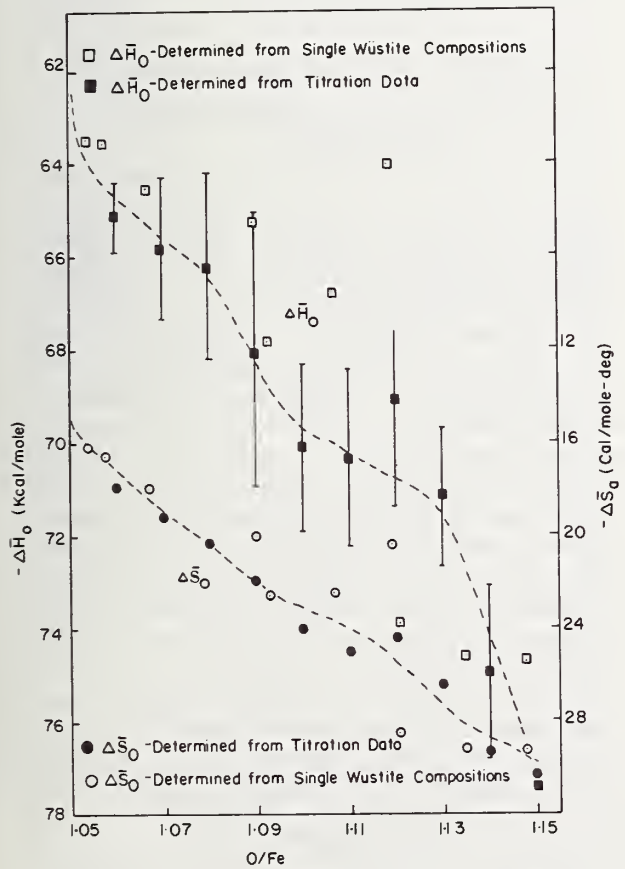

FIGURE 8. *Partial molal quantities $\Delta\bar{H}_O$, $\Delta\bar{S}_O$ for wüstite.*

compound in a second stoichiometric compound. Thus, considering $FeO_{1.05}$ and Fe_3O_4 as the two components, the enthalpy of formation per gram atom (see table 7) as a function of composition does indeed lie very close to the extrapolated line drawn between $FeO_{1.05}$ and Fe_3O_4.

Discussion

The question of whether diffusion is fast enough in the oxygen-rich compositions to eliminate polarization of the cell causing non-equilibrium conditions must be considered. It has been proposed by Raleigh [24] that diffusivities lower than 10^{-5} cm^2/sec can lead to excessive times for the elimination of concentration gradients. Diffusion constants between 2×10^{-5} and 1×10^{-7} cm^2/sec have been reported for iron in wüstite at 1000 °C. [25–28]. Most of the reported data indicates that the diffusion constant for iron in wüstite decreases with increasing oxygen content and, that in magnetite, it is two orders of magnitude lower than in $FeO_{1.05}$. Thus, assuming that diffusion of iron was rate controlling, then during the titration of oxygen into FeO_y, polarization should occur with the following relation holding:

$$\frac{d[O^{=}]}{dt} > \frac{d[Fe^{+2}]}{dt}. \qquad (19)$$

With the rate of arrival of $O^{=}$ ions at the ZrO_2–FeO_y interface greater than the transport of Fe^{2+} to this interface, the oxygen potential would change rapidly and, indeed, a blocking layer of Fe_3O_4 would result eventually and be recorded by a marked change in cell voltage. It is noteworthy that the presence of any Fe_3O_4 at the zirconia interface would result in 400 to 500 mv change in cell voltage. Using the same logic an attempt was made to oversaturate the interface by titration of oxygen for the purpose of measuring the mobility of holes or the predominant conducting species in wüstite. However, titration of 11.8 ma into FeO_y for 75 min. at 1084 °C at a current density of 12.5 ma/cm^2 did not result in any polarization. Assuming a mobility of 0.11 cm^2/volt sec for holes and with the number of vacancies equal to number of holes, the current calculated with the known dimensions and emf across the FeO_y electrode, required to achieve this mobility, was approximately three orders of magnitude greater than 11.8 ma.

An experiment which also provides information on the diffusion of iron in the FeO system was performed by Barbi [29]. The purpose of his experiment was to determine the free energy of formation of Al_2O_3 from the following cell:

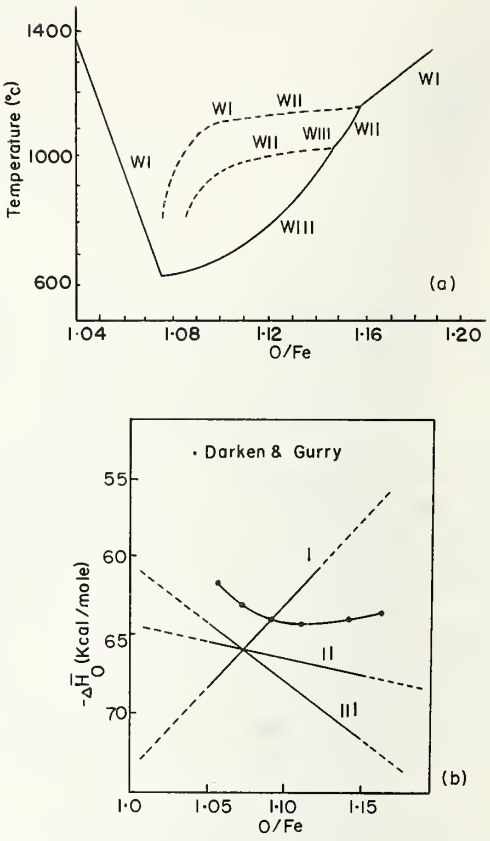

FIGURE 9a. *Fe-O phase diagram after Kleman [12].*

9b. $\Delta\bar{H}_O$ *as a function of different wüstite, after Kleman [12].*

Current was passed through the anode resulting in reduction of the Al_2O_3 film on the Al metal, and oxygen entering the cathode oxidized the Fe-Fe_xO to Fe_2O_3. Measurement of cell emf versus time after titration resulted in two regions of constant cell voltage. The constant emf indicates that a two-phase region is being reduced. The difference in cell voltage between these two constant-emf regions corresponded to the change in oxygen potential between the two-phase equilibria Fe_2O_3-Fe_3O_4 and Fe-Fe_xO. A typical time required for reduction from Fe_2O_3 back to the Fe-Fe_xO mixture was 10 minutes for a titration current of 3 ma for 25 minutes at 639 °C. This rapid reduction certainly indicates that equilibrium is achieved rapidly in the Fe-O system.

Another question to consider is the effect of impurities on defect phases noted. The purity of iron was examined by starting with a sample of pure zone-refined iron (< 25 ppm impurities) and

$$\text{Pt, Graphite, Al} + Al_2O_3 \;\Big|\; \begin{matrix} ThO_2 \\ \text{15 mole \% } LaO_{1.5} \end{matrix} \;\Big|\; \text{Fe} + Fe_xO\text{, graphite, Pt.}$$

titrating oxygen into the iron until the Fe-Fe_xO boundary composition was exceeded (Sample C—cell III). Titration was performed at temperatures between 900 and 1000 °C in order to reduce any effect due to reaction between platinum and the iron sample. Assuming a composition of $FeO_{1.05}$ as the iron-rich boundary, the error in the number of coulombs titrated to this boundary was 0.9 percent, which is well within weighing errors for the 92.2 mg sample of iron. The results of the 1100 °C isotherm are shown in figure 4. The only discernible difference was a 3 mv higher cell potential at the high oxygen compositions compared to other experiments at the same temperature on different samples.

The results of this study support and perhaps can be used to explain various observed phenomena in the iron-oxygen system. Consider the transition in wüstite from a p- to n-type semiconductor. The arrows in figures 3–6 indicate the pressures [20] where the p-n transition occurs. It has been reported that the conductivity becomes insensitive to oxygen pressure beyond the transition point and the composition of this transition decreases with increasing temperature [20]. The transition appears to correspond to the inflection point of the curves which indicates a change in the activity-composition coefficient. The change of the coefficient is certainly suggestive of a change in defect structure. It is noteworthy that Kleman [12] apparently interpreted this effect as a phase change within the wüstite region. The results of this study between 950 and 1200 °C do not substantiate his proposed diagram (fig. 9). The presence of any two-phase field within his diagram would certainly have been observed with the sensitive coulometric titration technique employed in this study. It is easy to understand how such an interpretation could be made, based on plots of log P_{O_2} versus O/Fe ratio which do show changes in slope.

A plot of log P_{O_2} versus $1/T$, corresponding to the oxygen pressure at which p-n transition occurred, showed two distinct slopes. The partial molal enthalpy of oxygen was 67.0 kcal/mole between 950 and 1100 °C and 45.8 kcal/mole between 1100 and 1300 °C. It is noteworthy that at lower temperatures the wüstite compositions where the transition occurs are $FeO_{1.10}$ to $FeO_{1.11}$, and that the 67 kcal/mole corresponds to the partial molal enthalpy of oxygen determined for this composition range.

Libowitz [30] has recently derived a model expression relating the activity of oxygen ($P_{O_2}^{1/2}$) to the deviation in stoichiometry δ in $FeO_{1+\delta}$. The model is based on the assumption that the principal defect is a complex composed of two iron vacancies associated with an Fe^{+3} interstitial as proposed by Roth [31]. The model equation was applied to the isotherms in this study. It was found that the expression predicted the P_{O_2} versus O/Fe dependence fairly well between $FeO_{1.05}$ and $FeO_{1.11}$ and at temperatures between 1057 and 1200 °C. The correlation between the model and the titration data provided additional support for the selection of the (1057 to 1200 °C) temperature range in which to determine the thermodynamic functions of wüstite. Below this range the correlation was unsatisfactory. It is interesting to note at this point that Koch [32] has recently observed by high-temperature x-ray diffraction that vacancies form clusters around iron ions, presumably Fe^{+3} ions, and that reflections exhibit characteristics of superlattice lines indicating ordering.

Conclusions

The usefulness of a solid electrolyte galvanic cell in determining phase boundaries and thermodynamic functions in the iron-oxygen system has been demonstrated. Coulometric titration of oxygen through calcia-stabilized zirconia makes it possible to explore the entire iron-oxygen system with one experiment.

The activity of oxygen as a function of wüstite composition was determined at temperatures between 1057 and 1200 °C. The results led to the determination of partial molal quantities for the solution of oxygen in $FeO_{1.05}$ for all wüstite compositions FeO_y. It is noteworthy that the partial molal enthalpy of oxygen appeared to remain constant between $FeO_{1.10}$ and $FeO_{1.13}$ before again becoming more negative.

A statistical mechanical model, developed by Libowitz, based on Fe^{+3} interstitials associated with two Fe vacancies, predicted correctly the P_{O_2} versus O/Fe dependence at temperatures between 1000 and 1200 °C.

The writers are indebted to the Research Committee of the University of Utah for providing funds for the research. The principal author is grateful to Brig. General Raymond A. Gilbert and the Air Force for affording the opportunity to continue studies in the Ph. D. program.

References

[1] Kalevi Kiukkola, High-Temperature Electrochemical Study of Uranium Oxides in the UO_2-U_3O_8 Region, Acta. Chem. Scand., **16**, 327–345 (1962).

[2] R. N. Blumenthal, J. B. Moser, and D. H. Whitmore, Thermodynamic Study of Nonstoichiometric Niobium Pentoxide, J. Am. Ceram. Soc., **48**, 617–622 (1965).

[3] R. N. Blumenthal, and D. H. Whitmore, Thermodynamic Study of Phase Equilibria in the Titanium-Oxygen Sys-

tem within the $TiO_{1.95}$-TiO_2 Region, J. Electrochem. Soc., **110**, 92–93 (1963).

[4] Giovanni B. Barbi, The Stability of Wüstite by Electromotive Force Measurements on All-Solid Electrolytic Cells, J. Phys. Chem., **68**, 2912–2916 (1964).

[5] R. F. Ksenofontova, I. A. Vasil'era, Ya. I. Gerasinov, The Thermodynamics of Tungsten Oxide of Variable Composition, Proc. Acad. Sci. USSR., Chem. Sect. **143**, 314 (1962). (In English)

[6] T. L. Markin and R. J. Bones, The Determination of Changes in Free Energy for Uranium Oxides Using a High Temperature Galvanic Cell, part I, At. Energy Res. Estab. (Gr. Brit.) report no. 4040 (April 1962).

[7] Kalevi Kiukkola, and Carl Wagner, Measurements on Galvanic Cells Involving Solid Electrolytes, J. Electrochem. Soc., **104**, 379–386 (1957).

[8] C. B. Alcock, S. Zadon, B. C. H. Steele, A Thermodynamic Study of Dilute Solutions of Defects in the Rutile Structure TiO_{2-x} and $Ti_{0.5}NB_{0.5}O_{2+x}$, paper presented at British Ceramic Society meeting on Thermodynamics of Ceramic Systems, 19–21, University of London, April 1966.

[9] L. S. Darken and R. W. Gurry, The System Iron-Oxygen. I. The Wüstite Field and Related Equilibria, J. Am. Chem. Soc., **69**, 1398–1412 (1945).

[10] H. F. Rizzo, Thermodynamics of the Fe-O System by Coulometric Titration in High Temperature Galvanic Cells, unpublished Ph.D. Thesis, University of Utah (1967).

[11] R. A. Meussner, L. E. Richards, and C. T. Fujii, Studies of High-Temperature Materials (Properties of FeO), Report of NRL Progress, Naval Research Laboratory, Washington, D.C., pp. 26–28, Dec. 1965.

[12] M. Kleman, Thermodynamic Properties of Ferrous Oxide and Application of Experimental Results to Equilibrium Phase Diagram, Mem. Science Review Metall., **62**, 457–469 (1965).

[13] J. Chipman, Molten Metals, Slags and the Third Law, Pure and App. Chem., **5**, 669–681 (1962).

[14] G. L. Humphrey, E. G. King, and K. K. Kelley, U.S. Bur. of Mines Rep. Invest., No. 4870 (1952).

[15] C. E. Wicks and F. E. Block, Thermodynamic Properties of 65 Elements—Their Oxides, Halides, Carbides, and Nitrides, Bull. 65, U.S. Bur. Mines, pp. 57–59 (1963).

[16] H. F. Rizzo, R. S. Gordon, I. B. Cutler, The Determination of Phase Boundaries and Related Thermodynamic Properties in the Fe-O System by Coulometric Titration, to be published.

[17] H. F. Rizzo, R. S. Gordon, and I. B. Cutler, Evidence for the Existence of More Than One Defect Phase Between Wüstite and Magnetite, unpublished work to be published.

[18] J. H. Swisher, and E. T. Turkdogen, Solubility Permeability, and Diffusivity of Oxygen in Solid Iron, Trans. AIME, **229**, 426–31 (1967).

[19] I. Bransky and D. W. Tannhauser, High Temperature Defect Structure of Ferrous Oxide, Trans. AIME, **239**, 75–80 (1967).

[20] G. H. Geiger, R. L. Levin, and J. B. Wagner, Jr., Studies on the Defect Structure of Wüstite Using Electrical Conductivity and Thermoelectric Measurements, J. Phys. Chem. Solids, **27**, 947–956 (1966).

[21] D. S. Tannhauser, Conductivity in Iron Oxides, J. Phys. Chem. Solids, **23**, 25–34 (1962).

[22] Pierrie Vallet and Paul Raccah, Contribution of the Study of the Thermodynamic Properties of Ferrous Oxide, Mem. Scien. Rev. Metall., **62 (1)**, 1–29 (1965).

[23] S. M. Ariya and M. P. Morozova, E. Vol'f, The Chemistry of Compounds of a Variable Composition (English Translation), Zh. Neorgan. Khim U.S.S.R. **11**, 13–22 (1957).

[24] D. O. Raleigh, Solid State Electrochemistry, Progress in Solid State Chemistry, **3**, 83–134 (1966).

[25] P. F. J. Landler and K. L. Komarek, Reduction of Wüstite Within the Wüstite Phase in H_2-H_2O Mixtures, Trans. AIME, **236**, 138–149 (1966).

[26] L. Himmel, R. F. Mehl and C. E. Birchenall, Self-Diffusion of Iron in Iron Oxides and the Wagner Theory of Oxidation. Trans. AIME, **197**, 827–843 (1953).

[27] R. L. Levin, J. B. Wagner, Jr., Reduction of Undoped and Chromium-Doped Wüstite in Carbon Monoxide-Carbon Dioxide Mixtures, Trans. AIME, **233**, 159–167 (1965).

[28] C. T. Fujii and R. A. Meussner, Determination of Chemical Diffusion Coefficient of Iron in Wüstite at 1000 °C, Report of NRL Progress, PB 174294, Naval Research Laboratory, Washington, D.C., pp. 27–28, March 1967.

[29] Giovanni B. Barbi, Thermodynamic Functions by E. M. F. Measurements on Solid Galvanic Cells in Non-Stationary Conditions, Systems $Al + Al_2O_3$, Trans. Faraday Soc., **62**, 1989–1595 (1966).

[30] G. G. Libowitz, Defect Complexes and Microdomains in Oxides, paper presented at this conference.

[31] W. L. Roth, Defects in the Crystal and Magnetic Structures of Ferrous Oxide, Acta. Cryst., **13**, 140–149 (1960).

[32] F. Koch, Private Communication.

[33] S. J. Ariya, M. P. Morozova, and A. L. Shneider, I. The Thermodynamics of Ferrous Oxide, J. General Chem. U.S.S.R., **24**, 37–42 (1954).

[34] L. Himmel, Self Diffusion of Iron in Iron Oxides and the Wagner Theory of Oxidation, unpublished Ph. D. Thesis, Carnegie Institute of Technology, Pittsburgh, Pa. (1953).

The Mechanism of Oxygen Self-Diffusion in Nickel and Cobalt Oxides

M. Hoch and R. Szwarc

Materials Science Program
University of Cincinnati
Cincinnati, Ohio 45221

The cation diffusion coefficients and hole conductivity data in FeO, CoO, and NiO were correlated assuming a vacancy mechanism for cation diffusion and a hopping mechanism for hole diffusion. The cation diffusion coefficients in $Fe_{1-\delta}O$, $Co_{1-\delta}O$, and $Ni_{1-\delta}O$ were shown to be proportional to the concentration of vacancies δ in the cation lattice with identical pre-exponential and exponential terms. The hole diffusion coefficients have the same pre-exponential term as that for cation diffusion, but the activation energy depends on the bonding of the hole to the respective ion. Only one of the two holes created by the introduction of a cation vacancy takes place in the conduction process.

The sintering kinetics of pure and doped nickel and cobalt oxides were studied in an effort to elucidate the mechanism of oxygen self-diffusion in these oxides. Both initial and intermediate sintering models were used to study the oxygen diffusion coefficients. Doping with monovalent lithium ions increased the oxygen diffusion coefficient. Addition of trivalent chromium ions decreased the oxygen diffusion coefficient, although the effect was not as great as in the case of lithium. The defect responsible for oxygen self-diffusion in CoO and NiO is thus a complex, made up of an oxygen vacancy and two electron holes ($V_0\oplus\oplus$). This model was used to calculate the Schottky product in NiO and CoO; they were found to be equal.

This research has been supported in part by the Air Force Materials Laboratory, Research and Technology Division, Air Force Systems Command, United States Air Force, under Contract No. AF 33(615)-2746.

Experimental Evidence for Highly Mobile Electrons in MnO and NiO at High Temperature

D. S. Tannhauser,[1] N. M. Tallan [2] and M. Gvishi

Department of Physics

Technion—Israel Institute of Technology, Haifa, Israel.

The measured Hall mobility in MnO and NiO near 1000 °C, is n-type in the range where the conductivity is p-type. For MnO, where the measurements extend into the n-type conductivity range, this gives directly $\mu_n^H = 10$ cm$^2/V \cdot$ sec. For NiO the analysis is indirect, it relies on a model with negligible Hall mobility of the holes, and on the experimental value of the optical band gap. The value calculated is $\mu_n^H \geq 30$ cm$^2/V \cdot$ sec.

The drift mobility of holes in the compounds MnO, FeO, CoO and NiO is about 0.1–1 cm$^2/V \cdot$ sec at $T \geq 1000$ °C. This low mobility is connected with the fact that the holes move in the d-levels of the cations, however the question whether the motion is by band conduction or by small polaron hopping is not settled. We would like to present experimental evidence that in MnO and in NiO the mobility of the electrons is much larger than that of the holes. The evidence for MnO is much more direct than that for NiO.

Hed and Tannhauser [1][3] combined conductivity with gravimetric measurements on MnO at $T \geq 1100$ °C. The partial pressure of oxygen in the atmosphere surrounding the sample (established by mixing CO_2 and CO in measured ratios $q = P(CO_2)/P(CO)$) controlled the deviation from stoichiometry and therefore also the concentration of holes and electrons. It was found that the conductivity goes through a minimum at $q = 1$, holes dominate the conductivity at $q > 1$ and electrons at $q < 1$. The detailed analysis of the conductivity and gravimetric data gave $\mu_p^D = 0.2$ cm$^2/V \cdot$ sec at 1200 °C, and $\mu_n^D/\mu_p^D \geq 10$ at the same temperature; the lower limit reflecting the fact that the weight change in the n-type region was immeasurably small. μ_n^D and μ_p^D are the drift mobilities of electrons and holes. Thermoelectric measurements in ref [1] and similar data of McKinzie [2] confirmed that $\mu_n^D/\mu_p^D > 1$, but the numerical value of this ratio could not be accurately determined because of the uncertain values of the heat of transport.

Recent Hall effect measurements gave a ratio of $\mu_n^H/\mu_p^H \cong 50$ at 943 °C, where μ^H are the Hall mobilities. An a-c Hall effect apparatus with a 510 cps electric current and a 2 cps magnetic field was used [3]. The data (see fig. 1) were taken on a single crystal of MnO in which the charge carrier concentrations were varied by a factor of 30 through control of $P(O_2)$, spanning the range from electron controlled to hole controlled conductivity. The Hall effect stayed n-type in all the range where we could measure. Figure 1 shows that the dependence of the measured μ_{Hall} on $P(O_2)$ agrees with the theory $[\mu_{\text{Hall}} = \mu_n^H(1-\alpha/b)/(1+\alpha)$ where $\alpha = p\mu_p^D/n\mu_n^D$ and $b = \mu_n^H/\mu_p^H]$ for a two carrier semiconductor with $\mu_n^H = 10$ cm$^2/V \cdot$ sec and $\mu_n^H/\mu_p^H \cong 50$. For the highly mobile electrons it is fair to assume that $\mu_n^H \cong \mu_n^D$ and furthermore the Hall mobility of the holes, which is 0.2 cm$^2/V \cdot$ sec, agrees fairly well with their drift mobility extrapolated from the data of ref [1]. It is therefore likely that the value of μ_n^D/μ_p^D at 943 °C is also 50, in agreement with the estimate of ref. [1]. μ_p^H could not be measured directly because of electrical noise generated by the contacts at high deviations from stoichiometry.

In NiO similar measurements were made at 1007 °C. In this compound, similarly to MnO, the Hall effect was n-type, while the conductivity was clearly p-type both by its dependence on $P(O_2)$ and by thermoelectric data over the whole range of measurement.

The relation $\mu_{\text{Hall}} = C\sigma^{-2}$ was found to fit the data over the range of measurement (see fig. 2). An explanation based on the two carrier model can be given, however, here the relation $\mu_p^D = \mu_p^H$ does not hold. It is known from conductivity vs. $P(O_2)$ experiments that $\alpha \gg 1$ and therefore $\alpha = K\sigma^2$ so that the above equation gives

$$\mu_{\text{Hall}} = \mu_n^H(1/\alpha - 1/b) = K\mu_n^H\sigma^{-2} - \mu_p^H$$

and this fits the experimental curve provided

[1] At present at the Division of Engineering, Brown University, Providence, R.I. 02912.

[2] On leave from Aerospace Research Laboratories, Wright-Patterson Air Force Base, Ohio 45433.

[3] Figures in brackets indicate the literature references at the end of this paper.

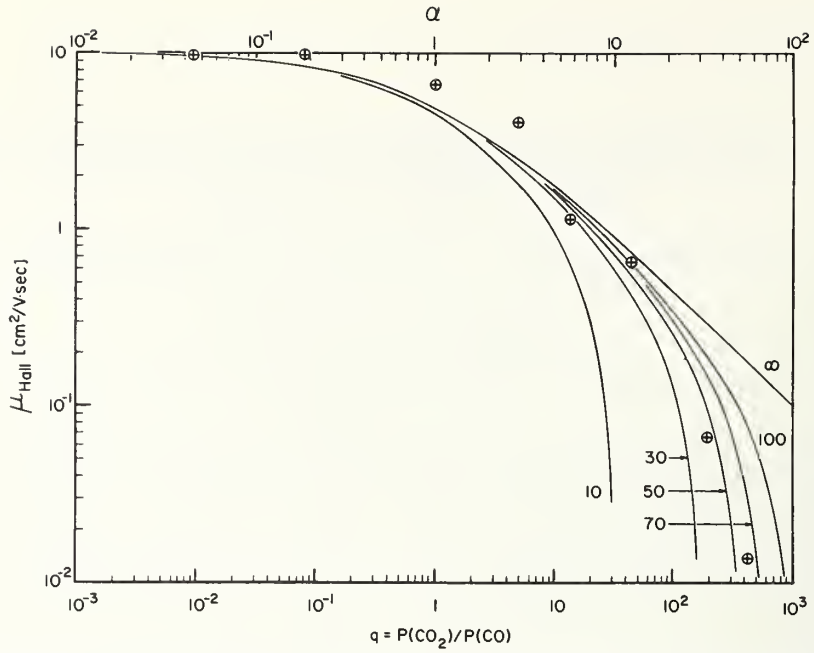

FIGURE 1. *The Hall mobility* μ_{Hall} *of MnO at 943 °C plotted against* $q \equiv P(CO_2)/P(CO)$.

⊕ are experimental points, the lines are theoretical curves drawn with the assumption $\mu_n^H = 10$ cm²/V sec and various values of $b \equiv \mu_n^H/\mu_p^H$. Values of $\alpha = q^{2/3}$ are also given on the abscissa.

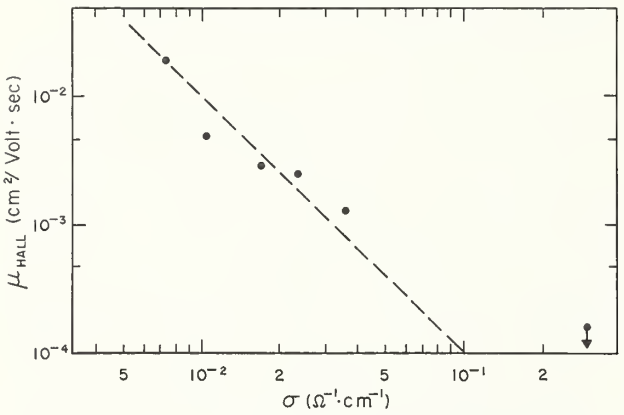

FIGURE 2. *The Hall mobility* μ_{Hall} *of NiO at 1007 °C plotted against the conductivity* σ.

The dashed line represents the relation $\mu_{\text{Hall}} = C\sigma^{-2}$. The point at $\sigma = 3 \times 10^{-1}$, which was taken in air, represents an upper limit only.

$\mu_p^H \ll \mu_{\text{Hall}}$ at the low σ end of the measurement range. Therefore $\mu_p^H \ll 2.10^{-2}$ cm²/$V \cdot$ sec while $\mu_p^D \cong 0.5$ cm²/$V \cdot$ sec. The relation $\mu_p^H \ll \mu_p^D$ might be explained by a recent theory by Maranzana [4] which has already been used by van Daal and Bosman [5] to explain their results for Li-doped NiO; alternatively it might point to hole conduction by small polarons where the ratio μ_p^H/μ_p^D depends very sensitively on the details of the model chosen.

The electron mobility μ_n cannot be directly calculated in the case of NiO, the experimental data giving only the value of the product $n\mu_n^2$. Estimating the product $n \cdot p$ from the optical band gap ($\Delta E = 4$ eV) gives $\mu_n \geq 30$ cm²/$V \cdot$ sec, depending on whether the effective density of states for electrons is taken as $N_e = 1$ per ion-pair or $N_e < 1$.

It is a priori reasonable that the mobility of electrons in transition metal oxides is much larger that that of the holes, since electrons are presumably located in the 4*s* states of the cations which have considerably larger overlap than the 3*d* states. The high values of μ_n in MnO and NiO support this picture and it is therefore reasonable to assume that electrons move by band conduction in these oxides.

There is also experimental evidence from thermoelectric data that electrons play a role in CoO, however no measurements of the electron mobility are available.

This work was partially sponsored by the Aerospace Research Laboratories under Contract No. AF 61(052)–825 with the European Office of Aerospace Research, U.S. Air Force.

References

[1] A. Z. Hed and D. S. Tannhauser, J. Chem. Phys. **47**, 2090 (1967).
[2] H. McKinzie, Ph. D. Thesis, Arizona State University (1967).
[3] N. Z. Lupu, N. M. Tallan and D. S. Tannhauser, Rev. Sc. Instr. **38**, 1658 (1957).
[4] F. Maranzana, Phys. Rev. **160**, 421 (1967).
[5] H. J. van Daal and A. J. Bosman, Phys. Rev. **158**, 736 (1967).

High Temperature Defect Structure and Electrical Properties of NiO

I. Bransky

Israel Institute of Technology

and

N. M. Tallan

Aerospace Research Laboratories
Wright-Patterson Air Force Base, Ohio 45433

Although there is general agreement that pure NiO is an oxygen excess semiconductor throughout its stability range and that the predominant defects are metal vacancies and holes, both singly ionized [1, 2][1] and fully ionized [3] vacancies have been proposed. There has been a similar lack of agreement concerning the nature of the charge carrier transport mechanism. Although most of the early investigations on Li-doped NiO concluded that the charge carrier transport in NiO is thermally activated, as expected for small polarons in the hopping regime, several recent investigations have presented evidence for a narrow band conduction mechanism at temperatures below about 1000 °C [4, 5].

The objective of this study was the determination of the temperature and oxygen partial pressure dependence of the electrical conductivity and Seebeck coefficient of NiO above 1000 °C. Both single crystal and polycrystalline specimens were studied. The single crystal specimens were epitaxially grown on MgO crystal substrates by the technique of vapor decomposition of $NiBr_2$. The polycrystalline samples were prepared by oxidation of spectroscopically pure nickel foil.

The various oxygen partial pressures required were established using pure oxygen, oxygen-argon mixtures, or CO-CO_2 mixtures. Four terminal conductivity measurements were made to eliminate contact resistances. An a-c bridge operating at 80 cps was used after preliminary measurements showed no frequency dependence of the conductivity up to 20 Kcps. The thermal emf measurements were made by heating one end of the specimen to establish a steady state temperature gradient in it, and then measuring the voltage developed between the pure platinum legs of two thermocouples, one at each end of the specimen. Although in all cases the voltage developed was significantly larger than the residual voltage at zero temperature gradient, the thermal emf values reported were obtained by least-square analysis of many determinations at different temperature gradients.

The time required for a 0.33 mm thick single crystal specimen to attain steady-state conduction values, after isothermal changes in the ambient oxygen partial pressure, was determined as a preliminary step in the conductivity studies. Above 1200 °C the apparent equilibration was accomplished within ten minutes; below 1200 °C, considerably longer times had to be allowed to obtain reproducible, meaningful results. The oxygen partial pressure dependences of the conductivity of single crystal and polycrystalline specimens at constant temperature were of the form $\sigma \propto P(O_2)^{1/x}$, where x varied from 4.1 ± 0.1 at 1000 °C to 4.3 ± 0.1 at 1600 °C. This pressure dependence is consistent with the defect formation reaction $\frac{1}{2}\ O_2\ (\text{gas}) \rightleftharpoons O_o + V'_m + \oplus$, describing the formation of single ionized metal vacancies and holes.

The temperature dependence of the single crystal and polycrystalline specimen conductivities were identical between 800 and 1500 °C. Assuming a pre-exponential T^{-1} dependence in the conductivity, and therefore plotting log σT versus T^{-1}, an activation energy for conduction of 1.03 ± 0.02 eV was found. Since the observed pressure dependence of the conductivity suggests the formation of singly ionized metal vacancies and holes, this activation energy for conduction includes the energy of formation of the defects, $\Delta H_f/2$, and any motional energy of the hole.

The Seebeck coefficient, $\alpha = \text{emf}/\Delta T$, was measured against platinum on a single crystal specimen. All Seebeck coefficient determinations made were p-type, indicating a predominance of positive

[1] Figures in brackets indicate the literature references at the end of this paper.

charge carriers. A value for α was obtained at each temperature studied by a least squares analysis of at least twenty measurements of the voltage developed across the specimen as a function of the temperature gradient imposed. The Seebeck coefficient was found to be exponentially temperature dependent with an activation energy of 0.66 ± 0.03 eV. In an extrinsic p-type semiconductor, $\alpha = k/e$ (ln $N_v/p + A$), where N_v is the density of states and A is the kinetic energy transported by the charge carrier. The energy of formation of the defects, $\Delta H_f/2$, is therefore 0.66 eV if N_v is temperature independent, as generally assumed for a localized carrier model, and 0.75 eV if N_v varies as $T^{3/2}$, as in the case of a broad-band semiconductor. These values for $\Delta H_f/2$ are in reasonable agreement with values of 1.36 ± 0.04 eV [2] and 1.5 ± 0.2 eV [3] for ΔH_f obtained from conductivity measurements alone.

The activation energy for conduction 1.03 eV, containing both $\Delta H_f/2$ and any energy required for the motion of the carriers, is therefore significantly larger than the value of $\Delta H_f/2$ found from Seebeck coefficient measurements at high temperatures. This is in direct support of the applicability of a localized model for the charge carrier and a hopping model for its transport mechanism at high temperatures. Subtracting the value 0.66 eV for $\Delta H_f/2$ from the energy for conduction, a value of 0.37 eV for the motional energy of the hole is obtained.

References

[1] H. H. v. Baumbach and C. Wagner, Z. Physik. Chem. **B24**, 59 (1934).
[2] N. G. Eror, Thesis, Northwestern Univ., 1965.
[3] S. P. Mitoff, J. Phys. Chem. **35**, 882 (1961).
[4] A. J. Bosman and C. Crevecoeur, Phys. Rev. **144**, 763 (1966).
[5] I. G. Austin, A. J. Springthorpe, B. A. Smith and C. E. Turner, Proc. Phys. Soc. (London) **90**, 157 (1967).

Ionic Conductivity in Oxides:

Experimental Problems
Survey of Existing Data

L. Heyne

Philips' Research Laboratories
Eindhoven, Holland

Electrically insulating oxides may show electronic as well as ionic conduction when heated to a high temperature. To characterize this high temperature conductivity, it is necessary to separate both contributions and to study their dependence on oxygen pressure and doping. The theory is discussed on which methods for determination of the conductivity components are based. Starting from general charge transport equations, it is possible to express electronic and ionic currents in terms of two gradients; that of the electrochemical potential of electrons, and that of the chemical potential of oxygen. The first is measured with metal contacts, the second determined by the local oxygen partial pressure. The basic assumption is made, that local thermodynamic equilibrium between all charge carriers and the lattice is undisturbed by current flow. In practice, different boundary conditions can be obtained by a choice of electrodes with special properties with respect to reversibility or blocking action. This opens the possibility of the determination of transport numbers. Four different situations will be considered: both contacts reversible and in the same atmosphere; both contacts reversible but at different oxygen pressures; blocking of the ion current; blocking of the electron current. Special attention is paid to the question of how close the situation on which the quantitative evaluation of the experiment is based is approximated by the practical arrangement. Finally, a short review is given of the most important properties of those oxides, about which dependable quantitative information is available in literature.

Key Words: Blocking electrodes, electronic conductivity, ionic conductivity, reversible electrodes, thermodynamic equilibrium, transport numbers.

1. Introduction

The electrical conductivity of solids can be a consequence of the presence of mobile electronic charge carriers as well as of ionic charge carriers. In the general case both types of conduction are present simultaneously. The total electrical conductivity must then be characterized by the partial conductivities of electrons and holes and of the different ionic species that can be present. In an important respect mixed ionic and electronic semiconductors differ essentially from purely electronic semiconductors. This is a consequence of the fact that, since ionic conduction forms an integral part of the total conductivity, the substance can come easily into equilibrium with the surrounding atmosphere. This means that significant values of conduction parameters can only be determined if due care is taken to control the composition of the sample. This can be done by controlling the surrounding gas atmosphere, or by equilibrating the sample with a solid in which the thermodynamic potential of one of the components of the sample is fixed (for a binary substance). This solid can often be chosen as one of the electrical contacts.

In this survey attention will be concentrated only on those aspects of mixed conduction that have a direct bearing on the methods of determination of the various components of the conductivity. The description of ionic conductivity in terms of fundamental lattice properties and lattice defects will not be undertaken here [1]. [1]

A complete characterization of the electrical conductivity of an oxide consists of the determination of the electronic and ionic partial conductivities as a function of the oxygen partial pressure (or the deviation from stoichiometry) and of the concentration of added impurities. A knowledge of these dependences can lead to a quantitative description of the solid under consideration in terms of the thermodynamics of lattice defects.

Here, only the ionic conductivity caused by ionic species of the compound itself will be considered. This means that it will be assumed that the mobility of foreign ions is essentially zero and, therefore, that the only influence of their possible presence

[1] Figures in brackets indicate the literature references at the end of this paper.

is on the thermodynamic equilibrium between the intrinsic lattice defects. Through this influence the ionic conductivity and the self diffusion coefficients might be modified. It must, however, be kept in mind that this assumption is arbitrary, and that it is not justified in many practical cases.

To explain the methods that can be used to determine the components of the electrical conductivity separately, it is necessary to give a short discussion of the movement of the charge carriers under the influence of an electrical field and a concentration gradient.

The movement of ions in a crystalline solid can only take place by the movement of lattice imperfections. As a consequence, the transport can be described in two different ways.

In the first way, an average mobility is attributed to the main ionic components of the crystal. Although the value of this mobility depends on the fraction of those ions that are in a favourable position to move (e.g., interstitial ions), and on the mobility of these ions, the latter are not introduced as such in the analysis. Therefore, it is unnecessary to have a detailed knowledge of the actual model valid for the substance under consideration. The transport coefficients (mobility and diffusion coefficient) are considered as empirical quantities, the gradients occurring in the transport equations are those of electrical and thermodynamic potentials. This method was used by C. Wagner in his original treatment of transport in growing tarnishing layers [2].

In the second way of treatment, attention is focussed on the moving species themselves, the actual lattice defects present. The real transport properties of these defects and their concentrations enter into the transport equations. Thus a detailed model is required. From such a model the mobility could, in principle, be calculated. The chemical potentials that are introduced into the equations, are the so-called virtual chemical potentials of the defects [3]. In his review of Wagner's equations, Kröger compares both ways of description [4].

2. The General Transport Equation

We will start using the description in terms of defects. The quantity j_k is the electrical current density connected with the flow of particles of type k having a charge $z_k q$, where q is the absolute value of the electronic charge. The concentration of these particles is n_k, their mobility v_k and their diffusion coefficient D_k. The partial current density can then be written:

$$j_k = -n_k|z_k|qv_k \operatorname{grad} V - D_k z_k q \operatorname{grad} n_k; \quad (1)$$

V denotes the electrical potential.

Here it is assumed, that no cross effects take place, like those present in the general transport equations of irreversible thermodynamics [5]. This means that, apart from the interaction through the electrical field, the currents and gradients of one particle species do not influence the flow of other species. Furthermore, only isothermal situations are considered.

We introduce the electrochemical potential η_k, which is connected to the chemical potential μ_k and the electrical potential by

$$\eta_k = \mu_k + z_k q V,$$

where

$$\mu_k = \mu_{k0} + kT \ln n_k. \quad (2)$$

Furthermore, we use the Einstein relation:

$$D_k = \frac{kT}{|z_k|q} v_k. \quad (3)$$

We obtain:

$$\boxed{j_k = \frac{-\sigma_k}{z_k q} \operatorname{grad} \eta_k.} \quad (4)$$

Here $\sigma_k = n_k|z_k|qv_k$ is the partial conductivity associated with the particle species k.

If the particles considered are not defects, but lattice ions themselves, eq. (4) is still valid; η_k is in that case not the virtual electrochemical potential of the defects, but the real electrochemical potential of the corresponding ions. Since, not considering the sign, both electrochemical potentials differ only by a constant, their gradients are equal.

3. Electronic Transport

Now, for the moment, we confine our attention to the electronic component j_e of the current only. This is composed of a contribution by electrons and holes:

$$j_e = j_n + j_p. \quad (5)$$

Thus

$$j_e = \frac{\sigma_n}{q} \operatorname{grad} \eta_n - \frac{\sigma_p}{q} \operatorname{grad} \eta_p. \quad (6)$$

Here η_n and $-\eta_p$ are equivalent to the quasi Fermi potentials of electrons and holes, as used in semiconductor physics. Following Stieltjes [6] we write this in the form

$$j_e = \frac{\sigma_n + \sigma_p}{q} \operatorname{grad} \eta_n - \frac{\sigma_p}{q} (\operatorname{grad} \eta_n + \operatorname{grad} \eta_p). \quad (7)$$

Now we assume, that the thermodynamic equilibrium between electrons and holes is not disturbed by the current flow. This assumption excludes effects of injection or extraction, like those occurring near *p-n* junctions in diodes and transistors. This equilibrium situation has the consequence that:

$$\text{grad } \eta_n + \text{grad } \eta_p = 0. \tag{8}$$

So the electronic current becomes:

$$j_e = \frac{\sigma_n + \sigma_p}{q} \text{ grad } \eta_n = \frac{\sigma_e}{q} \text{ grad } \eta_n = -\frac{\sigma_e}{q} \text{ grad } \eta_p. \tag{9}$$

4. Ionic Transport

We proceed now, by assuming that two ionic species also contribute to the current transport. Let them be characterized by indices 1 and 2. Carrying out the same procedure again, we find for the total ionic current density $j_i = j_1 + j_2$:

$$j_i = -\frac{\sigma_1 + \sigma_2}{z_1 q} \text{ grad } \eta_1 + \frac{\sigma_2}{q}\left(\frac{1}{z_1} \text{ grad } \eta_1 - \frac{1}{z_2} \text{ grad } \eta_2\right). \tag{10}$$

We assume now that, at each point, the thermodynamic equilibrium between the ionic species is undisturbed by the current flow. This thermodynamic equilibrium can be expressed by a reaction equation like:

$$|z_2| M^{|z_1|+} + |z_1| X^{|z_2|-} \rightleftarrows M_{|z_2|} X_{|z_1|}. \tag{11}$$

The equilibrium condition requires the equality of the sums of the chemical potentials on both sides of this equation,

$$|z_1| \mu_2 + |z_2| \mu_1 = \mu_{MX}. \tag{12}$$

(In the indices we write MX instead of $M_{z_2} X_{z_1}$) This equation is also valid for the gradients:

$$|z_1| \text{ grad } \mu_2 + |z_2| \text{ grad } \mu_1 = \text{grad } \mu_{MX}. \tag{13}$$

For small defect concentrations μ_{MX} is constant and consequently:

$$\text{grad } \mu_{MX} = 0. \tag{14}$$

Furthermore, the gradients in the chemical potentials may be replaced by gradients in electrochemical potentials since the electrical terms balance out. Thus we obtain:

$$|z_1| \text{ grad } \eta_2 + |z_2| \text{ grad } \eta_1 = 0. \tag{15}$$

This relation, introduced into (10), gives the result:

$$j_i = j_1 + j_2 = -\frac{\sigma_1 + \sigma_2}{z_1 q} \text{ grad } \eta_1 = -\frac{\sigma_i}{z_1 q} \text{ grad } \eta_1 = -\frac{\sigma_i}{z_2 q} \text{ grad } \eta_2. \tag{16}$$

This is the ionic equivalent of eq (9).

Note, that we tacitly changed over from virtual chemical potentials of defects to chemical potentials of ions.

5. Total Current

Now the total electrical current density j_t, flowing in a mixed conductor when gradients in the electrical potential and in chemical potential are present simultaneously follows from (9) and (16):

$$j_t = j_e + j_i = \frac{\sigma_e}{q} \text{ grad } \eta_n - \frac{\sigma_i}{z_1 q} \text{ grad } \eta_1. \tag{17}$$

This can be written:

$$j_t = \frac{\sigma_e + \sigma_i}{q} \text{ grad } \eta_n - \frac{\sigma_i}{q}\left(\frac{1}{z_1} \text{ grad } \eta_1 + \text{grad } \eta_n\right). \tag{18}$$

If the thermodynamic equilibrium between ions and electrons is locally undisturbed, the following equilibrium reaction equations can be considered:

$$X^{|z_2|-} + |z_2| h \cdot \rightleftarrows X^*, \qquad M^{|z_1|+} + |z_1| e' \rightleftarrows M^*. \tag{19}$$

(M^* is a neutral metal atom, X^* one of the metalloid, $h \cdot$ is an electron-hole, e' an electron). We then have the relations:

$$\mu_2 + |z_2| \mu_p = \mu_X, \qquad \mu_1 + |z_1| \mu_n = \mu_M. \tag{20}$$

These can be written in terms of gradients, and electrochemical potentials can be introduced. We obtain:

$$\begin{aligned} \text{grad } \mu_M &= \text{grad } \mu_1 + |z_1| \text{ grad } \mu_n \\ &= \text{grad } \eta_1 + |z_1| \text{ grad } \eta_n, \\ \text{grad } \mu_x &= \text{grad } \mu_2 + |z_2| \text{ grad } \mu_p \\ &= \text{grad } \eta_2 + |z_2| \text{ grad } \eta_p. \end{aligned} \tag{21}$$

Under the assumed conditions eq (18) reduces to

$$jt=\frac{\sigma_t}{q}\,\text{grad}\,\eta_n-\frac{\sigma_i}{qz_1}\,\text{grad}\,\mu_M=-\frac{\sigma_t}{q}\,\text{grad}\,\eta_p-\frac{\sigma_i}{qz_2}\,\text{grad}\,\mu_X \tag{22}$$

Here use is made of eq (15) and of the fact that z_1 is positive and z_2 is negative.

6. Electrode Processes

In order to be able to make use of the equations obtained, it is necessary to consider a specific situation. In such a situation, the processes taking place at the free surfaces or at the electrodes determine the boundary conditions under which the current equations must be solved. Therefore we shall spend a few moments to look at these processes in some detail.

From standard semiconductor practice we know that transfer of electrons (or holes) from a contact to a semiconductor is not always as easy as, for example, between two metals. We distinguish two extremes. At so called "ohmic contacts," no appreciable potential drop arises when a current is passed in either direction. "Blocking or rectifying contacts" allow no significant current to pass in one direction. Intermediate cases often occur in practice. The behaviour of a contact can be described in terms of the work functions of the metal and the semiconductor. In practice it is often difficult to make contacts with desired characteristics.

With respect to the ionic currents, the same problems arise as in wet electrochemistry. Apart from energy barriers that may exist, equivalent to those occurring in blocking electronic contacts (activation polarization in wet electrochemistry), here current limiting may also take place as a consequence of the material transport accompanying the current flow. When, for example, gas is evolved in the electrode reaction, the difficulty in its transport away is even greater than in the case of a liquid electrolyte, where the solubility is generally higher and where bubbles may be formed. The equivalent of the latter would be destructive in the solid state situation [7]. Because of the low solubility and diffusion coefficient of gases in solids, the electrode reactions are confined to the immediate vicinity of the three-phase boundary: electrode – electrolyte – gas phase.

The uncertainties in electrode properties do not interfere seriously in the determination of the total conductivity, since by the use of a four point method or by measurements with alternating current, disturbing electrode effects can be avoided.

With d-c measurements, the electrode effects must be taken into account. However, these effects are not always a disadvantage. To the contrary we will see that a proper choice of the electrodes can, in some cases, open the possibility of separating the electronic and ionic contributions to the conductivity. This was first recognized for the case of silver sulphide by Wagner [8] and by Hebb [9]. The methods were summarized by Wagner [10, 11].

For the moment, we shall assume that, by the choice of certain electrodes, we can determine the electrode properties at will. We will apply the current eqs (9), (16), and (22) to four situations where:

1. completely reversible electrodes are present as well for electrons as for ions, so that the current flow is not influenced in any respect, or
2. no current is supplied to the sample externally, or
3. only electrons are allowed to pass through the sample via the electrodes, or
4. only ions are entering and leaving the sample through reversible electrodes.

These different situations can often be approximated in practice often to such an extent, that meaningful interpretation of measurements in terms of the formulae to be derived below can be made. In the following we will consider oxide samples only.

6.1. Completely Reversible Electrodes

Samples with completely reversible electrodes are represented schematically in the figures 1a and 1b. In figure 1a the sample is in equilibrium with the electrodes consisting of the metal component M of the oxide MO; in figure 1b it is in equilibrium with the oxygen present in the surrounding atmosphere through the porous inert electrodes. In the latter situation, the composition of the oxide can be changed by variation of the oxygen partial pressure of the atmosphere. Thus, the influence of this partial pressure on the conductivity can be studied.

For evaluation of the current densities eqs (9) and (16) are valid. Since the assumed reversibility of the electrodes has the consequence, that the oxide stays in equilibrium everywhere in the sample, no concentration gradients are formed. This means, that grad η in eqs (9) and (16) can be replaced by zq grad V (see eq (2)).

$$j_i=-\sigma_i\,\text{grad}\,V,\ \text{and}\ j_e=-\sigma_e\,\text{grad}\,V. \tag{23}$$

This is simple Ohm's law behaviour.

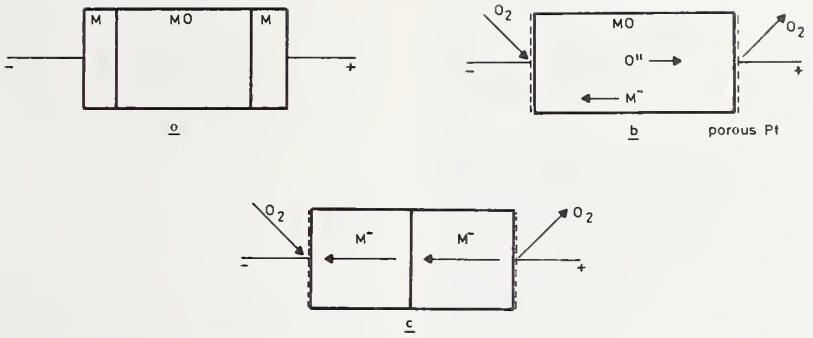

FIGURE 1. *Mixed ionic and electronic conductor between reversible electrodes.*
a. The metal component M used as electrode; b. Porous inert electrodes in an atmosphere with defined oxygen partial pressure: c. Transport by metal ions causes weight changes of anode and cathode tablets.

The ionic contribution to the current can be found by determination of the weight increase of the cathode and the corresponding decrease in weight of the anode in the situation of figure 1a or, in figure 1b, by the measurement of the oxygen taken up or evolved at the corresponding inert electrodes. In this way the ionic transport number is found:

$$t_i = \frac{\sigma_i}{\sigma_i + \sigma_e} = \frac{j_i}{j_i + j_e}. \qquad (24)$$

Note that in this way *no information* is obtained about the ionic specie which is responsible for the transport ($M^{\cdot\cdot}$ or O''). To get this information the method of Tubandt [12] can be used. Here the sample is composed of two (or more) tablets pressed together. By weighing before and after current flow the transport of matter is determined (fig. 1c). When only oxygen is mobile, no weight changes take place, mobile metal ions cause an increase in weight of the cathode tablet. Similar effects can be seen if inert markers are used.

An important matter of consideration is to what degree the ideal reversible electrode can be approximated in practice. It will be clear, that there must be a driving force to get a flow of oxygen into the sample at the cathode and out of it at the anode (fig. 1b). So, fundamentally, the boundary regions cannot be in exact equilibrium with the gas phase. This deviation from equilibrium depends strongly on the structure of the contact material and sample surface. They determine the effective length of the three phase boundary, where the electrode reactions take place and the ease of diffusion of the gas to this region. Slow gas diffusion causes stronger deviations, the higher is the current density and the lower is the gas pressure.

It must be recognized further that, for instance at the cathode, O_2 molecules must be split up into atoms and then be ionized. Thus the electrode must be an efficient catalyst for these reactions, whatever the physical meaning of this statement may be. Since these reactions are thermally activated processes, a strong temperature dependence of their effect must be expected. This is in contrast with gas diffusion limitations, which exhibit only a slight temperature dependence.

The flow limitations mentioned cause polarization voltages to be built up in the electrode regions. These can effect the apparent conductivity measured. Moreover, if reversibility of the electron transfer is assumed, such a polarization voltage increases the electronic component of the current flow at the contact. Since the effects will in general not be equal at both electrodes, the current flow will cause a net loss or gain of oxygen. This change in composition influences the conductivity components again, so that erroneous results will be obtained.

The occurrence of these phenomena can often be detected by a gradual change in the current after the application of a constant voltage or, inversely, a gradual change in voltage after the switching on of a constant current.

An experimental example is given in figure 2.[2] Here the voltage between two thinly sputtered Pt electrodes on a sample of stabilized zirconia (15 mol percent CaO) is recorded against time.

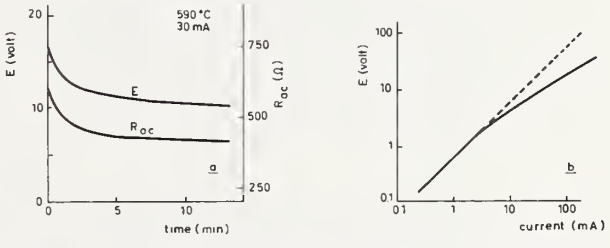

FIGURE 2. *Experimental stationary voltage vs. time (a) and voltage vs. current (b) curves of a ZrO_2-CaO sample in air with contacts acting as reversible electrodes at low current density and showing polarization at higher current densities*
The polarization causes oxygen loss and as a consequence additional electronic conduction (drop in a-c resistance).

[2] Details will be published elsewhere.

290-621 O-68—11

Ambient was air at both electrodes, the temperature 550 °C. A second curve gives the resistance which was measured simultaneously by means of a small superimposed alternating current.

Both curves indicate that a decrease in bulk resistance takes place during current flow, which must be attributed to a loss of oxygen. [3] This oxygen deficiency results in the appearance of appreciable electronic conductance. (At the oxygen pressure used the initial conductivity was at least for 99.99 percent ionic.) This electronic conductivity was confirmed by a determination of the amount of oxygen transported. The latter showed a corresponding decrease in time, like the resistance.

This experiment shows that the speed of take up of oxygen at the cathode may be limiting. The magnitude of the effect depends strongly on the electrode preparation, and it is only present at relatively high applied voltages (or current densities) and low temperatures. Moreover, it is more pronounced at lower oxygen pressures (at the cathode). The effect is also clearly evident from a current-voltage plot using the final values (fig. 2b). The strong temperature dependence at a certain current density indicates that a thermally activated process like O_2-dissociation or solid state diffusion is the cause, rather than a limited gas diffusion rate.

6.2. No Current Supply. Sample Between Different Oxygen Partial Pressures

We will consider an oxide sample which separates two regions where constant oxygen partial pressures are maintained, and where the boundaries of the sample can be considered to be in equilibrium with the corresponding oxygen partial pressures. In figure 3a an example is sketched; another example can be a layer of oxide on a metal (fig. 3b). Electronic contacts may be present to measure the potential difference, but are not used to supply an electric current.

Under this condition, j_t in eq (22) is zero, so that also using eq (8) and putting $z_2=-2$ we obtain:

$$\text{grad } \eta_n = -\frac{\sigma_i}{2\sigma_t} \text{ grad } \mu_O = -\frac{1}{2} t_i \text{ grad } \mu_O$$

$$= -\frac{t_i}{4} \text{ grad } \mu_{O_2}. \qquad (25)$$

Integrating between the boundaries I and II, we can obtain a value for the difference in the electrochemical potential of the electrons at both sides. This difference is just $-q$ times the value of the voltage that can be measured between two identical

[3] See section 7.1.

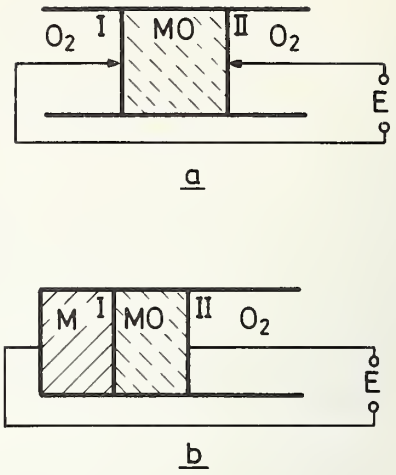

FIGURE 3. *Galvanic cells with an oxide as electrolyte acting between different oxygen chemical potentials*

a. Differing oxygen pressures at both sides. b. Oxygen potential fixed by metal electrode on one side. The latter is the case, when an oxide layer is growing on a metal.

metal electrodes (the chemical potentials and derived quantities are expressed per atom here instead of the usual gramatom). We thus obtain:

$$E = -\frac{1}{q}\int_I^{II} d\eta_n = \frac{1}{4q}\int_I^{II} t_i d\mu_{O_2}. \qquad (26)$$

If the oxygen potential difference is small, so that t_i can be considered as a constant (equal to an average value $\bar{t}_i$), we get simply:

$$E = \frac{1}{4q}\bar{t}_i\,(\mu_{O_2}^{II} - \mu_{O_2}^{I}), \qquad (27)$$

or, since $\mu_{O_2} = \mu_{O_2}^{\circ} + kT \ln p_{O_2}$

$$E = \bar{t}_i \frac{kT}{4q} \ln \frac{p_{II}}{p_I}. \qquad (28)$$

These are the well known expressions given by Wagner [2] for a galvanic cell with a mixed conductor as electrolyte. They allow a direct determination of the ionic transport number from a measurement of the type represented in figure 3a. To determine the oxygen pressure dependence of the transport number, both pressures in the compartments I and II have to be varied simultaneously, but, in order to use eqs (27) or (28), only a small relative difference between p_{II} and p_I is allowed. With a cell of the type of figure 3b this is not possible.

The oxygen dependence of the transport number can still be obtained with this set-up when E as a function of p_{II} is determined. This can be seen as follows. Writing eq (26) in the form containing

$kT \ln p_{O_2}$ instead of μ_{O_2} and differentiating with respect to the upper integration limit we obtain:

$$\left(\frac{dE}{d\ln p_{O_2}}\right)_{\text{at } p_{O_2}=p_{II}} = \frac{kT}{4q}(t_i)_{\text{at } p_{O_2}=p_{II}}. \qquad (29)$$

So the ionic transport number and its pressure dependence can be obtained from the slope of an experimental E versus $\ln p_{II}$ plot.

Often the oxygen pressures in the two regions I and II are fixed by filling them with a mixture of a metal with its oxide. This provides an easy experimental technique in which the specimen is lightly pressed between two different tablets composed of the two metal-metal oxide mixtures and placed in an inert gas atmosphere in a furnace. The tablets can serve as electrical contacts. The oxygen chemical potential difference can be found from the thermodynamic data of the oxide used [15–21].

However, only a limited number of oxygen potentials are available in this way, and the oxygen pressures differ very often by many orders of magnitude. So the average transport number so obtained from eq. (27) is a rather inexact quantity, unless it happens to be unity.

Moreover, if the transport number $t_i < 1$ an ion current flows, and the oxide mixtures have to supply or take up oxygen. Since the electrode reactions take place at the interface, diffusion processes in the metal-metal oxide tablet must prevent exhaustion of one of the components there. At moderate temperatures this is impossible and the method fails [22].

A check can be obtained by building up a cell with the same electrode tablets, but with a purely ionic conductor as an electrolyte (e.g., $ZrO_2 - CaO$). A current is passed through this cell that gives a mass transport comparable with the expected value in the open circuit situation of the original test cell. Only if the emf. assumes a stationary value immediately after the interruption of the current, and independent of its direction of flow, meaningful values of the transport number can be obtained from the original cell. The author's experience with these cells at temperatures below 1000 °C have made him rather pessimistic about the value of the method for quantitative measurements. However, this method remains useful to ascertain whether an ionic transport number is unity or not at any pressure in the range between the equilibrium pressures of the tablets.

It may be worth recalling, that using an electrolyte in which it is well established that $t_i = 1$ in the region of interest, the tablet method can be used with advantage to determine thermodynamic data of one of the electrode systems [15, 23–29].

The set-up of figure 3a requires an inert wall forming a gas-tight fit to the sample in order to separate the two gas compartments [30]. This is also necessary to guarantee the one-dimensional geometry that was assumed in the calculation.

Since this is difficult to realize in most cases, the set-up of figure 4a has been chosen by various workers. The sample is clamped between the ends of ceramic tubes, through which the reference gases can flow. Here the requirements for gas tightness are not so high, since the reference oxygen pressures are determined by streaming gas mixtures. However, effects at the outer boundary, where the gas pressures are not well defined and where surface properties may be decisive, may spoil the homogeneous field distribution inside the sample.

Mitoff [31] avoided these complications by the use of a guard electrode on which a potential is imposed equal to the measured potential in the center of the sample (fig. 4b). The influence of electronic currents through the gas phase, which at high temperatures result from thermionic emission [32], is also minimized by this arrangement.

Another practical difficulty met in this kind of experiment at high temperatures is the occurrence of stray thermal emf's. These may be considerably higher than the electrochemical potentials to be measured. Therefore, they must be reduced as much as is possible by careful design of the apparatus and control of the gas flows. However, they may not be completely eliminated in many cases, and means to change the reference atmospheres from left to the right and visa-versa are required to separate the thermal and electrochemical effects. It must be kept in mind that both the thermal emf and the transport number depend on the oxygen pressure. This means that a simple correction by substraction of the voltage obtained with identical atmospheres at both sides is not justified.

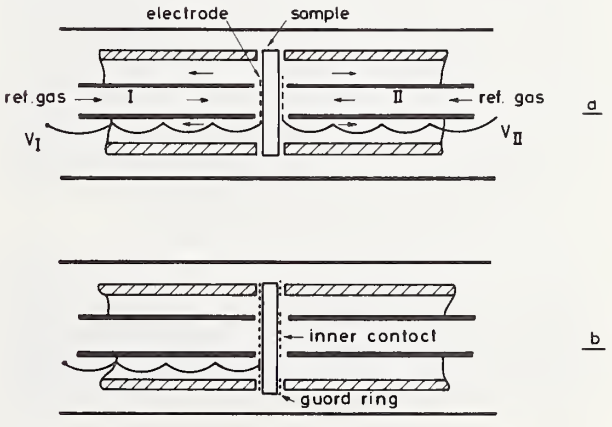

FIGURE 4. *Practical galvanic cell arrangements with the oxygen pressures obtained by gas streams*
a. Two-contact arrangement. b. Guard ring added to avoid surface effects.

A more fundamental difficulty lies in the assumption, made in the derivation of the equations, that the boundaries of the sample are in thermodynamic equilibrium with the corresponding gas phases. The fact that no current is supplied externally is not relevant as before, since, if $t_i \neq 1$, a material transport still takes place through the sample; only the sum of the currents j_e and j_i equals zero.

If for instance the surface reaction between oxygen in the gas phase and in the solid is slow, and from experience with oxygen isotope exchange it is known that this is often the case [33–37], jumps in the thermodynamic potential of oxygen may occur at the surfaces. In such cases the measured emf. will be too low.

A way to check if this effect interferes would be to repeat the same measurement with different sample thicknesses so that the oxygen flow is varied with the same chemical potential difference. If necessary, extrapolation to infinite thickness would give the correct result.

The value of the partial currents $j_i = -j_e$ flowing through the sample follows directly from the eq (9) when the value for grad η_e as found from eq (25) is inserted

$$j_e = -j_i = \frac{\sigma_e}{q} \text{ grad } \eta_n = \frac{-\sigma_e}{4q} t_i \text{ grad } \mu_{O_2}. \quad (30)$$

This can also be written:

$$-j_e = j_i = \frac{\sigma_t}{4q} t_e t_i \text{ grad } \mu_{O_2} = \frac{1}{4q} \frac{\sigma_i \sigma_e}{\sigma_i + \sigma_e} \text{ grad } \mu_{O_2}. \quad (31)$$

In the arrangement of figure 3b this current is proportional to the rate of growth of the oxide MO on the metal M.[4] Eqs (31) are forms of the well known Wagner's equations [2] for the rate of growth of oxide layers on metals and leads to a parabolic rate law since grad μ_{O_2} at constant oxygen pressure changes inversily proportional to the thickness of the layer. From the equations it can be seen that the lower of the two types of conductivities determines the oxidation rate. So ionic transport numbers can be determined from this reaction rate if the oxide is a predominantly electronic conductor.

In the opposite case where $t_e \ll t_i$ the transport of electrons is rate limiting and can be determined from the material transport. In a setup like that of figure 3a and measurement of the oxygen permeation the electronic transport number in stabilized zirconia and hafnia can be determined.[5] The availability of gas tight tubes of these materials makes such a determination of the electronic conductivity (through eq (30)) in them very easy; even the presence of electrodes is not necessary.

6.3. Only Electrons Allowed to Pass Sample

6.3a. Voltage Chosen to Stop Ion Current

An important variation of the last mentioned kind of experiment consists of the application of a voltage (or, what is equivalent, the passage of a current) that is chosen in such a way that the growth of the oxide layer or the permeation of the oxygen is just stopped. In that situation, instead of the total current being zero, only the flow of the ionic component is stopped. This means that according to eq (16):

$$\text{grad } \eta_1 = \text{grad } \eta_2 = 0. \quad (32)$$

In combination with eq (21) and eq (8) this has the consequence that

$$\text{grad } \eta_n = \frac{-1}{|z_2|} \text{ grad } \mu_X = \frac{-1}{2|z_2|} \text{ grad } \mu_{O_2}. \quad (33)$$

The applied voltage, E_{stop}, can thus be found as (see eq (26)):

$$E_{stop} = V_{II} - V_I = \frac{-1}{q} \int_I^{II} d\eta_n = \frac{1}{2|z_2|q} (\mu_{O_2}^{II} - \mu_{O_2}^{I}). \quad (34)$$

By comparison with eq (27) we see that this voltage is equal to the emf. that would be developed, if the oxide were a purely ionic conductor. Furthermore, since the current flowing is all electronic, an average electronic conductivity can be found directly (from eq (9) in integrated form).

An experiment of this kind is described by Jörgensen [38], who studied the oxidation of silicon. As has been stressed by Kröger [39], this kind of experiment allows an unequivocal determination of the charge ($|z_2|$) of the moving ionic specie. This is important because it is *not self evident* that the defects responsible for the current transport have the charge which corresponds to the conventional charge attributed to the ions.

It must be remarked, that, on behalf of clarity, this was tacitly assumed in many of the equations used so far.

6.3b. Blocking Electrode(s) for Ionic Currents

A second way to block the ionic current in oxides is the use of contacts that are impermeable to and do not take up or supply oxygen. The application of a small voltage causes only a temporary ion flow.

[4] Here, and in what follows, we assume that transport of material in uncharged form does not take place.

[5] See section 7.1.

After some time a concentration gradient is built up and no ion current flows any more: the cell is polarized. In this polarized condition the electron current is responsible for the complete electric current, just as in the situation of the last section. So eqs (33) and (34) are also valid here, only the potential difference $V_{II}-V_I$ is the applied voltage here and the difference in $\mu_{O_2}^{II}$ and $\mu_{O_2}^{I}$ is established automatically as a consequence of the applied voltage and the damming up of the mobile ions.

The current in the final stationary state is given by eq (9)

$$j_t = j_e = \frac{\sigma_e}{q} \text{ grad } \eta_n. \tag{35}$$

This can be written also, according to eq (33) and since $|z_2| = 2$:

$$j_t = j_e = -\frac{\sigma_e}{4q} \text{ grad } \mu_{O_2}. \tag{36}$$

Here σ_e is in general dependent on μ_{O_2}, $\sigma_e = \sigma_e(\mu_{O_2})$, and thus dependent on the applied voltage. Integration over the sample thickness L gives:

$$j_t L = -\frac{1}{4q} \int_I^{II} \sigma_e(\mu_{O_2}) \, d\mu_{O_2}. \tag{37}$$

Only for small applied voltages, corresponding to small differences in μ_{O_2}, a meaningful average electronic conductivity $\bar{\sigma}_e$ can be put before the integral, resulting in:

$$j_t L = -\frac{\bar{\sigma}_e}{4q} \int_I^{II} d\mu_{O_2} = \frac{-\bar{\sigma}_e}{4q} (\mu_{O_2}^{II} - \mu_{O_2}^{I}) = -\bar{\sigma}_e (V_{II} - V_I). \tag{38}$$

However, one inconsistency is present in our treatment so far. By means of the applied voltage only the difference $\mu_{O_2}^{II} - \mu_{O_2}^{I}$ is determined, and not the value of each of them. Because of the perfect blocking action of the electrodes, as was assumed in the beginning of this section, the possibility of fixation of the μ_{O_2} by exchange with the surrounding gas atmosphere is excluded. So the oxygen potential is only determined by the *initial* composition of the sample, and depends on the way of its pretreatment.

To obtain meaningful results, one must be *certain* that, during the establishment of the stationary, polarized state, no oxygen loss or gain whatsoever could have happened. However, this certainty is hard to obtain: in practice it is likely that some change in composition occurs. Therefore it is advisable to use one blocking contact only, and allow the sample to come into equilibrium with the atmosphere by the use of a reversible electrode for the other contact. Of course a metal-metal oxide mixture or the metal component of the oxide itself would do as well.

We assume now that electrode I is chosen as the reversible one and that, consequently $\mu_{O_2}^{I}$ has a well defined value. Then $\mu_{O_2}^{II}$ is fixed by the applied voltage (see eq (34)):

$$\mu_{O_2}^{II} = \mu_{O_2}^{I} + 4qE. \tag{39}$$

In the same way, the oxygen potential at a position x in the sample, where, with a metallic probe, a voltage $E(x)$ is measured with respect to the reference electrode I, is found as

$$\mu_{O_2}^{x} = \mu_{O_2}^{I} + 4qE(x). \tag{40}$$

Using this equation in eq (36) and solving for $\sigma_e(\mu_{O_2}^{x})$ gives

$$\sigma_e(\mu_{O_2}^{x}) = \frac{-j}{(dE/dx) \text{ at } x}. \tag{41}$$

This probe method was introduced by Hebb [9] in the case of Ag_2S.

Wagner [10] suggested a method to obtain the μ_{O_2} dependence without the use of probes. Differentiation of eq (37) with respect to the upper integration limit (introducing eq (39) and solving for $\sigma_e(\mu_{O_2}^{II})$ gives

$$\sigma_e(\mu_{O_2}^{II}) = L \frac{dj}{dE}. \tag{42}$$

So the electronic conductivity component is obtained from the slope of the j versus E plot which is measured in the final polarized situation. The corresponding μ_{O_2} is given again by eq (39).

The integration of eq (37) can be performed, if it is assumed that the electron (or hole) mobility is independent of the composition of the substance. In that case, the oxygen pressure dependence of σ_e results only from the concentration dependences of the electrons and holes (n and p). According to eq (2), n can be expressed in terms of μ_n:

$$n(x) = n_1 \exp \frac{\mu_n(x) - \mu_n^{I}}{kT}. \tag{43}$$

Here n_1 is the electron concentration at the reversible electrode I, and $n(x)$ that at the position x. With the eqs (33) and (40) this can be transformed into:

$$n(x) = n_1 \exp \frac{-qE(x)}{kT}. \tag{44}$$

Since the electron conductivity σ_n is proportional to n, we can also write:

$$\sigma_n(x) = \sigma_{n1} \exp \frac{-qE(x)}{kT}. \tag{45}$$

For holes the equivalent expression is found:

$$\sigma_p(x) = \sigma_{p1} \exp \frac{qE(x)}{kT}. \tag{46}$$

So, $\sigma_e(x)$ in eq (37) can be replaced by

$$\sigma_e = \sigma_n + \sigma_p = \sigma_{n1} \exp \frac{-qE(x)}{kT} + \sigma_{p1} \exp \frac{qE(x)}{kT}. \tag{47}$$

When also E is introduced for μ_{O_2}, we find, after integration of eq (37) between $E=0$ and $E=E$,

$$j_t = j_e = \frac{-kT}{qL}\left[\sigma_{n1}\left(1 - \exp\frac{-qE}{kT}\right) + \sigma_{p1}\left(\exp\left(\frac{qE}{kT}\right) - 1\right)\right]. \tag{48}$$

A typical shape of the curve representing this j versus E dependence for the polarized state is given in figure 5. It shows three regions: a low voltage region where the electronic conductivity is n-type, a relatively flat portion corresponding to intrinsic electronic conductivity, and a second rising part at higher voltages corresponding to high oxygen pressures and p-type conductivity. The slope of the curve is a measure of the electronic conductivity according to eq (42). It must be remarked that in many practical cases only a part of this general curve can be realized because of the limited range of oxygen pressures in which the oxide under consideration is thermodynamically stable.

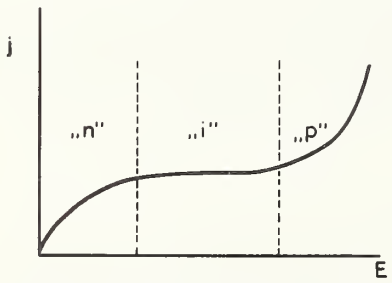

FIGURE 5. *Typical stationary current versus voltage curve for a polarized cell*

The oxygen pressure at the reversible reference electrode is assumed to be so low that the current is n-type when a low positive voltage E is applied to the blocking electrode. At a higher voltage, part of the oxide becomes high ohmic (electronically). At still higher voltages, the region near the positive contact becomes p-type.

The polarized cell technique described has been successfully applied to the silver, copper and lead halides [40, 41, 42]. In applications to oxides the determination method consisting of the passage of a constant current and observation of the final stationary voltage has been described [43, 44, 45]. However, a reversible reference electrode was not used in these cases. An analyses according to eq (48) was applied to $ZrO_2.CaO$ and $ThO_2.Y_2O_3$ by Patterson et al. [46].

It seems useful to discuss the limitations of this method as applied to oxides in some detail. As has already been discussed, the fixation of the oxygen potential at one electrode is important. For instance, it is unsatisfactory to make measurements in a vacuum, as was done by Danforth and Bodine [43] in a study of ThO_2-crystals. The oxygen partial pressure of a practical vacuum is undefined.

An interfering process takes place at the free sides of the sample, on which no contact material can be present to close off the surrounding gas. The uniformity of the gradients inside the sample may be spoiled and O_2-exchange with the atmosphere takes place. Thus the current in the final stationary state may not depend only on the applied voltage, but also on this oxygen exchange rate. In most practical cases it will not be possible to close off the sides and the only measure that can be taken to reduce this disturbance seems to be the use of thin samples and, possibly, a guard ring technique.

Furthermore, the degree of blocking of the electrode is difficult to ascertain. Any leak of oxygen through the contact gives rise to a stationary final current, just as that arising from the electronic conductivity. The temperature dependence may, sometimes, give an indication of what process might be responsible, as shown by Vest and Tallan [45], but cannot be used as a general criterion. It is evident that the kind of electrode and its way of application are very important in this respect.

This is demonstrated in figure 6. Shown are some recordings of the voltage versus time when a constant current (10 $\mu A/cm^2$) is switched on and off with three different kinds of Pt–electrodes and with different oxygen pressures. The sample was calcia-stabilized zirconia, its conductivity at the temperature concerned (550 °C) was less than 10^{-2} percent electronic (determined by the oxygen permeation technique).

Note the difference from the experiment shown in figure 2—the coordinate values are in millivolts and seconds; in figure 2, in volts and minutes. The contacts used in the former experiment behaved like those in figure 6a with small currents and thus

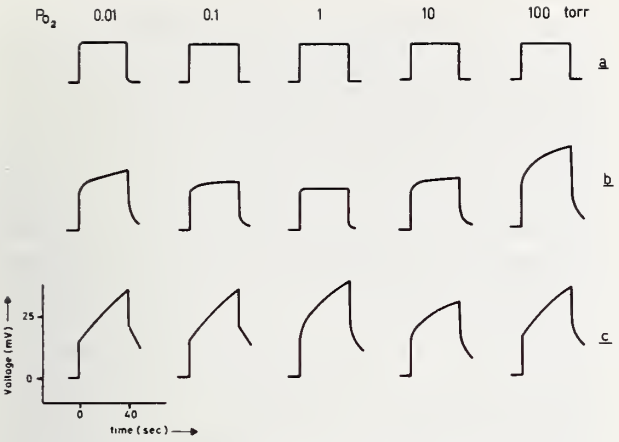

FIGURE 6. *Experimental current vs. time curves for ZrO_2-CaO during a current pulse of 40 seconds and 10 $\mu A/cm^2$*

Different types of electrodes and different oxygen pressures were used. The building up of a polarization voltage occurs only when some ion blocking takes place; a. reversible electrodes of thinly sputtered platinum; b. more densely sputtered platinum electrodes block at high and low oxygen pressures; c. painted platinum electrodes show more blocking action.

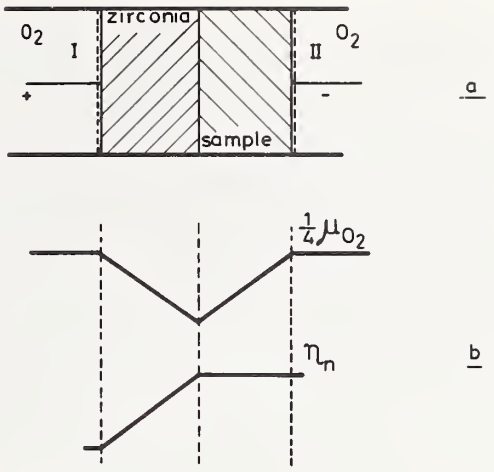

FIGURE 7. *a. Blocking of electronic current by an ionic conductor as electrode.*

b. Distribution of oxygen chemical potential and electron electrochemical potential in sample (right) and ionic electrode (left).

were perfectly reversible in this current and voltage range.

In conclusion, we can remark that the polarization technique, which is in principle capable of the detection of very small electronic contributions to the conductivity, seems in the practical application to oxides only dependable for the determination of substantial electronic transport numbers. Results can only be trusted quantitatively if care has been taken to fix the composition of the sample, if only low polarization voltages have been used, and if the use of different blocking electrodes gave consistent results.

6.4. Only Ion Current Allowed

While, in the preceding section, ion current blocking was discussed, now the blocking of electrons will be considered. This can be achieved by the use of a purely ionic conductor, exhibiting negligible electronic conductivity, as an electrode. The situation is most simple if the ionic conductance of this electrode is much higher than that of the sample under test. Then, when a current flows, the voltage drop over this electrode caused by the current can be neglected. This intermediate electrode, as well as the opposite side of the sample, are provided with reversible electrodes. These are in contact with the same surrounding, oxygen-containing, atmosphere (see fig. 7a).

If the applied potential difference $V_{II}-V_I=E$ is so small that no electrolysis products can be formed at the interface, the distribution of two different potentials is as represented in figure 7b. Since in the sample $j_e=0$ it follows from eq (9) that $\Delta\eta_n=0$. So the total applied η_n-difference ($=-qE$) appears over the ionic conductor. Consequently, a drop in oxygen chemical potential of $\Delta\mu_{O_2}=4qE$ builds up over it. As both contacts are in the same atmosphere, a corresponding inverse oxygen potential difference appears over the sample.

The ionic current through the sample is given by:

$$j_i=\frac{\sigma_i}{2q}\,\text{grad}\,\eta_2 \qquad \text{(see eq (16))}.$$

Furthermore, according to eq (21):

$$\text{grad}\,\eta_2=\tfrac{1}{2}\,\text{grad}\,\mu_{O_2}-2\,\text{grad}\,\eta_n.$$

Because here grad $\eta_n=0$, this becomes grad $\eta_2=\frac{1}{2}$ grad θ_{O_2}. Thus, for the current density we find:

$$j_i=\frac{\sigma_i}{4q}\,\text{grad}\,\mu_{O_2}. \tag{49}$$

If σ_i is independent of the oxygen pressure, or if the applied voltage is sufficiently low so that σ_i can be considered as constant, integration gives

$$j_i=-\frac{\sigma_i E}{L}. \tag{50}$$

So, it is just as if no electronic conductivity existed in the sample, and as if the voltage was applied directly. In fact the ionic conductor has the function of presenting an oxygen atmosphere (different from that of the surroundings) and the electrical current is a measure for the oxygen penetration through the sample which occurs as a consequence of the applied oxygen pressure difference.

Practical difficulties are likely to be met again by the processes taking place at the sides of the sample and with exchange of oxygen between the solid-solid interface and the surrounding atmosphere. They have to be solved by closing off the sides or, perhaps, by the use of a guarded electrode arrangement. So far no studies are known by the author where this method has been used in oxide research.

An important variation results when electrode II is blocking for ions. Any current passed through the system enriches or impoverishes the sample with oxygen. In this way, by measuring the equilibrium voltage (= equilibrium pressure) after a certain amount of charge has been passed as a function of this amount, the solubility of oxygen as a function of the oxygen pressure can be measured. This method of "potentiometric titration" has for instance been used by Alcock and Belford to determine the solubility of oxygen in liquid lead, and recently, by Alcock, Zador and Steele to study the nonstoichiometric oxides TiO_2, NbO_2, and $Ti_{\frac{1}{2}}Nb_{\frac{1}{2}}O_2$ [47].

7. Survey of Existing Data

At present, dependable quantitative knowledge about ionic conductivity is only available for a limited number of oxides. Only a short review will be given here and it will be restricted to well established data for some important refractory oxides.

7.1. Stabilized Zirconia

The literature on stabilized zirconia is very extensive and still rapidly growing. The ionic conductivity of rare earth doped zirconia was already recognized by Nernst in the year 1899 [48]. Schottky in 1935 [49] suggested the use in fuel cells and Baur and Preis [50] investigated this application experimentally in 1937. Their emf measurements proved the predominant ionic character of the conductivity. Wagner explained this by the assumption of the presence of mobile oxygen vacancies (1943) [51]. Confirmation was obtained by the comparison of x-ray and pycnometer densities by Hund [52] and by comparison of oxygen self diffusion data with the conductivity [37, 53]. The correlation factor [37] appeared to correspond to a vacancy mechanism. The cation mobility is very low [54].

The influence of the dope concentration on the conductivity has been studied extensively [55–67]. It appears that a maximum in the conductivity occurs somewhat above the lowest doping level that is required to make the cubic structure stable. For calcia the maximum is situated at 12 mol percent CaO. For rare earth doping, it lies between 8 and about 12 mol percent. The conductivity maximum shifts to higher percentages in the direction Sc, Yb, Gd, Sm, Nd, i.e., in the direction of higher ionic radius and with higher temperatures. The highest conductivity is found for the smaller ions (Sc).

The activation energy is minimum for the highest conductivity and increases from there with higher concentrations and also with increasing ionic radii [57, 58, 62].

From this experience it is clear that the ionic conductivity is more determined by the mobility of the oxygen ions, than by the vacancy concentration.

At 1000 °C slow irreversible changes take place in the lattice which are accompanied by a decrease in conductivity. Annealing at about 1300 °C restores the original conductivity, which has remained ionic in character [63–67]. X-ray and neutron diffraction studies indicate that some ordering mechanism takes place. A practical study by Takahashi et al. [66] reveals that for an Yb_2O_3 or Y_2O_3 content above 10 percent, annealing at 1000 °C does not influence the 1000 °C conductivity. But the 600 °C conductivity decreases somewhat after a 1000 °C anneal.

The ionic transport number measured by direct transport and emf. methods appears to be 100 percent within experimental error at near atmospheric pressures, and also at such low oxygen pressures as coexistent with H_2O+O_2 or $CO+CO_2$ mixtures or with metals like Fe, Ni, Cr [15, 68, 69].

But at very low pressures, e.g., as low as in equilibrium with metallic Zr, the transport number drops because the increased electron conductivity predominates [21, 30, 46, 70, 71, 72].

This effect can be observed directly by transport measurement of zirconia in a reducing atmosphere [14] and is most easily demonstrated by trying to electrolize oxygen out of a gas system which contains no oxygen or reducible compounds. The zirconia is reduced itself in this way, but, at low current densities, no metallic Zr is formed. This can be seen from the equilibrium potential after the current is interrupted, which is lower than would correspond with free Zr [72]. The drop in resistance shown in figure 2 is caused by the same effect. The resistance increase found by Strickler et al. [61] upon electrolysis in a reducing atmosphere (ZrO_2-Y_2O_3) is not understandable in this respect, and is opposite to the author's experience (with ZrO_2-CaO).

The small contribution of electronic conductivity at higher pressures can be obtained from oxygen permeability measurements as were performed by Smith et al. [73] as a function of pressure (difference). The $p^{1/4}$ law found can be explained from the most simple defect model with hole conduction

and a concentration of ionized oxygen vacancies fixed by the calcium concentration.

Analysis of Smith's data with the help of eq. (30) and resistance data from ref. [55] yields a transport number for holes at 1275 °C and 25 torr oxygen pressure of about .05 percent. The activation energy is 2.5 eV, so is about two times higher than that for ion transport. Our measurements at lower temperatures confirm the activation energy, but yielded higher values. At 730 °C the electronic transport number found was 3.10^{-4} for ZrO_2 with 15 mol percent CaO.

Predominant electronic (*n*-type) conductivity appears with the addition of comparatively small amounts of V_2O_5 [45] or Ta_2O_5 [74], which act as donors. A solution for the problem of why such a small donor concentration in the presence of a much higher acceptor (Ca) concentration can give *n*-type conductivity was proposed by Kröger [75]. He assumed that the greater part of the effectively negatively charged calcium ions form neutral associates with the oxygen ion vacancies.

In this way, the acceptor character of the calcium is annihilated and only a small concentration of five-valent ions acting as donors are sufficient to compensate the rest of the (unassociated) calcium ions and give rise to *n*-type conductivity.

The oxygen movement takes place through the vacancies neighbouring calcium ions and is possible because of the high concentrations present.

A Mössbauer study [76] of iron-57, and mechanical or electrical loss measurements [77] (for ThO_2-CaO) point to the presence of acceptor-vacancy associates.

7.2. Pure Monoclinic Zirconia

The low temperature modification of zirconia is monoclinic. Its electrical conductivity was studied by Rudolph [78], by Kofstad and Ruzicka [79] and, most recently, by Vest, Tallan and Tripp [80]. According to the last mentioned investigators the conductivity is mainly electronic and is proportional to $p_{O_2}^{1/5}$ at pressures above 10^{-8} atm. The conductivity curve shows a flat portion between 10^{-8} and 10^{-21} atm. and increases towards lower pressures. In the defect model proposed, completely ionized zirconium vacancies are assumed. However, the possibility of the existence of such highly charged defects was doubted by Kröger [75], who argues that association with ionized oxygen vacancies is more probable.

7.3. Pure Tetragonal Zirconia

This modification is stable at high temperatures. Electrical conductivity measurements performed by Vest and Tallan [81] showed only a very weak oxygen pressure dependence in the temperature range 1300 to 1700 °C. A shallow minimum in the conductivity-pressure curve was found near 10^{-7} atm. at 1300 °C, which shifts to higher pressures at increasing temperature. Polarization measurements revealed mixed ionic and electronic conductivity. The ionic contribution was dominant at 1300 °C and practically pressure independent, the electronic part showed a pronounced minimum, with *n*- and *p*-type branches at low and at high pressures. Oxygen dependences in these branches approximated $p_{O_2}^{-1/6}$ and $p_{O_2}^{1/6}$ laws. At higher temperatures, the electronic transport number increases to about $\frac{1}{2}$ (1600 °C).

7.4. Stabilized Hafnium Oxide

The properties of calcia stabilized hafnia were investigated by Johansen and Cleary [57], yttria stabilized hafnia was studied by Robert, Deportes and Besson [82]. As is to be expected, the conductive properties are very similar to those of stabilized zirconia. Even the slow irreversible changes near 1000 °C take place in Y-stabilized hafnia [82].

From the oxygen permeation data of Smith et al. [73] it can be calculated that the electronic transport number is also of the same order of magnitude as in zirconia.

Pure monoclinic hafnia can be studied in a greater temperature range than monoclinic zirconia because of the higher transformation temperature. Tallan, Tripp and Vest [83] found, as with zirconia, electronic (*p*-type) conductivity at oxygen pressures higher than 10^{-6} atm. (between 1000 and 1500 °C). The pressure dependence was again as $p_{O_2}^{1/5}$. The ionic contribution was low, as was checked by polarization measurements with blocking electrodes.

7.5. Thorium Oxide

Thorium oxide exhibits mixed conduction, as was demonstrated by Danforth and Bodine [43, 44] by a polarization technique. More quantitative results were obtained by Rudolph [78]. By means of galvanic cell measurements Subbarao, Sutter and Hrizo [84] found that the ionic transference number of Y-doped thoria at near atmospheric oxygen pressure was lower than unity and dependent on the Y-content. Alcock and Steele [21, 30] established a value of unity at low oxygen pressures. Their galvanic cell measurements demonstrate that this is also the case at such extremely low oxygen partial pressures that stabilized zirconia would become electronically conductive.

Results by Lasker and Rapp [22] and Bauerle [85] show that a pressure independent conductivity plateau exists at pressures below about 10^{-6} atm.

of oxygen. This corresponds to purely ionic conductivity. At higher pressures p-type conductivity comes up, increasing with a $\frac{1}{4}$ power of the pressure. The ionic conductivity plateau increases with dope (Y) concentration up to about 15 mol/$YO_{1.5}$ and decreases with higher dopant content. The results for "pure" thoria indicate that the properties are still determined by the presence of unknown impurities.

Density measurements performed by Wimmer, Bidwell and Tallan [86] indicate that oxygen vacancies are responsible for the ionic conductivity. The activation energies for the electronic conductivity and for the ionic conductivity are both about equal to 1 eV, so that the transport number does not change appreciably with the temperature.

7.6. Cerium Dioxide

In the older literature about cerium dioxide ionic conduction was sometimes suggested [87], but measurements were also interpreted in terms of electronic conduction [88, 89]. Ionic conductivity was proved by Neuimin and Pal'guev [89] and identified by mass transport measurements as oxygen conductivity [90]. The passage of a direct current may result in a reduction of the CeO_2, while at the same time the conductivity increases, as was shown by Kevane et al. [91]. Cerium oxide doped with La_2O_3 was studied by Takahashi, Ito and Iwahara [92]. A maximum in conductivity was found near a content of 10 mol percent. Emf. measurements show that the conductivity is 100 percent ionic at near atmospheric oxygen pressures if more than 2.5 percent of La_2O_3 is present. At lower oxygen pressures reduction takes place giving rise to n-type conductivity.

7.7. Ternary Mixed Crystals

Mixed crystals in the system $ZrO_2 - CeO_2 - Y_2O_3$ were studied by Robert et al. [82]. They found that the cubic structure was stabilized already with 3 mol percent Y_2O_3 when part of the ZrO_2 was replaced by CeO_2 (in the ratio $ZrO_2 : CeO_2 : Y_2O_3 = .90 : .07 : .03$). However, the maximum conductivity still appeared at 8 mol percent, just as in the case with zirconia. The value of the maximum did not differ appreciably from the zirconia case.

7.8. Aluminum Oxide

The conductivity studies of alumina do not give sufficient information about the ionic contribution [100, 101]. Preliminary galvanic cell measurements by R. W. Cooper on single crystals [102] indicate an appreciable ionic component. This is also found by Schmalzried [71] for sintered alumina.

7.9. Yttrium Oxide

Cell measurements by Tare and Schmalzried [103] at 825 °C indicate purely ionic conduction in the oxygen pressure range 10^{-6} to 10^{-17} atm. However, measurements by the polarization technique performed by Tallan and Vest [104] on purer samples and at higher temperatures indicate only a very small ionic contribution. This was even so at the oxygen pressure where the conductivity is minimum.

7.10. Beryllium Oxide

The electrical conductivity and self diffusion coefficients of BeO have been studied intensively [18, 105–116]. It is well established now that the conductivity is of mainly ionic character over a wide range of oxygen pressures and at temperatures up to 1600 °C [18, 110, 111, 112, 113], although mainly electronic conduction was proposed by Pryor [109]. Comparison with self diffusion data of oxygen and beryllium [105] indicates that the beryllium ions must be responsible for the current transport. The value of the correlation factor points to a vacancy mechanism [111, 112].

The conductivity versus $1/T$ curve shows an activation energy of about 2.6 eV. It was assumed that this conductivity is extrinsic and caused by unknown impurities [112, 116].

At temperatures below 1000 °C, a much smaller slope was found [112] and it was suggested that in this region the current passed through a second phase formed at the grain boundaries. This would result from impurities present in a concentration above the solubility limit at the lower temperatures.

7.11. Magnesium Oxide

After some interpretation difficulties of earlier results [93], Schmalzried [94] and Mitoff [95] agreed about the mixed character of the electrical conductivity of MgO. The ionic transport number depends on the temperature and on the oxygen partial pressure [18, 96, 31, 71]. It is maximum at about 10^{-5} atm. oxygen and decreases when the temperature is increased from 1000 to 1500 °C. Comparison of self diffusion data for oxygen [97] and for Mg [98] leads to the conclusion that the ionic current is carried by magnesium ions. The total electrical conductivity is influenced by the addition of Ni [99].

8. References

[1] A. B. Lidiard, Ionic Conductivity, in: Encyclopaedia of Physics, Vol. XX (Ed. S. Flügge), Springer Verlag, Berlin, 1956, p. 246.

[2] C. Wagner, Z. physik. Chemie, **B21,** 25 (1935). Z. physik. Chemie, **B32,** 447 (1936). See also the review in K. Hauffe, Oxidations of Metals, Plenum Press, New York (1965).
[3] F. A. Kröger, F. Stieltjes and H. J. Vink, Philips Research Repts. **14,** 557 (1965).
[4] F. A. Kröger, Chemistry of Imperfect Crystals, North Holland Publishing Cy, Amsterdam, Ch. 21 (1964).
[5] S. R. de Groot, Thermodynamics of Irreversible Processes, North Holland Publishing Cy., Amsterdam (1951).
[6] F. Stieltjes. Philips Research Repts. **17,** 337 (1962).
[7] M. V. Perfil'ev and S. F. Pal'guev, Trans. (Trudy) No. 6, Inst. of Electrochem. Urals Ac. Sc., Electrochem. Molten and Solid Electrolytes, Vol. 3, p. 97, p. 105.
[8] C. Wagner, Z. physik. Chem. **B21,** 42 (1933). Z. physik. Chemie **B23,** 469 (1934).
[9] M. H. Hebb, J. Chem. **20,** 185 (1952).
[10] C. Wagner, Proc. 7th meeting Int. Comm. on Electrochem. Thermodynamics and Kinetics, Lindau (1955), Butterworth, London, p. 361 (1957).
[11] C. Wagner, Z. Elektrochemie **60,** 4 (1956); ref. [4], Ch. 22.
[12] C. Tubandt, Handb. Experimentalphysik, Eds. Wien and Harms, **12,** part 1, Akademische Verlagsgesellschaft, Leipzig, p. 412 (1933).
[13] Z. S. Volchenkova and S. F. Pal'guev, Transactions (Trudy) of the Institute of Electrochemistry No. 1, Electrochem. of Molten and Solid Electrolytes, Consultant Bureau, New York, p. 97 (1961).
[14] J. L. Weininger and P. D. Zemany, J. Chem. Phys., **22,** 1496 (1954).
[15] K. Kiukkola and C. Wagner, J. Electrochem. Soc., **104,** 308 (1956) and J. Electrochem. Soc., **104,** 379 (1956).
[16] H. Peters and G. Mann, Z. Electrochemie, **63,** 244 (1959).
[17] H. Schmalzried, J. Chem. Phys. **33,** 940 (1960).
[18] S. F. Pal'guev and A. D. Neuimin, Sovj. Phys. Solid State **4,** 629 (1962).
[19] S. F. Pal'guev and A. D. Neuimin, Trans. (Trudy) of the Institute of Electrochemistry No. 1, Electrochem. of Molten and Solid Electrolytes, Consultant Bureau, New York, p. 90 (1961).
[20] S. P. Mitoff, J. Chem. Phys. **33,** 941 (1960); J. Chem. Phys., **36,** 1383 (1962).
[21] C. B. Alcock and B. C. H. Steele, in: Science of Ceramics, Vol. II, Ed., G. H. Stewart, Trans. Brit. Cer. Soc. (1964), Academic Press, London, p. 397 (1965).
[22] M. F. Lasker and R. A. Rapp, Z. Physik. Chemie N.F., **49,** 198, p. 211 (1966).
[23] H. Peters and H. H. Möbius, Z. Physik. Chemie, Lpz. **209,** 298 (1958).
[24] H. Schmalzried, Z. Physik. Chemie N.F., **25,** 178 (1960).
[25] T. N. Rezukhina and Z. V. Proshina, Russ. J. Phys. Chem., **36,** 333 (1962).
[26] T. N. Rezukhina, V. A. Levitskii and N. M. Kazimirova, Russ. J. Phys. Chem., **35,** 1305 (1961).
[27] V. I. Lavrent'ev, V. A. Levitskii and F. A. Kuznetskov, Russ. J. Phys. Chem., **35,** 671 (1961).
[28] R. W. Taylor and H. Schmalzried, J. Phys. Chem., **68,** 9 (1964).
[29] G. B. Barbi, J. Phys. Chem., **68,** 1025 (1964).
[30] B. C. H. Steele and C. B. Alcock, Trans. Metall. Soc. AIME, **233,** 1359 (1965).
[31] S. P. Mitoff, J. Chem. Phys. **41,** 2561 (1964).
[32] J. P. Loup and A. M. Anthony, Rev. Hautes Temp. Réfract., **1,** 15 (1964).
[33] R. Haul, D. Just and G. Dümbgen, Sauerstoffdiffusion in Oxygen, in Reactivity of Solids, Ed. J. H. de Boer, Elsevier, Amsterdam, p. 65 (1961).
[34] R. Haul and D. Just, J. Appl. Phys. suppl., **33,** 487 (1962).
[35] R. Haul ånd G. Dümbgen, J. Phys. Chem. Solids, **26,** 1 (1965).
[36] J. Nováková, K. Klier and P. Jíru, Exchange Reactions Between Solid Oxides and Oxygen Molecules, in Reactivity of Solids, Ed. G. M. Schwab, Elsevier, Amsterdam, p. 269 (1965).
[37] L. A. Simpson and R. E. Carter, J. Am. Cer. Soc., **49,** 139 (1966).
[38] P. J. Jorgensen, J. Chem. Phys., **37,** 874 (1962).
[39] F. A. Kröger, Proc. Brit. Cer. Soc., **1** 167, p. 170 (1964).
[40] B. Ilschner, J. Chem. Phys., **28,** 1109 (1958).
[41] J. B. Wagner and C. Wagner, J. Chem. Phys., **26,** 1597 (1957).
[42] J. B. Wagner and C. Wagner, J. Electrochem. Soc., **104,** 509 (1957).
[43] W. E. Danforth and J. H. Bodine, J. Franklin Inst., **260,** 467 (1955).
[44] W. E. Danforth, J. Franklin Inst., **266,** 483 (1955).
[45] R. W. Vest and N. M. Tallan, J. Appl. Phys., **36,** 543 (1965).
[46] J. W. Patterson, E. C. Bogren, and R. A. Rapp, J. Electrochem. Soc., **114,** 752 (1967).
[47] C. B. Alcock and T. N. Belford, Trans. Faraday Soc., **60,** 822 (1964), C. B. Alcock, S. Zador and B. C. H. Steele, Proc. Brit. Cer. Soc., **8,** 231 (1967), B. C. H. Steele, this Conference.
[48] W. Nernst, Z. Elektrochemie, **6,** 41 (1900).
[49] W. Schottky, Wiss. Veröff. Siemenswerke, **14,** H2, 1 (1935).
[50] E. Baur and H. Preis, Z. Elektrochemie, **43,** 727 (1937).
[51] C. Wagner, Naturwissenschaften, **31,** 265 (1943).
[52] F. Hund, Z. Physik. Chemie, **199,** 142 (1952).
[53] W. D. Kingery, J. Papis, M. E. Doty and D. C. Hill, J. Am. Cer. Soc., **42,** 393 (1959).
[54] W. H. Rhodes and R. E. Carter, 64th Ann. Meeting Am. Cer. Soc., New York, 1962, Abstract in: Bull. Am. Cer. Soc., **41,** 283 (1962).
W. H. Rhodes and R. E. Carter, J. Am. Cer. Soc., **49,** 244 (1966).
[55] J. M. Dixon, L. D. Lagrange, U. Merten, C. F. Miller and J. T. Porter, J. Electrochem. Soc., **110,** 276 (1963).
[56] T. Y. Tien and E. C. Subbarao, J. Chem. Phys., **39,** 1041 (1963).
[57] H. A. Johansen and J. G. Cleary, J. Electrochem. Soc., **111,** 100 (1964).
[58] H. Tannenberger, H. Schachner and P. Kovacs, Proc. 1res Journées Intern. d'Etude des Piles à Combustible, Brussels, Part III, p. 19 (1965).
[59] H. H. Möbius, Z. Chemie, **2,** 100 (1962); **4,** 81 (1964).
[60] H. H. Möbius, H. Witzmann and G. Pröve, Z. Chemie, **4,** 195 (1964).
[61] D. W. Strickler and W. G. Carlson, J. Am. Cer. Soc., **47,** 122 (1964).
[62] D. W. Strickler and W. G. Carlson, J. Am. Cer. Soc., **48,** 286 (1965).
[63] E. C. Subbarao and P. H. Sutter, J. Phys. Chem. Solids, **25,** 148 (1964).
[64] R. E. Carter and W. L. Roth, General Electric Rept. No. 63-RL-3479M (1963).
[65] R. Collongues, Ann. Chim. (Paris) **8,** 395 (1963).
[66] T. Takahashi and Y. Suzuki, to be published in Proc. II^{mes} Journées Internat. d'Etude des Piles à Combustibles, Brussels (1967).
[67] J. E. Bauerle and J. Hrizo, Westinghouse Techn. Rept. Sept. 30, 1964 thru March 31, 1965, Program Code No. 4980, p. 14.
[68] J. Weissbart and R. Ruka, J. Electrochem. Soc., **109,** 723 (1962).
[69] J. Weissbart and R. Ruka, Rev. Sci. Instr. **32,** 593 (1961).
[70] H. Schmalzried, Z. Elektrochemie, **66,** 572 (1962).
[71] H. Schmalzried, Z. Physik. Chemie N.F. **38,** 87 (1963).
[72] D. T. Bray and U. Merten, J. Electrochem. Soc., **111,** 447 (1964).

[73] A. W. Smith, F. W. Meszaros and C. D. Amata, J. Am. Cer. Soc., **49**, 240 (1966).
[74] A. G. Buyers, J. Am. Cer. Soc., **48**, 122 (1965).
[75] F. A. Kröger, J. Am. Cer. Soc., **49**, 215 (1966).
[76] A. J. Panson, M. Kuriyama and R. J. Ruka, Westinghouse Techn. Rept. Sept. 30, 1964 thru March 31, 1965, Program Code No. 4980, p. 4.
[77] J. B. Wachtman, cited by A. D. Franklin in *Physics and Chemistry of Ceramics*, Ed. C. Klingsberg, Gordon and Breach, New York, p. 83 (1963).
[78] J. Rudolph, Z. Naturforsch., **14a**, 727 (1959).
[79] P. Kofstad and D. J. Ruzicka, J. Electrochem. Soc., **110**, 181 (1963).
[80] R. W. Vest, N. M. Tallan and W. C. Tripp, J. Am. Cer. Soc., **47**, 635 (1964).
[81] R. W. Vest and N. M. Tallan, J. Am. Cer. Soc., **48**, 472 (1965).
[82] G. Robert, C. Deportes and J. Besson, to be published in Proc. II^{mes} Journées Intern. d'Etude des Piles à Combustible, Brussels (1967).
[83] N. M. Tallan, W. C. Tripp and R. W. Vest, J. Am. Cer. Soc., **50**, 279 (1967).
[84] E. C. Subbarao, P. H. Sutter and J. Hrizo, J. Am. Cer. Soc., **48**, 443 (1965).
[85] J. E. Bauerle, J. Chem. Phys., **45**, 4162 (1966).
[86] J. M. Wimmer, L. R. Bidwell and N. M. Tallan, J. Am. Cer. Soc., **50**, 198 (1967).
[87] U. Croatto and A. Mayer, Gazz. Chim. Ital., **73**, 199 (1943).
[88] W. Noddack and H. Walch, Z. Physik. Chemie, **211**, 194 (1959).
[89] A. D. Neuimin and S. F. Pal'guev, Trans. Inst. Elektrokhim, Akad. Nauk SSSR, Ural'sk Filial No. 3, 141 (1962).
[90] L. D. Yushina and S. F. Pal'guev, Trans. (Trudy) No. 4 of the Institute of Electrochemistry, Urals Academy of Science, Electrochemistry of Molten and Solid Electrolytes, vol. 2, Consultants Bureau, New York, p. 74 (1964).
[91] C. J. Kevane, E. L. Holverson and R. D. Watson, J. Appl. Phys. **34**, 2038 (1963).
[92] T. Takahashi, K. Ito and H. Iwahara, Proc. I^{res} Journees Internat. d'Etude des Piles à Combustible, Brussels, p. 42 (1965).
[93] S. P. Mitoff, J. Chem. Phys., **31**, 1261 (1959).
[94] H. Schmalzried, J. Chem. Phys., **33**, 940 (1960).
[95] S. P. Mitoff, J. Chem. Phys., **33**, 941 (1960).
[96] S. P. Mitoff, J. Chem. Phys., **36**, 1383 (1962).
[97] Y. Oishi and W. D. Kingery, J. Chem. Phys., **33**, 905 (1960).
[98] R. Lindner and G. D. Parfitt, J. Chem. Phys., **26**, 182 (1957).
[99] M. O. Davis, J. Chem. Phys., **38**, 2047 (1963).
[100] J. Cohen, Am. Cer. Soc. Bull., **38**, 441 (1959).
[101] J. Papis and W. D. Kingery, J. Am. Cer. Soc., **44**, 459 (1961).
[102] R. W. Cooper, quoted by F. A. Kröger, ref. [39].
[103] V. B. Tare and H. Schmalzried, Z. Physik. Chemie N.F., **43**, 30 (1964).
[104] N. M. Tallan and R. W. Vest, J. Am. Cer. Soc., **49**, 401 (1966).
[105] J. B. Holt, Univ. California, Lawrence Radiation Lab. Rept. UCRL 6940 (1962).
[106] S. Austerman, J. Nucl. Mat., **14**, 248 (1964).
[107] H. J. de Bruin and G. M. Watson, J. Nucl. Mat., **14**, 239 (1964).
[108] J. B. Holt, J. Nucl. Mat., **11**, 107 (1964).
[109] A. W. Pryor, J. Nucl. Mat., **14**, 258 (1964).
[110] C. F. Cline, H. W. Newkirk, R. H. Condit and Y. Hashimoto, Am. Cer. Soc. Bull., **43**, 664 (1964); 17th Pacif. Coast Reg. Meeting Am. Cer. Soc., Oct. 30 (1966).
[111] H. W. Newkirk and C. F. Cline, Univ. California, Lawrence Radiation Lab. Rept. UCRL 7261 T (1964).
[112] H. J. de Bruin, G. M. Watson and C. M. Blood, J. Appl. Phys., **37**, 4543 (1966).
[113] C. F. Cline, J. Carlberg and H. W. Newkirk, J. Am. Cer. Soc., **50**, 55 (1967), C. F. Cline, H. W. Newkirk, R. H. Condit and Y. Hashimoto, this Conference.
[114] R. H. Condit and Y. Hashimoto, J. Am. Cer. Soc., **50**, 425 (1967).
[115] H. J. de Bruin, G. M. Watson, C. M. Blood and D. Roman, Phil. Mag., **16**, 427 (1967).
[116] S. B. Austerman and J. W. Wagner, J. Am. Cer. Soc., **49**, 94 (1966).

Measurement of High-Temperature Thermodynamic Properties of Non-Stoichiometric Oxides Using Solid State EMF and Coulometric Techniques

B. C. H. Steele

Imperial College, London, England

The relative partial molar free energy of oxygen in a number of non-stoichiometric oxides, TiO_2, VO_2, NbO_2, MoO_2, UO_2, has been measured as a function of composition and temperature (700 to 1100 °C) using galvanic cells incorporating solid oxide electrolytes. The data have been analysed to find the region of nonstoichiometry over which the dilute solution laws can be applied and the associated values for the partial heats of solution of oxygen are briefly reviewed. A coulometric technique was successfully employed to vary the oxygen content of certain of the oxides, and the advantages and present limitations to this method of controlling the composition of non-stoichiometric oxides are discussed with reference to the different cell assemblies and oxide systems examined.

Key Words: Coulometric titration, free energy, galvanic cell, nonstoichiometry, solid oxygen electrolyte.

1. Introduction

Thermodynamic studies of non-stoichiometric oxides can help to clarify current theoretical problems associated with the properties of these phases of variable composition. In any metal oxide system for example, it is important to know the composition range over which the simple Wagner-Schottky model for nonstoichiometry is applicable. This model requires random non-interacting defects (Henrian dilute solution behaviour) and is characterised by a constant partial molar heat of solution over the relevant composition range. If the model is applicable then the postulated defect equilibria can also be expressed in terms of simplified mass-action constants in which activities are replaced by concentrations of the appropriate species [1].[1] These regions of complete disorder are, however, difficult to establish experimentally as the partial molar free energy-composition isotherms become very steep when the metal/oxygen ratio approaches the stoichiometric value (figs. 1a and 1b).

As the deviations from exact stoichiometry increase interaction between the defects can result in the formation of 'micro-domains' in which the defects may be considered to be ordered [2]. This ordering process can produce a series of ordered intermediate phases of definite compositions and structures as exemplified by the Magneli structures in Ti_nO_{2n-1}, V_nO_{2n-1}. Under these conditions the partial molar heat of solution is no longer an invariant function of composition, and activity coefficients should be introduced into the relevant mass action expressions, although many theoretical models have been proposed which do not comply with this requirement.

It is obviously important to obtain data on the thermodynamic stability and composition range of these ordered intermediate phases as their existence is obviously fundamental to an understanding of mass transport processes in oxide crystals, and thus to the mechanisms involved in ionic diffusion, ionic conductivity, and solid state reactions. Thus ordered intermediate phases, which often appear only after long annealing times, seem to be only slightly more stable than the disordered parent structure from which they are derived. Moreover, differences in the thermodynamic stability of the individual intermediate phases also appear to be very small [3, 4] and difficult to determine by conventional gas equilibration techniques using CO-CO_2 or H_2-H_2O mixtures.

In view of the preceding comments it is apparent that use of a solid state coulometric technique to control the composition of a non-stoichiometric phase offers many potential advantages. This technique was employed by Wagner et al. to control the stoichiometry of sulphides [5, 6] and tellurides [7], and more recently has been used to study the thermodynamics of UO_{2+x} [8], TiO_{2-x} [9], NbO_{2-x} [9], FeO_{1+x} [10]. A titration, for example, of 0.01 coulombs (10μA for 16.7 mins.) involves the mass transfer of 10^{-7} equivalents (8×10^{-7} gms) of oxygen. For a 100 mg sample of an oxide MO possessing an atomic weight of 100, this transfer of

[1] Figures in brackets indicate the literature references at the end of this paper.

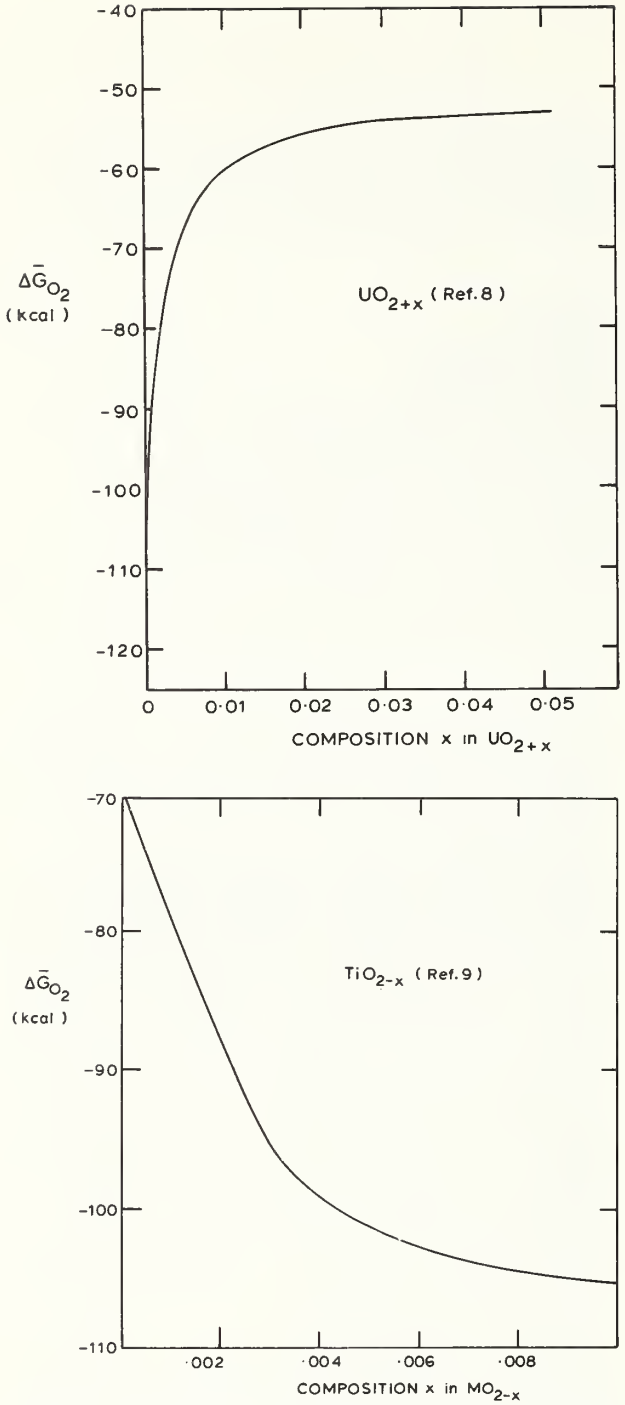

FIGURE 1. *Relative partial molar free energy (ΔG_{O_2}) composition isotherms for TiO_{2-x} and UO_{2+x} at 1000 °C.*

oxygen represents a change in the oxygen/metal ratio of approximately 0.0001. Furthermore the emf of these solid state galvanic cells can often be measured with a precision of ± 1 mV or better which corresponds to an uncertainty of ± 100 cal. in the derived partial molar free energy data for the solution of oxygen.

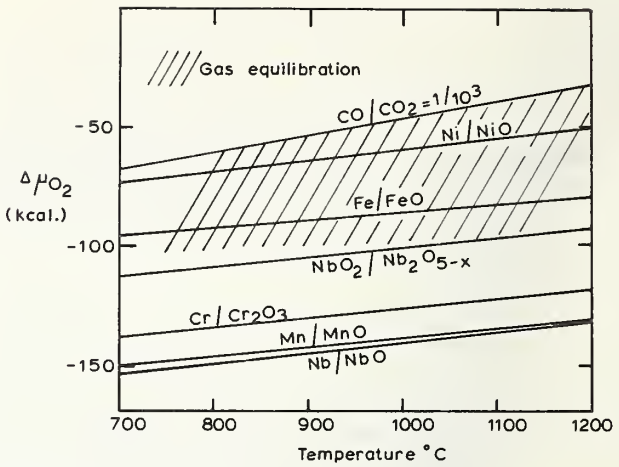

FIGURE 2. *Oxygen chemical potentials of selected metal-metal oxide systems as a function of temperature.*

It is also possible using this technique to measure oxygen partial pressures outside the range that can be conveniently established by conventional gas equilibration techniques (see fig. 2). The low oxygen chemical potentials associated with the Nb-NbO [11] and Mn-MnO [12] systems depicted in figure 2, for example, have been studied using thoria based solid oxide electrolytes; the relevant oxygen partial pressures at 1000 °C possessing values of $10^{-24.8}$ and $10^{-24.3}$ atm. respectively.

To date, however, it has proved impossible to exploit all the potential advantages of this solid state coulometric technique and it is opportune therefore to consider recent applications of this technique to non-stoichiometric studies in order to examine some of the current experimental problems.

2. Experimental

The procedures generally employed for high temperature equilibrium emf measurements using galvanic cells incorporating solid oxide electrolytes have recently been reviewed elsewhere [13] and it is only necessary therefore to describe those additional features particularly relevant to the solid state titration techniques.

2.1. Selection of Electrolyte Material

Solid oxide solutions based on ZrO_2 or ThO_2 have invariably been selected as the electrolyte material, and available data listed below clearly indicate that in these materials the cationic contribution to the ionic conductivity is many orders of magnitude smaller than the oxygen ion conductivity and may be neglected for most applications.

$Zr_{0.85}Ca_{0.15}O_{1.85}$:

$D_{O^{2-}}$ (1000 °C) $= 8 \times 10^{-8}$ cm^2 sec.$^{-1}$ [37]

$D_{Zr^{4+}}$ (1000 °C) $= 5 \times 10^{-18}$ cm^2 sec.$^{-1}$ [38]

$D_{Ca^{2+}}$ (1000 °C) $= 3 \times 10^{-18}$ cm^2 sec.$^{-1}$ [38]

ThO_2:

$D_{O^{2-}}$ (1000 °C) $= 2 \times 10^{-11}$ cm^2 sec.$^{-1}$ [39]

$D_{Th^{4+}}$ (1000 °C) $= 2 \times 10^{-16}$ cm^2 sec.$^{-1}$ [40].

The magnitude of the electronic conductivity is more uncertain and is of course dependent upon the oxygen partial pressure. Using the Hebb-Wagner polarisation technique Rapp [14] has recently determined the electronic conductivity in $Zr_{0.85}Ca_{0.15}O_{1.85}$ and $Th_{0.85}Y_{0.15}O_{1.925}$, and the results for 1000 °C are summarised in figure 3. Oxygen permeability measurements of Roberts and Fabre also indicate comparable electronic transference numbers (10^{-2}–10^{-3}) at the higher oxygen partial pressures. Particular attention should be paid to these permeability measurements which have included studies on selected commercially available electrolyte materials now being used in many industrial and University laboratories; and it must be recognised that the flux of oxygen through these commercial materials is often much higher than would be predicted from the electronic transference numbers determined for similar electrolyte compositions prepared in the laboratory [15, 16].

Polarisation studies made at Imperial College [17] suggest that the onset of significant *n*-type conduction (> 1 percent) occurs at oxygen partial pressures significantly greater than those reported by Rapp and a tentative value for this *n*-conduction in $Zr_{0.85}$-$Ca_{0.15}O_{1.85}$ has also been included in figure 3.

Accurate data for the electronic transference number is not only necessary for precise coulometric titrations but is also important because the presence of an electronic conductivity allows a continuous flux of oxygen ions to pass through any galvanic cell possessing a finite emf. For example a $Zr_{0.85}Ca_{0.15}O_{1.85}$ pellet of 1 sq. cm. cross-section and 1 mm thickness will possess a resistance of 2.5 ohms at 1000 °C. If the observed emf is 500mV then an electronic transference number of 10^{-2} could allow a current of 2mA to flow assuming that the electrochemical reactions at the electrodes are not rate-controlling. In the absence of appropriate precautions this oxygen flux could significantly change the composition of the non-stoichiometric phase under investigation.

2.2. Reference and Working Electrodes

For coulometric titrations it is generally desirable to have separate reference and working electrodes to avoid excessive polarisation at both the working electrode and the relevant variable composition phase electrode. It should be noted that large concentration polarisation voltages may cause reduction of the solid oxide electrolyte thus introducing an unknown electronic contribution to the titration current.[2] To minimise polarisation effects the electrode materials should exhibit both large exchange currents and large diffusion coefficients to avoid concentration gradients. Information relating to the electrochemical kinetics of systems involving solid oxide electrolytes is meagre but activation polarisation is probably not important, and attention should be devoted to minimising the concentration polarisation effects. Porous platinum oxygen electrodes, for example, exhibit insignificant overpotentials [18] at 1000 °C even at current densities approaching 100μA cm^{-2}.

[2] Using a pure oxygen reference electrode the voltage which can be applied across a cell incorporating $Zr_{0.85}Ca_{0.15}O_{1.85}$ as the electrolyte should not exceed about 1 volt at 1000 °C and 1.5 volts at 500 °C. Higher voltages will electrolyse the solid and give rise to electronic conduction. By combining the oxygen chemical potential at which significant electronic conduction (0.1%) occurs with that imposed by the reference electrode, the maximum applied voltage can be determined using the well known relationship: $\Delta\mu_{O_2} = -zEF$.

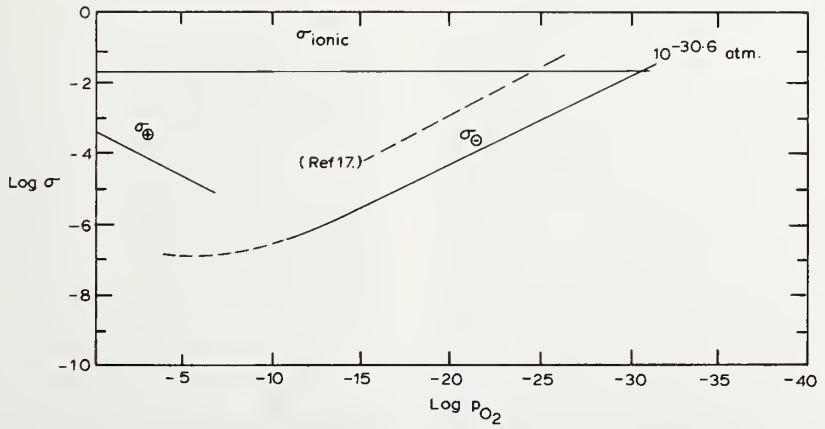

FIGURE 3. *Ionic and electronic conductivities as a function of oxygen partial pressure for $Zr_{0.85}Ca_{0.15}O_{1.85}$ at 1000 °C [14].*

The oxygen chemical potentials in equilibrium with many non-stoichiometric phases of interest, however, possess relatively low values, and as it is advantageous to avoid large chemical potential gradients then alternative reference and working electrodes must be used. Porous platinum electrodes in contact with $CO-CO_2$ mixtures could be used but present design problems if separate working and reference electrodes are to be employed. Saturated liquid metal electrodes (e.g., Pb—PbO [19] or Sn—SnO [20]) are attractive because the relatively high oxygen diffusion coefficients in liquid metals ($\sim 10^{-5}$ cm^2 sec) ensures small concentration overpotentials, and these electrodes can be incorporated into relatively simple cell assemblies [21]. It is easiest, however, to specify solid reference and working electrodes, and both Ni–NiO and Fe–FeO compacts have been employed for this purpose. Cation diffusion rates in the former system, however, are comparatively slow [22] (10^{-10}–10^{-11} cm^2 sec^{-1} at 1000 °C) and Ni–NiO electrodes can exhibit significant overpotentials [23] at 1000 °C even at current densities as low as 5μA cm^{-2}. Iron-wüstite electrodes (D_{Fe} values in FeO vary from 10^{-5}–10^{-7} cm^2 sec^{-1} at 1000 °C) can sustain much higher currents ($\sim 100\mu$A cm^{-2} at 1000 °C) without excessive departures from the equilibrium potential and are generally to be preferred, although reaction with the electrolyte material may sometimes produce erroneous voltages. If the non-stoichiometric phase under examination constitutes the other electrode then polarisation of this electrode will often determine the maximum titration current which can be applied. For example during studies involving coulometric titrations from an Fe–FeO electrode into a wüstite electrode of variable composition, currents as high as 1000μA cm^{-2} were employed by Rizzo et al. [10] without excessive polarisation effects. Coulometric titration experiments by Alcock et al. [9] also involving an Fe–FeO working electrode but with non-stoichiometric rutile ($D_{O^{2-}}$ at 1000 °C: 10^{-13} cm^2 sec^{-1} [25]) as the other electrode material, were limited, however, to currents of 1–5μA cm^{-2}, and even with these small currents subsequent equilibration took at least 24 hours. This need to restrict titration currents to small values for certain electrode systems has lead to developments in the cell design which are described in section 2.3.

Another factor which should always be considered when coulometric titrations involve solid electrodes is the influence of the three phase region where the electrolyte, electrode, and gas phase are all in contact. It is always possible that oxygen ions discharged in the vicinity of this region could form gaseous molecules which would not contribute to changes in the composition of the non-stoichiometric electrode phase.

2.3. Cell Assemblies

Typical cell arrangements that have been used to examine the thermodynamics of variable composition phases are depicted in figures 4–6. Cell assemblies I and II (fig. 4) have been successfully used for many years at Imperial College for equilibrium emf measurements [11, 12, 26]. A special feature of this design is the provision of two separate electrode compartments to eliminate gas phase transfer between the two electrodes via CO and H_2 impurities. The side reactions associated with this process can produce erroneous mixed potentials. Both designs (I and II) can be operated with two separate purified streams of argon or under vacuum conditions (10^{-5}–10^{-6} Torr).

Type I was adopted by U.K.A.E.A., Harwell, for solid state coulometric studies on UO_{2+x} [8] and the accompanying research programme was successfully completed without any major practical difficulties. Studies on TiO_{2-x} and NbO_{2-x} [9] using the type II cell configuration, however, produced many experimental problems which were principally caused by the excessive times required for equilibration following a coulometric titration. Cell assemblies III and IV (fig. 5) were therefore developed in attempts to overcome the limitations

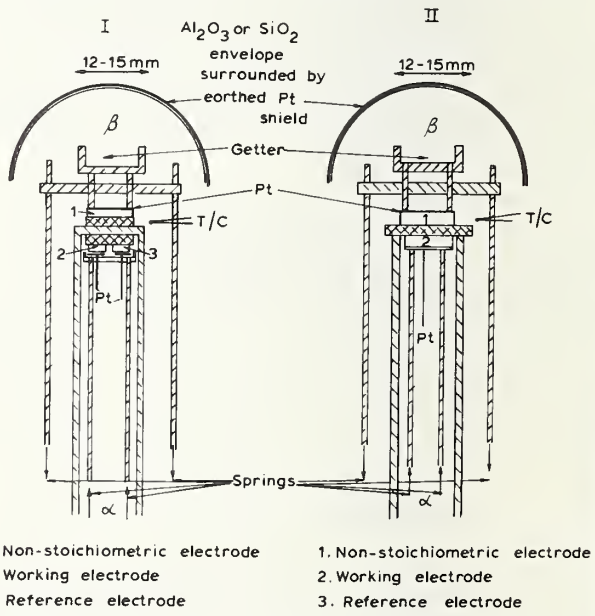

FIGURE 4. *Cell assembly for solid state coulometric titrations (Types I and II).*

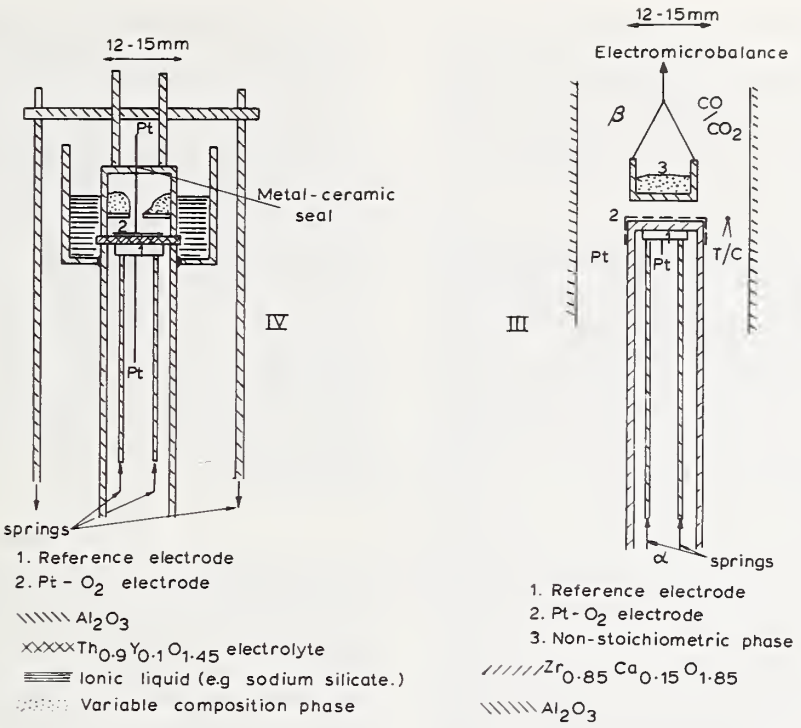

FIGURE 5. *Cell assembly for solid state coulometric titrations (Types III and IV).*

imposed by the relatively slow solid state diffusion processes.

In the type III cell arrangement powdered material consisting of the relevant non-stoichiometric phase was placed in an appropriate inert container and suspended from an electro-microbalance having a sensitivity of $\pm 10^{-5}$ gm. The compositions of both the powdered material and a known volume of a recirculating mixture of CO and CO_2 mutually adjusted to their appropriate equilibrium values and the associated oxygen chemical potential was determined using the solid oxide electrolyte galvanic cell. By means of a coulometric titration a known amount of oxygen was then introduced into the compartment marked β containing the non-stoichiometric phase. The additional oxygen was distributed between the non-stoichiometric phase and the CO–CO_2 mixture. The weight change of the powdered material was recorded by the electro-microbalance, and the oxygen chemical potential developed by the new CO–CO_2 ratio obtained from the relevant e.m.f. measurement. All the measurements should be consistent with the appropriate oxygen mass balance values. It has been impossible, however, to obtain consistent reproducible data with this type III cell arrangement due to problems associated with the oxygen permeability of the zirconia electrolyte tube, and difficulties in selecting the optimum quantities of non-stoichiometric powder and surrounding CO–CO_2 mixture.

In another cell arrangement, type IV depicted in figure 5, an attempt has been made to provide the powdered non-stoichiometric phase with its own gaseous environment in an impermeable alumina crucible, and to alter the composition of this environment (CO–CO_2, or H_2–H_2O) by coulometric titrations using a porous Pt oxygen electrode, which was connected to the external circuit via a platinum-alumina seal incorporated into the alumina container. The relevant surfaces of the alumina container and oxide electrolyte pellets were prepared with a final polish of ¼ micron diamond paste, pressed firmly together, and a relatively impermeable seal was obtained by immersing the alumina-electrolyte interface in an ionic liquid. A sodium silicate having the composition, Na_2O, SiO_2, 25:75 mole percent and melting point ~ 800 °C was usually employed as the sealing fluid. Applications of this modified technique have so far been confined to the TiO_{2-x} system, and preliminary experiments have been encouraging. The gas electrode has allowed titration currents of up to 50μA to be used without excessive polarisation, and subsequent equilibration times have been reduced to 1–3 hours (cf. solid TiO_{2-x}) electrodes. However, at compositions approaching stoichiometry (x in $TiO_{2-x} < 0.001$), and at tempera-

290-621 O-68—12

tures in the range 900 to 1100 °C, the recorded e.m.f.'s exhibited a continual drift with time (1–5 mV per hour) which indicated that the experimental assembly was not sufficiently impermeable to prevent changes in the oxygen content of the gaseous environment of the non-stoichiometric powder.

Two other cell assemblies are depicted in figure 6. Type V has been used by Tretyakov [27] and Flengas [25] to measure equilibrium oxygen chemical potentials of various metal/metal oxide systems. Using a similar configuration it should be possible to vary the composition of a powdered non-stoichiometric phase contained within the solid oxide electrolyte tube. In practice, however, oxygen permeability through the electrolyte tube could be a major problem.

Rapp [29] has designed the type VI cell assembly to determine the solubility and diffusion coefficients of oxygen in solid copper, and the same arrangement can in principle be used to study the thermodynamic behaviour of any solid variable composition phase. The configuration has the advantage of allowing oxygen to be titrated across both faces of the pellet and at the same time minimising the surface area of the pellet in contact with the surrounding gaseous phase.

3. Results

3.1. UO_{2+x}

Using a coulometric technique Markin [8] determined the partial molar free energies of solution of oxygen ($\Delta\overline{G}_{O_2}$) in UO_{2+x} as a function of composition. The reported values are in general agreement with gas equilibration studies and have been the basis for many theoretical models of the defect structure of UO_{2+x} [30]. The high mobility of oxygen ($D_{O_2-} = 10^{-9}$–10^{10} cm^2 sec^{-1} at 1000 °C [31], within

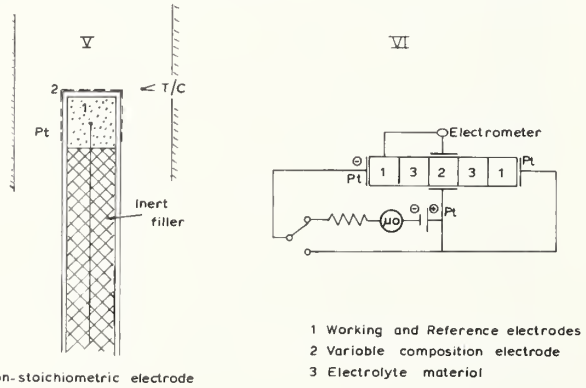

FIGURE 6. *Cell assembly for solid state coulometric titrations (Types V and VI).*

the nonstoichiometric UO_{2+x} phase undoubtedly contributed to this successful application of the coulometric technique. It would be interesting, however, to measure the partial molar heat of solution of oxygen ($\Delta\overline{H}_{O_2}$) at compositions much closer to stoichiometry than those investigated by Markin and his co-workers [8] in an attempt to establish the range of composition for which the simple Wagner-Schottky model is applicable (constant $\Delta\overline{H}_{O_2}$). These studies would be particularly valuable in view of the $\Delta\overline{H}_{O_2}$ values recently determined calorimetrically by Dodé et al. [32]. These coulorimetric values are not in agreement with those derived from the coulometric studies, and additional experiments are required to clarify this uncertainty.

3.2. TiO_{2-x}

Experimental problems associated with coulometric studies on this oxide have already been mentioned in preceding sections, and the results have also been examined in some detail elsewhere [9]. These results are compared in figure 7 with other data obtained using thermogravimetric techniques [33, 34] and the logarithmic plot indicates some difference in the values of the pressure dependence of the defect concentration. The slopes of the isotherms, however, are very sensitive to small changes in the reported composition values which are subject to errors of at least 0.001 in the values of x.

It is more interesting to compare the $\Delta\overline{H}_{O_2}$ values reported as a function of composition in figure 8. The agreement ($\Delta\overline{H}_{O_2} = 108 \pm 5$ kcal) between values obtained in using a thermogravimetric [34], conductivity [35] and coulometric [9] technique is encouraging. Also taking into consideration the different origins of the various TiO_{2-x} samples it does appear that the $\Delta\overline{H}_{O_2}$ values refer to the intrinsic defect properties of rutile and are not determined by the presence of aliovalent cation impurities. Also noteworthy is the comparatively large composition range extending up to a defect concentration of approximately 3×10^{-3} at 1000 °C for which the simple Schottky-Wagner model appears to be applicable (constant $\Delta\overline{H}_{O_2}$). At higher concentrations the partial molar heat term is a function of composition indicating that interaction between the defects is becoming important.

3.3. NbO_{2-x}

Attempts to control the composition of NbO_{2-x} using the coulometric technique and the type II cell assembly (fig. 4) were unsuccessful [9]. Although it

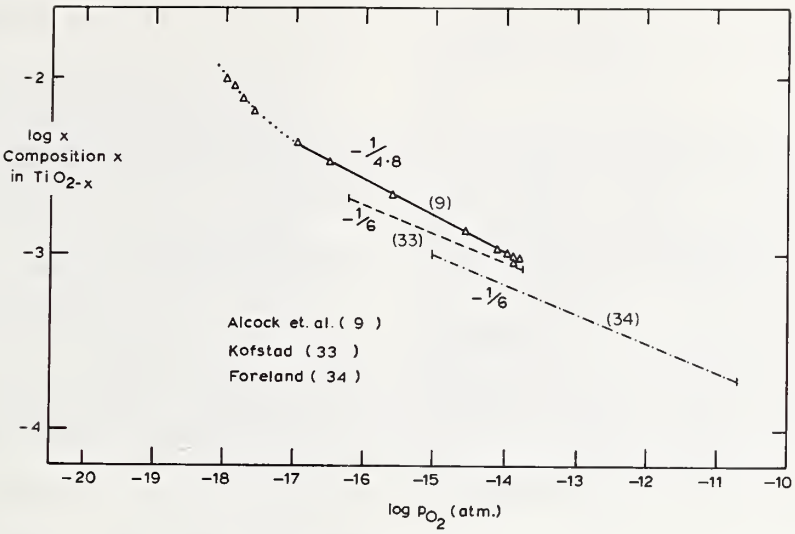

FIGURE 7. *Comparison of results at 1000 °C for the variation of oxygen partial pressure with composition of TiO_{2-x} using a logarithmic plot.*

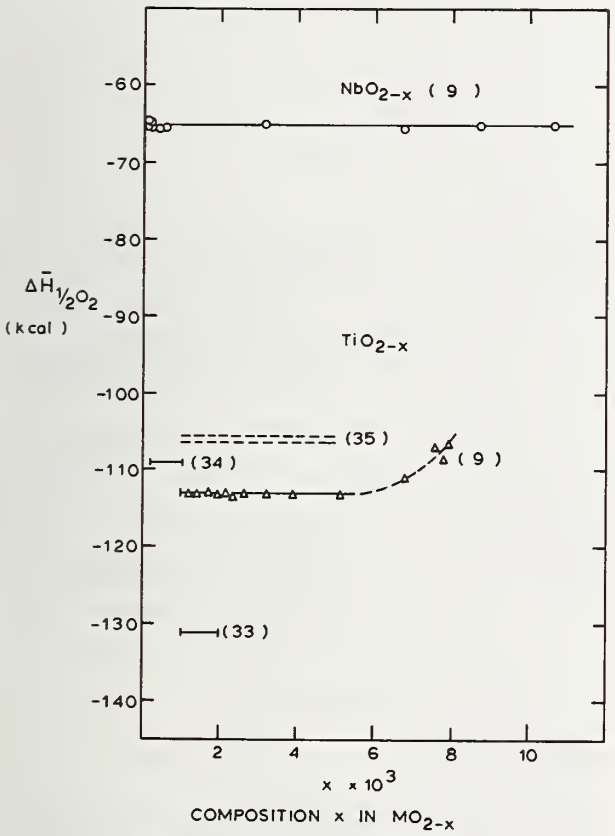

FIGURE 8. *Comparison of partial molar heats of solution of oxygen as a function of composition for TiO_{2-x} and NbO_{2-x}.*

appeared feasible to add oxygen quantitatively to the oxygen-deficient NbO_2, it was found impossible to reverse the process and remove oxygen quantitatively. The slow diffusion process within NbO_{2-x} and the low oxygen chemical potentials involved (-100 kcal $> \Delta\mu_{O_2}$ (1000 °C) > -130 kcal) probably both contributed to the failure of the technique on this occasion. The dependence of composition on the oxygen chemical potential was therefore determined [9] by equilibrating NbO_2 pellets in fixed pH_2/pH_2O gas mixtures, followed by emf measurements and gravimetric analyses. These data produced a constant value for $\Delta\bar{H}_{1/2O_2}$ (-65 kcals) over a wide range of composition (fig. 8), and long annealing times (~ 100 hrs) for compositions exhibiting large departures from stoichiometry ($x \sim 0.01$) failed to produce any evidence for ordering processes due to the absence of any super lattice lines (x-ray examination), or changes in the values for $\Delta\bar{H}_{1/2O_2}$. It would be interesting to examine whether the composition of this phase could be controlled by coulometric titrations using the modified Type IV cell assembly (fig. 5).

3.4. VO_{2-x} and MoO_{2-x}

Problems associated with the fabrication of dence strong pellets of MoO_{2-x} and VO_{2-x} have necessitated that coulometric studies [36] on the thermodynamic properties of these phases be conducted with powdered samples suspended from an electrical microbalance in the type III cell configuration (fig. 5). As reported earlier (section 2.3), however, it proved impossible to adequately control the oxygen content of the gas phase due to the permeability of the zirconia electrolyte tube and these studies have so far been inconclusive.

4. Conclusions

The present survey indicates that solid state coulometric titrations can provide a convenient

and reliable method for investigating the thermodynamics of nonstoichiometric phases possessing high ionic mobilities and equilibrium oxygen partial pressures in the range, $10^{-8} > p_{O_2}$ atm (1000 °C) $> 10^{-16}$ atm (e.g., UO_{2+x} and FeO_{1+x}). However, slow solid state diffusion processes combined with relatively fast reactions between nonstoichiometric electrode materials and the surrounding gaseous environment at present severely limit the application of this technique. Further developments of the method are probably dependent upon the design of alternative cell assemblies which are able to maintain the appropriate equilibrium oxygen partial pressure above the nonstoichiometric phase, and thus allow the relevant electrode system at any given temperature and composition to behave as an invariant system.

The comments on the modified cell designs are based on experimental work performed by Miss S. Zador and Mr. J. Chan of the Metallurgy Department, Imperial College.

5. References

[1] C. Wagner, Thermodynamics of Alloys (Publ. by Addison-Wesley, Reading, Mass. (1952).
[2] J. S. Anderson and B. G. Hyde, J. Phys. Chem. Solids, 1967, **28**, 1393–1408.
[3] S. Kachi and P. Roy, Phase Equilibrium Studies and Transitions in the System V_2O_3–V_2O_5, presented at the 67th Annual Meeting, American Ceramic Society, 15th May, 1965 (Basic Science Division No. 80–B–65).
[4] A. S. Khan, Intermediate Oxides of Vanadium and Titanium, D. Phil. Thesis, Oxford University, November 1967.
[5] C. Wagner, J. Chem. Phys., **21**, 1819 (1953).
[6] J. B. Wagner and C. Wagner, J. Chem. Phys., 1957, **26**, 1602.
[7] K. Kiukkola and C. Wagner, J. Electrochem. Soc., 1957, **104**, 379–386.
[8] T. C. Markin and R. J. Bones, United Kingdom Atomic Research Authority, Report No. 4178.
[9] C. B. Alcock, S. Zador and B. C. H. Steele, Proc. Brit. Ceram. Soc. 1967, No. 8, 231–245.
[10] H. F. Rizzo, R. S. Gordon, and I. B. Cutler, Determination of Thermodynamic Properties in Single Phase Wüstite by Coulometric Titration in a High Temperature Galvanic Cell, presented at the National Bureau of Standards Conference on 'Mass Transport in Oxides' (24th October 1967).
[11] B. C. H. Steele and C. B. Alcock, Trans. A.I.M.E. 1965, **233**, 1359–67.
[12] C. B. Alcock and S. Zador, Electrochim. Acta, 1967, **12**, 673–7.
[13] B. C. H. Steele in Electromotive Force Measurements in High Temperature Systems, to be published by the Inst. of Mining and Metallurgy, London, April, 1968.
[14] P. W. Patterson, E. C. Bogren, and R. A. Rapp, J. Electrochem. Soc. 1967, **114**, 752–758.
[15] E. W. Roberts, Permeability Studies on Refractory Oxide Systems, Ph.D. thesis, Leeds University U.K. (September, 1966).
[16] R. Fabre, Etude de la Permeabilite aux Gaz des Ceramiques d'oxydes a Haute Temperature, doctoral thesis, Grenoble University, France (July, 1967).
[17] H. Smith, Metallurgy Department, Imperial College, private communication.
[18] S. V. Karpachev, A. T. Filyayev, and S. F. Palguev, Electrochim, Acta., **9**, 1681–5 (1964).
[19] C. B. Alcock and T. N. Belford, Trans. Faraday Soc. 1964, **60**, 822–835.
[20] C. B. Alcock, and T. N. Belford, Trans. Faraday Soc. 1965, **61**, 443–453.
[21] G. P. Stavropoulos, Physicochemical Studies Associated With the Electrochemical Measurement of the Solubility of Oxygen in Liquid Sodium, Ph.D. thesis, London University, June 1967.
[22] J. S. Choi and W. J. Moore, J. Phys. Chem. 1962, **66**, 1308–11.
[23] B. C. H. Steele, Thermodynamic Studies Using Galvanic Cells With Solid Electrolytes, Ph.D. thesis, London University, July 1965.
[24] L. Himmel, R. F. Mehl and C. E. Birchenall, Trans. A.I.M.E., 1953, **197**, 827–843.
[25] R. Haul and G. Dumbgen, J. Phys. Chem. Solids, 1965, **26**, 1–10.
[26] A. Kubik and C. B. Alcock, Metal Sci. J., 1967, **1**, 19–24.
[27] Y. D. Tretyakov, Inorg. Materials, 1966, **2**, 432–6.
[28] G. G. Charette and S. N. Flengas, Dept. of Metallurgy and Materials Science, University of Toronto, Canada, submitted for publication in J. Electrochem. Soc.
[29] R. A. Rapp, Mixed Conduction in Solid Oxide Electrolytes, presented at the I.A.E.A. Conference in Vienna, Sept. 1967.
[30] L. E. J. Roberts and T. L. Markin, Proc. Brit. Ceram. Soc. No. 8, 201–217 (1967).
[31] A. B. Auskern and J. Belle, J. Chem. Phys. 1958, **28**, 171.
[32] M. Dodé and P. Gerdanian, Comptes Rendues 1966, **262**, 796–799.
[33] P. Kofstad, J. Phys. Chem. Solids, 1962, **23**, 1579–1586.
[34] K. Forland, Acta Chem. Scand., 1964, **18**, 1267.
[35] R. N. Blumenthal, J. Coburn, J. Baukus, and W. M. Hirthe, J. Phys. Chem. Solids 1966, **27**, 643–654.
[36] S. Zador, Metallurgy Department, Imperial College, Private Communication.
[37] L. A. Simpson and R. E. Carter, J. Am. Ceram. Soc. 1966, **49**, 139–144.
[38] W. H. Rhodes and R. E. Carter, J. Am. Ceram. Soc. 1966, **49**, 244–249.
[39] H. S. Edwards, A. F. Rosenburg and J. T. Bittel, Tech. Doc. Report No. A5D–63–635 (1963), General Electric Co.
[40] R. J. Hawkins, Cation Diffusion in Fluorite Lattices, Ph. D. thesis, London University, Feb. 1967.

Interdiffusion Coefficients From Electronic Conductivity Measurements—Application to Cu_2O

R. H. Campbell, W. J. Kass and M. O'Keeffe

Chemistry Department, Arizona State University, Tempe, Arizona 85281

The interdiffusion of oxygen and cuprous oxide has been followed by monitoring the electrical conductivity of single crystal cuprous oxide specimens. The measured values are in good agreement with the values calculated from the tracer diffusion coefficient of copper and the departure from stoichiometry using the Darken equation.

Key Words: Cuprous oxide, electrical conductivity, interdiffusion, nonstoichiometry.

Introduction

In many non-stoichiometric oxides with ionized vacancies, the conductivity is proportional to the departure from the ideal composition. This is the case for example in CoO [1].[1] In Cu_2O the conductivity is accurately proportional to the square root of the copper vacancy concentration (as shown by the oxygen pressure dependence of conductivity [2] and departure from stoichiometry [3]). It would appear possible therefore to use conductivity as a measure of composition of the sample, and indeed several authors [4] have used this fact to follow the kinetics of interdiffusion in oxides.

It is necessary however to proceed with caution as in general the apparent conductance of an inhomogeneous sample is not proportional to the average concentration of defects. Provided that there is local electrical neutrality (i.e., in the absence of a space charge), it is possible however, to relate the local conductivity σ to the local concentration of defects, c.

Theory

We have considered the case of a rectangular prism $-a_1 < x_1 < a_1, -a_2 < x_2 < a_2, -a_3 < x_3 < a_3$ with porous electrodes on the x_1, x_2 faces so that the conductance can be measured in the x_3 direction. We suppose that the initial conductivity σ_i is due to an initial homogeneous concentration of defects c_i. For times greater than zero the surface concentration is held at c_f so that the conductivity comes to a value σ_f as $t \to \infty$. The concentration at any point in the material is then given by the well-known expression

$$c(x_1, x_2, x_3) = c_f - (c_f - c_i)S(\xi_1)S(\xi_2)S(\xi_3), \quad (1)$$

where

$$S(\xi_1) = (2/\pi) \sum_{n=0}^{\infty} [(-1)^n/(n+1/2)]$$

$$\exp[-\beta_i(n+1/2)^2\pi^2] \cos[(n+1/2)\pi\xi_i], \quad (2)$$

and in turn

$$\xi_i = x_i/a_i; \quad \beta_i = Dt/a_i^2. \quad (3)$$

The local conductivity is $\sigma(x_1, x_2, x_3)$ and as discussed above we have

$$\sigma(x_1, x_2, x_3) = A[c(x_1, x_2, x_3)]^m, \quad (4)$$

with A a constant and m usually 1 or ½.

The apparent conductivity, $\bar{\sigma}$, measured in the x_3 direction is obtained by multiplying the conductance of the sample by the length/area ratio and is related to the local conductivity by

$$\bar{\sigma} = \frac{a_3}{2a_1a_2}\left[\int_{-a_3}^{a_3} \frac{dx_3}{\int_{-a_1}^{a_1}\int_{-a_2}^{a_2} \sigma\, dx_2\, dx_1}\right]^{-1} \quad (5)$$

From eqs (5), (4) and (1) one obtains after some manipulation

$$\sum \equiv \frac{\sigma_f - \bar{\sigma}}{\sigma_f - \sigma_i} = \frac{1}{1-\alpha}\left[1 - \left(\int_0^1 I^{-1}\, d\xi_3\right)^{-1}\right], \quad (6)$$

[1] Figures in brackets indicate the literature references at the end of this paper.

where $I=\int_0^1\int_0^1 [1+(\alpha^{1/m}-1)S(\xi_1)S(\xi_2)S(\xi_3)]^m \, d\xi_1 d\xi_2$,

and $\alpha=\sigma_i/\sigma_f$.

It is of interest to compare Σ as given by eq (6) with the corresponding quantity $W\equiv(w_f-w)/(w_f-w_i)$ where w_f and w_i are the final and initial amounts of defects. The explicit expression for W is given in ref. [4].

In figure 1 we show W and Σ as a function of the dimensionless quantity Dt/a_3^2 for various shape samples and values of σ_f/σ_i for the case $m=1$. It may be seen that in general W and Σ are very close to each other for long, thin samples when σ_f/σ_i is not very different from unity. In other cases however the assumption that $\Sigma=W$ may lead to large errors in the calculated diffusion coefficients.

Application to Cuprous Oxide

Attempts to study interdiffusion in cuprous oxide using a vacuum microbalance technique were severely limited by the nature of the material. Specifically, at temperatures above 1000 °C evaporation is very rapid so that the small weight changes upon change of stoichiometry are hard to determine. At lower temperatures the cuprite phase field is very narrow, again precluding reliable measurements. For these reasons we decided to resort to electrical measurements in this system.

Two single crystal specimens were used; sample 1 was $4.50\times4.65\times6.34$ mm and sample 2 was $1.91\times1.91\times15.9$ mm. In each case the conductivity was measured along the longest direction using two probes. After equilibration at low oxygen pressure, oxygen was rapidly admitted to the sample and the conductivity monitored as a function of time. Strictly, in order to use the expressions derived above for Σ, porous contacts covering the whole face of the crystal should be used. The use of smaller contacts is likely to be less serious in the case of sample 2. As conductivity changes are very rapid, the sample current with known constant applied voltage was recorded with a recorder speed of 6 inches/minute. Plots of Σ versus log t were superimposed on theoretical plots of Σ versus log (Dt/a_3^2) calculated according to eq (6). The difference in the abscissa of the two plots is equal to log (D/a_3^2) so that D is readily calculated. As the conductivity is very temperature sensitive it is quite possible to measure erroneous values of σ_f; however, this becomes evident when the experimental curve is compared to the theoretical curve, and any experimental results differing significantly from the theory were rejected.

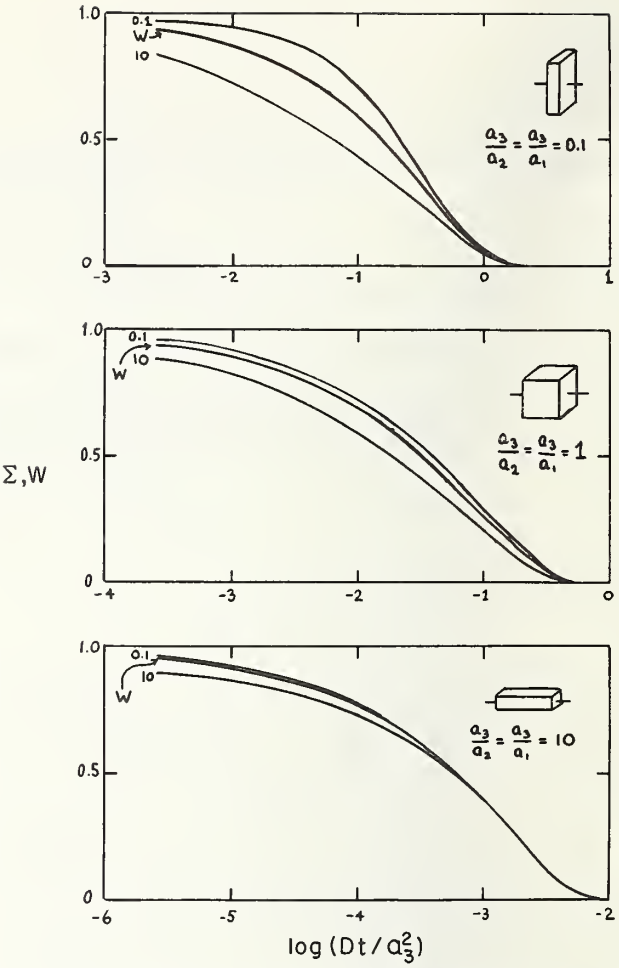

FIGURE 1. *Thereotical curves for conductivity and weight change as a function of time for various shape samples.*

The numbers on the curves are the values of σ_i/σ_f. The curves labeled W refers to weight change, the others to conductivity change.

Because of the very rapid diffusion observed there was considerable scatter of the experimental results. These are reported in table 1 with results for each crystal at each temperature reported as an average. The results for sample 2 were in general better and are in fair agreement with the theoretical values (discussed below). The results for sample 1 are too high; it is not clear at present whether this is due to the fact that the experimental conditions did not conform to the boundary conditions used in deriving eq. (6) or whether effects such as surface diffusion are significant.

Theory for Cuprous Oxide and Comparison With Experiment

We can calculate the expected interdiffusion coefficient as follows. Neglecting oxygen diffusion, which has been shown to be very much slower than copper diffusion [5], the rate of interdiffusion of

oxygen and Cu_2O_{1+x} is given by the Darken equation [6]

$$\widetilde{D} = (1/f) D^*_{Cu} (\mathrm{dln}\, a_{Cu} / \mathrm{dln}\, c_{Cu}), \tag{7}$$

where $\widetilde{D}$ is the measured interdiffusion coefficient, D^*_{Cu} is the tracer diffusion coefficient and f is a correlation factor to take into account the fact that successive jumps of the tracer atom will not be random. For a face-centered cubic lattice (as in the case for Cu^+ in Cu_2O) $f = 0.78$. In the final factor in eq. (7) a_{Cu} is the activity of copper in cuprous oxide and c_{Cu} the concentration of copper.

According to Moore and Selikson [7] at an oxygen pressure of 0.1 torr

$$\log_{10} D^*_{Cu} = -1.36 - 7900/T. \tag{8}$$

We have also that

$$a^2_{Cu} a_o = a_{Cu_2O},$$

where a_o is the activity of oxygen and to an excellent approximation a_{Cu_2O} is constant, so that

$$\mathrm{dln}\, a_{Cu} = -(1/2)\, \mathrm{dln}\, a_o \tag{9}$$

or, as a_o is proportional to the square root of the oxygen pressure,

$$\mathrm{dln}\, a_{Cu} = -(1/4)\, \mathrm{dln}\, P_{O_2} \tag{10}$$

In terms of the stoichiometric excess of oxygen, x, we have also for the concentration of copper, measured in fraction of sites occupied,

$$c_{Cu} = (2 - x)/2 \tag{11}$$

or, recalling that $x \ll 1$,

$$\mathrm{dln}\, c_{Cu} = -dx/2 \tag{12}$$

so that finally

$$\mathrm{dln}\, a_{Cu} / \mathrm{dln}\, c_{Cu} = (1/2x)\, (\mathrm{dln}\, P_{O_2} / \mathrm{dln}\, x) \tag{13}$$

O'Keeffe and Moore [3] found by direct gravimetry that at $P_{O_2} = 0.1$ torr

$$\log_{10} x = 0.02 - 4760/T' \tag{14}$$

and

$$(\mathrm{dln}\, P_{O_2} / \mathrm{dln}\, x) = 3.7 \tag{15}$$

Substituting into eq. (7) the appropriate values from eqs. (8), (13), (14) and (15), we obtain finally for the calculated rate of interdiffusion

$$\log_{10} \widetilde{D} = 1.00 - 3140/T \tag{16}$$

It should be remarked at this point that the only assumptions made about the mechanism of diffusion are (a) that oxygen diffusion is negligibly slow and (b) that the correlation factor is 0.78. In particular it should be emphasized that if there is a diffusion potential and there is ambipolar diffusion of mobile holes and less mobile vacancies this factor is already included in the term $(\mathrm{dln}\, a_{Cu} / \mathrm{dln}\, c_{Cu})$ in eq. (7). This point has been discussed at some length elsewhere [8]; the general validity of eq. (13) is illustrated by a consideration of two specific models in the appendix.

We turn now to a comparison of the experimental results with the theoretical expression, eq (16). In table 1 we have recorded the experimental interdiffusion coefficients for both samples at a number of temperatures. Also in the table are the diffusion coefficients calculated from eq (16). For sample 2 the agreement with the calculated values is very good; sample 1 gives values that are consistently too high. We believe that the discrepancy for sample 1 arises because the theoretical conductivity curves were calculated for contacts covering the whole face of the crystal, whereas in fact "point" contacts were used. As the area of the contact faces was small in comparison to the area of the other faces for sample 2, the error should not be so great for this sample.

The agreement between theory and experiment for sample 2 is very gratifying when it is recalled that the results of three separate measurements (interdiffusion, tracer diffusion and nonstoichiometry) are being compared. The most difficult measurement is that of the degree of nonstoichiometry, x, and we consider the present measurements to be a valuable confirmation of the order of magnitude at least of the previously reported results.

The $\widetilde{D}$ reported here may be interpreted as a vacancy diffusion coefficient. The very high dif-

TABLE 1. *Measured and calculated values of* $\log_{10} \widetilde{D}$ *in* Cu_2O.

T °C	Sample 1 [a]	Sample 2 [a]	Calculated [b]
933 ± 1	−3.4 (1)	−3.6 (2)	−3.60
973 ± 1	−3.15 (5)	−3.4 (2)	−3.52
1001 ± 1	−3.2 (3)	−3.75 (4)	−3.46
1032 ± 1	−2.6 (2)	−3.45 (3)	−3.40
1064 ± 1	−2.5 (2)	−3.4 (5)	−3.36

[a] Numbers in parentheses are the number of separate measurements at that temperature.

[b] Calculated from eq (16).

fusion coefficients are in accord with the observation that internal equilibrium can readily be reached in cuprous oxide down to very low temperatures [2, 9]. It is worth remarking also that in general cation mobility is very high in the chalcogenides of the univalent metals.

This research was supported by the Air Force Office of Scientific Research, Office of Aerospace Research, United States Air Force, under AFOSR grant Nr. AF-AFOSR-717-65.

Appendix

We consider here more fully the question of a diffusion potential and demonstrate that the validity of eq (13) is not dependent on a particular model for the incorporation of oxygen in cuprous oxide. Two possible models are considered:

(a) production of neutral cation vacancies

$$\text{crystal} \rightarrow V_{Cu} + Cu_{(gas)}; \tag{A1a}$$

(b) production of charged (ionized) vacancies

$$\text{crystal} \rightarrow V_{Cu}^{n-} + ne^{+} + Cu_{(gas)}. \tag{A1b}$$

In either case, assuming as before that the activity of the crystal is constant, and assuming local thermodynamic equilibrium, we have the equilibrium constants:

$$a_{Cu}a(V_{Cu}) = K_a, \tag{A2a}$$

$$a_{Cu}a(V_{Cu}^{n-})a^{n}(e^{+}) = K_b. \tag{A2b}$$

Here the activities, a, are defined in terms of the *electrochemical* potential μ, by

$$a = \exp[(\mu - \mu^{\circ})/RT]. \tag{A3}$$

In a dilute solution of ions of charge Z

$$a = c \exp(Ze\phi/kT), \tag{A4}$$

where Z is the valence of the ion, c is the concentration, measured most conveniently as site fraction, and ϕ is the local electrostatic potential. Thus

$$a(V_{Cu}) = x/2,$$

$$a(V_{Cu}^{n-}) = (x/2) \exp(-ne\phi/kT),$$

$$a(e^{+}) = (nx/2) \exp(e\phi/kT).$$

The equilibrium constants of eqs (A2) now become

$$a_{Cu}(x/2) = K_a, \tag{A5a}$$

$$a_{Cu}(x/2)(nx/2)^{n} = K_b. \tag{A5b}$$

It should be noted that the local electrostatic potential does not appear in these expressions.

It is now possible to evaluate the terms in eq (13); as previously we restrict ourselves to the situation where $x \ll 1$ so that $\ln c_{Cu} \approx (-x/2)$, and obtain:

$$\text{Case (a)} \quad d\ln a_{Cu}/d\ln c_{Cu} = (2/x); \tag{A6a}$$

$$\text{Case (b)} \quad d\ln a_{Cu}/d\ln c_{Cu} = [2(n+1)/x]. \tag{A6b}$$

On the other hand using eq (10) it may be seen that from eqs (A5):

$$\text{Case (a)} \quad d\ln P_{O_2}/d\ln x = 4; \tag{A7a}$$

$$\text{Case (b)} \quad d\ln P_{O_2}/d\ln x = 4(n+1). \tag{A7b}$$

In both cases eqs (A6) and (A7) yield

$$d\ln a_{Cu}/d\ln c_{Cu} = (1/2x)(d\ln P_{O_2}/d\ln x), \tag{13}$$

as we set out to demonstrate.

Finally it may be remarked that the result, eq (15), quoted indicates strongly that case (a) obtains in cuprous oxide (cf. eq (A7a)). Recent high temperature Hall-effect measurements [10] confirm this observation.

References

[1] B. Fisher and D. S. Tannhauser, J. Electrochem. Soc., **111**, 1194 (1964).
[2] R. S. Toth, R. Kilkson and D. Trivich, Phys. Rev., **122**, 482 (1961); M. O'Keeffe and W. J. Moore, J. Chem. Phys., **35**, 1324 (1961).
[3] M. O'Keeffe and W. J. Moore, J. Chem. Phys., **36**, 3009 (1962).
[4] J. B. Price and J. B. Wagner, Z. phys. Chem. (N.F.), **49**, 257 (1966); L. C. Walters and R. E. Grace, J. Phys. Chem. Solids, **28**, 245 (1967); D. G. Thomas, J. Phys. Chem. Solids, **3**, 229 (1957).
[5] W. J. Moore, Y. Ebisuzaki and J. Sluss, J. Phys. Chem., **62**, 1438 (1958); M. O'Keeffe, Y. Ebisuzaki and W. J. Moore, J. Phys. Soc. Japan, **18**, 131 (1963).
[6] L. S. Darken, Trans. Met. Soc. AIME, **175**, 184 (1948).
[7] W. J. Moore and B. Selikson, J. Chem. Phys., **19**, 1539 (1951); **20**, 927 (1952).
[8] M. O'Keeffe, Diffusion in Oxides and Sulfides in Sintering and Related Phenomena (G. C. Kuczynski, Ed.), Gordon and Breach, N.Y. (in press).
[9] M. O'Keeffe and F. S. Stone, Proc. Roy. Soc. (Lond.), **A267**, 501 (1962).
[10] H. L. McKinzie and M. O'Keeffe, Phys. Lett. **24A**, 137 (1967).

A Chemla Experiment in BeO [1]

C. F. Cline, H. W. Newkirk, R. H. Condit, and Y. Hashimoto

Lawrence Radiation Laboratory, University of California, Livermore, California 94550

The drift of Be^7 tracer in BeO at 1550 °C under the influence of an externally applied d-c electric field was determined by a sectioning technique. Reasonable agreement was obtained with the Nernst-Einstein relation.

Key Words: Diffusions, electrical conductivity, tracer diffusion.

The drift of a radioactive tracer under the influence of a d-c electric field has been described by Chemla [1] [2] and referenced by others [2, 3]. In this case, the diffusion equation for a cation tracer is

$$\frac{dc}{dt}=D\frac{d^2c}{dx^2}-\mu E\frac{dc}{dx}, \tag{1}$$

where C is the concentration of the tracer, D is the diffusion coefficient, μ is the ion mobility of the tracer, and E is the electric field strength. For an anion, the term in E would be positive. The net effect of the electric field is simply to displace the center of gravity of the diffusion distribution profile by a distance,

$$\Delta x=\mu Et. \tag{2}$$

There is no other distortion of the distribution profile if the field is homogeneous in the region of diffusion. Experimentally, two flat slabs are pressed together with a thin layer of radiotracer between them, and a high-temperature anneal is carried out with the electric field imposed normal to the plane. The resultant distribution of tracer can be analyzed in terms of the distance, x, from the initial interface,

$$C(x)/C_0=\frac{1}{\sqrt{4\pi Dt}}\exp-\frac{(x-\Delta x)^2}{4Dt} \tag{3}$$

where C_0 is the initial amount per unit area and $C(x)$ is the concentration at a distance, x. Thus, the mobility can be found from an experimental determination of the center of gravity of the profile since the maximum of the bell-shaped profile moves away from the interface with a velocity, μE. The diffusion coefficient can be obtained in the usual way from the shape of the profile, i.e., from plot of log C versus $(x-\Delta x)^2$.

The work reported here was concerned with measurement of the mobility of Be^7 tracer in BeO. The material used was the same as that previously employed in studies of self-diffusion in BeO [4]. It was 98 percent dense, contained grains averaging 30 microns, major impurities were Al (200 ppm) and Si (50 ppm). BeO has the hexagonal, wurtzite crystal structure, and there is a preferred crystallographic orientation among the grains; the majority of the c-axes of the crystallites were at right angles to the field direction. Three pieces were prepared with front and back sides made parallel, the tracer was deposited on the polished faces by a technique previously described [4], and the individual pieces were assembled as shown in figure 1. The attachment of electrodes to the stack and the placement of electrodes used to measure the potential drop across each interface are also shown. Platinum electrodes were used on the end samples, and a potential of 30 volts was supplied throughout the run. The current passing through the assembly was monitored by a recording ammeter. The duration of the anneal was 5.15×10^5 seconds and the temperature 1550 °C. While there was a considerable voltage drop at the electrode BeO interface, the field strength was only about 10.0 volts per centimeter in the neighborhood of the tracer.

Following the anneal, the distribution of tracer in the region between the samples 1–2 and 2–3 was determined by sectioning. The resulting concentration profile is shown in figure 2.

If the tracer had behaved ideally, the profiles in figure 2 would follow eq (3) and have a relatively smooth, displaced bell shape. However, there is some barrier to completely free interchange of

[1] Work performed under the auspices of the U.S. Atomic Energy Commission.

[2] Figures in brackets indicate the literature references at the end of this paper.

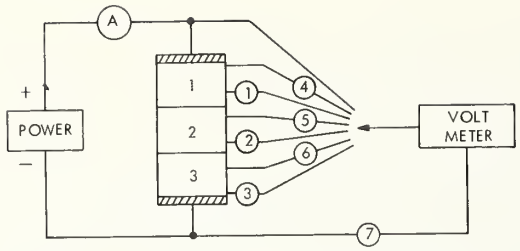

FIGURE 1. *Circuit diagram.*

tracer between pieces of BeO. One also sees an apparent decrease in activity concentration near the surface, but this is probably due to slight pitting of the specimens when they are pulled apart after the anneal. The tails of the profiles are enhanced by grain boundary diffusion.

Since the 1–2 interface exhibited much greater surface holdup (fig. 2) than the 2–3 interface, the latter was used for all calculations. The displacement of the center of gravity of the diffusion profile can be estimated as 20 microns for interface 2–3. In both cases, the drift of the tracer was toward the cathode. Using this displacement and a field gradient of 10 V/cm, the mobility calculated from eq (2) is found to be 3.9×10^{-10} cm^2-volt^{-1}-sec^{-1}

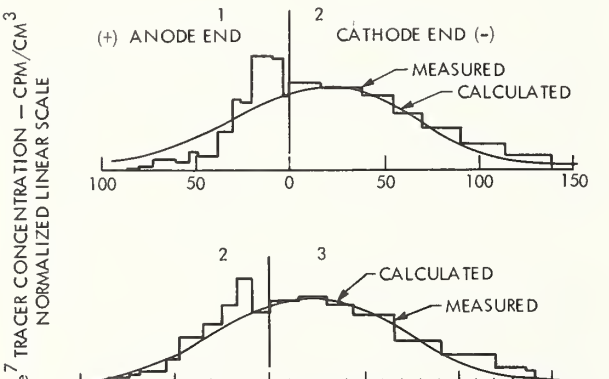

FIGURE 2. *Be^7 tracer distribution profiles.*

It now becomes possible to calculate the diffusion coefficient for Be^{+2} ions from the mobility through use of the Nernst-Einstein relationship,

$$D_i=\frac{\mu RT}{zF} \tag{4}$$

where R is Boltzmann's constant, 8.31 joules deg^{-1} mole^{-1}, F is a Faraday, 9.65×10^4 coulomb mole^{-1} and Z, the charge per ion, is 2. One finds at the 2–3 interface, $D_i=3.05\times10^{-11}$ cm^2-sec^{-1}.

The diffusion coefficient as obtained by tracer techniques, D_{sd}, is related to that obtained from ionic transport measurements, D_i, by the correlation coefficient [2, 3],

$$f=D_{sd}/D_i. \tag{5}$$

Using 0.78 for f [5, 6, 7], one calculates a D_{sd} of 2.38×10^{-11} cm^2-sec^{-1}. Substituting the time and D_{sd} back into eq (3), one can calculate the diffusion profile. This calculated curve is shown in figure 2, and it appears to agree fairly well with the measured points. The diffusion coefficient calculated here is only about 40 percent of the value to be expected on the basis of previous measurements [4]. But this is not a serious disagreement in view of the scatter in the data.

In conclusion, it has been found that Be tracer migrates toward the cathode at a rate which tends to support the view that electrical conductivity in BeO is by a mechanism involving beryllium ion diffusion.

The authors are indebted to Prof. C. E. Birchenall and Drs. L. Himmel and R. Borg for reviewing the manuscript.

References

[1] M. Chemla, Diffusion of Radioactive Ions in Crystals, Ann. Phys. (Paris) ser. 13, **1**, 959. Also UCRL-Trans 1038(L) (1956).

[2] A. B. Lidiard, Ionic Conductivity, Handbuch der Physik **20**, 246 (1957).

[3. J. R. Manning, Isotope Effect in an Electric Field and Jump Frequencies for Diffusion in Ionic Crystals, J. Appl. Phys. **33**, 2145 (1962).

[4] R. H. Condit and Y. Hashimoto, Self-Diffusion of Beryllium in Beryllium Oxide, J. Am. Ceram. Soc. **50**, 425 (1967).

[5] K. Compaan and Y. Haven, Correlation Factors for Diffusion in Solids, Part 2—Indirect Interstitial Mechanism, Trans. Faraday Soc. **54**, 1498 (1958).

[6] H. J. de Bruin, G. M. Watson, and C. M. Blood, Cation Self-Diffusion and Electrical Conductivity in Polycrystalline BeO, J. Appl. Phys. **37**, 4543 (1966).

[7] C. F. Cline and H. W. Newkirk, Electrical Transport Processes in Beryllium Oxide, to be published.

Self-Diffusion of Oxygen in Neodymium and Samarium Sesquioxide

G. D. Stone, G. R. Weber and L. Eyring

Department of Chemistry, Arizona State University, Tempe, Arizona 85281

The oxygen self-diffusion coefficients were measured for Nd_2O_3 (*A*-type) and Sm_2O_3 (*B*-type) and an estimate was made for the diffusion coefficient of Er_2O_3 (*C*-type) at 1000 °C using the method of isotope exchange. The rate of change of ^{18}O in the gas phase in equilibrium with a solid sample was measured by a mass spectrometer. The enriched oxygen gas was circulated over the sample and through a leak valve which continuously admitted a small amount of the gas directly into the analyzer of the mass spectrometer. The solid samples were in the form of spheres prepared in an argon plasma. Over the range of pressures used (30 to 300 mm Hg), there was no pressure dependence noticed. The self-diffusion coefficients as a function of temperature, determined in the range of 700 to 1000 °C using an exact solution of Fick's second law with a first order exchange reaction at the surface, were

$$Sm_2O_3\ (99.9\%),\quad D = 9.2\times10^{-6}\exp(-23.5\pm2\ \text{kcal}/RT)$$
$$Sm_2O_3\ (99.998\%),\ D = 6.0\times10^{-6}\exp(-21.3\pm.5\ \text{kcal}/RT)$$
$$Nd_2O_3\ (99.999\%),\ D = 1.3\times10^{-4}\exp(-31.\ \pm2.\ \text{kcal}/RT)$$

The value for the diffusion coefficient of Er_2O_3, estimated at 1000 °C, was 10^{-14} cm²/sec. The low value measured for the heat of activation and the lack of pressure dependence indicated that the diffusion was probably extrinsic. While the systematic errors were large, the measured values for the heats of activation indicated a possible correlation to structure and the lanthanide contraction.

Key Words: Oxygen isotope exchange, rare-earth oxides, self diffusion.

1. Introduction

In the study of the rare earth oxides, there have been many indications that oxygen is much more mobile than the cations. For example, in praseodymium and some of the other rare earth oxides of variable valence, tensimetric studies have shown that the solid reaches equilibrium with oxygen very rapidly after a change in the oxygen gas pressure. This has been observed as low as 400 °C; far below the Tammann temperature where the cations should be mobile [1, 2].[1] In the oxidation of praseodymium metal, scratches on the surface appeared unchanged after the formation of a dense oxide layer upon complete oxidation, indicating that oxygen was the mobile species [3]. Oxygen mobility has also been shown to be important in the vacuum reduction of $PrO_{1.71}$ where the self-diffusion coefficients for oxygen for particles 0.5 microns in diameter have been estimated to be [4]

$$D = 1.5\times10^{-9}\ \text{cm}^2/\text{sec at 990 °C}$$
$$D = 1.7\times10^{-11}\ \text{cm}^2/\text{sec at 700 °C.}$$

In a more recent study on the oxidation of rare earth metals, an estimate of 10^{-8} cm²/sec at 1600 °C was made for the self-diffusion coefficient of oxygen through the oxide coating [5]. Using slightly reduced Y_2O_3 (*C*-type) and Er_2O_3 (*C*-type), diffusion coefficients for oxygen were recently given as a function of temperature by the relations [6]

$$Y_2O_3,\ D = 7.24\exp(-58.6\ \text{kcal/RT}),\quad \text{for 1000 to 1500 °C}$$
$$Er_2O_3,\ D = 1.22\exp(-47.8\ \text{kcal/RT}),\quad \text{for 850 to 1250 °C.}$$

All of these measurements indicated that the self-diffusion coefficient of oxygen in the rare earth oxides appeared to be much greater than those observed for some other transition metal oxides; for example, TiO_2 has a value about 10^{-13} cm²/sec at 1000 °C [7].

In order to improve understanding of the apparent high mobility of oxygen, it was desirable to measure the self-diffusion of oxygen and its temperature and pressure dependence by a more direct method. The method chosen for the study was that of heterogeneous isotope exchange. This study was

[1] Figures in brackets indicate the literature references at the end of this paper.

of fixed valence oxides to see if a correlation could be made between the diffusion coefficients and structure. However, the apparatus was designed to study either fixed or variable valence materials. Since the high temperatures used in the preparation of the samples and the conditions of the exchange experiments did not allow the use of one cation for the three major polymorphic forms of the sesquioxide (*A*, *B*, and *C*-type), three different rare earths were used: Nd_2O_3 (*A*-type), Sm_2O_3 (*B*-type), and Er_2O_3 (*C*-type).

The structures of the *A*, *B*, and *C*-form rare earth oxides may be viewed as being derived from the fluorite structure characteristic of the dioxides of these elements. In the fluorite structure each metal atom is coordinated with eight oxygen atoms at the corners of a cube with all coordination cubes sharing edges. Alternatively one may view the structure as tetrahedrally coordinated oxygen atoms in which all tetrahedra share edges.

In terms of MO_8 coordination cubes the *C*-type structure is seen as six coordinated MO_6V_2 (V symbolizes an oxygen vacancy) cubes with the two vacancies occurring either on the face (in 75 percent of the cases) or body diagonals. The *A* and *B*-type are seen as structures in which distorted MO_8 coordination cubes provide the correct stoichiometry by shearing to allow face sharing as well as edge sharing as has been illustrated by Eyring and Holmberg [1]. Actually changes in M-O distances suggest seven coordination for *A* type and six and seven for *B*-type.

From the alternate viewpoint Caro [8] has illustrated how these structures may be considered as three dimensional arrangements of OM_4 tetrahedra in which sheets of $(MO)_n^{n+}$ polymers are seen to be separated by oxygen layers. In either view the oxygens are not all equivalent and one would expect the oxygen transport properties to be determined by the mechanism of transport which would be sensitive to the structures and the interatomic distances.

2. Apparatus

A block diagram of the system used is shown in figure 1. The total system included gas preparation and storage, vacuum pumping and pressure measurement, and exchange and analysis sections. A more detailed drawing of the exchange and analysis section is shown in figure 2. The enriched oxygen was prepared by electrolysis of water enriched with ^{18}O using NaOH as an electrolyte. Any carbon dioxide absorbed in the water was removed by repeatedly freezing the liquid and evacuating

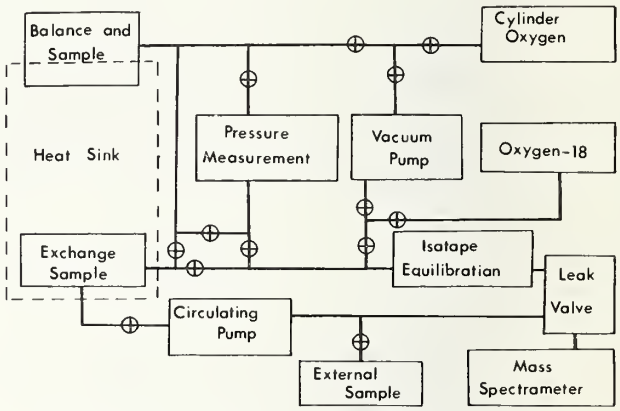

FIGURE 1. *Apparatus for oxygen isotope exchange.*

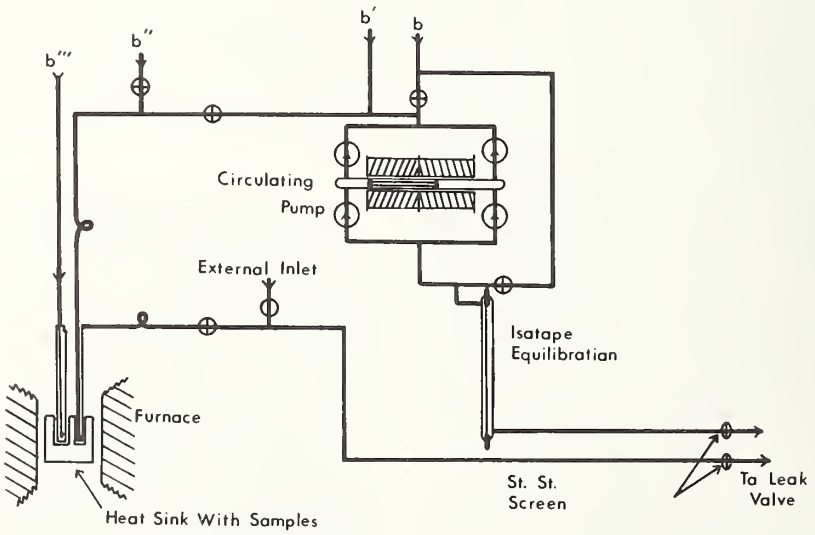

FIGURE 2. *Samples and gas flow.*

the gas over the ice. Any hydrogen in the oxygen was removed by oxidation catalyzed by Pd coated asbestos heated to 400 °C. The cylinder oxygen, containing the normal isotopic concentration of ^{18}O, 0.2 percent, and the enriched oxygen both had the water removed by dry ice traps before storage in evacuated flasks. Mass spectrometric analysis of the enriched oxygen showed only slight increase in impurities over that normally measured as background in the mass spectrometer.

The system was designed so that the gas in all sections could be evacuated or its pressure measured. For gas pressures above 1 mm Hg, a mercury manometer was used. A spiral gauge, used as a null meter, isolated the system from mercury.

The system had been designed to determine the composition as well as measure the rate of exchange for the rare earths of variable valence. For this reason two samples are shown in Figures 1, 2, and 3. Only one sample, the exchange sample,

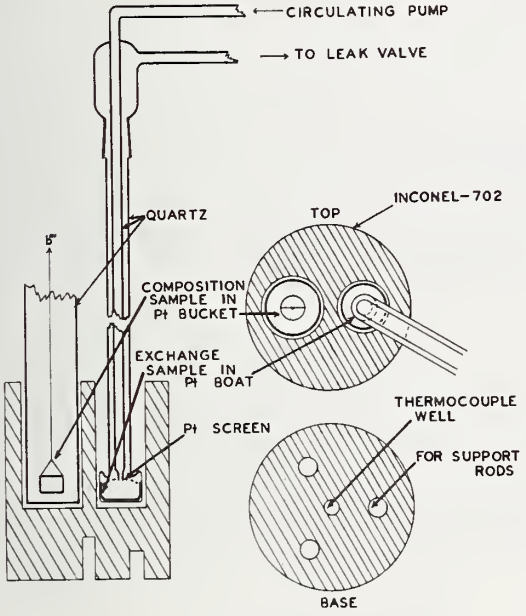

FIGURE 3. *Samples and heat sink.*

was used for the materials of fixed valence; Sm_2O_3, Nd_2O_3, and Er_2O_3. The furnace was designed, with top and bottom auxiliary heaters and an Inconel metal block, so that there would be a six inch constant temperature zone. The temperature gradient of this zone was measured by difference thermocouples (Pt/Pt + 10 percent Rh) inside the furnace next to the furnace tube. The measured gradient was always kept within 1°. The temperature itself was controlled electronically to within 0.1° at 1000 °C with the temperature being measured at the Inconel block with a Pt/Pt + 10 percent Rh thermocouple.

The gas used for the isotope exchange was mixed and circulated using a magnetically operated, internal circulating pump over the sample and through the leak valve as is shown in figures 3 and 4. The Granville-Phillips leak valve allowed

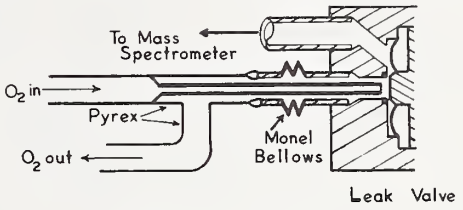

FIGURE 4. *Gas sampling.*

only a small amount of the gas to pass continuously into the analyzer section of the CEC 21–130 mass spectrometer. Even after twenty-four hours, the amount of gas lost from the system through the leak valve was less than could be measured as a pressure change. Separate experiments using nitrogen in one section mixed at a certain instant with oxygen in the other established the time required for gas mixing by the pump and indicated the lack of serious memory effects in the continuous sampling technique.

It took 3.5 seconds for the gas to go from the sample to the leak valve, hence all measured times had to be corrected by this amount. Jíru and Nováková [9, 10] found that the equilibrium concentration of the isotopes in the various molecules of oxygen, $^{16}O^{16}O$, $^{16}O^{18}O$, and $^{18}O^{18}O$, was not always maintained. Therefore, a heated Pt + 10 percent Rh wire was used as a catalyst to see if this would cause a problem for the rare earth oxides. It was found that equilibrium was established in all runs reported here since the temperature of the sample container was above 700 °C. A run made at 1000 °C without a sample indicated that no correction was necessary under the conditions of the experiments.

3. Operating Procedure

Before an exchange study was carried out the sample was heated in vacuum to 1000 °C in order to remove adsorbed gases. After the experimental temperature had been set, one of two procedures was used. One procedure, which would have been appropriate for samples of variable valence, used cylinder oxygen in the sample volume and enriched oxygen in the rest of the system. In this case the circulating pump mixed the gases as well as circulated them. In another procedure, the sample volume was initially evacuated and enriched oxygen was admitted from the rest of the exchange system at the beginning of the run. Tests on a sample of

Nd_2O_3 indicated that there was only a slight difference between the diffusion coefficients measured by the two methods. In either case, the amount of gas added was determined from the measured pressures and temperatures and the previously calibrated volumes.

The $^{16}O^{16}O^+/^{16}O^{18}O^+$ ratios were measured with the mass spectrometer to determine the rate of change of ^{18}O concentration in the gas above the exchanging sample. After an experiment on a sample at one temperature was finished (this normally took one hour) cylinder oxygen was added at 200 mm Hg to the evacuated exchange system. The temperature was taken above 800 °C, and the ^{18}O was removed from the solid by back exchange. The procedure was repeated four times with the fourth batch of cylinder oxygen being left overnight. The isotopic concentration of the solid was determined from this last back exchange and in every case was 0.2 percent ^{18}O. With this procedure it was possible to use the same sample for a variety of runs.

4. Samples and Sample Preparation

The enriched water, used in the preparation of the ^{18}O enriched oxygen gas, was obtained from Yeda Research and Development Co. and had a listed enrichment of 1.66 percent ^{18}O and 0.14 percent ^{17}O.

The solid samples, Sm_2O_3 and Er_2O_3 were obtained from Research Chemicals. The purity for two of the samples of Sm_2O_3 and for Er_2O_3 was 99.9 percent. The higher purity sample of Sm_2O_3 was 99.998 percent. Trona supplied the 99.999 percent purity Nd_2O_3. All of the purities listed are with respect to rare earths.

The procedure for the preparation of spheres from these starting materials consisted of two main steps; sintering in vacuum at 1700 °C and melting in an argon plasma. Before sintering it was usually necessary to heat the fresh sample in a Pt crucible in air to 900 °C to remove any hydroxide or carbonate that had formed on standing. The samples were also kept in argon or vacuum at every stage of their preparation to prevent the readsorption of H_2O or CO_2. Since not all of the sintered powder that was put through the plasma melted to form spheres, the spheres were separated by rolling them away from the odd shaped powder on a glass plate held at a slight incline. The spheres were then separated according to size by sieves.

Microscopic examination of the whole spheres at 50× and of cut spheres at 400× indicated that 5 percent were not melted throughout. The rest of the spheres appeared to be homogeneous and transparent to translucent. Under a polarizing microscope, there was no evidence that the spheres were single crystals. There was no appreciable change in the appearance of the spheres after repeated reaction and back exchange.

5. Computation

Solutions of Fick's second law for the isotopic exchange of a solid with a well-stirred gas of limited volume have been given by several authors including J. Crank [11] and R. Haul and coworkers [12, 13]. Preliminary results with the rare earth oxides indicated that the simpler solution given by Crank could not be used. It was necessary to consider a phase boundary reaction as well as diffusion in the first portion of the reaction. A solution for this case has been obtained by Haul et al. [13]. Their solution is:

$$\frac{P-P_1}{P_2-P_1}=\sum_{n=1}^{3}\frac{Z_n^2-Z_n\left(\frac{S\sqrt{D}}{3}-\frac{K}{\sqrt{D}}\right)}{(Z_n-Z_{n+1})(Z_n-Z_{n+2})}\,eerfc(-Z_n\sqrt{t})$$

where the Z_n are the roots of the equation

$$Z^3+Z^2\left(\frac{K}{\sqrt{D}}-\frac{S\sqrt{D}}{3}\right)+Z\frac{KS}{\lambda}-\frac{KS^2\sqrt{D}}{3\lambda}=O$$

and $Z_4=Z_1$, $Z_5=Z_2$.

The solution was obtained by making the assumption that in the subsidiary equation, given below, cosh qa can be replaced by sinh qa.

$$\overline{P}=\frac{\lambda(P_2-P_1)\left[aq\cosh qa\left(\frac{Ka}{D}-1\right)\sinh qa\right]}{3K\left[\left(1+\frac{\lambda Z}{3K}\right)\left(q\cosh qa-\frac{1}{a}\sinh qa\right)+\frac{\lambda Z}{SD}\sinh qa\right]}$$

where $q^2=Z/D$.

From the definition of q it can be seen that this is certainly valid when D is small enough. However, the values measured in the present work were fairly large ($D \approx 10^{-10}$). Therefore, it became necessary to know how closely the approximate and exact solutions agreed. Thus the diffusion equation was solved using the method of the Laplace transform and the boundary conditions given by Haul et al. [13]. The result is:

$$\frac{P-P_1}{P_2-P_1}=\frac{\lambda}{1+\lambda}+\frac{54Q^2}{\lambda}\sum_{n=1}^{\infty}\frac{e^{-\alpha_n^2 S^2 Dt/9}}{\alpha_n^4+3\alpha_n^2\left(3Q^2-Q-\frac{6Q}{\lambda}\right)+\frac{81Q^2(1+1/\lambda)}{\lambda}}$$

where the α_n are the roots of

$$\tan \alpha_n=\frac{9\alpha_n Q-\alpha_n^3\lambda}{3\alpha_n^2\lambda Q+9Q-\alpha_n^2\lambda}$$

where $Q=\frac{K}{DS}$.

The above equation reduces to that of Crank in the limit as K approaches infinity.

The agreement between the two solutions is good until the reaction is very nearly complete. For the approximate solution the error function of a real variable was calculated using a rational approximation [14] and the error function of a complex variable was calculated using an infinite series approximation [14]. When using the exact solution twenty terms in the series were summed. Both equations were used in the analysis of the data. The diffusion coefficients obtained by the two equations were essentially the same except in a few instances when the diffusion coefficients were large. All calculations were performed on a CDC-3400 computer which carried ten digits. The time required for the calculations by the two equations was comparable.

5.1. List of Symbols

P = isotope content in the gas at $t=t$
P_2 = isotope content in the gas at $t=o$
P_i = isotope content in the solid at $t=o$
n_g = moles of exchanging atoms in the gas
n_s = moles of exchanging atoms in the solid
$\lambda = n_g/n_s$
D = Diffusion coefficient
S = specific surface = 3/radius of the sphere
K = phase boundary reaction constant
z = parameter of the Laplace integral

$$\int_0^{\infty} e^{-zt}p(t)\,dt=\bar{p}(z)$$

6. Results

6.1. Sm_2O_3 Experiments

Using 99.9 percent and 99.998 percent Sm_2O_3, three different samples were used to obtain the diffusion coefficients and the phase boundary reaction constants listed in table 1.

When the logarithm of the diffusion coefficients were plotted against $1/T$. as shown in figure 5, two

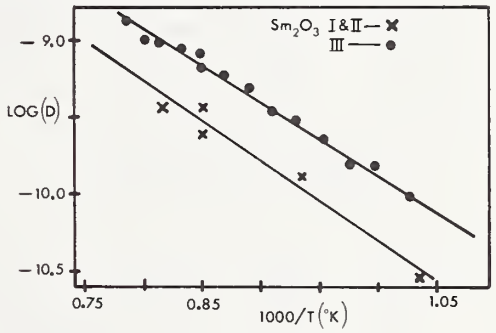

FIGURE 5. *Sm_2O_3 Temperature dependence of* D.

separate lines were obtained. One line corresponds to the 99.9 percent sample and the other to the 99.998 percent purity sample. It can be seen that the slopes are the same within the limits of error and only the intercepts are different. When expressed in equation form:

Sm_2O_3 (99.9%),

$$D=9.2\times10^{-6}\exp(-23.5\pm2\ \text{kcal}/RT)$$

Sm_2O_3 (99.998%),

$$D=6.0\times10^{-6}\exp(-21.3\pm.5\ \text{kcal}/RT).$$

The variation with pressure, as shown in figure 6, indicates that there is no pressure dependence

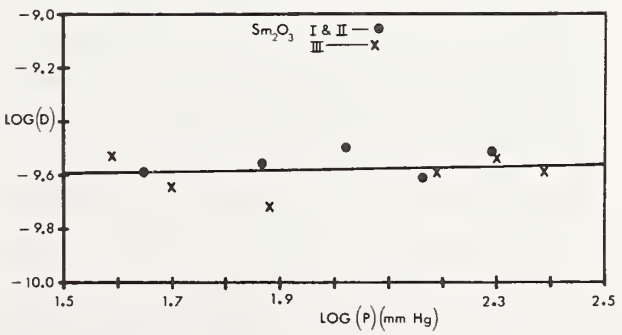

FIGURE 6. *Sm_2O_3, Pressure dependence of* D.

TABLE 1. *Samarium sesquioxide*

Temperature sample (°C)	Pressure mm of Hg	D cm²/sec	K cm/sec
Sample I: 1.3449 gm, 99.9% purity, spheres 0.111 ± 0.038 mm diameter			
696.20	63.45	2.947×10^{-11}	6.454×10^{-8}
794.10	64.20	1.237×10^{-10}	4.150×10^{-7}
899.50	64.10	3.530×10^{-10}	1.803×10^{-6}
793.10	119.85	1.135×10^{-10}	4.702×10^{-7}
793.10	214.10	9.000×10^{-11}	5.926×10^{-7}
Sample II: 1.3980 gm, 99.9% purity, spheres 0.111 ± 0.038 mm diameter			
907.60	44.80	2.542×10^{-10}	1.806×10^{-6}
950.20	44.80	3.278×10^{-10}	3.579×10^{-6}
906.80	73.75	2.740×10^{-10}	1.643×10^{-6}
907.50	104.70	3.125×10^{-10}	2.542×10^{-6}
907.60	145.40	2.197×10^{-10}	2.983×10^{-6}
907.10	196.45	2.756×10^{-10}	2.116×10^{-6}
Sample III: 0.8973 gm, 99.998% purity, spheres 0.160 ± 0.017 mm diameter			
702.50	38.70	9.309×10^{-11}	2.287×10^{-7}
725.50	38.75	1.435×10^{-10}	2.000×10^{-7}
749.50	38.30	1.556×10^{-10}	3.433×10^{-7}
774.10	37.55	2.196×10^{-10}	5.087×10^{-7}
798.50	38.85	2.937×10^{-10}	8.545×10^{-7}
822.90	38.85	3.430×10^{-10}	1.208×10^{-6}
848.70	38.80	4.608×10^{-10}	1.725×10^{-6}
874.90	38.95	5.742×10^{-10}	2.106×10^{-6}
901.30	38.95	7.695×10^{-10}	2.777×10^{-6}
900.30	38.75	6.397×10^{-10}	2.762×10^{-6}
924.50	39.15	8.416×10^{-10}	4.819×10^{-6}
953.50	38.90	9.491×10^{-10}	4.195×10^{-6}
973.10	38.80	1.001×10^{-9}	6.535×10^{-6}
998.70	38.60	1.221×10^{-9}	6.363×10^{-6}
799.90	50.10	2.250×10^{-10}	7.768×10^{-7}
799.40	76.15	1.894×10^{-10}	9.994×10^{-7}
[a] 799.40	105.95	1.359×10^{-10}	7.462×10^{-7}
799.50	154.35	2.535×10^{-10}	9.287×10^{-7}
799.50	201.50	2.846×10^{-10}	7.428×10^{-7}
799.40	245.95	2.543×10^{-10}	7.968×10^{-7}

[a] This datum was not used for the least squares equation or plot since it was outside the limits of error using Chauvenet's Criterion [15].

within the limits of error. The slope of the line is 0.04 ± 0.07.

The phase boundary reaction constant as a function of temperature can be expressed:

Sm_2O_3 (99.9%), $K = 7.4 \exp(-35.6 \pm 0.5 \text{ kcal}/RT)$

Sm_2O_3 (99.998%), $K = 1.9 \exp(-31.3 \pm 0.8 \text{ kcal}/RT)$.

The pressure dependence expressed as a slope can be written as

Sm_2O_3 (99.9%), 0.17 ± 0.1

Sm_2O_3 (99.998%), -0.04 ± 0.04.

6.2. Nd_2O_3 Experiments

Using 99.999 percent Nd_2O_3 spheres, three different samples were used to obtain the diffusion coefficients and phase boundary reaction constants listed in table 2. For the temperature dependence, two samples of different size were used in order to check the validity of the equation. It was assumed that if a surface process were important but not correctly accounted for by the phase boundary reaction constant, different diffusion coefficients would have been obtained. Since the agreement was good, both sets of data were used to give the temperature dependence as shown in figure 7 and given in the equation

$$D = 1.3 \times 10^{-4} \exp(-31.0 \pm 2.0 \text{ kcal}/RT).$$

TABLE 2. *Neodymium sesquioxide.*

Temperature Sample (°C)	Pressure mm of Hg	D cm²/sec	K cm/sec
Sample I: 1.2529 gm, 99.999% purity, spheres 0.160 ± 0.017 mm diameter			
900.20	36.30	1.023×10^{-9}	4.814×10^{-6}
900.00	87.55	1.047×10^{-9}	1.004×10^{-5}
899.90	99.25	7.810×10^{-10}	9.137×10^{-6}
902.90	139.50	9.694×10^{-10}	1.113×10^{-5}
898.10	178.70	1.242×10^{-9}	1.235×10^{-5}
897.60	286.05	1.129×10^{-9}	3.829×10^{-4}
Sample II: 0.99279 gm, 99.999% purity, spheres 0.163 ± 0.014 mm diameter			
706.80	74.75	1.741×10^{-11}	1.629×10^{-7}
780.10	76.85	6.700×10^{-11}	6.300×10^{-7}
852.90	78.30	1.740×10^{-10}	1.978×10^{-6}
924.20	77.05	3.701×10^{-10}	3.789×10^{-6}
1002.80	75.90	7.300×10^{-10}	6.641×10^{-6}
Sample III: 0.96250 gm, 99.999% purity, spheres 0.0965 ± 0.0085 mm diameter			
717.00	73.65	2.132×10^{-11}	3.218×10^{-7}
788.80	73.00	5.686×10^{-11}	1.306×10^{-6}
854.50	73.35	1.011×10^{-10}	3.982×10^{-6}
920.90	73.26	2.785×10^{-10}	1.056×10^{-5}

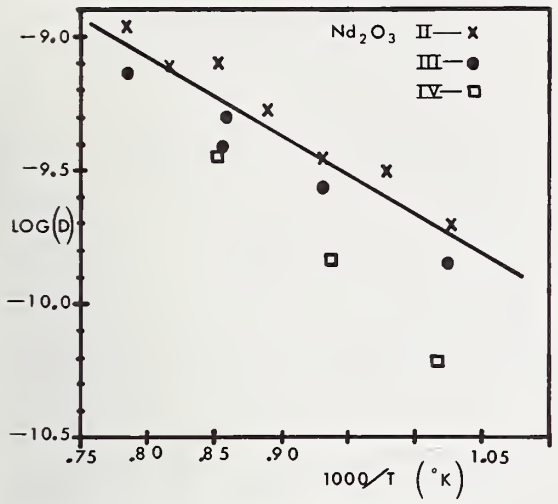

FIGURE 7. *Nd_2O_3, Temperature dependence of* D.

Again there appears to be no pressure dependence as can be seen in figure 8 where the slope was calculated to be 0.08 ± 0.06.

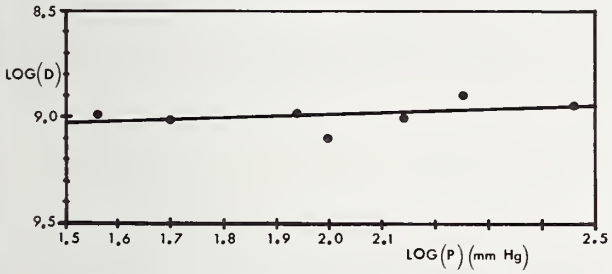

FIGURE 8. *Nd_2O_3, Pressure dependence of* D.

The phase boundary reaction constants as a function of temperature can be expressed

$$Nd_2O_3(V), K = 2.5 \times 10^2 \exp(-40.3 \pm 0.1 \text{ kcal}/RT)$$

$$Nd_2O_3(VI), K = 1.7 \exp(-31. \pm 2. \text{ kcal}/RT)$$

6.3. Er_2O_3 Experiment

It was found in an attempt to measure the diffusion coefficient of oxygen in Er_2O_3 that the rate of exchange was much slower than had been observed for Nd_2O_3 or Sm_2O_3. While it was possible to make an estimate of the diffusion coefficient, it was not possible to determine it accurately. The design of the apparatus did not allow higher temperatures to be used in order to increase the measured rate of exchange. The estimated diffusion coefficient at 1000 °C was 10^{-14} cm^2/sec.

7. Discussion

In the presentation of results the only errors listed were those obtained as deviations from a line determined by a linear least squares treatment. The magnitude of systematic errors could be calculated from the variation of the sphere size and inaccuracies in pressure, temperature, and volume measurements, with the result that the diffusion coefficients could be in error by 10 to 15 percent, the heats of activation by ± 4 kcal/mole, and the logarithm of the pre-exponential factor by ± 1. The systematic errors would probably be of the same order of magnitude as errors determined from the scatter if different samples were used for each experimental point.

The low values measured for the heat of activation and the lack of pressure dependence suggest that extrinsic diffusion is important. It is possible that the defect concentration is controlled by impurities, such as Ca, Mg, and Si which have a maximum listed concentration of 0.01 percent by weight. Since the pre-exponential term in extrinsic diffusion is controlled by the concentration of defects, the difference observed for Sm_2O_3 99.9 and 99.998 percent might just be due to the differences in the concentration of these impurities.

If there was a difference in the defect concentration between the slightly reduced Er_2O_3 and spheres, it is possible to explain the different diffusion coefficients observed for these two samples by a change in the pre-exponential term D_o. For example, if the value for the heat of activation for slightly reduced Er_2O_3 [6] is assumed to be correct, by using a pre-exponential term of 10^{-5} cm^2/sec, similar to that measured for Sm_2O_3 and Nd_2O_3, the diffusion coefficient is close to 10^{-14} cm^2/sec at 1000 °C as was observed for the exchange with spheres.

Considering the heats of activation measured and the above assumption, it is possible to explain qualitatively the reported results. Since in the case of extrinsic diffusion the heat of activation would be the energy of motion, differences in the interatomic distances along the jump path would be expected to produce differences in the activation energies. For the same rare earth cation the density increases or average interatomic distance decreases as the structure changes from *C* to *B* to *A*-type sesquioxide [16]. While the limits of error and the use of different cations makes it difficult to reach any definite conclusion, Nd_2O_3 (*A*-type) does have a greater activation energy than Sm_2O_3 (*B*-type) as might be expected from the oxide type. While no activation energy was measured by isotope exchange for Er_2O_3, if the 47.8 kcal/mole [5] is correct, it must be assumed that the lanthanide contraction has decreased the interatomic distances to such an extent that even though the structure is *C*-type, the energy of activation is greater than that observed for the *A*-type and *B*-type sesqui-

290-621 O-68—13

oxides measured. This ionic radius effect can also be used to explain why the difference between Sm_2O_3 and Nd_2O_3 was not greater.

Before the diffusion experiments can be expected to yield unambiguous information about the transport mechanism the effect of structure alone must be explored. (Such a study is presently underway with *B* and *C*-type $GdO_{1.5}$.) It will also be necessary to clarify further whether or not the diffusion is indeed extrinsic and if so to what type of defect it is due.

It is a pleasure to express appreciation to the United States Atomic Energy Commission for their support of this work. Dr. S. H. Lin provided many interesting and enthusiastic discussions concerning the solution of the diffusion equation.

8. References

[1] L. Eyring and B. Holmberg, Adv. Chem. Ser., **39**, 46 (1963).
[2] B. G. Hyde, D. J. M. Bevan, and L. Eyring, Phil. Trans. Roy. Soc., London, Ser. A, **259**, 583 (1966).
[3] K. Vorres, Ph.D. Thesis, State University of Iowa, Iowa City, Iowa (1958). K. S. Vorres and L. Eyring, "Rare Earth Research" (E. V. Kleber, Editor) The Macmillan Co., New York (1961).
[4] U. Kuntz and L. Eyring, Kinetics of High Temperature Processes, Ed. W. D. Kingery, Cambridge Technology Press (1959), p. 59.
[5] J. Brett and L. Seigle, J. Less-Common Metals, **10**, 22 (1966).
[6] C. D. Wirkus, M. F. Berard, and D. R. Wilder, J. Am. Ceram. Soc., **501**, 113 (1967).
[7] R. Haul, G. Dümbgen, and D. Just, J. Phys. Chem. Solid, **26**, 1 (1965).
[8] P. Caro, Inorg. Chem., In press.
[9] P. Jíru and J. Nováková, Coll. Czech. Chem. Commun., **28**, 1 (1963).
[10] P. Jíru, K. Klier, and J. Nováková, J. Catal., **2**, 479 (1963).
[11] J. Crank, Mathematics of Diffusion, Clarendon Press, Oxford, 1956.
[12] P. C. Carman and R. A. Haul, Proc. Roy. Soc., **A222**, 109 (1954).
[13] R. Haul, G. Dümbgen, and D. Just, Z. Phys. Chem. NF, **31**, 309 (1962).
[14] Handbook of Mathematical Functions—AMS55 (M. Abramowitz and I. A. Stegun, editors) U.S. Department of Commerce, National Bureau of Standards.
[15] A. G. Worthing and J. Geffner, Treatment of Experimental Data, John Wiley & Sons, Inc., New York (1943).
[16] G. Brauer, Progress in Science and Technology of the Rare Earths, Vol. 2, Ed. L. Eyring, Pergamon Press, New York (1966).

Oxygen Transport During Oxidation

John B. Lightstone [1, 2] and J. Paul Pemsler [1]

A large volume fraction of potential short circuit paths for diffusion was shown to exist in the oxide formed on Zr by oxidation between 500 and 1000 °C in oxygen. The results of oxygen tracer experiments were also in agreement with a short circuit diffusion mechanism of oxygen transport. The assumption of line diffusion was shown to imply intuitively reasonable values of both the grain boundary thickness and the ratio of the oxygen line diffusion coefficient to the lattice diffusion coefficient.

X-ray line broadening measurements were used to estimate the grain size of the oxide. The assumption was made in the interpretation of the data that strain contributions to the line breadth may be neglected. The average grain was calculated to be approximately 300 Å.

The small grain size and a possible high dislocation density associated with a martensitic transformation imply a high volume fraction of potential short circuit paths for diffusion. The mechanism of oxidation was studied in an attempt to demonstrate that transport of oxygen along these short circuit paths is the predominant mechanism of film growth.

Zr was oxidized at 500, 600, 750, and 910 °C in O_2^{16}, and the oxidation continued in O_2^{18}. A new method of general application in diffusion problems was used for studying the movement of the oxygen tracer. The oxide was sputtered in a beam of argon ions at a rate of 1 micron per hour into a mass spectrometer. The O^{18} profile was determined with a resolution of 0.015 microns.

The fraction O^{18} exchanged in a volume very near the surface was always less than unity. The fraction increased with time in O_2^{18} for the same initial time in O_2^{16} at a given temperature.

Arguments are presented against an explanation of these observations in terms of a surface exchange limited reaction, or in terms of an O^{18} interstitial diffusion followed by exchange with O^{16} in normal sites. However, the evidence against a surface exchange limited reaction is not conclusive.

The observations of the fraction O^{18} exchanged in a volume very near the surface are explained by suggesting that many of the oxygen atoms are not taking part directly in the diffusion process. Transport is occurring predominantly through easy diffusion paths. There is also a slow exchange between O^{18} in these short circuit paths and O^{16} in the lattice, so that the fraction exchanged near the surface increases with time.

The fraction exchanged after very short times such that there is a negligible contribution from lattice diffusion to the diffusion profile is used to estimate the volume fraction of short circuit paths. An estimate of the volume fraction of short circuit paths obtained in this way is combined with a value of the average grain size from x-ray line broadening measurements to derive an apparent grain boundary thickness on the assumption that grain boundaries are the only short circuit paths available. At 600 °C this implies a grain boundary thickness of 14 Å. This result is similar to values reported in metals, and is intuitively reasonable. This is regarded as evidence in favor of the model.

Observations of the O^{18} profile after very short times in O_2^{18} were used to derive a line diffusion coefficient for oxygen. The increase with time of the fraction exchanged in a volume near the surface was used to calculate an oxygen lattice diffusion coefficient. The ratio of the line diffusion coefficient to the lattice diffusion coefficient was 9×10^7 at 600 °C. This ratio is similar to values obtained in metals, and is cited as indirect justification of the model.

Nickel oxidation at 1000 °C was studied by a similar tracer technique. The fraction exchanged in a volume very near the surface was in this case unity. The shape of the diffusion profile was consistent with a model of material transport in which there is a significant contribution from oxygen lattice diffusion.

[1] Ledgemont Laboratory, Kennecott Copper Corp., Lexington, Mass. 02173.
[2] Now at Union Carbide Corp., Linde Division, Tonawanda, N.Y. 14152.

Mechanical and Dielectric Relaxation of Hopping Electrons and the Ionic Defects in Reduced Rutile (TiO_{2-x})

W. W. Scott and R. K. MacCrone [1]

School of Metallurgy and Materials Science
University of Pennsylvania, Philadelphia, Pennsylvania 19104

Non-stoichiometry in transition metal oxides involves the formation of ionic defects. For oxygen deficient n-type oxides, the primary ionic defects are oxygen vacancies and/or cation interstitials. These ionic defects are positively charged and at low temperatures trap electrons into states centred on one of several nearest neighbour cation sites. Some general features of the electron localization are briefly discussed.

An electric field or a mechanical stress may induce electron hopping between two such cation sites and give rise to a discrete dielectric or mechanical relaxation. The orientation dependence and "selection rules" of such relaxations provides a powerful method of investigating the ionic defects and complexes. In the particular case of reduced Rutile several dielectric relaxations and their corresponding anelastic relaxations are observed. The orientation dependence, and impurity dependence, of the dielectric relaxations indicates the presence of oxygen-vacancies in association with extrinsic trivalent impurities and also Ti^{+3} interstitials which may be associated with two impurities.

Key Words: Cation interstitial, nonstoichiometry, oxygen vacancy, rutile.

1. Introduction

Mass transport in oxides occurs by the diffusion of ionic defects. In all but the simplest cases, more than one kind of ionic defect is involved, since at high temperatures various interactions may occur and defect complexes may be formed. Thus, experiments which measure the combined effect of several defects cannot easily yield unambiguous conclusions about the individual defect types involved. Selective experiments which enable specific defect types to be identified and their concentrations determined are therefore of great importance.

Dielectric and anelastic relaxation measurements near and above room temperature have proved to be valuable in identifying specific ionic defects, where the ion itself moves between equilibrium positions. This paper describes how at low temperatures in a reduced transition metal oxide, TiO_2, electron hopping gives rise to dielectric and anelastic relaxations, and how these relaxations may be used to characterize the ionic defect types. The experimental method should be applicable to other transition metal oxides.

The basic mechanism involves the ionic defect centres (e.g., oxygen vacancies) which are positively charged and which trap electrons at low temperatures. These electrons are not in hydrogenic states centered about the particular ionic defect but in states centered around one of several surrounding nearest neighbor cations. This can be schematically represented as follows:

$$X^{n-1}\ \boxed{O_v}\ X^n.$$

An equivalent configuration of equal energy but of opposite dipole moment is

$$X^n\ \boxed{O_v}\ X^{n-1}.$$

An alternating electric field will induce backward and forward electron hopping, which under appropriate conditions of temperature, frequency, and orientation will give rise to a Debye type dielectric relaxation [1–5].[2] A theoretical discussion has been given by Fröhlich, Machlup and Mitra [6].

2. Experimental Results and Discussion

Dielectric relaxation measurements at low temperatures with the electric field parallel to [001] have shown [7, 8] the existence of two pronounced re-

[1] Present address: Department of Materials Engineering, Rensselaer Polytechnic Institute, Troy, New York 12181.
[2] Figures in brackets indicate the literature references at the end of this paper.

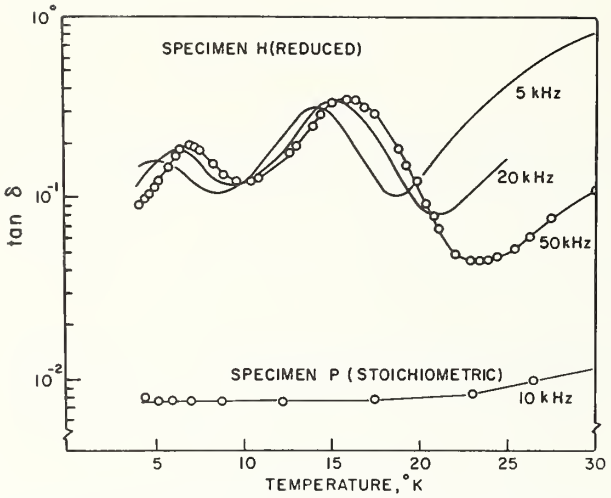

FIGURE 1(a). *Typical dielectric loss as a function of temperature of reduced Rutile, showing two relaxation processes.* E || [001].

$Q = 1.0 \pm 0.5 \times 10^{-3}$ eV with pre-exponential factor $\tau^* = 10^{-6}$ sec.

The higher temperature peak, Peak II at 17 °K, has been shown to be most likely due to electron hop I at the Ti^{+3} interstitial, which may be associated with two trivalent substitutional impurities as indicated in figure 3. The relaxation time for this peak was found to have an activation energy $Q = 2.0 \pm 0.5 \times 10^{-2}$ eV with pre-exponential factor $\tau^* = 10^{-7}$–10^{-8} sec.

The identification of the two relaxations shown in figure 1(a) with the specific electron hops and ion cores indicated was deduced from experiments in which the orientation of the electric field E was varied with respect to the crystallographic axes and from experiments in which the trivalent substitutional impurity was varied.

Figure 1(b) shows the behaviour when the elec-

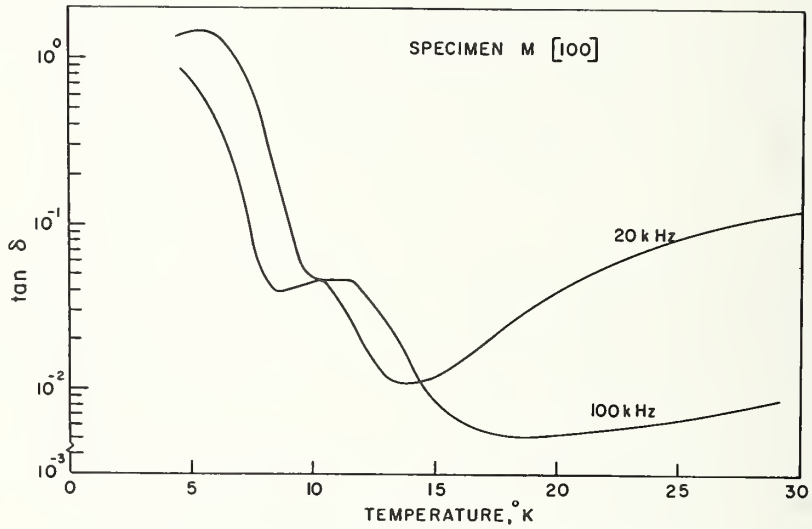

FIGURE 1(b). *Typical dielectric loss vs. temperature for* E || [100].
Note the absence of the Peak at 17 °K. The small peak, at ≈ 11 °K, is believed due to electron hopping around a Y^{-1} centre.

laxation peaks, figure 1(a) (The temperature region above 30 °K is obscured in these measurements due to the formation of a Shottky barrier layer as the Fermi level rises with temperature.). A comprehensive discussion of the structural origin of these relaxations has been given [7, 8]. The salient features are summarized below; the details will be found in refs. 7 and 8.

The low temperature peak, Peak I at 6 °K, has been shown to be due most likely to electron hopping at an oxygen vacancy in association with one trivalent substitutional impurity. This complex defect has two, almost equi-energetic ion core configurations. These core configurations are shown in figures 2(a) and (b), which also indicate the proposed electron hops. The relaxation time τ for this peak was found to have an activation energy

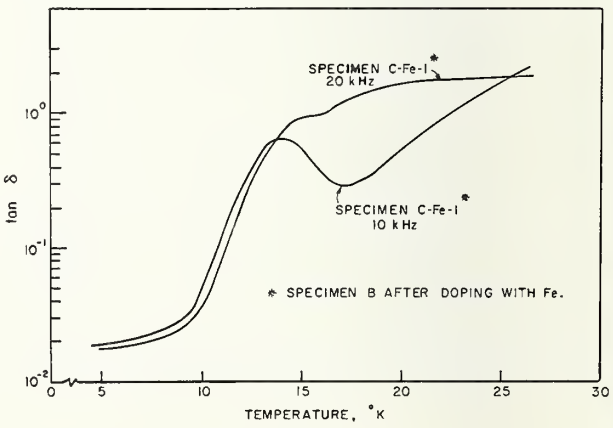

FIGURE 1(c). *Dielectric loss vs. temperature for specimen containing increased trivalent substitutional impurity.* E || [001].

tric field is parallel to [100], the specimen with electric field parallel to [110] behaving similarly. In both cases the higher temperature peak is absent since the hopping mode 2, figure 3, cannot be excited for these field directions.

Figure 1(c) shows the behaviour of a specimen in which the trivalent substitutional impurity had been increased. In this case Peak I is absent due to the proposed formation of $(O_v - Y_2)$ neutral complex defect centres [9] which cannot trap electrons. The formation of this (neutral) complex defect probably follows the equations

$$O_v^{+2} + Y^{-1} \underset{\longrightarrow}{K_1(T)} (O_v - Y)^{+1}$$

$$(O_v - Y)^{+1} + Y^{-1} \underset{\longrightarrow}{K_2(T)} (O_v - Y_2^0).$$

By increasing the concentration of the effectively negative trivalent impurity Y^{-1}, the equilibrium is driven towards the right, since Haul and Dumbgen [10] have shown experimentally that the concentration of oxygen vacancies remains fixed.

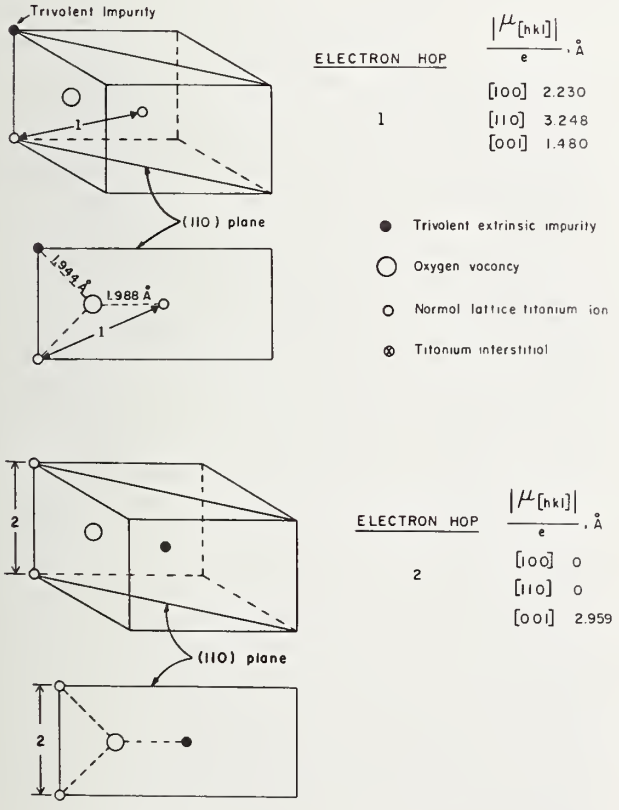

FIGURE 2. *Oxygen vacancy with one associated trivalent impurity.*
(a) [100], [110], and [001] components of dipole moment, μ
(b) only [001] component of μ.

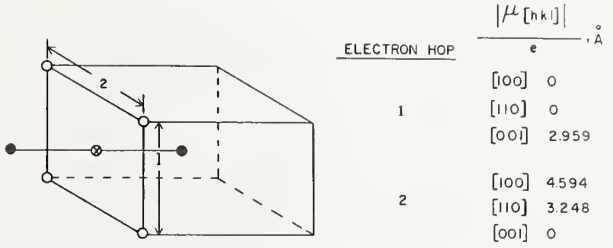

FIGURE 3. *Titanium interstitial associated with two trivalent impurities.*

The intermediate temperature peak, Peak III (which is obscured in figure 1(a)) is also due to electron hopping at some ionic core. Since this relaxation shows the same orientation dependence as Peak I, and apparently does not depend on the trivalent impurity concentration, this ion core has been proposed as a simple substitutional pentavalent impurity present in our boules. The relaxation time for this peak was found to have an activation energy $Q = 8.0 \pm 0.5 \times 10^{-3}$ eV and $\tau^* 10^{-7}$ sec.

There are two major theoretical aspects that are of interest concerning the localization of the electrons and the intercationic hopping as envisaged:

(i) the symmetry properties of the defects and the selection rules for observable relaxations and
(ii) the nature of the electron states.

2.1. The Symmetry Properties

The symmetry properties and selection rules of defects in general, have been discussed by Wachtman [11], and by Nowick and Heller [12]. These references should be consulted for further details.

2.2. The Electron States

Consider the oxygen vacancy shown in figure 2(a). If the cation sites were strictly equivalent, the ground state wave functions of the electron would be symmetric or anti-symmetric combinations of wave functions centered on the cation sites. Transitions between these non-polar states would thus not give rise to a dielectric relaxation. As discussed in detail in [8], transitions between the ground state and some polar excited state will give rise to a relaxation but cannot be the cause of the dielectric relaxations observed here; the transition rate would be too rapid. Therefore, the supposition that the two cation sites are equivalent must be abandoned. The non-equivalence of the two cation sites may arise in one of two ways:

(i) the "reaction field" of the lattice, polarized by the electric dipole, is

different at the two cation sites [8], or
(ii) the relative displacements of the two cations with respect to some symmetry centre are different.

It is not known which of these two effects is dominant. In any event, a perturbation on the non-equivalence of the cation sites may be produced by the application of a mechanical stress in an analogous way to the perturbation produced by an electric field.

To specifically check this prediction, low temperature mechanical loss measurements were made on a specimen of lightly reduced rutile in an apparatus described elsewhere. The specimen orientation was such that an alternating compressive and tensile stress was applied along the [101] direction. This direction was chosen since electrons at all three of the proposed defect centres will be active if the centres are present. The results are shown in figure 4(a). (Note that in these

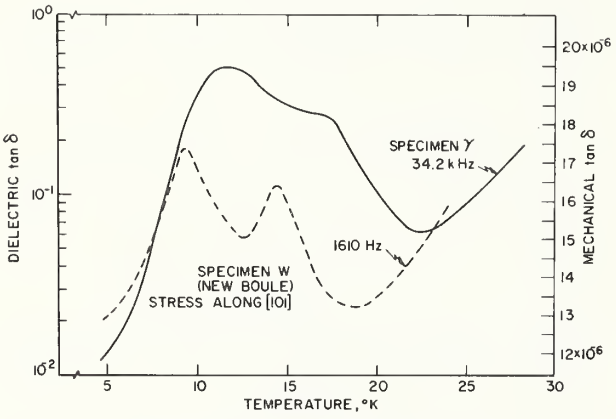

FIGURE 4(a). *Mechanical loss versus temperature in reduced rutile (dotted line) showing two relaxation processes.*
The correlation with the dielectric relaxations (solid line) should be noted.

specimens Peak I is not present due to the presumed large trivalent impurity content [8].) The one to one correspondence between the dielectric relaxations and the mechanical relaxations is most satisfactory. It is interesting to note that, where comparison is possible i.e., Peak II and Peak III, the activation energies Q and pre-exponential factors τ^* are the same for the mechanical and dielectric relaxations. The values of Q and τ^* describing electron hopping in Rutile are comparable to those reported by Volger [5] for electron hopping in Fe_2O_3.

The mechanical loss measurements reveal in addition other relaxations at temperatures 42 and 55 °K (fig. 4(b)). These relaxations (provided of course that they are electrically active) have not been observed in vacuum reduced rutile since the formation of a Schottky surface barrier obscures

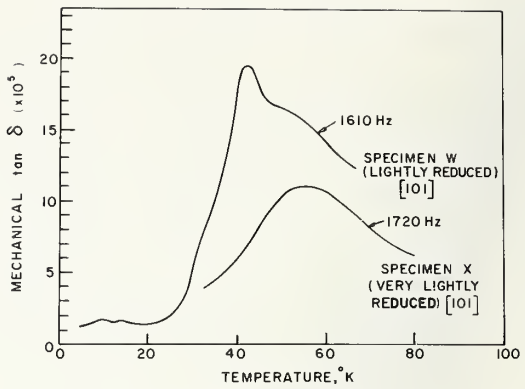

FIGURE 4(b). *Mechanical loss vs. temperature in reduced rutile for two states of reduction.*

bulk dielectric phenomena at temperatures above 30 °K. Mechanical measurements do not have this disadvantage.

The most powerful approach in identifying any active defect is to study the symmetry properties of the resulting relaxations. Such an investigation is currently in progress on the peaks at 50 °K. Any serious ion core model must await the results of these experiments.

3. Conclusion

Low temperature dielectric and mechanical relaxation due to intercationic hopping at ionic defect centres has been shown to be a useful method of investigating ionic defect centres in transition metal oxides. Using this technique, the orientation dependence of the dielectric relaxations that occur in reduced Rutile indicates the presence of oxygen vacancies in association with one trivalent substitutional impurity (fig. 2(a) and (b)) as well as the presence of Ti^{+3} interstitials (fig. 3). A one to one correlation between dielectric relaxations and mechanical relaxations has been established for two distinct electron hops. In addition, new electron hops at ~ 50 °K have been found.

From a theoretical point of view, the localization of electrons in this way requires that two cation sites, equivalent in the lattice, be unequivalent when adjacent to an intrinsic ionic defect with an electron localized on one of the cations. In this connection the mechanical relaxation indicates that a mechanical stress, as expected, alters the potential inequivalence sufficiently to induce transitions between the two sites. It is not known whether the cation site inequivalence is due to polaron effects or to electrostatic effects within the ion core.

Finally, the magnitude of the dielectric relaxations may be used to determine the number of electrons involved quite accurately (on the order of 10^{16} cm^{-3} in fig. 1), since the electric dipole

moments can be reasonably estimated. There is probably a fairly good correlation between the electron concentration and ionic defect centre concentration, although at these temperatures the effect of other polar or non-polar donor or acceptor states may be important in the Fermi statistics of these wide gap materials.

The authors would like to express their appreciation to Dr. Jerome R. Long for helpful discussion and the editors of The Physical Review for permission to reproduce figures 1 to 3. The financial support of the Advanced Research Projects Agency is also gratefully acknowledged.

4. References

[1] J. W. Verwey, Semi-conducting Materials, Butterworths, p. 151 (1951).

[2] J. Volger, J. M. Stevels, C. van Amerongen, Philips Research Reports, **10**, 260 (1955).

[3] N. R. Freyman, et al., J. Phys. et Raduim **17**, 806 (1956).

[4] W. A. Joffe, Silikattechnik **10**, 599 (1959); Fiz. Tv. Tela **4**, 669 (1962).

[5] J. Volger in Progress in Semiconductors, Vol. 4, Ed.: A. Gibson, Wiley, p. 205 (1960).

[6] H. Fröhlich, S. Machlup and T. K. Mitra, Phys. Kondensierten Materie **1**, 359 (1963).

[7] L. A. K. Dominik and R. K. MacCrone, Phys. Rev. **156**, No. 3, 910 (1967).

[8] L. A. K. Dominik and R. K. MacCrone, Phys. Rev. **163**, No. 3, 756 (1967).

[9] * The oxygen vacancy O_v^{+2} is effectively positive with a double charge.

A trivalent substitutional impurity is effectively negatively charged in the rutile lattice, and is given the symbol $^{Y-1}$.

[10] R. Haul and G. Dumbgen, J. Phys. Chem. Solids **26**, 1 (1965).

[11] J. B. Wachtman, Jr., Phys. Rev. **131**, 517 (1963).

[12] A. S. Nowick and W. Heller, Advances in Physics **XIV**, No. 54, 101 (1964).

Purity and Perfection of Research Specimens of Oxides[1]

J. W. Cleland

Solid State Division, Oak Ridge National Laboratory
Oak Ridge, Tennessee 37830

Specific examples of the effects of pre-purification, crystal growth, characterization, and research involving oxides in the Research Materials Program of the Solid State Division of the Oak Ridge National Laboratory were selected to indicate the current status of the purity and perfection of these particular materials, and to examine the primary experimental problems that stand in the way of better research materials. The coded and filmed collection of data sheets, abstracts, reports, open literature publications, and bibliographies of the Research Materials Information Center, various publications of the Electronic Properties and Defense Ceramics Information Centers, and the contents of a number of journals and books gave information on the initial purification, crystal growth, and final characterization of some general classes of oxides, as well as a number of specific materials of interest. A number of individual research groups were contacted to obtain current information on the purity and perfection of those oxides of particular interest to their own research program.

Key Words: Characterization, crystal growth, oxide crystals, purity.

1. Introduction

The purpose of this survey was to ascertain the present status regarding the purity and perfection of research specimens of oxides. Progress in understanding the fundamental properties and the ultimate range of properties in many materials has been severely limited by a lack of pedigreed samples of sufficiently high purity and crystalline perfection. Extensive tests on ultra-pure specimens, or on specimens that contain a known amount of a specific impurity, are required.

The Research Materials Program of the Solid State Division of the Oak Ridge National Laboratory (ORNL) is concerned with developing the necessary techniques required for the growth of ultra-high purity and of controlled impurity research specimens (usually single crystal) of a composition, quality, purity, and perfection required in materials research. The choice of materials for consideration has been made, for the most part, on the basis of the potential gain to a fundamental understanding of a given material that may result from an intensive investigation by a number of research groups, and on the basis of an expressed need for a specific research material. Certain research materials that have not been investigated previously are being produced with new techniques of purification and crystal growth.

The entire program involves a number of research divisions at ORNL and other AEC installations. The Analytical Chemistry Division has provided a variety of special analytical techniques, and a program of research on improvement in analytical techniques. Most of the work on crystal growth has been carried out by research groups within the Metals and Ceramics and the Solid State Divisions of ORNL, and these groups have also conducted a wide variety of physical property measurements that characterize the end-product. Selected samples have been supplied to other research groups within and without ORNL for comparative analyses, cooperative measurements that increase the characterization, and for special experiments of interest to the AEC.

Information concerning the availability of and need for high-purity research materials has always been difficult to obtain; hence, the Research Materials Information Center (RMIC) [1][2] was established as a part of the Research Materials Program to collect and provide information on the initial purification, crystal growth, final characterization, and availability of research quality specimens to both producers and users. Ready access to its accurate up-to-date listing of available materials eliminates much duplication of effort to produce materials that are already available elsewhere. A simultaneous listing of research materials that are desired but are not available has served to focus the attention of researchers on promising new areas of investigation.

The American Ceramic Society has published a compilation [2] of selected engineering property

[1] Research sponsored by the U.S. Atomic Energy Commission under contract with Union Carbide Corporation.

[2] Figures in brackets indicate the literature references at the end of this paper.

data of the physical, thermal, and mechanical properties of a large number of single and mixed oxides. The separate listing of 1026 data sources or references is of value in obtaining information on purity and perfection that was not a part of the collection of engineering properties. The Defense Ceramic Information Center (DCIC), Battelle Memorial Institute, Columbus, Ohio, collects, interprets, and disseminates technical information to qualified requestors on materials composition, processing, fabrication, property and performance data, and fundamental aspects of processing and behavior. The Electronic Properties Information Center (EPIC), Air Force Systems Command, Hughes Aircraft Company, Culver City, California, has compiled information on the electronic properties of Al_2O_3, BeO, MgO, CdO, PbO, and ZnO in separate data sheet publications that are available from the Defense Documentation Center, Alexandria, Virginia.

Review articles [3] by E. A. D. White and R. G. Bautista and J. L. Margrave were of considerable value in obtaining information. A report [4] of the Materials Advisory Board, the International Conference on Crystal Growth [5], and the newly formed Materials Research Bulletin, Journal of Crystal Growth, and Journal of Materials Science provided additional information of value.

The coded and microfilmed collection of data sheets, abstracts, reports, and open literature publications of the RMIC, and the data sheets and data sources of the other publications named above gave information on the initial purification, crystal growth, and final characterization of general classes of oxides, as well as specific materials of interest. It is evident that individual authors, sponsoring organizations, and journal referees or editors must share the blame for minimizing or deleting the information that concerns the actual purity or perfection of the specific material under investigation. Most of the publications referred to the material as good quality, reasonable purity, or as single crystal; however, the actual sample was seldom identified in quantitative terms of specific impurity content or lattice perfection. It is hoped that the above mentioned new publications (and the old) will alleviate this problem.

A number of individuals and research groups were contacted to obtain up-to-date information on the purity and perfection of those oxides of particular interest to them. No attempt was made to contact every individual or group, hence, the information as received was incomplete; however, the cooperation of those who furnished information contributed in large measure to the aim and intent of this survey.

The RMIC, already described, answered more than 2400 inquiries from 940 individuals in 27 countries during the period from July, 1966, to July, 1967. Table 1 is a tabulation of requests received for information regarding the availability of single crystals of a particular material, arranged in order of the number of requests during the period from July, 1966, to July, 1967. This list does not include the requests for other information, such as purification, crystal growth techniques, or specific property measurements, but only the direct requests for availability of single crystals.

2. Specific Materials

2.1. Magnesium Oxide

Single crystals of MgO are advertised as available from Electronic Space Products, Inc., General Electric Co., Norton Co., Monocrystals, Inc., Muscle Shoals Electrochemical Corp., Semi-Elements, W. & C. Spicer, Ltd., England, and yet other sources of a commercial or research nature. A large number of detailed analyses of both starting material and final product appear in the literature; however, the end result is 99.9 percent (3*N*) or at most 99.99 percent (4*N*) purity. This is not surprising since most crystal growers have employed the same type of starting material, and since a few companies have served as producers for a number of crystal brokers or vendors.

An example of the complexity of analytical techniques for materials is that of a long-term contract between the Jet Propulsion Laboratory and the Battelle Memorial Institute for The Development of Chemical Analysis Techniques for Ad-

TABLE 1. *Single Crystal Requests Through The Research Materials Information Center (July 1966–July 1967)*

Crystal	Number of Requests	Crystal	Number of Requests
MgO	17	KCl	8
ZnO	16	Te	8
$BaTiO_3$	15	Fe_3O_4	7
CdS	14	CaF_2	7
Ge	12	Ni	7
graphite	12	NiF_2	7
ZnS	12	Si	7
PbTe	11	SrO	7
TiO_2	11	FeF_2	6
ZnSe	11	MnO	6
ZnTe	11	W	6
BaO	11	AlN	5
HgS	10	PbS	5
NiO	10	PbSe	5
BaS	9	SrTe	5
ThO_2	9		

vanced Materials. The intent of this contract is the complete chemical characterization of the oxides of Mg, Al, Ca, and Zr, and the carbides of Ta, Hf, Nb, and Zr. The progress to date on one starting material (Fischer M–300 magnesia powder) is that it has been standardized in terms of F, Si, S, Cl, and Ca.

The primary technique for single crystal growth of pure and of doped crystals of MgO is the arc fusion between carbon electrodes of precalcined or sintered material at temperatures in excess of 2800 °C. A. Rabenau [6] has described a typical furnace, melting procedure, and technique for selected doping. The Atomic Energy Research Agency, Harwell, England, had a contract with W. & C. Spicer, Ltd., for arc fusion growth of single crystals of MgO, and the Research Materials Program at ORNL has purchased the right from that company to duplicate the furnace design and crystal-growth techniques.

Table 2 indicates the analyses of magnesia powder as obtained after isostatic compaction and following arc fusion. It is evident that the initial purities of the starting material and the electrodes, and the maintaining of purity during calcining, sintering, isostatic compaction, fusion, ball mill grinding, and refusion were the factors that determined the purity of the end product.

The MgO crystals were of reasonable purity (4*N*) and perfection; however, many of the melts gave crystals that exhibited an internal cloud or murkiness that may have been due to hydroxyl or water vapor in the starting powder. The Research Materials Program at ORNL will investigate [7] some additional prepurification techniques, prolonged vacuum baking at an elevated temperature before isostatic compaction, a close control of purity during compaction and fusion, and high temperature vacuum annealing of the fused crystals in an attempt to improve the quality.

Figure 1 indicates the optical absorption coefficient at 2850 Å of MgO quenched in argon and irradiated with ^{60}Co gamma rays versus the concentration of iron (from chemical analysis) for a wide variety of single crystals measured by Y. Chen and W. Sibley of the Solid State Division of ORNL [8]. Also shown are similar data for MgO with 200 to 5000 ppm of iron, obtained by R. W. Davidge of AERE, Harwell, England, after heating the crystals in air at 1400 °C [9]. The figure shows that the optical absorption coefficient depends markedly on the concentration of iron in the MgO.

It must be stated that most of the published work on diffusion, plastic deformation, and optical absorption studies on MgO would have benefited from better crystals. The status-quo is that of single crystals of several tens of cubic centimeters maximum size, 4*N* purity, internal cloud due to hydroxyl or water vapor, and lots of experimental problems to solve before better crystals can be provided.

2.2 Zinc Oxide

The final report of a contract between the Advanced Research Projects Agency and the Radio Corporation of America on "The Synthesis and Characterization of Electronically Active Materials" contains the statement by L. R. Weisberg that "ZnO was chosen for study because it is versatile, useful, and enigmatic". The author continues that "The means and mechanisms of energy transfer in ZnO are still obscure". The files of the RMIC contain many references to crystal growth of ZnO during the past five years by hydrothermal, flux growth, traveling solvent, vapor reaction, thin-film sputtering, and other techniques. The

TABLE 2. *Analysis of magnesia powder and single crystals of MgO (ppm) compact and crystal analyses at ORNL*

Impurity	Ca	Na	Pb	Ba	Mn	Zr	As	Cr
Powder [a]	35	.....	25	40	3	trace	10	.....
Compact [b]	29	25	< 0.8	< 20	1.5	< 1	< 3	24
Single crystal [c]	20–30	1–3	< 0.5	< 2	< 1	1–5	< 5	< 5
Impurity	**Ti**	**N**	**P**	**S**	**Fe**	**Si**	**Al**	**Zn**
Powder [a]	.....	.....	25	250	8	20	80	20
Compact [b]	< 30	< 1	8.5	140	11	76	50	< 50
Single crystal [c]	< 5	1–5	< 3	< 2	2–10	15–39	30–40	1–10

[a] Powder and analysis from the Kanto Chemical Co., Japan.
[b] Same powder, compacted at Atomic Energy Research Agency, Harwell, England; analyzed at Oak Ridge National Laboratory.
[c] Average values for crystals from 18 arc fusions by W. & C. Spicer, Ltd., England; analyses at Oak Ridge National Laboratory.

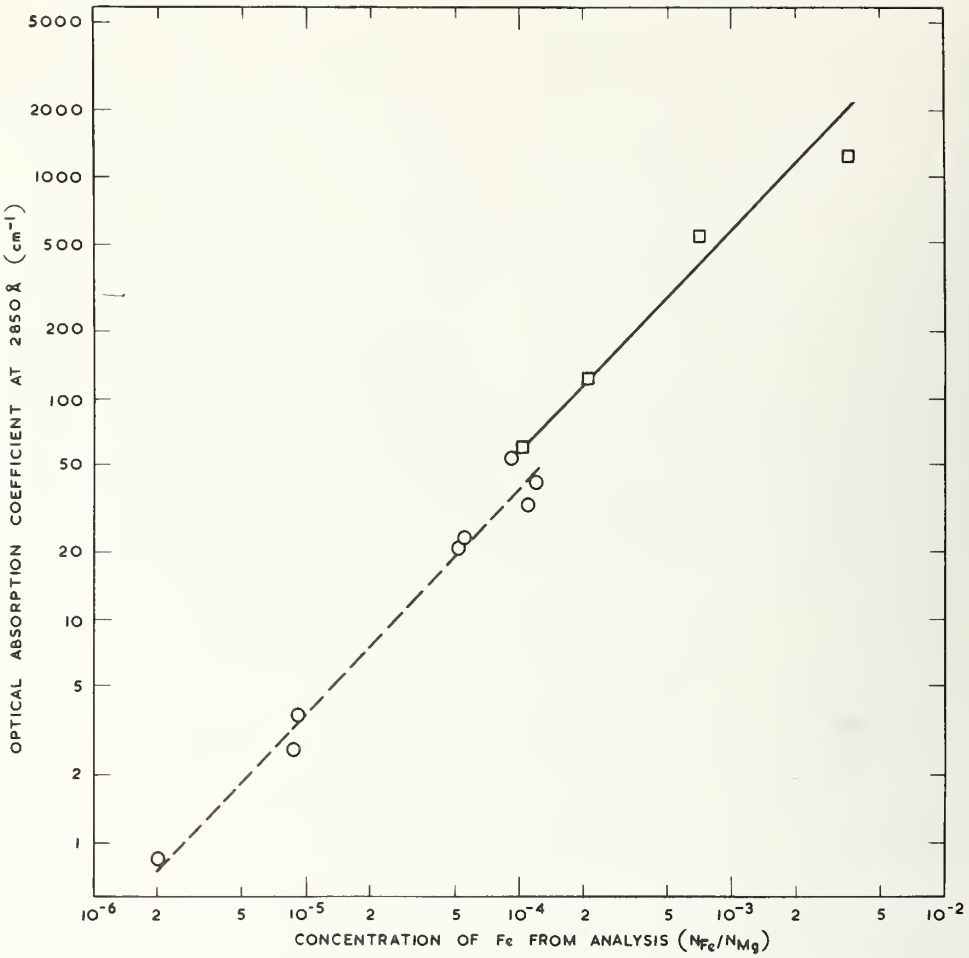

FIGURE 1. *Variation of absorption in MgO at 2850 Å wavelength with iron content.*
○—saturation level on γ irradiation (Chen and Sibley); ◇—saturation level on heating in air at 1400 °C.

Airtron Division of Litton Industries has produced ZnO hydrothermally, and this material is commercially available. Y. S. Park and D. C. Reynolds [10] have grown crystals by subliming both ZnS and ZnSe to have them react with oxygen in an argon gas flow.

Figure 2 is a photograph of single crystals of ZnO, available commercially in research quantities [11]; Table 3 gives the results of an emission spectrograph analysis (typical data but not guaranteed values). The status-quo for ZnO, therefore, is that of raw, uncut, hexagonal crystals up to 6 mm diameter, with less than 50 ppm impurity content as detected by emission spectroscopy or available in the *Z*-axis wafer form, either undoped or doped with lithium. It is hoped that a commercial availability of research specimens of reasonable purity will serve to make ZnO less enigmatic.

2.3. Calcium Oxide

Single crystals of CaO of 2N or 3N purity are advertised for sale from Electronic Space Products, Inc., Muscle Shoals Electrochemical Corp., Semi-Elements, W. & C. Spicer, Ltd., and yet other commercial producers. Table 4 represents typical data for the Spicer product. These crystals are listed as 3N purity, and they vary from colorless transparent to cloudy or milky. It has been stated that the cloud can be removed by annealing at 1800 °C. F. Galtier and R. Collongues [12] have recently reported the production of single crystals of CaO by the Verneuil method in a plasma furnace. They state that the crystals are as large as 7 mm diameter by 20 mm long, are perfectly transparent, and that they exhibit a remarkable chemical inertia in that they can be stored under water for several weeks without change. No information is available as to the actual purity and perfection of these crystals; however, the fact that they are transparent and unaffected by water would suggest that a considerable improvement has been made in the quality of single crystals of CaO.

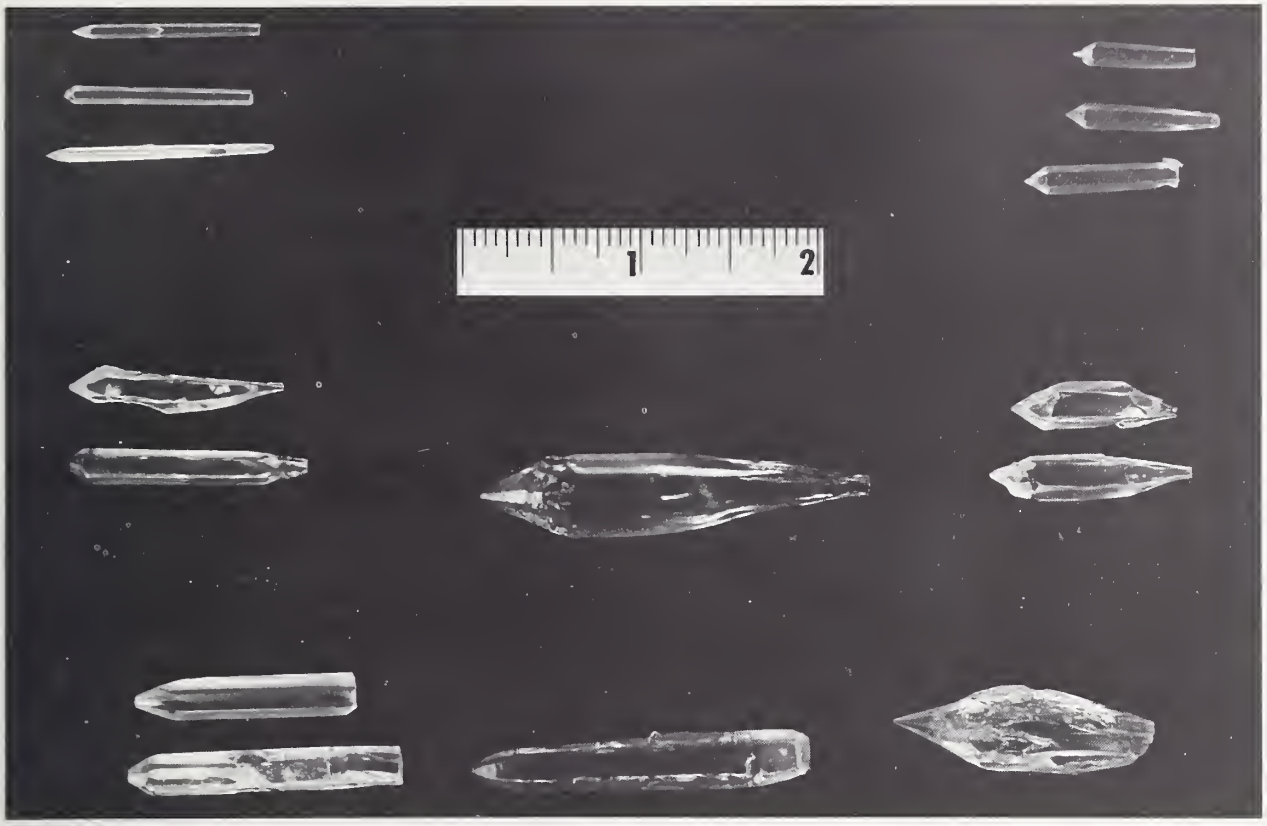

FIGURE 2. *Single crystals of ZnO.*

2.4 Barium or Strontium Oxide

During the period from July, 1966, to July, 1967, the RMIC received 12 requests for single crystals of BaO; however, they had no information concerning a commercial or research producer. R. J. Gambino [13] produced single crystals of Eu-doped BaO or SrO by a modified Verneuil technique, and G. E. Pynchon and E. F. Sieckmann [14] grew single crystals of "good optical quality" in a graphite resistance furnace by the method of ohmic heating; however, the maximum size of these crystals was listed as 1 mm^3. The pioneering effort of the group at Cornell University [15] has not been continued due to a lack of research quality specimens.

2.5 Zirconia and Hafnia

Analytical data exist for single crystals of zirconia, ZrO_2, and hafnia, HfO_2, that have been produced in a number of modifications. Pure zirconia has been used to produce crystal fragments up to 7 cm^3 volume with no visible crystal planes [16] as: (*a*) opaque green to white crystals, (*b*) gray to black crystals that possibly contain hydrogen in the lattice, and (*c*) gray to black crystals with a surface coating of golden appearance [17]. On calcination both (*b*) and (*c*) revert to (*a*). Transparent crystals up to 0.5 cm^3, varying in color from pale straw to dark brown, have been grown [16] with additives of 9 percent wt. calcia or 14.5 percent wt. yttria. The maximum impurity level is about 700 ppm excluding hafnia, and Ruh and Garrett [18] have published a full analysis for about 90 elements. Chase and Osmer [19] have produced single crystals of zirconia and hafnia from a PbF_2 fused salt system, and have also reported on flux crystal growth of other materials [20].

2.6 Titanium Dioxide or Oxide

The files of the RMIC list 9 commercial and 7 research producers of single crystals of material that are identified as TiO_2, Ti_2O_3, or TiO and are labeled as reasonably pure or of good quality. The literature as available, however, is almost devoid of any indication as to the purity and perfection of such crystals; not even the stoichiometry is indicated. Additional work involving the Verneuil, flame fusion, float zone, hollow cathode plasma torch, or chemical transport [21] techniques are required before one can discuss the purity and perfection of these materials.

TABLE 3. *Emission spectograph analysis of single crystals of zinc oxide (ppm) made by the 3M Co., Dielectric Materials and Systems Division*

Element	Detection limit	Quantity
Ag	< 1.0	< 1.0
Cu	< 1.0	8
Cd	3	.....
Ti	< 1.0	.....
V	< 1.0	< 1
Cs	< 1.0	< 1
Sn	< 1.0	1.5
Mo	< 1.0	.....
Be	< 1.0	.....
Al	3	< 3
Bi	< 1.0	.....
In	3	.....
Ge	< 1.0	.....
Fe	< 1.0	< 1
Cr	< 1.0	< 1
Ni	< 1.0	.....
Si	5	< 5
Sb	10	.....
Mg	< 1.0	< 1
Pd	3	.....
Mn	< 1.0	.....
B	< 1.0	5
Te	10	.....
As	10	.....
Ba	3	.....
Li	< 1.0	< 1
K	3	3
Na	< 1.0	3

(Typical data but not guaranteed values. The sample was ground in a boron carbide mortar and pestle.)

TABLE 4. *Analysis of single crystals of calcium oxide (ppm) from W. & C. Spicer, Ltd.*

Impurity	Al	Fe	Mg	Mn	Si	Sr
		< 50	< 200	< 50	< 100	< 100
Impurity	Ag Be Cr	Ba Cu Ga Mo	Co Pd Ti	Ce Ni Pb Sn	Cd	Be Na Cr
				< 50	< 100	< 100

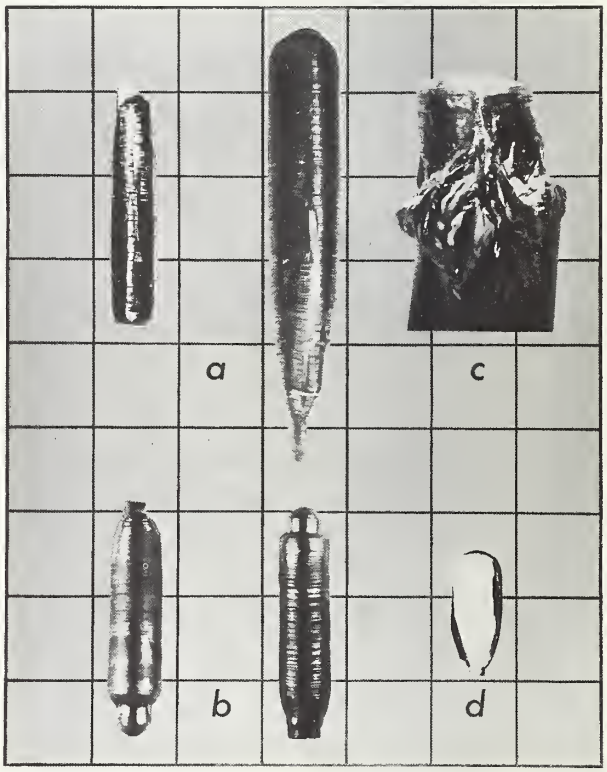

FIGURE 3. *Metal oxide crystals prepared by the arc-transfer method.*
(a) NiO; (b) CoO; (c) Tracking in NiO; (d) Cleaved boule of CoO (1 cm/div).

3. Crystal Growth Techniques

3.1 Arc-transfer Method for Metal Oxides

A major advance in crystal growth of oxides has been the arc-transfer method developed by J. R. Drabble and A. W. Palmer [22] of the University of Exeter, England. They strike a d.c. arc between a sintered feed rod (cathode) and the crystal being grown (anode); the oxides of Co, Fe, Ni, Ti, and V have been grown. B. A. Smith and I. G. Austin [23] of the University of Sheffield, England, have extended the arc-transfer technique to produce pure and Li-doped crystals of NiO and CoO. Figure 3 is a photograph of typical crystals of NiO and CoO, and tracking in NiO. The typical crystal is 5–9 mm diameter × 1–2 cm long.

Several other systems were explored using the arc-transfer method. Transport was usually observed in experiments involving Fe, Mn, Ti, V, Cr, and Cu but the product often contained mixed phases of more than one oxide. Only negligible growth was observed for MnO, Cr_2O_3, Al_2O_3, and ZrO_2. There is little if any data available on the purity and perfection of the oxide crystals produced by arc-transfer.

3.2 Epitaxial Deposition of Metal Oxides

Also of interest is the work of Robinson, White, and Roy [24] of the Materials Research Laboratory at the Pennsylvania State University on epitaxial deposition of NiO, CoO, FeO, Co_3O_4, and Fe_3O_4

on to single crystal MgO by the hydrolysis of the gaseous anhydrous metal bromide. Repeated deposition has permitted the growth of crystals up to 1 mm thick, and with a substantial increase in purity. The dislocation count for NiO was only 10^3 to 10^5 cm^{-2}.

3.3 Internal Centrifugal Zone Growth of UO_2 and 50–50 ThO_2–UO_2

A second major advance in the growth of single crystal oxides is the internal centrifugal zone growth technique developed by A. T. Chapman and G. W. Clark [25] of the Research Materials Program at the Oak Ridge National Laboratory. Figure 4 is a schematic drawing of the equipment to grow single crystals of UO_2. One starts with a sintered rod having a void in the bottom to permit insertion of a (single crystal) seed. The thin metal shields of Mo are used for inductive coupling to the coil until the temperature is such that the coil couples directly to the material. The dual action of rotation and translation circulates the molten material inside its own crucible, and deposits a single crystal with the preferred orientation of the seed crystal. This technique should be applicable to any high melting point material whose electrical conductivity at elevated temperatures will permit eddy current heating. Large grains of 50–50 ThO_2–UO_2 have been grown, also single crystals of isotopically enriched UO_2 for which economy of material is enhanced by retention within its own crucible. Figure 5 is a photograph of a cross section through a typical ingot.

There are 6 commercial and 9 research producers of single crystals of UO_2 listed in the files of the RMIC, and A. T. Chapman [26] is actively engaged in a program involving a comparison of material from different sources by etch pit, electron diffraction, and electron microscope techniques. This work was discussed at a recent meeting of the Nuclear Society of the American Ceramic Society and will be submitted for publication.

3.4. Flux Growth of ThO_2 and CeO_2

A major interest of the Solid State Division at the Oak Ridge National Laboratory is electron spin resonance (ESR) measurements on single crystals of ThO_2 and CeO_2 as doped with Gd, Dy, Er, or Yb. Figure 6 is a photograph of a single crystal of ThO_2, an optically transparent tetrahedron about 3 mm on edge, grown from a molten lithium ditungstate solvent by C. Finch and G. W. Clark [27] of the Research Materials Program at ORNL. These crystals contain less than 500-ppm W and less than 50-ppm Li as major impurities. Lanthanide- or uranium-doped single crystals of ThO_2 and CeO_2 have also been grown, and the glove box facilities of the Transuranic Research Laboratory at ORNL are currently being used to incorporate Cm, Am, and other transuranic elements. R. C. Linares [28]

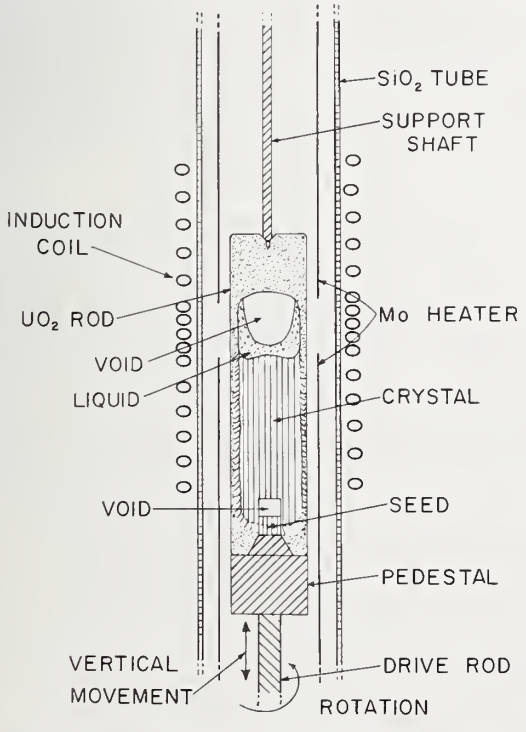

FIGURE 4. *Equipment for the internal centrifugal zone growth of single crystals of uranium dioxide.*

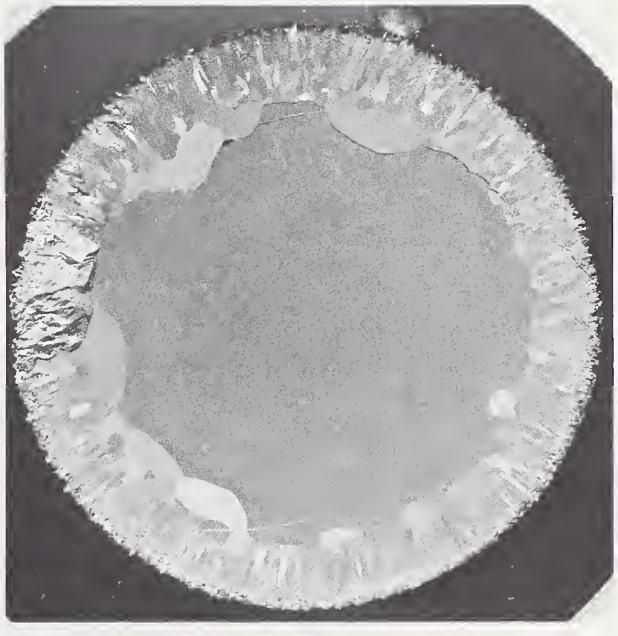

FIGURE 5. *Cross section through an ingot of uranium dioxide grown by internal centrifugal zone growth.*

290-621 O-68—14

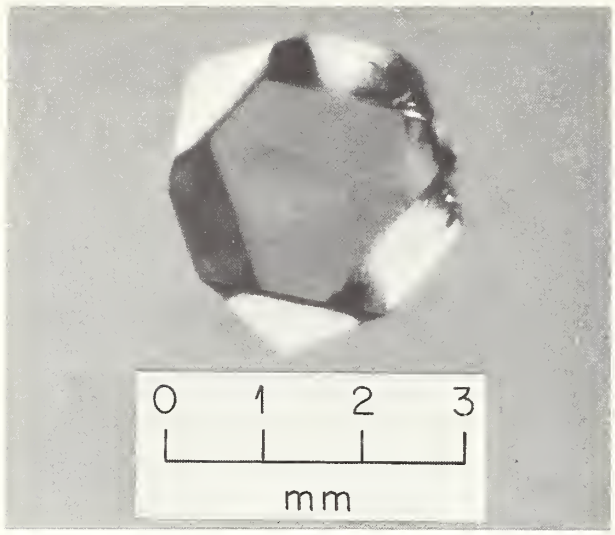

FIGURE 6. *Octahedral ThO_2 single crystal grown from $Li_2O \cdot 2WO_3$ solvent at 1280 °C.*

reported on the growth and properties of ThO_2 and CeO_2 as possible laser materials. Three different flux systems were used, and the optical radiation damage and possible laser properties were examined. The author concluded that a laser crystal can probably be produced if one can devise a technique to remove excess lead from the system.

3.5. Electron-Beam Float-Zone Growth of Laser Host Materials

Sapphire (alpha alumina) and ruby ($Al_2O_3:Cr^{3+}$) have been produced by flame fusion, hydrothermal, flux, Czochralski, electron-beam float-zone, hollow cathode plasma beam, and vapor deposition techniques. The files of the RMIC list 9 commercial and 5 research sources and more than 80 papers on growth techniques since 1965. These papers do not include the large number of proprietary or in-house reports of a number of commercial producers. Papers A–1, B–2, B–7, B–8, B–11, B–14, E–1, and E–14 of the International Conference on Crystal Growth, 1967 [5] concern either sapphire or ruby, and a great deal of information is available only in contract reports to the Air Force Cambridge Research Laboratory, Office of Naval Research, and to other government agencies. The long-standing program of research on "Crystal Growth and Characterization" of the National Bureau of Standards was changed on July 1, 1966, to a program of research on "Crystal Growth and Characterization and High Temperature and Laser Materials."

W. Class et al. of the Materials Research Corporation have reported extensively [29] on electron-beam float-zone processing of aluminum oxide, yttrium aluminum garnet, and multiply doped garnets. Large single crystals of sapphire have been grown that are optically clear, have a typical dislocation density from 10 to 10^4 cm^{-2}, and are completely clear of lineage boundaries. A typical chemical analysis is 20 ppm Fe, Ni, 10 ppm Cr, Cu, less than 10 ppm Ti, Si, and B, less than 5 ppm Sn, and less than 1 ppm Mn, Mg, Pb. The electron-beam float-zone technique uses surface tension to support a molten zone that traverses the crystal. The purification arises for the most part not from zone refining, but from selective distillation of higher vapor pressure impurities. This is an advantage for sapphire, but a distinct disadvantage for ruby in which one obtains a radial distribution or coring of the chromium.

3.6. Hollow Cathode Plasma Growth of Laser Host Materials

Yet another important technique in crystal growth of oxidic materials is the hollow cathode plasma beam process described by W. Class et al. [29] and by W. Class [30]. The advantages of this process are that one can operate at pressures up to 3 Torr with virtually any gas and without any thermionic electron emitter that might serve as a source of contamination. Float-zone purification and single crystal growth of yttrium aluminum garnet, yttrium aluminate, erbium aluminum garnet, erbium aluminate, and the oxides of yttrium, erbium, thulium, lanthanam, zirconium, titanium, and aluminum have been carried out with this type of hollow cathode. The crystalline perfection appears quite good under crossed polaroids; however, this technique is just started, and there are no data on purity and perfection.

3.7. Czochralski Growth of Laser Host Materials

Charvat et al. [31] and Keig et al. [32] of the Crystal Products Division of the Union Carbide Corporation, Indianapolis, Indiana, have reported extensively on the Czochralski growth of ruby and Nd^{3+}-doped YAG. The most important characteristic for a laser host material is the optical quality, and the purity of the starting material is of utmost importance since impurities can precipitate during cooling to form minute but well dispersed inclusions. These are difficult to detect, but are a real problem since they cause a localized absorption of optical energy under high-power Q-switched light operation and can lead to damage within the crystal. The most informative techniques for optical quality are Schlieren photography and Twyman-Green interference. Good quality laser ruby has less than 1 fringe per cm of rod length,

where these fringes are due to strain or to uneven distribution of solute. Crystals have been grown that are 5 cm diameter by 30 cm long, with no misorientations that can be detected by chemical etching or the Schultz-Wei technique. The dislocation densities measured on the basal and prismatic planes are 10^4 and 10^5 cm^{-2}, respectively. The starting material for Czochralski growth of ruby has 20 to 30 ppm of cation impurities. Elimination of rare-earth impurities is of extreme importance for Nd^{3+} YAG, since these have optical absorption tails that extend into the infrared region. Faceting and core formation are also a problem with this material.

4. Summary

The introductory lecture at the Santa Fe Conference on Radiation Effects in Semiconductors (to be published by Plenum Press) was presented by Dr. J. W. Corbett, General Electric Research Laboratories, Schenectady, New York, on the subject of "Important Unanswered Problems." Dr. Corbett used three slides as a part of his lecture that read: What are the impurities; is that all the impurities, and are you sure? It is felt that these questions are equally applicable to the purity and perfection of oxide materials; that solid state chemistry is as important as solid state physics; and that crystal growth and characterization are as important as research on oxide materials. Progress in understanding the fundamental properties and the ultimate range of properties depends, therefore, on a continued improvement in the purity and perfection of research specimens.

5. References

[1] The author is indebted to Mr. T. F. Connolly, Director, and to Dr. H. S. Pomerance of the Research Materials Information Center for a great deal of assistance in assembling the information for this survey. Solid state crystal producers and users are urged to contact the RMIC, Bldg. 3001, Oak Ridge National Laboratory, P.O. Box X, Oak Ridge, Tennessee 37830 for data sheets to record their product or crystal desires.

[2] Engineering Properties of Selected Ceramic Materials, 1966, compiled and edited by Battelle Memorial Institute (American Ceramic Society, 1966).

[3] The Growth of Oxide Single Crystals from the Flux Melt, by E. A. D. White; High Temperature Techniques, by R. G. Bautista, in Techniques of Inorganic Chemistry, vol. 4 (Interscience Publ., 1966).

[4] Report MAB 229, The Characterization of Materials, Materials Advisory Board (1967).

[5] Proc. Intern. Conf. on Crystal Growth, J. Phys. Chem. Solids, Pergamon Press (1967).

[6] Z. Rabenau, Chemie Ingenieur Technik **36,** 542 (1964).

[7] C. T. Butler and J. R. Russell, Solid State Division, Oak Ridge National Laboratory, are in charge of the program of research on MgO.

[8] Y. Chen and W. A. Sibley, Phys. Rev. **154,** No. 3, 842 (1967).

[9] R. W. Davidge, J. Matl. Sci. **2,** 339 (1967). I am indebted to Dr. Davidge for this figure.

[10] Y. S. Park and D. C. Reynolds, J. Appl. Phys. **38,** No. 2, 756 (1967).

[11] Minnesota Mining and Manufacturing Company (3M), Dielectric Materials and Systems Division, 2501 Hudson Road, St. Paul, Minnesota 55119. I am indebted to Dr. Robert D. Carlton for the photograph and table of spectrographic data.

[12] F. Galtier and R. Collongues, C. R. Acad. Sc. Paris **C264,** 87 (1967).

[13] R. J. Gambino, J. Appl. Phys. **36,** 656 (1965).

[14] G. E. Pynchon and E. F. Sieckmann, Phys. Rev. **143,** No. 2, 595 (1966).

[15] R. L. Sproull, W. C. Dash, and W. W. Tyler, Rev. Sci. Instr. **22,** 410 (1951).

[16] Personal communication with N. Quinn, W. & C. Spicer, Ltd.

[17] F. K. McTaggart, Nature **199,** 4981 (1963).

[18] R. Ruh and H. Garrett, J. Am. Ceram. Soc. **47,** No. 12, 627 (1964).

[19] A. B. Chase and J. A. Osmer, Am. Mineralogist **51,** 1808 (1966).

[20] A. B. Chase and J. A. Osmer, J. Am. Ceram. Soc. **50,** 327 (1967).

[21] T. Niemyski and W. Piekarczyk, J. Crystal Growth **1,** 177 (1967).

[22] J. R. Drabble and A. W. Palmer, J. Appl. Phys. **37,** 1778 (1966).

[23] B. A. Smith and I. G. Austin, J. Crystal Growth **1,** 79 (1967). I am indebted to Dr. I. G. Austin for permission to use the photograph.

[24] L. B. Robinson, W. B. White, and R. Roy, J. Mtrls. Sci. **1,** 336 (1966).

[25] A. T. Chapman and G. W. Clark, J. Am. Ceram. Soc. **48,** 494 (1965). I am indebted to G. W. Clark for the drawing and photograph.

[26] A. T. Chapman, School of Ceramic Engr., Ga. Inst. of Tech., Atlanta, Ga. 30332, personal communication.

[27] C. B. Finch and G. W. Clark, J. Appl. Phys. **36,** 2143 (1965); **37,** 3910 (1966). I am indebted to G. W. Clark for this photograph.

[28] R. C. Linares, J. Phys. Chem. Solids **28,** 1285 (1967).

[29] W. Class, H. R. Nasor, and G. T. Murray, Crystal Growth, J. Phys. Chem. Solids (Pergamon Press) 1967; AFCRL–67–0723 report (unpublished).

[30] W. Class, Research/Development (September 1967).

[31] F. R. Charvat, J. C. Smith, and D. H. Nestor, Crystal Growth, J. Phys. Chem. Solids (Pergamon Press) (1967).

[32] G. A. Keig, D. H. Nestor, and P. E. Otten, SRCR–67–5, Annual Technical Report, Office of Naval Research (unpublished).

The Growth of Oxide Single Crystals By Chemical Transport

Robert Kershaw and Aaron Wold

Department of Chemistry and Division of Engineering

Brown University, Providence, R.I. 02912

The growth of relatively large ferrite single crystals (5mm on an edge) was accomplished by an improved chemical transport procedure. Magnetite crystals were analyzed and found to have the composition $Fe_{2.99}O_4$. Dry hydrogen chloride was used as the transporting agent and there was no apparent evidence of chloride contamination in the final crystals.

Key Words: Chemical transport, crystal growth, ferrite crystals.

Chemical transport reactions have been used [1][1] to prepare single crystals of iron (II) diiron (III) tetroxide (magnetite) and other ferrites which comprise the majority of all known ferrimagnetic materials. Previously, Smiltens [2] had prepared well characterized iron (II) diiron (III) tetroxide crystals using a modified Bridgman-Stockbarger technique. The crystals were grown under a CO_2 atmosphere and then CO was introduced and the ratio of these gases changed gradually as the temperature was varied during the cooling process. This maintained the proper oxygen pressure necessary for the preparation of stoichiometric crystals. The techniques of flame fusion [3] and hydrothermal growth [4] have also been used to grow ferrite crystals, but their quality, in general, has usually been poor. In addition, a cobalt ferrite crystal was grown by Ferretti et al. [5] from the melt at 1600 °C under an oxygen pressure of 790 p.s.i. Chemical analysis of a portion of the crystal gave a ferrous ion content of 1.3 percent. Kunnmann et al. [6] reported that the simple ferrite spinels crystallize readily from the ternary flux system $MO\text{-}Na_2O\text{-}Fe_2O_3$. Crystals of $CoFe_2O_4$ were grown from a mixture of 1.5 moles of $CoFe_2O_4$ and 1 mole of $Na_2Fe_2O_4$ utilizing a platinum wire cold finger. The crystals grown were approximately 1 inch in diameter and 3/4 inch thick. However the crystals were not dense and appeared to have many defects. Nickel ferrite crystals were also grown by Kunnmann et al. [7] from sodium ferrite flux by a modified Czochralski method. The crystals were analyzed and corresponded to $Ni_{1.01}Fe_2O_{4.01}$. All of the latter methods were difficult to carry out and the results hard to reproduce.

Relatively pure crystals of magnetite and the other ferrites can, therefore, best be grown by the method of chemical transport. In this method [1, 8] the charge material reacts with the transporting agent to form a more volatile compound. This vapor diffuses along the tube to a region of lower temperature, where some of the vapor undergoes the reverse reaction. The starting compound is reformed and the transport agent is liberated. The latter then diffuses to the hot end of the tube and again reacts with the charge. Under the proper conditions the compound may be deposited as crystals. This may be illustrated with Fe_3O_4 where the transport using HCl as the transport agent occurs by the reversible reaction

$$Fe_3O_4 + 8\ HCl \rightleftharpoons FeCl_2 + 2\ FeCl_3 + 4\ H_2O.$$

The above reaction is illustrated in figure 1, and may also be used to prepare crystals of other ferrites such as $NiFe_2O_4$, $CoFe_2O_4$.

Experimental Procedure

The pure starting compounds were prepared by the method of Wickham et al. [9]. In this method precursors are reacted to form the pyridinates $M_3Fe_6(CH_3CO_2)_{17}O_3OH \cdot 12Py$; and then careful decomposition of the pyridinates results in well-crystallized, stoichiometric ferrites.

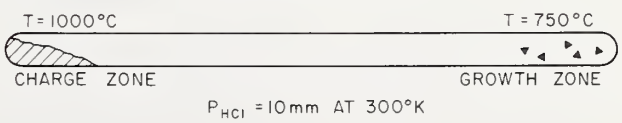

FIGURE 1. *Transport process.*

[1] Figures in brackets indicate the literature references at the end of this paper.

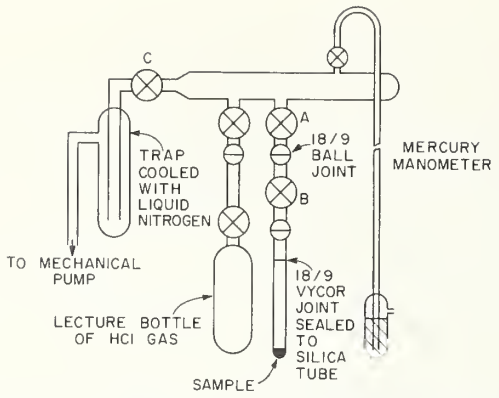

FIGURE 2. *Vacuum system used to prepare transport tubes.*

The transport tube used for single crystal growth is prepared by closing one end of a ten inch length of 13 mm. I.D. silica tubing and sealing the other end to an 18|9 vycor ball joint. After the tube has been cleaned with aqua regia and dried a one gram charge of ferrite is added through a long-stemmed funnel, and the tube is connected to stopcock on the vacuum system shown in figure 2. When the pressure in the system has been reduced to less than 10^{-3} Torr the sample is outgassed by heating to about 300 °C. Stopcock *C* is then closed, and HCl gas is let in to a pressure of 10 Torr, as measured with the mercury manometer. Stopcocks *A* and *B* are then closed, the joint between them separated, and the transport tube sealed off to a length of 8 inches with an oxy-hydrogen flame. This tube is then centered in the transport furnace and the temperature controller themocouples are placed at its ends. A Hevi-Duty MK2012 furnace, rewired to give two independently controllable temperature zones was used in these experiments. It was found that a two cm. thick firebrick baffle was needed at the junction of the two zones in order to obtain a satisfactory temperature profile in this relatively large diameter (6 cm.) furnace. The temperature of the empty, or growth zone is raised to 1000 °C, while the end of the tube with the powder, or charge zone, is left at room temperature. This back transport lasts for 24 hours, and cleans the growth zone of stray nuclei by causing them to transport to the charge zone, where they cannot interfere with crystal growth. The growth zone temperature is then lowered to 750 °C and the charge zone raised to 1000 °C. Transport is allowed to proceed for 10 days, after which time the charge zone temperature is reduced to 750 °C. In about one hour, when equilibrium has been re-established, both heaters are turned off. When the furnace has cooled to room temperature (usually overnight) the transport tube is removed and opened.

Properties

Crystals grown by chemical transport are well-formed octahedra, with shiny faces measuring up to 5 mm on an edge. X-ray patterns of the ground-up crystals were identical to that of the starting material. The results of chemical analysis of a typical magnetite run are given below. There was no evidence of chloride in the final transported crystals, although traces might be expected.

	Total iron	Iron (II)	Formula
Calculated	72.36%	24.12%	
Found (Powder)	72.66%	23.78%	$Fe^{II}_{.99}Fe^{III}_{2.03}O_4$
Found (Crystal)	72.83%	23.65%	$Fe^{II}_{.98}Fe^{III}_{2.01}O_4$

References

[1] Z. Hauptman, Czech. J. Phys., **B12**, 148 (1962).
[2] J. Smiltens, J. Chem. Phys., **20**, 990 (1952).
[3] R. Lappa, Przegland Telekomunikacyjng **31**, 229 (1958).
[4] N. Yu Ikornikova, Dokl. Akad. Nauk. USSR, **130**, 610 (1960).
[5] A. Ferretti, R. J. Arnott, E. Delaney and A. Wold, J. Appl. Phys., **32**, No. 5, 905 (1961).
[6] W. Kunnmann, A. Wold and E. Banks, J. Appl. Phys., **33**, No. 3, 1364 (1962).
[7] W. Kunnmann, A. Ferretti and A. Wold, J. Appl. Phys., **34**, No. 4 (Part 2), 1264 (1963).
[8] R. Kershaw and A. Wold. Accepted by Inorganic Syntheses.
[9] D. G. Wickham, E. R. Whipple and E. G. Larson, J. Inorg. Nucl. Chem., **14**, 217 (1960).

Panel Discussion

A. S. Nowick, Columbia University, Chairman
R. E. Carter, General Electric Company
J. H. Crawford, Jr., University of North Carolina
A. B. Lidiard, United Kingdom Atomic Energy Research Establishment, Harwell
D. H. Whitmore, Northwestern University
Y. Haven, Wake Forest University
J. B. Wachtman, Jr., National Bureau of Standards

The purpose of the panel was to summarize and comment upon the status of the field of mass transport in oxides. It was hoped that the discussion would focus attention on important new ideas that have arisen in the conference, and would also point out possible avenues of approach that had been missed or were not sufficiently emphasized earlier in the conference. To accomplish this objective, the chairman selected a number of key questions. In each case, at least one member of the panel presented the principal discussion, following which the other panel members and the audience contributed to the general discussion. In what follows, we shall present the questions posed, the principal discussions, and selected points from the general discussion.

Importance of a Better Fundamental Understanding

Question:

Is a better understanding of the fundamentals of ionic mass transport in oxides really needed in modern technology?

Principal Discussion (R. E. Carter):

The present question can be approached by considering three questions raised by Dr. R. Thomson of ARPA at the start of the conference:

1. What is the state of our knowledge of ionic transport in oxides?
2. What should be the goal of work on metal oxides?
3. Who is going to do the required work?

What then is the state of knowledge of transport in oxides and how useful is this knowledge to modern technology? Historically most of the work in oxides has been done by what might be called high temperature physical chemists, modern ceramists and metallurgists. These people have by and large gathered data to enter into analyses which were quite approximate (simple mass action equations, isolated defects, and activity coefficients of one). The motivation has been to understand various processes such as metal oxidation, sintering, electroconductivity, plastic deformation, and chemical synthesis. In general, to understand these processes has not required data of high precision. Also, as Professor Birchenall pointed out, many of the measurements have been made on commercially available material because these are the materials in which it is desired to understand the processes. These investigators have been fairly successful in meeting the over-all goals that were set up. It may then be said that our understanding of technologically important processes such as sintering is reasonably good. The principal problem in sintering is one of models and, in the case of oxides on which the better transport data has been gathered, understanding is not limited by the absolute accuracy of the available diffusion coefficients. Clearly this is not the case for all ceramic materials and an excellent case may be made for better transport data on oxides of specific interest. There seems to be little likelihood, however, that such data will improve our general understanding of the important processes involving metal oxides.

Dr. Thomson's second question, the goal of work on ionic transport in oxides, is related to the use to be made of the data. Several speakers at this conference have presented strong arguments asking for more accurate mass transport measurements both in the intrinsic and extrinsic ranges. The attainment of this accuracy will do much to improve the liaison between people interested in technological aspects of diffusion and those interested in the more fundamental studies, which should be one of the goals of any diffusion study in oxides. However, many of the processes that we wish to understand are not really controlled by ionic motion, but are strongly influenced by other aspects, such as interfaces and grain boundaries.

I think, therefore, that investigators working with oxides now appear to be at a crossroads. They can refine their techniques, work on better characterized materials, and develop better theories of the defect state. They can then hope or assume that this knowledge will be applicable to commercial materials and processes. Alternatively they can examine their

processes directly and look at interfaces and grain boundaries which may be controlling the rate of the ionic transport of interest, an approach which is often ignored by those concerned primarily with ionic motion. The greatest progress would appear to come from exploring both of these approaches, which should ideally compliment one another.

Finally, who is going to do the work which will permit a better understanding of oxides? The technologists, the ceramists and metallurgists, will no doubt continue to work on materials that, by physicists' standards, are impure and poorly characterized, and they will probably move into more complex areas like surfaces, interfaces, and grain boundaries. The physicist, who makes precise measurements and develops theories, will move from the halides to the oxides. The rate of this move will be approximately proportional to the availability of high quality specimens. In this respect, it is clear that "nothing succeeds like success." Dr. Cleland stated that he had more requests for MgO than any other oxide. At the present time, MgO is probably available in the highest purity and crystal perfection of any of the oxides and probably better work has been done on MgO than on any other oxide. While the strength of the physicist is his ability and interest in making precise measurements and developing exact theories, his weakness is his lack of interest in making good specimens. By and large he waits until good specimens are provided. As expressed by Werner Kanzig, "first come the crystals, then the good measurements, and then the theory."

General Discussion:

Several people felt that Dr. Carter had overrated the state of our knowledge and the usefulness of presently available measurements for technological purposes. The extremely poor reproducibility of diffusion data was particularly cited. These are so poor that, with much of the data it becomes impossible to maximize diffusion-controlled properties. Examples were also given of our inability to use refractory metals for high temperature structural applications because of inability to protect them from oxidation. Also, the processing of electronic ceramic materials (e.g., ferrites, ferroelectrics) is in a poor state because of inability to control sintering and grain growth. Further emphasis was also given in the discussion to the importance of processes other than mass transport that must also be better understood, e.g., grain growth during sintering, adhesion of scale, etc. Such processes will undoubtedly remain the limiting factors in technological processes unless their understanding is also advanced.

The question of proper characterization of the specimens being studied was also discussed. Obviously, only very pure or carefully doped specimens allow for a meaningful study. It is senseless to try to develop a complex theory from precise data if these data apply only to the particular specimen which was studied. A complete chemical analysis is the minimum characterization which is now acceptable. With this analysis there should be given the statistical distribution of the impurity contents.

Value of Alkali Halide Work

Question:

What can we learn from all of the past work on the alkali halides, and can we be misled by applying these results too directly to the oxides?

Principal Discussion (J. H. Crawford, Jr.):

As to the desirability of taking alkali halides as our point of departure in investigating oxides, I would like to make a few general remarks. Firstly, there is a tremendous inheritance available to us from the long standing research program on alkali halides which dates back to the early thirties. This inheritance is not only valuable to investigations of defect behavior in oxides but has profoundly influenced the development of solid state chemistry and physics as it pertains to non-metallic systems. We cannot ignore it. The concepts of point defects, composite imperfections, the mechanisms of their creation thermally and by radiation, the role of defects in diffusion processes, solid state reactions, etc., we largely owe to studies of imperfections in alkali halides.

A second point concerns the importance of trace impurities in determining physical behavior of non-metals: This has been vividly demonstrated through investigations of alkali halides. Radiation response (the yield of color centers), defect aggregation processes and related phenomena have been shown to depend sensitively upon the presence of certain types of impurities in very small concentration. Without the availability of high-purity alkali halide crystals which could then be doped to the desired level with the desired impurity, it is doubtful that this impurity sensitivity could have been explored. At this point we should acknowledge that in many systems impurity sensitivity may not be nearly so great as in the alkali halides and that some equally dominating structural characteristic may be the focus of deviations from intrinsic behavior. For example nonstoichiometry which is notorious in the oxides of transition metals may be the main point of interest.

Nevertheless, the importance of alkali halides as a simple model for defect behavior and mass transport in binary systems is clearly evident, whatever ultimate modifications to such a model might be necessary to make it applicable to a given oxide

system. As a matter of fact, modifications to the simple model are always necessary in order to utilize the body of knowledge available. To use a specific case, let's consider how the concepts are transferred from alkali halides to MgO. Here we must examine differences as well as similarities. The predominant distinction is that MgO is a divalent binary system with the consequence that the binding energy and the energies of formation and motion of cation and anion are considerably higher than for an alkali halide with the same lattice spacing. This means among other things that for a given impurity content one must go to a much higher temperature range than in an alkali halide to reach the domain of intrinsic (as contrasted with impurity-sensitive) behavior as applied to mass transport. Another consequence has to do with possible stable impurity-defect complexes: Whereas a divalent cation in an alkali halide introduces a single vacancy which can be bound to an impurity to form a dipolar complex, a cation impurity with one surplus charge in MgO can account for only one-half of a cation vacancy and the number of stable and metastable complexes is large, e.g., an impurity-vacancy complex still bearing a negative charge, and neutral I_2V complexes with a variety of configurations. It is interesting to note that the I–V complex by virtue of its charge can drift in an applied electric field and contribute to the ionic conductivity. Another difference is radiation response; Sibley and coworkers at ORNL have shown that although color centers can be readily created in MgO by fast neutrons and 1.5 Mev electron irradiation, their creation is evidently caused by a knock-on process rather than a radiochemical one since x rays and γ rays are incapable of producing *F*-centers. On the basis of the difference in valence alone it is evident that we face a much greater range of complexity in both number and response of imperfections. This should not necessarily be taken as a disadvantage since by proper use of some elements of this complexity it is possible to gain a deeper insight into the nature of the defects and their interactions. Nevertheless, it must be admitted that getting a specimen of MgO sufficiently pure to lower the intrinsic range of behavior into an experimentally convenient temperature range may be a difficult task.

General Discussion:

It was pointed out that in the study of nonstoichiometric oxides one might encounter new phenomena not previously seen in the alkali halides. One such effect is the ordering of defects to produce distinct phases of material, as described in the paper by Libowitz. Another telling point made was that alkali halides are essentially completely ionic whereas many important oxides and oxide systems are virtually covalent. Therefore, it would be very advantageous to have another well understood prototype material at the other end of the scale. Unfortunately with the best of these, i.e., an elemental material such as silicon or diamond, it is difficult to make a connection with the processes expected in a binary oxide. Nevertheless a predominantly covalent III–V or II–VI compound might be helpful to use as a guide.

Importance of Theory

Question:

What role can theory play in the development of the subject of mass transport?

Principal Discussion (A. B. Lidiard):

One must consider two principal parts of the theory (i) the underlying mechanics of the defect solid, its energy levels and states, the configurations of individual defects and so on and (ii) the statistical mechanics of defect solids, generally in or near thermodynamic equilibrium. Since models provided by this second part of the theory have formed the basis for most of the discussion at this conference I will deal with this part first.

Statistical mechanics of systems in thermodynamic equilibrium. Here one is interested in partial thermodynamic quantities, dependence of composition upon oxygen partial pressure, etc. Past discussions [1, 2][1] have generally been in terms of model systems of non-interacting point defects—the direction in which the subject was very successfully launched many years ago by Wagner. The extension of these models requires us first to specify the interactions between defects and then to calculate their effect upon the statistical properties. At long-range the dominant interactions between defects bearing a net charge are undoubtedly Coulombic. The only way of handling these which is sufficiently simple to be easily and universally applied is that provided by Debye-Hückel theory: more elaborate and accurate calculations for simple systems show that it is only qualitatively correct [3]. However, since, as Prof. Slifkin's review (this conference) showed, these Coulombic defect interactions are qualitatively important at concentrations even as low as 0.1 atomic percent they must certainly be important at 5 or 10 percent (as e.g., in nonstoichiometric FeO, UO_2 etc.) and it is certainly desirable therefore to make much wider application of the Debye-Hückel description even though it may be only approximate.

The evaluation of defect interactions at small separations is more difficult and depends strongly upon defect structure and details of the inter-

[1] Figures in brackets indicate the literature references at the end of this discussion.

atomic interactions. Evidently when the defects have a complex or unsymmetrical structure (as in the Roth model for Fe vacancies in $Fe_{1-x}O$) this interaction depends on the mutual orientation of the defects. However, even for the simple example of two vacancies in a metal the interaction depends strongly on the direction of the axis of the pair relative to the crystal axes; it is not a simple function of separation as suggested by continuum theories[4]. It is unlikely that theory can provide much insight into the interactions occurring at small separations in the absence of reasonable models for the substances of interest; these are only likely to emerge from a general and basic study of their physical properties. However one aspect of the interaction of complex and unsymmetrical defects can be handled without difficulty and that is "hindrance" effects i.e., the way in which one defect by its extension prevents another defect from occupying a certain number of neighbouring sites. The influence of these hindrances on the predicted composition isotherms was illustrated by the work of Libowitz on $Fe_{1-x}O$. I would interpret this work (which neglects other interactions) as showing the importance of hindrances but not necessarily the unimportance of those features omitted from the calculation (e.g., interactions at short and long-range). It is implied by these remarks that it is adequate to regard the oxide as a perfect lattice containing a statistical distribution of atomic defects—a distribution which can be determined by application of the methods of statistical mechanics. Of course, the model of interacting defects allows the possibility of cooperative ordering phenomena—as was recognised roughly twenty years ago, particularly by Anderson. It has been used by others since, notably by Libowitz for metallic hydrides [5]. The Anderson treatment was based on the simple Bragg-Williams approximation and the theory of physically simplified order-disorder systems (e.g., the Ising model) has now become mathematically very sophisticated. It is possibly time that theorists interested in the field of cooperative phenomena turned their attention to more elaborate models. The occurrence of Magneli phases seems to present a rather striking problem for the theory of these oxides and one where it is not, however, evident that the atomic defect model is a good starting point.

Statistical mechanics of non-equilibrium systems; diffusion etc. Considering kinetic processes, one sees first that for dilute systems of defects one has a fairly good theoretical framework already available. This was reviewed by Manning (this conference). The scheme is sufficiently general to be useful but it needs to be filled out experimentally by the determination of parameters such as the various defect jump rates and activation energies by which the model is specified. This is being done successfully in some metals and alkali halides and in principle could be done also for the closely stoichiometric oxides like MgO etc.

When one turns to concentrated systems (high defect concentrations, chemical diffusion couples, etc.) there is very little to go on. Manning has made many of the extensions of the kinetic theory necessary to deal with chemical diffusion in metals. This gives hope that a similar development of practical value could be made to oxide systems.

In this situation perhaps the most that can be done is to relate experimental results to a general phenomenological scheme adequate to distinguish clearly the different diffusion coefficients which arise (as e.g., in oxidation, interdiffusion of two oxides, tracer diffusion etc.). Such a scheme is provided by the phenomenological equations of irreversible thermodynamics [2]. However, it should be noted that this scheme of equations can make only very limited physical predictions in the absence of either experimental or theoretical knowledge of the behaviour of the phenomenological coefficients as functions of concentration. Howard and I have elsewhere [6] discussed the form of these phenomenological coefficients in dilute systems in both ionic compounds and metals. Although for more concentrated systems the scheme cannot predict much that is physically new, it may be very useful for keeping clear the differences in the nature of the diffusion coefficients measured in different experiments. While this is true for binary systems it is even more true for ternary systems on which there appears often to be an interesting limitation (Cooper, this conference). One should recognise however that the scheme of phenomenological equations one is concerned with here introduces six independent phenomenological coefficients for an isothermal ternary systems, each of which is a function of composition and temperature, and that it is very unlikely that these can all be determined by experiment—simply because there are not enough independent experiments which one can do. Further progress depends upon being able to obtain insight into the form and magnitude of these coefficients from defect models.

States, Energy Levels, etc. of Individual Defects. Although this subject logically preceeds that of the statistics of systems containing defects I deal with it last since it was discussed less frequently at the present conference. In this part of the subject we are almost always concerned with very low concentrations of defects when we are using spectroscopic methods; these methods (optical—especially on zero-phonon and other sharp lines, e.s.r. etc.) give important information about the

structural and electronic symmetry of the defects being studied (cf. the papers of Henderson and Kemp, this conference). The theory of the electronic states of these electron-excess colour centres in the alkaline earth oxides (F-centers and their aggregates especially) has been taken over from the alkali halides with little modification of principle and is very successful. Much less has been done on the electron-deficient centres (trapped holes) and rather little on the states of defects in transition or actinide oxides except for the study of impurity states. The complex structures inferred for the iron vacancy in $Fe_{1-x}O$ and the oxygen interstitial in UO_{2+x} from the long wavelength neutron scattering studies of these materials have not received a fundamental explanation.

Turning now to the calculation of defect formation and migration energies I would say this problem does not look very straightforward. Boswarva's results presented to this conference showed a consistency of different variants of the ionic model for the alkali halides that was lacking for the alkaline earth oxides. This is perhaps partly enhanced by the unreliability of the necessary but quite basic experimental data (e.g., compressibilities). It is likely that the models used for calculating defect migration energies, etc. will only give useful results if they are developed as part of the general solid state physics of these materials. Here the work on lattice vibrations which Slater reviewed can play a very important part. One can see in particular that good shell models have been built up for many materials from neutron scattering experiments but have not yet been much used for defect calculations although the way to do so is pretty clear. It would help considerably to know the predictions of these models for the alkaline earth oxides, UO_2 etc.

In oxides like $Fe_{1-x}O$ and UO_{2+x} it is much more important to know the electronic and charge states of the defects. Thus in considering the interstitial configuration in UO_{2+x} it is important to know whether the electron holes are localised near the oxygen interstitial. From measurements of partial thermodynamic quantities and from electrical measurements on nonstoichiometric UO_2 one can say that it is certain not both holes are so localised. It is not, however, clear that both of them are nonlocalised (inferences have generally been made by comparison with models which omit interactions). If one of the two holes is localised on or near the oxygen interstitial, then a much more elaborate calculation is needed; the atoms whose interaction one is attempting to deal with, are thus not in the same charge states as those which determine the lattice vibrations, elastic constants etc. Familiar examples of the importance of electronic state in determining the equilibrium atomic configuration of the center are provided by the alkali halide hole centers V_k, H etc., which have ⟨110⟩ axes of symmetry. Fundamental discussions of the dependence of configuration upon the electronic state of simple vacancy centers in a fully covalent system (diamond) have been given recently [7].

General Discussion:

The importance of three-body forces (cf. the departure from the central-force Cauchy relations for MgO) was mentioned as a possible source of difficulty in defect calculations. Lidiard's reply referred to Slater's view, presented to the conference, that noncentral forces are not very important for the overall dynamical properties, and suggested the same may be true of defect properties. Explicit attention to the role of three-body forces in defect properties has thus far only been given for the inert-gas solids [8].

References

[1] For an introduction see P. G. Shewmon, Diffusion in Solids, Chap. 5, McGraw Hill Book Co., New York (1963).

[2] For a full and modern account of all aspects of mass transport in solids see Y. Adda and J. Philibert, La Diffusion dans les Solides. Presses Univer staires de France, Paris (1966). For oxides see especially **II**, Chap. XIX.

[3] Review by A. R. Allnatt, Adv. in Chemical Physics, **11**, 1 (1967).

[4] J. R. Hardy and R. Bullough, Phil. Mag. **15**, 237 (1967).

[5] G. G. Libowitz, J. Appl. Phys. Suppl. **33**, 399 (1962).

[6] R. E. Howard and A. B. Lidiard, Reports on Progress in Physics, **27**, 161 (1964).

[7] J. Friedel, G. Leman and M. Lannoo, Phys. Rev. **164**, 1056 (1967) also M. Lannoo and A. M. Stoneham. J. Phys. Chem. Sol., in press.

[8] See e.g. the review by G. L. Pollack, Rev. Mod. Phys. **36**, 748 (1964); also R. Bullough, H. R. Glyde and J. A. Venables, Phys. Rev. Letts. **17**, 249 (1966).

Analysis of Diffusion Data

Question:

Why are data on mass transport in oxides generally so poor and what can be done to overcome the obstacles to better measurements? Also, what are the relationships between the various types of diffusion data which are being obtained?

Principal Discussion I (D. H. Whitmore):

This conference has certainly pointed up emphatically the need to differentiate clearly between the various kinds of diffusion coefficients being evaluated for oxide systems. To date, many of the diffusion experiments conducted on oxides have been concerned with either: (a) the measurement of the diffusivity of the cationic species in a "pure" simple oxide, utilizing an appropriate radioactive tracer of that species and a sectioning method or a decrease-in-surface radioactivity method; or (b) the measurement of the diffusivity of oxygen, using an oxygen isotope exchange method which

may involve either sectioning the specimen after the diffusion anneal or sampling to determine the composition of the gas phase surrounding the diffusion specimen as a function of time. It is mainly these experimentally-derived diffusion coefficients which are of interest to the theorist because they serve as a basis for comparison with the corresponding diffusivities which he derives from his atomistic theory of diffusion processes in oxides.

On the other hand, the technologist concerned with sintering, oxidation processes, etc., may be more interested in the chemical or interdiffusion coefficient which is derived by analyzing the concentration profile in an oxide solid solution formed by interdiffusion between the two different component oxides forming the diffusion couples. This latter diffusion coefficient is a phenomenological one and, as Dr. Lidiard has already remarked, is usually not related in a simple manner to the diffusion coefficients for the individual species in the oxide solution being studied.

If we consider first cation tracer and oxygen ion diffusion measurements that have been carried out on simple oxide systems by different investigators, the reproducibility in the measured diffusivities is generally poor. In fact, past experience indicates that the chance of one investigator's value agreeing with another's (measured under presumably identical experimental conditions) within 50 percent is fairly small. Since the reproducibility of a given tracer diffusion coefficient in a metal or alkali halide to within 2–5 percent is now a common occurrence, adapting the experimental techniques utilized by investigators in these fields to the study of cation and oxygen diffusivities in oxides might yield significant improvement in the oxide data. It has been reported that Argonne investigators working with simple oxides have succeeded already in achieving such reproducibilities for their cation tracer-diffusion coefficients when such experimental methods were employed.

The first serious problem facing the experimentalist undertaking the determination of the cation tracer diffusion coefficient in a given oxide is that of obtaining well-characterized oxide single crystals of extreme purity for his measurements. In contrast with the impurity levels obtainable in semiconductors and alkali halides, most oxides available today must be judged to be relatively impure materials. This may be a very serious problem if the oxide of interest falls into Professor Birchenall's "impurity sensitive" category, or less serious if it falls into his "impurity tolerant" category. Generally speaking, a precise knowledge of the dislocation density, impurity content and distribution, mosaic structure, etc. for the oxide crystal being studied is essential (although not usually done) if a meaningful understanding of mass transport behavior is desired from the experiment.

Next, in conducting a diffusion anneal of the simple oxide specimen (a binary thermodynamic system), the temperature, hydrostatic pressure and one other thermodynamic variable must be fixed in order to define unambiguously the thermodynamic state of the system (the oxide diffusion specimen) being investigated. In this case, it is often convenient to choose the thermodynamic activity of oxygen as the third independent variable since it may be controlled experimentally by regulating the composition and pressure of the gas atmosphere surrounding the specimen during its diffusion anneal. [To extend this consideration to the more general case of a multicomponent oxide system containing r components, we note that this case requires that $(r-1)$ independent variables be specified in addition to the temperature and pressure. The problem of which variables should be fixed in a chemical diffusion experiment involving a multicomponent oxide is frequently not a trivial one and warrants more careful consideration than has been given to it in several past diffusion investigations on oxides.]

The annealing operation for the specimen is certainly one of the most vital steps in the diffusion experiment. Component parts of the heating system like the furnace muffle, specimen container, radiation shields, etc., as well as the surrounding gas atmosphere, may serve to contaminate the specimen itself during the diffusion anneal. The precise measurement of the temperature of the anneal and its duration is important, and the former measurement may be a severe problem for the experimentalist when the anneal is being carried out at ultra-high temperature. It is likely that, for those oxides classified by Professor Birchenall as "impurity sensitive" or "borderline," the diffusion annealing ranges should have been extended to appreciably higher temperatures in order to insure that intrinsic diffusivities were indeed observed.

Measurement of the concentration profile of the diffusing species in the oxide specimen following the diffusion anneal has not received the attention it deserves in many laboratories involved in oxide diffusion experiments. Experience gained from diffusion investigations in metals or alkali halides has served to point up the value of determining the oxygen isotope or cation tracer concentration profile by either microtoming or precision grinding layer by layer off the diffusion specimen. The microtome sectioning technique might be used for oxides if a diamond knife were employed and the precision grinding methods, common for sectioning metal diffusion specimens, can readily be

modified for oxide specimens. Short-circuiting diffusion paths (dislocation pipes, cracks, etc.) may have a profound effect on the observed diffusion coefficient and are best detected by autoradiographic examination of oblique sections through the specimen.

Although Dr. Haven's discussion which follows deals with the subject of interdiffusion in detail, the measurement of a chemical diffusion coefficient has several unique problems not dealt with in the above remarks. One of these is the bonding together of the two halves of the diffusion couple so that there is no barrier to interdiffusion at this interface. This may be accomplished, for instance, by hot pressing the two pieces together in an induction-heated graphite die. The determination of the concentration profile may be undertaken with the aid of electron microprobe scanning parallel to the diffusion direction: this same technique should also prove useful in revealing short-circuiting diffusion paths in the specimen.

In summary, then, the problems currently encountered in diffusion experiments with oxides are invariably more severe than those encountered when dealing with metals or alkali halides. Some of the factors which are undoubtedly responsible for this present situation are: (1) the relatively impure and poorly characterized oxide single crystals available; (2) the contamination and temperature measurement problems arising because the diffusion anneals for the oxide specimens, of necessity, have to be conducted at extremely elevated temperatures; (3) the imprecision, achieved by the majority of the experimentalists who have investigated mass transport in oxides, in the evaluation of the concentration profile.

Principal Discussion II (Y. Haven):

The use of different diffusion coefficients calls for some caution, because they can be defined for different sets of gradients. A general discussion of such relationships, based on irreversible thermodynamics, is given by Howard and Lidiard (Reports on Progress in Physics **27**, 161 (1964)).

For a particular example one may decide to use one of the descriptions:

$$J_A = L_{11}(d\mu_A/dx) + L_{12}(d\mu_B/dx) + L_{13}(d\mu_C/dx) \quad (1)$$

$$= L'_{11}(dc_A/dx) + L'_{12}(dc_B/dx) + L'_{13}(dc_C/dx) \quad (2)$$

$$J_A = (L'_{11} - L'_{12})(dc_A/dx) \quad (3)$$

$$= (L'_{11} - L'_{13})(dc_A/dx) \quad (4)$$

where J_A is a current of A, the L's are coefficients and $d\mu/dx$ and dc/dx are gradients of chemical potential and concentration, respectively. Equations (3) and (4) follow from eq (2) with the assumptions

$$dc_A/dx = -dc_B/dx,\ dc_C/dx = 0$$

$$\text{and } dc_A/dx = -dc_C/dx,\ dc_B/dx = 0,$$

respectively.

Suppose A and B are isotopes and C is a second component.

When the tracer diffusion is considered one finds from (3)

$$D^*_{AB} = L'_{11} - L'_{12} = f(n/N)D_{\text{defect}} \quad (5)$$

where L'_{11} and L'_{12} are of the same order of magnitude. The result contains a factor (n/N) for the vacancy (or interstitial) concentration and a factor f for the correlations. D_{defect} is a diffusion coefficient defined for the random motion of defects.

It should be remembered that irreversible thermodynamics itself does not give factors like f or (n/N), which can only be incorporated by specific kinetic arguments. Equations like the Darken eq (6) cannot account for these.

One obtains rather simple relationships with the chemical diffusion coefficients, in cases where A and C have similar diffusion mechanisms, for example in an alloy AC. A diffusion coefficient described by eq (4) has the same structure as the tracer coefficient (3). In such a case usually the Darken equation gives a satisfactory description:

$$\tilde{D} = (D^*_1 N_3 + D^*_3 N_1)(1 + d \ln \gamma / d \ln N_1) \quad (6)$$

where the N's represent mole fractions.

In the case of oxides, however, if A and C represent cation and anion respectively, this procedure can be completely unsatisfactory, because the two components may travel on different sub-lattices, or may be coupled by electric forces. For example, in the interdiffusion of oxygen and cation a correlation factor is usually absent, also the factor (n/N) may appear in a different context.

In such cases one needs to go to the formula as developed by Schottky and Wagner (see paper by Heyne) and formulae for interdiffusion often take a form

$$D = 2D_A D_B/(D_A + D_B) \quad (7)$$

which equation can be encountered in ambipolar diffusion, or in the oxidation of metals.

If one component is slow, one may find for example

$$D = 2D_A. \quad (8)$$

Note the factor 2.

When a single phase oxide is subjected to a change of oxygen pressure, the attainment of equilibrium is governed by a diffusion coefficient (4) which takes the form

$$D = (L'_{11} - L'_{13}) = D_{\text{defect}} \tag{9}$$

Comparison of eq (9) with the tracer diffusion coefficient of eq (5) enables one to obtain separately the concentrations and mobilities of defects.

The latter information is to a certain extent lost, however, if the results are discussed in the language with chemical potentials as in eq (1), etc. (which may be the only feasible system).

For example, the rate constant for the oxidation of metals is in Wagner's theory presented in the form

$$k_m = -\frac{1}{|2A|}\frac{300}{F}\frac{1}{Ne}\int_{\mu_A(o)}^{\mu_A(\xi)} \sigma \cdot n_{\text{ion}} \cdot n_{\text{el}} d\bar{\mu}_A \tag{10}$$

where σ is a conductivity, n_{ion} and n_{el} are transference numbers for ionic and electronic transport, $\mu_A(o)$ and $\mu_A(\xi)$ are the electrochemical potentials at the boundaries of the oxide phase, and the other symbols have their usual meaning.

Only in the case that n_{el} is close to unity does the integrand represent the ionic conductivity and can it be replaced by a diffusion coefficient (hereafter denoted by the symbol D, and representing the sum of the diffusion coefficients of the ionic species involved, if properly normalized).

In more elementary approximations of eq (10) the conductivities (diffusion constants) may be independent of the position in the layer or rather independent of μ_A so that eq (10) can be integrated in a straightforward way to

$$k_m \approx D(\mu_A(\xi) - \mu_A(0)) \tag{11}$$

leading to Darken-type equations (except for a different type of summation of the D's). Such type of equations may be useful for the discussion of transport of oxygen through layers with a rather wide range of composition, because in these cases the diffusion coefficient may not be too strongly dependent on compositions. If this condition holds an equation for the chemical diffusion coefficient D in the form

$$D = (1/f)\alpha D_A^* \, (\partial \ln a_A / \partial \ln C), \tag{12}$$

where a_A is the activity of component A, may be quite appropriate, if α is a constant still to be determined for each particular case. However, if the D is dependent on composition an average D is measured which may differ considerably from D's measured in other ways.

Basically, eq (10) is derived with the assumption that the currents are throughout the layer the same, which condition can be maintained because the gradient of μ_A can adjust itself to this condition. However, in order to use such experiments for the determination of D's, one must ascertain that no barriers at the interfaces occur. Especially in such type of experiments large gradients may occur at one boundary, which may produce erratic results, because these gradients can be very sensitive to disturbances.

Many so-called irreproducible results are due to a lack of specific data on the thermodynamic circumstances.

A Materials Program?

Question:

Would it be desirable to select two or more particular oxides to serve as prototype materials, and to make interlaboratory comparisons on them? If so, which materials should be chosen, and how pure and well characterized would they have to be?

Principal Discussion (J. B. Wachtman, Jr.):

The uncertainty and lack of reproducibility which are frequently mentioned in connection with diffusion data make it very desirable to have some means of checking on both the experimental technique and on the specimens as possible sources of variability. Interlaboratory comparisons are a useful technique for assessing the accuracy of a given measurement and are sometimes also useful in helping to find the source of errors. For such comparisons, measurements must be made on the same specimen or on specimens having the same properties within the accuracy desired. For certain diffusion techniques, such as oxygen self-diffusion by gas sampling, it may be possible to use the same specimen in different laboratories, but diffusion experiments usually require destruction of the specimen so that reproducible specimens are needed.

A reasonable degree of reproducibility has been achieved in diffusion experiments on certain metals, alkali halides, and silver halides and one might consider the use of some of these materials as interlaboratory comparison specimens. The temperature range and the chemical environment (generally oxidizing) required for studies of diffusion in oxides do not favor the use of metals or halides, however. It appears that oxide specimens must be used for this purpose, but variation of composition and microstructure between nominally identical oxide specimens is thought to be one of the major sources of variability in diffusion data on oxides. If a re-

producible oxide can be obtained, it might be used to test the adequacy of experimental techniques which, when proven sound, could then be used to search for the sources of variability in other oxides. This proposed program would actually require a sequence of different oxide intercomparison specimens to correspond to the wide range of experimental conditions used for cation and anion diffusion in the various oxides being studied. The whole program would depend on producing one or more oxides which are sufficiently reproducible to serve as starting points.

The class of impurity-tolerant oxides discussed by Birchenall in this conference appears to offer the best prospects for such starting points. Diffusion in these oxides is dependent upon a very high concentration of point defects which is controlled by fixing the departure from stoichiometry through control of the activity of the major components or by fixing the amount of one additive at such a high level as to dominate other impurity effects. On this basis, the following list of oxides is suggested:

Material	Type and application
85 ZrO_2 + 15 CaO	Impurity-tolerant; oxygen self-diffusion
$Fe_{1-x}O$	Impurity-tolerant; cation self-diffusion
98.5 ThO_2 + 1.5 La_2O_3	Impurity-tolerant; variable mixed ionic and electronic conduction
MgO	Impurity sensitive; self-diffusion of both components, foreign cation diffusion.

The suggestion of calcia-stabilized zirconia as an interlaboratory comparison standard for oxygen self-diffusion was based on the comparatively good agreement in diffusion constants obtained by several different methods (see Birchenall's paper). It is known, however, that at 1000 °C the transport properties change slowly with time as ordered microdomains form. This might seriously limit the use of calcia-stabilized zirconia as a comparison standard at temperatures below 1400 °C. Wüstite was suggested for comparisons of cation self-diffusion, because it appears possible to fix a large departure from stoichiometry by using a practically achievable level of oxygen pressure, and because considerable work has been done on this system with results which show good consistency for oxides. Thoria containing lanthana or yttria was suggested as a mixed ionic and electronic conductor whose percentage of ionic conduction can be varied by varying the partial pressure of oxygen; this behavior is discussed in Heyne's paper in the present conference. Such a variable mixed conductor would be valuable in assessing experimental techniques for measuring ionic conductivity for comparison with diffusion data through the Nernst-Einstein relation. Heyne has discussed various experimental procedures all of which place strict requirements on electrodes as to their being reversible, or blocking to ionic current, or blocking to the electronic current. A controllable variable mixed conductor would permit checking some of the electrodes now used. Finally, the use of MgO as an impurity-sensitive comparison standard was tentatively proposed because much effort is being devoted to making better crystals (see the paper by Cleland) and a level of purity and perfection of MgO may be achieved which would permit its use to check experiments for contamination from supports and furnace atmosphere which may be a serious problem at the high temperatures used in diffusion studies in refractory oxides. In particular, oxygen self-diffusion usually involves a surface layer only a few microns thick and it is just this surface layer which is rather difficult to protect from contamination in the range of a few parts per million. It is frequently not appreciated how difficult it is to heat an oxide to 1800 °C without trace contamination of the surface.

General Discussion:

This was a lively discussion in which many participants, while generally agreeing that interlaboratory comparison specimens are desirable, pointed out a number of difficulties associated with the ones listed by Wachtman and suggested some other possibilities:

(1) There is some evidence that surface exchange of oxygen is the slow step for thoria and stabilized zirconia. This affects the diffusion profile obtained in a gas-solid experiment and would considerably complicate the analysis.

(2) The existence of time-dependent changes in the zirconia-calcia system associated with ordering of the cation sub-lattice was emphasized and the possibility was suggested that this may also occur in lanthana-doped thoria although no evidence was offered. The electrical conductivity depends on the grain size in calcia-stabilized zirconia which suggests a possible dependence of oxygen diffusion rate on grain size also.

(3) It was pointed out that a eutectoid reaction and precipitation of magnetite occurs in $Fe_{1-x}O$ so that heating and cooling the specimen would probably cause changes. In reply, it was argued that proper control of the activities of the com-

ponents of the system being studied, for sufficient time to achieve equilibrium, is an essential part of a diffusion experiment in a compound. The sensitivity of $Fe_{1-x}O$ to change of temperature and activities of components is thus a desirable feature of a standard specimen for checking experimental technique. This statement was accepted, but the original objection was clarified by pointing out that irreversible structural damage may occur in the process of precipitation and reheating. Thus, even if the specimen was equilibrated with respect to composition at the same temperature, structural damage might remain and affect diffusion values.

(4) Cobaltous oxide was suggested as a better possibility than ferrous oxide, although precipitation of a higher oxide is thought to occur in $Co_{1-x}O$ as well as in $Fe_{1-x}O$. This precipitation may not be an insuperable difficulty for either of the two oxides. The combination of choosing a small value for x and using a rapid heating and cooling schedule may sufficiently reduce structural damage.

(5) It was suggested that heavy doping of some oxide other than zirconia or thoria be tried to produce an impurity-tolerant standard; magnesium oxide doped with 5 percent alumina was suggested as an example. In reply, it was pointed out that while solid solution of Al_2O_3 in MgO is thought to exceed 5 percent at 2000 °C, precipitation of spinel would occur below 1700 °C. The general idea of heavy doping to produce a solid solution which is impurity-tolerant is attractive, but difficult to carry out because the possible existence of solid solution below 2 percent has not been investigated for most oxide systems. In those systems which appear to exhibit a large degree of solid solution the solid solution limit usually decreases rapidly with decreasing temperature, causing precipitation. In other cases (such as calcia-stabilized zirconia), the solid solution is metastable at intermediate temperatures and formation of microdomains occurs if time is allowed.

(6) The contamination of specimens during heating can be reduced by enclosing the specimen in a container of the same material. This may be a useful procedure in some diffusion experiments, but does introduce an additional complication in oxygen exchange experiments.

(7) Calcium oxide was suggested as an alternative to magnesium oxide because a material having cations and anions of approximately the same size and polarizability is desirable for comparison with alkali halides. The best understood of the alkali halides are those having ions of similar size such as NaCl or KCl.

Summary

The problem of mass transport in oxides may be divided rather naturally into two parts. The first part deals with the fundamental lattice defects present in pure (or, at least, well defined) single crystals and their role in mass transport. Here, the people studying oxides invariably look with admiration upon the experimental and theoretical achievements in similar studies of the alkali halides. There is little doubt that the alkali halides provide a natural starting point for the study of oxides because of the comparative simplicity of those materials as well as because of the accumulated information about defects in them. On the other hand, investigators of the oxides must be on the lookout for new phenomena, particularly those related to the higher valencies as well as the more covalent bonding of the oxides. As examples, the much greater deviation from stoichiometry in the oxides and the occurrence of microdomains should particularly be cited. If the lessons of the effects of purity in the alkali halides can be carried over to the oxides, it is clear that one cannot work too hard in the direction of improving the quality and purity of available oxide materials. In fact, it is doubtful if the intrinsic range of behavior can be observed for many of presently available oxide crystals.

For an advance in theoretical understanding, there is a great need to obtain good values for the formation and migration energies of the various predominant defects, in addition to information on defect symmetries and electronic charge states. At present, there is no expectation that theory alone can give meaningful values for these quantities. Rather, the experimentalist must supply the numbers which will then provide the basis for testing of theoretical models, the types of potentials to be employed, etc. This seems to be the best approach for advancing our theoretical understanding of defects in oxides. Such a program then requires the carrying out of such basic measurements as tracer diffusion of both cation and oxygen, ionic conductivity, transport number measurements, and where applicable, electron spin resonance and optical absorption. In all cases, extreme care is needed to fix the thermodynamic variables and to prevent contamination when measurements or heat treatments are carried out at very high temperatures. But all this care is not meaningful without good starting materials!

The need for better materials has been mentioned in the discussion at this conference, over and over again. It was particularly interesting to note how much debate arose over the proposal by Wachtman of four materials to serve as interlaboratory standards. The objections raised, particularly emphasized the complexity of structural and phase

changes that may be expected when solid solutions or highly nonstoichiometric oxides are chosen. Another factor that might be added here is the desire of solid-state scientists to make basic measurements on the purest and simplest materials, so that good data will have "handbook" value, especially to theoreticians. In this connection, the program of the Oak Ridge National Laboratory to prepare MgO crystals of high purity is probably most relevant. The availability of any one oxide of high purity and perfection will inevitably stimulate more reliable data and substantial interlaboratory comparison. In addition to the role of the national laboratories in producing such materials, however, industrial firms which produce or have a strong interest in a given oxide material should be made to feel a responsibility to the scientific community to produce a quantity of the best possible material. A striking example in the metals field, is the contribution that the American Smelting and Refining Company made some years ago, by producing and making available spectroscopically pure copper. This AS&R copper, which became the standard research material over a period of many years, was a major contribution to improved understanding of the noble metals.

And now, given this improved scientific understanding of defects and transport coming from better materials, more careful experiments, and theoretical calculation of defect parameters, how can this information be coupled to the practical technology of ceramic materials? This question apparently cannot readily be answered, unless we introduce a second group of problems in the study of oxides. Prominent among these problems are the following: (1) the study of the role of short-circuiting paths in diffusion and ionic conductivity, starting from very simple dislocation arrays; (2) the adhesion of scale during oxidation; (3) the kinetics and mechanisms of grain growth during sintering; and (4) the relation between chemical and tracer diffusion coefficients. To a purist in the field of point defects these problems may be of lesser interest, but, conversely, in real technological situations the intrinsic behavior of structurally perfect crystals may be of only minor importance. Instead, the process may be dominated by factors involved in the above, or similar, problems. Most of these problems received very little attention at this conference. For problem (4) there is an elaborate formal theory based on the thermodynamics of irreversible processes, but not much data in which the various diffusivities are all measured on a single system. Such a detailed study is required in order to determine which simplifying approximations can be introduced into the theory for a given diffusion problem.

It appears that only by expanded activity in this second group of problems, in parallel with the fundamental studies of lattice defects, can we anticipate a useful contribution to the understanding of technologically important processes.

290-621 O-68—15

NATIONAL BUREAU OF STANDARDS

The National Bureau of Standards[1] was established by an act of Congress March 3, 1901. Today, in addition to serving as the Nation's central measurement laboratory, the Bureau is a principal focal point in the Federal Government for assuring maximum application of the physical and engineering sciences to the advancement of technology in industry and commerce. To this end the Bureau conducts research and provides central national services in three broad program areas and provides central national services in a fourth. These are: (1) basic measurements and standards, (2) materials measurements and standards, (3) technological measurements and standards, and (4) transfer of technology.

The Bureau comprises the Institute for Basic Standards, the Institute for Materials Research, the Institute for Applied Technology, and the Center for Radiation Research.

THE INSTITUTE FOR BASIC STANDARDS provides the central basis within the United States of a complete and consistent system of physical measurement, coordinates that system with the measurement systems of other nations, and furnishes essential services leading to accurate and uniform physical measurements throughout the Nation's scientific community, industry, and commerce. The Institute consists of an Office of Standard Reference Data and a group of divisions organized by the following areas of science and engineering:

Applied Mathematics—Electricity—Metrology—Mechanics—Heat—Atomic Physics—Cryogenics[2]—Radio Physics[2]—Radio Engineering[2]—Astrophysics[2]—Time and Frequency.[2]

THE INSTITUTE FOR MATERIALS RESEARCH conducts materials research leading to methods, standards of measurement, and data needed by industry, commerce, educational institutions, and government. The Institute also provides advisory and research services to other government agencies. The Institute consists of an Office of Standard Reference Materials and a group of divisions organized by the following areas of materials research:

Analytical Chemistry—Polymers—Metallurgy — Inorganic Materials — Physical Chemistry.

THE INSTITUTE FOR APPLIED TECHNOLOGY provides for the creation of appropriate opportunities for the use and application of technology within the Federal Government and within the civilian sector of American industry. The primary functions of the Institute may be broadly classified as programs relating to technological measurements and standards and techniques for the transfer of technology. The Institute consists of a Clearinghouse for Scientific and Technical Information,[3] a Center for Computer Sciences and Technology, and a group of technical divisions and offices organized by the following fields of technology:

Building Research—Electronic Instrumentation — Technical Analysis — Product Evaluation—Invention and Innovation— Weights and Measures — Engineering Standards—Vehicle Systems Research.

THE CENTER FOR RADIATION RESEARCH engages in research, measurement, and application of radiation to the solution of Bureau mission problems and the problems of other agencies and institutions. The Center for Radiation Research consists of the following divisions:

Reactor Radiation—Linac Radiation—Applied Radiation—Nuclear Radiation.

---

[1] Headquarters and Laboratories at Gaithersburg, Maryland, unless otherwise noted; mailing address Washington, D. C. 20234.
[2] Located at Boulder, Colorado 80302.
[3] Located at 5285 Port Royal Road, Springfield, Virginia 22151.

NBS TECHNICAL PUBLICATIONS

PERIODICALS

JOURNAL OF RESEARCH reports National Bureau of Standards research and development in physics, mathematics, chemistry, and engineering. Comprehensive scientific papers give complete details of the work, including laboratory data, experimental procedures, and theoretical and mathematical analyses. Illustrated with photographs, drawings, and charts.

Published in three sections, available separately:

• Physics and Chemistry

Papers of interest primarily to scientists working in these fields. This section covers a broad range of physical and chemical research, with major emphasis on standards of physical measurement, fundamental constants, and properties of matter. Issued six times a year. Annual subscription: Domestic, $5.00; foreign, $6.00*.

• Mathematical Sciences

Studies and compilations designed mainly for the mathematician and theoretical physicist. Topics in mathematical statistics, theory of experiment design, numerical analysis, theoretical physics and chemistry, logical design and programming of computers and computer systems. Short numerical tables. Issued quarterly. Annual subscription: Domestic, $2.25; foreign, $2.75*.

• Engineering and Instrumentation

Reporting results of interest chiefly to the engineer and the applied scientist. This section includes many of the new developments in instrumentation resulting from the Bureau's work in physical measurement, data processing, and development of test methods. It will also cover some of the work in acoustics, applied mechanics, building research, and cryogenic engineering. Issued quarterly. Annual subscription: Domestic, $2.75; foreign, $3.50*.

TECHNICAL NEWS BULLETIN

The best single source of information concerning the Bureau's research, developmental, cooperative and publication activities, this monthly publication is designed for the industry-oriented individual whose daily work involves intimate contact with science and technology—*for engineers, chemists, physicists, research managers, product-development managers, and company executives.* Annual subscription: Domestic, $1.50; foreign, $2.25*.

*Difference in price is due to extra cost of foreign mailing.

NONPERIODICALS

Applied Mathematics Series. Mathematical tables, manuals, and studies.

Building Science Series. Research results, test methods, and performance criteria of building materials, components, systems, and structures.

Handbooks. Recommended codes of engineering and industrial practice (including safety codes) developed in cooperation with interested industries, professional organizations, and regulatory bodies.

Special Publications. Proceedings of NBS conferences, bibliographies, annual reports, wall charts, pamphlets, etc.

Monographs. Major contributions to the technical literature on various subjects related to the Bureau's scientific and technical activities.

National Standard Reference Data Series. NSRDS provides quantitative data on the physical and chemical properties of materials, compiled from the world's literature and critically evaluated.

Product Standards. Provide requirements for sizes, types, quality and methods for testing various industrial products. These standards are developed cooperatively with interested Government and industry groups and provide the basis for common understanding of product characteristics for both buyers and sellers. Their use is voluntary.

Technical Notes. This series consists of communications and reports (covering both other agency and NBS-sponsored work) of limited or transitory interest.

CLEARINGHOUSE

The Clearinghouse for Federal Scientific and Technical Information, operated by NBS, supplies unclassified information related to Government-generated science and technology in defense, space, atomic energy, and other national programs. For further information on Clearinghouse services, write:

Clearinghouse
U.S. Department of Commerce
Springfield, Virginia 22151

Order NBS publications from:
Superintendent of Documents
Government Printing Office
Washington, D.C. 20402

U.S. GOVERNMENT PRINTING OFFICE : 1968 OL—290-621